

IAP/ICP Final Report (2021 – Apr 2025) *Editor: Dr. Samir Mourad*

Legend:

- Still open
- In work
- completed



IAP/ICP Projects Actual Status Apr 2025



Still open issues:

2025: Mass Spectrometer, Cyclotron

- Responsible: Majd/Abdullah K.
- Due Date:
- Needed Budget:

X-Ray Detector (Scintillator) and X ray pattern (Laue pattern)



ICF Driver (light ion beam with pulsed powered diode and Marx Generator)

Needed Budget: 1000\$
Timeline: 3-9/25
Responsible:

ICF Target

Design
Timeline: 9/24
Responsible:
Design: Phys Funda M2 Group (

Realization
Needed Budget: 1000\$
Timeline: 2025
Responsible: Design: Phys Funda M2 Group (Ahmad)

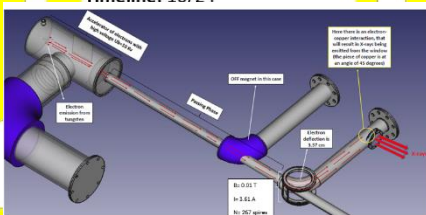
Magnetic Beam Deflection



TODO: Realization

Linear Accelerator (RF)

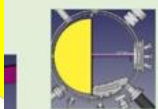
Needed Budget:
Timeline: 10/24



Electron Source

Flue Gas Heavy Metals Mass Spectrometer

Needed Budget: 2000\$
Timeline: Integration (9/24), Testing (9/24)
Responsible: Majd



IECF Device

Needed Budget: 5000\$
(Ultra High Vacuum Pump), D2



ICF Simulation

Fusion Process in Target
Timeline: 9/24
Responsible:

Last Update:
 15.04.2025 15:54

Content

Preface	11
1 Lists of Abbreviations and Symbols	15
1.1 LIST OF ABBREVIATIONS.....	15
1.2 LIST OF SYMBOLS.....	15
2 Summary	19
2.1 Actual Status of Projects in Apr 2025.....	19
2.2 IAP Physics Lab	20
2.3 Posters of partly realized projects	22
2.3.1 IAP Physics Lab Training Device.....	22
2.3.2 IECF (Inertial Electrostatic Confinement Fusion).....	24
2.3.3 X-Ray	26
2.3.4 Inertial Confinement Fusion.....	27
2.3.5 Mass Spectrometer	30
2.3.6 Plasma Code.....	36
2.4 Actual Status of projects	37
2.5 To be further realized.....	38
2.5.1 Cyclotron	38
2.5.2 Electrical Propulsion for Space	42
2.5.3 X-Ray Detection by Laue pattern	45
3 IAP-Physics Lab Testrig	50
3.1 Requirements for IAP-Physics Lab Testrig.....	50
3.1.1 System Requirements	50
3.1.2 Mechanical requirements:	50
3.1.3 Electrical requirements:.....	51
3.1.4 Magnetic requirements:.....	51
3.1.5 Safety requirements:	51
3.2 System Design and Mechanical Design of IAP-Physics Lab Testrig.....	52
3.3 Mechanical Realization of IAP-Physics Lab Testrig	55
3.4 IAP-Physics Lab Testrig Automation (Process control system).....	58
3.4.1 PLC control panel.....	59

Content

3.4.2	Instruments	59
3.4.3	Panel Wiring Diagram	60
3.4.4	Graphical User Interface (GUI).....	61
3.4.5	Modbus Address - Point Interface (PLC).....	61
3.5	IAP-Physics Lab Testrig Vacuum testing & X-Ray Testing.....	62
3.5.1	System Test Specification	62
3.5.2	System Test and Results	66
4	Electron Flux Measurement with Rogowski Coil.....	79
4.1	Introduction.....	80
4.1.1	Task	80
4.1.2	Current Transducer Approach.....	80
4.1	In terms of installation and connection	81
4.1.1	Questions:.....	81
4.2	Rogowski Coil Approach	82
4.2.1	In terms of alternating current measurement (AC), there are Rogowski Coil:	82
4.2.2	What is a Rogowski Coil?.....	82
4.2.3	How does a Rogowski Coil Work?.....	82
4.2.4	Rogowski Coil Current Sensor	83
4.2.5	Rogowski Coil Design	83
4.2.6	Rogowski Coil Integrator	85
4.2.7	Rogowski Coil.....	88
4.2.8	Construction of Rogowski coil	88
4.2.9	Design experiment of Rogowski Coil in laboratory	89
4.2.10	Design and construction of active integrator	90
4.2.11	Electronic tools used to create an active integrator	91
4.2.12	Using EagleCAD to create a schematic and to do switch to board	92
4.3	Construction of an active integrator connected to the coil in laboratory	94
4.3.1	The formulas that should be used after construction a rogowski coil:.....	95
4.3.2	Fix some errors in the installed electrical circuit in the lab	96
4.4	Comparison between op07cp and op77f.....	98
4.4.1	How to insert and use the OP77F code downloaded from the Internet into the LTspice:.....	100
4.4.2	The electronic circuit schematique in LTspice	103

4.4.3	Simulation (DC on pnt)	106
4.4.4	Add an input voltage to the schematic	110
4.5	Remaining tasks	112
4.6	Literature.....	113
5	X Ray and Gamma Ray Shielding	115
5.1	Introduction.....	116
5.2	Gamma ray	116
5.3	Protecting Against Exposure.....	119
5.3.1	Time, Distance and Shielding	119
5.3.2	Shielding of Gamma Radiation	121
5.3.3	Gamma Rays Attenuation.....	122
5.4	Pulsed power accelerators	128
5.4.1	Construction and operation	128
5.4.2	MAIN PARAMETERS OF ACCELERATOR.....	129
5.5	Monitoring Radiation Exposure	129
5.5.1	Measurement of beam current.....	129
5.6	DESIGN OF X-RAY ROOMS	131
5.6.1	Room size.....	131
5.6.2	Doors and Walls	131
5.6.3	Protective cubicle.....	132
6	X-Ray Generation and Detection (Master Thesis Final Version Sent Feb 2022)	133
6.1	Summary: Status Nov 21	134
6.2	Abstract	135
6.3	X-Ray Detection (Master Thesis Master Thesis Presentation 8.12.21).....	135
6.4	Introduction.....	146
6.5	Source	147
6.5.1	X-ray tube process	147
6.5.2	Selection of XRD Tubes According to Anode Material :	147
6.6	Detector	148
6.6.1	Concept of solid state radiation detectors:.....	148
6.6.2	Scintillators.....	150
6.6.3	Photodiode:	153
6.7	Realization of X-Ray Sensor in Nano satellite and laboratory testing	157

6.7.1	Detector.....	157
6.7.2	Electrical Circuit Testing with Oscilloscope.....	162
6.7.3	Preamplifier Design:.....	164
6.7.4	Testing X-ray sensor with X-ray source.....	166
6.8	Results in Time domain and in Frequency domain.....	173
6.9	Conclusion:.....	175
6.10	References.....	176
6.11	List of figures.....	176
6.12	List of Tables.....	177
6.13	Annex: Matlab code.....	177
7	RF Linear particle accelerator.....	179
7.1	Parts of LINAC and their functions.....	179
7.2	How it's Work.....	180
7.3	Electrons gun.....	181
7.4	High voltage power supply:.....	181
7.4.1	Vacuum of the tube accelerator:.....	183
7.4.2	Slit accelerator anode connected:.....	183
7.4.3	Slit accelerator anode disconnected:.....	183
	Tube accelerator:.....	184
8	Electron Source, LINAC (with glass tube), electromagnetic deflection of electrons and X-Ray Generation.....	187
8.1	LIST OF FIGURES.....	187
8.2	LIST OF TABLES.....	189
8.3	Basics concerning Generation and Accelerating Electrons.....	191
8.3.1	Cathode.....	191
8.3.2	Anode.....	192
8.3.3	Acceleration of electrons.....	192
8.4	Vacuum Pump.....	196
8.4.1	The fundamentals of vacuum theory.....	196
8.4.2	Basic vacuum system for our prototype.....	196
8.5	Electron gun Glass Tube LINAC Testing.....	197
8.5.1	System requirements.....	197
8.5.2	Mechanical requirements.....	197

8.5.3	Electrical requirements	197
8.5.4	Safety requirements	197
8.5.5	System test specification.....	197
8.5.6	System Test and Results	200
8.6	Basics concerning X-ray production (by collision of accelerated electrons on heavy metals)	222
8.6.1	The characteristic radiation.....	222
8.6.2	The target (copper).....	223
8.7	Detection of X-rays with Geiger Muller counter	224
8.8	Safety with X-rays working.....	225
8.9	X-Ray Protection Lead box design & Realization	226
8.9.1	Computer Aided Design (CAD).....	226
8.9.2	Realization.....	227
8.10	Basics concerning electron beam deflection by Helmholtz coil	228
8.10.1	Definition.....	229
8.10.2	Features.....	229
8.10.3	Mathematical formula	229
8.10.4	Manufacturing conditions.....	230
8.11	Helmholtz Coil Design.....	230
8.11.1	Fundamental Precepts	230
8.11.2	Computer Aided Design (CAD).....	231
8.11.3	Realization.....	232
8.12	Helmholtz coil test.....	234
8.12.1	Requirements	234
8.12.2	System test specification.....	235
8.12.3	System Test and Results	235
9	IECF (Inertial Electrostatic Confinement Fusion)	241
9.1	On www.aecenar.com	241
9.2	IAP-IECF Device Concept and Design	241
9.2.2	Our Device.....	253
9.2.3	IEC Device	255
9.2.4	Simulation	256
9.3	IAP-IECF Device Realization	273

Content

9.3.1	Introduction.....	277
9.3.2	Physics.....	277
9.3.3	Fuel of Fusor reactor	293
9.3.4	Electrical System.....	311
9.3.5	Mechanical system	333
9.3.6	Detectors	338
9.3.7	Vacuum tests.....	340
9.3.8	Searching for materials	356
9.3.9	Procurements	382
9.3.10	References.....	385
9.4	Open Tasks Status Apr 22 / Nov 23 for IECF.....	385
9.5	Neutron Production at FRANZ proton thruster in Frankfurt/Germany	386
10	Mass Spectrometer Concept	387
10.1	Basic Principles	391
10.1.1	Introduction.....	391
10.1.2	Measurement principles	392
10.1.3	Sampling.....	393
10.1.4	The Ion source.....	393
10.1.5	Magnetic Mass Analyser	394
10.1.6	Detectors	395
10.1.7	Mass Spectrometry / Gas Chromatography	399
10.1.8	VG-70S Magnetic Sector Mass Spectrometer.....	400
10.2	Our Device.....	401
10.2.1	Overview	401
10.2.2	Parts.....	404
10.2.3	Acceleration Slits	404
10.2.4	Magnet	405
10.2.5	Detector.....	405
10.2.6	406	
10.2.7	FreeCad.....	407
11	Mass Spectrometer Detector.....	409
11.1.1	Introduction.....	411
11.1.2	Faraday's cup (test module).....	412

11.1.3	Fundamental Precepts	412
11.1.4	Computer Aided Design (CAD).....	413
11.1.5	Realization.....	417
11.1.6	Electronics and Amplification Process:.....	421
11.1.7	In summary	422
11.1.8	Faraday Cut Detector Amplification Circuit	423
12	Mass Spectrometer Design and Realization based on Helmholtz Coils.....	426
12.1	SUMMARY	427
12.2	Introduction.....	427
12.3	Mass Spectrometer Requirements.....	427
12.3.1	System requirements:.....	427
12.3.2	Mechanical requirements:	428
12.3.3	Physical requirements:.....	428
12.3.4	Electrical requirements:	428
12.3.5	Magnetic requirements:.....	428
12.3.6	Safety requirements:	429
12.4	Mass spectrometer Design.....	429
12.4.1	Fundamental Concepts.....	429
12.4.2	Computer Aided Design (CAD).....	429
12.5	Mass Spectrometer Realization.....	432
12.6	Helmholtz coil with soft iron	436
12.6.1	Definition.....	436
12.6.2	Features.....	437
12.6.3	Mathematical formula	438
12.6.4	Manufacturing conditions.....	438
12.7	Requirements for Helmholtz coils.....	439
12.7.1	Mechanical requirements:	439
12.7.2	Electrical requirements:	439
12.7.3	Magnetic requirements:.....	440
12.8	Design of Helmholtz coil with soft iron	440
12.8.1	Fundamental Precepts	440
12.8.2	CAD.....	441
12.9	Realization of Helmholtz Coils	442

Content





12.10	Helmhotz Coils System Test Specification.....	442
12.11	Helmhotz Coils System Tests and Results	443
12.11.1	Test 22.09.23	443
12.11.2	Test 09.10.23	444
12.11.3	Test 20.10.23	447
12.12	Mass Spectrometer System Test Specification.....	449
12.12.1	00001: Ensure complete air evacuation	449
12.12.2	00002: Tungsten power supply.....	450
12.12.3	00003: First positively charged plate (trap) electron).....	450
12.12.4	00004: Second positively charged plate (ion repellent).....	450
12.12.5	00005: Obtain electrons.....	451
12.12.6	00006: Detector.....	452
12.12.7	00008: Power supply to the three plates (Acceleration zone).....	453
12.12.8	00009: Helmholtz coil.....	454
12.12.9	000010: Acceleration and Deviation.....	454
12.13	Conclusion and Perspectives for using Helmholtz Coils for Mass Spectrometer	456
12.14	Bibliography	456
12.15	LIST OF FIGURES.....	457
12.16	LIST OF TABLES	458
13	Mass Spectrometer Design, Simulation and Realization based on Iron Core Coils	461
13.1	ABSTRACT	462
13.2	CHAPTER 0: INTRODUCTION	462
13.3	CHAPTER I: BASICS.....	462
13.3.1	Mass Spectrometer Principle	462
13.3.2	Electromagnetism.....	466
13.3.3	Purification of Iron	475
13.3.4	Annealing	477
13.4	CHAPTER II: ELECTROMAGNETIC CONCEPTIONS	479
1.	Multi-solenoid Unit.....	479
2.	C-shaped Unit.....	482
13.5	CHAPTER III: REALIZATION, TESTS & DISCUSSION	493
13.5.1	Realization.....	493
13.5.2	Tests and Results	501





13.5.3	Calibrating Mass Spectrometer with Known Material Probes	507
13.6	CHAPTER IV: CONCLUSION & PERSPECTIVES.....	511
13.7	List of References	512
13.8	List of Figures.....	513
13.9	List of Tables.....	514
14	Electron Gun for Mass Spectrometer	517
14.1	Introduction.....	517
14.1.1	Structure and Function of an Electron Gun.....	517
14.1.2	Electric Fields and Electron Acceleration.....	517
14.1.3	Role of the Wehnelt Grid.....	518
14.1.4	High Vacuum (HV) Requirements and Materials	519
14.1.5	Magnetic Lenses and Electron Optics.....	519
14.2	Simulation.....	519
14.2.1	ElectronGun Outer Cover Design (Dec24/25)	522
14.2.2	Electron Entrance Realization Concept (4.1.25)	522
14.3	System Test Specification.....	522
14.4	Electron gun Test (15.3.25).....	531
14.5	References	536
15	Inertial Confinement Fusion (ICF)	537
15.1	Fundamentals.....	537
15.2	ICF Simulation Introduction and Theory	552
15.3	Our ICP-ICF Simulation Code	562
15.3.1	Documentation of the ICF_SIMULATION code.....	563
15.4	Design of IAP-ICF Device.....	575
16	ICF Light-Ion Driver: Marx Generator and Pulsed Powered Diode.....	577
16.1	Pulsed power diode accelerator	579
16.1.1	General Features:.....	579
References	591






Preface

In this report all activities concerning IAP (experimental physics) and ICP (theoretical and computational physics) in AECENAR are documented for the period 2021 – April 2025.

The following reports are part of the report:

<p>IECF</p>  <p>Inertial Electrostatic Confinement Fusion Reactor</p>	 <p>Inertial Electrostatic Confinement Fusor (IECF) Prototype Realization, Ver. March 2022</p>
<p>X-Ray</p> <p>X-Ray and Gamma ray shielding</p>  <p>M.K., 4.1.21</p>	 <p>MASTER THESIS</p> <p>In Order to Obtain the Research Master Or Physics of Radiation-Matter Interaction</p> <p>Presented and defended by: Yahya Al Abbouchi</p> <p>On 10th October 2021</p> <p><u>Title</u> X-Ray Detector for the Nano satellite IAP-SAT</p> <p>Supervisor Dr. Ahmad Osman</p> <p>Reviewer Prof. Adnan Naja Prof. Hassan Amoud</p>
<p>Mass Spectrometer Concept</p>	<p>Mass Spectrometer with Deflection based on Helmholtz Coils</p>

 <p style="text-align: center;"> Magnetic Sector Mass Spectrometry </p> <p style="text-align: center;"> Author: Maryam Abdel-Karim </p> <p style="text-align: center;"> Last Update: 22.12.21 </p>	  <p style="text-align: center;"> MEMORY </p> <p style="text-align: center;"> In order to obtain the RESEARCH </p> <p style="text-align: center;"> In PIRM: Physics of Radiation-Matter Interaction </p> <p style="text-align: center;"> Presented and Supported by: Asmaa Ahmad El Mir Jan 2023 </p> <p style="text-align: center;"> <u>Title</u> Evolution of mass spectrometer device for the detection of combustion gases from municipal waste </p> <p style="text-align: center;"> Supervisor Prof. Ahmad Osman Readers Dr. Hamed Khatib Dr. Adnan Naja </p> <p style="text-align: center;"> <small>Lebanese University-Faculty of sciences</small> </p>
<p style="text-align: center;"> Mass Spectrometer Based on Iron Core </p> <hr/>  <p style="text-align: center;"> MASTER THESIS </p> <p style="text-align: center;"> In order to obtain the PROFESSIONAL MASTER Energetics </p> <p style="text-align: center;"> Insured by: Faculty of Sciences of the Lebanese University </p> <hr/> <p style="text-align: center;"> Presented and defended by: Omar Ali Zreika </p> <p style="text-align: center;"> On October, 2024 Title Mass Spectrometer for Detection of Toxic Metals in Municipal Waste Incineration Flue Gas </p> <hr/> <p style="text-align: center;"> Supervisor Dr. Samir Mourad </p> <p style="text-align: center;"> Reviewers Dr. Ahmad El Mol </p>	
<p>Electron Source and LINAC</p>	

 <p>MEMORY</p> <p>In order to obtain the</p> <p>RESEARCH</p> <p>In</p> <p>PIRM: Physics of Radiation-Matter Interaction</p> <p>Presented and Supported by:</p> <p>Rouayda Muhammad Sakka</p> <p>January 2024</p> <p>Title</p> <p>Development of the integration and commissioning of a physics laboratory training device with X-ray production.</p> <p>Supervisor</p> <p>Prof. Adnan Naja</p> <p>Readers</p> <p>Dr. Ahmad Osman</p> <p>Dr. Hassan Amoud</p> <p><small>Lebanese University-Faculty of sciences</small></p> 	 <p>AECENAR Association for Economical and Technological Cooperation in the Euro-Asian and North-African Region www.aecenar.com</p>  
	<p><u>Electrofilter</u> Measurement with Rogowski Coil</p> <p>Author: Louay Indakji</p> <p>Last update: 08.06.2021</p>

1 Lists of Abbreviations and Symbols

1.1 LIST OF ABBREVIATIONS

HCL	: Hydrogen Chloride
HF	: Hydrogen Fluoride
Hg	: Mercury
SO ₂	: Sulfur Dioxide
CAD	: Computer Aided Design
FreeCAD	: a CAD software
PCB	Printed Circuit Board
Op-amps	: operational amplifier
Max	: maximum
Min	: minimum
ICF	: Inertial Confinement Fusion
CAD	: Computer Aided Design
IECF	: Inertial Electrostatic Confinement Fusion
PLCS	: Industrial Programmable Automation Systems
FreeCAD	: A CAD software
MISTLETOE	: Graphical User Interface
PLC	: Programmable Logic Controller (Industrial Programmable Logic Controller)
LINAC	: Linear accelerator

1.2 LIST OF SYMBOLS

R_m	: Average resistance	Ω
U	: Potential difference	V

E	: Electric field	Vm^{-1}
U_b	: Acceleration voltage	V
d	: Distance between cathode and anode	m
F	: Electric force	N
e	: Charge of an electron	C
W	: Electrical work between the cathode and the anode	I
E_c	: Kinetic energy	J or ev
m	: Mass of an electron	Kg
V	: Speed of the electron	ms^{-1}
V_f	: Final velocity of the electron	ms^{-1}
m_r	: Relativistic mass of an electron	Kg or ev.C^{-2}
C	: Speed of light	ms^{-1}
γ	: Lorentz factor	
V_r	: Relativistic speed of an electron	ms^{-1}
V_c	: Classical speed of an electron	ms^{-1}
X	: Position of the electron	m
t	: Time	s
has	: Acceleration of the electron	ms^{-2}
R	: Radius of the circular trajectory of the electrons	m
B	: Magnetic field	T
q	: Charge	C
E_K	: K-shell binding energy	ev
E_L	: Binding energy of the L layer	ev
E_M	: M-shell binding energy	ev
$E_{K\alpha}$: Difference between K-shell energy and L-shell energy	ev
$E_{K\beta}$: Difference between K-shell energy and M-shell energy	ev
I	: Intensity of the current flowing through the two coils	HAS
N	: Number of turns	

R'	: Radius of each coil	m
d'	: Distance between two coils	m
D	: Diameter of each coil	m
μ_0	: Vacuum permeability	Hm^{-1}
x	: Distance measured along the central axis of the coils	m
V	: Volume of the ionization chamber	m^3
IE_1	: First ionization energy	ev
IE_2	: Second ionization energy	ev
m	: Mass of an ion	Kg
Z	: Electric charge of an ion	
R	: radius of curvature of an ion	m
E_c	: Kinetic energy of an ion	J or ev
q	: Charge	C
U	: Potential difference	V
v	: Speed of an ion	ms^{-1}
F	: Magnetic force	N
B	: Magnetic field	T
U_{off}	: Offset voltage offset	V
A_{v}	: Voltage gain	
$CMRR$: Common mode rejection ratio	dB
μ_0	: Vacuum permeability	H/m
μ_r	: Relative permeability of magnetic material	

Lists of Abbreviations and Symbols

μ	: Magnetic permeability of the material	H/m
I	: Current intensity flowing through the two coils	HAS
D	: Diameter of each coil	m
N	: Number of turns	
R'	: Radius of each coil	m
d'	: Distance between two coils	m
x	: Distance measured along the central axis of the coils	m

2 Summary

2.1 Actual Status of Projects in Apr 2025

Legend:

- Still open
- In work
- completed

بِسْمِ اللَّهِ الرَّحْمَنِ الرَّحِيمِ



IAP/ICP Projects Actual Status Apr 2025



Still open issues:

2025: Mass Spectrometer, Cyclotron

- Responsible: Majd/Abdullah K.
- Due Date:
- Needed Budget:

**X-Ray Detector
(Scintillator)
and X ray pattern
(Laue pattern)**

Needed Budget:
Timeline:
Responsible:

**ICF Driver (light ion beam
with pulsed powered diode
and Marx Generator)**

Needed Budget: 1000\$
Timeline: 3-9/25
Responsible:

ICF Target

Design

Timeline: 9/24
Responsible:
Design: Phys Funda M2 Group (

Realization

Needed Budget: 1000\$
Timeline: 2025
**Responsible: Design: Phys Funda
M2 Group (Ahmad)**

Magnetic Beam Deflection

Needed Budget: 1000\$
Timeline: 10/24
Responsible: Abdullah Q.

Linear Accelerator (RF)

Needed Budget:
Timeline: 10/24
Responsible:

**Flue Gas Heavy Metals
Mass Spectrometer**

Needed Budget: 2000\$
**Timeline: Integration
(9/24), Testing (9/24)**
Responsible: Majd

Cyclotrone

TODO: Realization

Electron Source

ICF Simulation

**Fusion Process in
Target**
Timeline: 9/24
Responsible:

IECF Device

Needed Budget: 5000\$
**(Ultra High Vacuum
Pump), D2**

2.2 IAP Physics Lab

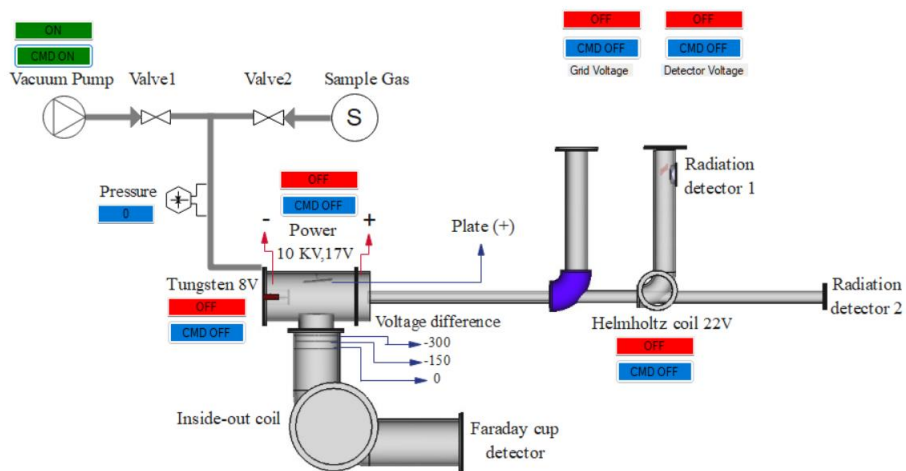




Mass_Spectrometer


Control

Mass Spectrometer




2.3 Posters of partly realized projects


2.3.1 IAP Physics Lab Training Device



AECENAR
Association for Economical and Technological Cooperation
in the Euro-Asian and North-African Region

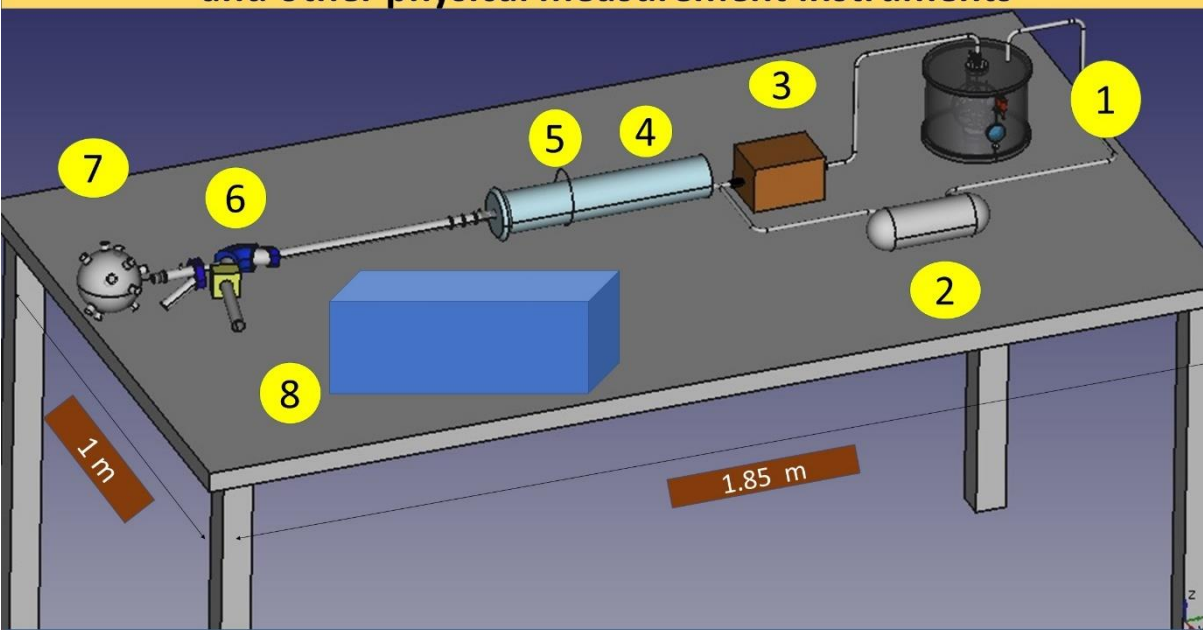
TECDA





IAP
INSTITUTE FOR
ASTROPHYSICS

System design of a physics lab training device with Rogowski Coil and other physical measurement instruments



1-Inertial electrostatic confinement fusion (IECF) : is a class of fusion power devices that use electric fields to confine the plasma rather than using magnetic fields.

2-Vacuum pump: a vacuum pump is a device that draws gas molecules from a sealed volume in order to leave behind a partial vacuum .The function of a vacuum pump is to generate a relative vacuum within the capacity to avoid collision of particles with air particles.

3-High voltage Supply (48 kV) .

4- LINAC: Linear particle accelerator is a type of particle accelerator that dramatically increases the kinetic energy of charged subatomic particles or ions by subjecting the charged particles to a series of oscillating electrical potentials along a line of linear beam.

5- Rogowski Coil : an electrical device that is used to measure current.

6- Magnetic sector mass spectrometer: In mass spectrometry, ions are generated from a sample to be analyzed. These ions are then separated and quantitatively detected. Separation is achieved on the basis of different trajectories of moving ions with different mass/charge (m/z) ratios in electrical and/or magnetic fields.

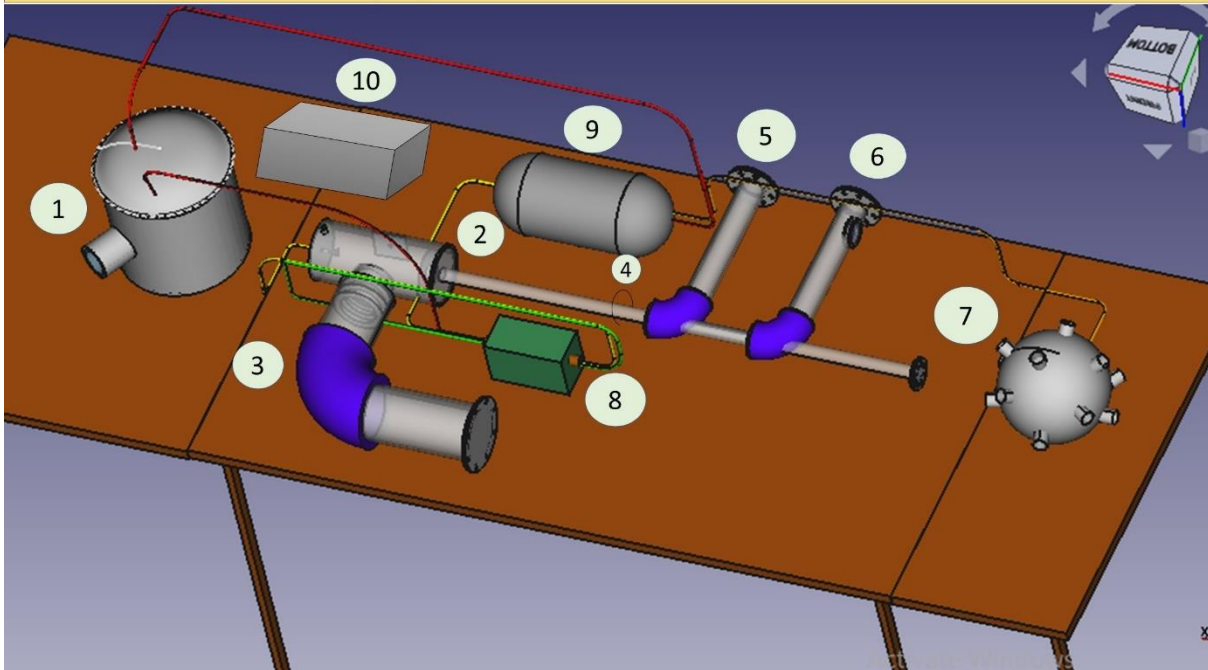
7- Inertial confinement fusion (ICF) target : a fusion energy target device were a high energy beam (here: electron beam) initiates nuclear fusion reactions by compressing and heating the target which is filled with thermonuclear fuel .

8- Control Box: sensors/actuators interface, PLCs, Connection to computer (data visualization and processing).

Rouwayda Sakka, Asmaa El Mir, Jana Hammoud

@AECENAR/ August 2022

System design of a physics lab training device with Rogowski Coil and other physical measurement instruments



1-Inertial electrostatic confinement fusion (IECF) : is a class of fusion power devices that use electric fields to confine the plasma rather than using magnetic fields.

2-Electron accelerator : production of beams of electrons.

3-Magnetic sector mass spectrometer: In mass spectrometry, ions are generated from a sample to be analyzed. These ions are then separated and quantitatively detected. Separation is achieved on the basis of different trajectories of moving ions with different mass/charge (m/z) ratios in electrical and/or magnetic fields

4-Rogowski Coil : an electrical device that is used to measure current.

5-Electron beam: This tube is ready for another application in the future.

6-Interaction electron-copper: production of X-ray.

7- Inertial confinement fusion (ICF) target : a fusion energy target device were a high energy beam (here: electron beam) initiates nuclear fusion reactions by compressing and heating the target which is filled with thermonuclear fuel .

8-High voltage Supply (48 kV) .

9-Vacuum pump: a vacuum pump is a device that draws gas molecules from a sealed volume in order to leave behind a partial vacuum .The function of a vacuum pump is to generate a relative vacuum within the capacity to avoid collision of particles with air particles.

10- Control Box: sensors/actuators interface, PLCs, Connection to computer (data visualization and processing).

Rouwayda Sakka, Asmaa El Mir

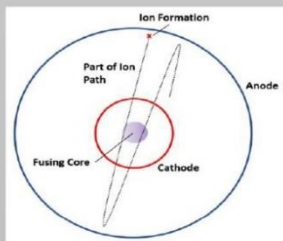
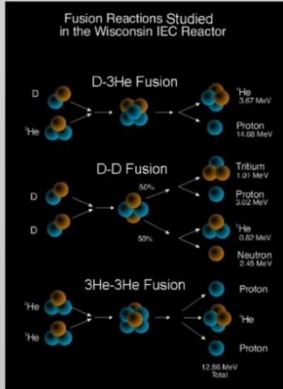
@AECENAR/ November 2022

2.3.2 IECF (Inertial Electrostatic Confinement Fusion)

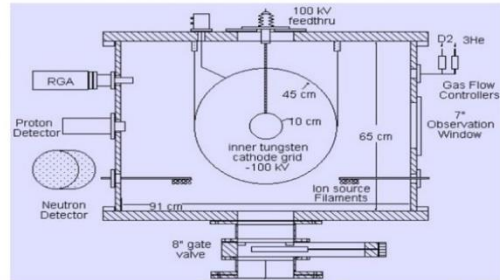


Principles

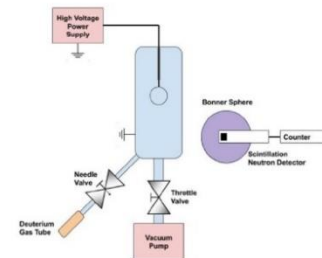
Inertial electrostatic confinement fusion does not rely on any magnetic field, and instead uses an electric field to perform the plasma confinement. The device is formed by arranging two spherical metal meshes concentrically and putting an extremely large voltage across them, typically 10 to 100 kV in vacuum. The meshes are supported by a high-voltage stalk. Fusion fuel, in this case deuterium, is then released into the chamber where the large voltage ionizes a portion of the gas. These positively charged ions are accelerated by the electric field toward the center of the device, where most will pass straight through the cathode at the center and out the other side due to the large gaps in the metal mesh. Once on the other side, the electric field slows the ions and eventually turns them back towards the center, setting up a recirculation. The ion density in the center increases, and eventually fusion occurs. This does not require nearly as large a machine as the tokamak: typical IEC devices comfortably sit on tabletops.



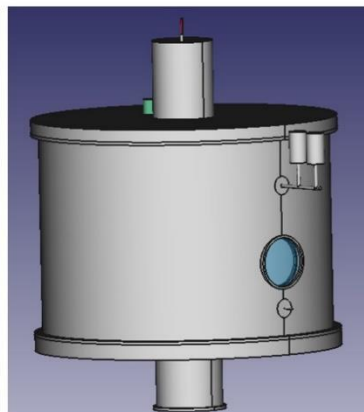
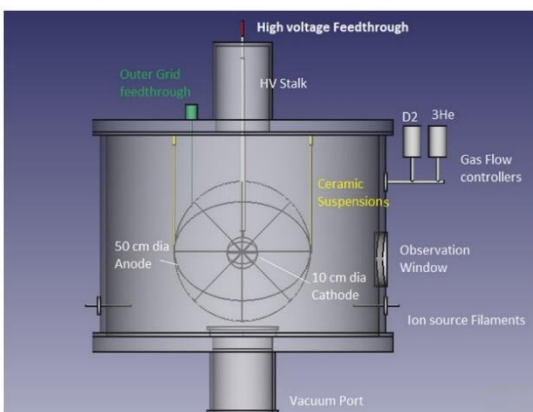
Inertial Electrostatic Confinement Fusor



University of Wisconsin-Madison IEC Device



Part	Description	Material	Size
Anode wire	grounded,	stainless steel	45 cm diameter grid of stainless-steel wire
Cathod wire	-100KV DC, supported on a 200 kV vacuum feed-through. input power levels exceeding 8.5 kW at voltages ranging from -25 kV to -185 kV and at currents from 30-75 mA.	tungsten	10 cm diameter coarse-grid sphere of 0.8 mm tungsten wire
stalk (will hold the cathod)	stainless steel tubing Quartz tubing non-porous high alumina ceramic (Alumina ceramic (Aluminum Oxide or Al2O3) is an excellent electrical insulator)	stainless steel, quartz, alumnia	0.64 cm dia stainless 70 cm 1.28 cm dia quartz 55 cm 0.95 cm dia quartz 60 cm 1.91 cm dia Alumina 31 cm
Vacuum chamber	cylindric, base pressure of 2 x 10 ⁻⁷ torr, Experiments run steady-state within the limitations of chamber heating	Aluminum	91 cm diameter, 65 cm tall
Deuterium/ He gas tube	Electronically controlled gas flow regulators adjust the fuel flow ratio and amount into the system.		
Ion Source Filaments	2 filaments a discharge voltage and current of 80V and 200-500mA is maintained	thoriated tungsten filaments	
vacuum pump	450 l/s turbo pump		
high voltage supply	provides up to 200 kV at 75 mA		
neutron detector	helium proportional counter neutron detector, placed 60 cm from the center		

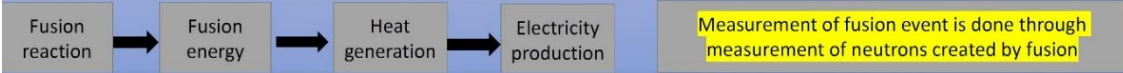


FreeCAD

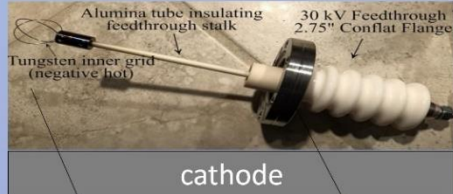
Maryam Abdel-karim
@AECENAR / July 2021

Introduction:

Fusion takes place only when the average kinetic energy of nuclei is sufficiently raised (to overcome the coulomb barrier) by accelerating their speed and increasing the density of nuclei in the center of the Inertial Electrostatic Confinement (IEC) reactor. This is achieved by creating a potential between electrodes, i.e. a sufficiently high voltage is created between cathode and the external sphere (anode).



- To operate the fusor, it requires fuel particles to be accelerated which are introduced into the fusor in the form of a gas (deuterium gas) injected into the vacuum chamber through a precisely regulated valve, which will become ionized in a strong electric field.
- In our case, the avalanche of electrons causes through high voltage.
- The 2nd stage of ionized gas is a formation of quasi-neutral plasma, concentrated in the center of the hollow cathode (poisor), and this is observed by a sudden increase in the current between the electrode followed by a drop in voltage.
- Our cathode (concentric in the chamber) consists of a 30 kV crosshead with a 2.75" stainless steel flange, an insulating aluminum tube crosshead rod and the negative hot inner grid of the tungsten filament with its stainless steel base that connects the inner grid with the crossing pin. This grid is a combination of 3 rings forming a sphere with a diameter 20% of that of the external sphere (anode).



Cylindrical shape :

This is the most common shape for vacuum chambers.

Allowable external pressure:

If $D0/t \geq 10$

Eq.1: $P_a = 4B/3(D0/t)$

Eq.2: $P_a = 2AE/3(D0/t)$

If $D0/t < 10$

Eq.1: $P_a = B/(R0/t)$

Eq.2: $P_a = 0.0625E/(R0/t)^2$

Allowable stress:

- 1-It is the amount of force exerted on an object, divided by its cross section $\sigma = F/A$.
- 2-Deformation, due to applied forces, is of two types :elastic and plastic ; $\epsilon = \Delta L/L$
- 3-Elastic limit : corresponds to the point where the material begins to deform plastically.
- 4-Safety factor : $r = (\text{Elastic limit}) / (\text{Work or design constraint})$.

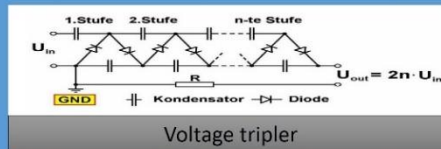
- The conditions of pressure, high voltage between electrodes and electrodes distance should be such that voltage breakdown in the plasma\electron cloud will be prevented, i.e.electric discharges between the electrodes are unwanted.

- Plasma turns into poison if a mean free path of ions has been reached : $l = k_b T / (\sqrt{2} n d^2 p)$.
- For $l > 2R$; recirculation occurs.
- The fusion rate (D-D) : $F = (1/2)n^2 (\sigma V)$

Electrical system:

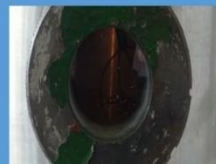


It is necessary to isolate the voltage tripler , by putting it in a suitable box filled with sunflower oil (about 6 liters).



Results of tests:

So far our test results have achieved an 80% reduction in air leakage and the pressure gauge indicates that the vaccum pump has extracted 900 mbar from the chamber. The desired result is to reach approximately 95% vaccum for a good fusion reaction.



2.3.3 X-Ray

Introduction مقدمة X-RAY GENERATION

X-RAY:
An X-ray is a penetrating form of high-energy electromagnetic radiation. Most X-rays have a wavelength ranging from 10 picometers to 10 nanometers, corresponding to frequencies in the range 30 petahertz to 30 exahertz (30x10¹⁵ Hz to 30x10¹⁸ Hz) and energies in the range 124 eV to 124 KeV. X-ray wavelengths are shorter than those of UV rays and typically longer than those of gamma rays.
Y-RAY: (Figure 1)
A gamma ray (symbol γ), is a penetrating form of electromagnetic radiation arising from the radioactive decay of atomic nuclei. It consists of the shortest wavelength electromagnetic waves and so imparts the highest photon energy.
A gamma ray refers to the high-frequency electromagnetic radiation of a photon whose wavelength is less than about ten nanometers (<10–8 m), which corresponds to frequencies above about 30 petahertz (>3 × 10¹⁶ Hz).

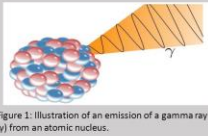


Figure 1: Illustration of an emission of a gamma ray (γ) from an atomic nucleus.

X-
الأشعة السينية هي شكل من أشكال إشعاع الكهرومغناطيسي عالي الطاقة. معظم الأشعة السينية لها طول موجي يتراوح بين 10 بيكومتر و 10 نانومتر ، وهو ما يقابل الترددات في النطاق 30 بيتاهرتز إلى 30 إكساهرتز (30 × 10¹⁵ هرتز إلى 30 × 10¹⁸ هرتز) والطاقات في النطاق 124 إلكترون فولت إلى 124 كيلو فولت. أطوال موجات الأشعة السينية أقصر من تلك الخاصة بالأشعة فوق البنفسجية وأطول من تلك الخاصة بأشعة جاما.
أشعة جاما (الرمز γ) هي شكل من أشكال الإشعاع الكهرومغناطيسي الناتج عن الاضمحلال الإشعاعي للنواة الذرية. يتكون من أقصر طول موجي.
تعتبر الأشعة جاما الإشعاع الكهرومغناطيسي من أقصر ترددات يكون عليه لنوع من جزيئات عالية التردد ($\gamma > 10^{-8}$ م) ، وهو ما يتوافق مع ترددات أعلى من 30 بيتاهرتز ($> 3 \times 10^{16}$ هرتز).

Sources مصادر

The x-ray source consists of a vacuum tube including a tungsten filament covered with a metal cathode (preferably tungsten) and a copper (or any element having an atomic number between 20 and 80). A high potential electric source is applied between the anode and the cathode that will result in electrons being accelerated from cathode to anode. Once the electrons hit the anode at high speed, x-rays are generated.
يتكون مصدر الأشعة السينية من أنود مطروح يتشكل على خطوط تستكس مطواة بمهبط معدني (غالبًا التنجستن) وأنود (أو أي عنصر له رقم ذري بين 20 و 80) ، يتم تطبيق مصدر كهربائي على الإمكانات بين الأنود والكاثود مما يؤدي إلى تسريع الإلكترونات من الكاثود إلى الأنود. بمجرد أن تصطدم الإلكترونات بالمهبط الموجب بسرعة عالية ، يتم إنشاء الأشعة السينية.
إن خطوط الكاثود المستخدمة لتوليد الأشعة السينية من الإلكترونات ليست سوى خطوط خفيفة معدنية من 24 فولت DC والتي تستهلك 200 مللي أمبير من تيار مستمر بتردد جبر العازل.

Figure 2: X-RAY generation

Figure 3: X-Ray plant

Protecting Against Exposure الحماية من التعرض

Time: is an important factor in limiting exposure to the public and to radiological emergency responders. The amount of radiation exposure increases and decreases with the time people spend near the source of radiation. The maximum time to be spent in the radiation environment is defined as the "stay time". The stay time can be calculated using the following equation: $Stay\ Time = Exposure\ Limits/Dose\ Rate$.
Distance: can be used to reduce exposure. The farther away people are from a radiation source, the less their exposure. Doubling the distance from a point source of radiation decreases the exposure rate to 1/4 the original exposure rate. Halving the distance increases the exposure by a factor of 4. How close to a source of radiation can you be without getting a high exposure? It depends on the energy of the radiation and the size (or activity) of the source. Distance is a prime concern when dealing with gamma rays, because they can travel at the speed of light. Alpha particles can only travel a few inches and beta particles about 10 feet.
Shielding: As ionizing radiation passes through matter, the intensity of the radiation is diminished. Shielding is the placement of an "absorber" between you and the radiation source. An absorber is a material that reduces radiation from the radiation source to you. Alpha, beta, or gamma radiation can all be stopped by different thicknesses of absorbers. Shielding material can include barrels, boards, vehicles, buildings, gravel, water, lead or whatever else is immediately available.

Figure 4: Principles of Radiation Protection - Time, Distance, Shielding

X-RAY DETECTION

1. Scintillators

Scintillators are materials in which large fractions of incident striking particles or radiation are absorbed and transformed into detectable visible or near visible light photons, later converted into an electric signal. They are used in many applications especially those require high energetic particles or hard X-rays that are not directly detectable by semiconductor detectors.

2. Detection of the Scintillation Light:

To understand the optical properties of silicon, one needs to analyze its band structure. Photon absorption through electronic transitions between different bands can occur only if the total energy and momentum of the system is conserved. The interaction of photons with silicon mainly occurs by the excitation of electrons from the valence band or impurity states into higher available energy states. But there is also the probability for excitations within the same band. For certain photon energies the joint density of states of the conduction and valence band becomes maximum. This leads to the so called Van Hove singularities in the joint density of states. Two regimes with an excitation energy E1 and E2, give rise to Van Hove singularities, hence to characteristic points of the absorption of silicon at E1 and E2.

3. Quantum efficiency

The quantum efficiency of semiconductor radiation detector defines its sensitivity to the incident radiation. In other term, η tells how many photons will be stopped by the detector sensitive area when irradiated by an incident beam.

4. Signal amplification and readout electronics:

CAMEX is a special electronic chip designed for pnCCD to amplify and sample the signals received from the parallel channels. In pnCCD the system must have a USB 2.0 cable B, with at least 3 meters as length (for safety purpose), to connect it with the control device (PC).
The system can be divided into 2 subcategories:
The plant side where the X-Ray setup is set, and the user side where all the controls are set.

X-RAY Control system

The X-Ray process control system to be implemented should have the following technical requirements:
The user must be able to control the X-Ray system through Graphic User Interface (GUI).
The user must be able to monitor Photodiodes (sensor) data on a well-organized GUI.
The system must have a USB 2.0 cable B, with at least 3 meters as length (for safety purpose), to connect it with the control device (PC).
The system can be divided into 2 subcategories:
The plant side where the X-Ray setup is set, and the user side where all the controls are set.

Arduino
Power circuit breaker: Turns on/off all the system (220V)
Vacuum Pump switch: Turns on/off the vacuum pump
Controller: The controller used is Arduino UNO. A USB 2.0 Cable type B is used to connect X-ray plant and the control station. It is used to control the relay box according to operator's command (from the user-end GUI) and send back the data coming from photodiodes (sensors).
Relay kit: Controlled contacts (2 channels).
User-End GUI
The GUI interface is shown in the image below. It is divided into 2 sections; The Power and monitoring, and control.
Figure 3, shows GUI when it is in the disconnecting state, where the filament and the high voltage buttons are deactivated (white boxes) where the connecting button is activated and red tinted which indicates the disconnecting statement with Arduino. If the connection box does not get red tinted, this indicator means that NO COM Port available. Hence, check the Arduino cable connection with the PC.

MATLAB
Figure 1. fitting curve
Figure 2. fourier transform

2.3.4 Inertial Confinement Fusion



بِسْمِ اللَّهِ الرَّحْمَنِ الرَّحِيمِ

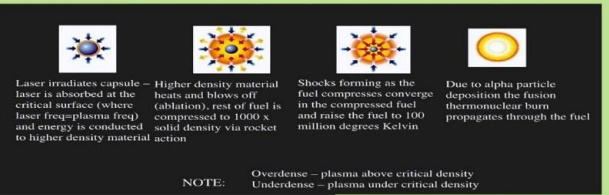
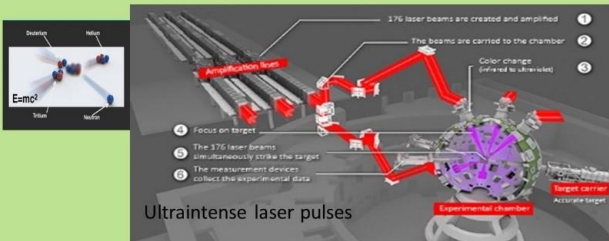


High energy laser induced plasma physics demonstration device

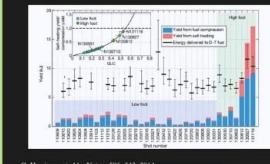
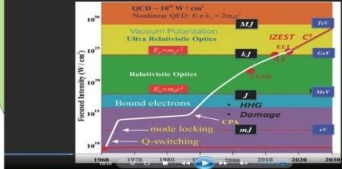
فيزياء البلازما و تكنولوجيا الليزر

A. Principles of fusion: Mass turns into energy

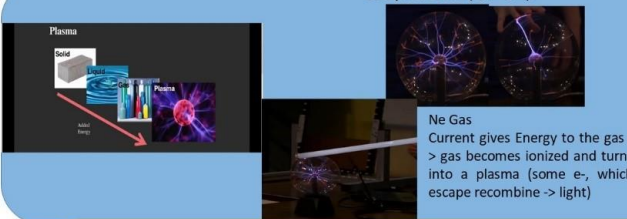
According to our understanding of modern physics, matter is made of atoms. Their constituents are positively charged nuclei surrounded by negatively charged electrons. Two light nuclei, when they approach each other, undergo, with a certain probability depending on their separation, a fusion reaction. Figure below depicts the reaction of heavy hydrogen and super-heavy hydrogen, deuterium and tritium (known as isotopes of hydrogen), to give helium (an α particle) and a sub-atomic particle, the neutron. Energy is gained in the process, which is carried away as kinetic energy by the helium atom and the neutron. At the same time, mass is lost: the combined mass of the products is lower than that of the reactants. Compared with a conventional (carbon) combustion process the energy gain is greater by six orders of magnitude! In principle numerous nuclei could be used as fuel in a fusion power plant. The advantage of deuterium and tritium is their high reaction probability.



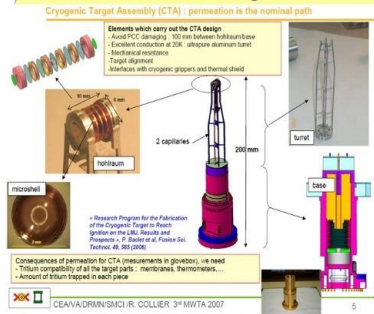
Making powerful lasers



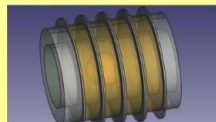
Cold plasma ball (بلازما بارد):



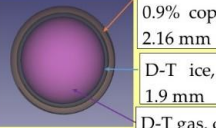
C. FreeCAD design



Hohlraum



Capsule



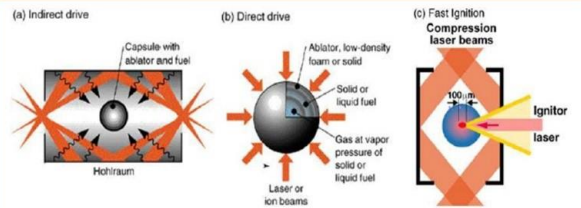
Beryllium doped with 0.9% copper, diameter: 2.16 mm
D-T ice, diameter: 1.9 mm
D-T gas, diameter: 1.74 mm

Clean energy for the future

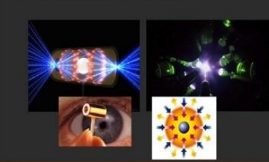
طاقة نظيفة للمستقبل

B. Concepts and stage of development of inertial fusion

- Glass pellets are thin-walled hollow glass spheres filled with the D-T mixture
- The D-T mixture is filled with an overpressure of approx. 6 bar, which achieves a certain recompression.
- The thin sheath consists of a heavy material of high atomic number, e.g. Gold



Inertial Confinement Fusion

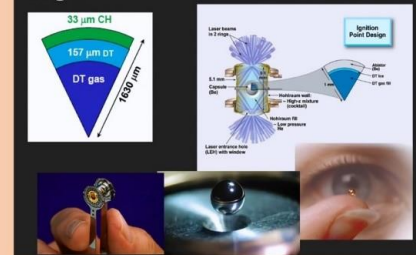


Numbers

7 million cm/s
Ablation velocity: $\sim 10^7$ cm/s
Implosion velocity: $\sim 10^7$ cm/s
Ablation pressure: 100s Mbar
Peak pressure: 100s Gbar (pressure amplification due to spherical convergence)
Energy for ignition: ~ 1 MJ

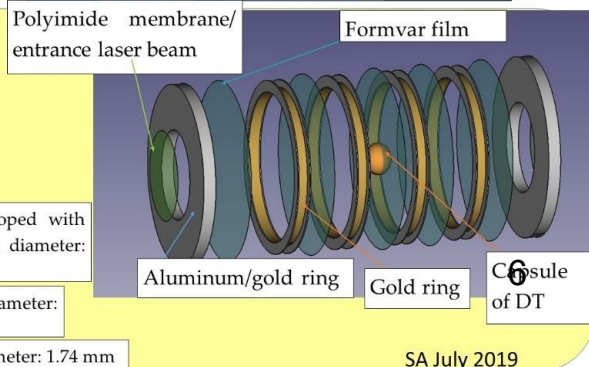
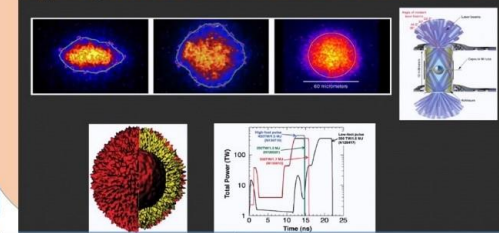
Laser → Through gold → X-Rays

Targets



- Hohlraum wall: gold
- very precise fine mechanics
- Cost of the target: about 1Mio. \$

Happening in the hohlraum: 50 measurement instruments



SA July 2019

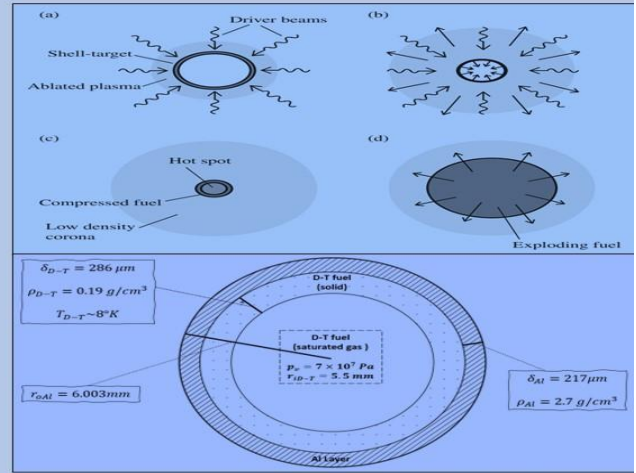


Last edited 4/12/2025 6:06:43 PM

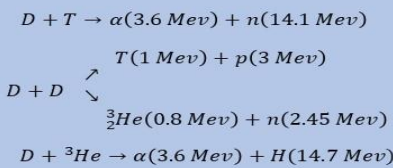
بِسْمِ اللَّهِ الرَّحْمَنِ الرَّحِيمِ

Overview of Inertial Confinement Fusion(ICF)

- The object of this method is to exploit nuclear energy.
Confinement is a necessary condition for fusion to occur, In ICF the only mean of confinement is the fuel's inertia!
Nuclear fuel is put in a spherical capsule (typically a couple millimeters in radius) usually made of gold or Aluminum.
The fuel pellet is irradiated with high intensity Laser beams from all directions, which drive the evaporation of the outer surface, this causes it to ablate outward compressing the fuel with extreme pressure so that the inner core reaches extreme density and temperatures, initiating nuclear fusion.



It is most common to use Deuterium and Tritium (isotopes of Hydrogen) as fuel (D-T fuel) If so, the most occurring nuclear reactions are



Energy Balance

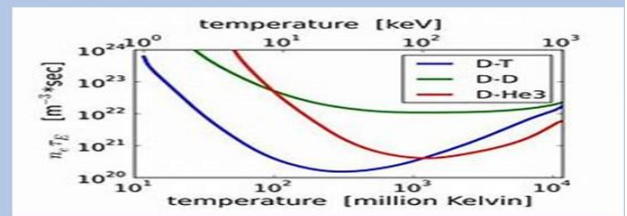


By equating energy losses to gains we arrive at the Lawson criterion for ICF

n tau_E = (3kT) / (1/4 <sigma v> beta Q_{D-T} - C_b sqrt(T))

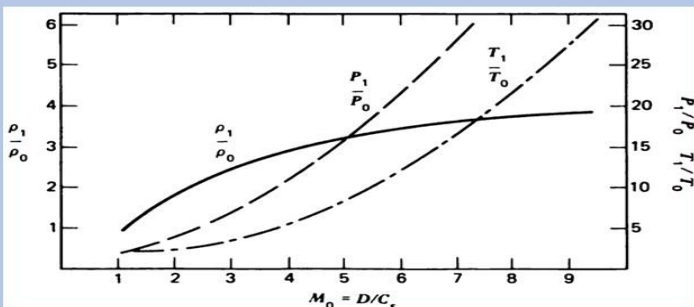
Where

- <sigma v> is the reaction rate
Q_{D-T} is the energy released from D-T reaction
beta is the fraction of Q_{D-T} that gets absorbed by the fuel
T is the temperature, k the Boltzmann constant
n is the particle density
And most importantly tau_E is the confinement time, it is a measure of the time needed by the plasma to dissipate its thermal energy.

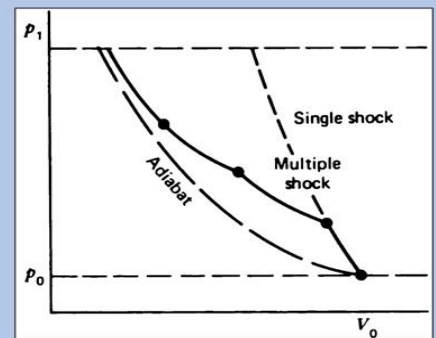


Shock-waves propagation

The dominant mechanism for heating the fuel is the shock-heating; as the outer surface is ablated off, shock-waves are created which propagate through the fuel and converge at the center.



Ratios of the density, pressure and temperature after the shock to their initial values in term of the Mach number... Look how density approaches a limit while temperatures and pressure increase indefinitely. This is one downside of shock-heating.



One way around this issue is to hit the pellet with multiple light pulses, the effect of the multiple small shocks thus generated is to increase the density with a controllable increase in temperature.

If we treat the ion gas a perfect (with ideal gas ratio gamma), then these ratios are given by the Hugoniot-Rankine relations;

p2/p1 = (2 gamma M1^2 - gamma + 1) / (gamma + 1) * ((gamma + 1) M1^2) / ((gamma - 1) M1^2 + 2)

T2/T1 = 1 + [2 * (gamma - 1) / (gamma + 1)] * [(gamma M1^2 + 1) / M1^2] * (M1^2 - 1)


conclusion

The basic ideas of inertial confinement fusion: Fulfill the Lawson criteria. Extra density, short time, high temperature by applying strong external forces.




2.3.4.1 Light-ion Driver for ICF

Association for Economical and Technological Cooperation in the Euro-Asian and North-African Region
www.aecenar.com



Pulsed diode accelerator



General features:

Considered E.M pulse compressors; consists of discharging electrical energy from the Marx generator into a pulse forming line where a short high energy pulse is formed and then applied to the diode via the transmission line.

Max Generator

{energy storage + voltage multiplication from the charge-discharge phenomenon of the capacitor}

E.M high voltage but

Pulse rise time is too slow

Pulse forming lines

{compress electrical energy into a short, fast pulse, this will multiply the voltage}

E.M of high voltage

+ Short and fast

Transmission line

{make the E.M more intense (beam)}

E.M intense high voltage

+ Short and fast

Diode

{when the high voltage pulse reaches the cathode, its voltage will create an emission of an intense field on the cathode tip which produces a plasma on the surface of the cathode and is translated by an intense current of electrons directing towards the anode}

Types of accelerators:

1-Marx Generator:

- The Marx generator designed for voltage multiplication.
- The generator is used as an energy storage element, at relatively low voltages; and when triggered, the 1st switching voltage drops, which increases the voltages across the remaining switches, causing a self-triggering chain reaction, until a high voltage pulse is obtained at the load.

Wave erection Marx:

- The Marx transient wave erection differs from the previous Marx circuit in its use of stray capacitance effects.
- A voltage wave propagates towards the load with increasing intensity, triggering successive switchings faster and faster until it reaches the load with a rise time inside (ns) and low jitter for output voltages of several certain (kv) at moderate energies per pulse.

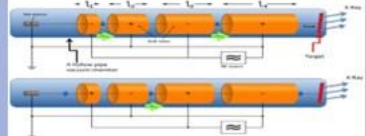
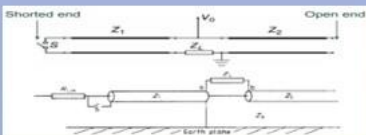
Large and Moderate generator systems	Compact and Solid state generator systems
<ul style="list-style-type: none"> Used as pulse charging subsystems in larger pulsed power applications. 	<ul style="list-style-type: none"> Designed to have pulse widths narrow enough to directly drive some applications.
<ul style="list-style-type: none"> Have low repetition rates, either because of the capacity of the power supply or because of the thermal stability of the load. 	<ul style="list-style-type: none"> Tend to run at higher rep rates to increase the average energy delivered to the load.
<ul style="list-style-type: none"> Resistive load works well (resistors reduce load efficiency). 	<ul style="list-style-type: none"> Resistors are replaced by inductors to allow fast and efficient charging (the addition of mutual coupling between the two inductors increases system performance).

2-linear accelerator:

Linear Particle Accelerator (LINAC) is a type of particle accelerator that dramatically increases the kinetic energy of charged subatomic particles or ions by subjecting the charged particles to a series of oscillating electrical potentials along a line of linear beam.

How it works:

- The source gives electrons which are accelerated towards the 1st drift tube due to their negative potential and the (+) tube; when these electrons enter the tube, the R. F source changes the polarity.
- The electrons leave the tube due to its inertia and then they are pushed by the 1st tube and attracted by the second in the same direction.
- When these electrons accelerate, their speed increases and they travel greater distances at the same time. As the electron velocity approaches C, the velocity increase will be small, and the electrode lengths will be $\sim t$.



Pulse forming line(PFL):

-A transmission line of any geometry of length l and characteristic impedance Z_0 makes a pulse forming line (PFL), which when combined with a closing switch SS makes the simple transmission line pulser.

-But the impulse generated in a suitable load is only equal to $(V_0/2)$; to avoid this problem, we will use Bulmeim PFL.


Electron Gun:

Electron guns include a cathode (tungsten filament), where electrons are produced, the cathode is at negative potential in the range [-30kv to - 150kv], there is a vacuum gap between cathode and anode which is at ground potential. The anode has a hole, so electrons are accelerated towards it and then pass through the hole. They then move at constant speed until they hit the target, where they release their kinetic energy in the form of heat and X-rays.





When the slit is disconnected, the electrons stayed around the tungsten filament (cathode).

When the slit anode is connected, the electrons are accelerated and then pass through the slit.





Transformer (2kv, 30VA, 50Hz)




The best type of power supply to use would probably be a (roughly) 20KV DC flyback transformer. However, we did not have a flyback power supply on hand, so I used a rectified sign transformer.

The electron beam is visible because there is low pressure gas in the tube. The electrons strike the gas molecules and give them energy, which is then released as light.







Vacuum of the tube accelerator (Amocanali pump)

Notes:

The transformer (of 12 kv) is an output in AC mode; for converted to DC mode, we use 4 diodes; and to multiply the applied voltage, this transformer is connected to a 2-stage voltage multiplier circuit, which provides a total voltage of 48 Kv [$U_{out} = 2 \times n \times U_{in}$]. To avoid jumping the voltage of the capacitor pins, this multiplier circuit is isolated and made in an oil bath.

Rouwayda Sakka, Asmaa El Mir & Ali Obeid

@AECENAR/August 2022

2.3.5 Mass Spectrometer

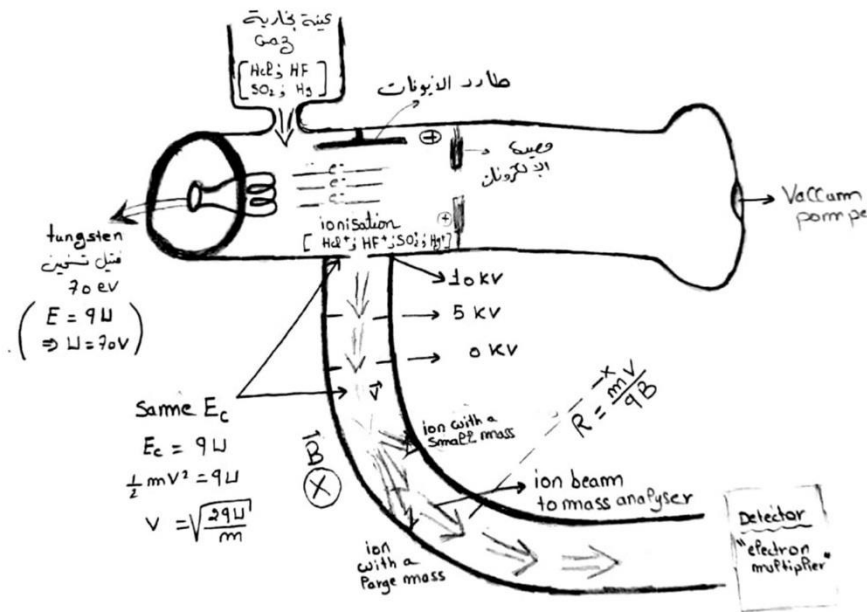
2.3.5.1 Magnetic Beam Deflection



Mass spectrometer

Goal: Detection that there are no toxic gases emitted by the combustion of waste, after the operation of the filtration, and this by using the mass spectrometer.

introduction:



A mass spectrometer produces ions from a sample to be analyzed. These ions are separated and detected quantitatively. The separation is achieved based on the different trajectories of ions moving at different ratios (mass/charge) in an electric and/or magnetic field.

The command is:

Step 1: Ionization: Atoms are ionized by removing one or more electrons to produce positive ions. This is also generally true for those that are said to form negative ions (such as chlorine) or not to form ions (such as argon). Mass spectrometers always work with positive ions.

Step 2: Acceleration: The ions are all accelerated to have the same kinetic energy.

Step 3: Deviation: The ions are then deflected according to their mass by a magnetic field. The lighter they are, the more deflection they have. The degree of deviation also depends on the number of positive charges on the ion, i.e., the number of electrons removed in the first step. The more charged the ion, the greater the deviation.

Step 4: Detection: Electronically detect the ion beam passing through the machine

List of components	Quantity	Description	We have $R = (m \cdot 2 \cdot U / q \cdot B^2)$; For a magnetic field $B = 60 \cdot 10^{-2} \text{ T}$, and a potential difference $U = 10 \text{ kv}$, we obtain the values of the radius as below :		
Metal plate	2	Slight positive charge	Gas type	Mass m (Kg)	Radius R (m)
Slits	3	2 acceleration slits [slight negative potential (10 kv and zero Kv)] 1 focusing slit [extremely high voltage (5Kv)]	HCl	$5.76 \cdot 10^{-26}$	0.14
Metal Coil	1	Tungsten filament	HF	$3.2 \cdot 10^{-26}$	0.11
Magnet	1	Strong magnetic field is applied perpendicular to the motional direction of the ions	SO2	$10.24 \cdot 10^{-26}$	0.19
Vacuum pump	1	10^{-7} mbar	Hg	$32 \cdot 10^{-26}$	0.33
Electron multiplier	-----		<div style="display: flex; justify-content: space-around;"> <div style="border: 1px solid black; border-radius: 50%; padding: 10px; width: 40%;"> <p>Note: The most suitable detector in mass spectrometry is the electron multiplier, because of the low sensitivity and the slow response time of a Faraday cut.</p> </div> <div style="border: 1px solid black; border-radius: 50%; padding: 10px; width: 40%;"> <p>Note: It is important that the ions produced in the ionization chamber flow freely through the machine without colliding with air molecules.</p> </div> </div>		
Metal or glass tube	2	1 horizontal tube 1 curved tube			
voltage	1	70 v (to heat the filament)	<p>Note : working with toxic gases is at low pressure and normal temperature.</p>		

Magnetic sector mass spectrometry

Introduction:

In mass spectrometry, one generates ions from a sample to be analyzed. These ions are then separated and quantitatively detected. Separation is achieved on the basis of different trajectories of moving ions with different mass/charge (m/z) ratios in electrical and/or magnetic fields.

في مقياس الطيف الكتلي يتم توليد الأيونات من خلال عينة لتحليلها. يتم فصل الأيونات واكتشافهم بشكل كمي. يتحقق فصلهم تبعاً لمسار حركتهم باختلاف الرابطة بين الوزن والشحن الخاص بكل أيون.

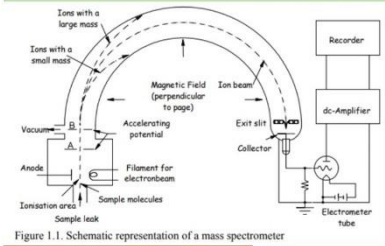


Figure 1.1. Schematic representation of a mass spectrometer

1. A small amount of a compound is evaporated.
2. The vapor molecules are now ionized by an electron beam (filament heating). Ionization is achieved by loss of valence electrons (positive ions).
3. The ions are accelerated by an electrostatic field ($A > B$).
4. Positive ions are expelled from the ionization chamber by a small positive charge.
5. Application of a magnetic field perpendicular to the direction movement of the ions. Fast moving ions following a circular trajectory due to Lorentz acceleration whose radius is determined by the mass-to-charge ratio of the ion and the intensity of the magnetic field.
6. The ions collide on a collector electrode.
7. The resulting current is amplified and recorded as a function of the force caused by the magnetic field or the accelerating voltage.

Note: The resulting mass distribution is characteristic for that given molecule.

Sampling:

A compound is supplied to a mass spectrometer as a vapor from a reservoir (reservoir pressure > 10 to 20 times the ionization chamber pressure). If the sampling cannot be carried out, we pass to the direct insertion of the sample.

يتم ادخال المركب في مقياس الطيف عن طريق تبخيره، إذا لم يتحقق ادخال العينة بهذه الطريقة نلجأ إلى الإدخال المباشر.

- The boiling of the fluid <150°C → evaporates at ambient temperature.
- The boiling of the fluid >150°C → heating the tank.

Ion source:

The sample vapor molecules are bombarded with electrons of about 70 e.v, which are generated by heating a metal wire [tungsten or rhenium]. A voltage of about 70 V (from 50 to 100 V) accelerates these electrons towards the anode. During bombardment, 1 or more electrons can be removed from neutral molecules to give radicals positively charged molecular ions; these ions gain enough excess energy to break one or more bonds, thus producing fragment ions.

يتم قصف جزيئات بخار العينة بالكترونات تبلغ قوتها 70 فولتاً تقريباً، والتي يتم إنشاؤها عن طريق تسخين سلك معدني [تنجستن أو رينيوم]. يعمل الجهد البالغ حوالي 70 فولت (من 50 إلى 100 فولت) على تسريع هذه الإلكترونات نحو القطب الموجب. أثناء القصف، يمكن إزالة 1 أو أكثر من الإلكترونات من الجزيئات المحايدة لإعطاء الجذور أيونات جزيئية موجبة الشحنة؛ تكتسب هذه الأيونات طاقة زائدة كافية لكسر رابطة أو أكثر، وبالتالي إنتاج شظايا الأيونات.

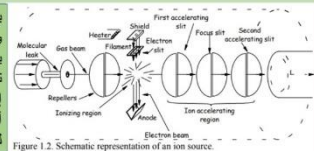


Figure 1.2. Schematic representation of an ion source.

Magnetic Mass Analyzer :

At the exit of the source, the kinetic energy of the ions is:

$E_k = (mv^2)/2 = qVs$. This ion is subjected to a magnetic force: $F_m = qvB$. The ion follows a circular path of radius r so that the centrifugal force balances the magnetic force:

$$qvB = (mv^2/r).$$

The ions leaving the source: $mv^2 = 2qVs$.

The ratio is then: $m/q = (r^2 \times B^2) / 2Vs$. [bending magnet].

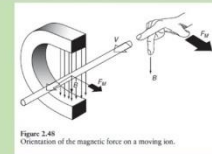


Figure 2.48. Illustration of the magnetic force on a moving ion.

Detectors:

- The ions pass through the mass analyzer and are then detected and transformed into a signal that can be used by a detector. The detectors are able to generate, from the incident ions, an electric current proportional to their abundance.
- The detection of ions is always based on their charge, their mass or their speed. Some detectors (Faraday cup) are based on DC load current measurement. Others (electron multipliers) are based on the kinetic energy transfer of incident ions.
- The number of ions leaving the analyzer is quite low; a large amplifier is often necessary to obtain a usable signal.
- Ion detectors are divided into 2 classes: some detectors are designed to count ions of one mass at a time and therefore detect the arrival of all ions sequentially at one point. Other detectors have the capacity to count several masses and to detect the arrival of all the ions simultaneously along a plane.
- The efficiency of these detectors decreases when the mass of the ion increases; for this reason, the development of new detectors, which eliminate these limitations, is necessary.

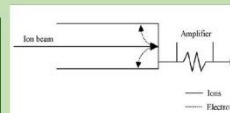


Figure 3.1. Schematic diagram of a Faraday cup.

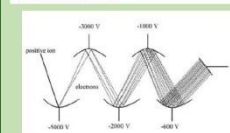


Figure 3.2. Schematic diagram of electron multiplier. The first dynode is a conversion dynode to convert ions into electrons.

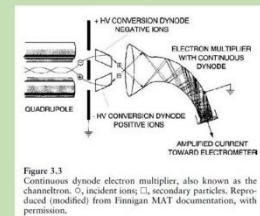
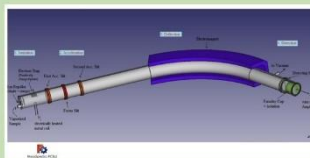
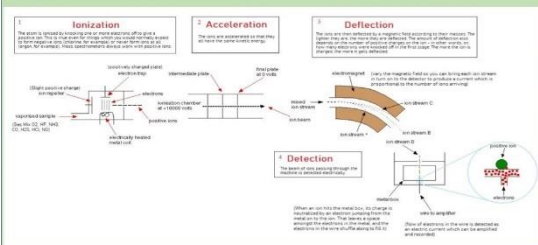


Figure 3.3. Continuous dynode electron multiplier, also known as the channeltron. O₁: incident ions, O₂: secondary particles. Reproduced (modified) from Finnigan MAT documentation, with permission.

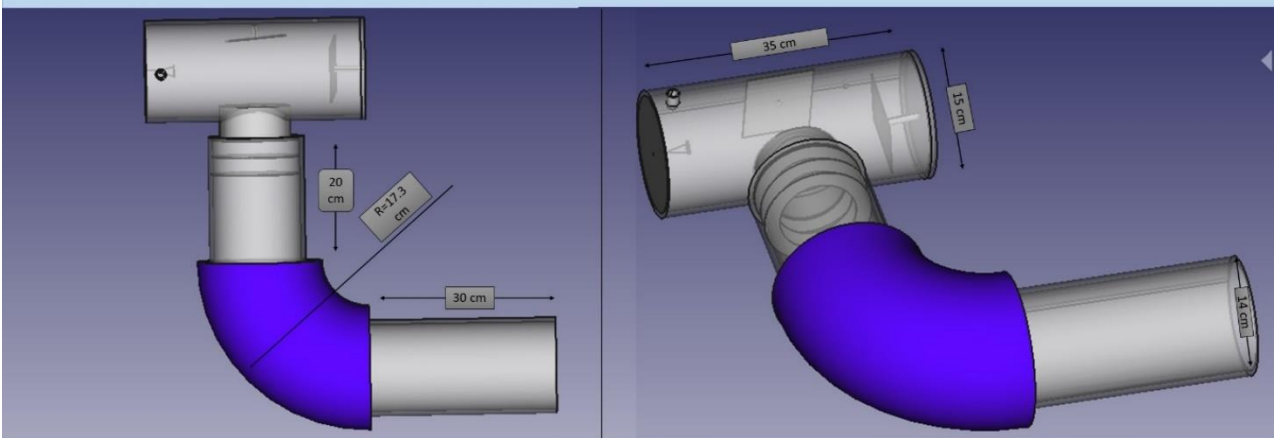
Our device:



Parts	Qty	Description
Metal Plate	2	slight positive charge
Slits	4	2 acceleration slits (slight negative potential) 1 Focusing Slit (extremely high voltage) 1 Detecting Slit
* metal coil	1	Tungsten filament
electromagnet	1	strong magnetic field is applied perpendicular to the motional direction of the ions
Vacuum pump	1	10 ⁻⁷ mbar
Faraday cup	1	
Amplifier	1	
Metal Tube	3	2 horizontale tubes 1 curved tube 60°

Mass spectrometer

Goal: Detection that there are no toxic gases emitted by the combustion of waste, after the operation of the filtration, and this by using the mass spectrometer.



A mass spectrometer produces ions from a sample to be analyzed. These ions are separated and detected quantitatively. The separation is achieved based on the different trajectories of ions moving at different ratios (mass/charge) in an electric and/or magnetic field.

The command is:

Step 1: Ionization: Atoms are ionized by removing one or more electrons to produce positive ions. This is also generally true for those that are said to form negative ions (such as chlorine) or not to form ions (such as argon). Mass spectrometers always work with positive ions.

Step 2: Acceleration: The ions are all accelerated to have the same kinetic energy.

Step 3: Deviation: The ions are then deflected according to their mass by a magnetic field. The lighter they are, the more deflection they have. The degree of deviation also depends on the number of positive charges on the ion, i.e., the number of electrons removed in the first step. The more charged the ion, the greater the deviation.

Step 4: Detection: Electronically detect the ion beam passing through the machine

List of components	Quantity	Description
Metal plate	2	Slight positive charge
Slits	3	2 acceleration slits [slight negative potential (300 v and zero v)] 1 focusing slit [extremely high voltage (150 v)]
Metal Coil	1	Tungsten filament
Magnet	1	Strong magnetic field is applied perpendicular to the motional direction of the ions
Vacuum pump	1	10 ⁻⁷ mbar
Electron multiplier	-----	
Stainless Steel tube	3	2 horizontal tube 1 curved tube
voltage	1	17 v (to heat the filament)

We have $R = (m \cdot 2 \cdot U / q \cdot B^2)$, and $v = (2 \cdot q \cdot U / m)^{1/2}$; For a magnetic field $B = 20 \cdot 10^{-2}$ T, and a potential difference $U = 300$ v, we obtain the values of the radius and the velocity as below :

Gas type	Mass m (Kg)	Radius R (m)	Velocity v (cm/s)
HCl	$5.76 \cdot 10^{-26}$	0.073	408
HF	$3.2 \cdot 10^{-26}$	0.056	547
SO2	$10.24 \cdot 10^{-26}$	0.098	306
Hg	$32 \cdot 10^{-26}$	0.173	173

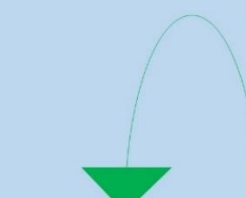
Note: working with toxic gases is at low pressure and normal temperature.

Note: it is important that the ions produced in the ionization chamber flow freely through the machine without colliding with air molecules.

Note: The most suitable detector in mass spectrometry is the electron multiplier, because of the low sensitivity and the slow response time of a Faraday cut.



The curved tube (where is the magnetic field applied)



Length of the ionization chamber (~ 35 cm)



Cross sectional diameter of two horizontal tubes (~ 14 cm)



Cross sectional diameter of the ionization chamber (~ 15 cm)

Mass Spectrometer Detector

Mass spectrometer sensor

Introduction:

A mass spectrometer is a device that can detect charged particles such as ions, protons, and electrons by separating them according to their mass-to-charge ratio using a magnetic field. Followed by a detector that receives these particles and transforms them into an electric signal. This signal is amplified by an amplifier circuit so that it can be recorded.

Objective:

To make a mass spectrometer to identify the composition of any gas for these molecules: HCl, HF, SO₂, and Hg, with their respective quantities.

Structure and roles

1. Analyzer:

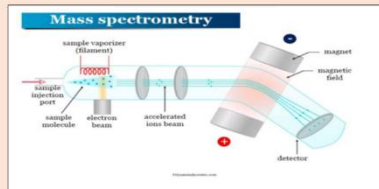


Fig. 1.1: The analyzer of the spectrometer

The analyzer is one of the three main parts of the mass spectrometer that has **three essential stages**:

Ionization, Acceleration, and Separation.

- Ionization: the sample of gas that needs a study is injected into a chamber that has a heat filament and electron gun that allow the gas to become charged (ionized).

- Acceleration: the sample is then accelerated using a magnetic field due to its charge.

- Separation: the accelerated ions go through another magnetic field parallel to their direction but this time to change their direction, since all ions have the same charge, they will experience the same moving force. However, due to the different masses of each ion, they will move in a different directory i.e., the heavier the ion the longer the arc will take.

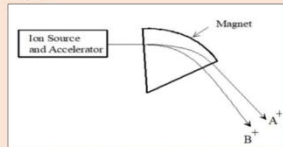


Fig.1.2: ion A+ and B+ separated using a magnet.

For the wanted sample:

1.4 Measurement of physical quantities

We have $B = (m \cdot 2\pi \cdot U / e \cdot h)^{1/2}$, and $v = (2\pi \cdot U / m)^{1/2}$. For a magnetic field $B = 20 \cdot 10^{-2}$ T, and a potential difference $U = 100$ V, we obtain the values of the radius and the velocity as follows:

Gas type	Mass m (kg)	Radius R (m)	Velocity v (m/s)
HCl	$5.76 \cdot 10^{-26}$	0.073	408
HF	$3.2 \cdot 10^{-26}$	0.056	547
SO ₂	$10.24 \cdot 10^{-26}$	0.098	306
Hg	$32 \cdot 10^{-26}$	0.173	173

3. Amplification circuit:

The electric charge is a property that is constant for all electrons and protons. In the mass spectrometer currently being worked on, the particles of interest are ionized so that all molecules become ions with one less electron which makes them positively charged thus for large ion currents, 1 ion (+1) has: 1.6×10^{-19} Coulombs and that means 1 ion/second is 1.6×10^{-19} A or 1.6×10^{-4} fA.

Even with the ability to collect charge efficiently, the need to amplify the current input of Faraday's cups so it can be measured and recorded vital.

In that sense, an amplification circuit is introduced to solve this problems.

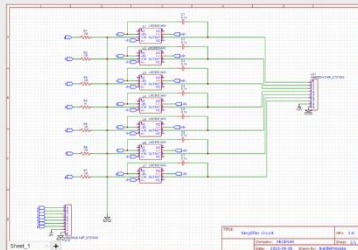


Fig.4: Schematic of the amplifier circuit for faraday's cup

2. Detector:

The detector is the second main part of the mass spectrometer that allows us to know the location of ions when they exit the analyzer and thus know their masses. There are several types of detectors out there, but it was chosen to use "Faraday's Cup" as a detector.

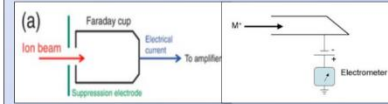


Fig. 2.1: Faraday's Cup

The Faraday's cup works based on the principles of electrochemistry and the conservation of electric charge.

Electrochemical process is the core principle behind Faraday's cup. When charged particles, such as ions or electrons, encounter a conductive surface (the collection surface of the cup), they can transfer their charge to that surface. This transfer of charge is facilitated by an electrochemical reaction between the charged particles and the conductive material of the cup's electrode.

This reaction creates a potential difference between the electrodes and the current integrator circuit which induce electric current that flows through an external circuit connected to the cup. This current is proportional to the number of charged particles that have been collected by the cup. By measuring this electric current, the number of charged particles that have impacted the cup's surface.

When the ions collide with the plate it induces a current equal to its charge, therefore the more ions the higher the current and thus the bigger the signal allowing us to know the quantity.

When designing a Faraday's Cup, a few considerations should be considered:

1. Material Selection:

A conductive material with high thermal and electrical conductivity. Commonly used materials are stainless steel and brass.

2. Cup Geometry:

The cup's geometry is critical for efficient ion collection and minimizing losses due to scattering.

3. Aperture Size:

The aperture size should be optimized to allow ions of interest to pass through while minimizing the passage of unwanted neutral particles or larger molecular clusters.

4. Electric Isolation:

The Cup must be electrically isolated from the analyzer to prevent interference with the magnetic fields used in it.

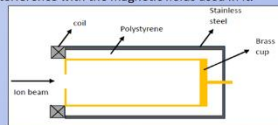


Fig.2.2: model #1 of Faraday's cup module #1

In the above fig., the brass cup is the collector; Polystyrene is not only an electric insulator, but also a shield against outside noise. The stainless steel is a protective casing, and finally, the coil, when electrified is going to induce a magnetic field that will prevent unwanted charged particles from interfering with the signal (protecting from potential inside noise).

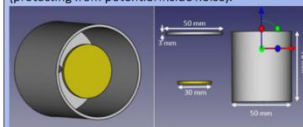


Fig.3: Module 2 made and ready to test.

As it is observed, each electrode signal of the faraday's cup must be amplified individually as it is too low and vulnerable to noise, thus the use of a mechanism that transfers the signal to the amplifier in series format instead of parallel (like a multiplexer) is unlikely due to noise.

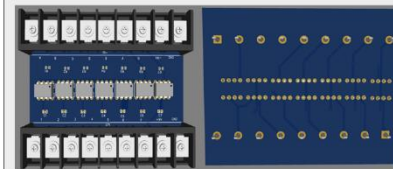


Fig.5: The front -back image of the amplifier circuit (3D)

About the LMC 6001 Op-Amp:

Input bias current (max) = 25 fA
Vos (offset voltage at 25°C) (max) = 0.35 mV
Total supply voltage (+5 V = 5, ±5 V = 10) (max) = 15.5 V
Total supply voltage (+5 V = 5, ±5 V = 10) (min) = 4.5 V
Large signal voltage gain (A) = 1400V/mV or 1400000 times the input.
So, if the input is 1nV the output will be 1.4 mV.

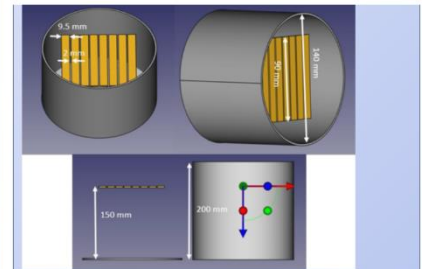
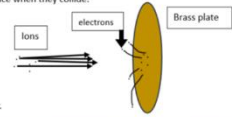
Yellow is brass, gray is stainless.

When the ion beam collide with the plate electrochemical reaction between them will transfer the charge to the plate that will generate current through the wire into the electrometer.

It is important to note that this design is not efficient as module 1 due to the possibility of the ion to bounce off electrons off the surface is a process called "electron scattering" which involves the interaction of atoms or particles with the electrons in the material of the conductive plate. This interaction can lead to changes in the direction and energy of the electrons as they bounce other charged particle off the plate's surface when they collide.

This will prevent an accurate measurement as these electrons carry charge that will be lost and thus current change.

However, this problem can be solved by implementing a tiny change that will be mentioned later.



In this module the "electron scattering is not yet solved; however, the introduction of rectangular brass plates is to make this detector an array one.

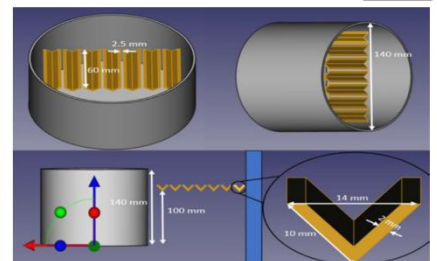
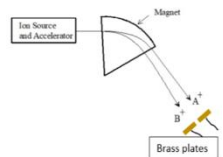
The problem with faraday's cup is that it can only be used to detect only one type of ions in the mass spectrometer unless a flight time analysis was implemented which is not.

An array of faraday's cup can solve the problem as each plate can detect one type of ions according to their position (masses).

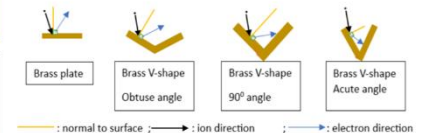
The accelerated ions go through a magnetic field which change their direction, since all ions in the experiment have the same charge, they will experience the same moving force. However, due to the different masses of each ion, they will move in a different directory i.e., the heavier the ion the longer the arc will take.

Looking at the diagram, it can be concluded that the more plates implemented the larger the ion type range that can be detected.

Which will directly affect module 4 the detector.



The final module reflects modules 5, but with replacing the plate-like brass into V-like shape. This will reduce the effect of "electron scattering" since when it happens the shot electrons will go in the direction of ion trajectory. This will leave the following cases:



What this shows is that the electrode shape actually matters because as the angle of the V-shaped is 180° (plate) or is obtuse the scattered electrons will leave; however, when it is 90° the electrons are more likely to hit the plate, but when it is acute angle the electrons are guaranteed to hit more than once which will drop the loss to minimum.

The LMC 6001 A1 Op-Amp was chosen for this application due to its high sensitivity and its low noise amplification process, since its Common-Mode Rejection Ratio (CMRR) is 83 dB, it means that the op-amp can effectively reject common-mode signals (inside noise). This is a desirable value for precision and sensitive applications. It means that the op-amp can amplify differential signals (signals that are in anti-phase on the inputs) while attenuating common-mode signals (signals that are in phase on the inputs).

Creating an electromagnetic coil for mass spectrometer for conducting tests on heavy ions (toxic metals)

System Requirements

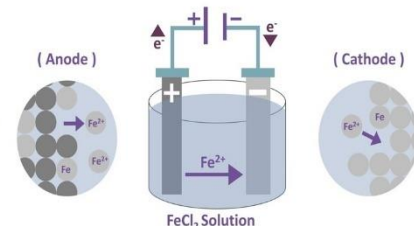
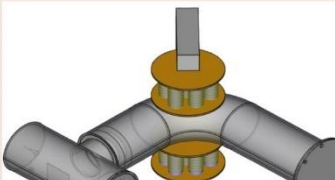
Coil Design

For Purification:

1. Electrolysis Cell: Container made of acrylic
2. Power Source: DC power supply
3. Anode: Impure Iron rod
4. Electrolyte Solution: FeCl₂ Solution
5. Cathode: Thin sheet of pure iron

In order to remove impurities from the iron, we use an electrolysis cell. The impure iron serves as the anode, while on the cathode side, we use another iron that will be purified.

The process known as **Electrolytic Refining Method**

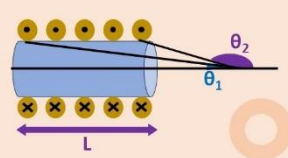
We have 2 identical units up and down to perform a uniform strong magnetic field.

Each unit contains 7 solenoids with a purified iron core which is cylindrical shape (20×100mm) and 70 turns of copper (2mm).

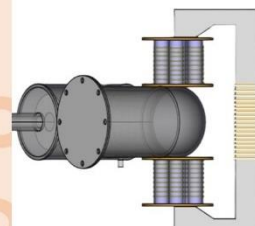
Magnetic field intensity is given by Biot Savart's Law as:

$$B = \frac{\mu NI}{2L} (\cos\theta_1 + \cos\theta_2)$$

B: magnetic field intensity in Tesla (T)
 μ: permeability of the core in Henry per meter (H/m)
 N: number of turns of the solenoid
 I: electrical current in Ampere (A)
 L: length of the coil in meter (m)



Biot-Savart Law


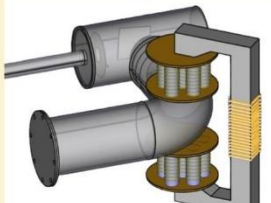


For Annealing:

1. Iron bar
2. Ethanol
3. Nitrogen gas
4. Muffle furnace

Temperature Controlling

For the process, purge the nitrogen gas in the furnace and set it between 800 and 850°C, then put the iron inside it until reaches the target temperature, and let it there for 1 hour, finally turn off the furnace and let the iron cooled slowly and normally.

The magnetic field intensity required for the analyzer in our mass spectrometer is ~ 0.2 T along 14 cm.

The model below inspired us to make the design.

We found that each solenoid can produce 0.11T along 14 cm distance, and since we have 2 units (up and down) the total magnetic field intensity will be 0.22T, if we use the following given for each solenoid:

μ = 4π × 10⁻⁷ × 4500 H/m
 N = 100 turns
 I = 6A

Using Biot-Savart law

If we succeed in achieving higher permeability, we'll require fewer turns.


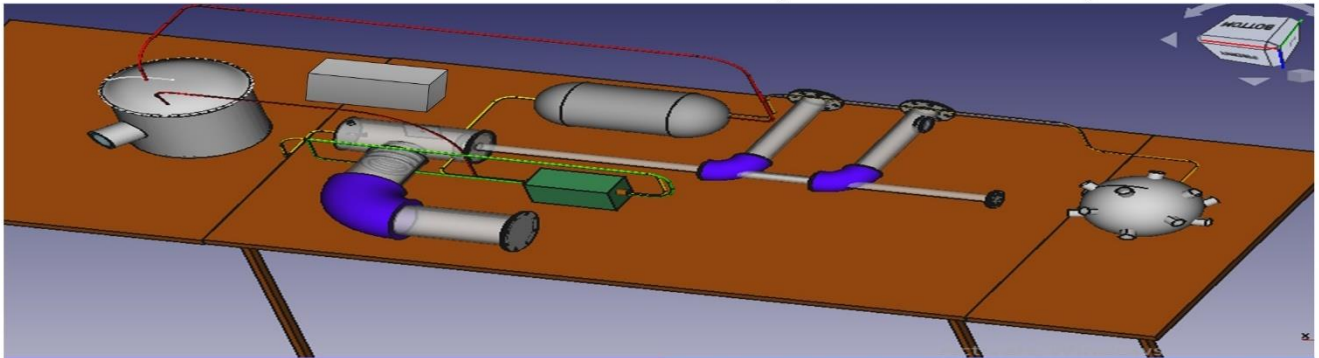
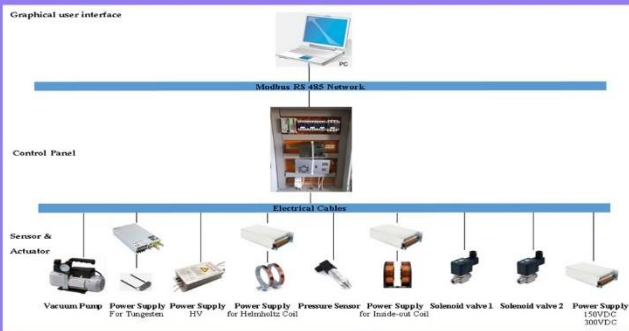


Image Source: WIKIMEDIA COMMONS

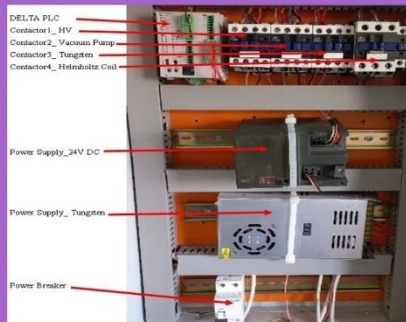
Control System For Mass Spectrometry



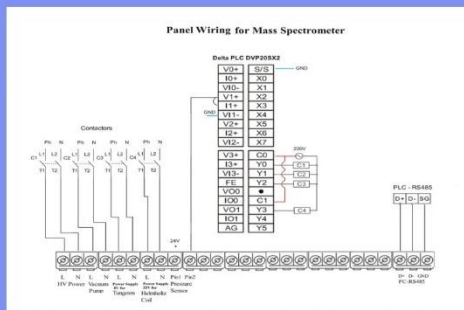
First it is important to know the sensor and actuators that will be wired to PLC therefore we place them in the control panel .
Program the PLC using DELTA WPLSoft.
Create the GUI using C#.net. Note that the addresses in PLC program differ from the addresses in C# code .



- Contactor1 is used to ON/OFF HV.
- Contactor2 is used to ON/OFF the vacuum pump.
- Contactor3 is used to ON/OFF the power supply applied to the tungsten (17V).
- Contactor4 is used to ON/OFF the power supply applied to the Helmholtz Coil.
- Power supply 24V DC is used to feed DELTA PLC.



Each of these components has the same COM C0. The phase of i element is connected to Yi output of the PLC as shown in the figure.



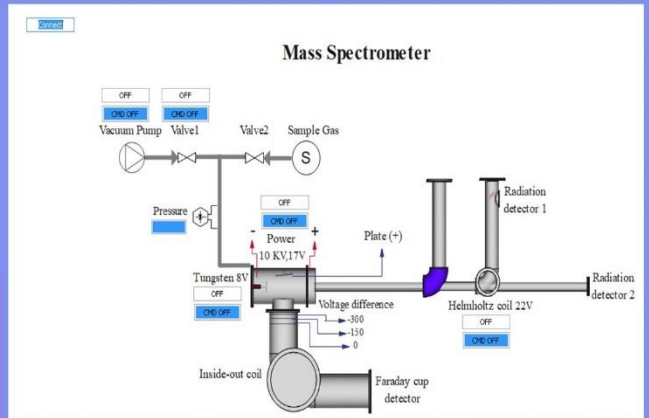
Components in coding and their addresses .

Mass Spectrometer	Current addresses inside (GUI)	Modbus-addresses (PLC)	Physical Address (PLC)
High Voltage Power	1280	1281	Y0
Vacuum Pump	1281	1282	Y1
Power Supply 8V for Tungsten	1282	1283	Y2
Power Supply 22V for Helmholtz Coil	1283	1284	Y3
Valve 1	1284	1285	Y4
Pressure Sensor	4100	4101	

Graphical user interface allows the user to control the components manually.

Each of Vacuum pump , Valve 1, Power (10KV,17V), Tungsten 8V and Helmholtz Coil have a command button ON/OFF and a button that shows its status.

Textbox Pressure shows the value of the pressure delivered from the pressure sensor through the PLC



Algorithm for Operating and Shutting Down the System

Action	Expected Result
<ul style="list-style-type: none"> Turn on the valve V1 and the pump Turn on the Power Supply P4 and P9 Burn the Tungsten by supplying it with P9 Connect the power supply P9 to the first plate Turn off the pump and the valve V1 Turn on the detector Turn on the valve (V2) for a few minutes. 	<ul style="list-style-type: none"> V1 is open, 95% Vacuum Continuous Power (17V) Get electrons around the Tungsten (the lamp will light) The first plate positively charged attracts the electrons towards it The air stopped and V1 is closed Detector is running The electrons will collide with the atoms of the vapor sample (Get ions with charge (+1)) Continuous power (300 V) Get magnetic field (B=0.2 T) The second plate positively charged repulses the ions out of the ionization chamber, and the ions enter the tube The ions that entered the tube will be accelerated The detector gives a signal (this indicates that the ions left the ionization chamber, entered the tube, accelerated by the plates, deflected by the magnetic field, and were detected) Ions acceleration stops, no signal will appear. Detector is not running. Magnetic field stops The second and the first plates are no longer charged and the lamp will turn off
<ul style="list-style-type: none"> Turn on P8 and P5 Turn on the Helmholtz Coil Connect the power supply P8 (150V) to the second plate 	
<ul style="list-style-type: none"> Connect the power supply P5 to the three plates in the tube Ions will be subjected to a magnetic field of B= 0.2 T when they pass through the curve 	
<ul style="list-style-type: none"> Turn off P5, the detector and the Helmholtz Coil 	
<ul style="list-style-type: none"> Turn off P8, P9 and P4 	

2.3.6 Plasma Code

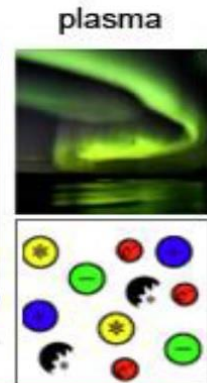
بِسْمِ اللَّهِ الرَّحْمَنِ الرَّحِيمِ



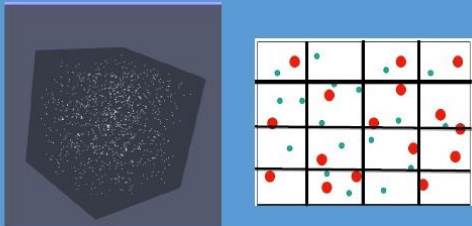
Particle simulation code (PSC - Plasma)

برنامج رقمي هدفه دراسة سلوك الجزيئات داخل البلازما.

Principles
 Plasma is considered the fourth state of matter. Plasma is a cloud of protons, neutrons and electrons where all the electrons have come loose from their respective molecules and atoms, giving the plasma the ability to act as a whole rather than as a bunch of atoms.
 The governing equations of intense laser plasma interaction, are the Vlasov-Boltzmann equations combined with Maxwell's equations in three spatial and momentum dimensions



Meshing
 The geometry used in this program is a cube. 1000 particles were studied (500 electrons and 500 ions) distributed randomly in the box.



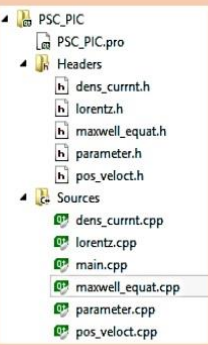
Equations
 The sequence followed in our program is:

```

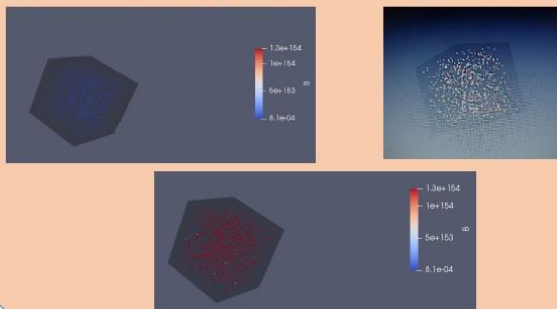
    graph TD
        A[Load Particle Distribution] --> B[Solve Particle EOM  
F_p -> (x_p, p_p)]
        B --> C[Model Surface Emission]
        B --> D[Monte-Carlo Collisions]
        C --> E[Particle Interpolation  
(E_i, B_i) -> F_p]
        D --> F[Extrapolate to Grid  
(x_p, p_p) -> (p_i, j_i)]
        E --> G[Solve Maxwell's Equation  
(p_i, j_i) -> (E, B)]
        F --> G
        G --> B
    
```

Using these equations:
 - Lorentz force: $\vec{F}_p = q\vec{E}_p + \frac{q}{m}(\vec{p}_p \times \vec{B}_p)$
 Position and velocity: $\frac{d\vec{v}_j}{dt} = \frac{q_j}{m_j}(\vec{E} + \frac{\vec{v}_j \times \vec{B}}{c})$
 $\frac{d\vec{x}}{dt} = \vec{v}$
 Density and current:
 $\rho(\vec{x}) = \sum_j q_j \delta(\vec{x} - \vec{x}_j)$
 $\vec{j}(\vec{x}) = \sum_j q_j \vec{v}_j \delta(\vec{x} - \vec{x}_j)$
 Maxwell equations to calculate E and B
 $\nabla \times \vec{E} = -\frac{1}{c} \frac{\partial \vec{B}}{\partial t}$
 $\nabla \cdot \vec{E} = 0, \quad \nabla \cdot \vec{B} = 4\pi\rho$
 $\nabla \times \vec{B} = \frac{4\pi\vec{j}}{c} + \frac{1}{c} \frac{\partial \vec{E}}{\partial t}$

Program
 The program is composed from 5 classes and the main program.
 After initializing the parameters and the initial condition using the class << parameter.cpp >>, the Lorentz force on each particle is calculated using the class << Lorentz.cpp>> then the new position and the velocity is calculated using the class << pos_veloct.cpp >>. The density and the current on the grid are calculated using the class << dens_currnt.cpp>>. Using these values and the Maxwell equations, the electric and magnetic field are calculated on each cell using the class << Maxwell_equat.cpp >>. Now the Lorentz force is recalculated and a new time step starts.



Results
 we can present any variable we want: velocity, electric field or magnetic field. The pictures below present the variation of the magnetic field with time. The magnetic field vary from time step to another as we can see in the pictures



Maryam Abdel-karim @AECENAR / IAP Aug. 2019

2.4 Actual Status of projects

Legend:

- Still open
- In work
- completed



IAP/ICP Projects Actual Status Apr 2025



Still open issues:

2025: Mass Spectrometer, Cyclotron

- Responsible: Majid/Abdullah K.
- Due Date:
- Needed Budget:

X-Ray Detector (Scintillator) and X ray pattern (Laue pattern)

Needed Budget:
Timeline:
Responsible:

ICF Driver (light ion beam with pulsed powered diode and Marx Generator)

Needed Budget: 1000\$
Timeline: 3-9/25
Responsible:

ICF Target

Design

Timeline: 9/24

Responsible:

Design: Phys Funda M2 Group (

Realization

Needed Budget: 1000\$

Timeline: 2025

Responsible: Design: Phys Funda M2 Group (Ahmad)

Magnetic Beam Deflection

Needed Budget: 1000\$
Timeline: 10/24
Responsible: Abdullah Q.

Linear Accelerator (RF)

Needed Budget:
Timeline: 10/24
Responsible:

Flue Gas Heavy Metals Mass Spectrometer

Needed Budget: 2000\$
Timeline: Integration (9/24), Testing (9/24)
Responsible: Majd

Cyclotrone

TODO: Realization

Electron Source

IECF Device

Needed Budget: 5000\$ (Ultra High Vacuum Pump), D2

ICF Simulation

Fusion Process in Target

Timeline: 9/24

Responsible:

2.5 To be further realized

2.5.1 Cyclotron



The Cyclotron



Definition
A cyclotron is a machine that accelerates charged particles or ions to high energies. It was invented to investigate the nuclear structure by E.O Lawrence and M.S Livingston in 1934.

Types of cyclotron
There are two types of cyclotrons, namely, synchronous and isochronous cyclotrons.

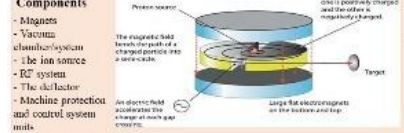
Synchrocyclotron: A modified cyclotron that obtains higher energy for charged particles by varying the mass change that the particles encounter as their velocity increases are called a synchrocyclotron.

Isochronous cyclotron: is an alternative to the synchrocyclotron. As stated above, in synchrocyclotron, the output beams come with a short gap. To avoid this short gap and get a continuous delivery of beam/particles, the use of isochronous cyclotrons is necessary.

Types of beams
Proton beams: the simplest type of cyclotron beam, proton beams are typically created by ionizing hydrogen gas.

H⁻ ions: Accelerating negative hydrogen ions simplifies extracting the beam from the machine. At the radius corresponding to the desired beam energy, a metal foil is used to strip the electrons from the H⁻ ions, transforming them into positively charged H⁺ ions. The change in polarity causes the beam to be deflected in the opposite direction by the magnetic field, allowing the beam to be transported out of the machine.

Heavy ion beams: Beams of particles heavier than hydrogen are referred to as heavy ion beams, and can range from deuterium nuclei (one proton and one neutron) up to uranium nuclei. The increase in energy required to accelerate heavier particles is balanced by stripping more electrons from the atom to increase the electric charge of the particles, thus increasing acceleration efficiency.



- Components**
- Magnets
 - Vacuum chamber/system
 - The ion source
 - RF system
 - The skid/structure
 - Machine protection and control system units.
- Uses/applications**
- Nuclear medicine: production of radioisotopes that are used in cancer treatment (targeted therapy).
 - PET: short lived positron-emitting isotopes (diagnosis & monitor).
 - Neutron production: production of high energy neutrons used for research, nuclear power plant test & cancer treatment.

Working principle

- Charged particle beam is accelerated using a high frequency alternating voltage applied to two "Dees" inside a vacuum chamber.
- Dees are placed opposite to each other creating an electric field.
- Two magnets are placed perpendicular to the "Dees", creating a magnetic field.
- Due to the presence of magnetic fields, particles in the cyclotron move in circular paths.
- Alternating voltage between the "Dees" creates the electric field that accelerates the particle.

Physics

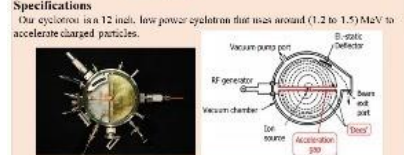
- Frequency of the voltage is equal to the frequency of the particle's cyclotron frequency.

$$f = \frac{qB}{2\pi m}$$

Where: B is the magnetic field strength
 q is the electric charge of the particle
 m is the relativistic mass of the charged particle

- energy of the particle depends on the strength of the magnetic field & the diameter of the Dees
- Centrifugal force: $F_c = \frac{mv^2}{r}$
- Lorentz's force: $F_D = qvB$

Solving for v & r : $F_c = F_D \Rightarrow \frac{mv^2}{r} = qvB \Rightarrow v = \frac{qBr}{m}$



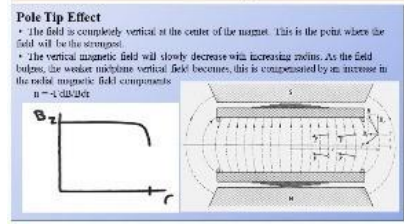
The Magnet

1.2 Tesla

- A proton circulating in a 1T has 15.2 MeV/revolution
- Each of the coils are energized by DC power supplies located in the control rack.
- Power leads should come from the slide boxes & connected terminals on the backside of the magnet.
- At full excitation, coils require 40 A.
- Impedance of each coil is 0.5 Ω .
- The Water Cooling system is used to de-ionize energy. We use two thermocouples as a backup, each placed on top and bottom and it actively being read by the PLC.
- The Field:
 - Before we can energize the power supplies, we need to enable the PLC's magnet permission.
 - We begin ramping up the current & hence the magnetic field.
- Magnetic field ramping could be visualized by a 3D compass.

$$B = \frac{\mu_0 n I}{2\pi r}$$

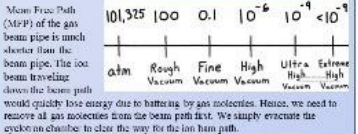
Where: B refers to the magnetic field strength in Tesla (T)
 μ_0 refers to the permeability of free space ($4\pi \times 10^{-7}$ T.m/A)
 I refers to the magnitude of the electric current in amperes (A)
 r refers to the distance in meters (m)



The Vacuum system

Vacuum chamber design:

- Brass accents
- Safety factor considered: max stress material can withstand / max stress material will encounter in a lifetime.
- Aluminum: body aircraft grade such as AL7075 for top and bottom lids.
- White teflon tape & tapered holes for pop seals, NPT (low pressure applications).
- O rings (Viton or brass-N) for id body seals.



The Deflector

The deflection channel intercepts the last turn of the cyclotron outward spiral beam. In a production machine, the beam is then guided onto a target where the nuclear interaction occur.

- Ion of specific velocities, determined by the deflector's electric field E , are transported to a phosphor coated collector plate.
- The deflection channel has a nominal radius of curvature, r_1 , of 1/2 inches and tangentially intercepts the cyclotron beam at a radius, r_2 , of 4.0 inches and transports it to a radius of 4.5 inches over 45° of arc.
- For an ion, charge q , of kinetic energy T or equivalently mass m in an axial magnetic field of B at 150° , the required deflecting electric field, E , is found to be:

$$E = \frac{2T}{q} \left(\frac{1}{r_1} - \frac{1}{r_2} \right) = \frac{qB^2 r_1^2}{m} \left(\frac{1}{r_1} - \frac{1}{r_2} \right)$$

The Vacuum system (continued)

Mean Free Path (MFP) of the gas beam pipe is much shorter than the beam pipe. The ion beam traveling down the beam pipe would quickly lose energy due to hitting by gas molecules. Hence, we need to remove all gas molecules from the beam path first. We simply evacuate the cyclotron chamber to clear the way for the ion beam path.

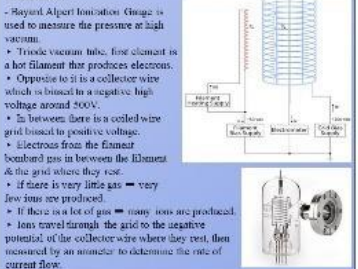
- In the rough regime, the (MFP) is actually still short enough that the gas acts viscously like a fluid; motion of gas molecules flow laminarily & exerts shear force on other gas molecules which makes pumping quite easy. We build a pump similar in that of a compressor known as a Rotary-Vane-pump.
- Flywheel expands gas on one side & compresses it on the other.
- On the expansion side, gas is drawn in viscously from the chamber & on the far side, gas is compressed & expelled into the atmosphere.
- Oil seals everything up & prevents the backflow of gas into the chamber.
- To measure the pressure in the rough vacuum, we use a thermocouple gauge, where the real conductivity is proportional to the (MFP).
- Filament connected to the thermocouple element which measures the temperature.
- A current is passed through the filament in the gauge depositing a constant amount of thermal power.
- If the gas surrounding filament is thermally conductive i.e. high pressure, the filament becomes cool as measured by the thermocouple element.

The Vacuum system (continued)

In the high vacuum regime, MFP is long enough so that the gas molecule spends much more time interacting with the walls of the chamber. This is known as "molecular flow".

In order to pump gas in this flow, use a diffusion pump that uses superheated jets of oil to capture individual gas molecules & pump them down & out of the chamber. To achieve this, the diffusion pump uses a parts:

1. Heater: resides at the bottom of the best chamber & boils oil forcing it upwards, interacting with the "chromium hair".
2. Chromium Hair: reduces the upward traveling gas back down so that any gas there would be deflected downwards.
3. Water cooling jacket: located inside the pump, which encloses the superheated boiling oil jet to travel back down to the boiler to be recycled.



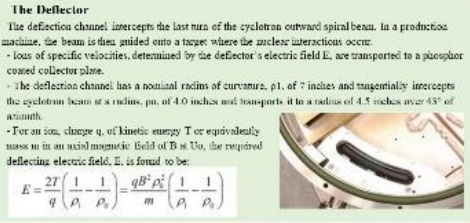
RF System

RF system design:

- Should be made of Copper or Brass
- Square wave is applied to Dees, the rest of the system is grounded
- 1/4-inch aluminum piping, positive work Deekin interior
- 1/4-inch copper refrigeration tubing
- Input coupling behind the coil
- Small motor driven trimmer capacitor adjustable from 4 to 30 pF
- Vacuum chamber, electrode system act as capacitor
- System is in parallel with an inductor & resonates of frequency $f = 1/(2\pi\sqrt{LC})$
- Values at most 2000 series of RF power
- Use a network analyzer to measure the resonant frequency of a tank circuit & identify the full width 45 max or bandwidth
- High quality means higher amplitude and narrow bandwidth.
- Low quality means lower amplitude and broader bandwidth. We choose Copper or silver-plated materials. $Q = \omega L / R$ (bandwidth)
- Dees voltage: time avg energy stored in the capacitor / time avg energy stored in inductor.

Ion source

- We set out to build a cold cathode Penning Ion Gauge (PIG) source
- It uses two tungsten cathodes pinned to stainless steel leads that are seated in boron-nitride cups which are housed in copper bases.
- The chimney, chimney bases, and HV lead shields are also all copper. Cooling is through conduction to the upper and lower chamber lids.
- Beam current from an arc current of 5 mA is sufficient for beam physics demonstrations, operating at greater currents quickly heats the phosphor screens.
- At 5 mA, the Mark-II PIG sources operate for greater than 40 hours without requiring servicing. Demanding greater arc currents reduces the source's lifetime.



The deflector installation consists of three major components:

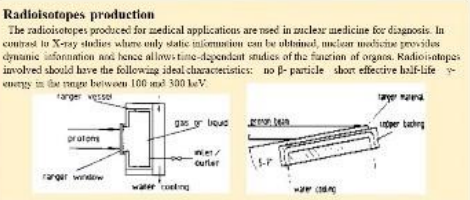
- The deflector assembly:
 - Two aluminum plates separated by stainless steel posts formed the skeletal structure. The septum's curve was machined as a stepped shelf along the inside edge of the top and bottom structural plates. A dim (0.005 inch thick) stainless steel strip was sealed against the step forming the septum.
 - This strips of aluminum matching the septum curvature were bolted into the shell changing the system in place and holding in operation.
 - The high voltage electrode was machined 3/8 inch thick from 7075 aluminum; each corner was rounded with a radius also of 3/8 inch.
 - The electric field: $E = \frac{0.9V}{r \ln \left(\frac{r+0}{r-0} \right)}$
 - The electrode was highly polished. It was supported from the back by the stem of two T Shaped Teflon insulators. Bosses were machined in the tips of each stem of the T-insulators, the bosses were seated in slots in top and bottom plates. The T-insulator stems were deeply counter-bored and finished with a blank through hole. Two tapered holes on the rear of the HV electrode, and Nylon screws secured the electrode to the base of the T-insulators. Electrical connector was made to the HV electrode by directly seating a HV ceramic vacuum feed-through conductor into a third and final clearance hole in the back of the electrode, and is captured by a set screw.

The phosphor screen detector:

- The screen was mounted at a 45° angle with respect to the incident beam and to the axis of a glass view port.
- The phosphor plate was separated from the carrier plate by 1/8-inch to keep the capacitance reasonably low.
- The carrier plate was clamped into the deflector assembly in a manner similar to the mounting of the septum. The center conductor of a coaxial cable was connected to the phosphor plate and the coax shield to the grounded carrier plate, the cable was routed to a DPC vacuum feedthrough connector.
- The electrical isolation and connectivity permits the phosphor plate to double as a Faraday collector. The low capacitance of the collecting plate should permit time-resolved electrical measurements of the impinging beam.

The high voltage power supply (HV):

- We cut the Herion 205A-50B
- This supply was also only a constant voltage simply requiring a current limiting resistor. The resistor was housed in an acrylic tube, capped at both ends, which was then externally covered to a grounded copper mesh.
- The high voltage was brought from the supply to the series resistor, and contained to the cyclotron chamber's HV vacuum bush using variable spray machine coaxial cable.



The production of radioisotopes used in nuclear medicine can be made with solid, gaseous and liquid targets.

The most important cyclotron produced isotopes for medical applications. Common isotopes for this radioisotope production are:

Radioisotope	Half-life (h)	Nuclear reaction	Bohring energy (MeV)
Gallium-67	78.3	Zn-69p,n(Ga-67)	25
Bromine-77	57	Kr-78p,n(Br-77)	30
		Rb-77- β^- -Kr-77- β^- -Br-77	
Rubidium-81	4.6	Kr-82p,n(Rb-81)	30
Indium-111	67.2	Cd-113p,n(In-111)	22
Iodine-123	13.2	Xe-124p,n(I-123)	30
		Cy-123- β^- -Xe-123- β^- -I-123	
Thallium-201	73.1	Tl-203p,n(Pb-201)	20
		Pb-201- β^- -Tl-201	
Fluorine-18	1.8	O-18p,p(F-18)	18

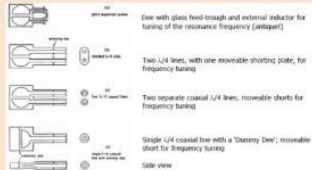
$$\langle U_x \rangle = \langle U_y \rangle = \frac{1}{2} L I^2 = \frac{1}{2} C V^2$$

$$V_{max} = \sqrt{\frac{2PL}{R_0 C}}$$



The Cyclotron Design

A 12-inch cyclotron is a compact and versatile particle accelerator that plays a crucial role in advancing research, diagnostics, and medical treatments. This innovative device utilizes the principles of electromagnetic fields to accelerate charged particles, propelling them to high energies for a wide range of scientific and medical applications. Materials Science, Particle Physics, Nuclear Physics Research, Cancer Therapy, Medical Isotope Production, Particle Acceleration).



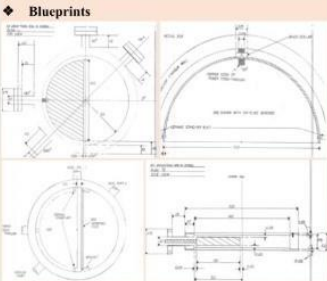
The original cyclotron had electrodes resembling the letter 'D'. In all classical cyclotrons, the DEEs are (capacitive) electrodes, inserted into the magnet gap, usually in the 'valley' of the pole plates. A shorted coaxial part (the inductive end) extends to the outside of the magnet yoke, thus completing the structures to 3/4 resonators.

- 1. Single DEE with Deflector:**
- Simplicity: A single DEE with a deflector setup is generally simpler in design and operation.
 - Energy Adjustment: It may be easier to adjust and control the energy of the accelerated particles with this setup.
 - Cost: It could be less expensive to build and maintain compared to a dual-DEE system.

- 2. Two DEEs:**
- Greater Energy Range: A dual-DEE cyclotron can provide a wider range of particle energies, which can be advantageous for various experiments.
 - Beam Intensity: Dual-DEE systems may offer better beam intensity and stability, especially at higher energies.
 - Versatility: They can accommodate a broader range of experimental requirements.

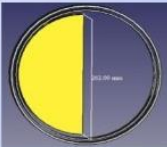


- Components**
- Our 12 inch cyclotron consists of:
1. DEE electrode
 2. Deflector
 3. Ion source PIG
 4. Flanges, Vacuum gauge & vacuum port
 5. Collector target port & Beam stopper
 6. Filament lead ports with gas inlet
 7. RF HV electrode
 8. CCD camera
 9. Deflector HV feedthrough
 10. RF pick-up probes.
 11. Shassy



1. DEE electrode

The DEE electrode is a critical component in the RF (Radio Frequency) acceleration process within a cyclotron. It provides the alternating electric field that allows charged particles to gain energy and accelerate as they move through the cyclotron's magnetic field.



- In a cyclotron, charged particles are injected into the central region, where a magnetic field causes them to move in a circular path. As they circulate, an alternating voltage is applied to the DEE electrodes.
- The DEE electrodes create an oscillating electric field within the gap between them. This electric field alternates in polarity as the particles move through it.
- The alternating electric field interacts with the charged particles in a way that synchronizes their motion with the changing field polarity. This synchronization allows the particles to gain energy with each revolution.
- By the time the particles reach the outer edge of the DEE electrodes, they have gained sufficient energy to be ejected from the cyclotron and directed toward a target or further stages of acceleration.
- Our cyclotron measure in diameter 12 inches which is 304.8 mm, DEE electrode measures 10 inches with is 262 mm

2. The Deflector

The deflector installation consists of three major components

- The deflector assembly,
- The phosphor screen detector
- The high voltage power supply.

Two aluminum plates separated by stainless steel posts formed the skeletal structure. The septum's curve was machined as a stepped shelf along the inside edge of the top and bottom structural plates.



A thin (0.005 inch thick) stainless steel strip was seated against the step forming the septum. Thin strips of aluminum matching the septum's curvature were bolted onto the shelf clamping the septum in place and holding its curvature.



The high voltage electrode was machined 3/8 inch thick from 7075 aluminum; each corner was rounded with a radius also of 3/8 inch.



3. Ion Source:

PI/G cold filament --c- emission

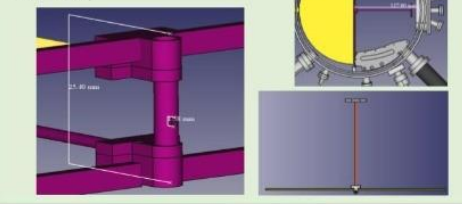
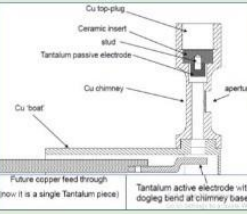
- Long warm up time (mins)
- Excellent lifetime
- Useful for low to medium Z
- High intensity

In our cyclotron, the height of the aperture is 1 inch tall which is 25.4 mm.

- The filaments length is equals to 5 inches or 127 mm that occupies half of the inner cylinder which is 10 inches

CHIMNEY: The inclusion of a chimney placed on top of the existing design will permit the thermionic electrons to travel to the median plane, thereby generating ions in the entire column.

A small aperture, 1/16 of an inch (1.5875 mm) in diameter, opening towards the DEE).



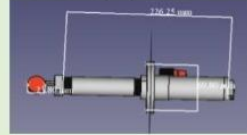
4. Flanges, Vacuum gauge & vacuum port

- Conflat flanges diameter: 2.75 inches (69.85 mm).
- Conflat flanges length: 1.5 inches (38.1 mm).
- Vacuum Wilson seal diameter: 1 inch (25.4 mm).
- Vacuum Wilson seal length: 2.5 inches (63.5 mm).



5. Collector target & Beam stopper

A copper beam stopper insert is a specific type of beam stopper designed to capture and absorb particle beams or radiation, particularly those generated in experiments or research applications. Copper is a common material used for such inserts due to its excellent thermal conductivity and radiation absorption properties. Placing the beam stopper insert behind the target has several advantages, but it should be carefully considered in the context of your experiment and its objectives.



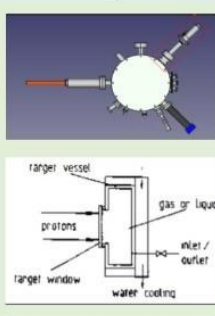
- Here are some reasons for placing a beam stopper insert behind the target material:
- Maximizing Interaction
 - Safety and Containment
 - Reducing Backscatter
 - Target Preservation

Collector Target

The choice of material for both the target body and window is dependent on the particular nuclide production process. Although a general rule does not exist, there are some aspects of the target bodies like activation, contamination, corrosion and cooling, which have to be considered. The parameters are influenced by the choice of bombarding particle, beam energy, beam current, material and solvent. The criteria for target-window materials should be the following:

- thickness of 1 – 200 mm
- pin-hole free
- high mechanical strength
- good thermal conductivity
- high melting point
- chemical resistance to oxidation

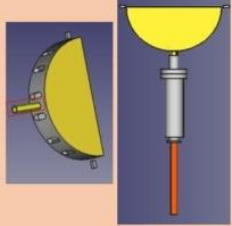
The target windows can be sealed either by O-ring or welding. This depends on the particular boundary conditions of cooling, temperature, pressure and radiation effects.



6. RF HV electrode

The high-voltage rod is positioned at the center of the cyclotron. It generates a high-frequency alternating current (AC) electric field. This alternating electric field accelerates charged particles placed in the center of the cyclotron.

- The choice of material for RF HV electrodes is crucial. It must have good electrical conductivity, high breakdown strength, and be able to withstand the thermal and electrical stresses associated with high voltages and RF fields.
- Common materials include copper, copper-plated materials, and other conductive metals.



7. CCD Camera

CCD (Charge-Coupled Device) cameras can be valuable tools for understanding and optimizing the performance of the cyclotron.

They are used in cyclotrons:

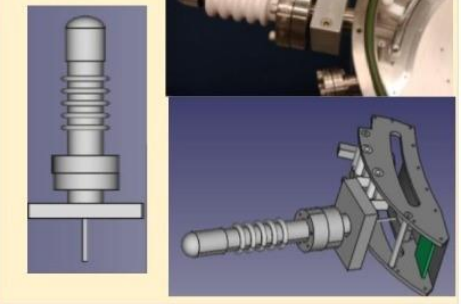
- Beam Profile and Emittance Measurements:
- Beam Position Monitoring
- Beam Spot Size and Intensity
- Radiation Detection
- Dosimetry and Radiation Safety
- Monitoring Cyclotron Components
- Data Acquisition
- Alignment and Calibration
- Visualization of Cyclotron Operation
- Beam Characterization

The location should provide a clear line of sight to the target or beam interaction region while ensuring the camera is shielded from radiation exposure.



8. Deflector HV feedthrough

Electrical connection was made to the HV electrode by directly seating a HV ceramic vacuum feed-through conductor into a third and final clearance hole in the back of the electrode.

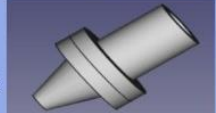


9. RF pick-up probes

An RF (Radio Frequency) pickup probe in a 12-inch cyclotron is a specialized component used for measuring and monitoring the RF electromagnetic fields within the cyclotron's radiofrequency cavity. RF pickup probes play a crucial role in ensuring the proper functioning and stability of the accelerator.

➤ Purpose:

- RF pickup probes are used to monitor the electric fields (E-fields) and magnetic fields (B-fields) inside the RF cavity of the cyclotron.
- They are essential for accurately measuring the RF frequency and field strength, ensuring that the particles are accelerated at the desired rate.



➤ Design:

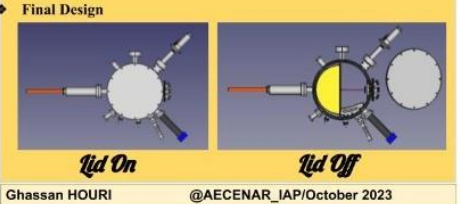
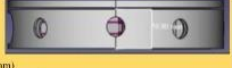
- RF pickup probes are typically designed as small, sensitive devices that can be inserted into the RF cavity of the cyclotron.
- They consist of electromagnetic sensors, such as dipole or loop antennas, that can detect the RF signals.
- The design may vary depending on the specific requirements of the cyclotron and the RF frequencies involved.

We place 2 RF pickup probes:

1. Since we have one DEE electrode, it should have its own RF pickup probe or set of probes to monitor the field at that location.
2. Beam Control and Stabilization: it helps maintain the desired resonance conditions and keep the particle orbits stable.

10. Shassy

- Outer cylinder is 12 inches in diameter (304.8 mm).
- Inner cylinder is 11 inches in diameter (279.4 mm).
- Gap size between two cylinders is 1 inch (25.4 mm)
- Inner cylinder and DEE Electrode is 0.5 inches (12.7 mm)
- Height is 2 inches (50.8 mm).



Ghassan HOURI @AECENAR_IAP/October 2023

❖ **Capacitance of cyclotrone**

- C is the capacitance in farads (F)

$C(t_{CT}=77.5\text{pF})$

❖ **The Magnet:**

- Magnetic Fields: Magnetic fields are used to exert forces on charged particles. In particle focusing, the magnetic field strength and direction are crucial for controlling particle paths.

$$B = \mu_0 I / g$$

μ_0 = permeability

I = intensity in Amp

g = height of air gap

❖ **Frequency:**

- $f = qB / 2\pi m = (1.602 \times 10^{-19})(1\text{T}) / 2(3014159)(1.6726219 \times 10^{-27}) = 15.2 \text{ MHz}$
- q is the charge of the proton (+1 elementary charge, approximately 1.602×10^{-19} Coulombs).
- B is the magnetic field strength (1 Tesla).
- π (pi) is approximately 3.14159.
- m is the mass of the proton (approximately $1.6726219 \times 10^{-27}$ kg)

❖ **Accelerating voltage**

- for a desired particle energy of 1.2 MeV and a magnetic field strength of 1 Tesla, we can use the following formula: $E = q \cdot V$
- E is the energy of the particle (1.2 MeV, which can be converted to joules).
- q is the charge of the particle 1.602×10^{-19} Coulombs
- V is the accelerating voltage.
- $V = E / q =$

❖ **Deflection voltage**

- $V_{def} = B \times R \times m \times v^2 / q \cdot d$.
- B is the magnetic field strength. = 1T
- R is the radius of the particle's path.

$$R = 2\pi \cdot m \cdot v / q \cdot B$$

- m is the mass of the proton (use the rest mass). = $1.6726219 \times 10^{-27}$ (kg)

- v is the velocity of the proton.

$$v = (q/B) \cdot (R/m)$$

- q is the charge of the proton = 1.602×10^{-19} (C)
- d is the distance of deflection.

- ❖ The voltage (V) required for a cyclotron is

$$V = qBR/\sqrt{2mE}$$

- V is the voltage in volts (V).
- q is the charge of the particle.
- B is the magnetic field strength.
- R is the radius of the cyclotron's path.
- m is the mass of the particle.
- E is the desired energy of the particle

- ❖ The radius of the particle's path in a cyclotron

$$\text{Radius } R = mv/qB$$

- R is the radius of the path.
- m is the mass of the particle.
- v is the velocity of the particle.
- q is the charge of the particle.
- B is the magnetic field strength.

Requirements

- Cyclotron Diameter: 12 inches (304.8 mm)
- Inner cylinder Diameter : 10 inches (254 mm)
- Magnetic field : 1 Tesla
- Desired energy: 1.2 MeV
- Cyclotron Frequency: 15 MHz
- ❖ Dee (electrode) Voltage

$$V_{DEE} \sim peak = \sqrt{2} V_{rms} = \sqrt{2PL/RC}$$

2.5.2 Electrical Propulsion for Space

AECENAR بسم الله الرحمن الرحيم
 Association for Economical and Technological Cooperation
 in the Euro-Asian and North-African Region



محطة تجريبية للدفع الالكتروني

Project of IAP institute by AECENAR

الهدف: عندما يكون القمر الاصطناعي في الفضاء، يحتاج إلى آلية تثبت و تصحح مساره. نستخدم لذلك الدفع الالكتروني، الذي لا يعمل إلا في غرفة فراغ. لدراسة فعاليته نحتاج لمنظومة من العدادات الكاشفة.

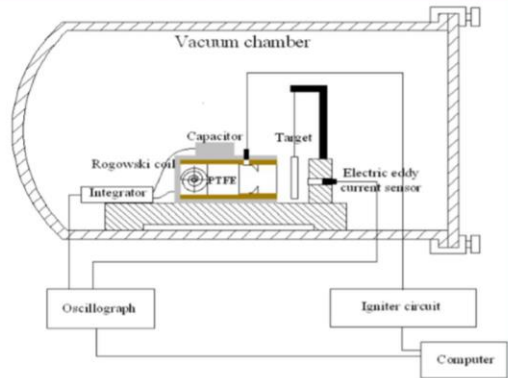
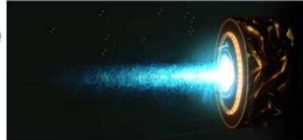


Figure 4. Schematic diagram of the experimental system

PPT

يتميز الPPT عن سائر منظومات الدفع الالكتروني بأنه سهل التصنيع ومثين فلا يتأثر كثيراً بالتصادمات الحاصلة في الفضاء.

الدفع الالكتروني

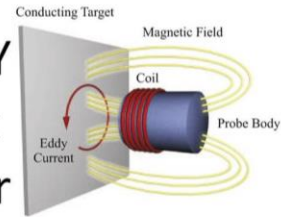


Pulsed Plasma Thruster

يتميز الدفع الالكتروني عن الدفع الكيميائي بأنه خفيف الوزن، لا يلوث، يمكن استخدامه لمدة طويلة في الفضاء (10 سنين)

عداد كاشف

EDDY current sensor



يقوم الECS بقياس فرق المسافة بين الtarget و الProbe الذي نشأ بتصادم البلازما بالهدف.

غرفة فراغ



تضيق الجزيئات في الهواء فلا تعطي مفعولها، و لا نستطيع أن نقيسها، و في حالتنا لا يتكون البلازما من الأصل إلا في غرفة فراغ شبه تام.

ROGOWSKI coil



يقيس الRC التيار (current) العائد بعد عملية الدفع.

Electrical Propulsion for Satellites

Electrical Propulsion Unit



Aluminium
Teflon
Plastic (isolator)
spark plug
Transformer



Vacuum Chamber



2.5.2.1 Rowowski Coil (Conceptional Realization done) for Electrical Propulsion Vacuum Chamber

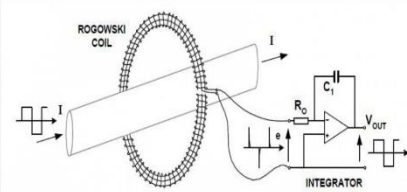


Theory

Rogowski Coil

Approach, Design and construction

Rogowski Coil:

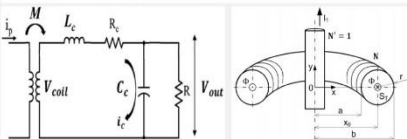


The Rogowski coil is defined as an electrical device that is used to measure alternating current (AC).

A Rogowski coil is an evenly wound coil with N number of turn and constant cross-section area A.

There is no metal core in a Rogowski coil.

The end terminal of the coil is returned through the central axis of the coil to another end.



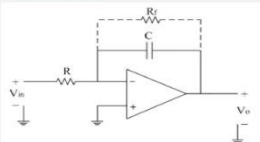
Rogowski coils work on the principle of Faraday's law.

When current passes through the conductor, it will create a magnetic field.

Due to an intersection with a magnetic field, a voltage is induced between the terminals of the Rogowski coil.

The output of Rogowski coils is connected with the integrator circuit.

Active integrator



$$Gain = \frac{V_{OUT_MAX} - V_{OUT_MIN}}{V_{IN_MAX} - V_{IN_MIN}}$$

$$Gain = \frac{R_f || X_C}{R_i}$$

Electro filter test and improvement

Design experiment of Rogowski Coil in Lab

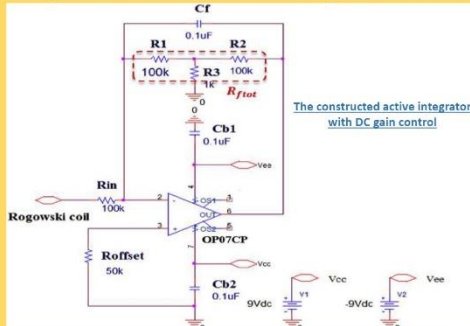


Rogowski Coil without integrator

The voltage produced by a Rogowski coil is:

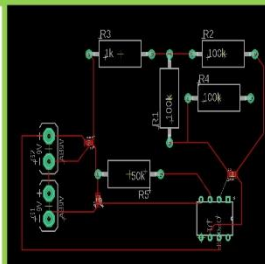
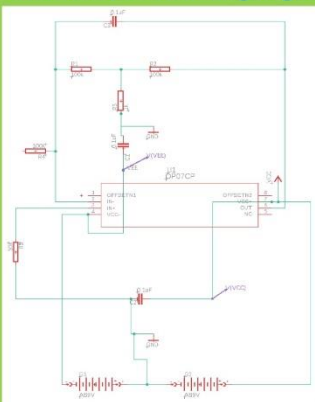
$$v(t) = \frac{-AN\mu_0}{l} \frac{di(t)}{dt}$$

Design and construction of Active Integrator



The constructed active integrator with DC gain control

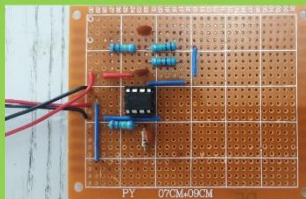
Schematic, Board using Eagle CAD



Using the schematic on Eagle CAD, we build the active integrator which is connected to the coil.

This is how we build the Rogowski Coil.

Construction of Rogowski Coil in Lab

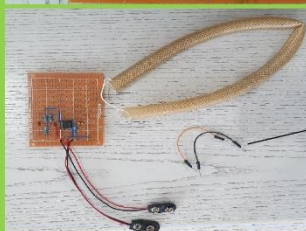


This integrator was selected ten times more than the time duration of the signal.

By connecting the output of Rogowski coil to the inverting input terminal of operational amplifiers, the input and output differ in phase and the role of this integrator is shown in equation:

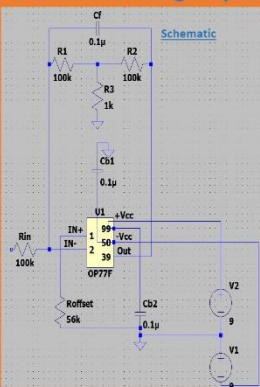
$$G(s) = -R_{fint} / R_{in}(1 + R_{fint}C_s)$$

Operational amplifier OP07CP has ultralow drift and high accuracy to form in-phase amplifier circuit.



All that remains is to mount the oscilloscope wires.

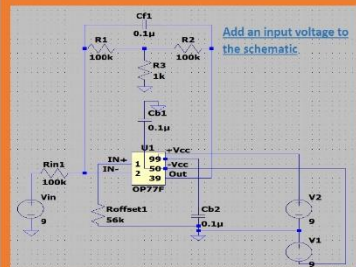
Simulation using LTspice



The operational amplifier OP07CP is the same as OP07C.

The OP77 is the next generation of the OP07.

By comparing the outputs of the two operational amplifiers, we demonstrate that we can use the OP77F instead of OP07CP in the simulation.



Simulation: DC operating point

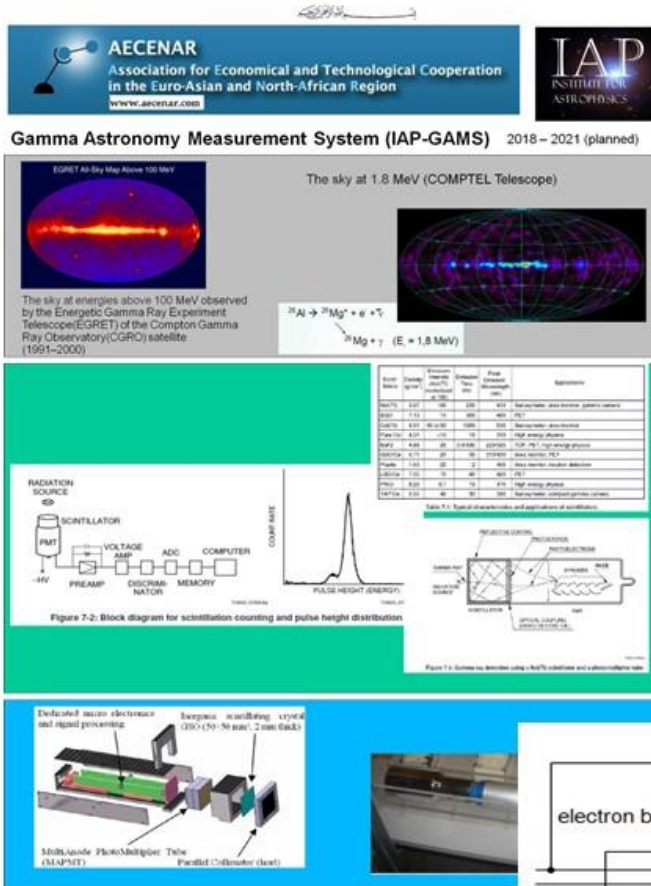


Results



2.5.3 X-Ray Detection by Laue pattern

03.04.2021



Master Thesis: Gamma/X-Ray detector development for IAP-SAT

Tasks:

1. Initializing documentation: 1. PhD ppn CCD, 2. x ray source/pulsed power accelerator / vaccum chamber technology
2. Source:
 - pulsed power diode accelerator in vaccum chamber
 - X-ray source (alternative: dentist x-ray source)
3. Building x-Ray detector: NaI scintillator + Si detector (PV cell)
4. Data Reduction SW (C++ with qt)
5. Testing: Laue diffraction patterns of plastic spheres

1

1. Initializing documentation: 1. PhD ppn CCD, 2. x ray source/pulsed power accelerator / vaccum chamber technology

Chapter 2 (Basics)

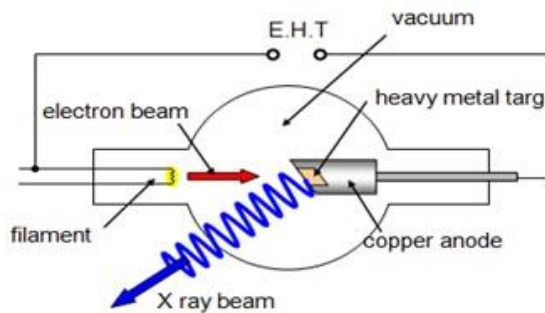
Timeplan

Topic	Timeline	Documentation
Initializing documentation	Dec 20 - 10.4.21	Completing Chapter 1 (Introduction, Task, Timeplan) Completing Chapter 2 (Basics)
Source: pulsed power diode accelerator in vaccum chamber (Design and Realization)	12.4.- 8.5.21 (3 weeks)	Chapter 3 (Contribution) Completing Chapter 3.1 (Realization of x-ray source)
Building x-Ray detector: Nal scintillator + Si detector (PV cell), CAMEX		Chapter 3 (Contribution) Completing Chapter 3.2 (Realization of detector)
Testing: Laue diffraction patterns of plastic spheres		
Data Reduction SW (C++ with qt)		

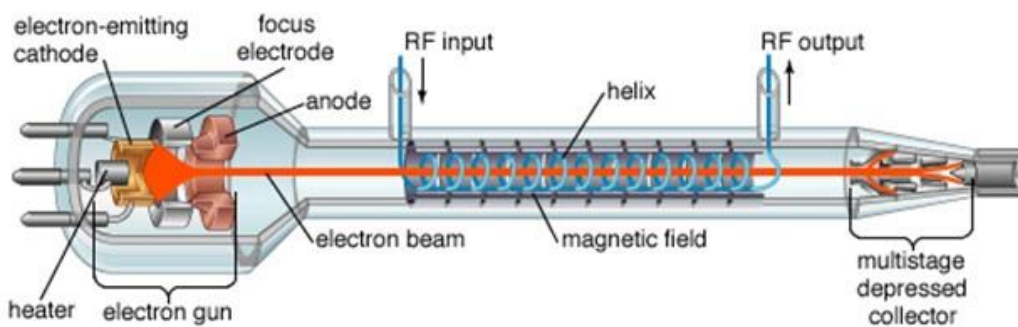
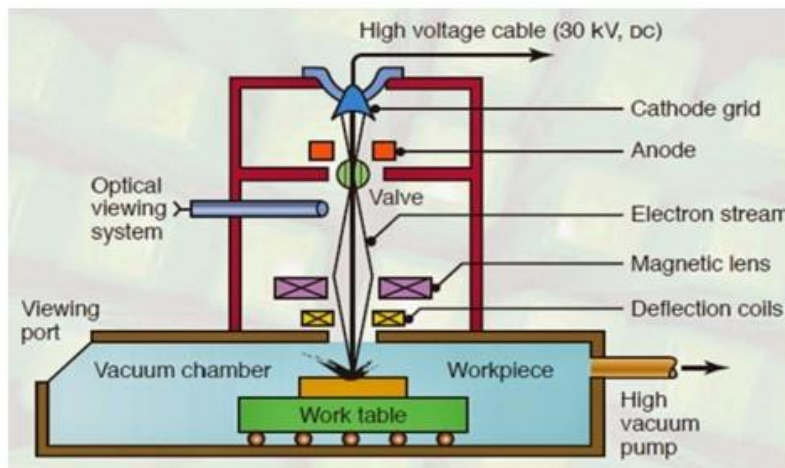
Remark: Vacuum Chamber Technology described in section IECF prototype realization

2. Source:

- pulsed power diode accelerator in vacuum chamber
- X-ray source (alternative: dentist x-ray source)



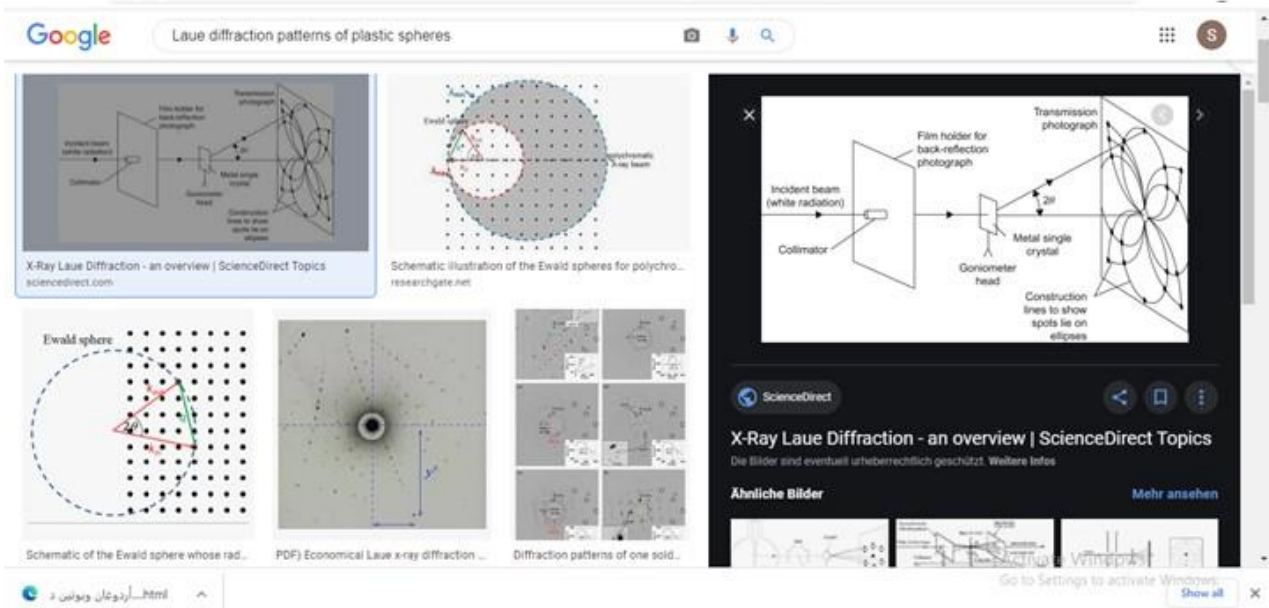
pulsed power diode accelerator



© 2004 Encyclopædia Britannica, Inc.

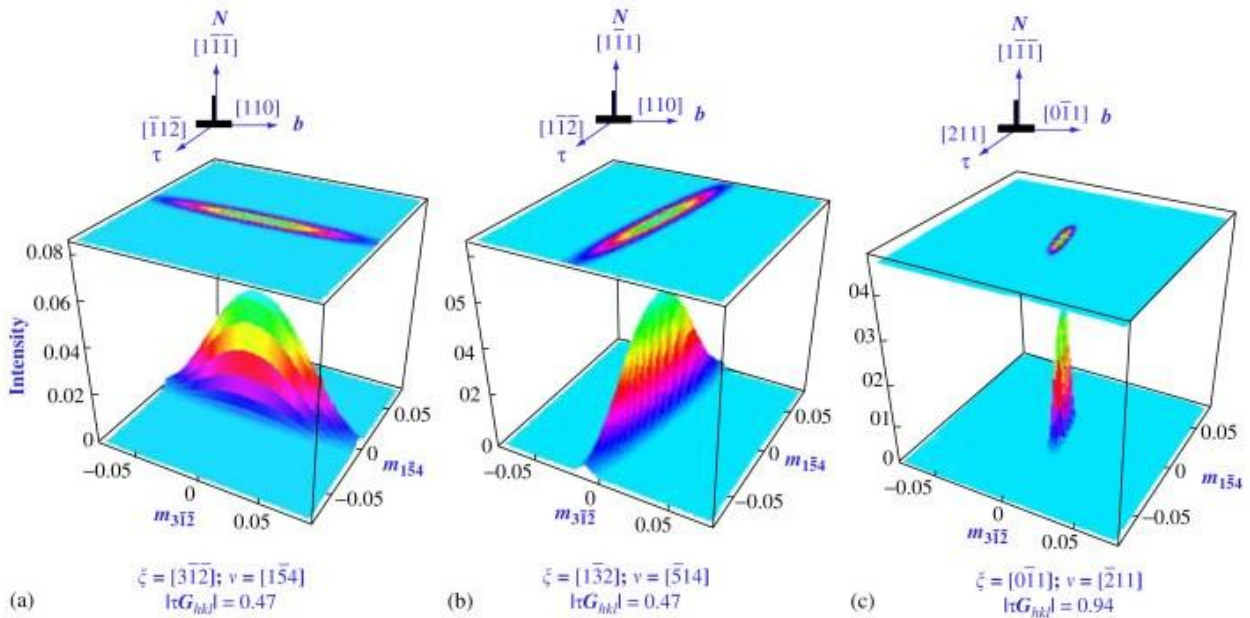
Remark: Source for X-Ray done in Master Thesis of Rouwayda Sakka

5. Testing: Laue diffraction patterns of plastic spheres



3.2 Natural Axes of the Laue Spot

To describe the intensity redistribution near a Laue spot, due to a particular set of dislocations, the mutual orientation of two planes are important (Figs. 5 and 8):



3 IAP-Physics Lab Testrig

Content taken from the following master thesis:



MEMORY



In order to obtain the

RESEARCH

In

PIRM: Physics of Radiation-Matter Interaction

Presented and Supported by:

Rouwayda Muhammad Sakka

January 2024

Title

Development of the integration and commissioning of a physics laboratory training device with X-ray production.

Supervisor

Prof. Aduan Naja

Readers

Dr. Ahmad Osman

Dr. Hassan Amoud

Lebanese University-Faculty of sciences

3.1 Requirements for IAP-Physics Lab Testrig

3.1.1 System Requirements

The electron accelerator must be able to produce electrons and accelerate them.

The Helmholtz coil must be able to deflect the trajectory of the electrons.

The target (made of copper) must be able to emit X-rays after collision with the electrons.

The detector must be able to detect X-rays.

3.1.2 Mechanical requirements:

The cathode must be able to withstand thermal and electrical stress.

The cathode must be tungsten.

The anode must be made of stainless steel.

The tube must be made of stainless steel.

The vacuum pump must be able to create a vacuum in the stainless steel tube.

The electron accelerator must be manufactured according to the mechanical design.

The Helmholtz coil is to be made from two pieces of plastic on which a copper strip is wound (Each piece is wound with 267 turns).

The target that emits X-rays when colliding with electrons must be made of copper.

The window must be made of glass to allow X-rays to pass through.

A camera must be placed inside the tube to be able to follow the trajectory of the electrons.

The detector must be placed outside the window to capture the X-rays and send a signal to the computer.

3.1.3 Electrical requirements:

A power supply must be capable of supplying 9V to tungsten.

Tungsten must be able to generate enough electrons to produce X-rays.

A power supply must be capable of providing a voltage of 10 kV.

A power supply must be capable of supplying a voltage of 21.7 V and a current of 3.61 A to the Helmholtz coil.

3.1.4 Magnetic requirements:

The Helmholtz coil must be able to generate the magnetic field necessary to deflect the electrons.

The Helmholtz coil must be able to generate a magnetic field of 0.01 T.

3.1.5 Safety requirements:

3.1.5.1 Electrical safety:

The anode, made of stainless steel, must be insulated from the tube to prevent voltage from extending and passing through the tube.

All electrical connections must be coated with the appropriate insulation depending on the current and voltage flowing through the connections.

9V cables and connections must be insulated with...

10 kV cables and connections must be insulated with...

21.7V cables and connections must be insulated with...

3.1.5.2 Radiological safety:

For X-ray protection, a metal box with a lead plate inside must be placed at the point of X-ray emission.

3.1.5.3 Chemical safety:

The lead must be completely enclosed to ensure that no toxic gases are emitted.

3.2 System Design and Mechanical Design of IAP-Physics Lab Testrig

In this chapter, we will examine two distinct aspects. The first will be devoted to mechanical design, covering the following elements: fundamental principles, Computer-Aided Design (CAD), and the implementation phase. The second will deal with automation, which involves the automatic collection and analysis of data using computerized systems.

We will have a particle source that will be accelerated by a potential difference. The accelerated particles, in this case electrons, will then enter a tube where their trajectory will be modified, leading to different avenues of study, each with a distinct objective. These electrons will either ionize the gases inside the mass spectrometer, follow a trajectory resulting in the production of X-rays, contribute to nuclear fusion reactions (ICF), or follow a trajectory that we envision as a future target.

To illustrate, to generate X-rays, we heat tungsten with 8 volts of power, acting as an electron source. These electrons are then accelerated by a 10 kV potential difference between the cathode and anode, resulting in uniform rectilinear motion. Then, a 0.01 T magnetic field deflects the electrons' trajectory over a radius of 3.37 cm, before they collide with a copper target placed at a 45-degree angle in another tube. This interaction generates X-rays. The resulting X-rays are detected using the "XR1 Pro" detector.

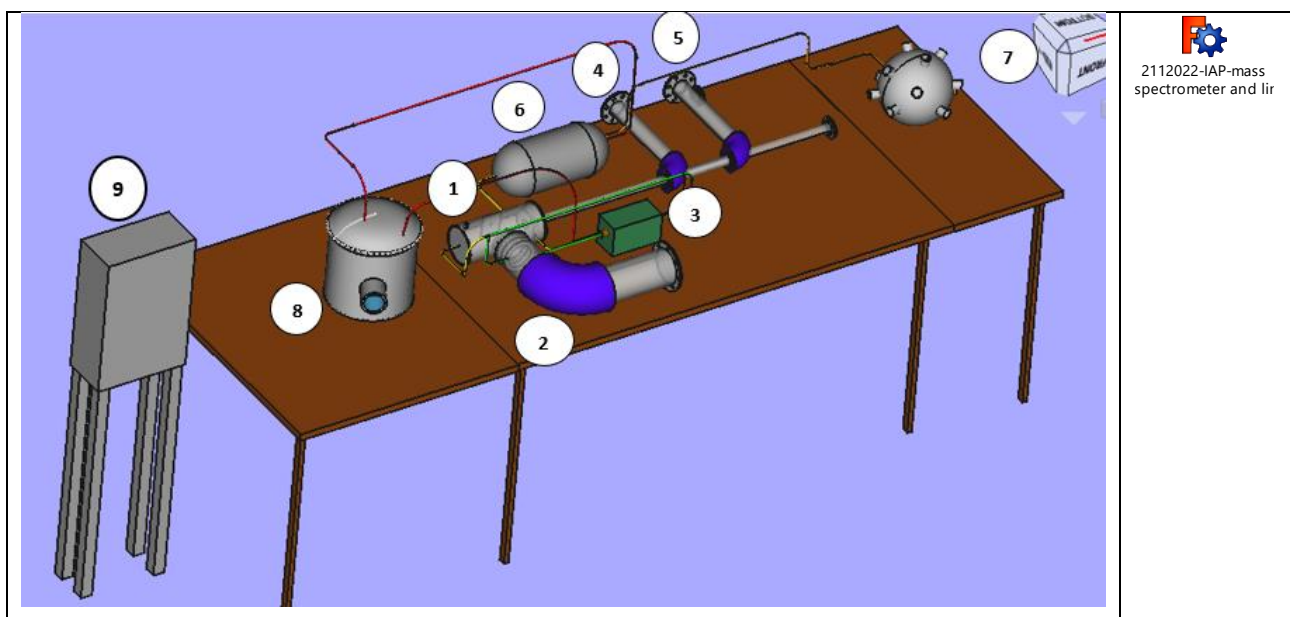


Figure II. 2: System design for a physics laboratory training device with some physical measuring instruments

1 - Electron Accelerator: Device for producing electron beams.

2 - Magnetic Sector Mass Spectrometer: In mass spectrometry, ions from a sample are generated, separated, and quantitatively detected according to their varied trajectories in electric and/or magnetic fields, based on their mass/charge ratios.

3 - High Voltage Power Supply (10 kV): Electrical device generating a high voltage of 10,000 volts.

4 - Electron Beam: This configuration is ready to be used for future application.

5 - Electron-Copper Interaction: Process to generate X-rays by interacting electrons with copper.

6 - Vacuum Pump: A device that sucks gas molecules into an enclosed space to create a partial vacuum. Its role is to generate a relative vacuum to prevent particle collisions with the air.

7 - Inertial Confinement Fusion (ICF) Target: A target structure in energetic fusion where a high-energy electron beam triggers nuclear fusion reactions by compressing and heating a target filled with thermonuclear fuel.

8 - Inertial Electrostatic Confinement Fusion (IECF): A class of energetic fusion devices that use electric fields to contain plasma, as opposed to magnetic fields.

9 - Control Box: Serves as an interface between sensors and actuators, with a connection to the computer for visualization and data processing, through programmable automated systems (PLCS).

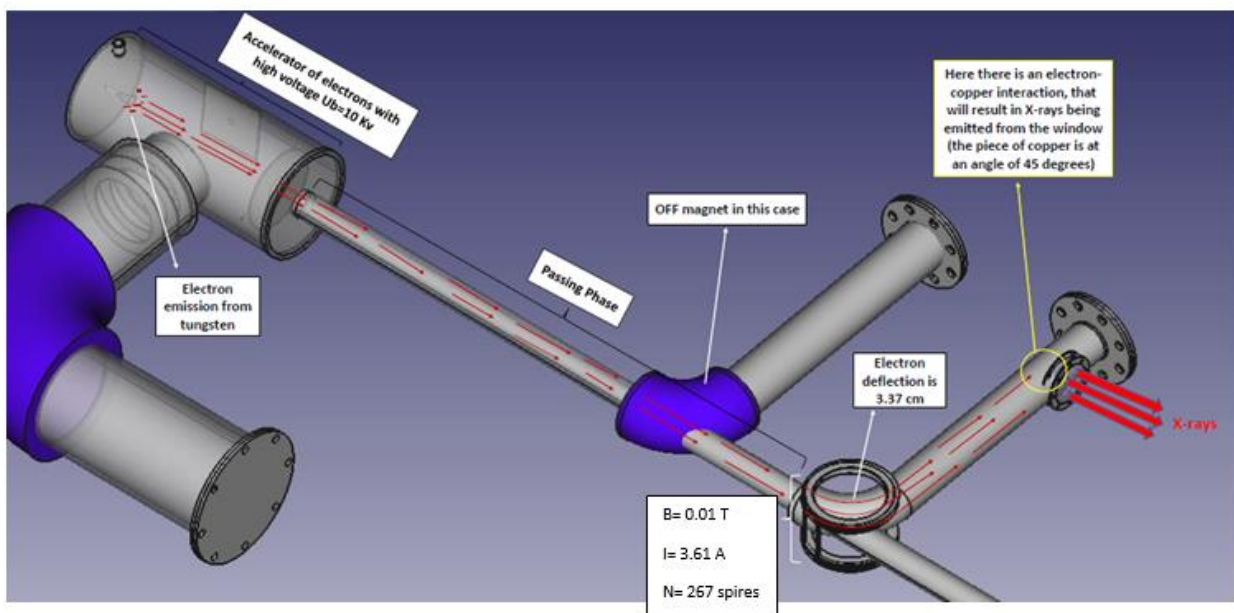


Figure II. 3: Trajectory of electrons before the production of the X-ray

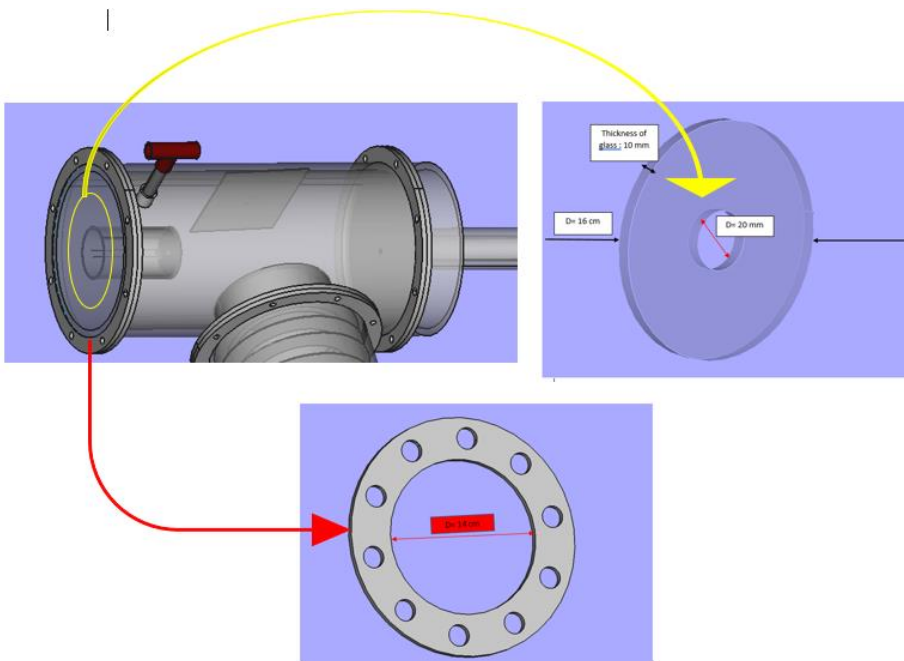


Figure II. 4: Glass disc for observing the electron beam

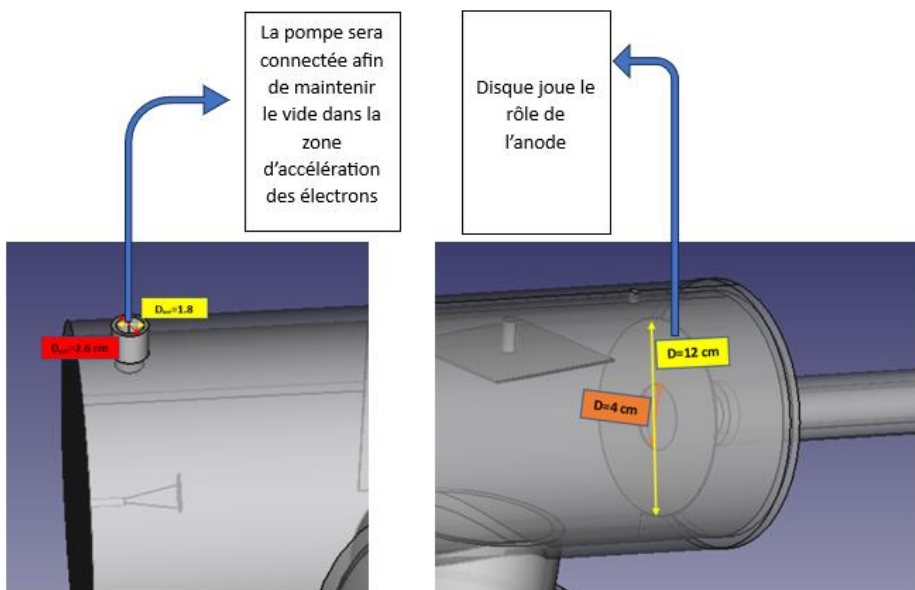


Figure II. 5: Measurement of certain components of the acceleration zone

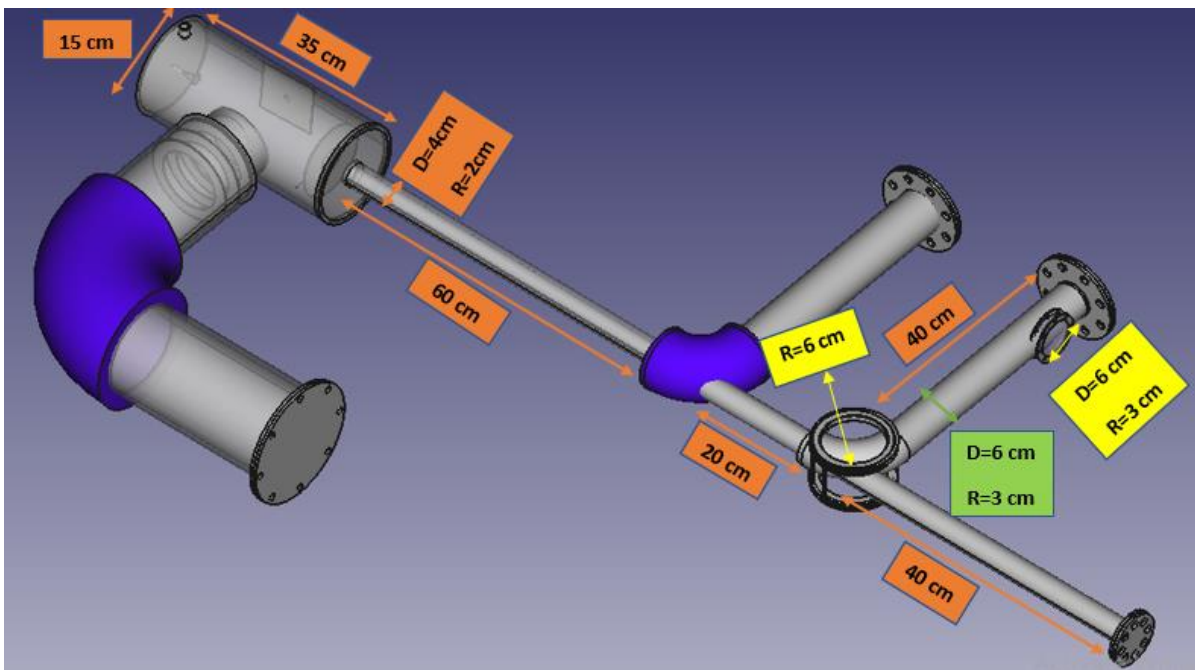
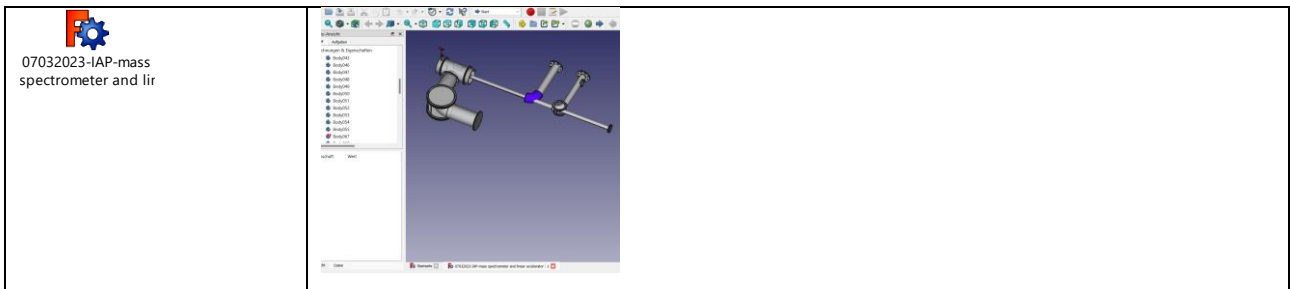


Figure II. 6: Specific measurements of the certain component of the prototype



3.3 Mechanical Realization of IAP-Physics Lab Testrig

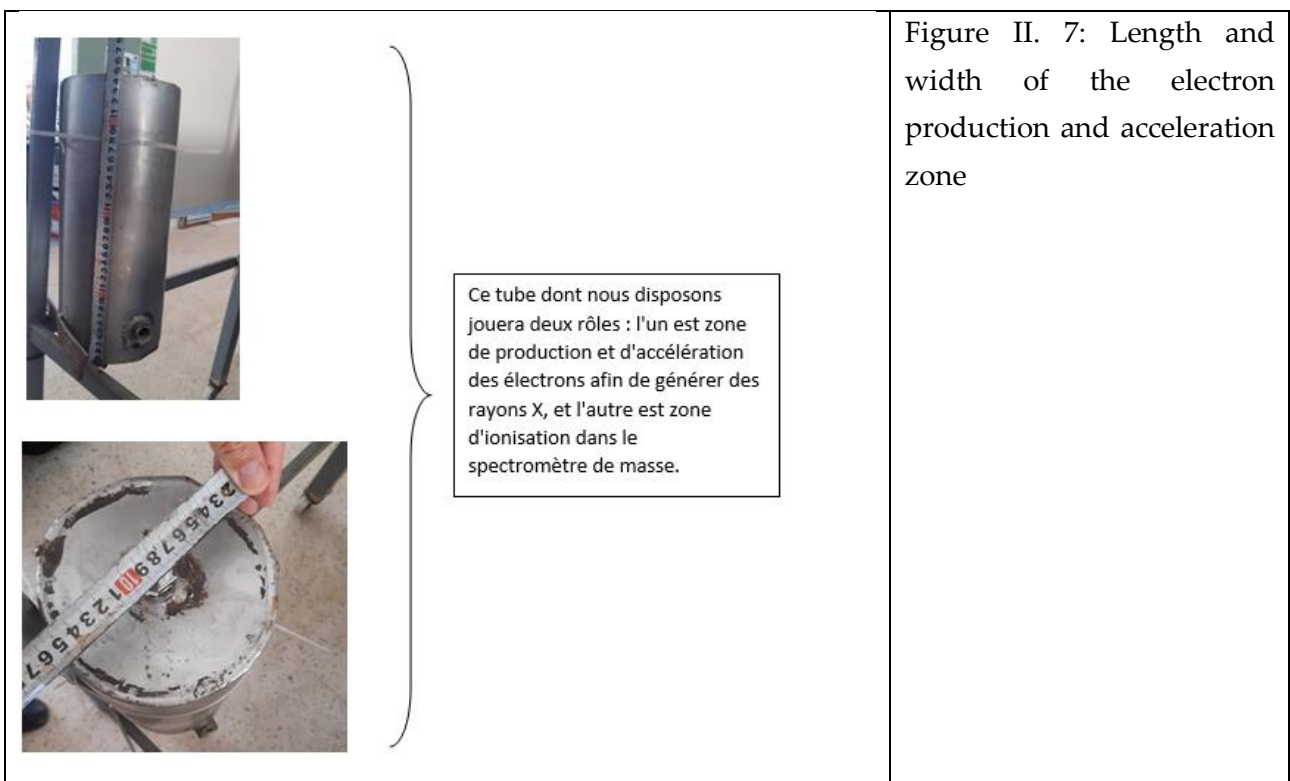


Figure II. 7: Length and width of the electron production and acceleration zone

Due to the availability of stainless steel components at the AECENAR Center, which can be used in the design of certain parts of our prototype, and considering the essential characteristics of stainless steel in terms of corrosion resistance, durability, ease of maintenance as well as flexibility in modification and welding, we made the decision to opt for the complete realization of the prototype in stainless steel.



Ce tube que nous avons
sera utilisé dans certaines
parties du spectromètre de
masse

Figure II. 8: Cross-sectional diameter of some mass spectrometer tubes



Figure II. 1: The curved tube where the magnetic field is applied



Figure II. 2: Preparing the window for X-rays with the appropriate flanges



Figure II. 3: Welding and Assembly of Prototype Components

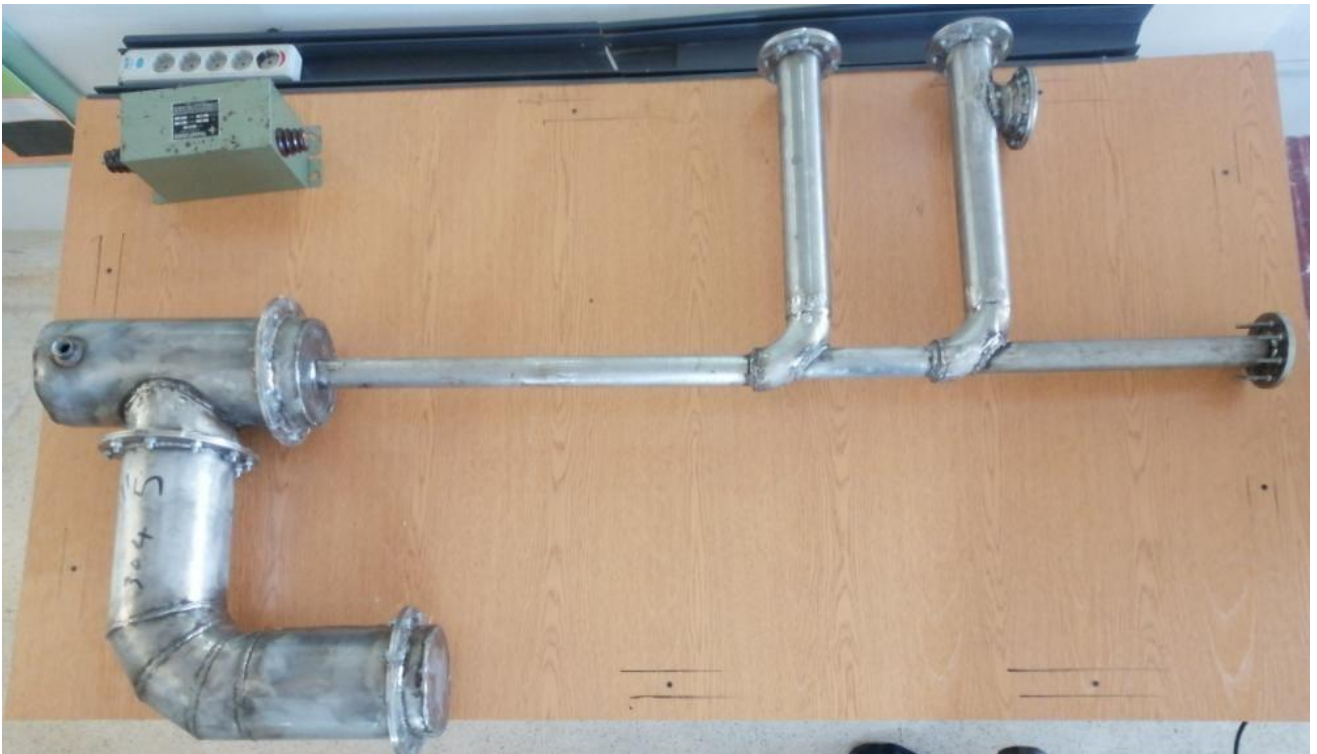


Figure II. 12: The assembled prototype also integrates the X-ray production device



Figure II. 13: Final Prototype with its Specialized Control Device

3.4 IAP-Physics Lab Testrig Automation (Process control system)

Graphical user interface



Modbus RS 485 Network

Control Panel



Electrical Cables

Sensor & Actuator



Vacuum Pump Power Supply For Tungsten Power Supply HV Power Supply for Helmholtz Coil Pressure Sensor Power Supply for Inside-out Coil Solenoid valve1 Solenoid valve2 Power Supply 150VDC 300VDC

Figure II. 24: Representative diagram of the Process Control System for IAP-PhysicsLab Testrig

3.4.1 PLC control panel

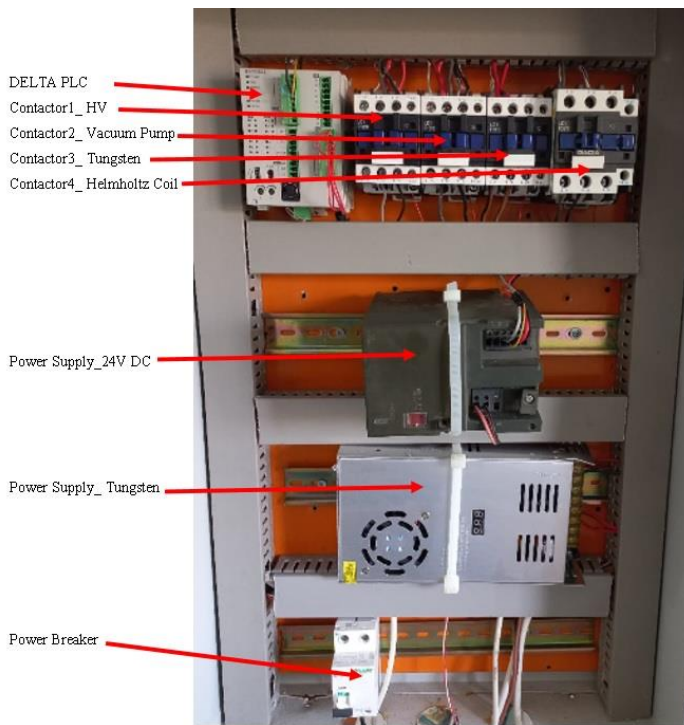


Figure II. 25: Representative diagram of the prototype control panel

3.4.2 Instruments



Figure II. 4: Some classifications of the constituent elements of the prototype

3.4.2.1 Electron gun filament (tungsten)



3.4.2.2 Radiation Detector (XR1 Pro)



3.4.2.3 Tesla Meter KT-102 (Measuring Range: 0-2500 mT)



3.4.3 Panel Wiring Diagram

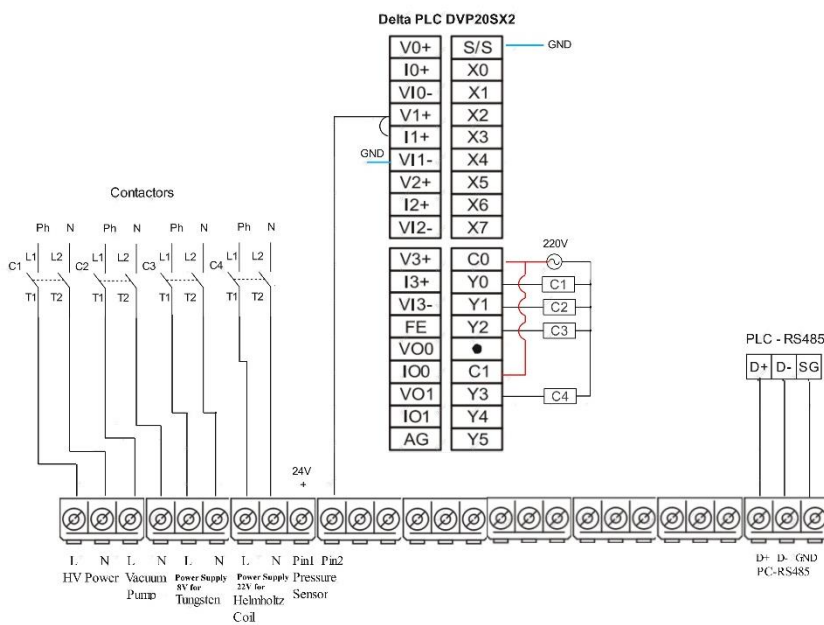


Figure II. 27: Representative diagram of the panel wiring

3.4.4 Graphical User Interface (GUI)

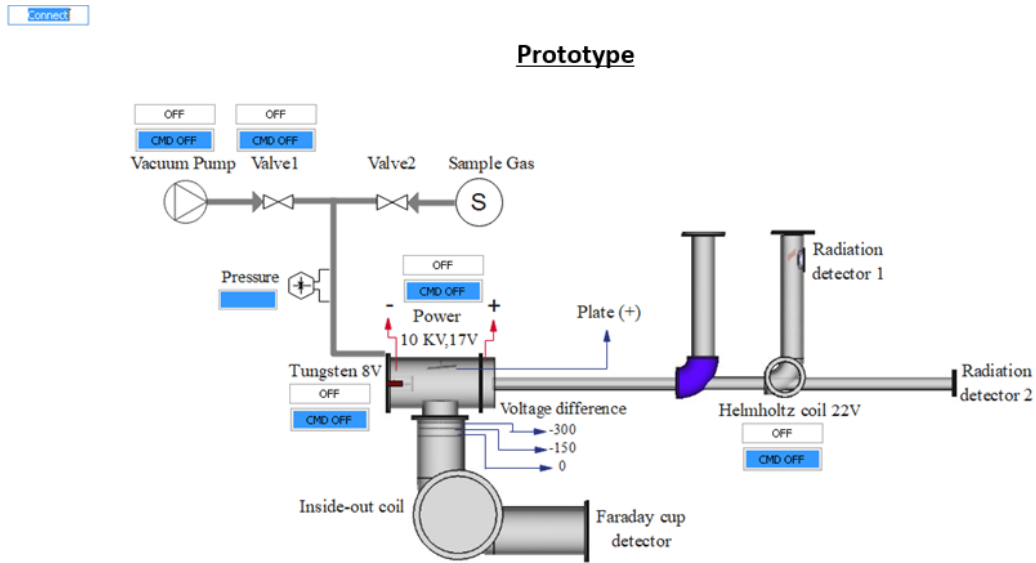


Figure II. 28: Representative diagram of the graphical user interface of the prototype

3.4.5 Modbus Address - Point Interface (PLC)

X-ray production	Modbus (PLC) addresses	Physical Addresses (PLC)
High voltage power	1280	Y0
Vacuum pump	1281	Y1
8V power supply for tungsten	1282	Y2
22V power supply for Helmholtz coil	1283	Y3
Valve 1	1284	Y4
Pressure sensor	4100	

3.5 IAP-Physics Lab Testrig Vacuum testing & X-Ray Testing

3.5.1 System Test Specification

00001: Ensure complete air evacuation

Stage	Description of the stage	Expected result
Precondition	The system is off	
Turn on the system	Turn on the pump	95% empty
Presence of a leak	Possibility of air leakage in certain places: welding-flanges-anode-cathode-tungsten-windows	Seal leaks
Turn off the system	Turn off the pump	The pump stops extracting air
Use of silicone	Apply silicone to the areas where there are air leaks	Stop leaks and achieve 95% vacuum when restarting the pump
Postcondition	The system is off	

00002: Tungsten power supply

Stage	Description of the stage	Expected result
Precondition	The system is off	
Turn on the system	Turn on the tungsten power supply	Obtain a continuous supply of 8 V
Turn off the system	Turn off the tungsten power supply	Continuous power supply stops
Postcondition	The system is off	

00003: Obtain electrons

Stage	Description of the stage	Expected Result
Precondition	The system is off.	
Turn on the pump	Turn on the pump	95% empty
Turn on the tungsten power supply	Turn on the tungsten power supply	Obtain a continuous supply of 8 V

Burning tungsten	Burn the tungsten by supplying it with 8V power	Get electrons around the tungsten (the lamp will light up)
Turn off the tungsten power supply	Turn off the tungsten power supply	The lamp will go out
Turn off the pump	Turn off the pump	The pump stops extracting air
Postcondition	The system is off	

00004: High voltage

Stage	Description of the stage	Expected Result
Precondition	The system is off	
Turn on the system	Turn on the high voltage	Obtain a continuous supply of 10 kV
Turn off the system	Turn off the high voltage	Continuous power supply stops
Postcondition	The system is off	

00005: Detector

Stage	Description of the stage	Expected result
Precondition	The system is off	
Turn on the system	Turn on the detector	The detector emits a signal when exposed to X-rays
Turn off the system	Turn off the detector	The detector is not working
Postcondition	The system is off	

00006: Acceleration of electrons

Stage	Description of the stage	Expected Result
Precondition	The system is off	

Turn on the pump	Turn on the pump	95% empty
Turn on the tungsten power supply	Turn on the tungsten power supply	Get a continuous power supply (8V)
Turn on the high voltage	Turn on the high voltage	Get a continuous power supply (10 kV)
Turn on the detector	Turn on the detector	The detector is working
Acceleration of electrons	Connect high voltage to the anode and cathode	X-ray emission (The detector emitting a signal will indicate that the electrons leaving the tungsten were accelerated as they passed between the anode and cathode, and struck the copper.)
Turn off the high voltage	Turn off the high voltage	No X-ray emission (the detector will not give a signal)
Turn off the detector	Turn off the detector	The detector is not working
Turn off the tungsten power supply	Turn off the tungsten power supply	The lamp will go out
Turn off the pump	Turn off the pump	The pump stops sucking air
Postcondition	The system is off	

00007: Helmholtz coil

Stage	Description of the stage	Expected result
Precondition	The system is off	
Turn on the system	Turn on the Helmholtz coil by supplying it with a supply of 21.7 V	Obtain a magnetic field ($B = 0.01 \text{ T}$)
Turn off the system	Turn off the Helmholtz coil	The magnetic field stops
Postcondition	The system is off	

00008: Electron deflection

Stage	Description of the stage	Expected result
Precondition	The system is off	
Turn on the pump	Turn on the pump	95% empty
Turn on the tungsten power supply	Turn on the tungsten power supply	Get a continuous 8V power supply
Turn on the high voltage	Turn on the high voltage	Get a 10 kV continuous power supply
Turn on the Helmholtz coil	Turn on the Helmholtz coil on the bent tube	Obtain a magnetic field ($B = 0.01 \text{ T}$)
Turn on the detector	Turn on the detector	The detector is working
Deflection of electrons	The electrons will be subjected to a magnetic field of $B = 0.01 \text{ T}$ as they pass through the curve	X-ray emission (The detector emitting a signal will indicate that the electrons leaving the tungsten were accelerated, passing between the anode and the cathode, deflected and struck the copper.)
Turn off the high voltage	Turn off the high voltage	DC power supply stops, No X-ray emission (the detector will not give a signal)
Turn off the detector	Turn off the detector	The detector is not working
Turn off the Helmholtz coil	Turn off the Helmholtz coil	The magnetic field stops
Turn off the tungsten power supply	Turn off the tungsten power supply	The lamp will go out
Turn off the pump	Turn off the pump	The pump stops extracting air
Postcondition	The system is off	

3.5.2 System Test and Results

3.5.2.1 Vacuum test 03-05-23

Analysis of test results:

To locate air leak locations, we applied soap and water to the surface of the device and then compressed the air inside;



Figure III. 1: Tools used to determine air leak locations

When we spot bubbles appearing, this indicates an air leak at that location.





Figure III. 2: Air leak locations

What we need to do:

We will redo the welding in the places where there were leaks during the previous welding.

We will be replacing the gasket on the flanges due to leaks.

3.5.2.2 Vacuum Test 9-6-2023

Analysis of test results:

First, we cleaned the stainless steel tube with special and precise tools;





Figure III. 3: During cleaning of the stainless steel tube

After cleaning, we noticed a small hole due to a soldering error.



Figure III. 4: An illustration of the device being prepared for welding improvement

To determine if there is still an air leak, we will retest the application of soapy water to the surface of the device and the air pressure inside the device.

When we spot bubbles appearing, this indicates an air leak at that location.



Figure III. 5: Carrying out a new check for the presence of air leaks

These flanges were leaking:



Figure III. 6: air leak locations

What we need to do: We will add silicone around the flanges.

3.5.2.3 X-ray test 03-07-23

Analysis of test results:

First, we started the pump and ensured the necessary vacuum;

Next, we turned on the tungsten via the control panel; We tried to power the tungsten with a voltage between 6 and 12 volts, but in this case, the tungsten drew more than 20 amps, causing the power supply to reduce the voltage to 3.5 volts. (The power supply we used can handle 0 to 20 amps);

Then we turned on the high voltage (10 kV), and the problem of electron leakage appeared at the ends of the cylinder, and the electrons did not penetrate the single hole in the plate,

but deflected to the screw on the plate (which indicates a problem in the uniform distribution of charges).

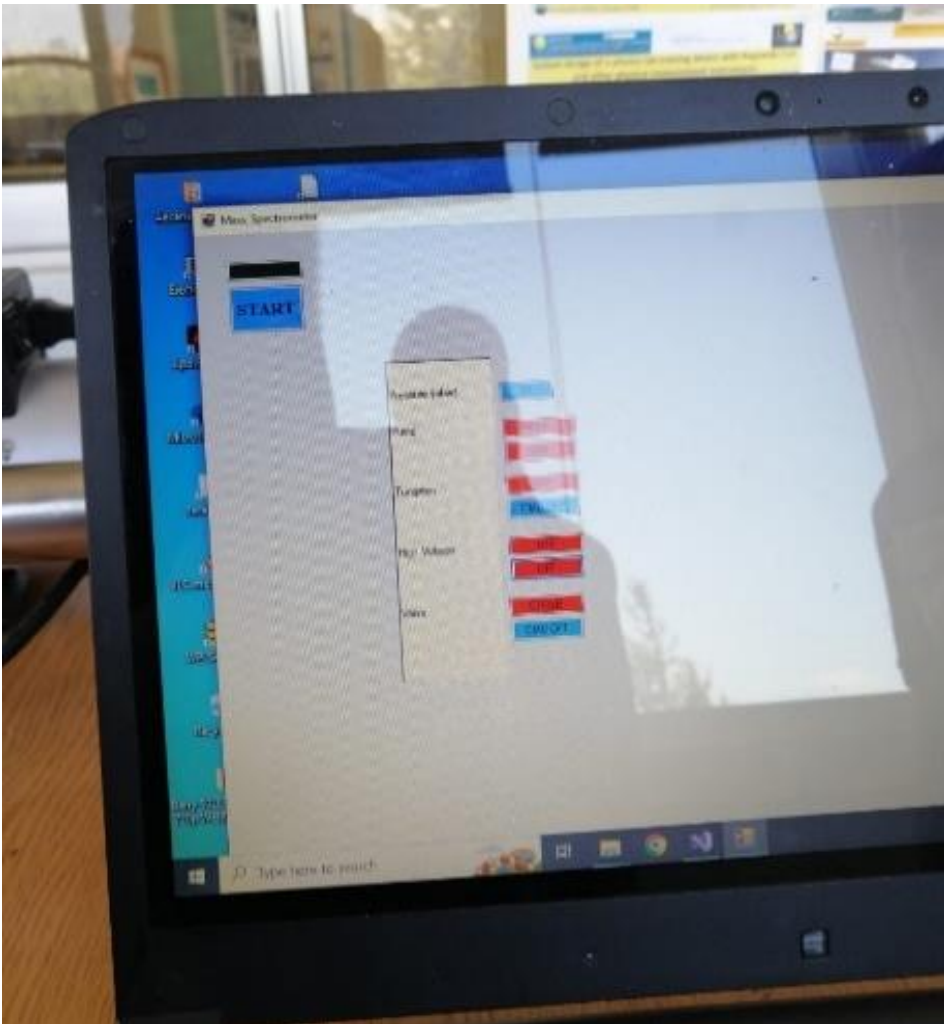


Figure III. 7: Control system





Figure III. 8: Power supply for tungsten

Figure III. 9: Alimentation d'une tension de 7 V au tungstène





Figure III. 10: Leakage and deflection of electrons towards the screw on the plate

What we need to do:

- We will use another power supply (from 0 to 200 A).
- We will remove the screw to distribute the loads evenly.

3.5.2.4 X-ray test 17_07_23

Analysis of test results:

We followed the same steps as in the previous test, but this time we used a power supply (capable of supplying up to 200 amps) responsible for supplying energy to the tungsten with a voltage range between 6 and 12 volts. Through it, we were able to supply tungsten with 6 to 8 volts, but when we gave 9 volts to the tungsten, it caused it to burn because it was consuming a high percentage of amps.

Then we turned on the high voltage, but the electrons didn't penetrate the hole; instead, they deflected in different directions away from the plate, indicating insulation problems. And there's still electron leakage around the cylinder.

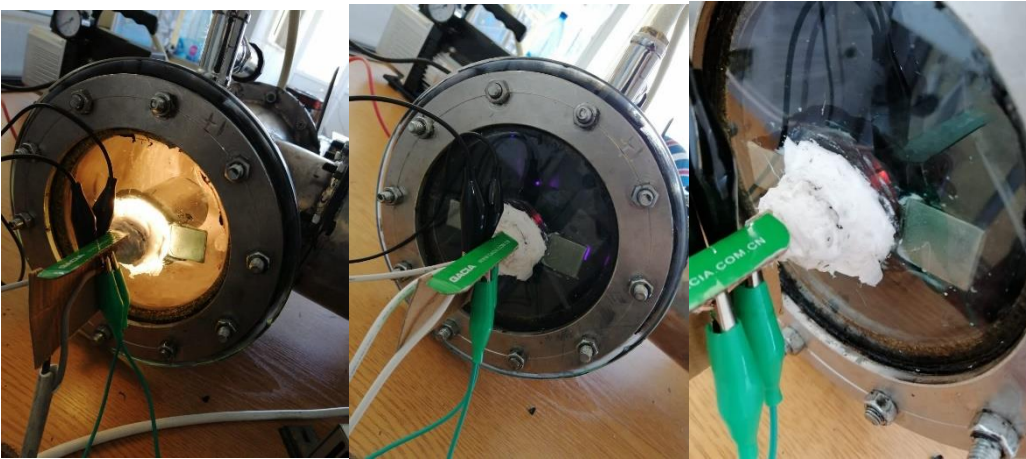


Figure III. 11: Leakage and deflection of electrons when applying 6 volts

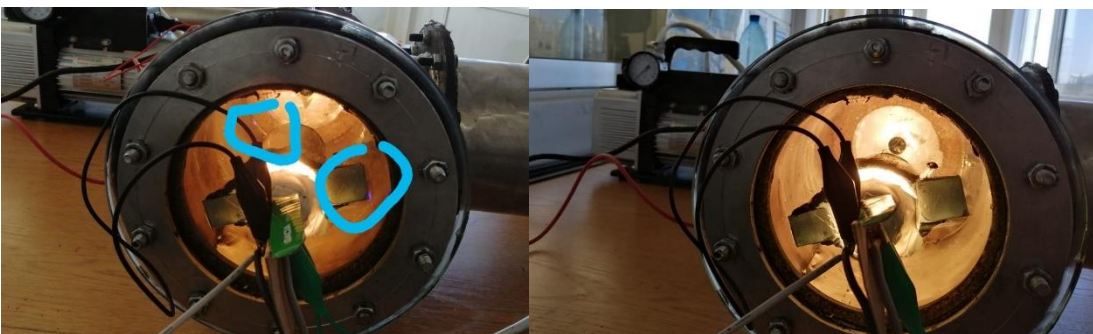


Figure III. 12: Leakage and deflection of electrons when applying 8 volts

WHAT WE NEED TO DO:

- We will wrap the plate with insulating rubber, while leaving the wall and what is adjacent to it ~ 2 cm without insulation.
- We will insulate the cylinder with rubber to prevent electron leakage.

3.5.2.5 X-ray test_24_07_23

Analysis of test results:

We followed the same steps as those adopted in the previous test, with the difference that we placed rubber on the disc to ensure insulation and left the hole and what is adjacent to it 2 centimeters without insulating them, and we covered the cylinder with black silicone to prevent any leakage of electrons.

When we gave 6 volts to the tungsten, we noticed that we still had electrons leaking from the cylinder, and although the electrons did not penetrate the hole in the disk, this time we came close to violating it, because they directed the electrons around the 2 centimeters left around the hole;

However, there is still another direction of electrons around the edges of the plate, indicating that there is still a problem with insulation.

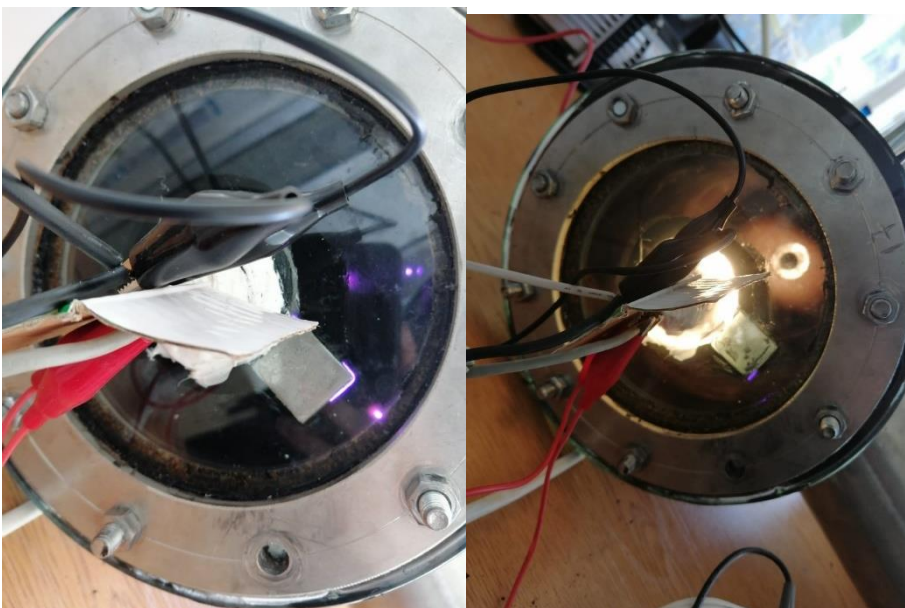


Figure III. 13: Persistence of electron leakage due to insulation problems

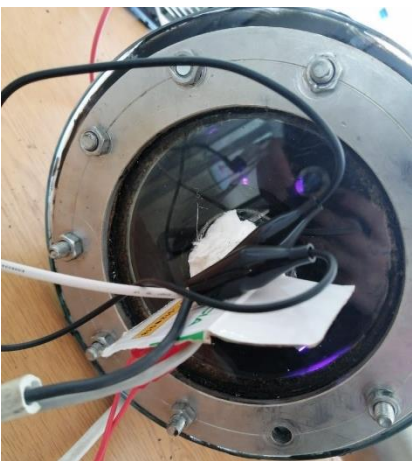
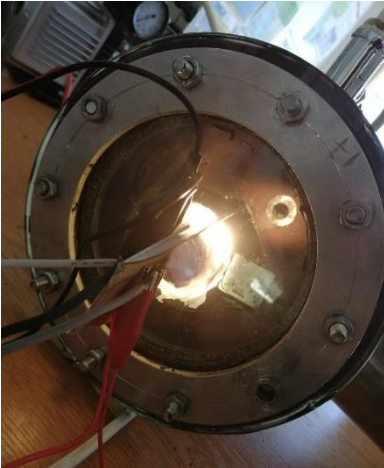


Figure III. 14: Approach of the electron line through the plate opening

Tests	Issue	Solution	Result
Vacuum test 03.05.23	Air leak	Re-weld in some areas and replace the gasket	Negative
Vacuum test 09.06.23	Air leak	Add silicone around the flanges	Positive
X-ray test 03.07.23	Tungsten drew over 20 amps,	Use another power supply and remove	Negative

	causing the power supply to reduce voltage to 3.5V instead of 8V + electron leakage + electron deflection on the plate due to lack of uniform charge distribution	the screw to distribute the loads evenly	
X-ray test 17.07.23	Tungsten burning at 9 V + insulation problem + electron leakage	Wrap the plate with insulating rubber and insulate the cylinder with rubber to prevent electron leakage	Negative
X-ray test 07/24/23	Another direction of electrons around the edges of the plate (insulation problem)	Replace the bolts on the plate flanges with rivets + replace the rubber with another type of insulation	-----

4 Electron Flux Measurement with Rogowski Coil

بِسْمِ اللَّهِ الرَّحْمَنِ الرَّحِيمِ



Electrofilter Measurement with Rogowski Coil

Author: Louay Indakji

Last update: 08.06.2021

4.1 Introduction

4.1.1 Task

Measure the current and voltage for different waste incineration (plastic, non-plastic, medical) with an electro filter voltage of 40 kV.

Master Thesis task

4.1.2 Current Transducer Approach

4.1.2.1 In terms of alternating current measurement (AC):

In Dommar store, there is a current transducer capable of measuring an alternating current between 0 and 5 A (shown in the figure). It transforms the current into an electric voltage between 0 and 10 V used in the control done through the computer. The figure also shows other characteristics of the current transducer.



Figure 1: current transducer.

However, standard current transducers available in the market are capable of measuring an up to 5A alternating current. In our case, the alternating current can have a current value up to 10A. A proposed solution is to use a transformer 10/5 (an input of 10A is reduced to 5A). In Dommar the available transformer is of 30/5. In this case the precision is lowered.

This Monday the store manager will contact and will let me know about the possibility of getting the 10/5 transformer from Beirut.

Price of the transducer: 50\$.

Price of the transformer: unknown. 6\$ (transformer 20/5).

4.1 In terms of installation and connection

As seen on the electrical panel board, the current transducer should be placed between the two circuit breakers available on the electrical panel board to be protected against temperate. The alternating current coming from the network is connected to the transducer in order to measure it.

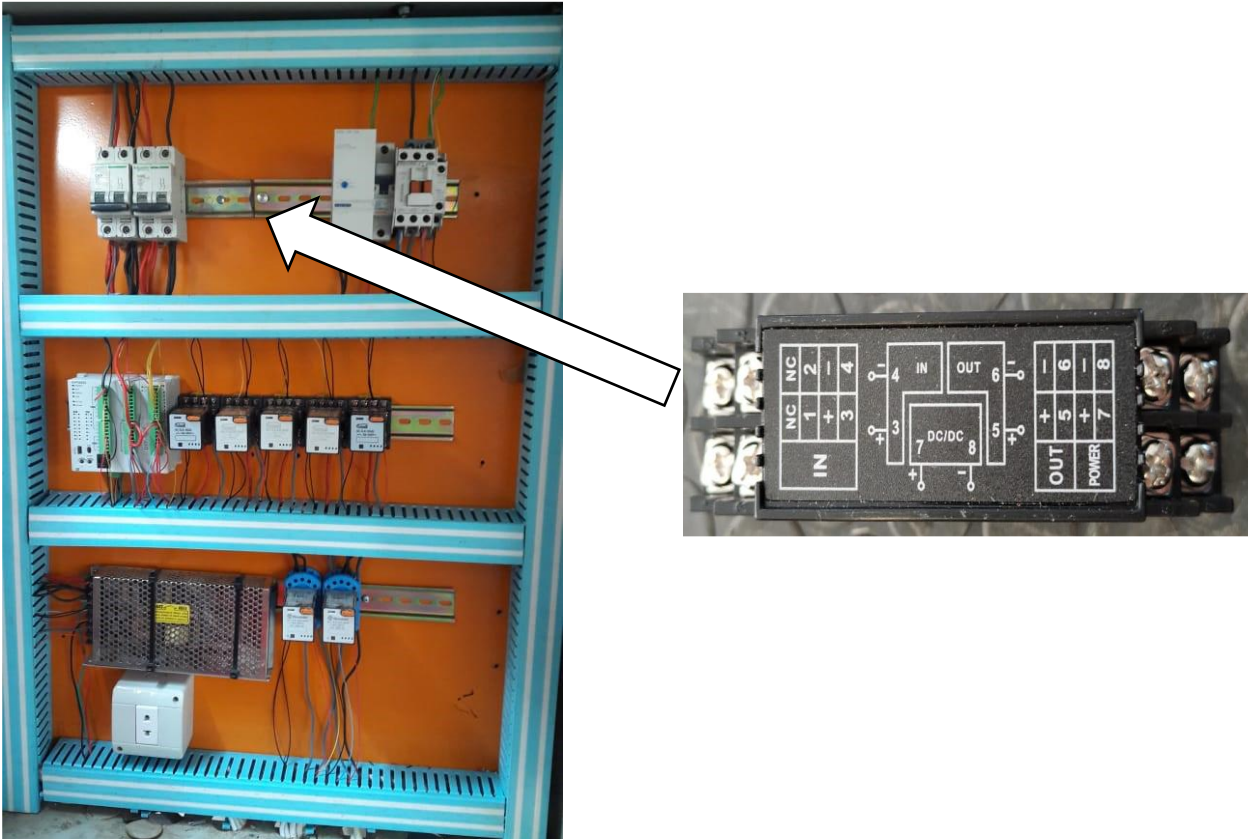


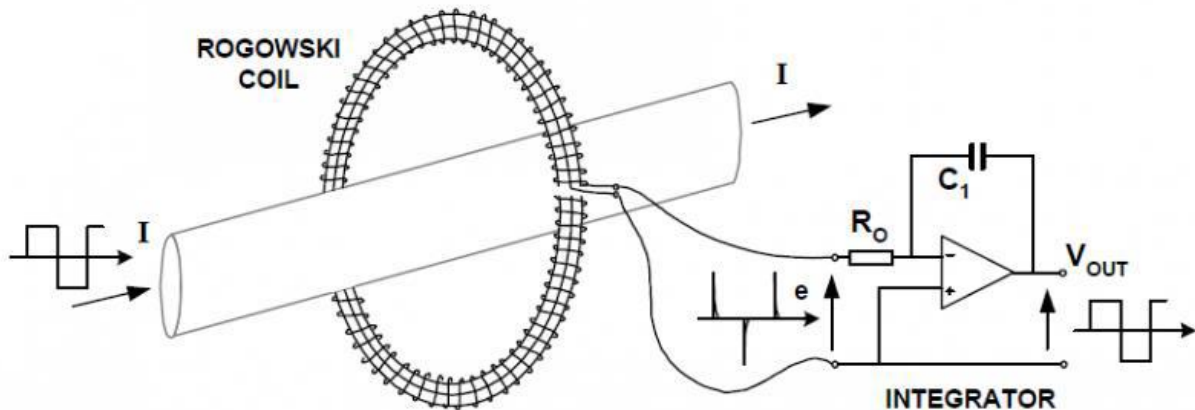
Figure 2: transducer installation.

4.1.1 Questions:

- 1) Where should we place the transformer?
- 2) Where is the network's wire? Is it the one going in from below the current breaker? Or the one going out form above?

4.2 Rogowski Coil Approach

4.2.1 In terms of alternating current measurement (AC), there are Rogowski Coil:



4.2.2 What is a Rogowski Coil?

The Rogowski coil is defined as an electrical device that is used to measure alternating current (AC). It is also used to measure the high-speed transient, pulsed current or sinusoidal current. The name Rogowski coil was named after the German physicist Walter Rogowski [1].

A Rogowski coil is an evenly wound coil with N number of turn and constant cross-section area A . There is no metal core in a Rogowski coil [1].

The end terminal of the coil is returned through the central axis of the coil to another end. Therefore, both terminals are at the same end of the coil [1].

This entire assembly wrapped around the current-carrying conductor whose current we need to measure [1].

4.2.3 How does a Rogowski Coil Work?

Rogowski coils work on the principle of faraday's law. It is similar to AC current transformers (CTs). In current transformers, the voltage induced in a secondary coil is proportional to the current flow through the conductor [1].

The difference between Rogowski coils and AC current transformers is in the core. In Rogowski coils, an air core is used and in the current transformer, a steel core is used [1].

When current passes through the conductor, it will create a magnetic field. Due to an intersection with a magnetic field, a voltage is induced between the terminals of the Rogowski coil [1].

The magnitude of voltage is proportional to the current passes through the conductor. Rogowski coils are close pathed. Generally, the output of Rogowski coils is connected with the integrator circuit. So, the coil voltage is then integrated to provide an output voltage that is proportional to the input current signal [1].

4.2.4 Rogowski Coil Current Sensor

Rogowski coil current sensors are preferred due to no magnetic saturation, no overheating, or no hysteresis loss. As such there are very low magnetic losses in Rogowski coils. And it has very low insertion impedance [1].

It is able to sense the current flowing through the conductor. Hence Rogowski coils can also function as current sensors [1].

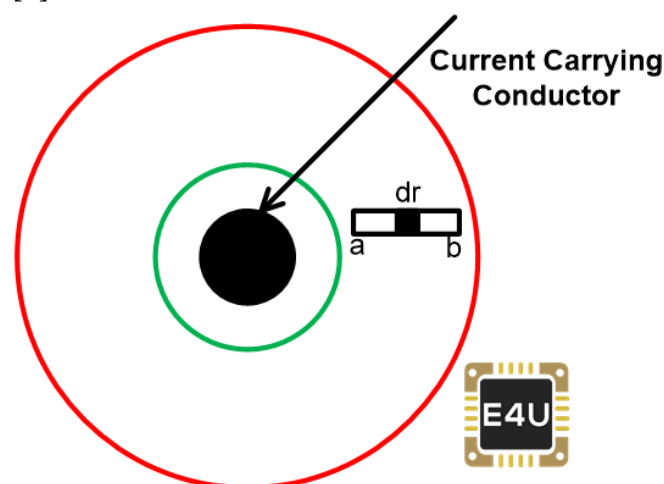
Rogowski coils are an air-cored toroidal winding wrapped on a conductor. For large currents, the output does not saturate due to the non-magnetic core [1].

It can be designed for a wide range of current measurements as well as protection applications. Rogowski coil sensor converts the input current to an output voltage. And it can sense the current flowing the conductor by integrating the output voltage [1].

There are two types of Rogowski coils; Rigid and Flexible [1].

4.2.5 Rogowski Coil Design

Consider the conductive element 'dr' at distance 'x' from the origin. The current-carrying conductor is placed at the center of the coil. The figure below shows the arrangement of a typical Rogowski coil [1].



As per biot-savart law, the magnetic strength at distance x is given by;

$$dH = \frac{I_{Primary}}{2\pi x}$$

The magnetic flux density at a point 'dr' is

$$dB = \mu \times dH$$

Where μ is the permeability of free space

From the above equations, the magnetic flux density due to a current flowing through the conductor is

$$dB = \mu \times \frac{I_{Primary}}{2\pi x}$$

The magnetic flux is given as

$$\phi = \int_a^b dB \times dA$$

Where dA is rectangular cross-section area for element 'dr' and that is given as

$$dA = dr \times h$$

$$\phi = \int_a^b \mu \times \frac{I_{Primary}}{2\pi x} \times dr \times h$$

$$\phi = \mu \times \frac{I_{Primary}}{2\pi} \times h \times \int_a^b \frac{1}{x} dr$$

Therefore, total flux is

$$\phi = \mu \times \frac{I_{Primary}}{2\pi} \times h \times \ln \frac{b}{a}$$

$$\frac{d\phi}{dt} = \frac{\mu \times h}{2\pi} \times \ln \frac{b}{a} \times \frac{dI_{Primary}}{dt}$$

As per Lenz's law, the voltage induced due to N turns is

$$V = N \times \frac{d\phi}{dt}$$

$$V = N \times \frac{\mu \times h}{2\pi} \times \ln \frac{b}{a} \times \frac{dI_{Primary}}{dt}$$

So, mutual inductance (M) for the Rogowski coil is

$$M = N \times \frac{\mu \times h}{2\pi} \times \ln \frac{b}{a} \times$$

Now, assume that sinusoidal current flowing through the conductor with an amplitude 'I_m' and frequency 'f'.

So, the voltage induced in the Rogowski coil is given by

$$V = M \times \frac{dI_m \sin(2\pi ft)}{dt}$$

$$V = M \times 2\pi f \times I_m \times \cos(2\pi ft)$$

At time t=0, the magnitude of voltage is maximum. So, the peak voltage is given as;

$$V_{Peak} = M \times 2\pi f \times I_m$$

RMS value of the voltage;

RMS value of an AC current represent the equal amount of power in DC current

$$V_{rms} = \frac{V_{peak}}{\sqrt{2}}$$

So,

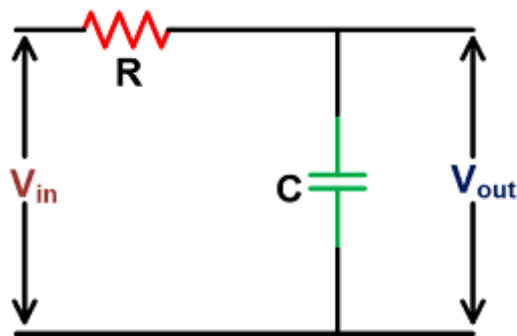
$$V_{RMS} = M \times 4.44f \times I_{RMS}$$

Hence, the induced voltage is proportional to RMS current flowing through the conductor and frequency of the current.

4.2.6 Rogowski Coil Integrator

According to components used in integrator, there are two types of integrator [1];

- Passive Integrator
 - Active Integrator
- i. Passive integrator



The value of R and C can be estimated by the below equations.

$$\tan(\phi) = \frac{X_c}{R}$$

$$X_c = \frac{1}{2\pi f C}$$

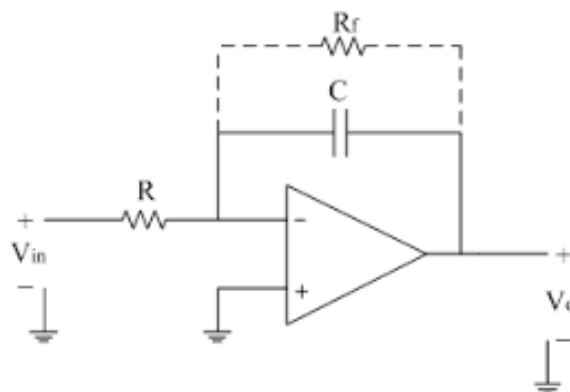
$$\tan(\phi) = \frac{1}{2\pi f C R}$$

$$RC = \frac{1}{2\pi f \tan(\phi)}$$

Where,

Φ = Target phase error
 X_c = Capacitive Impedance
 R = Resistance
 f = Input Frequency

ii. Active Integrator



Here, the RC element is in a feedback path of an Amplifier. The gain of the amplifier can be adjusted by using the below equation.

$$Gain = \frac{V_{OUT_{MAX}} - V_{OUT_{MIN}}}{V_{IN_{MAX}} - V_{IN_{MIN}}}$$

$$Gain = -\frac{R_F || X_C}{R_1}$$

1- Questions:

- a) which type of integrator should be used ?
- b) what is the system that must be installed to make a 0-10 volts control ?

4.2.7 Rogowski Coil

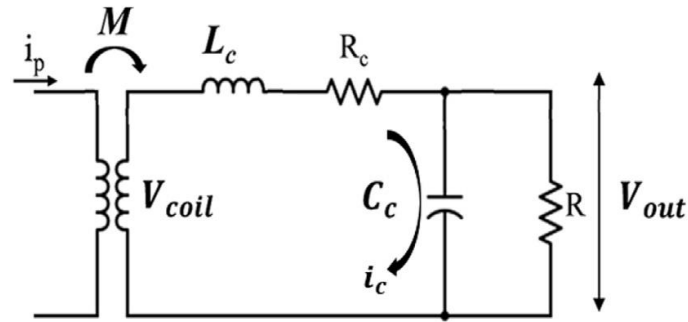


Fig.1: Lumped-element model of Rogowski coil.

$$V_{coil} = -n\mu_0 A \frac{dI}{dt} = \mp M \frac{dI}{dt} \quad [2]$$

4.2.8 Construction of Rogowski coil

Fig.2 Shows the schematic of the Rogowski sensor in the circular cross-section, which N , x_0 , a and b are the structural parameters of Rogowski coil [2].

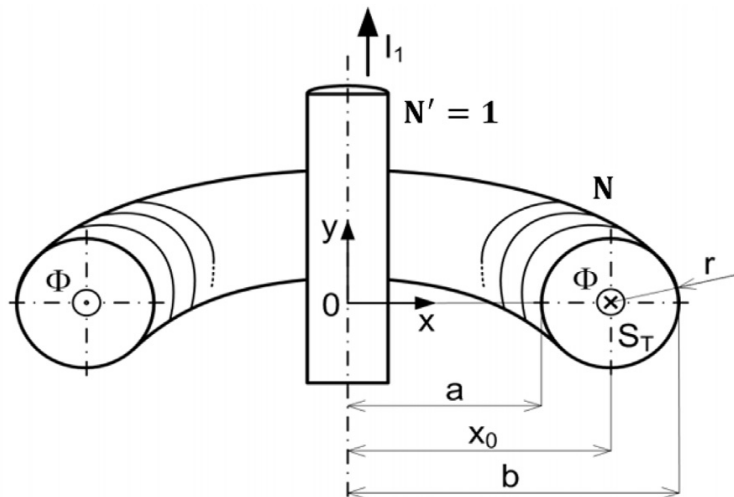


Fig.2: Circular cross-section Rogowski coil.

the optimal values of the structural parameters of the sensor, shown in table (1), were calculated. The sensor with the parameters of Table 1 was constructed [2].

Measured current	I_p	Main radius x_0 (cm)	13.17
Wire turns	3366	Wire diameter d(mm)/AWG	0.202
Core material	Teflon	Self-inductance L_c (mH)	1.702
Internal radius a(cm)	12.6	Distributed capacitance C_c (nF)	368.2
External radius b(cm)	13.74	Ohmic resistance $R_c(\Omega)$	72.42
Internal former radius $(b-a)/2$ without wire diameter (cm)	0.55	Terminal resistance $R(\Omega)$	50
		Calibration Coefficient kA/V	0.2

Tab.1: Structural Parameters of Rogowski coil for Alvand tokamak.

This sensor contains 3366 wire turns which is wrapped on a teflon non-magnetic core [2].

The Rogowski sensor produces an output voltage signal V_{out} equivalent to equation (13). Due to the factor N , the sensor output voltage has a high gain; therefore, the output signal will be easily distinguished from the noises of other parts of the system [2].

$$V_{out} = \mu A \frac{N dl}{l dt}$$

The winding was returned in the opposite direction to that of the pitch advancement turn along the central axis of the coil, in order to avoid the effect of a magnetic flux. In this case, both terminals are set at the same end of the coil. Therefore, interference of the unwanted magnetic fields is prevented [2].

4.2.9 Design experiment of Rogowski Coil in laboratory

I used a rubber tube, then I wrapped the turn of the coil around this tube .



Fig.3: Rubber tube.



Fig.4: Rubber tube with coils



Fig.5: Rogowski Coil without integrator.

4.2.10 Design and construction of active integrator

The DC-control active-type integrator was constructed. As shown in Fig.6 the time constant of this integrator was selected ten times more than the time duration of the signal [2]. By connecting the output of Rogowski coil to the inverting input terminal of operational amplifiers, the input and output differ in phase and the role of this integrator is shown in equation [2]:

$$G(s) = -R_{ftot} / R_{in}(1 + R_{ftot}C_c s)$$

Operational amplifier OP07CP has ultralow drift and high accuracy to form in-phase amplifier circuit [2]. The negative feedback resistance, R_{ftot} , is equivalent to the resistance

of R1, R2 and R3. This resistor, parallel to the Cf capacitor, provides a path to discharging the capacitor while the circuit is not operating and prevents its saturation [2]. The transfer function of the active integrator can be given by equation [2]:

$$G(s) = \frac{-[(R_1+R_2) + (R_1R_3+R_2R_3 + R_1R_2)]}{R_{in}(1 + [(R_1+R_2) + (R_1R_3+R_2R_3 + R_1R_2)]C_f s)}$$

The reconstructed signal of the measured current is amplified after the integration. The gain of this integrator is 10. Roffset is defined as Rin=R1 can eliminate the bias currents of operational amplifiers and the output offset voltage. Cb1 and Cb2 capacitors were added to remove noise on the input bias voltage [2].

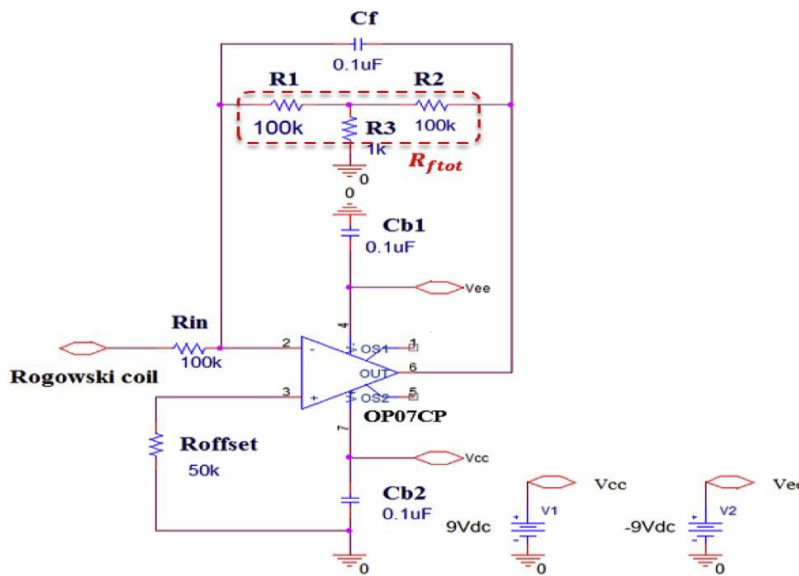


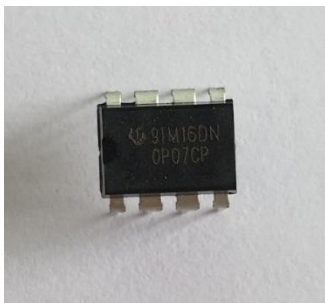
Fig.6: The active integrator with DC gain control. constructed

4.2.11 Electronic tools used to create an active integrator

There are:

Operational amplifier OP07CP,

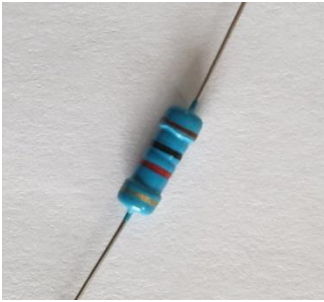
R1, R2, and Rin



R3



Roffset



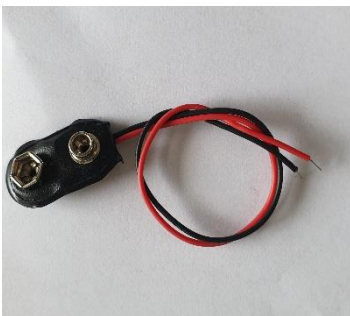
Cb1, Cb2, Cf





Battery 9v DC



Battery connecting tape



4.2.12 Using EagleCAD to create a schematic and to do switch to board

Schematic file	 louay.sch
Board file	 louay.brd

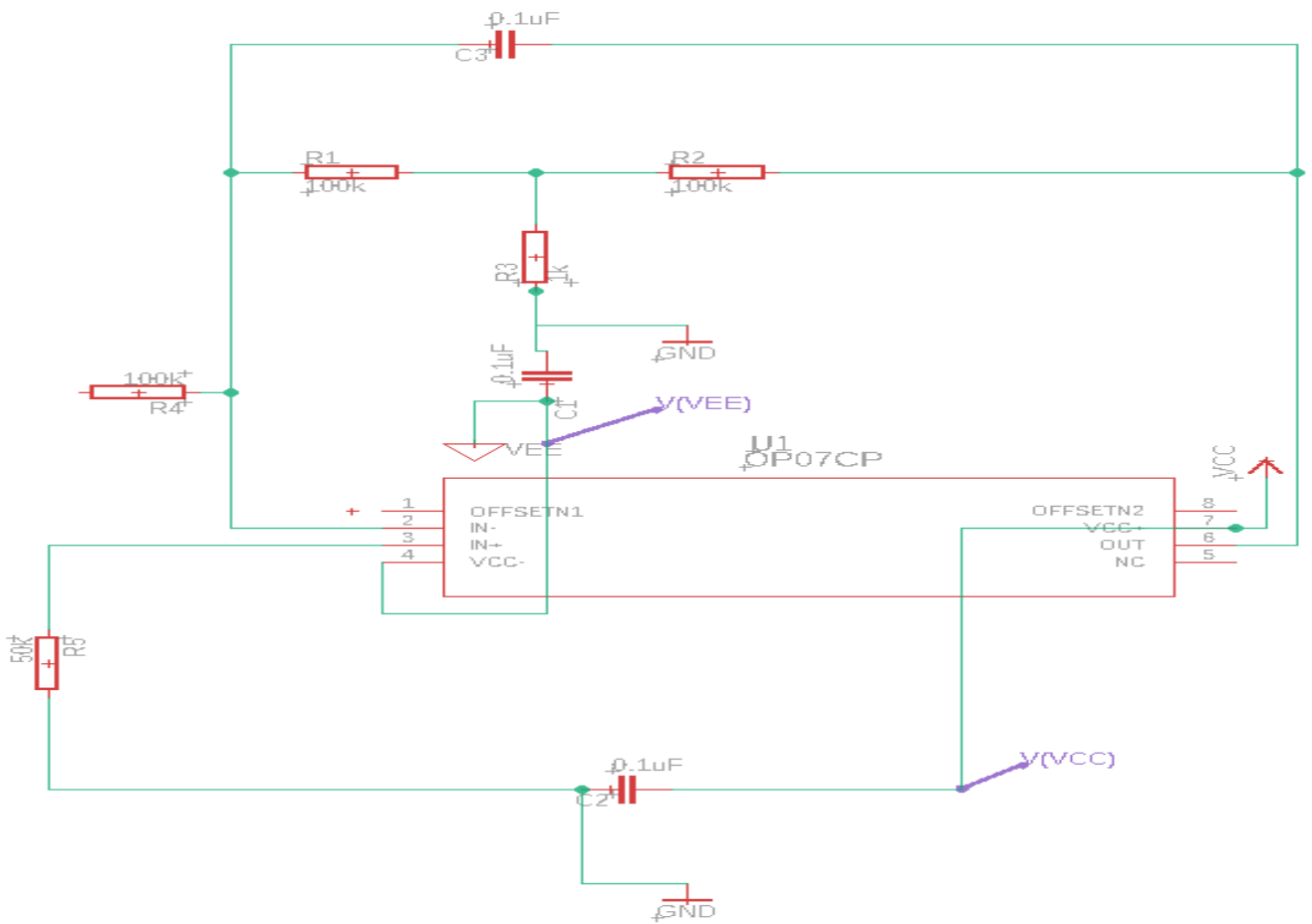


Fig.7: Schematic

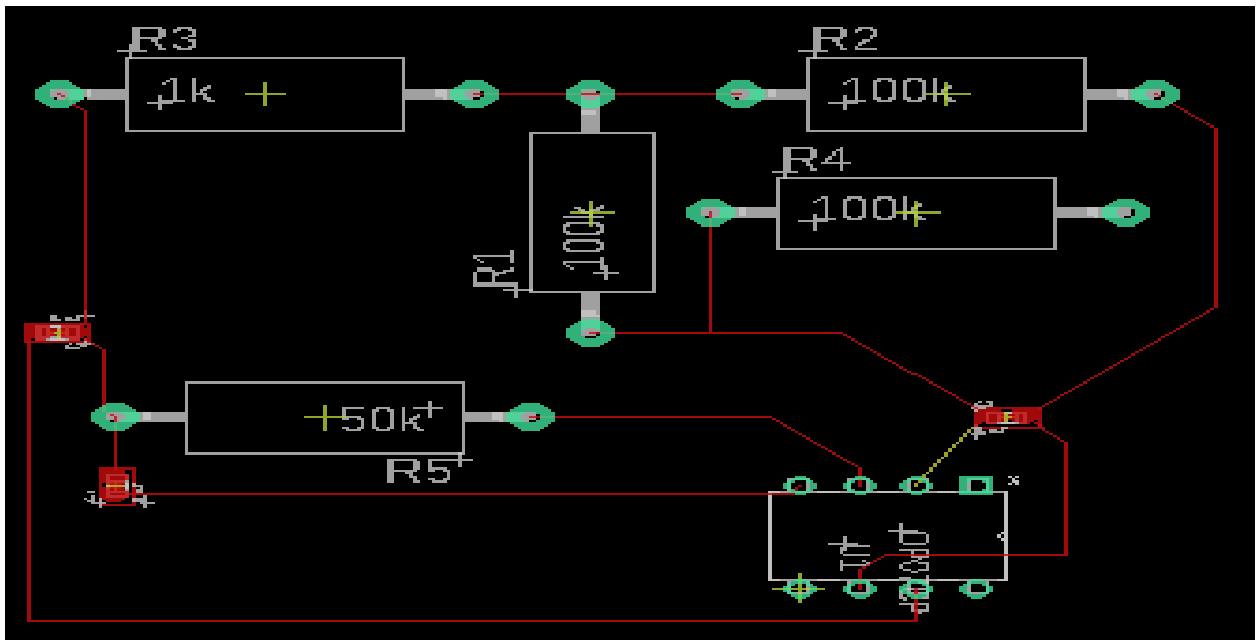


Fig.8: Board

4.3 Construction of an active integrator connected to the coil in laboratory

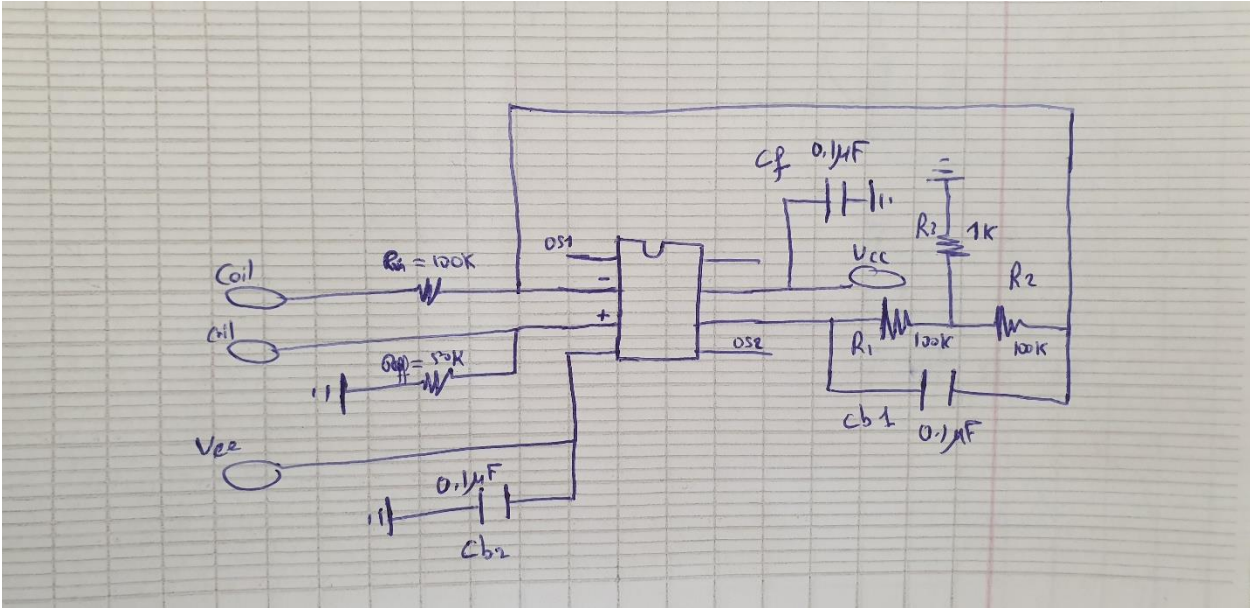


Fig.9: Electric circuit

Using the drawn circuit, we build the active integrator which is connected to the coil. This is how we build the Rogowski Coil.

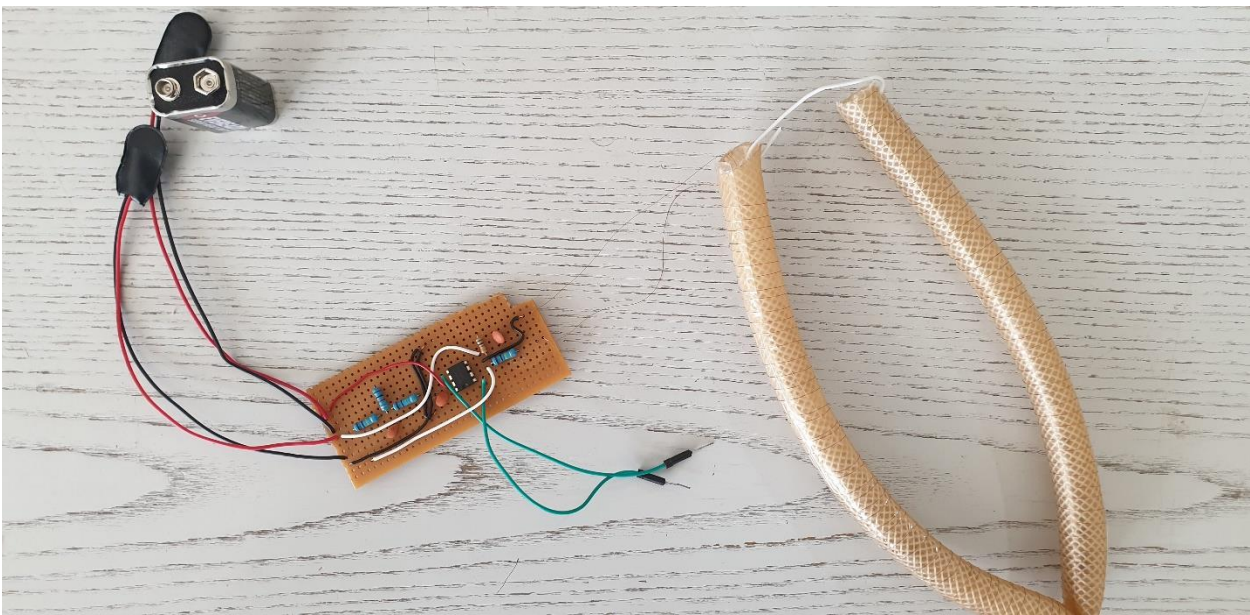


Fig.10: Rogowski Coil



NOTE: We need another battery 9v DC.

4.3.1 The formulas that should be used after construction a rogowski coil:

The voltage produced by a Rogowski coil is [3]

$$v(t) = \frac{-AN\mu_0}{l} \frac{dI(t)}{dt}$$

Where,

- $A = \pi r^2$, is the area of one of the small loops,
- N , is the number of turns,
- $l = 2\pi R$, is the length of the winding (the circumference of the ring),
- $\frac{dI(t)}{dt}$, is the rate of change of the current threading the loop,
- $\mu_0 = 4\pi \cdot 10^{-7}$, V·s/(A·m) is the magnetic constant,
- R , is the major radius of the toroid,
- r , is its minor radius.

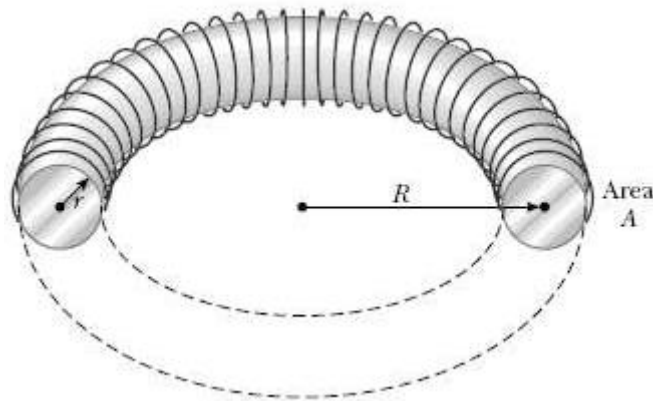


Fig.11: Major radius and minor radius of the toroid.

This formula assumes the turns are evenly spaced and that these turns are small relative to the radius of the coil itself [3].

The output of the Rogowski coil is proportional to the derivative of the wire current. The output is often integrated so the output is proportional to the wire's current [3]:

$$V_{out} = \int v dt = \frac{-AN\mu_0}{l} I(t) + C_{integration}$$

In practice, an instrument will use a lossy integrator with a time constant much less than the lowest frequency of interest. The lossy integrator will reduce the effects of offset voltages and set the constant of integration to zero [3].

At high frequencies, the Rogowski coil's inductance will decrease its output [3].

The inductance of a toroid is [3]:

$$L = \mu_0 N^2 (R - \sqrt{R^2 - r^2})$$

2) The values of the Structural parameters used in the construction of a rogowski coil:

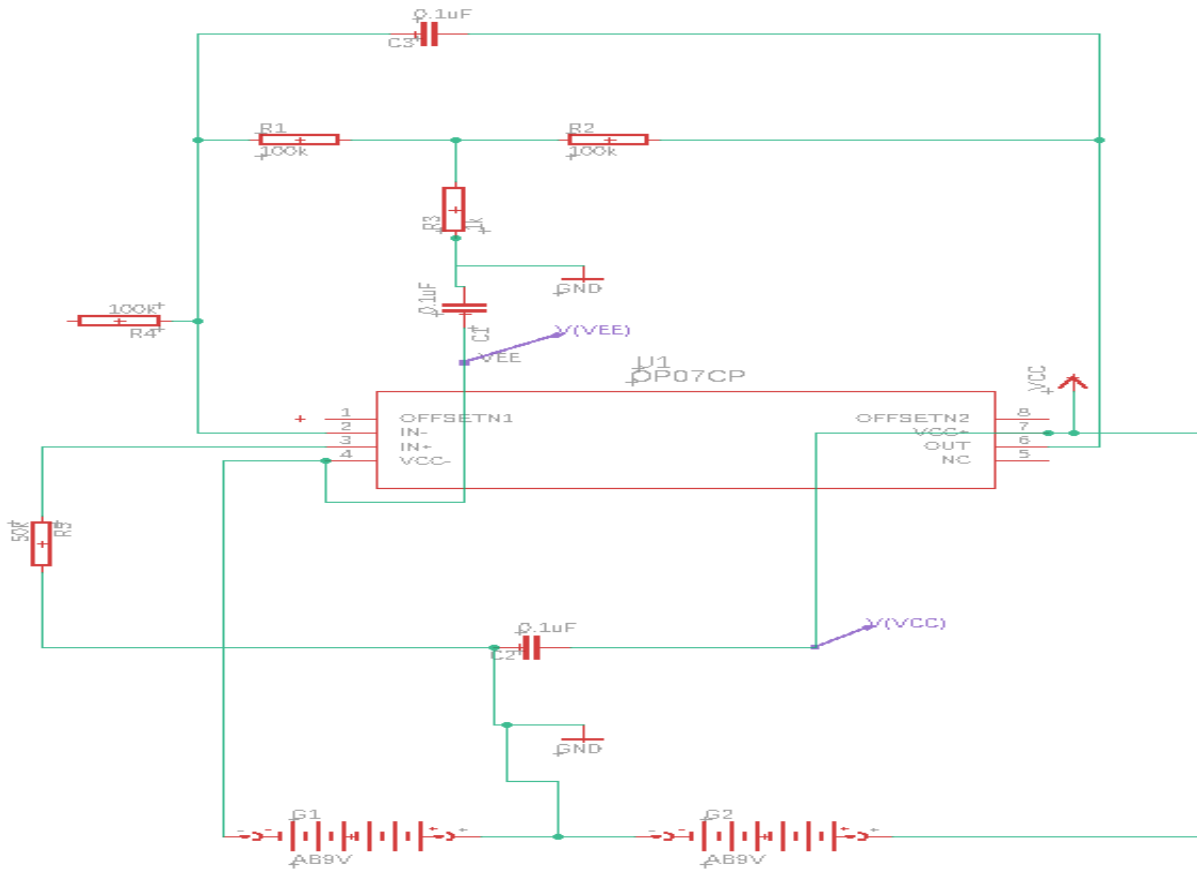
Parameters	Values
R1	100 kΩ
R2	100 kΩ
R3	1 kΩ
Rin	100 kΩ
Roffset	50 kΩ
C1 (Cb1)	0.1 μF
C2 (Cb2)	0.1 μF
C3 (Cf)	0.1 μF
Operational amplifier	OP07CP
Battery 1	9 Volts DC
Battery 2	9 Volts DC
N (Number of turns)	94 Turns
R (Major radius)	8 cm
r (Minor radius)	1 cm

Tab.2: Structural Parameters of Rogowski.

4.3.2 Fix some errors in the installed electrical circuit in the lab

- Common ground - Pin 5 is NC - Output is on pin 6 - Pin 8 and the ground are the OS

4.3.2.1 Update on EagleCAD





New Schematic file	 louay.sch
New Board file	 louay.brd

Fig.12: New schematic

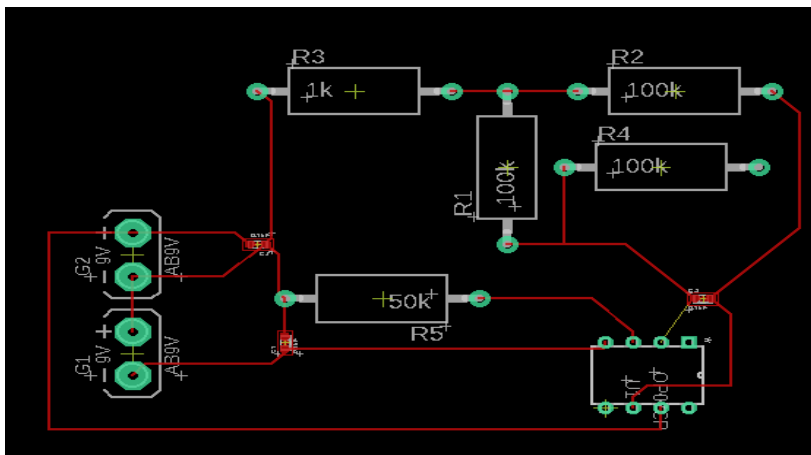


Fig.13: New Board

4.3.2.2 Update on the electrical circuit in lab

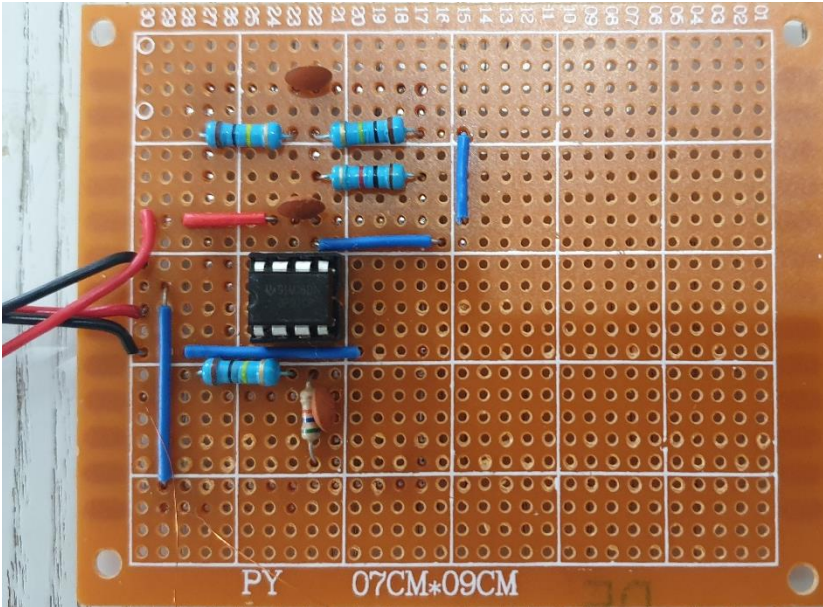


Fig.14: New Electrical circuit

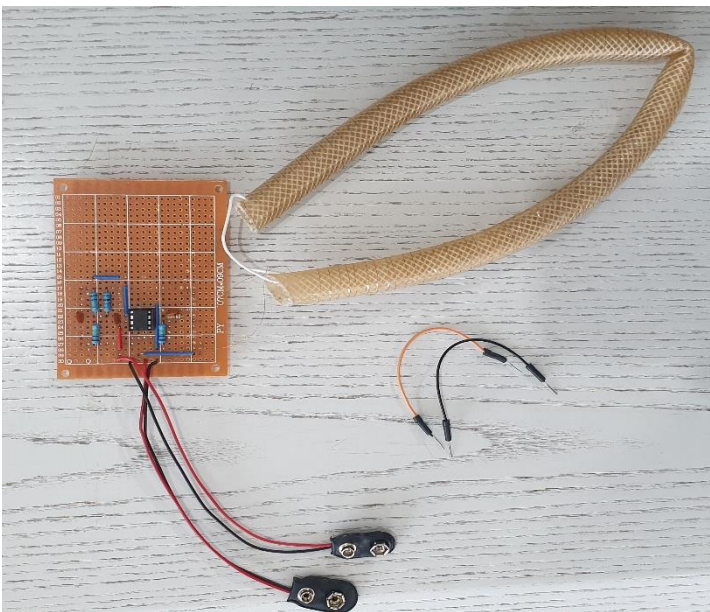


Fig.15: Rogowski Coil

Note: All that remains is to mount the oscilloscope wires.

4.4 Comparison between op07cp and op77f

The operational amplifier OP07CP is the same as OP07C, the OP77 is the next generation of the OP07.

Parameter	Symbol	Conditions	OP77E			OP77F			Unit
			Min	Typ	Max	Min	Typ	Max	
INPUT OFFSET VOLTAGE	V _{OS}		10	25		20	60	μV	
LONG-TERM STABILITY ¹	V _{OS} /Time		0.3			0.4		μV/Mo	
INPUT OFFSET CURRENT	I _{OS}		0.3	1.5		0.3	2.8	nA	
INPUT BIAS CURRENT	I _B		-0.2	1.2	2.0	-0.2	1.2	2.8	nA
INPUT NOISE VOLTAGE ²	e _{npp}	0.1 Hz to 10 Hz	0.35	0.6		0.38	0.65	μV _{pp}	
INPUT NOISE VOLTAGE DENSITY	e _n	f _O = 10 Hz f _O = 100 Hz ² f _O = 1000 Hz	10.3 10.0 9.6	18.0 13.0 11.0		10.5 10.2 9.8	20.0 13.5 11.5	nV/√Hz	
INPUT NOISE CURRENT ²	i _{npp}	0.1 Hz to 10 Hz	14	30		15	35	pA _{pp}	
INPUT NOISE CURRENT DENSITY	i _n	f _O = 10 Hz f _O = 100 Hz ² f _O = 1000 Hz	0.32 0.14 0.12	0.80 0.23 0.17		0.35 0.15 0.13	0.90 0.27 0.18	pA/√Hz	
INPUT RESISTANCE Differential Mode ³ Common Mode	R _{IN} R _{INCM}		26	45		18.5	45	MΩ GΩ	
INPUT RESISTANCE Common Mode	R _{INCM}		200			200		GΩ	
INPUT VOLTAGE RANGE	IVR		±13	±14		±13	±14	V	
COMMON-MODE REJECTION RATIO	CMRR	V _{CM} = ±13 V	0.1	1.0		0.1	1.6	μV/V	
POWER SUPPLY REJECTION RATIO	PSRR	V _S = 3 V to 18 V	0.7	3.0		0.7	3.0	μV/V	
LARGE-SIGNAL VOLTAGE GAIN	A _{VO}	R _L ≥ 2 kΩ	5000	12000		2000	6000	V/mV	
OUTPUT VOLTAGE SWING	V _O	R _L ≥ 10 kΩ R _L ≥ 2 kΩ R _L ≥ 1 kΩ	±13.5 ±12.5 ±12.0	±14.0 ±13.0 ±12.5		±13.5 ±12.5 ±12.0	±14.0 ±13.0 ±12.5	V	
SLEW RATE ²	SR	R _L ≥ 2 kΩ	0.1	0.3		0.1	0.3	V/μs	
CLOSED-LOOP BANDWIDTH ²	BW	A _{VCL} 1	0.4	0.6		0.4	0.6	MHz	
OPEN-LOOP OUTPUT RESISTANCE	R _O		60			60		Ω	
POWER CONSUMPTION	P _d	V _S = ±15 V, No Load V _S = ±3 V, No Load	50 3.5	60 4.5		50 3.5	60 4.5	mW	
OFFSET ADJUSTMENT RANGE		R _p = 20 kn		±3			±3	mV	

Fig.16: Electrical specifications of OP77F

PARAMETER	TEST CONDITIONS	T _A ⁽²⁾	OP07C			OP07D			UNIT	
			MIN	TYP	MAX	MIN	TYP	MAX		
V _{IO}	Input offset voltage	V _O = 0 V R _S = 50 Ω	25°C			150			μV	
			0°C to 70°C			250				
α _{VIO}	Temperature coefficient of input offset voltage	V _O = 0 V R _S = 50 Ω	0°C to 70°C			2.5			μV/°C	
	Long-term drift of input offset voltage	See				0.4			μV/mo	
	Offset adjustment range	R _S = 20 kΩ, See Figure 2	25°C			±4			mV	
I _{IO}	Input offset current		25°C			6			nA	
			0°C to 70°C			8				
α _{IIO}	Temperature coefficient of input offset current		0°C to 70°C			50			pA/°C	
I _{IB}	Input bias current		25°C			±12			nA	
			0°C to 70°C			±14				
α _{IIB}	Temperature coefficient of input bias current		0°C to 70°C			50			pA/°C	
V _{ICR}	Common-mode input voltage range		25°C			±13	±14	±13	±14	V
			0°C to 70°C			±13	±13.5	±13	±13.5	
V _{OM}	Peak output voltage	R _L ≥ 10 kΩ	25°C	±12	±13	±12	±13	V		
		R _L ≥ 2 kΩ		±11.5	±12.8	±11.5	±12.8			
		R _L ≥ 1 kΩ			±12		±12			
		R _L ≥ 2 kΩ		0°C to 70°C	±11	±12.6	±11		±12.6	

PARAMETER	TEST CONDITIONS ⁽¹⁾	OP07C	OP07D	UNIT	
		TYP	TYP		
V _n	f = 10 Hz	10.5	10.5	nV/√Hz	
	f = 100 Hz	10.2	10.3		
	f = 1 kHz	9.8	9.8		
V _{N(PP)}	Peak-to-peak equivalent input noise voltage	f = 0.1 Hz to 10 Hz	0.38	0.38	μV
I _n	Equivalent input noise current	f = 10 Hz	0.35	0.35	nV/√Hz
		f = 100 Hz	0.15	0.15	
		f = 1 kHz	0.13	0.13	
I _{N(PP)}	Peak-to-peak equivalent input noise current	f = 0.1 Hz to 10 Hz	15	15	pA
SR	Slew rate	R _L ≥ 2 kΩ	0.3	0.3	V/μs

Fig.17: Electrical specifications of OP07C

By comparing the outputs of the two operational amplifiers, we demonstrate that we can use the OP77F instead of OP07CP in the simulation because the output of the two operational amplifiers are very close and also because the spice model of OP07CP is not available on internet.

4.4.1 How to insert and use the OP77F code downloaded from the Internet into the LTspice:



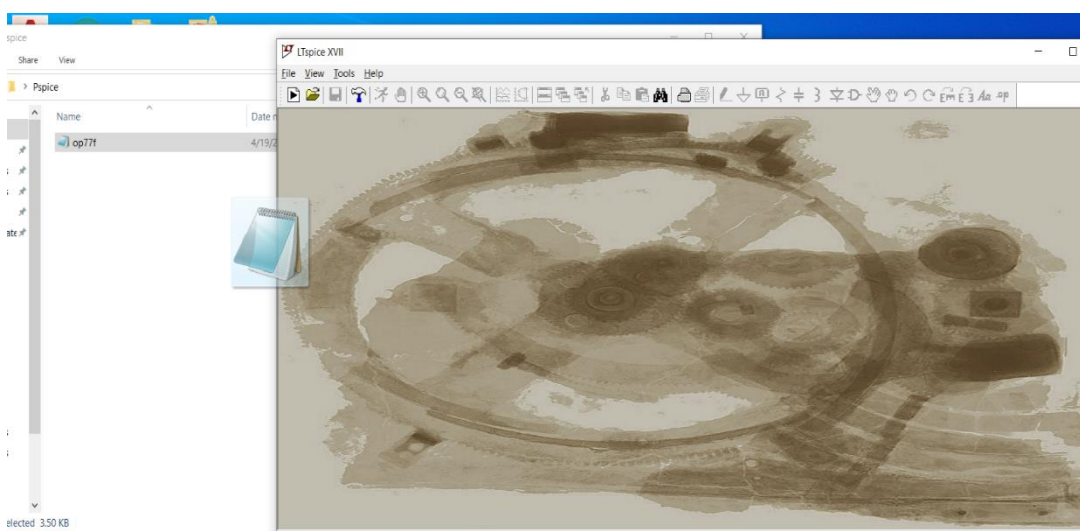


Fig.18: Step one

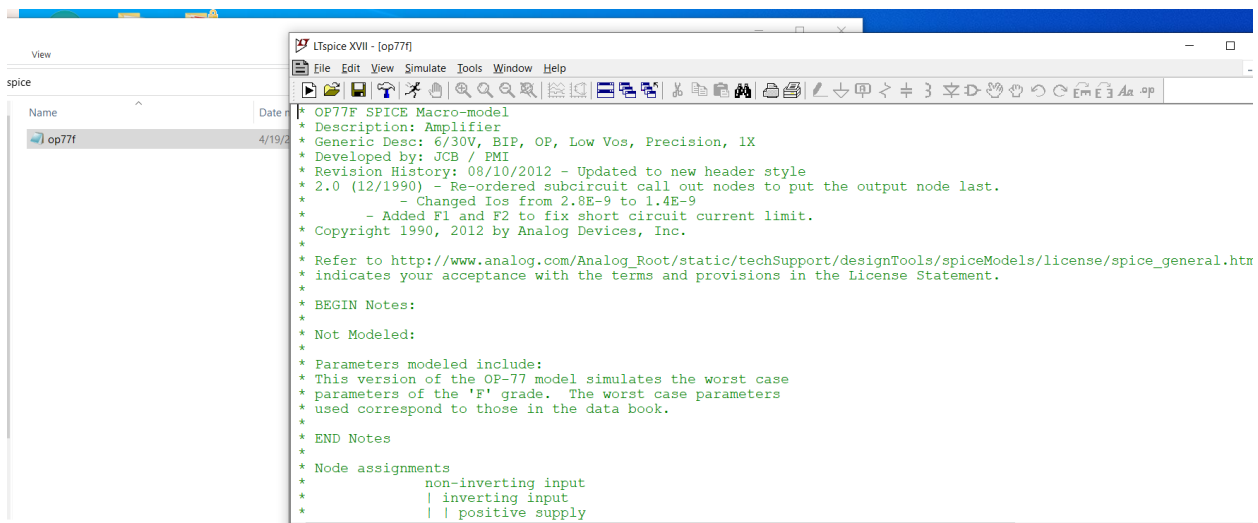


Fig.19: Step two

Electron Flux Measurement with Rogowski Coil

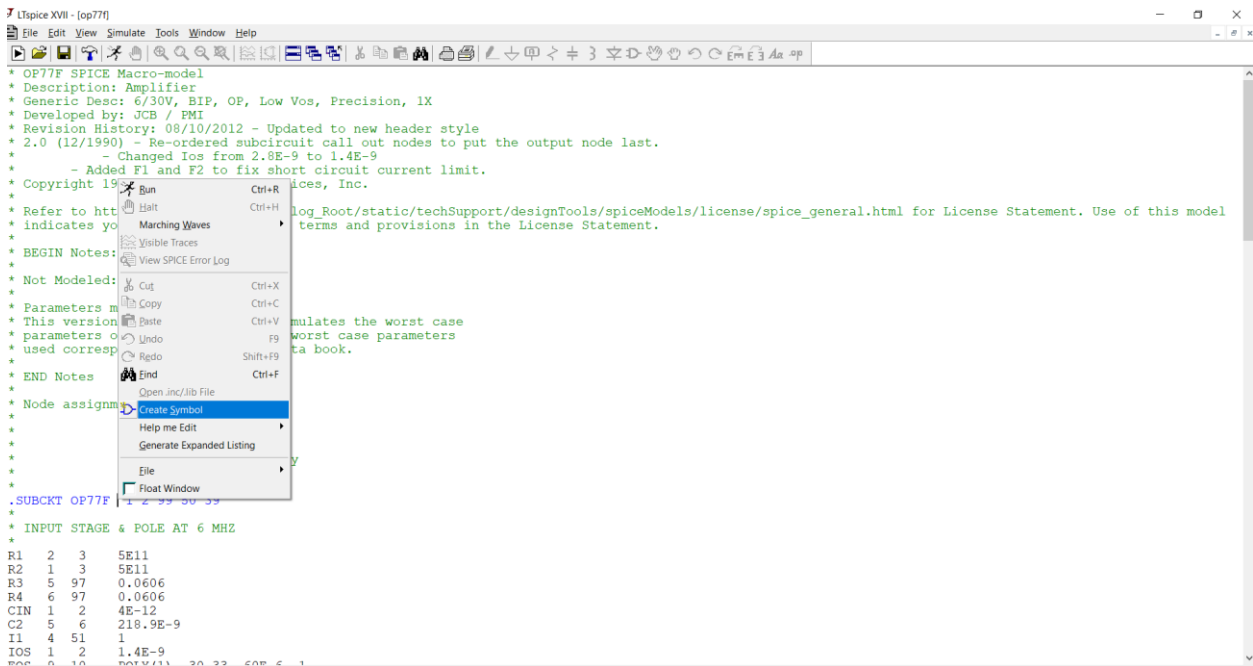


Fig.20: Step three

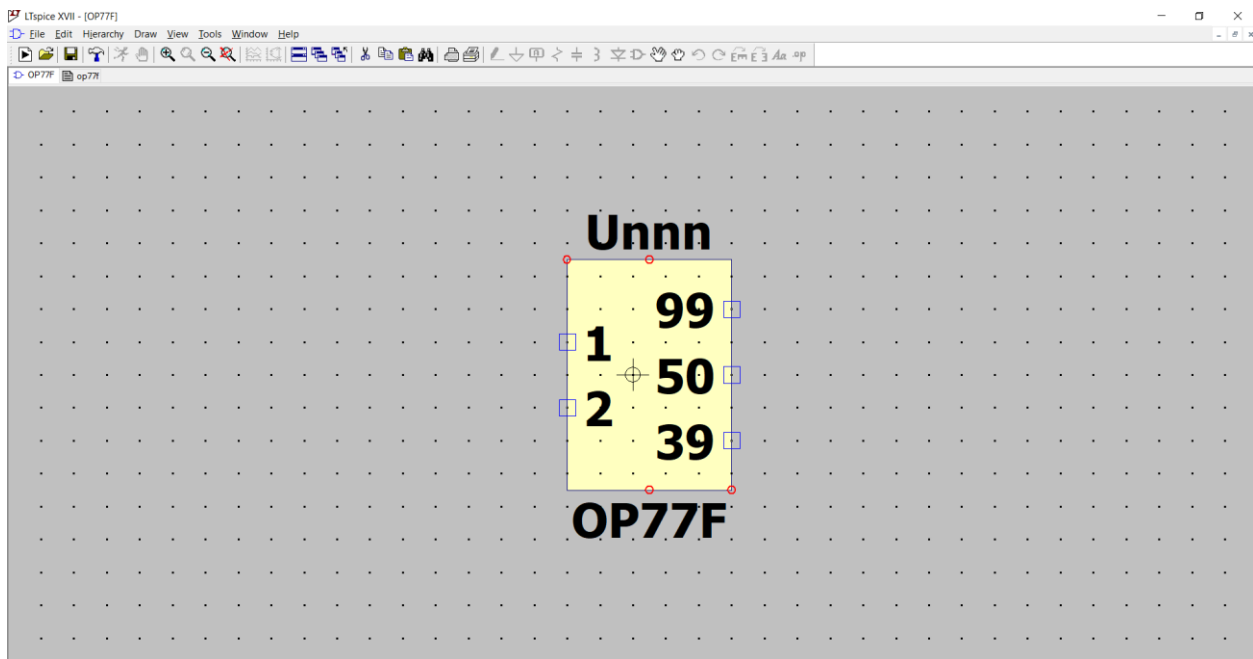


Fig.21: Step four

4.4.2 The electronic circuit schematique in LTspice

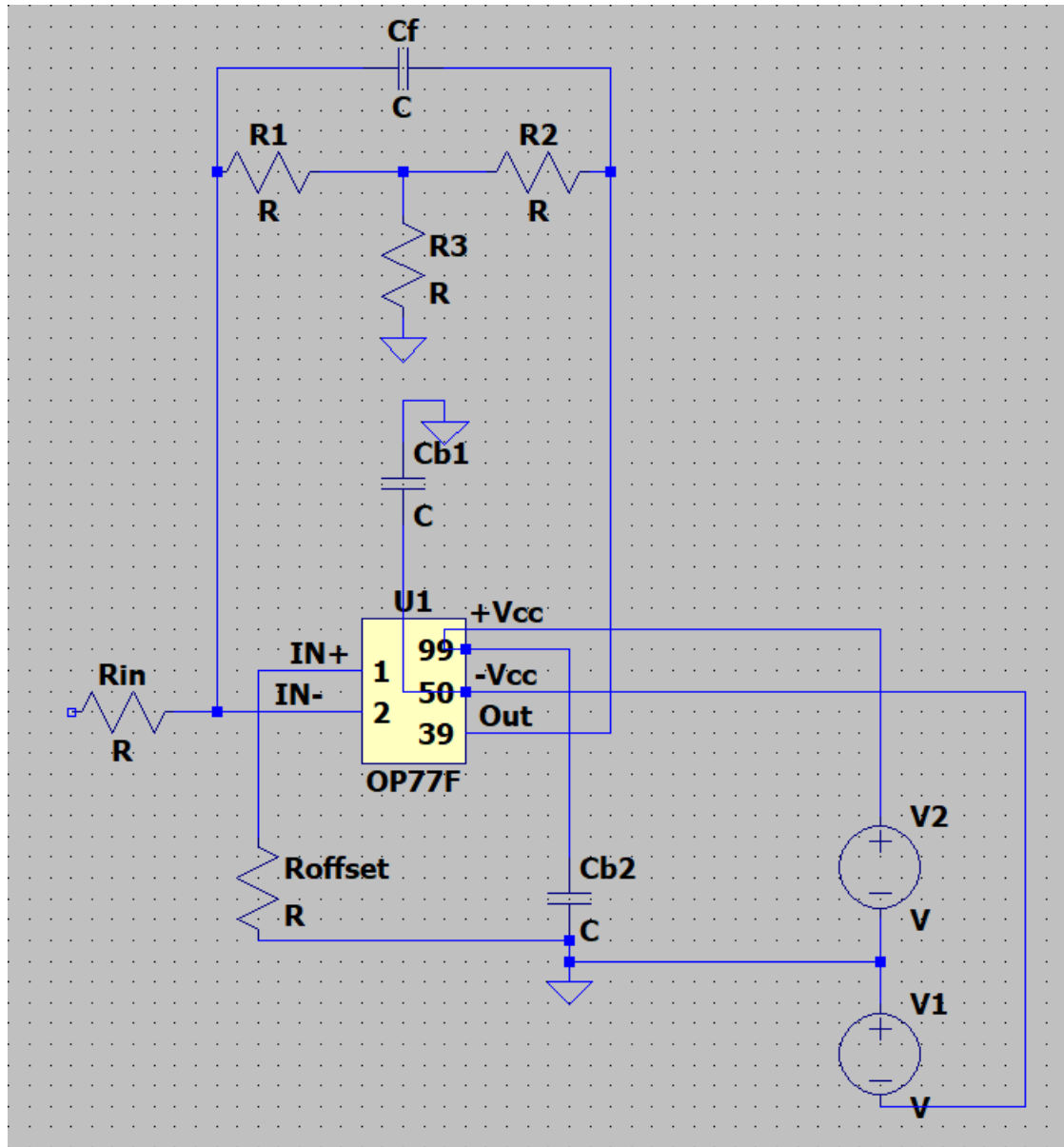


Fig.22: Schematic without values

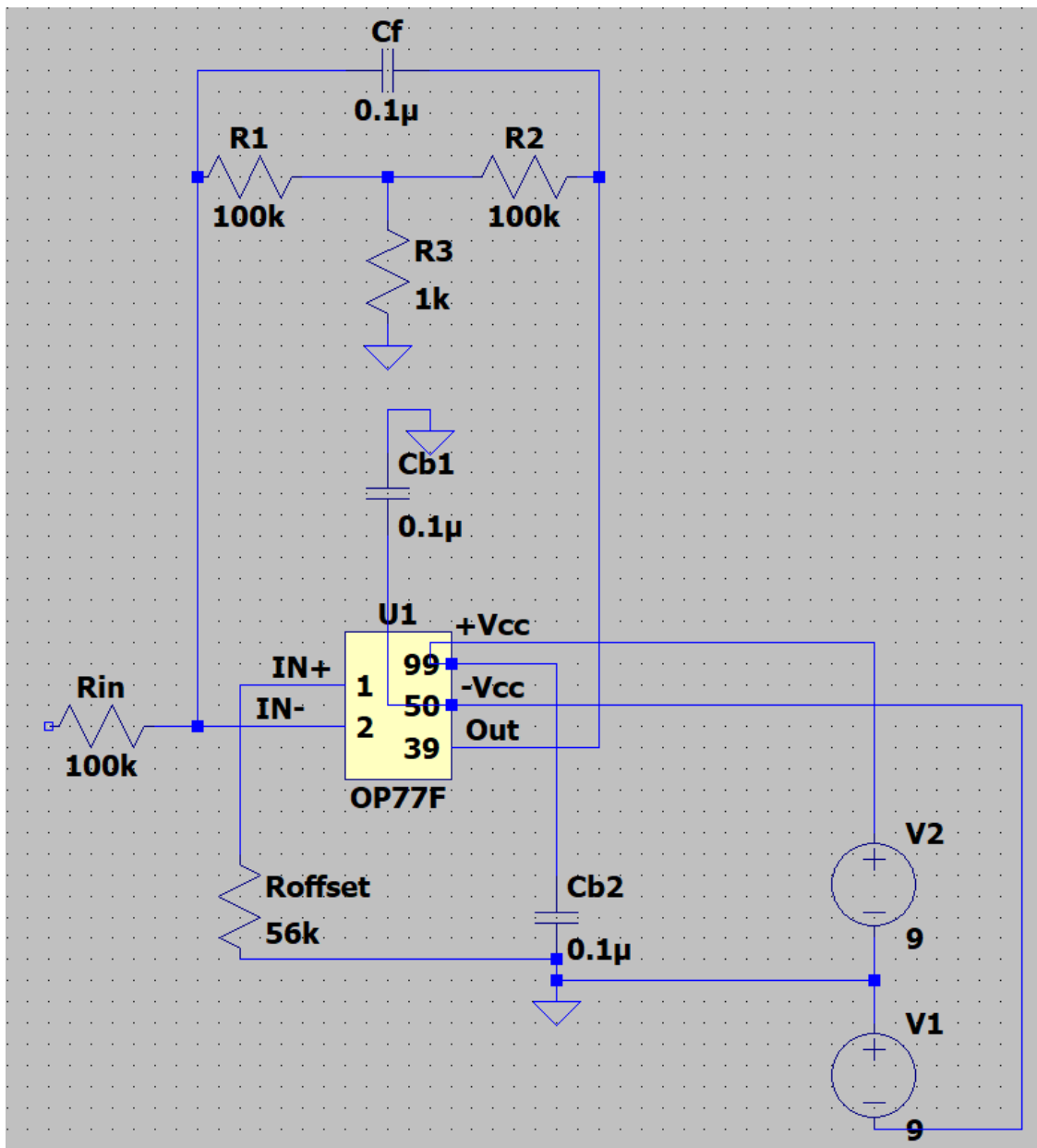


Fig.23: Schematic with values

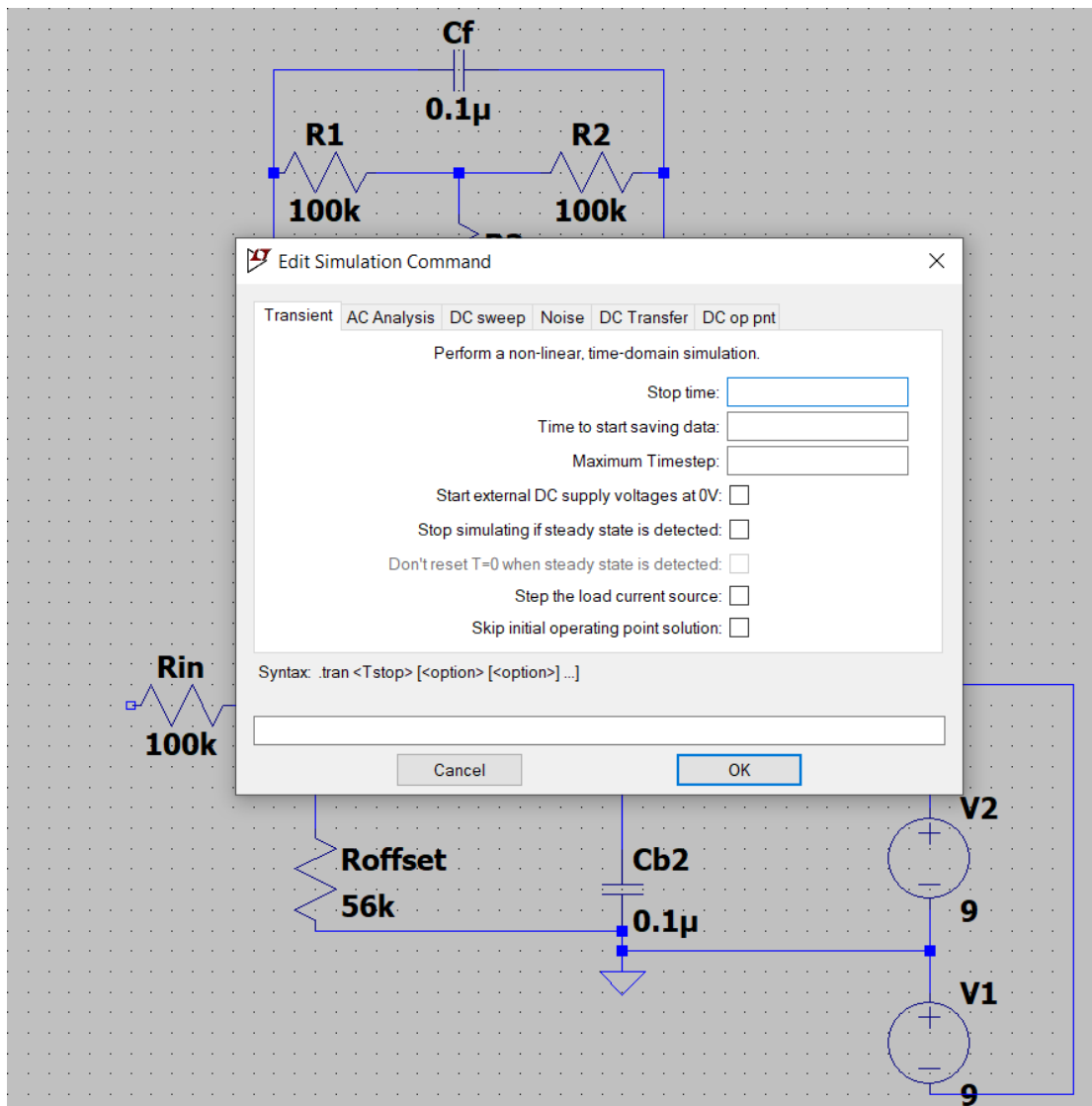


Fig.24: The six options of simulation

We use two options of simulation: (Transient) and (DC in ont)

4.4.3 Simulation (DC on pnt)

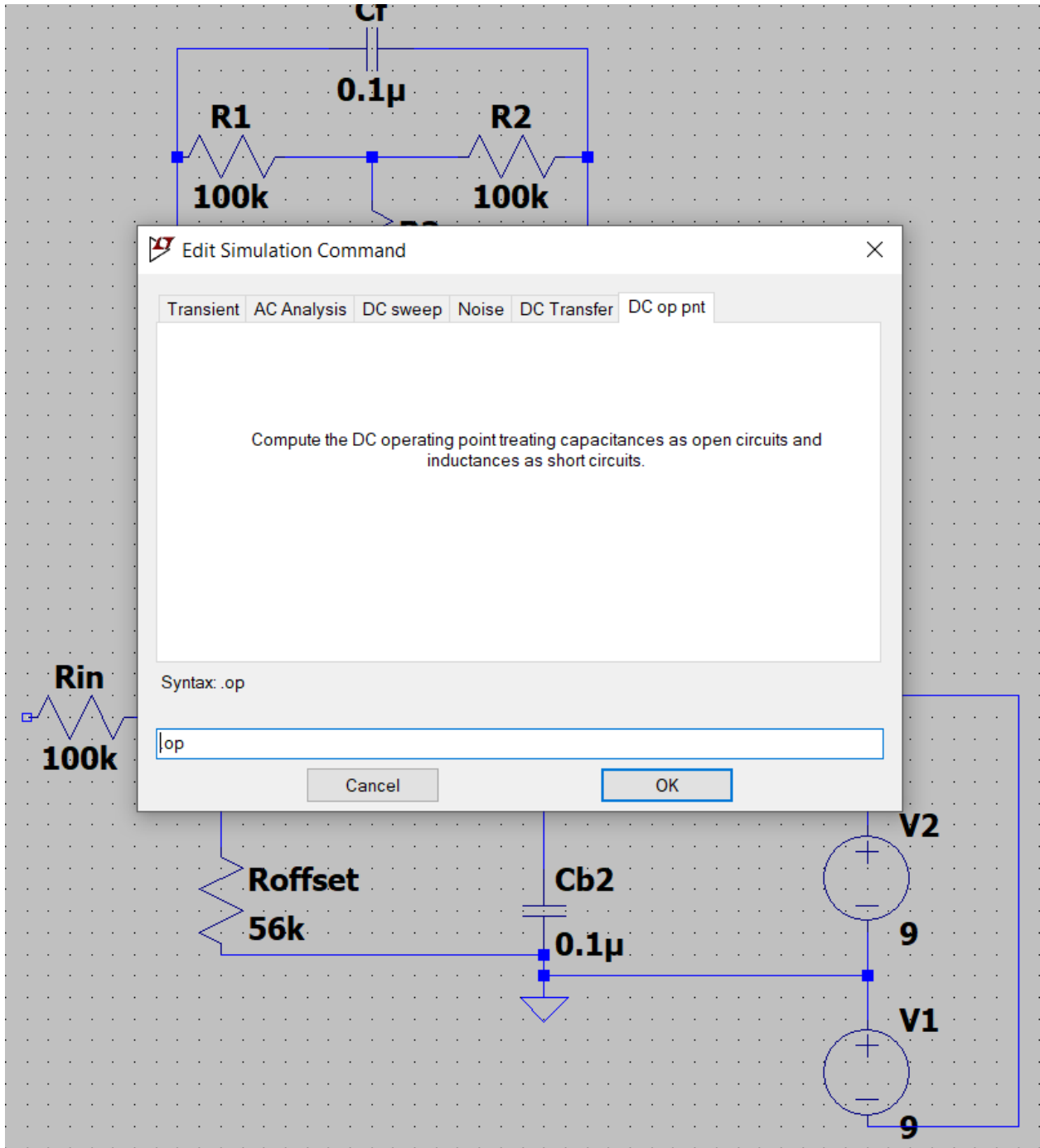


Fig.25: First simulation

```
* C:\Users\Loay\Desktop\LTSPICE INTEGRATOR.asc ×
--- Operating Point ---
V(in-) :      -0.000174724  voltage
V(in+) :      -0.000234725  voltage
V(+vcc) :      9          voltage
V(-vcc) :     -9          voltage
V(out) :      -0.00345361  voltage
V(n001) :     -3.55719e-005 voltage
V(nc_01) :    -0.000174724 voltage
I(Cb2) :      9e-019       device_current
I(Cb1) :      9e-019       device_current
I(Cf) :      -3.27889e-022 device_current
I(Roffset) :  -4.19152e-009 device_current
I(Rin) :      -2.71051e-025 device_current
I(R3) :      -3.55719e-008 device_current
I(R2) :      -3.41804e-008 device_current
I(R1) :      1.39152e-009  device_current
I(V2) :      -0.00149     device_current
I(V1) :      -0.00149003  device_current
Ix(u1:1) :    4.19152e-009 subckt_current
Ix(u1:2) :    1.39152e-009 subckt_current
Ix(u1:99) :   0.00149     subckt_current
Ix(u1:50) :   -0.00149003 subckt_current
Ix(u1:39) :   3.41804e-008 subckt_current
```

Fig.26: Results of first simulation

4.4.3.1 Simulation (Transient)

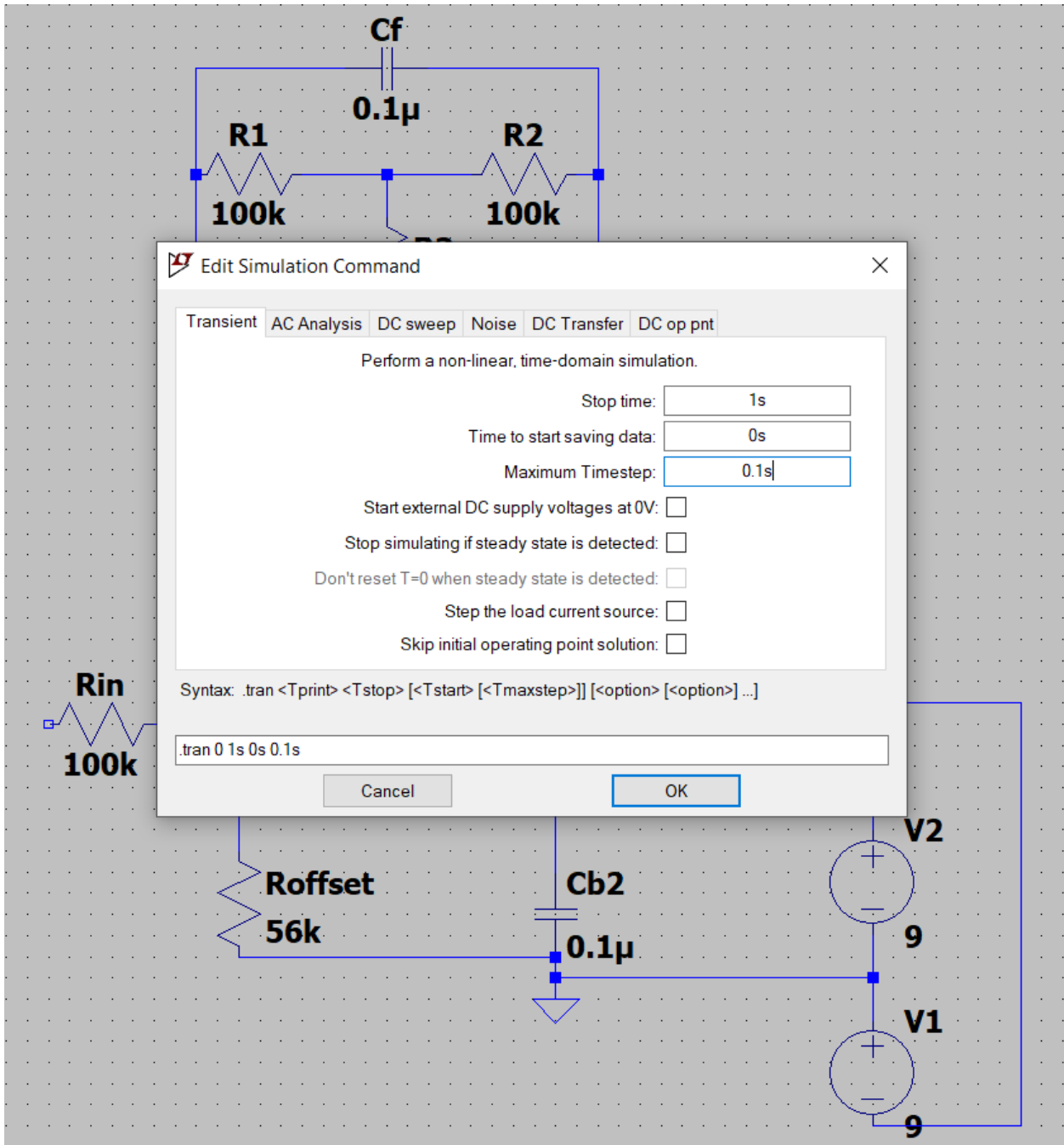


Fig.27: Second simulation

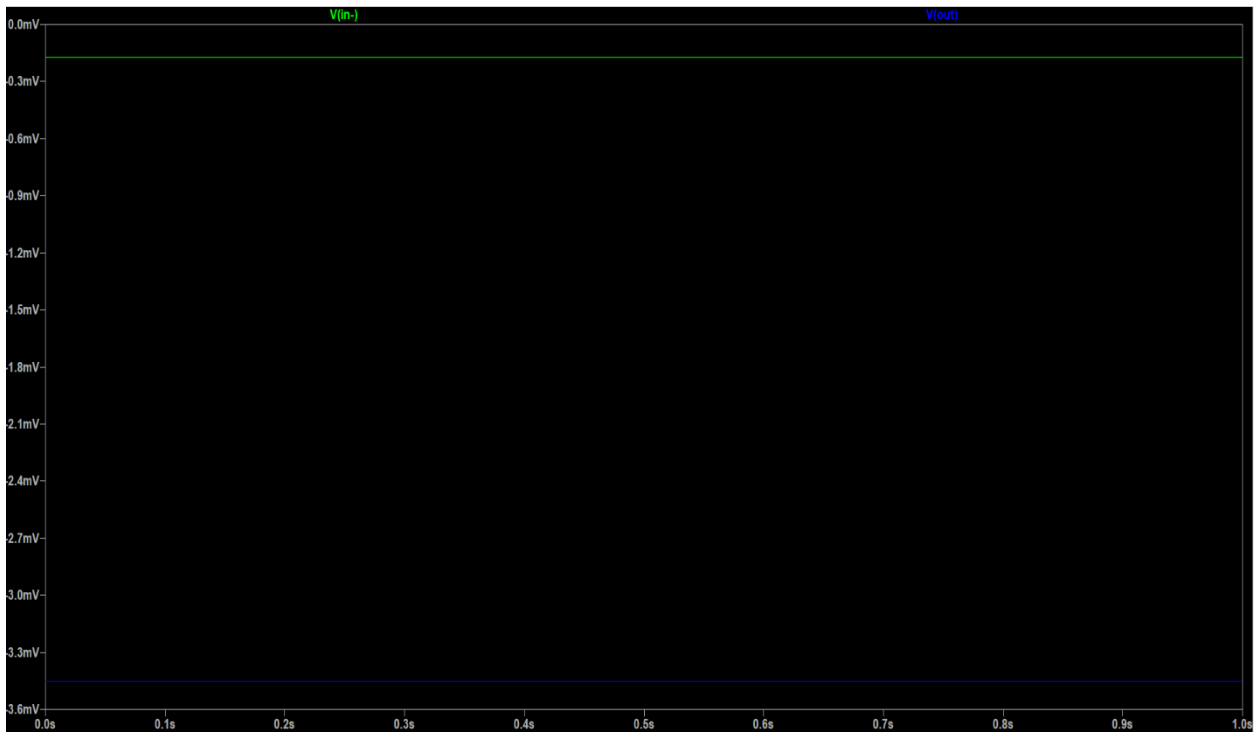
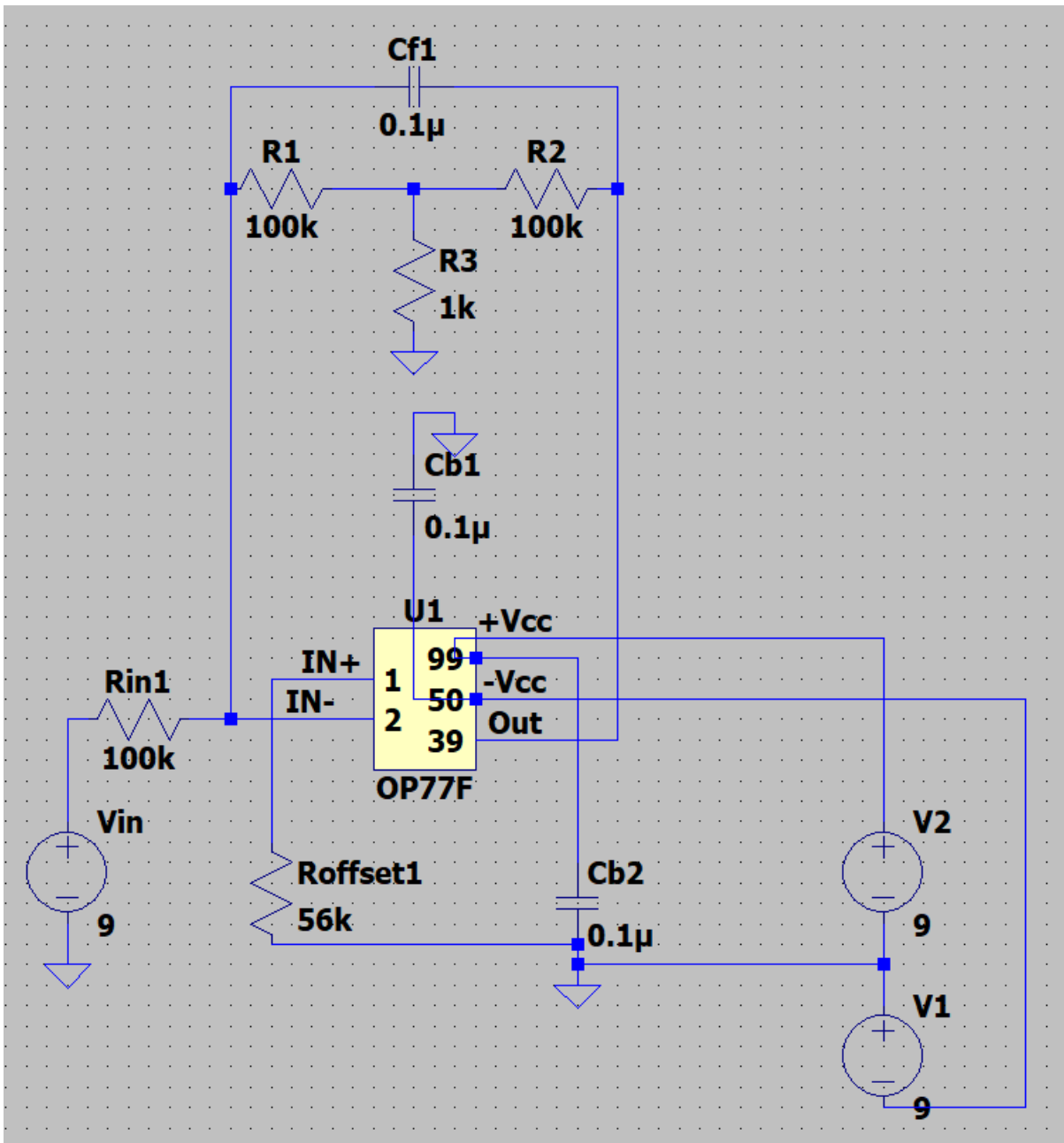
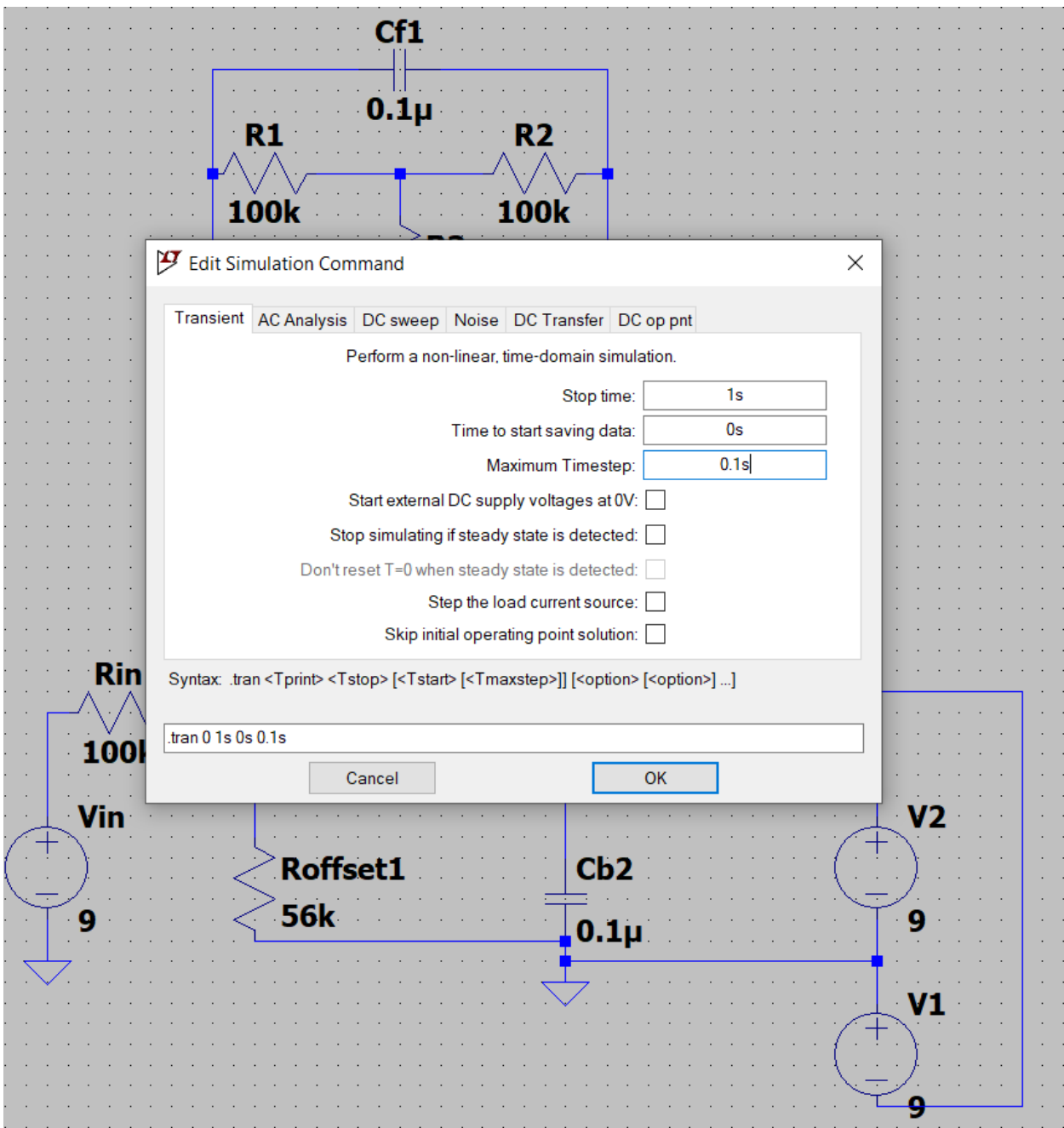
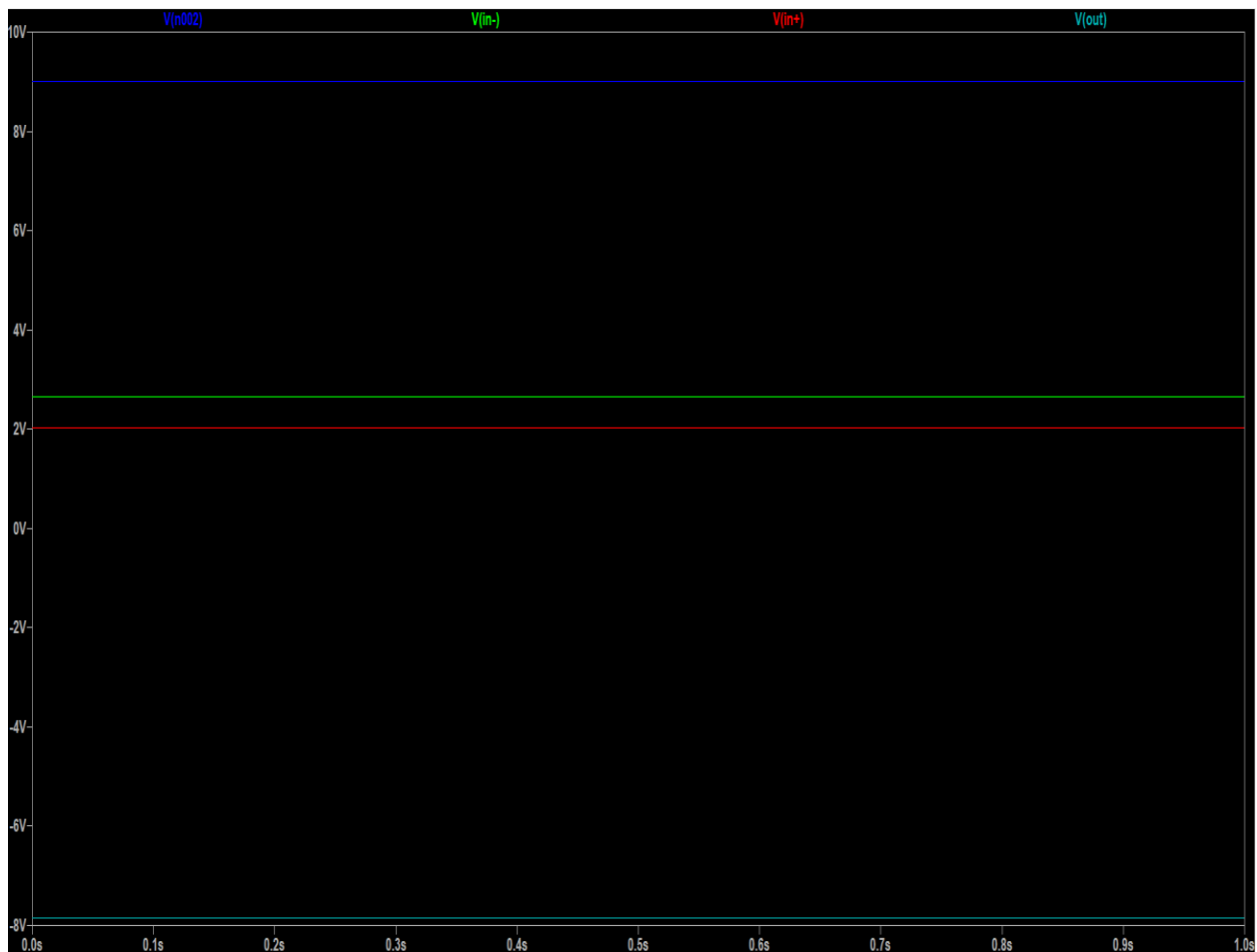


Fig.28: Results of second simulation

4.4.4 Add an input voltage to the schematic







4.5 Remaining tasks

1. First task: The Rogowski coil should be tested first by doing several measurements in the laboratory, and then plotting the voltage as a function of current. From this diagram, we can find out the equation that relates both voltage and current.
2. Second task: A numerical comparison should be made between the voltage values that we obtain through the equation we mentioned earlier and the theoretical equation in the article (the equation written on page 18).
3. Third task: When making sure that the comparison was close, then we must design and construct a small plastic house in order to put the Rogowski coil inside it, and of course there must be an exit for two electrical lines.
If the comparison is too far, another type of coil and another type of core should be used.
4. fourth task: In the fourth stage, the Rogowski coil must be given to a person specialized in the PLC to doing the power control system.
5. Final task: In the last stage, the Rogowski coil must be tested at the station. Of course, we must measure the current in the area located before the large voltage (40 KV), that is, directly before entering into the Electro filte . In other words, at the region where the voltage is found at its normal value (220 volts).

After that, there is a physical equation through which we can identify the value of the current in the Electro filter, which is:

$$V1/V2 = I2/I1$$

With,

V1= 220 v ,

$V_2 = 40 \text{ Kv}$,
 $I_1 =$ Done in final task ,
 $I_2 = ??$

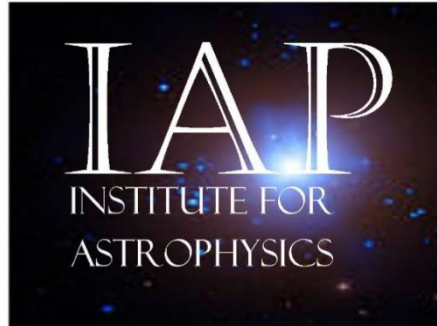
After we get the value of the current I_2 , we can evaluate the work and efficiency of this Electro Filter, and this is what we want to reach in this work.

4.6 Literature

- [1] <https://www.electrical4u.com/rogowski-coil/>
- [2] <https://www.sciencedirect.com/science/article/abs/pii/S1738573319301755>
- [3] https://en.wikipedia.org/wiki/Rogowski_coil

5 X Ray and Gamma Ray Shielding

X-Ray and Gamma ray shielding



M.K., 4.1.21

Table of Contents

X-Ray and Gamma ray shielding	115
Preface	Error! Bookmark not defined.
1 Introduction	116
1.1 Gamma ray	116
1.1.1 Description of Gamma rays	116
1.1.2 Characteristics of Gamma Rays / Radiation	117
1.1.3 Sources of Gamma rays	118
2 Protecting Against Exposure	119
2.1 Time, Distance and Shielding	119
2.2 Shielding of Gamma Radiation.....	121
2.3 Gamma Rays Attenuation	122
2.3.1 Linear Attenuation Coefficient	123
2.3.2 Validity of Exponential Law	126
2.3.3 Buildup Factors for Gamma Rays Shielding	127

3	Pulsed power accelerators	128
3.1	Construction and operation	128
3.2	MAIN PARAMETERS OF ACCELERATOR.....	129
4	Monitoring Radiation Exposure	129
4.1	Measurement of beam current.....	129
5	DESIGN OF X-RAY ROOMS	131
5.1	Room size.....	131
5.2	Doors and Walls.....	131
5.2.1	Lead equivalence	131
	Barium plaster	131
5.2.2	Windows and air conditioning units.....	131
5.3	Protective cubicle	132
	Figure 1: Illustration of an emission of a gamma ray (γ) from an atomic nucleus.....	117
	Figure 2: Total photon cross sections.Source: Wikimedia Commons	118
	Figure 3:Principles of Radiation Protection – Time, Distance, Shielding	121
	Figure 4: The relative importance of various processes of gamma radiation interaction with matter	123
	Figure 5: Dependence of gamma radiation intensity on absorber thickness	123
	Figure 6: Example of build-up of secondary particles. Strongly depends on character and parameters of primary particles	127
	Figure 7: The structure of electron accelerator.	129
	Figure 8:the diagram of beam parameters measurement system.....	130
	Figure 9:The monitoring screen for beam parameters measurement system.....	131

5.1 Introduction

In order to create a workplace isolated of the gamma radius ,we elaborated this document

5.2 Gamma ray

5.2.1 Description of Gamma rays

A gamma ray, or gamma radiation (symbol γ), is a penetrating form of electromagnetic radiation arising from the radioactive decay of atomic nuclei. It consists of the shortest wavelength electromagnetic waves and so imparts the highest photon energy.

A gamma ray refers to the high-frequency electromagnetic radiation of a photon whose wavelength is less than about ten nanometers ($<10^{-8}$ m), which corresponds to frequencies above about 30 petahertz ($> 3 \times 10^{16}$ Hz).

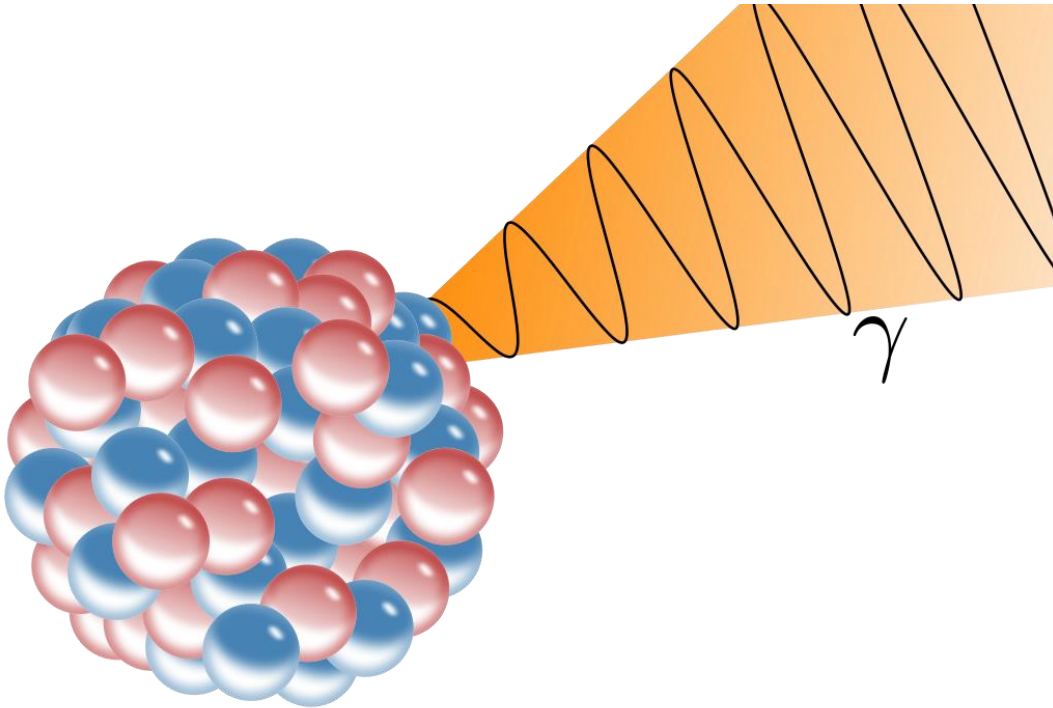


Figure 1: Illustration of an emission of a gamma ray (γ) from an atomic nucleus

Gamma rays from radioactive decay are in the energy range from a few kiloelectronvolts (keV) to approximately 8 megaelectronvolts (~ 8 MeV), corresponding to the typical energy levels in nuclei with reasonably long lifetimes. The energy spectrum of gamma rays can be used to identify the decaying radionuclides using gamma spectroscopy. Very-high-energy gamma rays in the 100–1000 teraelectronvolt (TeV) range have been observed from sources such as the Cygnus X-3 microquasar.

5.2.1.1 Characteristics of Gamma Rays / Radiation

Key features of gamma rays are summarized in following few points:

- ✓ Gamma rays are high-energy photons (about 10 000 times as much energy as the visible photons), the same photons as the photons forming the visible range of the electromagnetic spectrum – light.
- ✓ Photons (gamma rays and X-rays) can ionize atoms directly (despite they are electrically neutral) through the Photoelectric effect and the Compton effect, but secondary (indirect) ionization is much more significant.
- ✓ Gamma rays ionize matter primarily via indirect ionization.
- ✓ Although a large number of possible interactions are known, there are three key interaction mechanisms with matter.
 - Photoelectric effect
 - Compton scattering
 - Pair production
- ✓ Gamma rays travel at the speed of light and they can travel thousands of meters in air before spending their energy.

- ✓ Since the gamma radiation is very penetrating matter, it must be shielded by very dense materials, such as lead or uranium.
- ✓ The distinction between X-rays and gamma rays is not so simple and has changed in recent decades. According to the currently valid definition, X-rays are emitted by electrons outside the nucleus, while gamma rays are emitted by the nucleus.

Gamma rays frequently accompany the emission of alpha and beta radiation

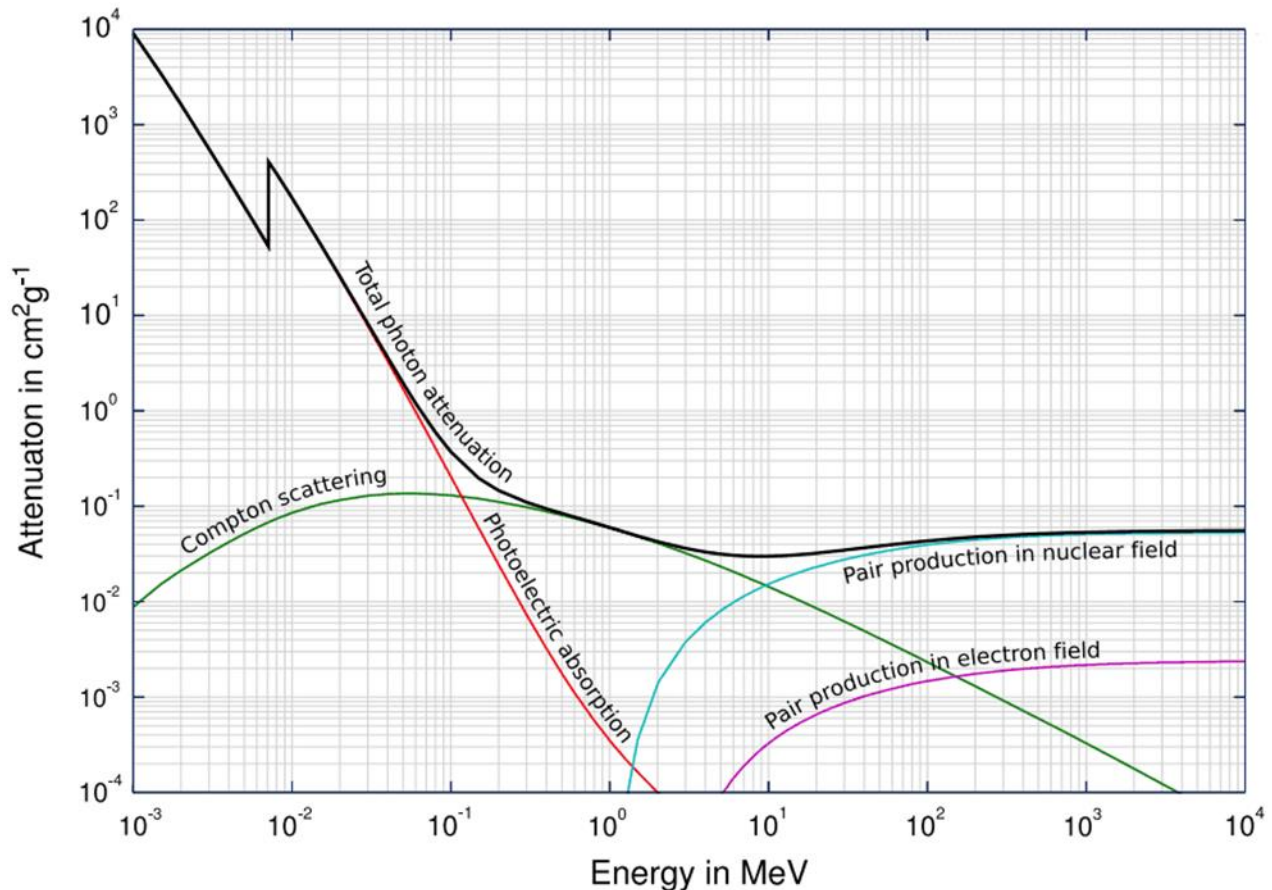


Figure 2: Total photon cross sections. Source: Wikimedia Commons

5.2.2 Sources of Gamma rays

Natural sources of gamma rays on Earth include gamma decay from naturally occurring radioisotopes such as potassium-40, and also as a secondary radiation from various atmospheric interactions with cosmic ray (are high-energy protons and atomic nuclei which move through space at nearly the speed of light. They originate from the sun, from outside of the solar system,[1] and from distant galaxies.) particles. Some rare terrestrial natural sources that produce gamma rays that are not of a nuclear origin, are lightning strikes and terrestrial gamma-ray flashes, which produce high energy emissions from natural high-energy voltages. Gamma rays are produced by a number of astronomical processes in which very high-energy electrons are produced. Such electrons produce secondary gamma rays by the mechanisms of bremsstrahlung, inverse Compton scattering and synchrotron radiation. A large fraction of such astronomical gamma rays are screened by Earth's atmosphere. Notable artificial sources of gamma rays include fission, such as occurs in nuclear reactors, as well as high energy physics experiments, such as neutral pion decay and nuclear fusion.

A sample of gamma ray-emitting material that is used for irradiating or imaging is known as a gamma source. It is also called a radioactive source, isotope source, or radiation source, though these more general terms also apply to alpha- and beta-emitting devices. Gamma sources are usually sealed to prevent radioactive contamination, and transported in heavy shielding.

5.3 Protecting Against Exposure

5.3.1 Time, Distance and Shielding

There are three general guidelines for controlling exposure to ionizing radiation:

- minimizing exposure time,

- maximizing distance from the radiation source,
- shielding yourself from the radiation source.

Time is an important factor in limiting exposure to the public and to radiological emergency responders. The amount of radiation exposure increases and decreases with the time people spend near the source of radiation. The maximum time to be spent in the radiation environment is defined as the “**stay time.**” The stay time can be calculated using the following equation:



Distance can be used to reduce exposure. The farther away people are from a radiation source, the less their exposure. Doubling the distance from a point source of radiation decreases the exposure rate to 1/4 the original exposure rate. Halving the distance increases the exposure by a factor of four. How close to a source of radiation can you be without getting a high exposure? It depends on the energy of the radiation and the size (or activity) of the source. Distance is a prime concern when dealing with gamma rays, because they can travel at the speed of light. Alpha particles can only travel a few inches and beta particles around 10 feet.

Shielding: As ionizing radiation passes through matter, the intensity of the radiation is diminished. Shielding is the placement of an “absorber” between you and the radiation source. An absorber is a material that reduces radiation from the radiation source to you. Alpha, beta, or gamma radiation can all be stopped by different thicknesses of absorbers.

Shielding material can **include barrels, boards, vehicles, buildings, gravel, water, lead** or whatever else is immediately available.

stop-alpha ALPHA – can be stopped after traveling through about 1.2 inches of air, about 0.008 inches of water, or a piece of paper or skin. A thin piece of paper, or even the dead cells in the outer layer of human skin, provides adequate shielding because alpha particles can’t penetrate it. However, living tissue inside the body offers no protection against inhaled or ingested alpha emitters.

stop-beta BETA – can only be stopped after traveling through about 10 feet of air, less than 2 inches of water, or a thin layer of glass or metal. Additional covering, for example heavy clothing, is necessary to protect against beta-emitters. Some beta particles can penetrate and burn the skin.

stop-gamma GAMMA: To reduce typical gamma rays by a factor of a billion, thicknesses of stop-gammashield need to be about 13.8 feet of water, about 6.6 feet of concrete, or about 1.3 feet of lead. Thick, dense shielding is necessary to protect against gamma rays. The higher the energy of the gamma ray, the thicker the shield must be. X-rays pose a similar challenge. This is why x-ray technicians often give patients receiving medical or dental X-rays a lead apron to cover other parts of their body.

Source: ANS, The Center for Nuclear Science and Technology Information (<http://nuclearconnect.org/know-nuclear/science/protecting#:~:text=Thick%2C%20dense%20shielding%20is%20necessary%20to%20protect%20against,apron%20to%20cover%20other%20parts%20of%20their%20body.>)

there are many many materials, which can be used for radiation shielding, but there are many many situations in radiation protection. It highly depends on the type of radiation to be shielded, its energy and many other parametres. For example, even **depleted uranium** can be used as a good protection from gamma radiation, but on the other hand uranium is absolutely inappropriate shielding of neutron radiation.

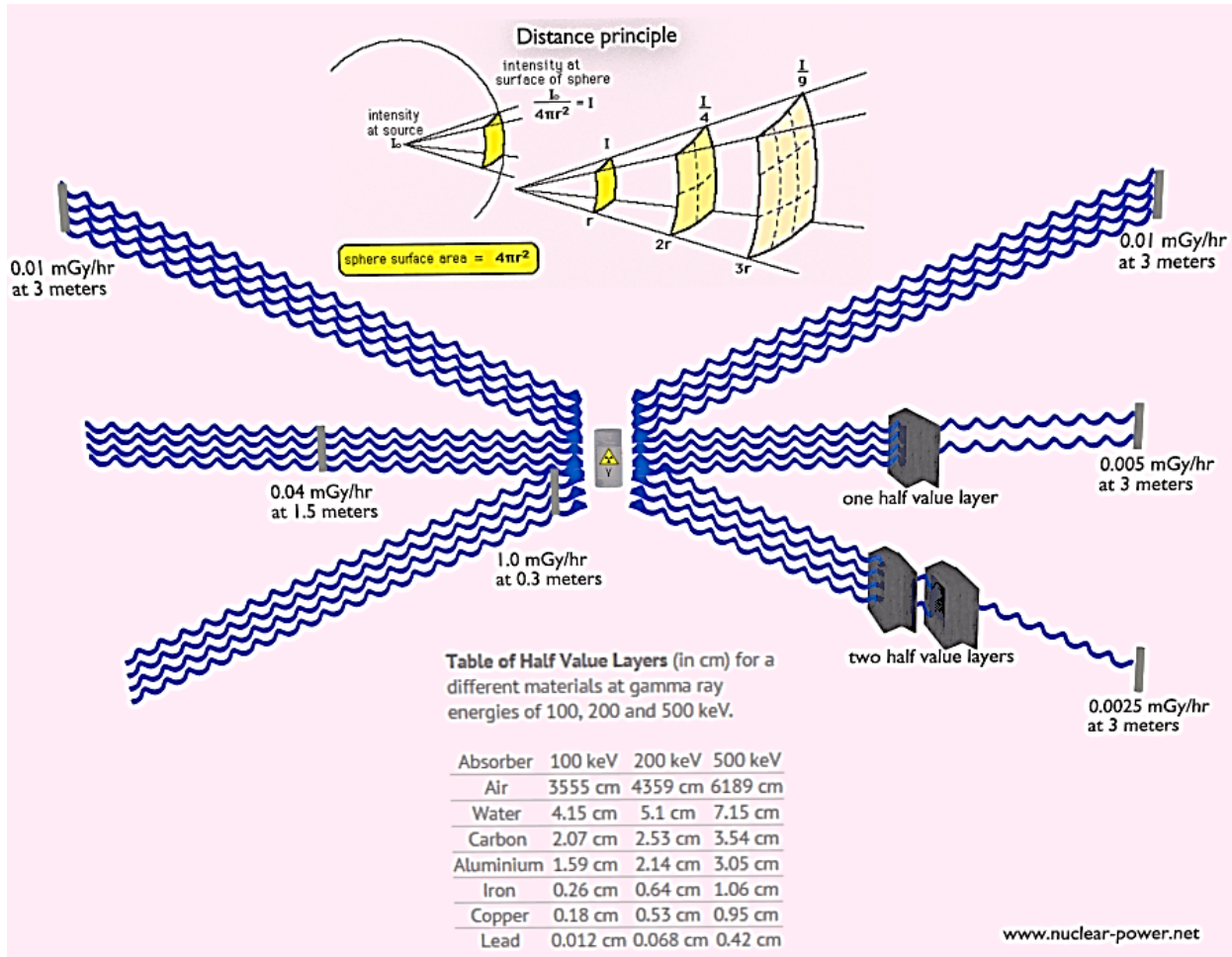


Figure 3: Principles of Radiation Protection – Time, Distance, Shielding

5.3.2 Shielding of Gamma Radiation

In short, effective shielding of gamma radiation is in most cases based on use of materials with two following material properties:

1. high-density of material.
2. high atomic number of material (high Z materials)

However, low-density materials and low Z materials can be compensated with increased thickness, which is as significant as density and atomic number in shielding applications.

A lead is widely used as a gamma shield. Major advantage of lead shield is in its compactness due to its higher density. On the other hand depleted uranium is much more effective due to its higher Z. Depleted uranium is used for shielding in portable gamma ray sources.

In nuclear power plants shielding of a reactor core can be provided by materials of reactor pressure vessel, reactor internals (neutron reflector). Also heavy concrete is usually used to shield both neutrons and gamma radiation.

Although water is neither high density nor high Z material, it is commonly used as gamma shields. Water provides a radiation shielding of fuel assemblies in a spent fuel pool during storage or during transports from and into the reactor core.

In general, the gamma radiation shielding is more complex and difficult than the alpha or beta radiation shielding. In order to understand comprehensively the way how a gamma ray loses its initial energy, how can be attenuated and how can be shielded we must have detailed knowledge of the its interaction mechanisms.

5.3.3 Gamma Rays Attenuation

The total cross-section of interaction of a gamma rays with an atom is equal to the sum of all three mentioned partial cross-sections: $\sigma = \sigma_f + \sigma_C + \sigma_p$

σ_f – Photoelectric effect

σ_C – Compton scattering

σ_p – Pair production

Depending on the gamma ray energy and the absorber material, one of the three partial cross-sections may become much larger than the other two. **At small values of gamma ray energy the photoelectric effect dominates. Compton scattering dominates at intermediate energies.** The **compton scattering also increases** with decreasing **atomic number of matter**, therefore the interval of domination is wider for light nuclei. Finally, electron-positron pair production dominates at high energies.

Based on the definition of interaction cross-section, the dependence of gamma rays intensity on thickness of absorber material can be derive. If monoenergetic gamma rays are collimated into a narrow beam and if the detector behind the material only detects the gamma rays that passed through that material without any kind of interaction with this material, then the dependence should be simple exponential attenuation of gamma rays. Each of these interactions removes the photon from the beam either by absorption or by scattering away from the detector direction. Therefore the interactions can be characterized by a fixed probability of occurrence per unit path length in the absorber. The sum of these probabilities is called the linear attenuation coefficient:

$$\mu = \tau(\text{photoelectric}) + \sigma(\text{Compton}) + \kappa(\text{pair})$$

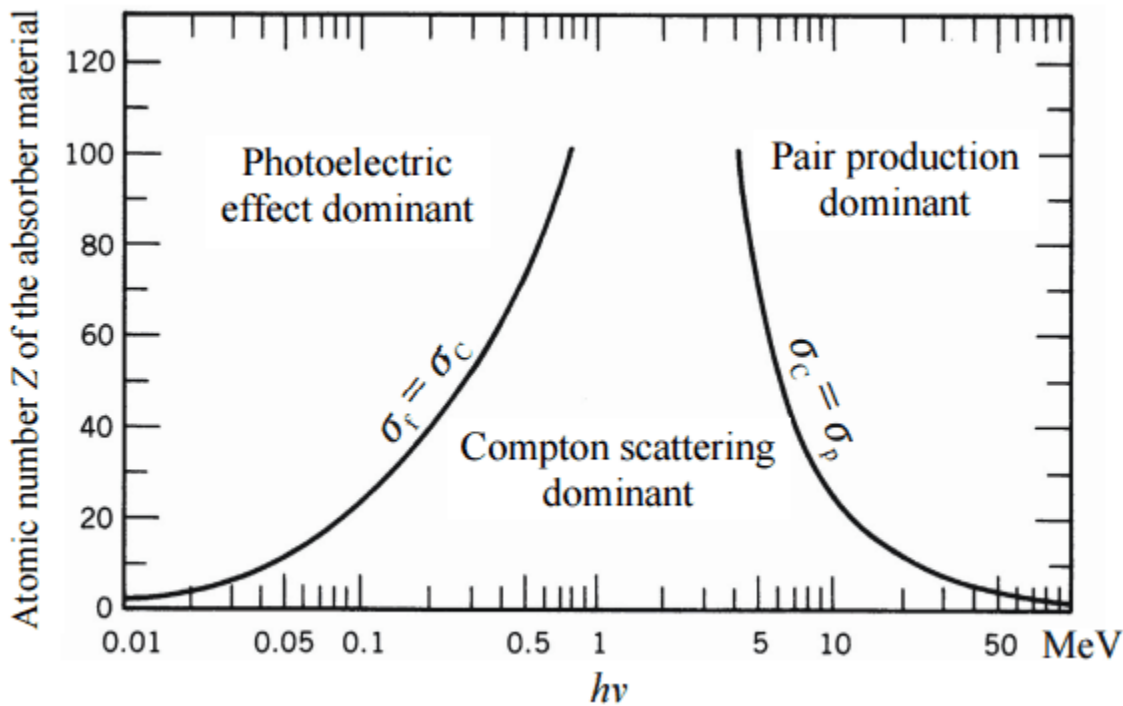


Figure 4: The relative importance of various processes of gamma radiation interaction with matter

5.3.3.1 Linear Attenuation Coefficient

The attenuation of gamma radiation can be then described by the following equation.

$I = I_0 \exp(-\mu x)$, where I is intensity after attenuation, I_0 is incident intensity, μ is the linear attenuation coefficient (cm^{-1}), and physical thickness of absorber (cm).

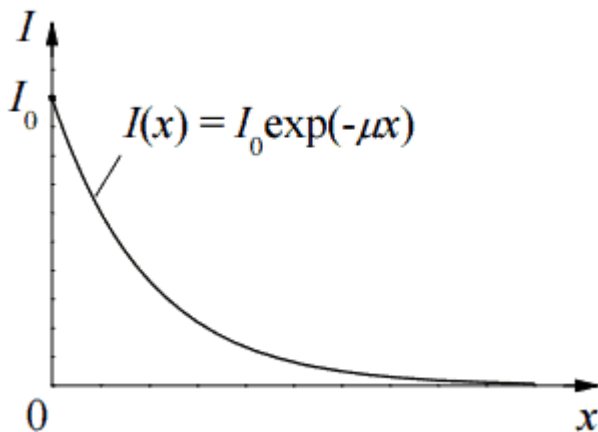


Figure 5: Dependence of gamma radiation intensity on absorber thickness

The materials listed in the table beside are air, water and a different elements from carbon ($Z=6$) through to lead ($Z=82$) and their linear attenuation coefficients are given for three gamma ray energies. There are two main features of the linear attenuation coefficient:

- The linear attenuation coefficient increases as the atomic number of the absorber increases.
- The linear attenuation coefficient for all materials decreases with the energy of the gamma rays.

Half Value Layer

The half value layer expresses the thickness of absorbing material needed for reduction of the incident radiation intensity by a factor of two. There are two main features of the half value layer:

- The half value layer decreases as the atomic number of the absorber increases. For example 35 m of air is needed to reduce the intensity of a 100 keV gamma ray beam by a factor of two whereas just 0.12 mm of lead can do the same thing.
- The half value layer for all materials increases with the energy of the gamma rays. For example from 0.26 cm for iron at 100 keV to about 1.06 cm at 500 keV.

Example:

How much water shielding do you require, if you want to reduce the intensity of a 500 keV monoenergetic gamma ray beam (narrow beam) to 1% of its incident intensity?

The half value layer for 500 keV gamma rays in water is 7.15 cm and the linear attenuation coefficient for 500 keV gamma rays in water is 0.097cm^{-1} . The question is quite simple and can be described by

$$I(x) = \frac{I_0}{100}, \text{ when } x = ?$$

following equation:

If the half value layer for water is 7.15 cm, the linear attenuation coefficient is:

$$\mu = \frac{\ln 2}{7.15} = 0.097\text{cm}^{-1}$$

Now we can use the exponential attenuation equation:

$$\begin{aligned} I(x) &= I_0 \exp(-\mu x) \\ \frac{I_0}{100} &= I_0 \exp(-0.097x) \\ \frac{1}{100} &= \exp(-0.097x) \\ \ln \frac{1}{100} &= -\ln 100 = -0.097x \\ x &= \frac{\ln 100}{0.097} = 47.47\text{ cm} \end{aligned}$$

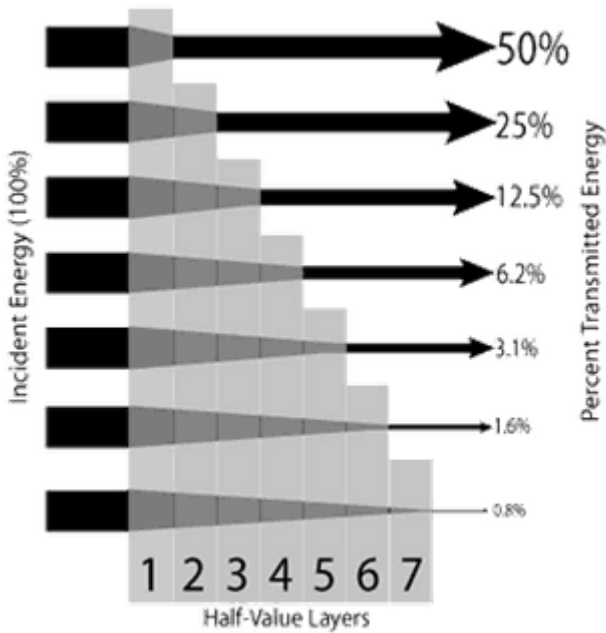
The required thickness of water is about 47.5 cm. This is relatively large thickness and it is caused by small atomic numbers of hydrogen and oxygen. If we calculate the same problem for lead (Pb), we obtain the thickness $x=2.8\text{cm}$.

Table of Linear Attenuation Coefficients (in cm^{-1}) for a different materials at gamma ray energies of 100, 200 and 500 keV.

Absorber	100 keV	200 keV	500 keV
Air	0.000195/cm	0.000159/cm	0.000112/cm
Water	0.167/cm	0.136/cm	0.097/cm
Carbon	0.335/cm	0.274/cm	0.196/cm

Aluminum	0.435/cm	0.324/cm	0.227/cm
Iron	2.72/cm	1.09/cm	0.655/cm
Copper	3.8/cm	1.309/cm	0.73/cm
Lead	59.7/cm	10.15/cm	1.64/cm

Half Value Layers



The half value layer expresses the thickness of absorbing material needed for reduction of the incident radiation intensity by a factor of two. With half value layer it is easy to perform simple calculations.

Source: www.nde-ed.org

Table of Half Value Layers (in cm) for a different materials at gamma ray energies of 100, 200 and 500 keV.

Absorber	100 keV	200 keV	500 keV
Air	3555 cm	4359 cm	6189 cm
Water	4.15 cm	5.1 cm	7.15 cm
Carbon	2.07 cm	2.53 cm	3.54 cm

Aluminium	1.59 cm	2.14 cm	3.05 cm
Iron	0.26 cm	0.64 cm	1.06 cm
Copper	0.18 cm	0.53 cm	0.95 cm
Lead	0.012 cm	0.068 cm	0.42 cm

Mass Attenuation Coefficient

When characterizing an absorbing material, we can use sometimes the mass attenuation coefficient. The mass attenuation coefficient is defined as the ratio of the linear attenuation coefficient and absorber density (μ/p). The attenuation of gamma radiation can be then described by the following equation:

$$I=I_0.e^{-(\mu/p).pl}$$

, where p is the material density, (μ/p) is the mass attenuation coefficient and pl is the mass thickness. The measurement unit used for the mass attenuation coefficient cm^2g^{-1} .

For intermediate energies the Compton scattering dominates and different absorbers have approximately equal mass attenuation coefficients. This is due to the fact that cross section of Compton scattering is proportional to the Z (atomic number) and therefore the coefficient is proportional to the material density p . At small values of gamma ray energy or at high values of gamma ray energy, where the coefficient is proportional to higher powers of the atomic number Z (for photoelectric effect $\sigma \sim Z^5$; for pair production $\sigma_p \sim Z^2$), the attenuation coefficient μ is not a constant.

5.3.3.2 Validity of Exponential Law

The exponential law will always describe the attenuation of the primary radiation by matter. If secondary particles are produced or if the primary radiation changes its energy or direction, then the effective attenuation will be much less. The radiation will penetrate more deeply into matter than is predicted by the exponential law alone. The process must be taken into account when evaluating the effect of radiation shielding.

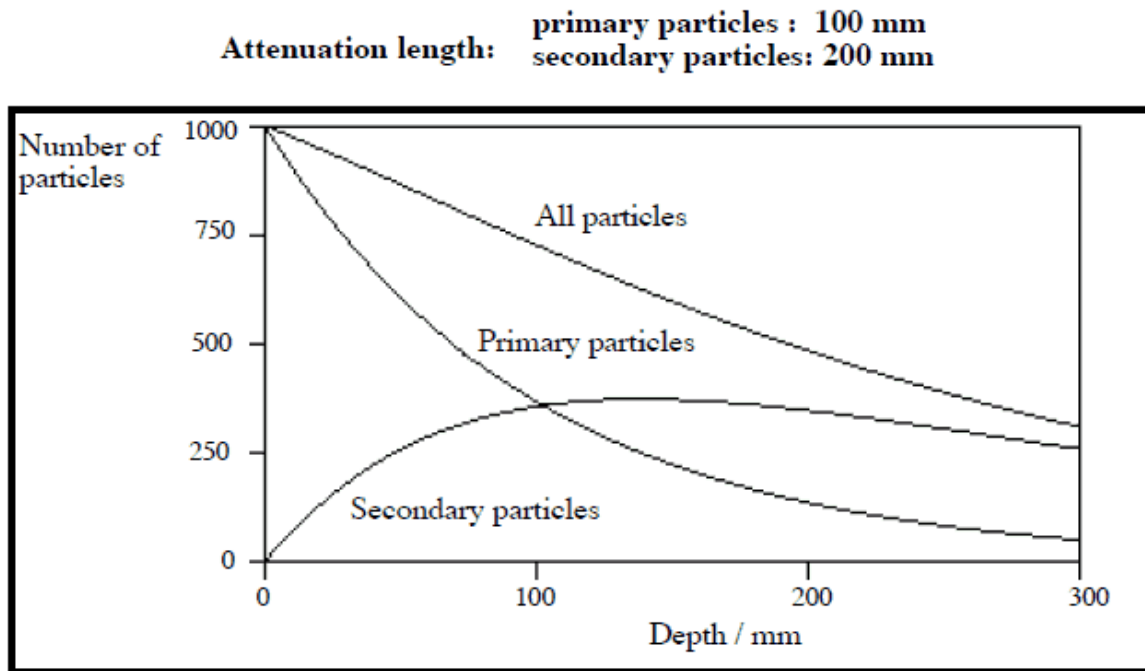


Figure 6: Example of build-up of secondary particles. Strongly depends on character and parameters of primary particles

5.3.3.3 Buildup Factors for Gamma Rays Shielding

The buildup factor is a correction factor that considers the influence of the scattered radiation plus any secondary particles in the medium during shielding calculations. If we want to account for the buildup of secondary radiation, then we have to include the buildup factor. The buildup factor is then a multiplicative factor which accounts for the response to the uncollided photons so as to include the contribution of the scattered photons. Thus, the buildup factor can be obtained as a ratio of the total dose to the response for uncollided dose.

The extended formula for the dose rate calculation is:

$$\dot{D} = \frac{kSE \frac{\mu_t}{\rho} B e^{-\mu D}}{4\pi r^2}$$

where

- k is a collective constant to convert energy fluence rate to dose rate; for gray/hour, k will have a value of 5.76×10^{-7}
- S is the source strength in s^{-1}
- E is the photon energy in MeV
- $\frac{\mu_t}{\rho}$ is the mass absorption coefficient for the material at the dose (values are available at NIST)
- B is the buildup factor (tabulated), which depends on the photon energy, the shield material and thickness, the source and shield geometry, and the distance from the shield surface to the dose point.
- μ is the linear attenuation coefficient for the photons in the shield material (values are available at NIST)
- D is the thickness of the shield

5.4 Pulsed power accelerators

Pulsed power accelerators have been used for many years as intense sources of X-rays.

The dominant trend in the development of pulsed power accelerator technology over the last decade has been towards higher power and shorter pulse widths.

Limitations in high voltage, high current switch performance, and in power flow through vacuum insulator housings led to the development of highly modular designs. This modular approach requires precise synchronization of the various modules and efficient methods of combining the power from these modules to drive a common load.

5.4.1 Construction and operation

The machines which have been constructed consist of three or more essential elements, an energy-storage device such as a Marx generator, a pulse-forming network, and a diode used for beam generation. The pulse line provides a fast-rise, short-duration pulse which is applied to the vacuum diode.

The pulsed electron accelerator consists from electron source with vacuum chamber for irradiation, Marx high voltage pulsed generator. Planar diode electron source has explosive emission cathode on the basis of carbon fiber materials and carbon nanotubes. The diameter of cathode is 1.0 – 10.0 cm. An anode is metal net from stainless steel. The pressure of residual gas in stainless steel vacuum chambers is 10^{-5} Torr. The nylon high voltage insulator has evacuated central metal electrode for connection with cathode. The Ti foil with thickness 15 microns uses for output electron beam from vacuum chamber to air. The two separated Marx generators with pulse duration 20 and 100-200 nsec are used in this accelerator in dependence on pulse duration. The regulation of output voltage from Marx generator realizes by variation of charging voltage and gas pressure in the sparks.

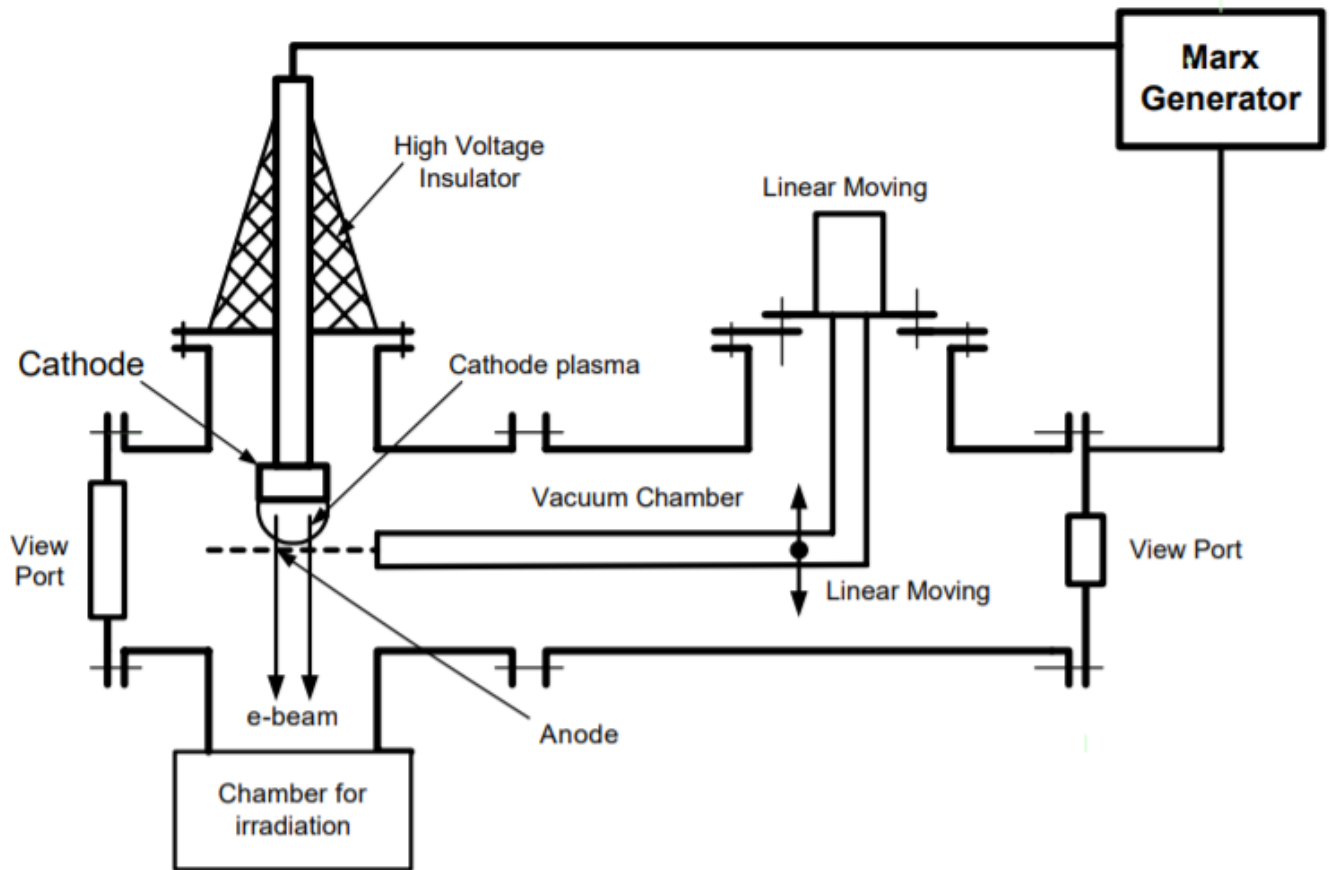


Figure 7: The structure of electron accelerator.

5.4.2 MAIN PARAMETERS OF ACCELERATOR

The main parameters of electron accelerator are next: 1. Kinetic energy.....200 – 400 keV. 2. Beam current.....10 – 1000 A. 3. Beam pulse duration20 and 100 nsec. 4. Repetition.....0.01 - 10 Hz. The change of pulse duration 20 and 100 nsec is realized by change of type for Marx generator.

5.5 Monitoring Radiation Exposure

Personal radiation detection devices (Luxel Aluminum Oxide or Thermo-Luminescence Dosimeters - TLD badges) are used to monitor the radiation dose that a wearer may have received from an exposure, but these devices offer no additional protection to the wearer. These devices measure exposure in only a small area of the body. The chances of these devices being located in an area of the body that is exposed is very small.

5.5.1 Measurement of beam current

The beam diagnostic includes the standard units. The current transformers (Rogowski Coils) and Faraday Cups are used for measurements of beam current. The high resistive dividers are used for measurements of accelerating voltage. The block-diagram of system for beam measurement is given on next Fig. This system uses PXI-1025, scope, switches and software LabVIEW 6.1. from National Instruments.

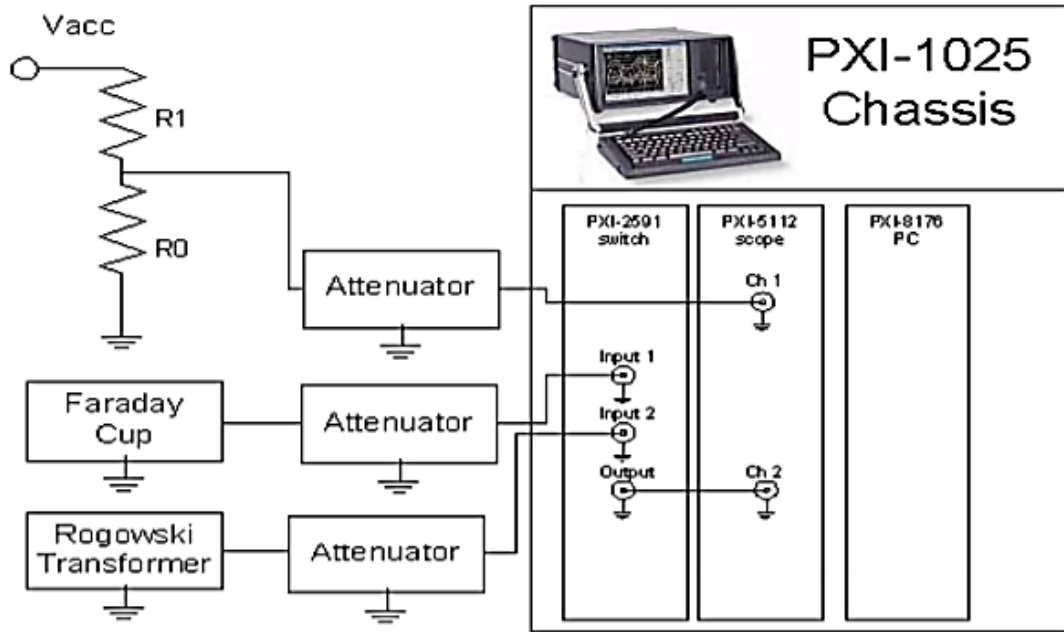


Figure 8: the diagram of beam parameters measurement system.

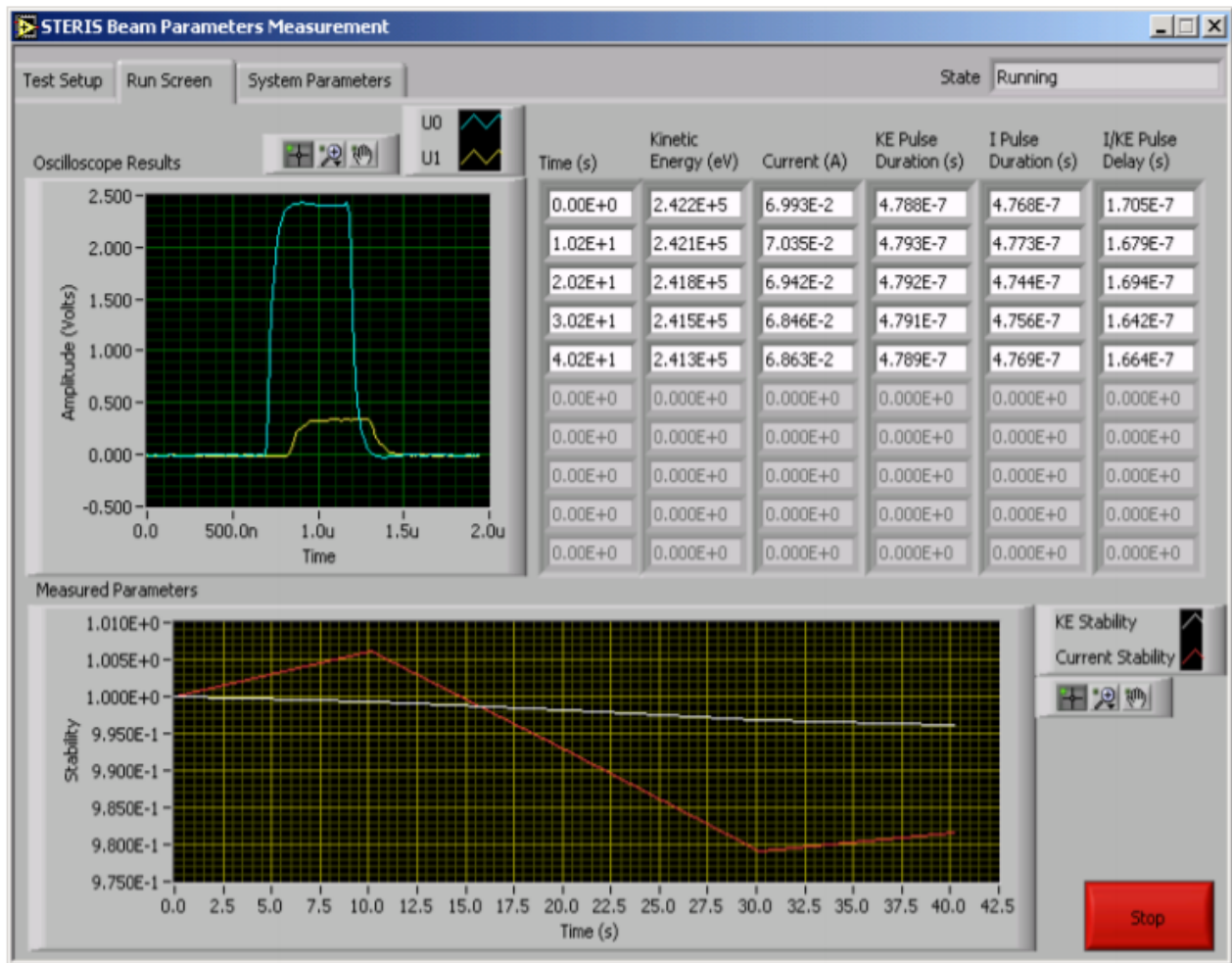


Figure 9: The monitoring screen for beam parameters measurement system

5.6 DESIGN OF X-RAY ROOMS

5.6.1 Room size

General radiographic rooms should be approximately $16m^2$. There should be sufficient space for a permanently built protective cubicle.

5.6.2 Doors and Walls

- Access doors should be of the sliding type giving better radiation protection.
- A clearing of 1.5 m is recommended. The overlap should be 100 mm each side.
- The doors should be lined with leadsheet of 2 mm thickness.
- The walls should be 230 mm kiln baked solid clay brick or 2 mm leadsheet sandwiched between partitioning or 115 mm brick with 6 mm barium plaster.
- Walls should be protected up to a height of 2.2 meter.

5.6.2.1 Lead equivalence

Material	Thickness of material (in mm)	Lead equivalence (in mm) at tube voltage	
		100 kV	150 kV
brick	115	1.0	0.9
brick	230	2.4	2.0
barium plaster	6	1.0	0.55
barium plaster	11		1.0

5.6.2.2 Barium plaster

Barium plaster mix:

1 part coarse barium sulphate

1 part fine barium sulphate, 1 part cement

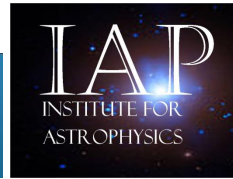
5.6.2.3 Windows and air conditioning units

- Windows and air conditioning units should be sited at least 2 m above the floor. Alternatively access near the window must be prevented effectively.
- Windows of upper floor x-ray rooms can be of normal height.

5.6.3 Protective cubicle

- A protective cubicle allowing space for the control as well as the operator should be constructed in the x-ray room.
- The cubicle should be located such that unattenuated direct scatter radiation originating on the examination table or the erect bucky do not reach the operator in the cubicle.
- The x-ray control for the system should be fixed within the cubicle and should be at least 1.02 m from any open edge of the cubicle wall which is nearest to the examination table.
- The size of the window should be at least 30 cm x 30 cm.
- The minimum height of the cubicle is 2.2 meter.
- The lead equivalence of the wall or panel as well as the protective glass should be at 2 mm, i.e., 230 mm brick or 115 mm brick barium plastered (6 mm) or 2 mm leadsheet.

6 X-Ray Generation and Detection (Master Thesis Final Version Sent Feb 2022)



Lebanese University

MASTER THESIS

In Order to Obtain the

Research Master

Of

Physics of Radiation-Matter Interaction

Presented and defended by:

Yahya Al Abbouchi

On 10th October 2021

Title

X-Ray Detector for the Nano satellite IAP-SAT

Supervisors

Dr. Ahmad Osman, Dr. Samir Mourad

Reviewer

Prof. Adnan Naja

Prof. Hassan Amoud

6.1 Summary: Status Nov 21



X-RAY

Introduction مقدمة

X-RAY GENERATION

X-RAY: An X-ray is a penetrating form of high-energy electromagnetic radiation. Most X-rays have a wavelength ranging from 10 picometers to 10 nanometers, corresponding to frequencies in the range 30 petahertz to 30 exahertz (30×10¹⁵ Hz to 30×10¹⁸ Hz) and energies in the range 124 eV to 124 KeV. X-ray wavelengths are shorter than those of UV rays and typically longer than those of gamma rays.

Y-RAY: (Figure 1) A gamma ray (symbol γ), is a penetrating form of electromagnetic radiation arising from the radioactive decay of atomic nuclei. It consists of the shortest wavelength electromagnetic waves and so imparts the highest photon energy. A gamma ray refers to the high-frequency electromagnetic radiation of a photon whose wavelength is less than about ten nanometers (<10–8 m), which corresponds to frequencies above about 30 petahertz (> 3 × 10¹⁶ Hz).

Y: أشعة غاما (الـ γ)، هي شكل من أشكال الإشعاع الكهرومغناطيسي عالي الطاقة. يحيط الأشعة غاما بطول موجي يتراوح من 10 بيكو متر إلى 10 نانومتر ، وهو ما يقابل الترددات في النطاق 30 بيتاهيرتز إلى 30 إكساهيرتز (30 × 10¹⁵ هرتز إلى 30 × 10¹⁸ هرتز) والطاقة في النطاق 124 إلكترون فولت إلى 124 ميجا إلكترون فولت. أشعة غاما هي الأشعة السينية أقصر من تلك الخاصة بالأشعة فوق البنفسجية وأطول من تلك الخاصة بأشعة جاما.

Y: أشعة جاما (الـ γ)، هي شكل من أشكال الإشعاع الكهرومغناطيسي الناتج عن التحلل الإشعاعي للنواة الذرية. يتكون من أقصر طول موجي.

تعطي الموجات الكهرومغناطيسية ونأمل أقصر طاقة للفوتون.

تتميز أشعة غاما على الإشعاع الكهرومغناطيسي عالي الودة الطولون بكون طول موجي أقل من حوالي عشرة نانومتر (< 10⁻⁸ م)، وهو ما يتوافق مع ترددات أعلى من حوالي 30 بيتاهيرتز (> 3 × 10¹⁶ هرتز).

Sources مصادر

The x-ray source consists of a vacuum tube including a tungsten filament covered with a metal cathode (preferably tungsten) and a copper (or any element having an atomic number between 20 and 80). A high potential electric source is applied between the anode and the cathode that will result in electrons being accelerated from cathode to anode. Once the electrons hit the anode at high speed, x-rays are generated.

يتمثل مصدر الأشعة السينية من اليون المفرغ على خطوط تصدق مغناطيسية. يتكون من أنود من التنجستن (مفضل التنجستن) والقطب (أو أي عنصر له رقم ذري بين 20 و 80). يتم تطبيق مصدر كهربي عالي على الأقطاب بين الأقطاب والكاثود، مما يؤدي إلى تسريع الإلكترونات من الكاثود إلى الأنود. بمجرد أن تصطدم الإلكترونات بالقطب الموجب بسرعة عالية ، يتم إنشاء الأشعة السينية.

X-ray: The x-ray source consists of a vacuum tube including a tungsten filament covered with a metal cathode (preferably tungsten) and a copper (or any element having an atomic number between 20 and 80). A high potential electric source is applied between the anode and the cathode that will result in electrons being accelerated from cathode to anode. Once the electrons hit the anode at high speed, x-rays are generated.

في خطوط الكاثود المستخدمة لتوليد أشعة من الأشعة السينية ، يتم تشغيلها بجهد 24 DC فولت (لا تعمل) والتي تتراوح من 200 إلى 2000 مللي أمبير من التيار المستمر يمر عبر الأنبوب.

X-ray: The anode used is a copper rod from Air conditioners. Tungsten anode is much preferred but it is not available. Numerous support screws are used to fix the anode in place.

X-ray: The cathode filament that is used to generate a cloud of electrons is nothing but a bulb light filament that is heated up by a DC voltage of 24 V (12 V didn't work) which will generate 200 mA of DC current passing through the filament.

X-ray: The anode used is a copper rod from Air conditioners. Tungsten anode is much preferred but it is not available. Numerous support screws are used to fix the anode in place.

Protecting Against Exposure الحماية من التعرض

Time is an important factor in limiting exposure to the public and to radiological emergency responders. The amount of radiation exposure increases and decreases with the time people spend near the source of radiation. The maximum time to be spent in the radiation environment is defined as the "stay time." The stay time can be calculated using the following equation: Stay Time = Exposure Limit/Dose Rate.

Distance can be used to reduce exposure. The farther away people are from a radiation source, the less their exposure. Doubling the distance from a point source of radiation decreases the exposure rate to 1/4 the original exposure rate. Halving the distance increases the exposure by a factor of four. How close to a source of radiation can you be without getting a high exposure? It depends on the energy of the radiation and the size (or activity) of the source. Distance is a prime concern when dealing with gamma rays, because they can travel at the speed of light. Alpha particles can only travel a few inches and beta particles around 30 feet.

Shielding. As ionizing radiation passes through matter, the intensity of the radiation is diminished. Shielding is the placement of an "absorber" between you and the radiation source. An absorber is a material that reduces radiation from the radiation source to you. Alpha, beta, or gamma radiation can all be stopped by different thicknesses of absorbers. Shielding material can include barrels, boards, buildings, gravel, water, lead or whatever else is immediately available.

Time: عامل مهم في الحد من التعرض للحماية والحد من التعرض الإشعاعي. تزداد كمية التعرض الإشعاعي وتقل مع مصدر الإشعاع. الحد الأقصى للوقت الذي يجب قضاءه في بيئة الإشعاع "وقت البقاء" يمكن حساب وقت البقاء باستخدام المعادلة التالية. وقت البقاء = الحد الأقصى للتعرض / معدل التعرض.

Distance: يمكن استخدام المسافة لتقليل التعرض. كلما بعدت عن مصدر الإشعاع، قل التعرض الإشعاعي. تضاعف المسافة من مصدر الإشعاع يقلل التعرض الإشعاعي بمقدار 1/4. تضاعف المسافة من مصدر الإشعاع يقلل التعرض الإشعاعي بمقدار 1/4. كلما قربت من مصدر الإشعاع، زاد التعرض الإشعاعي. كلما قربت من مصدر الإشعاع، زاد التعرض الإشعاعي. كلما قربت من مصدر الإشعاع، زاد التعرض الإشعاعي.

Shielding: كلما قربت من مصدر الإشعاع، زاد التعرض الإشعاعي. كلما قربت من مصدر الإشعاع، زاد التعرض الإشعاعي. كلما قربت من مصدر الإشعاع، زاد التعرض الإشعاعي.

X-RAY DETECTION

1. Scintillators

Scintillators are materials in which large fractions of incident striking particles or radiation are absorbed and transformed into detectable visible or near visible light photons, later converted into an electrical signal. They are used in many applications especially those require high energetic particles or hard X-rays that are not directly detectable by semiconductor detectors.

1. ديوذود: الديودات هي مواد يتم فيها امتصاص أجزاء كبيرة من الإشعاع وتحويلها إلى فوتونات ضوئية مرئية أو قريبة من الأشعة فوق البنفسجية، والتي يتم تحويلها لاحقًا إلى إشارة كهربائية. يتم استخدامها في العديد من التطبيقات خاصة تلك التي تتطلب جزيئات عالية الطاقة أو أشعة سينية صلبة لا يمكن اكتشافها مباشرة بواسطة أجهزة الكشف عن أشعة اليون.

2. Detection of the Scintillation Light:

To understand the optical properties of silicon, one needs to analyze its band structure. Photon absorption through electronic transitions between different bands can occur only if the total energy and momentum of the system is conserved. The interaction of photons with silicon mainly occurs by the excitation of electrons from the valence band or impurity states into higher available energy states. But there is also the probability for excitations within the same band. For certain photon energies the joint density of states of the conduction and valence band becomes maximum. This leads to the so called Van Hove singularities in the joint density of states. Two regimes with an excitation energy E1 and E2, give rise to Van Hove singularities. Hence to characteristic points of the absorption of silicon at E = E1 and E2.

2. الكشف عن ضوء السنتال: لفهم الخصائص البصرية للسيليكون ، يحتاج المرء إلى تحليل هيكل نطاق الطاقة الخاص به. يمكن أن يحدث امتصاص الفوتون من خلال الانتقالات الإلكترونية بين النطاقات المختلفة فقط إذا تم الحفاظ على الطاقة والزخم الكلي. التفاعل الرئيسي للفوتونات مع السيليكون يحدث عن طريق إثارة الإلكترونات من نطاق التكافؤ إلى نطاق التوصيل أو حالات الطاقة الممتلئة الأعلى. ولكن هناك أيضًا احتمال حدوث إثارة وإثارة نفس النطاقات. على نطاقات طاقة معينة من الفوتون ، تصبح الكثافة المشتركة لحالات التوصيل والطاقات المتكافئة ذات حواف في الكثافة المشتركة للنطاقات. هاتان نقطتان هامتان على نطاق E1 ، E2 ، يعزبان إلى ظهور الخصائص Van Hove ، وبالتالي إلى هاتين نقطتي الامتصاص السنتاليتين عند E = E1 ، E2.

3. Quantum efficiency

The quantum efficiency of semiconductor radiation detector defines its sensitivity to the incident radiation. In other term, η, tells how many photons will be stopped by the detector sensitive area when irradiated by an incident beam.

3. الكفاءة الكمومية: الكفاءة الكمومية هي كفاءة الإشعاع التي تقيس نسبة الفوتونات التي يتم إيقافها من قبل منطقة الكشف الحساسة عند التعرض لها.

4. Signal amplification and readout electronics:

CAMEX is a special electronic chip designed for pnCDD to amplify and sample the signals received from the parallel channels. In pnCDD used by eROSITA, three CAMEX are located at the endpoints of the 384 channels (each CAMEX connected to 128 channels).

4. إزارة التضخيم والإلكترونيات القراء: جزء هي رقاقة إلكترونية خاصة مصممة لـ pnCDD لتضخيم وعياد الإشارات المستلمة من القنوات المتوازية. في pnCDD المستخدمة في eROSITA ، يوجد ثلاث قنوات في كل قناة من 384 قناة (كل قناة متصلة بـ 128 قناة).

5. Spatial resolution:

The spatial resolution of the pnCDD mainly depends on the pixel size. The detector works on the principle of photon-charge conversion, the volume of the created charge cloud strongly contributes to the spatial resolution.

5. دقة المكان: دقة المكان في pnCDD بشكل أساسي يعتمد على حجم البكسل. يعمل الكاشف على مبدأ تحويل الفوتون إلى شحنة ، وحجم السحابة المشحونة الناتجة تساهم بقوة في الدقة المكانية.

6. Energy resolution:

The energy resolution of registered electrons can be determined by measuring the FWHM of the Gaussian energy distribution of a spectral peak centered at energy E of a monoenergetic X-ray line.

6. دقة الطاقة: يمكن تحديد دقة الطاقة للإلكترونات المسجلة عن طريق قياس FWHM من التوزيع الغاوسي لطاقة الفوتون المرصود نظريًا في الطاقة E. خط الأشعة السينية أحادية الطاقة.

7. Time resolution:

The sum of the integration time (exposure time), charge transfer and readout times from the cycle time and the frame rate.

7. وقت الوقت: مجموع وقت التكامل (التعرض) ، وقت نقل الشحنة وقراءة البيانات من وقت الدورة ووقت الإطار.

X-Ray Control system

The X-Ray process control system to be implemented should have the following technical requirements:

- The user must be able to control the X-Ray system through Graphic User Interface (GUI).
- The user must be able to monitor Photodiodes (sensor) data on a well-organized GUI.
- The system must have a USB 2.0 cable B, with at least 3 meters as length (for safety purpose), to connect it with the control device (PC).
- The system can be divided into 2 subcategories; The plant side where the X-Ray setup is set, and the user side where all the controls are set.

Arduino Code

- *Power circuit breaker: Turns on/off all the system (220V)
- *Vacuum Pump switch: Turns on/off the vacuum pump
- *Controller: The controller used is Arduino UNO. A USB 2.0 Cable type B is used to connect X-ray plant and the control station. It is used to control the relay box according to operator's command (from the user-end GUI) and send back the data coming from photodiodes (sensors).
- *Relay kit: Controlled contacts (2 channels).

User-End GUI

The GUI interface is shown in the image below. It is divided into 2 sections; The Power and monitoring, and control.

Figure 1, shows GUI when it is in the disconnecting statement, where the filament and the high voltage buttons are deactivated (white boxes) where the connecting button is activated and red tinted which indicates the disconnecting statement with Arduino. If the connection box does not red tinted, this indicator means that NO COM Port available. Hence, check the Arduino cable connection with the PC.

Matlab

The beam diagnostic includes the standard units. The current transformers (Rogowski Coils) and Faraday Cups are used for measurements of beam current. The high resistive dividers are used for measurements of accelerating voltage. The block diagram of system for beam measurement is shown in next Fig. This system uses PXI-1025, scope, switches and software LabVIEW 6.1. from National Instruments.

يتمثل تشخيص الحزمة (التي هي الوحدات القياسية) باستخدام ملفات روجوفسكي وأكوابك فارادي كأسل من أجهزة استشعار التيار. يتم استخدام مقاييس الجهد المقاوم لقياس الجهد التسارع. يتم استخدام مقاييس التيار من نوع PXI-1025 ، ومفاتيح وبرامج LabVIEW 6.1. من National Instruments.

6.2 Abstract

This work mainly consist to building an X-ray detector to place in Nano satellite launched into space to measure the incident energy and the intensity to which the satellite is exposed.

During this thesis, a PIN photodiode BPW34 in visible domain is used as detector to enhance quantum efficiency and response speed, and thus, we use a plastic scintillator on the top to convert X-ray into visible ray. In earth, there are not source of X-ray so we obliged to build one by using an evacuated X-ray tube to trying if our detector is functional or not. And a high voltage is applied to accelerate the electron beam between the cathode and the anode.

We have seen that when the high voltage is applied the short circuit is occur and we were electrocuted.

6.3 X-Ray Detection (Master Thesis Master Thesis Presentation 8.12.21)

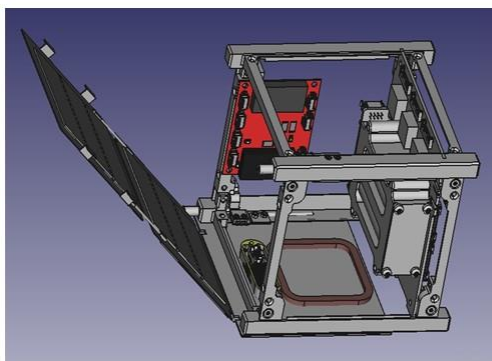


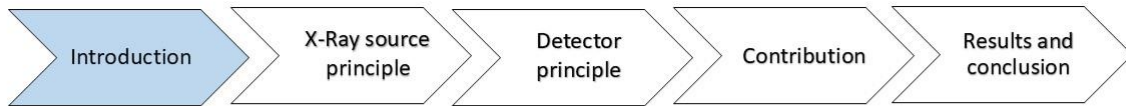
X-Ray detector for Nano satellite IAP-SAT
Presented by Yahya Al Abbouchi
In order to obtain the Research Master of Physics of
Radiation-Matter Interaction

Supervisor :
Dr. Ahmad Osman
Dr. Samir Mourad

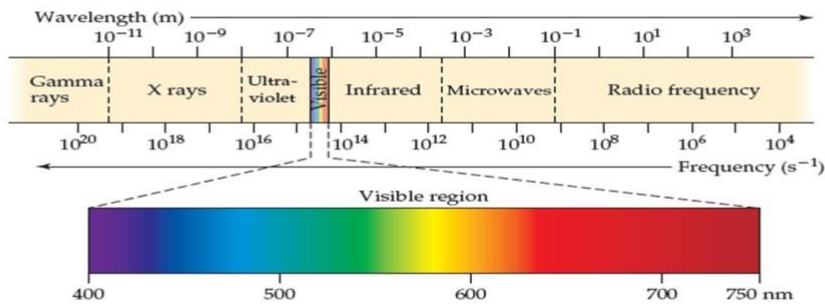
Reviewer:
Pr. Adnan Naja

the goal of building an X-Ray detector is for the purpose of Nano satellites
Launched in space to measure the both of the incident energy and
the intensity to which the Satellite is exposed

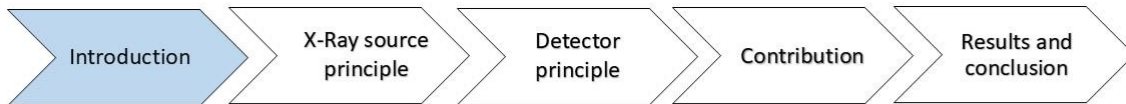




➤ Nature of X-Ray:



- ❖ X-Ray beam is a kind of electromagnetic radiation, in addition , relative to quantum mechanics the electromagnetic radiation can be considered as a set of particles.
- ❖ X-ray energy is measured in eV , where 1 eV is the energy of electron when applied a potential energy equal to 1 VOLT



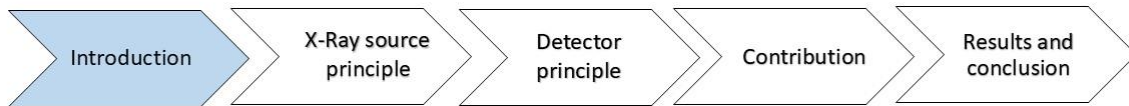
➤ In chapter 1 :

- ❖ We used an evacuated X-ray tube consist of aluminum filament as cathode and copper rod as anode.
- ❖ A high potential electric source is applied between the anode and the cathode that will result in electrons being accelerated from cathode to anode.

➤ In chapter 2 :

We will discuss the following title :

- ❖ the concept of solid state detector.
- ❖ An organic scintillators to convert the X-Ray into visible light.
- ❖ The type of radiation-matter interaction : photoelectric effect
And Compton scattering effect .
- ❖ The PIN photodiode used.
- ❖ The relation between the intensity and the mass coefficient attenuation.

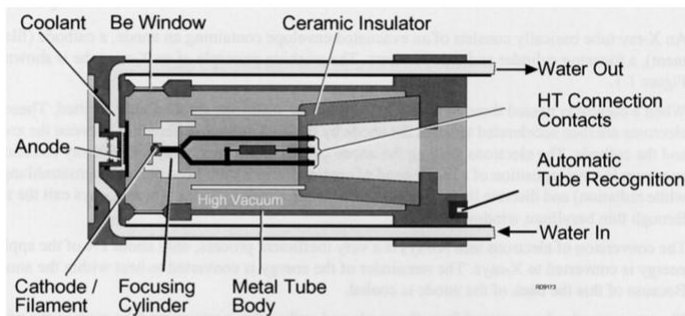
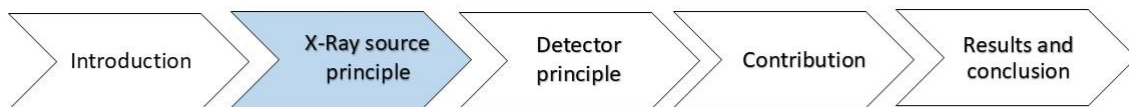


➤ In chapter 3 :

- ❖ A Cockcroft-Walton (voltage multiplier circuit) to achieve a high voltage around 48 KV
- ❖ Vacuum pump to pump the air outside the glass container
- ❖ Fixing all the parts together (source , vacuum pump , Cockcroft-Walton circuit)

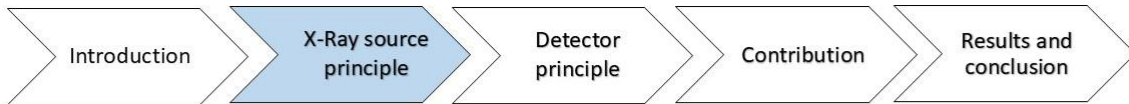
➤ In chapter 4 :

- ❖ We was analyze the light detected by the photodiode using MATLAB

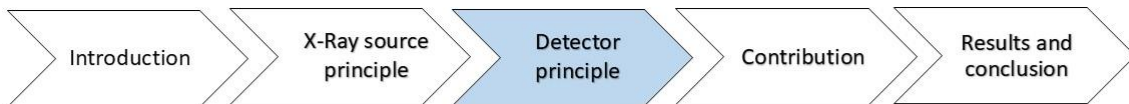


- ✓ As the energy is very high, 99% of input energy will lost as heat
- ✓ We must have to passing water through the anode to protect it from melting

- ✓ X-Ray source are created by bombarding a copper target with electrons inside a device known as X-Ray tube
- ✓ In X-Ray tube, the electron beam can flight from the cathode to the anode by applying a high
 - ✓ potential up to 60 KV

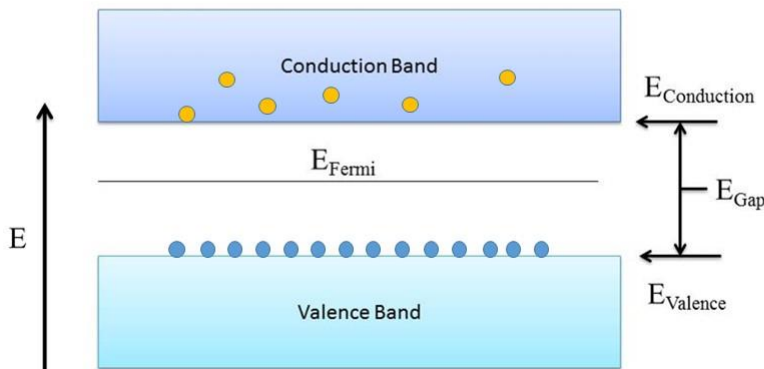


Anode material	Atomic number	Application
Copper (Cu)	29	Often used for most diffraction testing. Most widely used as anode material.
Moly (Mo)	42	Often used for testing on steels and metal alloys with elements in the range Titanium (Ti) (Z = 22) and Zinc (Zn) (Z = 30) as higher atomic number.
Cobalt (Co)	27	Suitable for ferrous samples, the Iron (Fe) fluorescence radiation it causes interference and cannot be eliminated by other way.
Iron (Fe)	26	Testing of ferrous samples. Again for use with metals instead of Co and Cr tubes in case we can't use.
Chromium (Cr)	24	Used for complex organic materials as well as strong radiative measurements on steel.
Tungsten (W)	74	Mostly used where the intense white spectrum is more important than the characteristic.

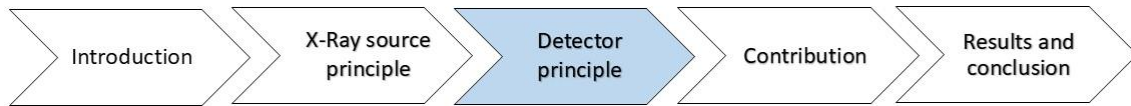


➤ Concept of solid state detector :

- Are manufactured from semiconductor materials that exploit the small gap between the valence band and conduction band.
- Silicon materials are the most widely used in detectors.

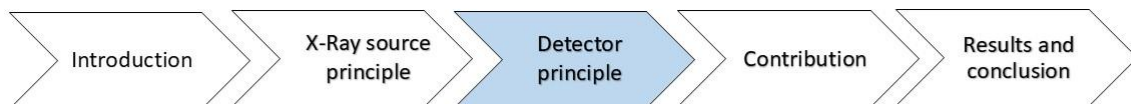


- An incident sufficient energy can ionize electrons from the valence Band to conduction band

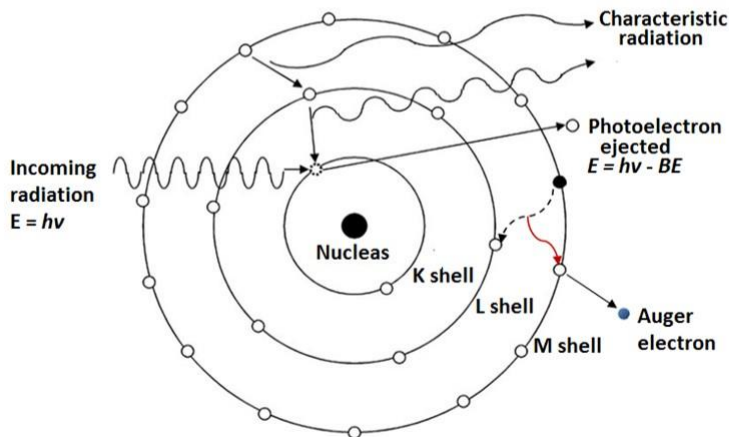


➤ Interaction X-ray with matter:

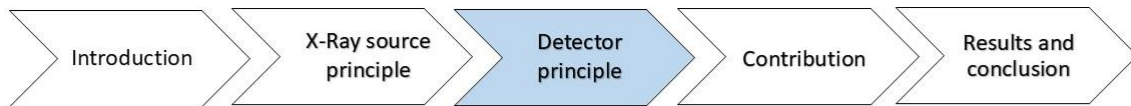
- ❑ Usually, in this type of work there are two kind of interaction :
photoelectric effect and Compton scattering effect.
- ❑ Compton scattering is dominate if $E > 55 \text{ K eV}$ and the photoelectric effect is the main contribution if $E < 55 \text{ K eV}$.
- ❑ In this thesis the max voltage is 48 K eV , so the Compton scattering is out of scope.



➤ Photoelectric effect :



The photon can be completely absorbed by the atom, their energy lead to the ejection Of an electron if that energy is bigger than binding energy

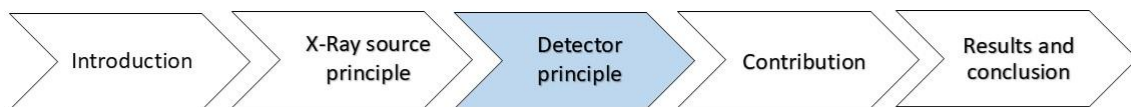


➤ Scintillators :

- ✓ Scintillators are materials can absorbed radiation and transform it to detectable visible or near visible light
- ✓ There are two type of scintillators : organic (plastic , liquid) and inorganics (crystals)

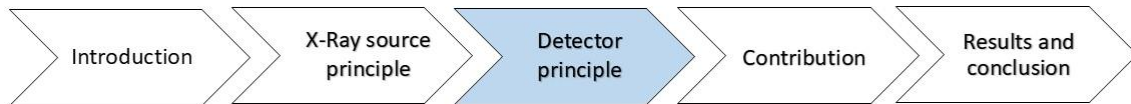
Comparison between organics and inorganics :

	Atomic number (z)	Density (g/cm ³)	Light yield (ph/Mev)	Detection efficiency	Energy resolution
Nal (Tl) (Crystal)	Z= 53	3.67	38000-55000	High detection efficiency	High energy resolution
Plastic scintillator	Z= 6	1	10000	Low detection efficiency	Low energy resolution

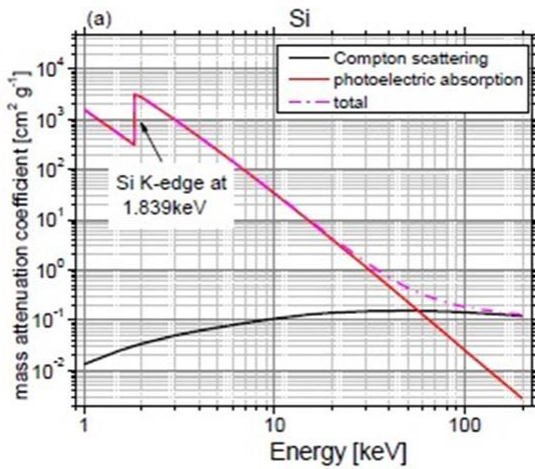


➤ Photodiode :

- ❖ The principle of the photodiode has a depleted semiconductor region
- ❖ For enhance the time response we need a thin depletion region and for achieve A high quantum efficiency the depletion region must be thick
- ❖ We use the PIN photodiode because the depletion region can be tailored To optimize the quantum efficiency and speed of response
- ❖ In addition, the PIN photodiode is a special type of p-n photodiode



➤ Attenuation coefficient of silicon :

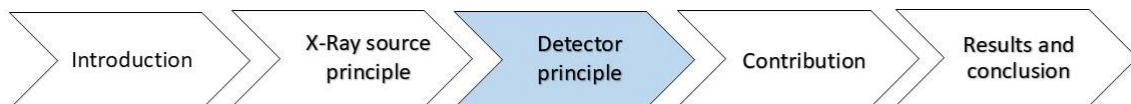


$$\frac{\mu}{\rho} = \frac{N_A \sigma}{M} \text{ (cm}^2/\text{g)}$$

with μ is the linear absorption coefficient with a unit cm^{-1} and ρ is the density of the material. N_A is the Avogadro number and M the molar weight.

The k-edge is the sudden increase in X-Ray absorption occurring when the photon interact With the electron in k-shell

On the other hand, the mass attenuation coefficient is increase when the atomic number Z is increase



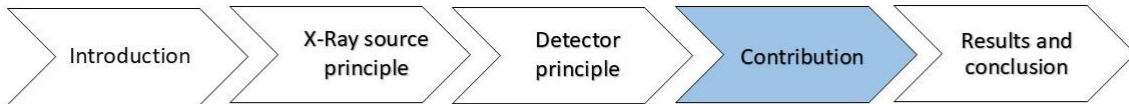
➤ Intensity of X-Ray :

When x-rays encounter any form of matter, along the thickness x , after the distance dx into the body, the X-rays intensity becomes decreasing because it's partly transmitted and partly absorbed.

$$\frac{dI}{dx} = -\mu I$$

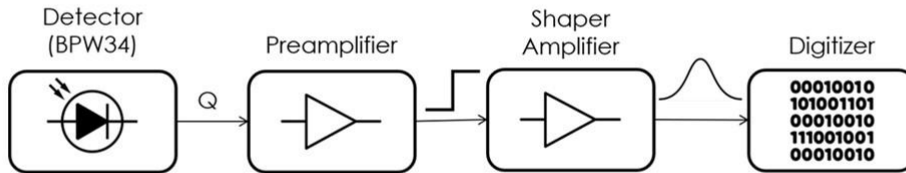
After integration along the direction x :

$$I = I_0 e^{(-\mu/\rho)\rho x}$$

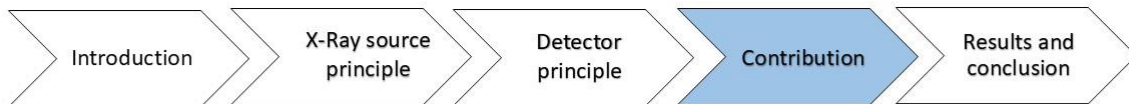


➤ X-Ray detector amplifier

The PIN photodiode (BPW34) have low-voltage input signal and have to be amplified
Via an extremely low-noise preamplifier.

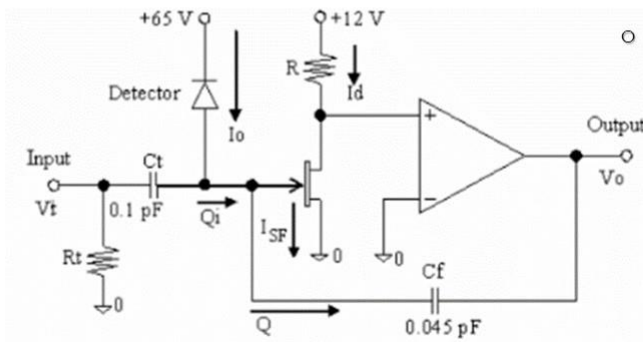


A shaping amplifier is used to make a reasonable signal shape that can be processed
And interpreted by a microcontroller

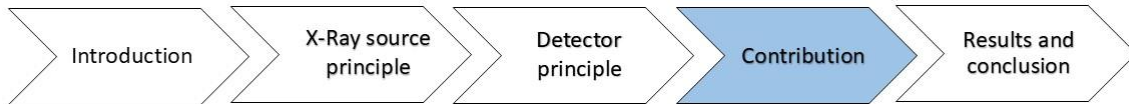


➤ Preamplifier design :

- After many experience to avoid noise, the preamplifier circuit design is shown in this figure below .



- A JFET transistor should be used at the output of the detector with low capacitance junction To collect the charges from the detector .



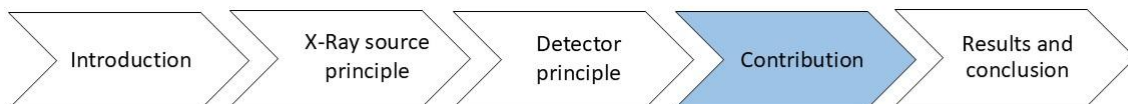
➤ X-Ray source container :

in this thesis the x-ray source consist of a vacuum tube including:

- ✓ An aluminum filament from a bulb light (cathode)
- ✓ A copper rod from air conditioners (anode)
- ✓ The support used for anode is also used to pump the air outside the glass container



- ✓ The vacuum pump used has a rating of 600 torr
Which is 79% of vacuum



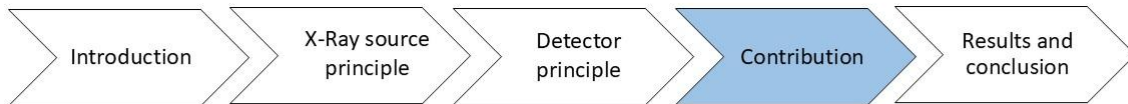
➤ Glass container :

At first, a cubic shape container was used but it could not stand the pressure difference.



So instead of this we use a circular shape with a thickness of 3 mm can support the 79% of vacuum.



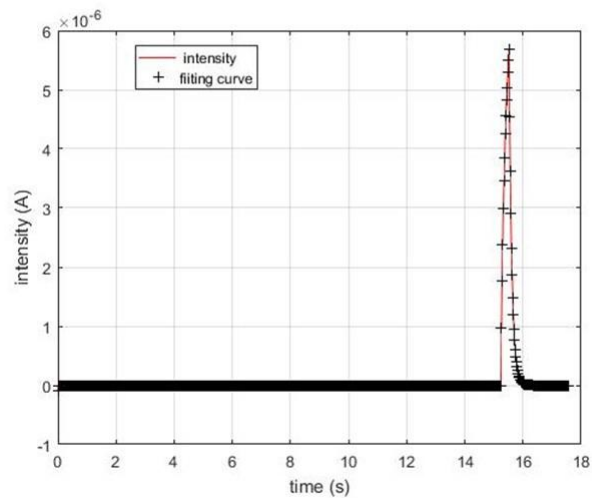
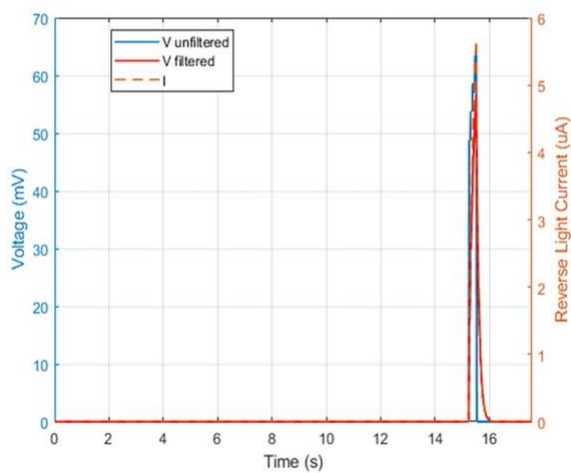
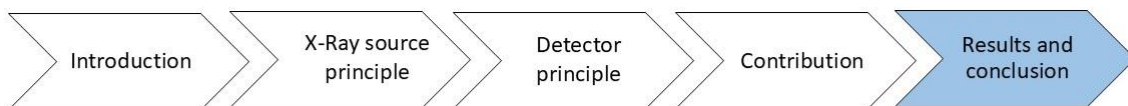
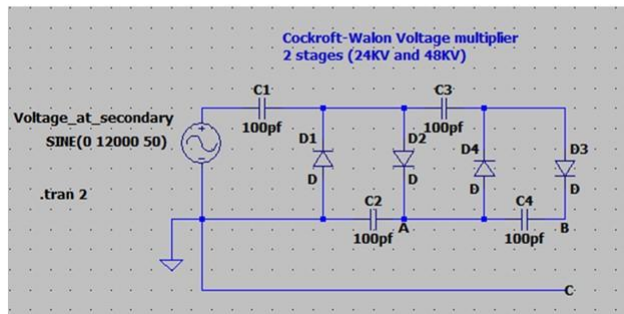


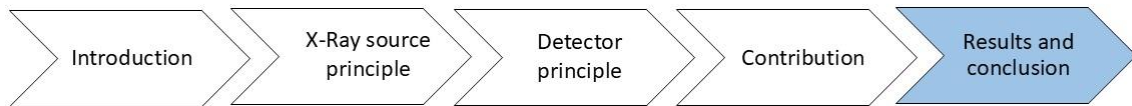
➤ **Transformer :**

In order to obtain 48 KV as an output voltage a step-up transformer 220V /12kV has been used

➤ **Cockcroft-Walton voltage multiplier:**

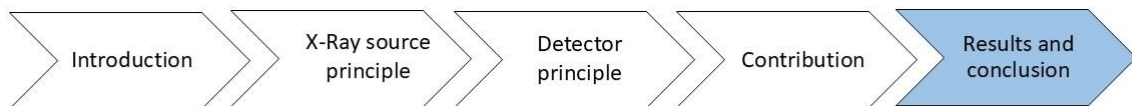
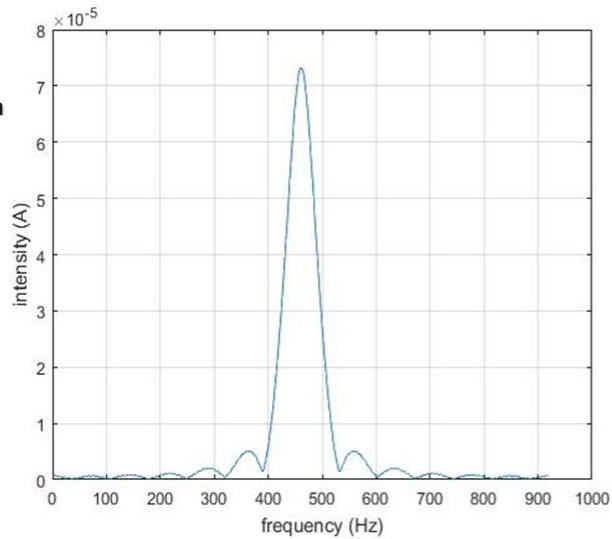
- ❑ The input of Cockcroft-Walton circuit is came from transformer which is 12KV
- ❑ The Cockcroft-Walton circuit is an electric circuit which convert low AC voltage Into high DC voltage





➤ **Fourier transform :**

As shown as in this fig. the frequency is of an order of 10^2 which mean the incident Radiation it's not an X-Ray



➤ **Conclusion:**

- We need a vacuum pump achieved 90% vacuum at least.
- High voltage up to 60 KV
- Reduce the distance between the cathode and anode to 3 cm instead of 35 cm
- Use a tungsten anode rather than copper anode
- Passing water through the anode to protect it from the melting
- A rotating anode can save the target for the long time

Note : the first three condition is enough to achieve an X-Ray radiation.

Thx for your attention

6.4 Introduction

In this thesis, an X-Ray detector device will be designed and implemented for Satellite purpose. The system is responsible to detect the quantity and intensity of X-rays on a satellite launched in the space.

An X-Ray beam is a kind of electromagnetic radiation which is the interference of electric field and magnetic field, both of which are propagated perpendicular to each other. As we know, the difference between all types of electromagnetic radiation lies in the wavelength and frequencies. On the other hand, relative to quantum mechanics the electromagnetic radiation can be considered as a set of particles that flight at speed of light and known as photons. [8]

The X-Ray energy is measured in electron-volt (eV), where 1 eV is the energy of electron when applied a potential energy equal 1 volt.

In chapter 1, naturally, we need a source to provide X-Ray and to give us the opportunity to conduct this experience. Accordingly, we used an evacuated X-Ray tube (most widely used) consist of aluminum filament (cathode) and copper rod (anode). To generate an electron beam inside the x-ray tube, a potential difference is applied then transform it into power in range of 35 to 60 kV.

In chapter 2, it include the concept of solid state detector, usually formed from semi-conductor materials(silicon the most widely used) and in this master thesis we used a PIN photodiode as detector to enhance quantum efficiency and response speed. In addition, we used an organic scintillators to convert the X-Ray into visible light (inorganics are better but more expensive), in this process the radiation-matter interaction can take place. Subsequently, in energy range = [1-150 keV] two types of interactions can occur: photoelectric effect, Compton scattering effect.

Also, the intensity will decrease while interaction because of the higher atomic number Z which in relation with the mass absorption coefficient of silicon, will discuss that in the chapter below.

In chapter 3, in order to obtain 48 KV as an output voltage, we should to use a transformer 220V/12KV, then will introduce the Cockcroft-Walton (voltage multiplier circuit) that convert low AC to high DC, In this thesis we use two stages of cockroft-walton each one consist two capacitors and 2 diode and finally in this way can achieve 48 KV.

Vacuum pump used has a rating of 600 torr while we need to 760 torr to achieve 100% vacuum. Will combine all parts together (source, vacuum pump , transformer , Cockcroft Walton) and will show the practical design procedure of the X-ray Source and detector. In addition to the hardware implemented and testing.

In chapter 4, the result will be obtained by turning on the high voltage where the detector is placed below the source on the same side of the anode. Thus, we use data reduction software (MATLAB) to analyze the spectrum we obtained and transform it to the frequency domain to make sure if the light detected is an X-Ray.

6.5 Source

X-ray sources are created by bombarding a tungsten target with electrons inside a device known as the x-ray tube.

An x-ray tube is a vacuum tube that converts electrical input power into x-rays, the tube must have: source of electrons, high voltage, metal target (often tungsten)

6.5.1 X-ray tube process

As pointed out by Coolidge in 1913, the filament tube is the most common type of laboratory X-ray source, the electron beam can fly from the cathode (filament) to the anode (target) by applying a high potential (up to 60 kV) between them. Once the electrons hit the target, it causes x-ray energy to be released from the metal's atomic structure. As the energy is very high, 99% of input energy will be lost as heat.

For this reason, we must have to pass water through the anode to protect it from melting (without water the tube can be damaged in seconds). [6]

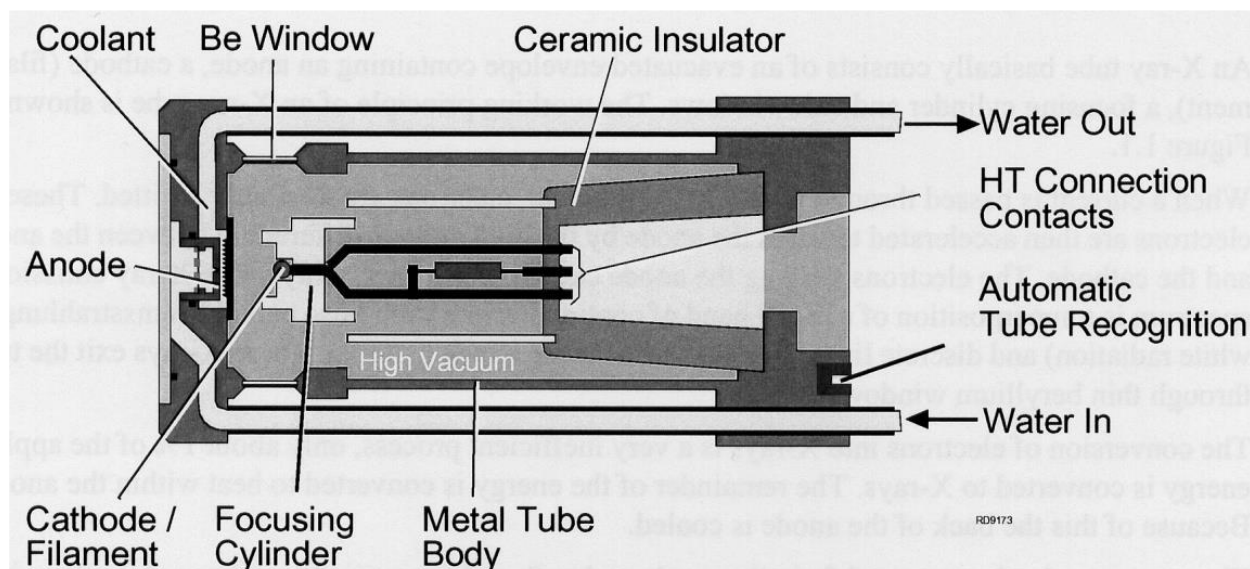


Figure 10: Component of X-ray tube.

6.5.2 Selection of XRD Tubes According to Anode Material :

Anode material	Atomic number	Application

Copper (Cu)	29	Often used for most diffraction testing. Most widely used as anode material.
Moly (Mo)	42	Often used for testing on steels and metal alloys with elements in the range Titanium (Ti) (Z = 22) and Zinc (Zn) (Z = 30) as higher atomic number.
Cobalt (Co)	27	Suitable for ferrous samples, the Iron (Fe) fluorescence radiation it causes interference and cannot be eliminated by other way.
Iron (Fe)	26	Testing of ferrous samples. Again for use with metals instead of Co and Cr tubes in case we can't use.
Chromium (Cr)	24	Used for complex organic materials as well as strong radiative measurements on steel.
Tungsten (W)	74	Mostly used where the intense white spectrum is more important than the characteristic.

Table 1: Comparison between different anode materials.

6.6 Detector

6.6.1 Concept of solid state radiation detectors:

Most of solid state detectors (SSDs) are manufactured from semiconductor materials that exploit the small energy gap between the both of the valence band and the conduction band. Hence, an incident sufficient energy can ionize electrons from the valence band to the conduction band creating holes . when applying an external electric field, the generated electron are produced a signal by drifting the electron and consequently the passage of an ionizing particle can be detected by collecting all the change carriers released by the energy deposition in the semiconductor. Since, the interaction between photons and matter is exploited the fundamental notion underlying the detection process is the x-ray interaction with matter.

The different types of this interaction in a range of energy equal to 150 KeV will be listed below:

6.6.1.1 Interaction of X-rays with matter :

In general, the most important variable that characterizes the X-ray radiations' penetration and diffusion is the probability per unit of path length. Where, a photon will interact with the body, which is commonly known as the attenuation coefficient " μ ". This quantity depends on the both of photon energy E and atomic number Z of the body. When the atom is exposed to radiation in the energy range 1~1000 keV, two types of interactions can occur: the photoelectric effect and the Compton Scattering effect. A pair production processes can take place at energie higher than 1022 Kev . However, such an energy level is out of scope in this thesis. For Si, the main contribution

to the attenuation coefficient comes from photoelectric process at energy $E < 55 \text{ KeV}$. As the energy increases, Compton scattering is dominates.

6.6.1.2 Photoelectric effect:

In this process, the photons can be completely absorbed by the atom, their energy lead to the ejection of an electron in condition of that energy must be larger than binding energy B_e . This process is known as “photoelectric effect”. The ejected electron is emitted with a kinetic energy equal to the difference between the both of incident photon energy and the binding energy of the electron:

$$K_e = E - B_e$$

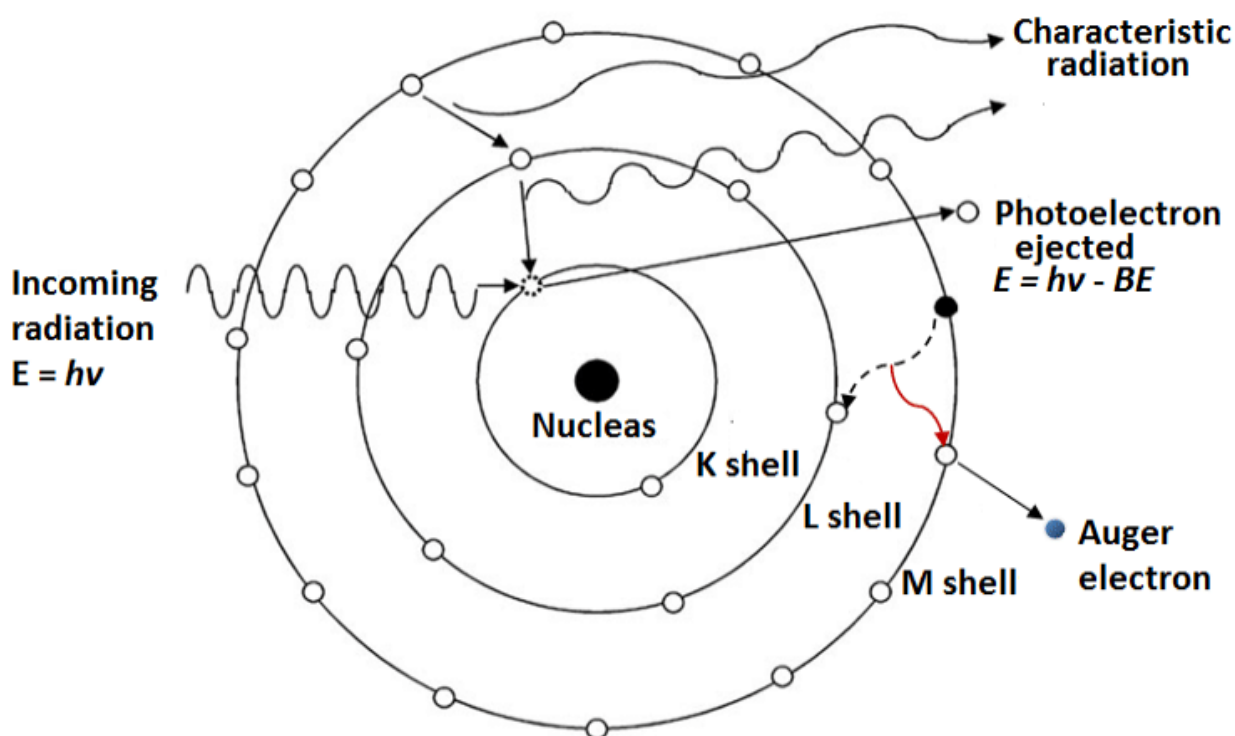


Figure 11: Principle of photoelectric effect.

2.1.4 Compton effect:

In 1927, Arthur Compton observed that when the incident photon energy “ E ” is much larger than the binding energy of the K-shell electron “ B_e ”, then, the ratio B_e / E can be neglected. Therefore, Compton discovered that, when the photon scatters after a corpuscular behavior of the incident photons on individual electrons, the binding energies of these electrons do not affect the interaction. Hence, this last can be ignored. This effect is known as “Compton scattering”. Furthermore, it is classified as an inelastic process. The following equation, below, describes the Compton effect mathematically:

$$E' = \frac{E}{1 + \epsilon(1 - \cos\theta)}$$

when the photon with energy E striking a quasi-free electron, this electron is scattered with an angle θ with energy E' , with $\epsilon = E/MC^2$. The Compton electron recoils at an angle θ' with energy $Ee' = E - E'$ that may adapt to any value between 0 and the so-called Compton edge, the backscattering energy. The specter of energy is continuous due to the secondary interactions with other atoms is measured through the detector. [1]

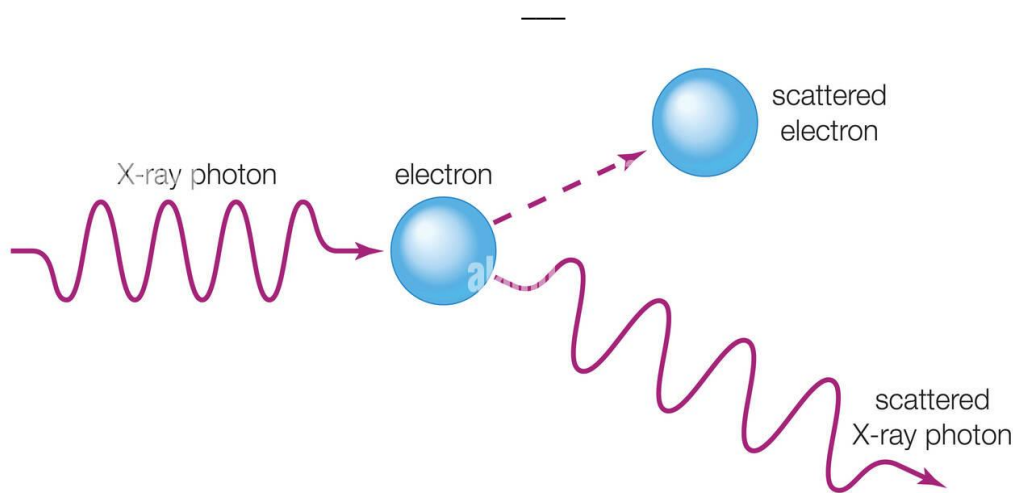


Figure 12: Principle of Compton effect.

6.6.1.3 X-ray intensity :

When x-rays encounter any form of matter, along the thickness x , after the distance dx into the body, the X-rays intensity becomes decreasing because it's partly transmitted and partly absorbed. The decrease in intensity is given by:

$$\frac{dI}{dx} = -\mu I$$

After integration along the direction x :

$$I = I_0 e^{-\mu x}$$

Where I and I_0 successively is the transmitted intensity and the initial intensity of the beam. Often, instead of μ , the mass absorption coefficient will be μ/ρ with ρ is the density of the body. Then: [8]

$$I = I_0 e^{(-\mu/\rho)\rho x}$$

6.6.2 Scintillators

Scintillator is a specific material that allows to absorb radiations and incident striking particles. Then, these absorbed radiations will be transformed into detectable visible or near-visible light photons.

Hence, into electric signal. Scintillator is used for many applications, specially that requires high energetic particles, or for indirect detectable hard x-ray applications.

There is two different types of scintillators: organic, and inorganic. It depends on the mechanism of light emissions and on the forming material of it. Organic scintillator is an aromatic hydrocarbon compounds containing a benzenic cycle. For instance, naphthalene ($C_{10}H_8$), and anthracene ($C_{14}H_{10}$) are classified as organic scintillator. While, inorganic scintillator is ionic crystals doped or undoped with an activator. For instance, $NaI(Tl)$, and $CsI(Tl)$ are classified as inorganic scintillator. This last one has a lattice effect as a mechanism of it. Where, the electrons in the valence band are bound at the lattice sites, while those in the conduction band are free to move throughout the crystal. If the incident radiation transfers sufficient energy, the electrons in the valence band can reach the conduction band leaving holes behind, the passage of ejected electrons through the crystal may ionize the crystal. If the incident energy is not sufficient, the electron of the valence band will not reach the conduction band and will form a bound state, called exciton, with the hole. [1]

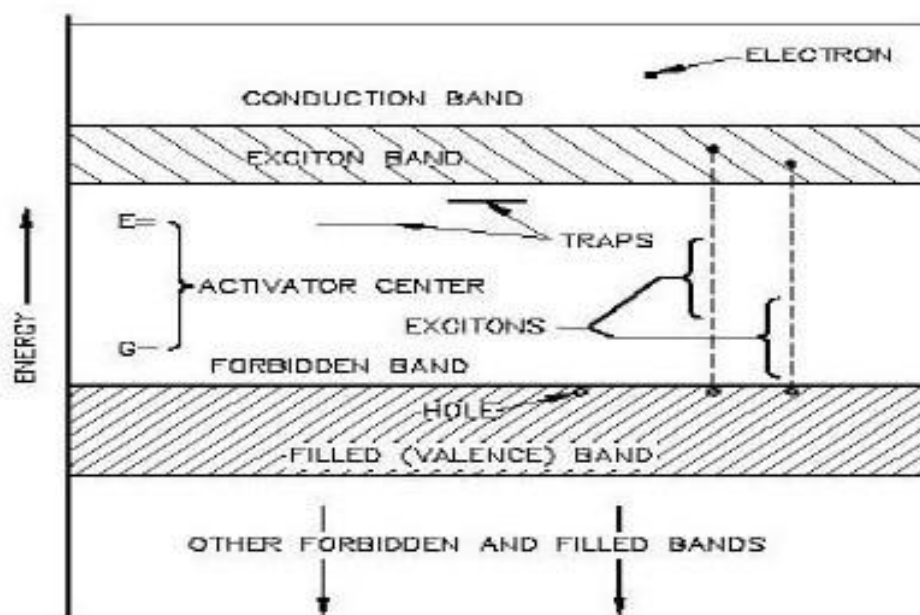
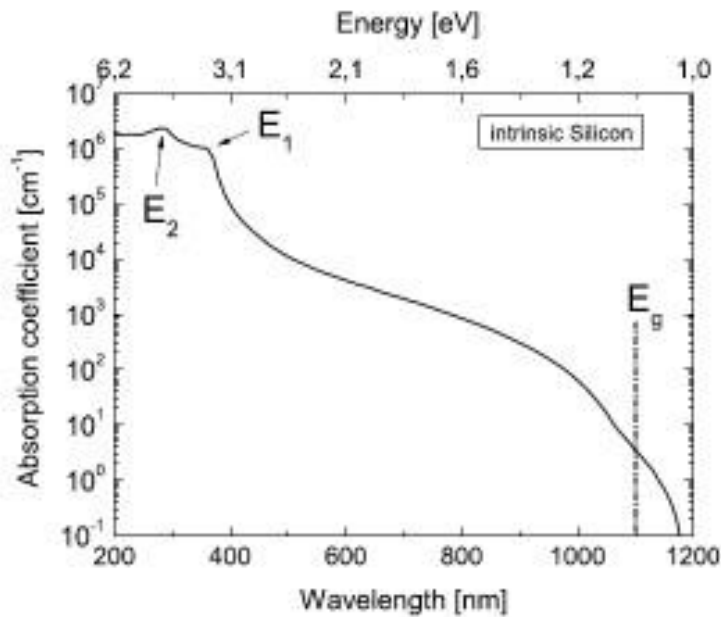


Figure 13: Electronic energy band of an inorganic scintillator doped with an activator

6.6.2.1 Detection of the Scintillation Light:

In order to understand how the scintillation light will be detected. The silicon properties, especially its band structures, should be known. When the system conserved its total energy and momentum, a photon absorption between different bands through an electronic transition will occur. Precisely, the interaction of photons with silicon occurs by the electrons excitation from the impurity states, into higher energy states (if it is available). In addition to, the probability of the excitation within the same band. Furthermore, there is a phenomenon, related to what had aforementioned, called "Van Hove singularities", that occurs when the conduction's joint density of the states and the valence band reach their maximum, for certain photon energy. In addition to that, when two regimes with an excitation energy E_1 , and E_2 meet the Van Hove singularities conditions. Then, the characteristic points of silicon absorption are at $E = E_1$ and E_2 . [1]



6.6.2.2 Optimization of the scintillator for indirect detectors:

As pointed out in [Martin, 2006] a scintillator for high resolution X-ray imaging should fulfil the following requirements:

According to Martin, 2006. To obtain a high X-ray resolution from a scintillator, firstly, the atomic number (Z) should be above 50 to maximize the efficiency of photon absorption, plus, the density should be higher than 5 g/cm^3 . Secondly, the wave length of the emissions have to well matched by photodiode, and the quantum yield should be greater than 15 photons/Kev . In addition, the scintillation efficiency should be linear with the X-ray flux, and the afterglow should be smaller than 4 decades of magnitude in 2 milliseconds. Finally, a good mechanical strength should be possessed, with the priority to for non-toxic and machinable ones. [2]

6.6.2.3 Ilastic Scintillators:

In contrast of inorganic, There are many organic materials scintillate upon irradiation. also, some organic scintillators have a crystal forms (e.g. anthracene and naphthalene), while the large number of organic scintillators are in form of liquids or plastics. They for the most part contain various aromatic compounds in the matrix, whose electronic states in π -molecular orbitals are promptly excited by traversing radiation to make excitons. consequently, excitons are captured by incorporated fluors and decay radiatively with visible photons generated.

Comparing with crystal scintillators, plastic scintillators presents a better radiation hardness and the environmental tolerance, which fits the outfield applications. Their quick response is adequate for the radiation flux measurements

In the other hand, plastic scintillators has some disadvantages such as the poorly light yield which equal to $10000 \text{ photons/MeV}$, a non-linear ionization energies, a low stopping powers and photoelectric peak ratio, due to the effectiveless atomic number ($Z \cong 6$) and the low density of polymer in it ($\sim 1 \text{ g/cm}^3$). In addition, this type of scintillators has no resolution information, that is needed for gamma-ray spectroscopy.[3]

6.6.2.4 Comparison between plastic and crystals scintillators

I. Energy resolution :

is amount of optical photons emitted per MeV of energy received by the crystals, and it depends with the intensity of the light yield (photons / MeV). And since the light yield of crystals scintillators is higher than plastic scintillators, the result is that the energy resolution of crystals scintillators is better.

II. Detection efficiency :

It is a function of the ability to attenuate photons and is expressed in terms of the mass absorption, which is proportional to the density and the atomic Z number. Same that energy resolution, the detection efficiency of crystals scintillators are better than the last one.

III. Quantum efficiency :

it means that how many photons will be stopped by the detectors, if scintillator is irradiated by an incident beam. For more detection efficiency, and a better energy resolution, the materials of high atomic number and high density is recommended.

Table 2: Comparison between the organics and inorganics scintillators

	Atomic number (z)	Density (g/cm³)	Light yield (ph/MeV)	Detection efficiency	Energy resolution
Nal (Tl)	Z= 53	3.67	38000-55000	High detection efficiency	High energy resolution
Plastic scintillator	Z= 6	1	10000	Low detection efficiency	Low energy resolution

6.6.3 Photodiode:

The principle of the photodiode has a depleted semiconductor region and the consequently separation of electrons and holes by the electric field. For fast detector requirement, we need to thin depletion region (time resolution). In contrast, to achieve a high quantum efficiency (the number of electron-holes pairs generated per incident photon) the depletion region must be thick enough so that a large part of the incident light can be absorbed. In addition to the reverse bonding between the quantum efficiency and the time response. Otherwise, in the visible and near-infrared wavelength range, photodiodes are typically reverse biased with moderate biases, as this reduces the carrier transit time and the diode capacitance (time resolution). However, for sure the reverse bias is below the breakdown voltage. [4]

6.6.3.1 p-n photodiode:

P-N photodiode has many important features. For instance, it has fast time response, noise equivalent power (NEP), and the quantum efficiency. Furthermore, when the depletion layer is striking by a flux of photon, with a generation rate equal to G_0 , then, a photo-generated current will take place and added to the diffusion current. [4]

6.6.3.2 PIN photodiode:

There are many type of p-n junction photodiodes used in this situation but the special one is the p-i-n photodiode detectors and is the most-common photodetectors used ,because the depletion zone thickness (the intrinsic layer = space charge) can be tailored to optimize the quantum efficiency and speed of response. [7]

6.6.3.3 p-n junction:

The difference of fermi levels in P-N junction cause a surplus carries' diffusion to the other material, until thermal equilibrium. In this situation, the fermi levels will be merged. Therefore, the remaining ions will create a depletion zone (a stable space charge region), where the electric field will stop further diffusion.

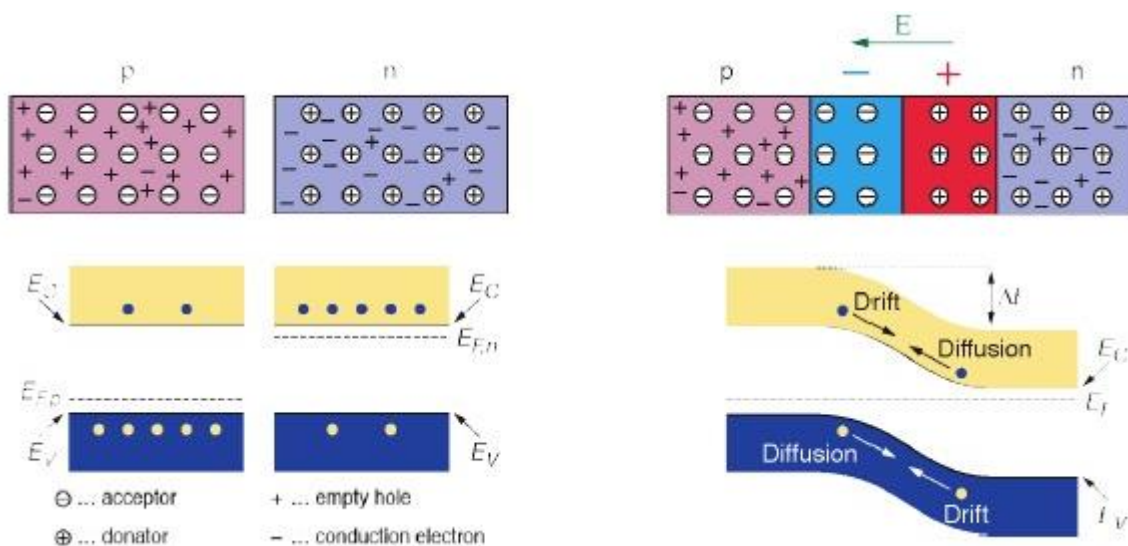


Figure 14: p-n junction process

When an external voltage is added. Where the cathode is connected to P side, and the anode for n side, the electrons and holes will be pulled out of the depletion zone. Thus, this zone will be enlarged, and the potential barrier will be higher (high electron volt). Hence, the diffusion across the junction will be suppressed, and the current will be reduced (known as “leakage current”). [5]

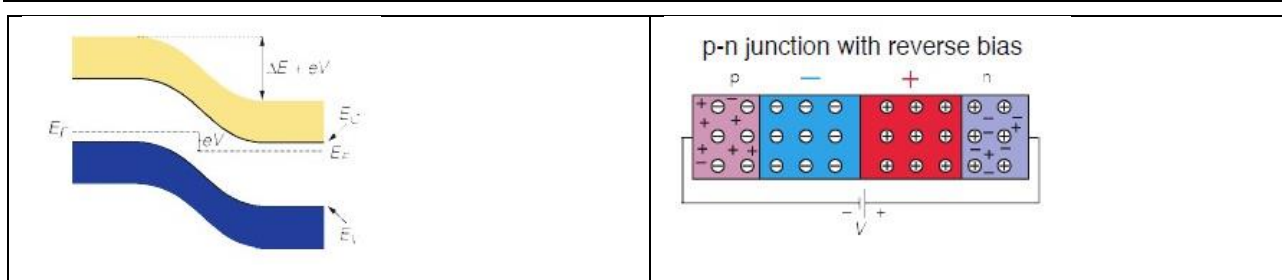


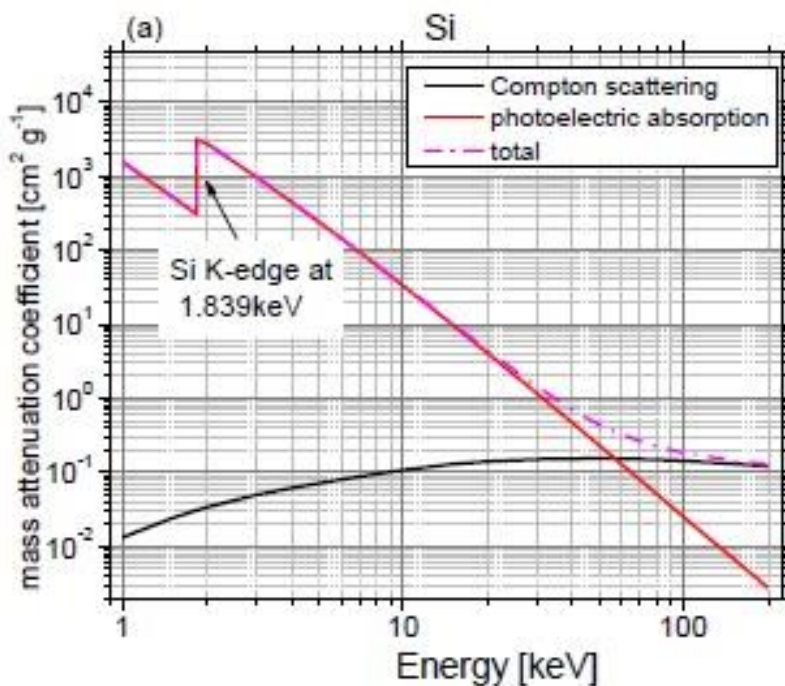
Figure 15: Reverse bias and p-n junction and energy diagram

6.6.3.4 Attenuation coefficients of Si:

In X-ray transport and the deposition of the photo energy calculations, an important coefficient known as “The masse attenuation” should be take into consideration.

$$\frac{\mu}{\rho} = \frac{N_A \sigma}{M} (cm^2/g)$$

with μ is the linear absorption coefficient with a unit cm^{-1} and ρ is the density of the material.



As shown in the figure, the photoelectric effect is the dominant interaction in Si with $E < 55\text{Kev}$. The strong decrease in the mass attenuation coefficient in k-edge at 1839 eV implies limitations in the detection capabilities of hard X-rays. The probability of the photoelectric effect and the Compton scattering are equally important at $E=55\text{ Kev}$. Around 200 keV, the total absorption is done from the compton effect.[1]

6.6.3.5 Characteristics of our photodiode:

- dimensions :Length = 5.4 mm ; Width = 4.3 mm ; height = 3.2 mm (5.4*4.3*3.2)

spatial resolution

- radiant sensitive area : 7.5 mm^2

- high photo sensitivity
- high radiant sensitivity
- angle of half sensitivity : $\theta = \pm 65^\circ$
- wavelength sensitivity : 430 to 1100 nm

sensitivity

- fast response time
- high speed photodetector

time resolution

Two essential characteristics to avoid destroy the photodiode is:

1. breakdown voltage : $V_R = 60 \text{ v}$
2. operating temperature range : -40 to 100 °C

The photodiode used is a BPW34 PIN photodiode type that have both of high speed and high radiant sensitivity, clear plastic scintillator on the top. It is sensitive to light which have a wavelength in the range of 430 to 1100 nm (visible light and near infrared radiation).

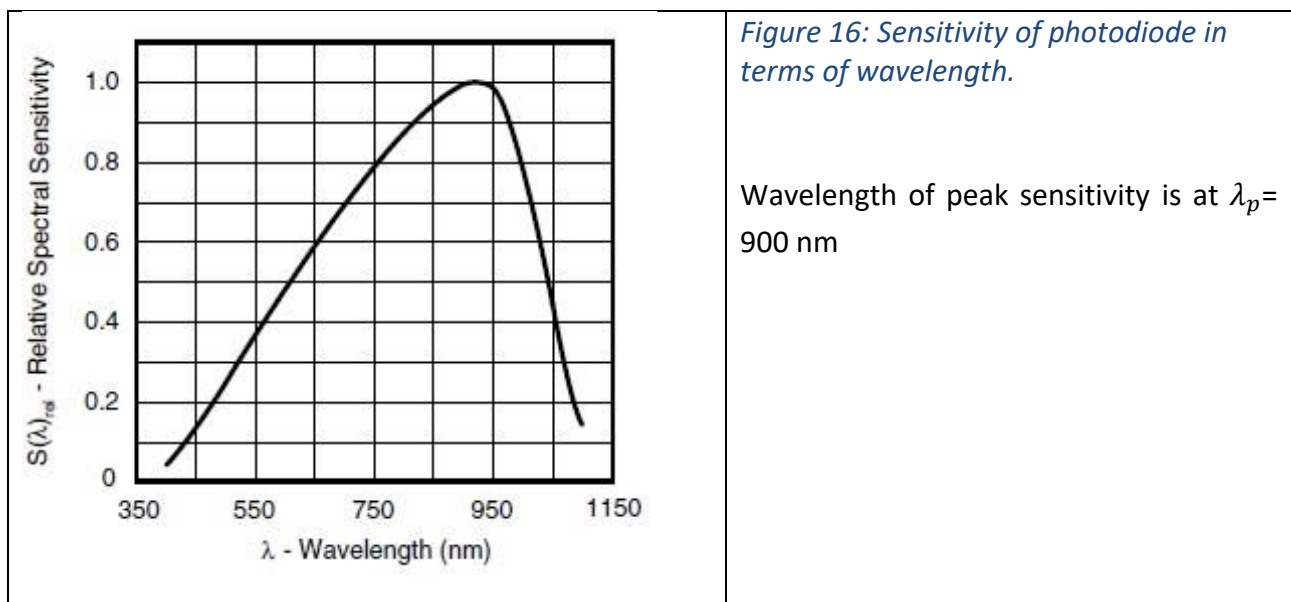
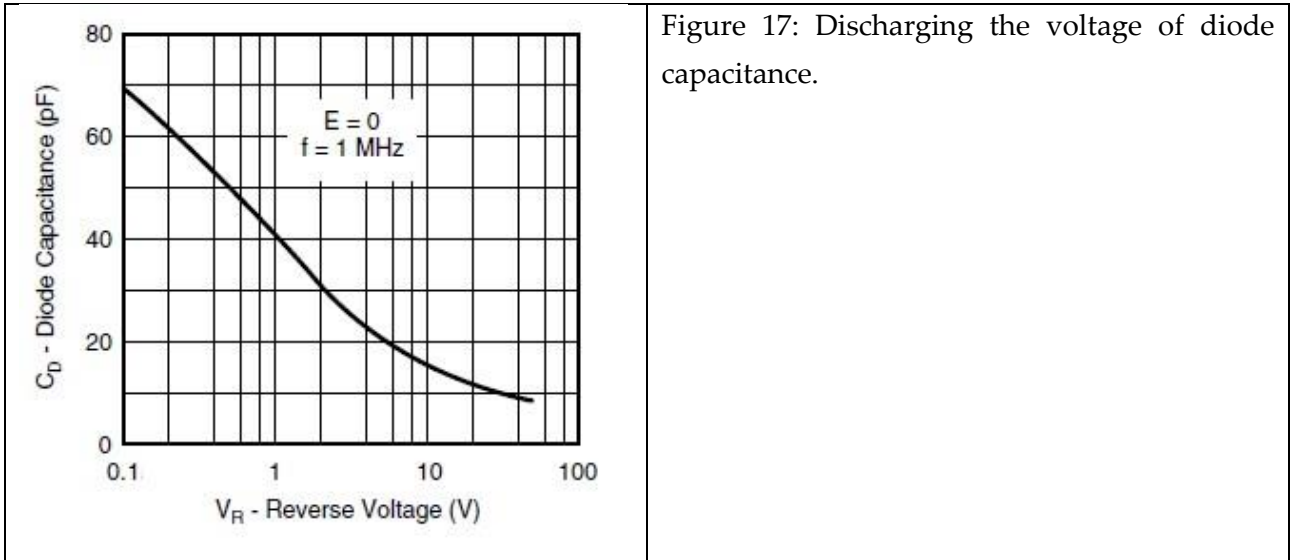


Figure 16: Sensitivity of photodiode in terms of wavelength.

Wavelength of peak sensitivity is at $\lambda_p = 900 \text{ nm}$

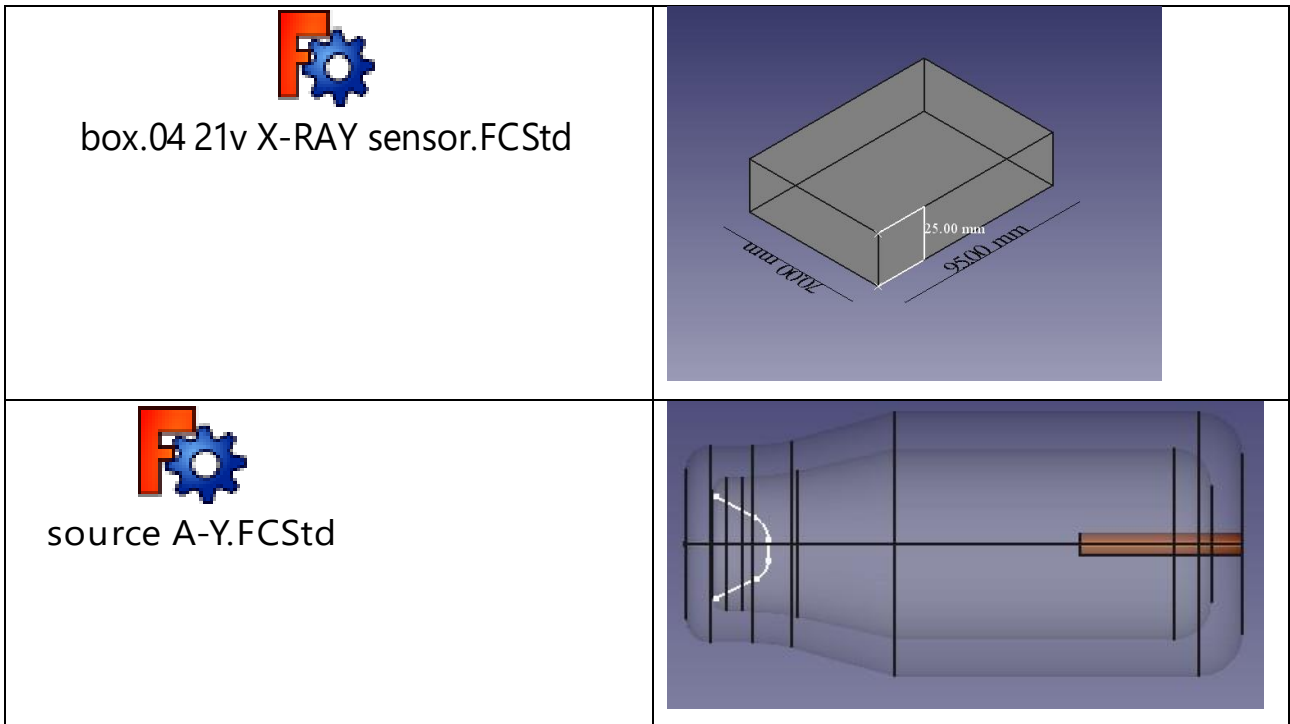
When the incident light is stopped, the diode capacitance will begins to give off its stored energy.



6.7 Realization of X-Ray Sensor in Nano satellite and laboratory testing

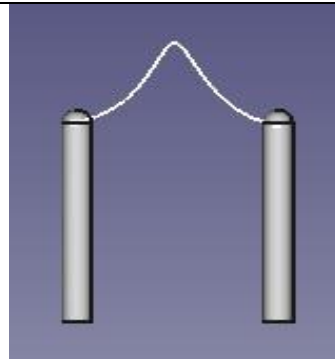
6.7.1 Detector

6.7.1.1 Box of X-RAY sensor

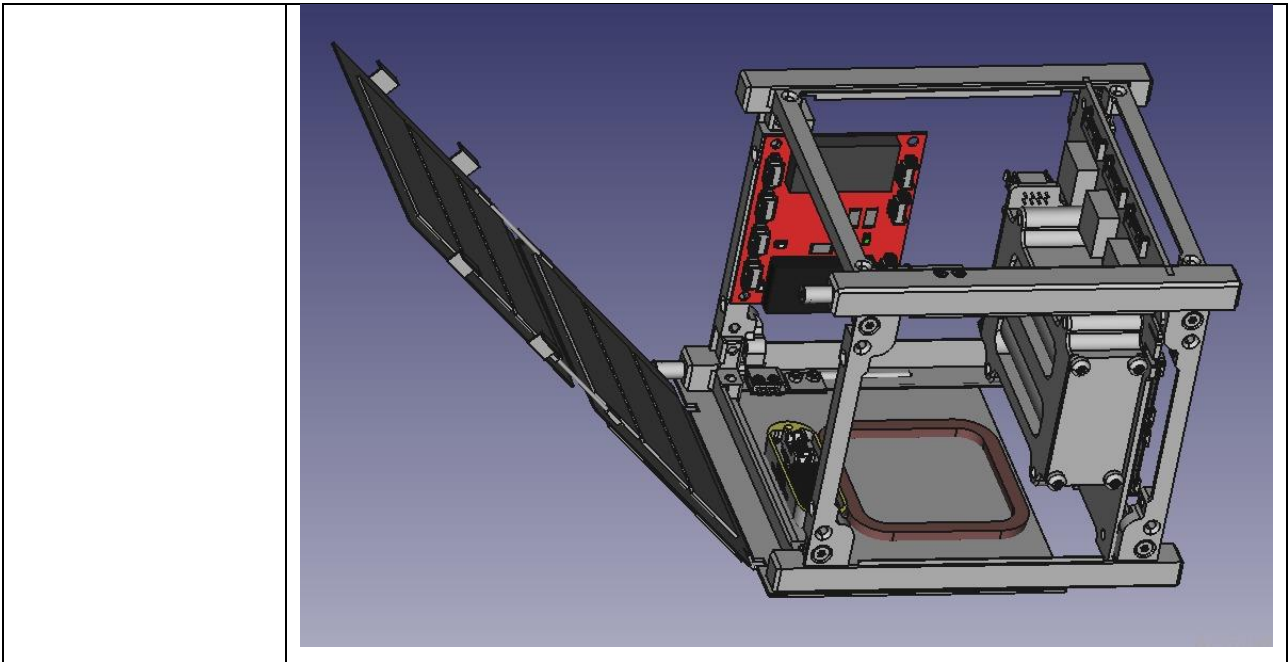




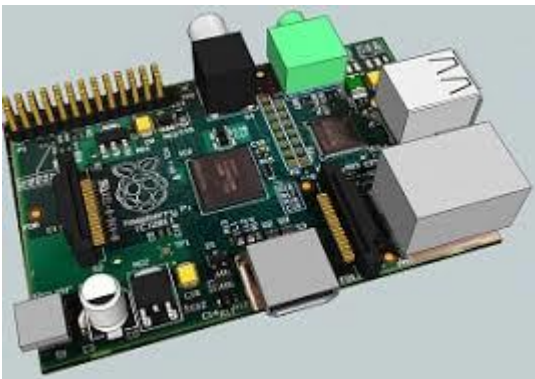
wire.FCStd



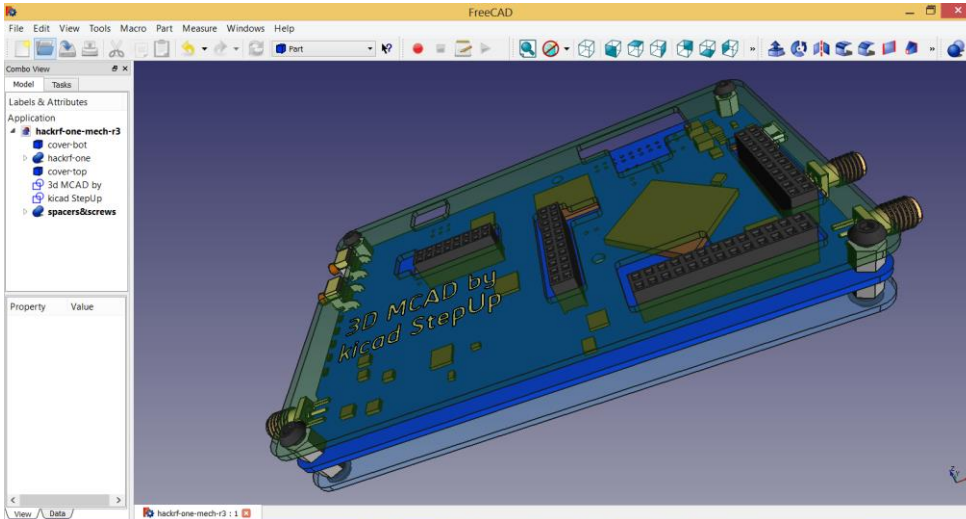
6.7.1.2 Integration of X-Ray Sensor into IAP-SAT:



Data Reduction Software on Raspberry Pi 3:



Communication of Sensor Data to Ground Station with HackRF:



6.7.1.3 X-Ray detector amplifier:

This project will present the design and implementation of an X-ray detector system that is based on low-cost PIN diodes (BPW34). General procedure of designing the preamplifier and shaping amplifier will be presented as well as the practical approach to implement this system.

Typically, the PIN diodes (detectors) have low-voltage output signal and have to be amplified via an extremely low-noise preamplifier. The preamplifier acts as a first stage in a chain of amplifiers that has very sensitive characteristics. Then, a shaping amplifier is used to make a reasonable signal shape that has the shape of a tail which can be processed and interpreted by a microcontroller. An ADC will then be used to transform these analog quantities to digital. figure 11 below shows the overall process of converting input charges from a detector into digital readable signal proportional to input charges.

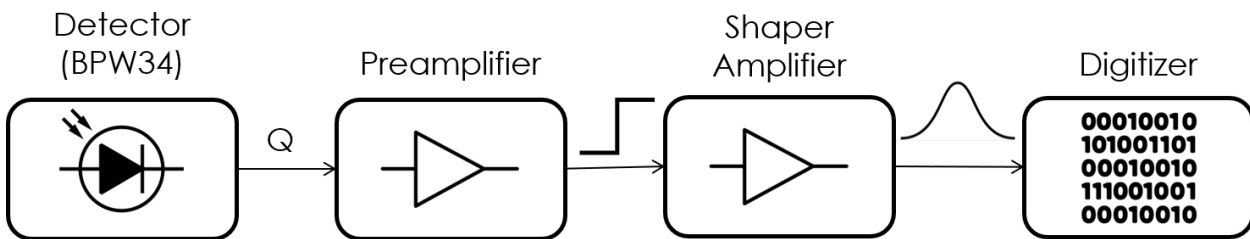


Figure 18: Silicon detector amplification stages

There are mainly 3 types of preamplifiers and are listed below. However, we are just interested in charge-sensitive preamplifiers which are the type used for charge detector applications.

- Voltage-sensitive preamplifier.
- Current-sensitive preamplifier.
- Charge-sensitive preamplifier.

6.7.1.4 charge amplifier

As mentioned before, the PIN diode, when used to detect X-rays, outputs a very weak charge pulse having a pulse width of several tens of nano seconds. Since the detector is can be modeled as a capacitive device, its impedance is high and the preamplifier should be designed according to this criterion. For these applications, an integrator amplifier (using capacitor feedback) is used since it has high impedance, integrates weak charge pulses and converts them to voltage pulses ready for further amplification.

The first stage of charge amplifier (preamplifier) is usually a low-noise FET and its open loop gain must be set high in a way that the second amplification stage is not influenced by the detector capacitance.

When X rays strike into the detector, signal charges Q_s are generated with an amplitude proportional to the particle energy. These signal charges are all integrated in the feedback capacitance C_f (since it can be approximated that the current entering the op amp is equal 0) and then a pulse output $e_{out}(t)$ is generated.

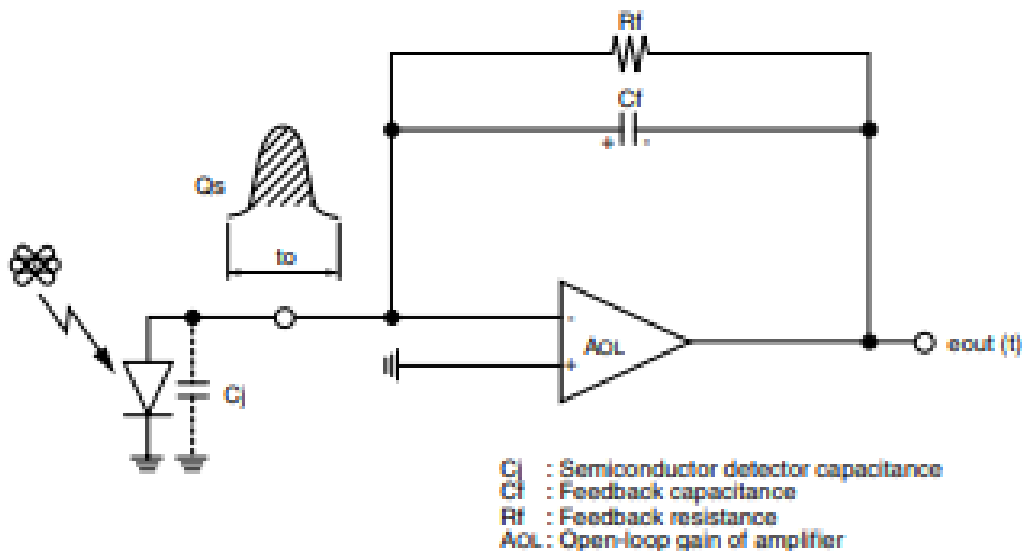


Figure 19: Amplifier circuit of incident power

In general, the following characteristics are required for the design of a good X ray charge amplifier:

- High gain
- Low noise (Excellent signal-to-noise ratio)
- Excellent integration linearity
- High speed rise time
- High temperature stability

6.7.1.5 gain

The gain of charge amplifier is given in 2 ways; amplifier gain alone or the gain for detector/amplifier together. Amplifier gain (G_c) which is also referred to charge gain is given as:

$$G_c = \frac{V_{out}}{Q_s} = \frac{1}{C_f} \left[\frac{V}{\text{Columb}} \right] \text{ or } \left[\frac{V}{\text{picoColumb}} \right] \quad (1)$$

The charge fall time of the amplifier can be determined by the feedback resistance and capacitor.

$$\tau_f = R_f C_f$$

Amplifier with detector gain can be referred to as sensitivity (R_s). Sensitivity is expressed as output voltage mV per one MeV of energy particle irradiated onto the detector. The amplitude of the signal charge obtained with a semiconductor detector is determined by the input particle energy such as X-rays and also by the material of the semiconductor.

$$Q_s = \frac{E \cdot e^-}{\varepsilon} \quad (2)$$

Where, E is the particle energy (MeV), e^- is the elementary charge ($1.6e^{-19}$ C), and ε is the energy required to create one electron/hole pair. For silicon, ε varies between 3.62 eV and 3.71 eV. From equations (1) and (2), amplifier's sensitivity can be written as:

$$R_s = \frac{V_{out}}{E} = \frac{e^-}{C_f} \cdot \frac{1}{\varepsilon} \left[\frac{mV}{MeV} \right] \quad (3)$$

6.7.1.6 Noises:

Noises in charge amplifiers come generally from 3 sources: Thermal noise of first-stage FET, shot noise caused by the gate current of the first stage FET and dark current of the detector, and thermal noise caused by the feedback resistance. The noise of the first-stage FET is given as:

$$en_1 = \sqrt{\frac{8}{3}} \cdot \frac{KT}{g_m} \quad (4)$$

Where, K is Boltzmann constant, T is the absolute temperature in Kelvin, and g_m is the mutual conductance of first-stage FET. The second noise source, shot noises, can be expressed as:

$$in = \sqrt{2q(I_G + I_D)} \quad (A/\sqrt{Hz}) \quad (5)$$

Where, q is the elementary charge, I_G is the gate leakage current of first-stage FET, and I_D is the dark current of the detector. The third and final source of noises can be presented as:

$$en_2 = \sqrt{4kTR_f} \quad (V/\sqrt{Hz}) \quad (6)$$

Where, R_f is the feedback resistance. From equations (4), (5), and (6), the total noise of a charge

amplifier can be written as:

$$en_t(jw) = en_1^2 \cdot \left(1 + \frac{C_{in}}{C_f}\right)^2 + \left[in^2 + \left(\frac{en_2}{R_f}\right)^2 \right] \cdot \frac{1}{(jwC_f)^2} \quad (7)$$

The first term is constant over the entire frequency range and amplified by the noise gain $(1 + \frac{C_{in}}{C_f})$ determined by the input capacitance. The second term component is constant regardless the input capacitance but it decreases with the frequency.

6.7.2 Electrical Circuit Testing with Oscilloscope

6.7.2.1 Experiment 1: I-V characteristics of BPW34 diode:

The I-V characteristics of a photodiode are studied with the same manner of an ordinary diode. The diode is studied under reverse voltage of 12 V to ensure its ionization and with a 100 ohms resistor to measure the current across it using an oscilloscope. A flash light from the phone is used as luminance input.

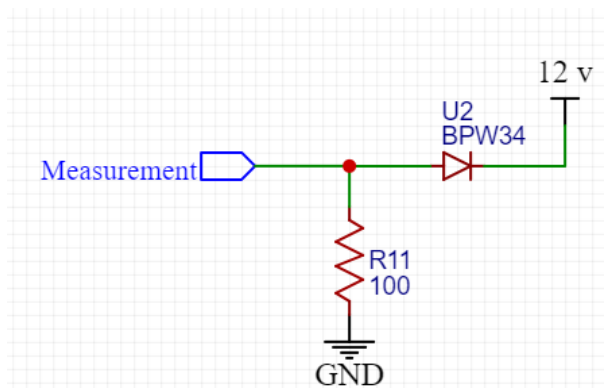
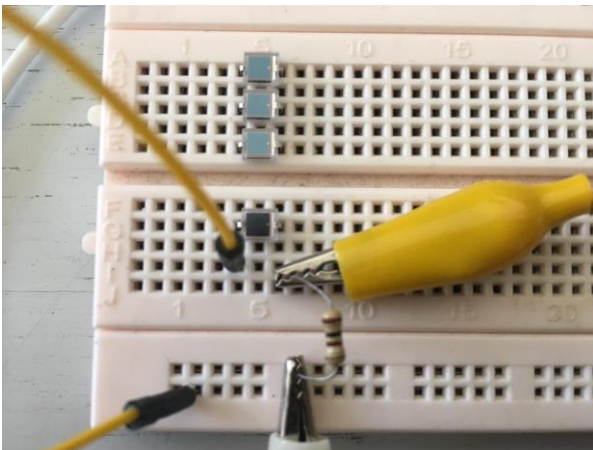


Figure 20: Circuit design of BPW3

6.7.2.2 Experiment 2: Preamplifier Design:

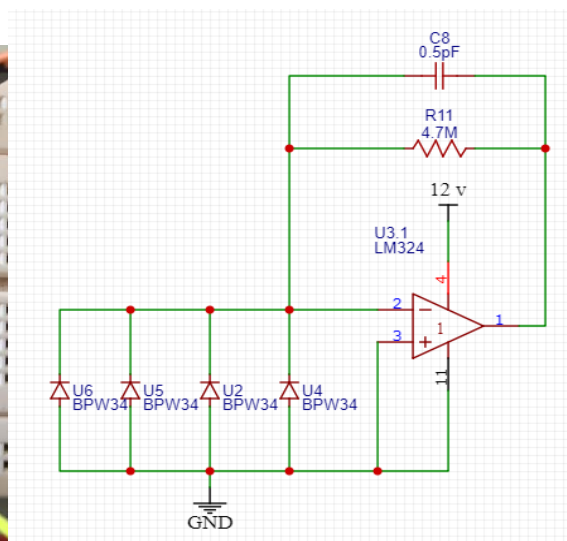
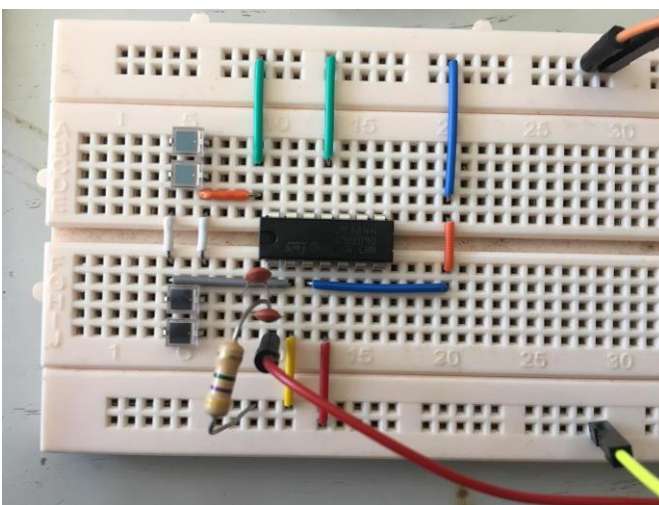


Figure 21: Preamplifier circuit design.

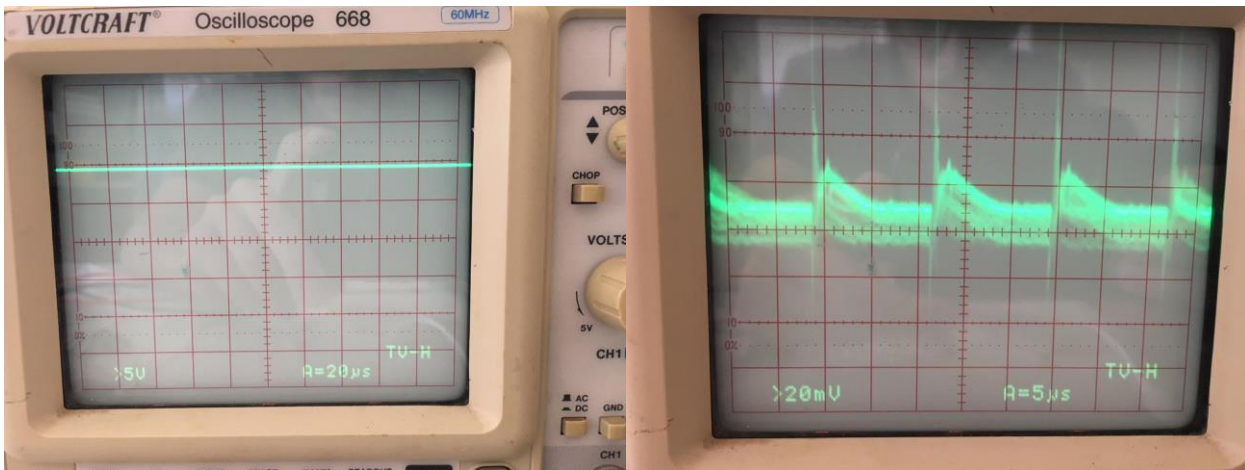


Figure 22: Voltage visualization on oscilloscope.

However, the output is constant (left figure) no matter how much light is presented at the photodiodes. After some modifications, a 10-pF capacitor is mounted between the photodiodes and the operational amplifier and it can be seen from the right figure above a nearly charging and discharging signal shape. **(FAILED)**

6.7.2.3 Experiment 3: Preamplifier Design:

Another experiment was done by presenting a bias voltage for the photo diodes by connecting a voltage divider network into the non-inverting operational amplifier pin. The output can still be seen as very noisy. **(FAILED)**

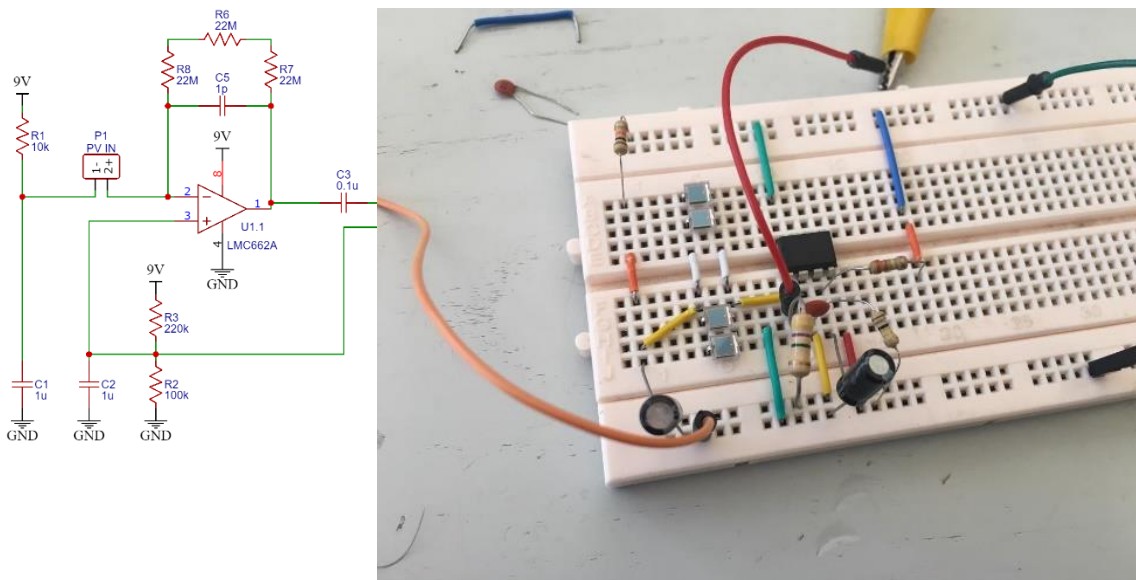


Figure 23: Preamplifier circuit (for another exp).

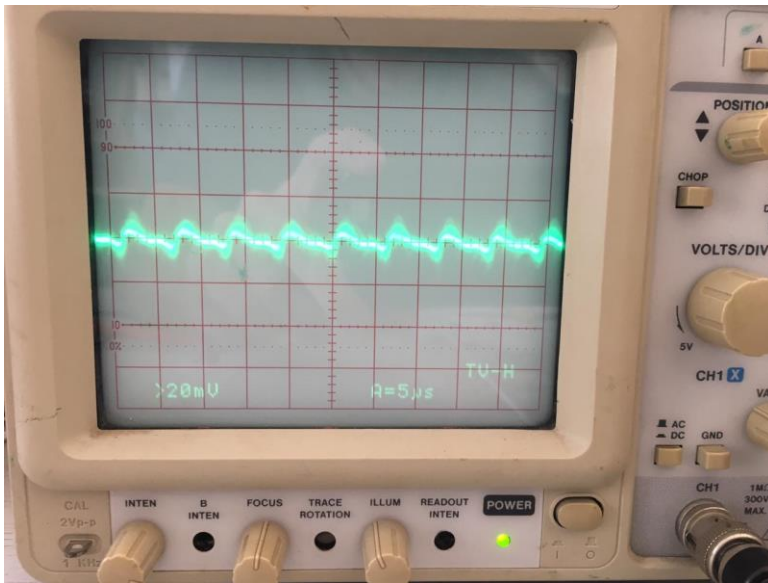


Figure 24: Voltage visualization on oscilloscope for sec exp.

6.7.3 Preamplifier Design:

The previous experiments gave unsatisfactory results due to several reasons, such as:

- A JFET transistor should be used at the output of the detector with low capacitance junction to collect the charges from the detector. JFET transistor suggestions can be: 2N4416, 2SK152, 2N6550.

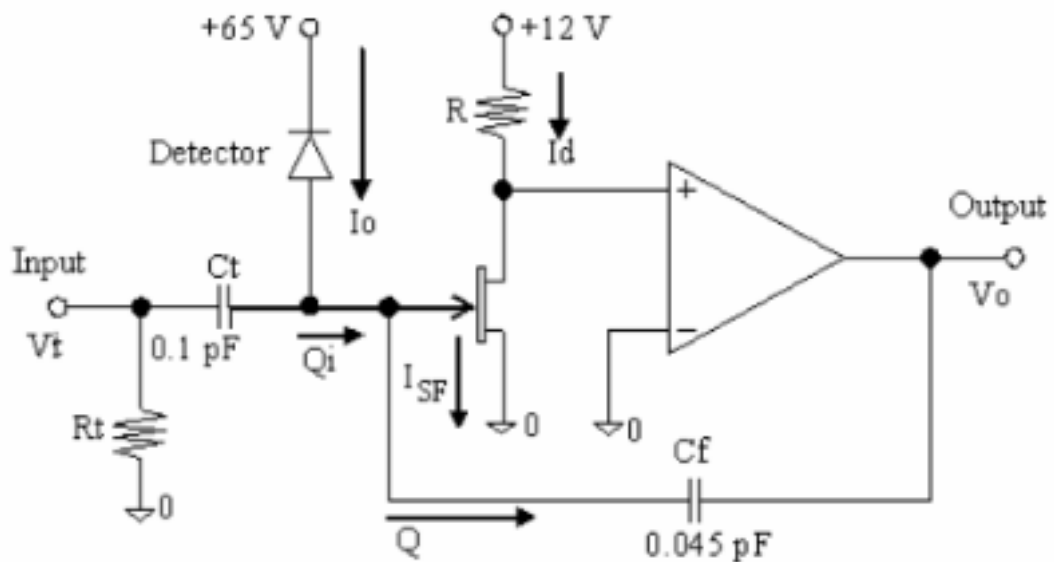


Figure 25: The used preamplifier circuit.

- Another operational amplifier with JFET input should be used such as TLE2072 or OPA324.

6.7.3.1 Monitoring:

Another approach was taken in order to monitor the energy received by the photodiodes. The photodiodes in this experiment were dealt with as current sources. A resistor is connected to the

reverse diodes in order to get a voltage image of the current. An Arduino Uno is used to read the voltage coming from the photo diodes through its analog pin A0 which will be then converted into current.

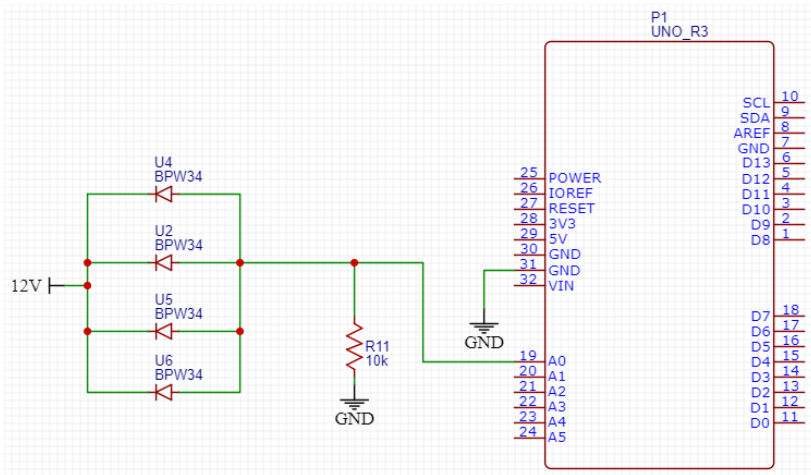


Figure 26: Circuit of the system.

The nominal voltage, when the diodes are exposed to normal room lights, was approximately 750 mV. When an external light source (phone flashlight) is exposed to the diode array at a distance of approximately 8 cm, the voltage rises to 1780 mV. A complimentary filter is used to filter out measurement noises which has the following form:

$$V_{filt} = \alpha \cdot V_{filt} + (1 - \alpha) \cdot V_{measured} \quad (8)$$

Where, α is a wheighing constant between 0 and 1 which prefers one variable over the other, where it was chosen as 0.8. The current is calculated by dividing the output voltage by the load resistance of 10 k ohms.

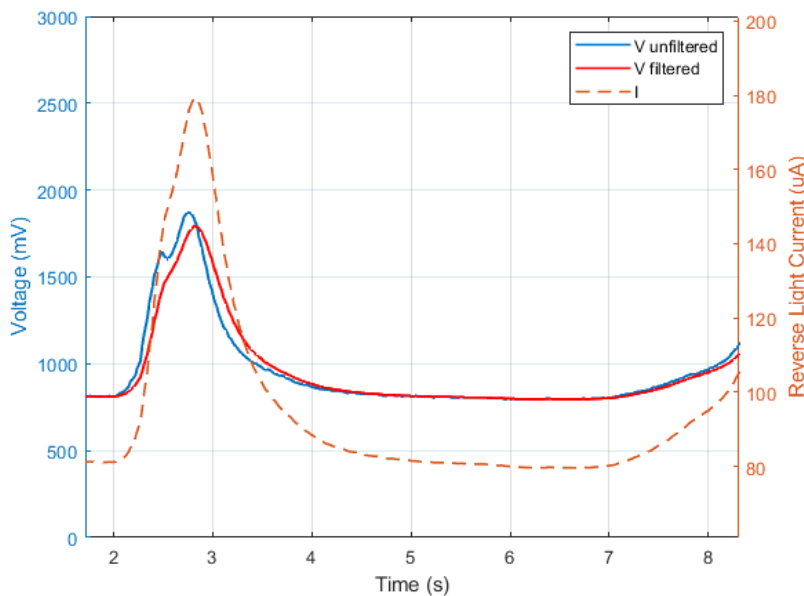


Figure 27: Testing diode for the visible light.

This experience depends on visible light by using flash light to make sure the diodes is working.

The light intensity, at this stage, can be calculated from the current graphs given by the datasheet of the BPW34 photodiodes. It is noteworthy that there are 4 diodes connected in parallel so the current is added.

6.7.4 Testing X-ray sensor with X-ray source

6.7.4.1 X-ray source overview, Parameters of our system

The X-ray source consists of a vacuum tube including an a tungsten filament as cathode and a copper rod as anode (or any element having an atomic number between 20 and 80). A high potential electric source is applied between the anode and the cathode that will result in electrons being accelerated from cathode to anode. Once the electrons hit the anode at high speed, x-rays are generated. The basic requirements used for building the x-ray test stand are:

Parameter	Value
Vacuum pump pressure	600 torr
Anode to cathode voltage	48 KV
Filament voltage	24 DCV
Cathode Material	Aluminum
Anode Material	Copper
Container	Glass
Container dimensions	50 cm length and 6 cm diameter

Table 3: Parameters of our system

Where a pressure of 760 torr represents 0% air inside the tube or 100 % vacuum. The used vacuum pump has a rating of 600 torr which is $\frac{600}{760} = 0.789$ or approximately 79% of vacuum.



Figure 28: Vacuum pump, 600 torr.

The cathode filament that is used to generate a cloud of electrons is nothing but a bulb light filament that is heated up by a DC voltage of 24 V (12 V didn't work) which will generate 200 mA of DC current passing through the filament.

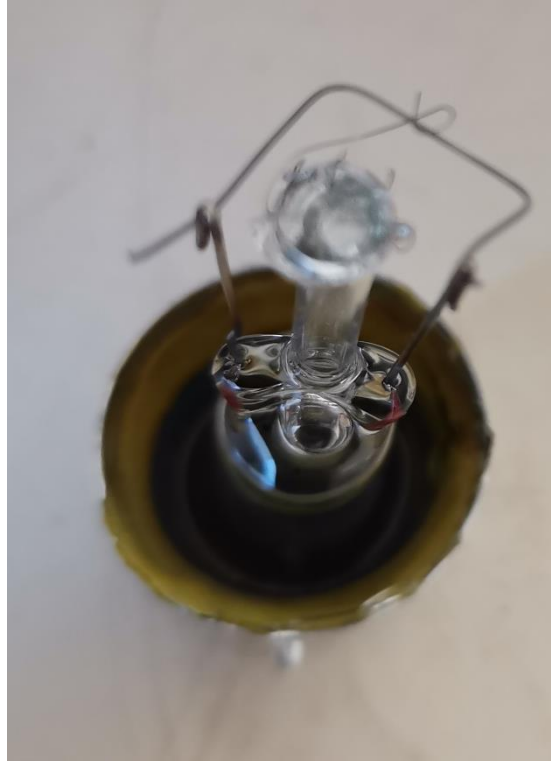


Figure 29: The cathode filament (tungsten).

The anode used is a copper rod from Air conditioners. Tungsten anode is much preferred but it is not available. Numerous support screws are used to fix the anode in place. The supports used for the anode are also used to pump the air outside the glass container.



Figure 30: Cooper rod used as anode.

6.7.4.2 The glass container - rectangle vacuum container was destroyed, circular tube was ok

At first, a cubic-shape glass container was designed to have a cubic-shape of 40x6x8 cm in dimensions. Once everything is fixed in place, the vacuum pump is ON.

After we turn on vacuum pump, the glass container is broke because the difference between atmosphere pressure and the inside pressure (evacuated region) becomes important.



Figure 31: Rectangle glass container

A circular-shaped glass container is now used with a thickness of 3 mm. Everything is fixed in place using silicone.

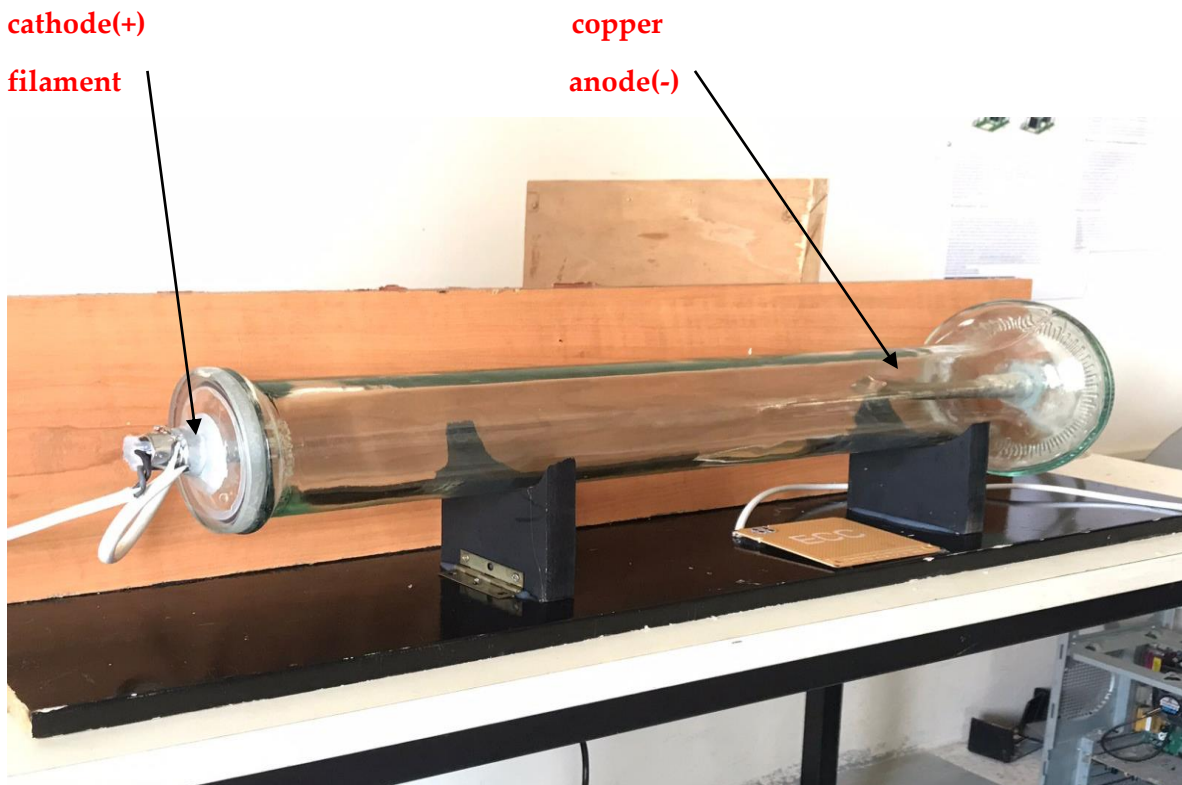


Figure 32: Cylindrical glass container that support 79% of Vacuum.

6.7.4.3 Cockcroft-walton voltage multiplier

There are many uses of high voltage DC power supply. High DC voltage is mainly used in the industries where the requirement of high dc power is necessary. High DC voltage power is widely used in research work in the field of applied physics and for testing purpose in industries. High voltage is used for dielectric and insulation testing of electrical equipment at power frequency. There are many applications of High voltage DC power in electrical engineering such as electron microscope, x-ray, electrostatic precipitators, particle accelerator, etc. Dielectric behavior of electrical equipment can be tested by giving high voltage DC supply as an input to them, where the surviving capacity of equipment can be tested at all conditions. The voltage given to the equipment should be greater than the normal DC voltage to find out equipment's sustaining capability of voltage and decide the voltage margin for the particular equipment.

The circuit Cockcroft Walton generator or voltage multiplier is an electric circuit which generates DC power at high voltage. This circuit was discovered much earlier by Heinrich in 1919. The circuit got named after the British and Irish physicist John Douglas Walton and Earnest Thomson Walton, who first used this circuit in 1932 to power their particle accelerator.

The main importance is given on designing of Cockcroft Walton Generator circuit, and its hardware implementation. It is a two stages voltage multiplier circuit having 220V AC as an input supply and 48 kV DC as an output voltage. The entire work is categories into two main stages. First stage deals with generation of high DC voltage using multiplier circuit and second stage deals with conversion of high DC voltage into standard pulse. Then, a hardware implemented of circuit is done in the laboratory.

6.7.4.4 voltage multiplier circuit

As the name suggests, the Cockcroft-Walton is a voltage multiplier circuit which has a multiplication factor of two. A voltage multiplier is an electrical circuit that converts low AC voltage into high DC voltage. It is made of a voltage multiplier ladder network of capacitors and diodes to generate high voltages.

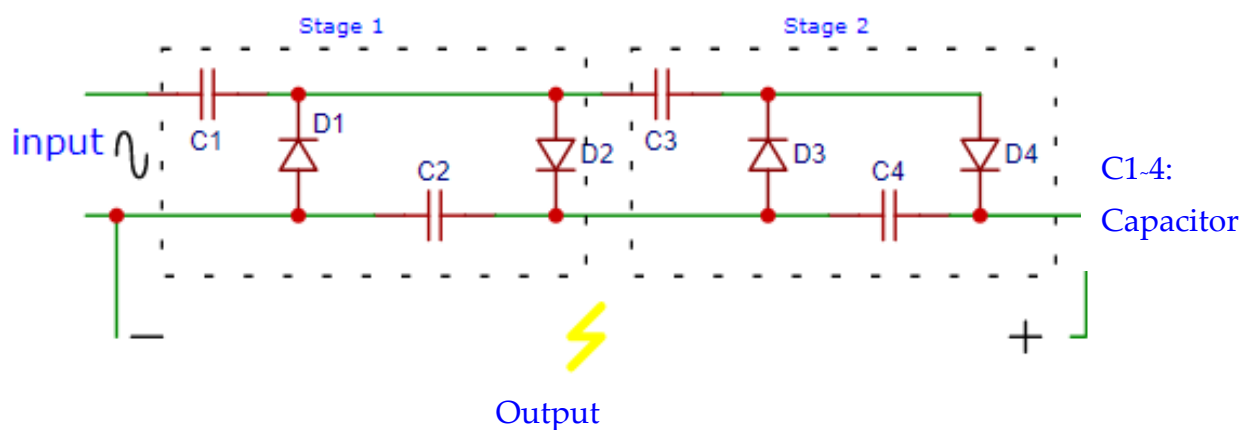


Figure 33: Basic voltage multiplier circuit of 2 stages

The above circuit shows a basic multiplier circuit which consist of two half-wave rectifier circuits. Through addition of second diode and capacitor, we can increase its output voltage. When the sinusoidal input voltage is positive capacitor C1 charges through diode D1 and when sinusoidal input voltage is negative, capacitor C2 charges through diode D2. The DC output voltage across the final stage presented by equation 1, below.

$$V_o = n \times 2 \times V_{peak} \quad (9)$$

Where, n represents the number of stages, where each stage consists of two diodes and two capacitors as shown figure 24 above.

6.7.4.5 Design criteria :

The design criteria describe the selection of different elements. This includes selection of number of stages for required output, selection of capacitors, selection of diodes.

Number of stage selection :

In order to obtain a desired output level, the number of stages in Cockroft-Walton voltage multiplier circuit should be selected. Therefore, the selection of stages should be accordance with required output voltage, and the voltage drop till last stage. In this work, the voltage drop is too small according to output voltage.

The number of stages is given in equation 2 below in equation (2).

$$n = \frac{v_{out} + V_{drop}}{2 \times V_{peak}} \quad (10)$$

Where:

n= Number of stages

v_{out} = Output Voltage

V_{drop} = Voltage drop till last stage

V_{peak} = Input peak voltage

Capacitors selection :

Generally, the size of capacitors used in the Cockroft-Walton multiplier circuit is directly proportional to frequency of its input voltage. For the frequency of 50 Hz, the selected capacitor is 100pF 30KV (code: 101k 30KV), as shown in figure 27 below. Therefore, it is better to select the capacitor of voltage rating twice (approximately) that of input voltage. In other word, the capacitor should voltage rating of 2 Vmax, where Vmax is the input voltage.

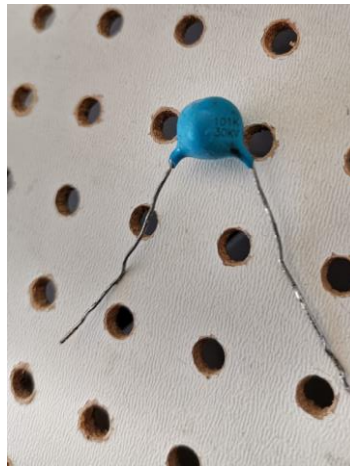


Figure 34: Capacitor 101k 30 kV

Therefore, for high voltage stage, capacitor pins should be good isolated for any potential electric arc. As shown in figure 28 below.

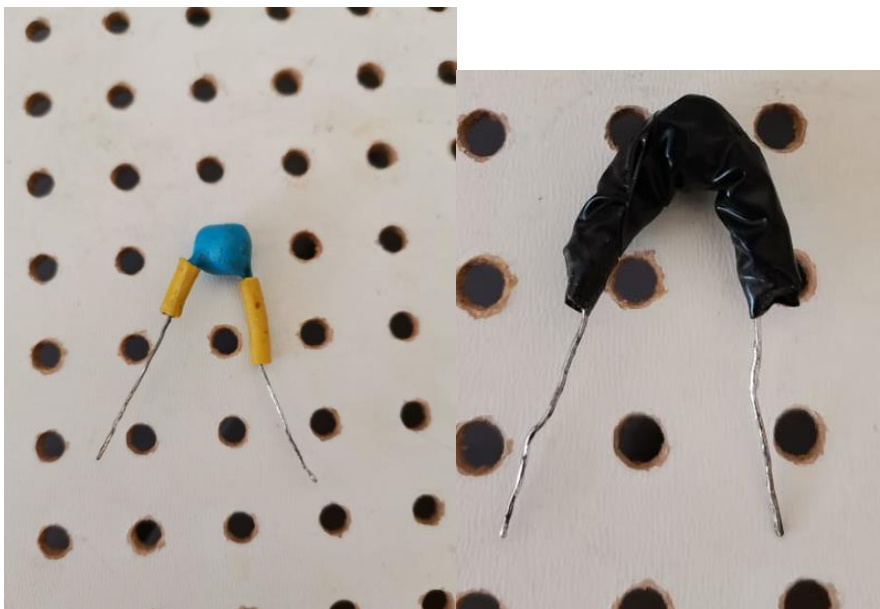


Figure 35: Capacitor isolated pins

Diodes selection:

Selection of diode depends upon maximum reverse voltage across the diode (peak reverse voltage). For safety purpose, the required diode should have 2 V_{max} as voltage rating. The selected diode is 2CLG30KV/0.5A, as shown figure 29. Where the voltage rating of this diode is 30 KV and current rating is 0.5 Ampere.



Figure 36: 2CLG30kV/0.5A

6.7.4.6 Step-up transformer:

In order to obtain 48KV as an output voltage from 220 V of input voltage, a step-up transformer 220/12KV 30 mA has been used, as shown in figure below. In this condition, the considered input voltage of Cockroft-Walton Voltage multiplier is 12KV. In other word, $V_{max}=12KV$.



Figure 37: 220V/12kV 30mA

6.7.4.7 High voltage generation simulation

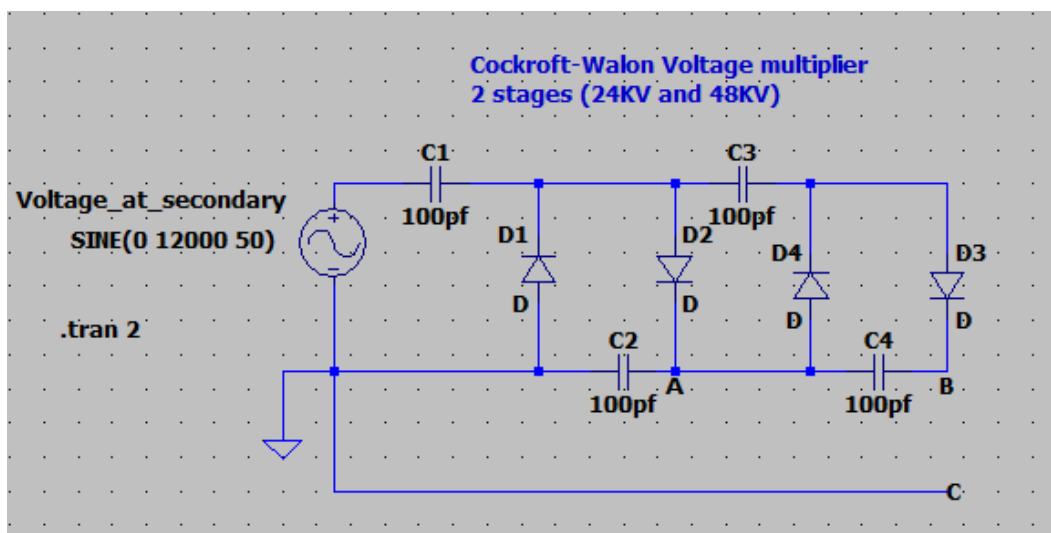


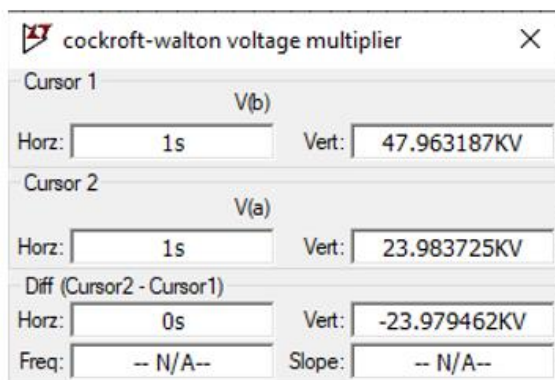
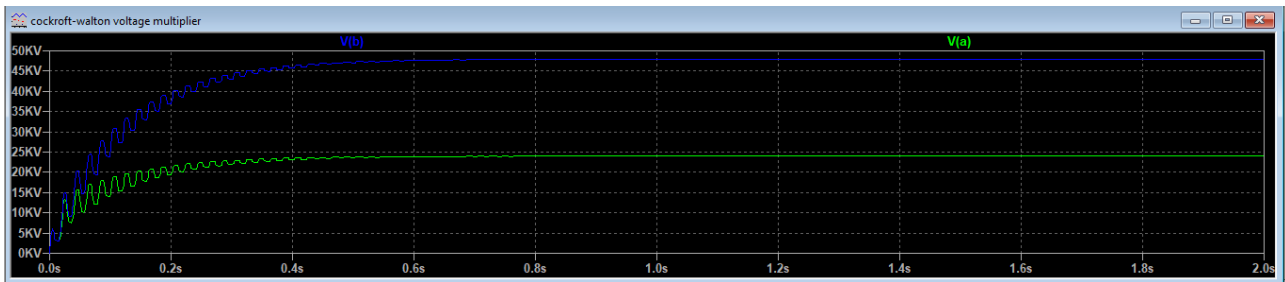
Figure 38: Generation of high DC voltage via LT spice Simulink

Figure 31 shows the simulation circuit of the Cockcroft-Walton voltage multiplier. Table 1 below shows the ratings for circuit parameters used for simulation.

Table 4: Circuit parameters

Parameter	Rating
Input voltage	12 KV
Input frequency	50 Hz
Capacitor	100pF 30Kv
Diode breakdown	30KV

6.7.4.8 Output of the stages



6.7.4.9 Data reduction software

MATLAB could be a numerical and graphical computer program bundle with numerical, graphical, and programming capabilities. It has built-in capacities to perform numerous operations, and there are tool kits that can be included to increase the capacities (e.g., for signal processing). There are adaptations accessible for diverse equipment stages, in both proficient and understudy versions.

6.8 Results in Time domain and in Frequency domain

After many experiments mentioned before in the chapter 3, finally, fixing all the components in the system (high voltage around 48 kv, vacuum pump, output circuit, glass container). The following results were obtained:

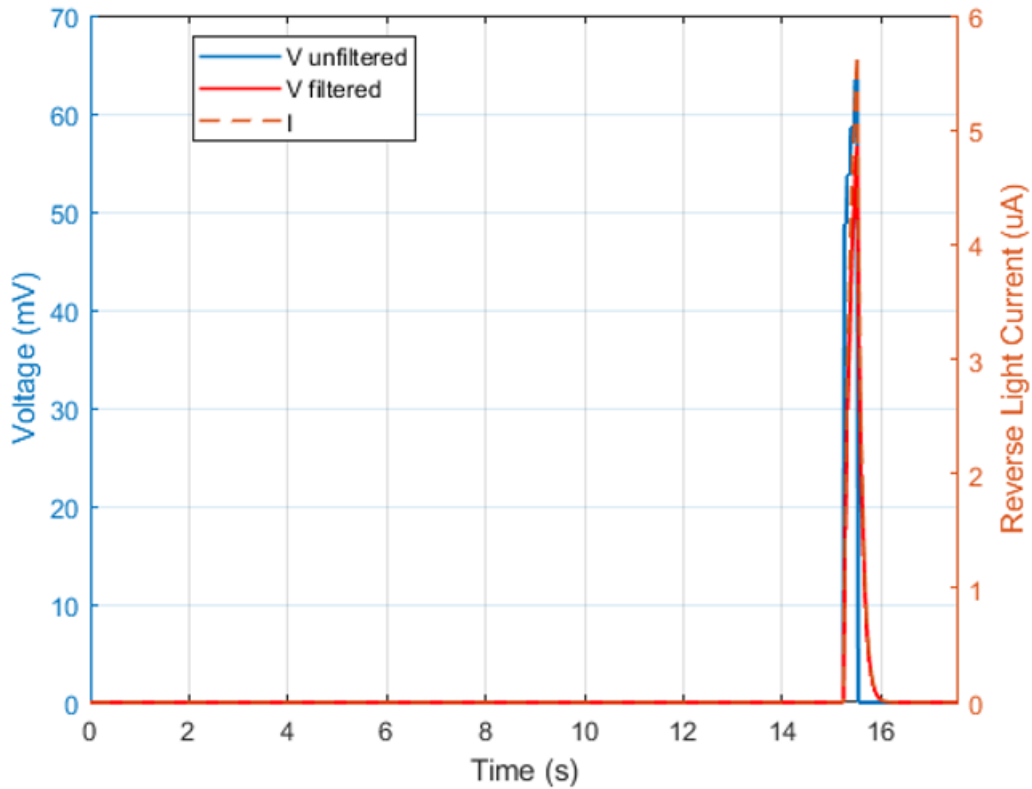


Figure 39: The spectrum detected via photodiode in terms of time with calculated current.

Although we know that the X-ray spectrum is continuous, the result obtained above shows a single peak because something wrong happen in high voltage, and thus, we were electrocuted (short circuit).

Unfortunately, the laboratory not equipped to protect us from high voltage.

For this reason , we will take this result and analyze it by converting it to frequency domain. If the frequency in a range of the X-Ray [$10^{15}hz$, $10^{20}hz$] this means that spectrum is specific to X-Ray radiations.

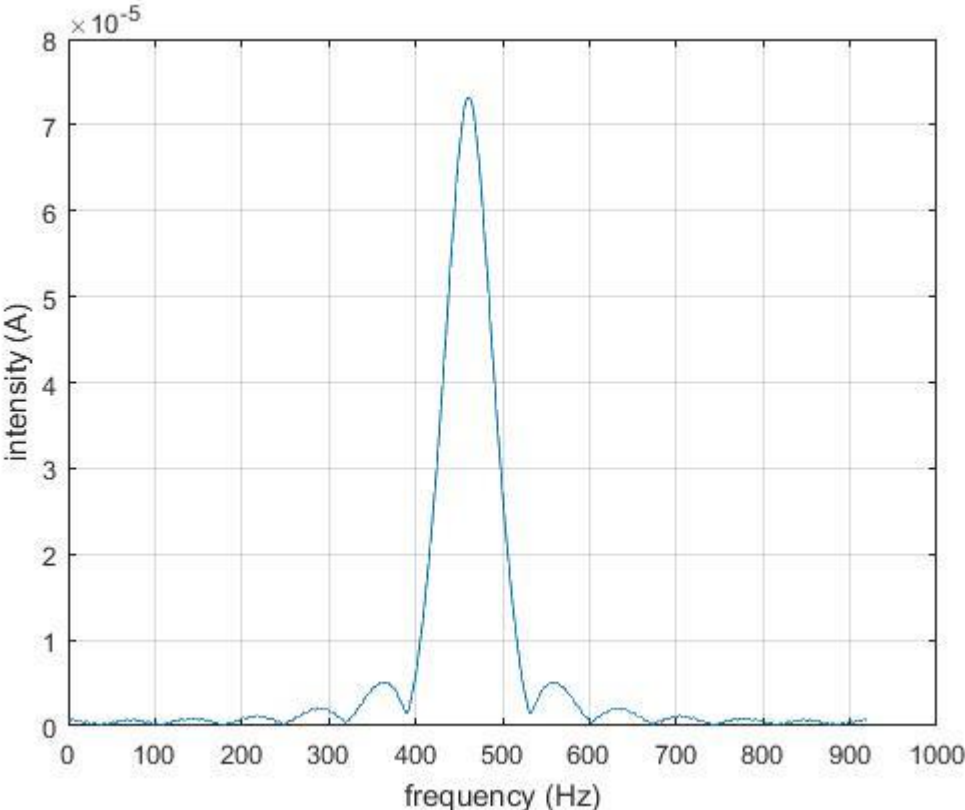


Figure 40: The result in frequency domain (Fourier Transform).

In the figure above the frequency is of an order of 10^2 , therefore, the light detected by the photodiode is not able to make an X-ray radiation.

6.9 Conclusion:

To conclude, after entering the data into (MATLAB), the frequency is shown in the figure above demonstrate that radiation detected by the photodiode is not an X-Ray because the frequency must be in range 10^{15} to 10^{20} Hz. Thus, there are many issues that caused the expected result not be appear and have to improve it.

First, determine and improve the high voltage up to 60 kV, in addition to improve vacuum pump to achieve 90% vacuum at least.

Secondly, the distance between cathode and anode must be close to each other (around 3 cm), moreover, the tungsten anode can be placed instead of the copper anode as it has a higher atomic number Z.

To avoid destroying the anode soon a rotating anode can be used, in this way the electron beam hits the anode in a different place each time, also, we must have to passing water through the anode to protect it from the melting.

6.10 References

1. Shokr, M., 2019. From pnCCD to pnCCD+ CsI (TI) scintillator: characterizations and applications.
2. Cecilia, A., 2012. *Crystals for indirect and direct detectors employed in X-ray imaging applications* (Doctoral dissertation, Verlag nicht ermittelbar).
3. Chen, Q., 2012. *Polymer Composites for Radiation Scintillation* (Doctoral dissertation, UCLA).
4. Grundmann, M., 2010. *Physics of semiconductors* (Vol. 11, pp. 401-472). Berlin: Springer.
5. Krammer, M., 2011. Silicon detectors. *Institute of High Energy Physics, Vienna, Austria*.
6. Mneke, D., environmental health & safety, 480 oak road, stanford, california 94305-8007
7. Sze, M.S., and Kwok, K., copyright 2007 by John Wiley & Sons, physics of semiconductor third edition, Department of Electronics Engineering National Chiao Tung University Hsinchu, Taiwan and Central Laboratory MVC (a subsidiary of ProMOS Technologies, Taiwan) San Jose, California. Published by John Wiley & Sons, Inc., Hoboken, New Jersey.
8. G. Rocha, J. and Lanceros-Mendez, S., 2011. Review on X-ray detectors based on scintillators and CMOS technology. *Recent Patents on Electrical & Electronic Engineering (Formerly Recent Patents on Electrical Engineering)*, 4(1), pp.16-41.

6.11 List of figures

Figure 1: Component of X-ray tube.....	147
Figure 2: Principle of photoelectric effect.....	149
Figure 3: Principle of Compton effect.....	150
Figure 4: Electronic energy band of an inorganic scintillator doped with an activator	151
Figure 5: Absorption coefficient of intrinsic at room temperature.....	Error! Bookmark not defined.
Figure 6: p-n junction process.....	154
Figure 7: Reverse bias and p-n junction and energy diagram.....	155
Figure 8: Absorption coefficient [cm^2g^{-1}] of silicon in terms of energy [Kev].....	Error! Bookmark not defined.
Figure 9: Sensitivity of photodiode in terms of wavelength.	156
Figure 10: Discharging the voltage of diode capacitance.....	157
Figure 11: Silicon detector amplification stages	159
Figure 12: Amplifier circuit of incident power.....	160
Figure 13: Circuit design of BPW3	162
Figure 14: Preamplifier circuit design.....	162
Figure 15: Voltage visualization on oscilloscope.	163
Figure 16: Preamplifier circuit (for another exp).....	163
Figure 17: Voltage visualization on oscilloscope for sec exp.....	164
Figure 18: The used preamplifier circuit.	164
Figure 19: Circuit of the system.	165
Figure 20: Testing diode for the visible light.	165
Figure 21: Vacuum pump, 600 torr.	166
Figure 22: The cathode filament (tungsten).	167
Figure 23: Cooper rod used as anode.	167

Figure 24: Rectangle glass container	168
Figure 25: Cylindrical glass container that support 79% of Vacuum.....	168
Figure 26: Basic voltage multiplier circuit of 2 stages	169
Figure 27: Capacitor 101k 3o kV	171
Figure 28: Capacitor isolated pins.....	171
Figure 29: 2CLG30kV/0.5A.....	172
Figure 30: 220V/12kV 30mA.....	172
Figure 31: Generation of high DC voltage via LT spice Simulink	172
Figure 32: The spectrum detected via photodiode in terms of time with calculated current.....	174
Figure 33: The result in frequency domain (Fourier Transform).....	175

6.12 List of Tables

Table 1: Comparison between different anode materials.	148
Table 2: Comparison between the organics and inorganics scintillators.....	153
Table 3: Different parameters of our system.....	166
Table 4: Circuit parameters	173

6.13 Annex: Matlab code

```

load data.txt
t=data(:,1); % time
v=data(:,3); % filtred voltage
v1= v*10.^-3;
r = 1e3 ;
I=v1/r;% current
%% figure(1) intensity in terms of time
figure (1)
    plot(t,I,'r')
    grid on
    xlabel ('time (s)')
    ylabel ('intensity (A)')
    xlim([ 14 , 16 ])
    %% curve fitting using smooth.spline
figure (2)
    plot(t,I,'r')
    hold on
    grid on
    xlabel ('time (s)')
    ylabel ('intensity (A)')
    lowess_large= smooth(t,I,.001,'lowess'); % fitting non parametric curve
    LL_plot = plot (t,lowess_large,'k+');
    legend ( ' intensity ' , 'fitting curve ' )
%% voltage in terms of time
figure(3)
    plot(t,v1,'b')
    grid on
    xlabel ('time (s)')
    ylabel ('voltage (v) ')
%% fourier transform
figure (6)
    f2ft=fft(lowess_large);

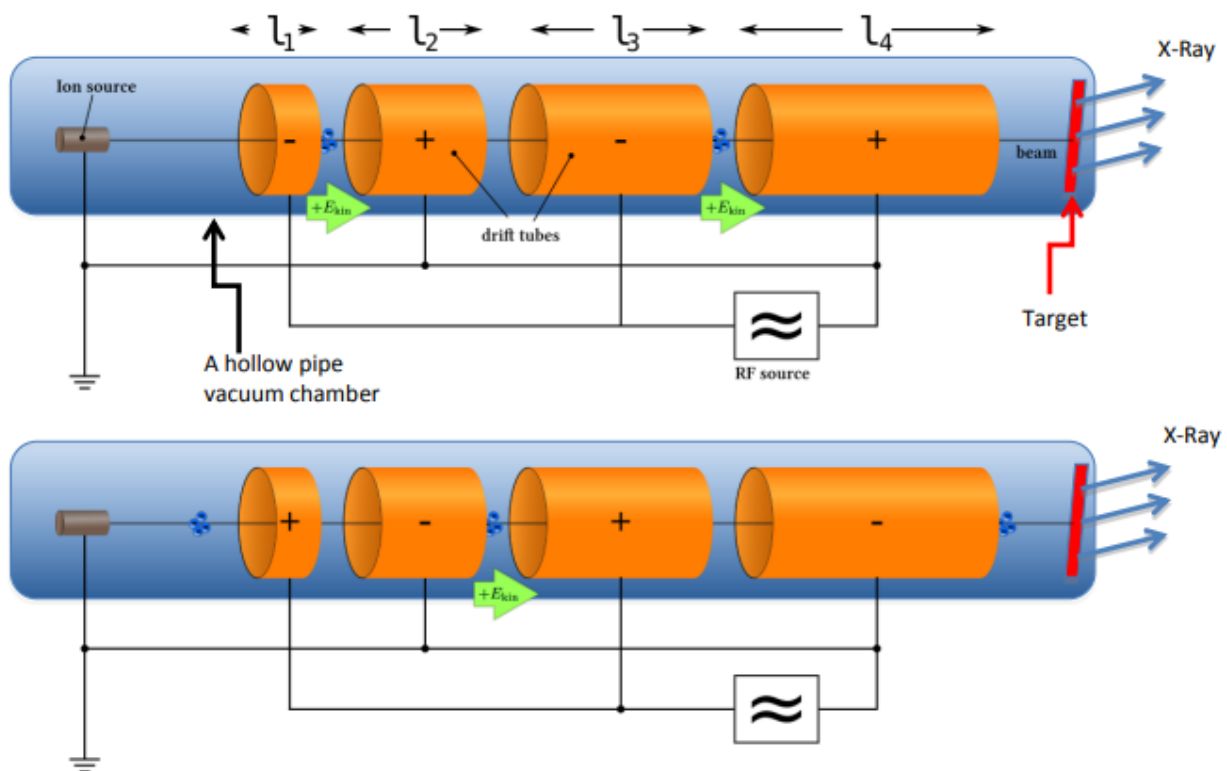
```

```
plot(fftshift(abs(f2ft)));  
grid on  
xlabel ( ' frequency (Hz) ' )  
ylabel ( ' intensity (A) ' )
```

7 RF Linear particle accelerator

A linear particle accelerators have many applications: they generate X-rays and high energy electrons for medicinal purposes in radiation therapy, serve as particle injectors for higher-energy accelerators, and are used directly to achieve the highest kinetic energy for light particles (electrons and positrons) for particle physics. Linear particle accelerator (often shortened to linac) is a type of particle accelerator that greatly increases the kinetic energy of charged subatomic particles or ions by subjecting the charged particles to a series of oscillating electric potentials along a linear beamline; this method of particle acceleration was invented by Leó Szilárd.

7.1 Parts of LINAC and their functions



The particle source (“Ion source” in Figure). The design of the source depends on the particle that is being moved. Electrons are generated by a cold cathode, a hot cathode, a photocathode, or radio frequency (RF) ion sources. Protons are generated in an ion source, which can have many different designs. If heavier particles are to be accelerated, (e.g., uranium ions), a specialized ion source is needed.

A high voltage source for the initial injection of particles.

A hollow pipe vacuum chamber. The length will vary with the application. If the device is used for the production of X-rays for inspection or therapy the pipe may be only 0.5 to 1.5 meters long. If the device is to be an injector for a synchrotron it may be about ten meters long. If the device is used as the primary accelerator for nuclear particle investigations, it may be several thousand meters long.

Within the chamber, electrically isolated cylindrical electrodes (“drift tubes”) are placed, whose length varies with the distance along the pipe. The length of each electrode is determined by the

frequency and power of the driving power source and the nature of the particle to be accelerated, with shorter segments ("11" in Figure) near the source and longer segments ("14" in Figure) near the target. The mass of the particle has a large effect on the length of the cylindrical electrodes; for example an electron is considerably lighter than a proton and so will generally require a much smaller section of cylindrical electrodes as it accelerates very quickly. Likewise, because its mass is so small, electrons have much less kinetic energy than protons at the same speed. Because of the possibility of electron emissions from highly charged surfaces, the voltages used in the accelerator have an upper limit, so this can't be as simple as just increasing voltage to match increased mass.

One or more sources of radio frequency energy ("RF source" in Figure), used to energize the cylindrical electrodes. A very high power accelerator will use one source for each electrode. The sources must operate at precise power, frequency and phase appropriate to the particle type to be accelerated to obtain maximum device power.

An appropriate target. If electrons are accelerated to produce X-rays then a water cooled tungsten target is used. Various target materials are used when protons or other nuclei are accelerated, depending upon the specific investigation. For particle-to-particle collision investigations the beam may be directed to a pair of storage rings, with the particles kept within the ring by magnetic fields. The beams may then be extracted from the storage rings to create head on particle collisions. Additional magnetic or electrostatic lens elements may be included to ensure that the beam remains in the center of the pipe and its electrodes. Very long accelerators may maintain a precise alignment of their components through the use of servo systems guided by a laser beam.

7.2 How it's Work

In source gives bunch of electrons which are then accelerated towards first drift tube (Bottom scheme in Figure) because of their negative potential and drift tube's positive potential. When electrons comes inside tube, in that moment RF source shifts its polarity. First drift tube then becomes negatively charged and second drift tube positively charged. Electrons comes outside of tube because of its inertia and in that moment they are pushed with first drift tube and attracted by the second one in the same direction (Top scheme in Figure). As electrons are accelerating, their velocity becomes bigger and they travel longer distance in the same time. That is the reason why drift tubes must be longer as electrons comes closer to target; because of their greater velocity. If very great velocity is needed, because of long drift tubes and big number of drift tubes, linac must be very long. As the particle bunch passes through the tube it is unaffected (the tube acts as a Faraday cage), while the frequency of the driving signal and the spacing of the gaps between electrodes are designed so that the maximum voltage differential appears as the particle crosses the gap. This accelerates the particle, imparting energy to it in the form of increased velocity. At speeds near the speed of light, the incremental velocity increase will be small, with the energy appearing as an increase in the mass of the particles. In portions of the accelerator where this occurs, the tubular electrode lengths will be almost constant.

7.3 Electrons gun

Electron guns comprise a cathode, where the electrons are produced. The cathode is at a high negative potential, typically in the range -30kV to -150kV . There is a vacuum gap between the cathode and an anode, which is at ground potential. The anode has a hole in it, so the electrons are accelerated towards it and then pass through the hole. They then travel at a constant speed (usually a third or more of the speed of light) until they impact on the work piece or target, where they release their kinetic energy as heat and X-rays.

Tungsten filaments are widely used in scanning electron microscopy. Of all metals in pure form, Tungsten has the highest melting point, the lowest vapor pressure, the lowest thermal expansion and a very high tensile strength which are ideal properties for making an electron source. The operational temperature of the Tungsten filament lies around 2800 Kelvin, The difference in temperature has a direct effect on the source.

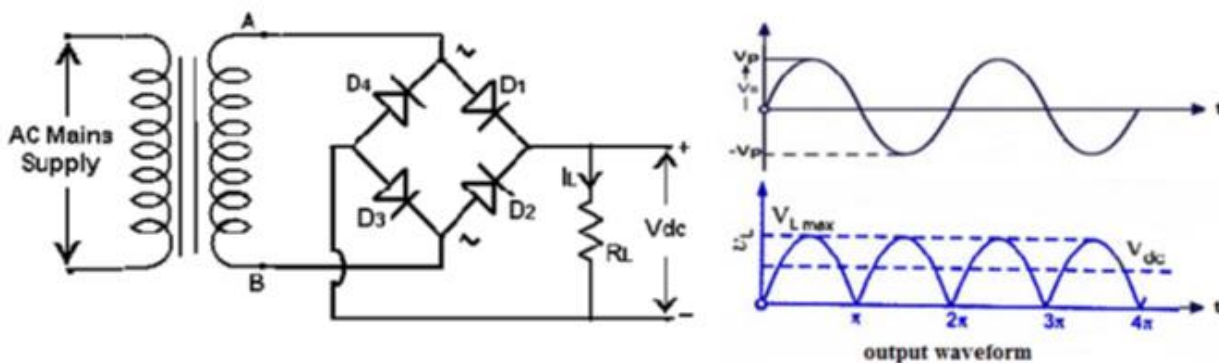
The electron beam is visible because there is a low-pressure gas in the tube. Electrons striking the gas molecules give them energy, which is then released as light.

7.4 High voltage power supply:

The cathode ray tube/gas discharge tube does not require any sort of specialized power supply. Any high voltage power supply that can produce over 10kV of potential difference will work.

The best type of power supply to use would probably be a (roughly) 20kV DC flyback transformer using a low current driver like a 555 oscillator and MOSFET. In fact, almost any of the "quick high voltage power supply" instructables we have here should work. However, we did not have a flyback power supply on hand, so I used a rectified sign transformer.

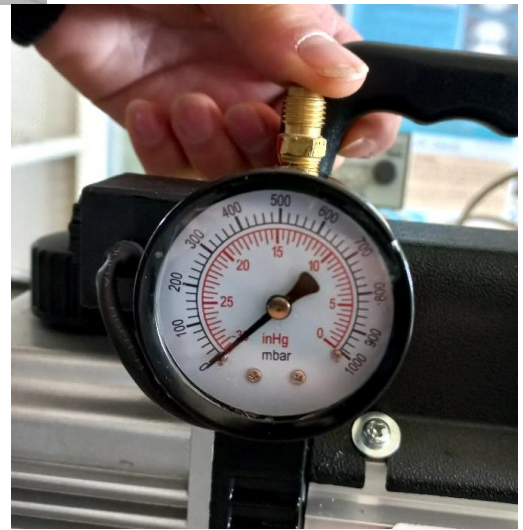
We've included an electrical schematic that shows how to hook the diodes up to the transformer.





Transformer (12kv, 30 mA, 50hz)

7.4.1 Vacuum of the tube accelerator:



Arnocanali pump

7.4.2 Slit accelerator anode connected:

When the slit anode is connected, the electrons are accelerated and then pass through the slit.

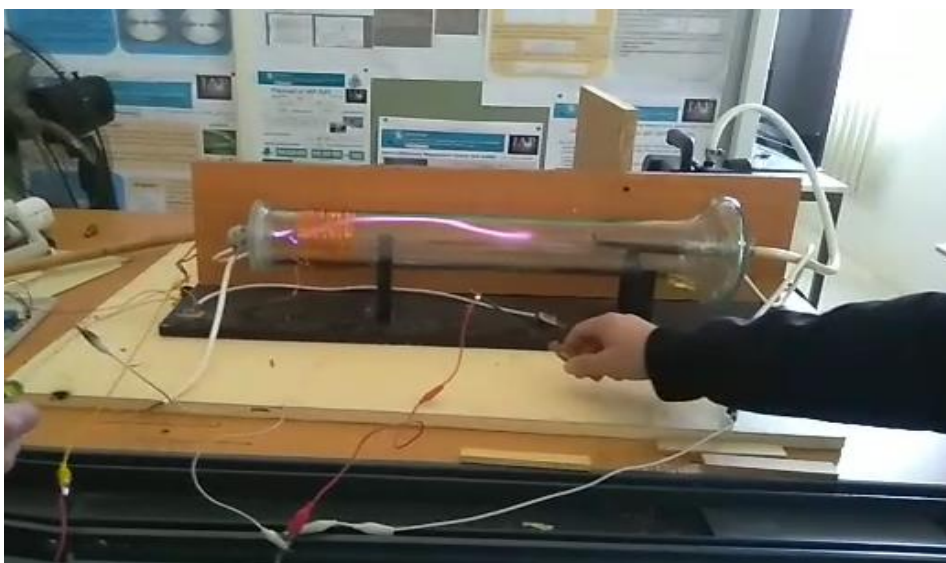


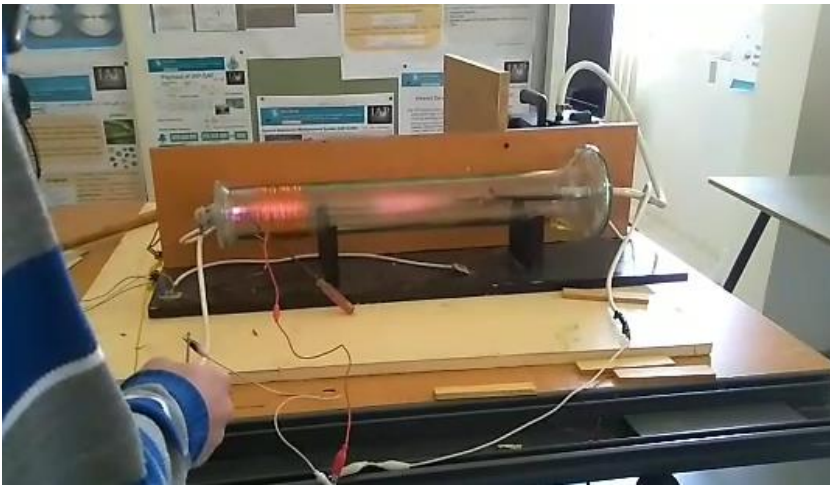
7.4.3 Slit accelerator anode disconnected:

When the slit is disconnected, the electrons stayed around the tungsten filament (cathode).



Tube accelerator:





The electrons beam pass from the cathode to the anode inside the accelerator tube.

8 Electron Source, LINAC (with glass tube), electromagnetic deflection of electrons and X-Ray Generation

Content taken from the following master thesis:



MEMORY



In order to obtain the

RESEARCH

In

PIRM: Physics of Radiation-Matter Interaction

Presented and Supported by:

Rouwayda Muhammad Sakka

January 2024

Title

Development of the integration and commissioning of a physics laboratory training device with X-ray production.

Supervisor

Prof. Adnan Naja

Readers

Dr. Ahmad Osman

Dr. Hassan Amoud

Lebanese University-Faculty of sciences

8.1 LIST OF FIGURES

Figure I. 1: Tungsten	191
Figure I. 2: Configuration of the electron gun	192
Figure I. 3: Comparison between classical speed and relative speed	194
Figure I. 4: Deflection of the electron trajectory under the effect of the magnetic field	195
Figure I. 5: explanatory diagram of the production of characteristic radiations	222
Figure I. 6: Graph representing the spectrum of X-ray	223
Figure I. 7: Energy levels of copper	223
Figure I. 8: Graph representing the X-ray spectrum for the copper	224
Figure I. 9: Representative diagram of a Helmholtz coil	230

Figure I. 10: X-ray detector type "XR1 Pro" 225

Figure I. 11: Arnocanali Bistaduim high pressure pump 42l/H 196

Figure II. 1: Schematic diagram of the FRANZ proton thruster with four target stations for neutron production **Error! Bookmark not defined.**

Figure II. 2: System design for a physics laboratory training device with some physical measuring instruments **Error! Bookmark not defined.**

Figure II. 3: Trajectory of electrons before the production of X-ray **Error! Bookmark not defined.**

Figure II. 4: Glass disc for observing the electron beam **Error! Bookmark not defined.**

Figure II. 5: Measurement of certain components of the acceleration zone **Error! Bookmark not defined.**

Figure II. 6: Specific measurements of the certain component of the prototype **Error! Bookmark not defined.**

Figure II. 7: Length and width of the electron production and acceleration zone **Error! Bookmark not defined.**

Figure II. 8: Cross-sectional diameter of some tubes of the 32 mass spectrometer **Error! Bookmark not defined.**

Figure III. 1: Previous experience of colleagues in generating electron beams 201

Figure III. 2: Air leak locations 202

Figure III. 3: a 55 neon lamp 202

8.2 LIST OF TABLES

Table I. 1: Comparison between the binding energy of the k-layer of copper and tungsten	195
Table I. 2: Disadvantages of some types of magnets	229
Table I. 3: Pressure ranges in vacuum technology	196

8.3 Basics concerning Generation and Accelerating Electrons

In order to analyze the structure of matter, it is necessary to build a device that produces X-rays. Therefore, in this chapter, we will cover the basics of X-rays, choosing the right pump, the right detector, as well as protection measures against these rays. And since the device will follow a path where electrons deflect before reaching the target and producing these rays, we must talk about the magnetic field responsible for the deflection of the electrons.

Before starting the production of X-rays, it is imperative to examine the most commonly used methods for their production. Two key mechanisms stand out: bremsstrahlung and characteristic radiation. The bremsstrahlung effect involves the interaction of highly energetic electrons with a target, such as tungsten or molybdenum, resulting in an abrupt slowing of the electrons and the production of continuous X-rays over a wide range of energies. Characteristic radiation, on the other hand, arises from specific interactions between the incident electrons and the target atoms, where an X-ray photon is emitted when the electrons fill the vacant electronic levels. This radiation has well-defined energies, providing a precise method for materials analysis.

In addition, we are exploring the innovative use of synchrotrons, which are particle accelerators that can achieve very high electron energies. In these devices, electrons circulate at high speeds in storage rings, subjected to intense magnetic fields, thus producing high-intensity and high-brightness X-rays. This advanced technique has essential applications in materials science and structural biology research.

In our study, we will take an innovative approach while respecting the fundamental principles of standard X-ray production. We will do this by heating tungsten to release electrons, which will then be accelerated by applying a potential difference. These electrons will then be directed towards the target where they will collide to produce X-rays. In the rest of our research, we will detail each step individually, outlining the pathway we will follow to ensure efficient and safe X-ray production in this particular configuration.

8.3.1 Cathode

In our experimental setup, the cathode plays a fundamental role as a negative electrode, made of tungsten, which has favorable electron emission properties when subjected to a heat source. The resistance of the tungsten used in our case is 0.21 ohm. Knowing that the first ionization energy of tungsten is about 7.6 eV, this corresponds to an initial energy of about 8 V required to heat the tungsten and allow the emission of electrons, in accordance with the process known as the "thermionic effect".



Figure I. 1: Tungsten filament

8.3.2 Anode

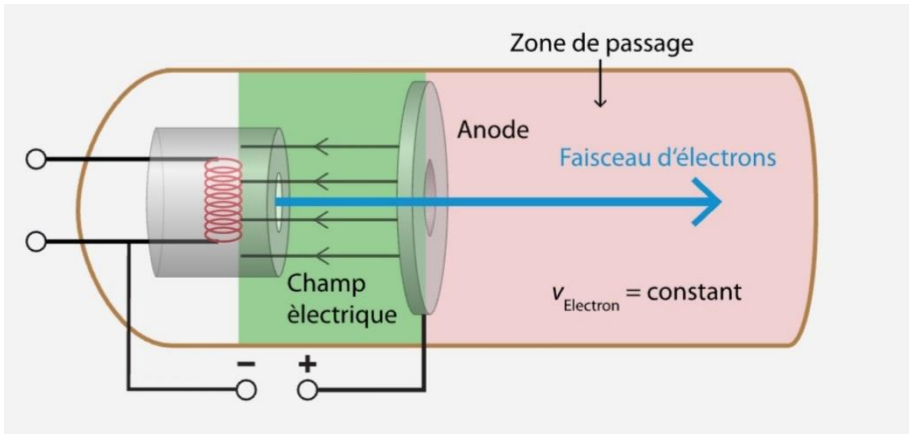


Figure I. 2: Electron gun configuration

The essential role of the anode in the X-ray tube is to receive the electrons emitted by the heated tungsten cathode and accelerate them towards the target. We use a positively charged anode in the form of a disc plate. This particular design includes a small central hole through which the electrons emitted by the cathode will pass in a straight line. The deliberate circular shape of the disc allows for an even distribution of electrical charges over the surface, thus ensuring that the electrons travel exclusively within the hole. This sophisticated anode design aims to optimize the efficiency of electron acceleration and ensure their precise path towards the target, thus contributing to the controlled and targeted production of X-rays for our study of the structure of materials.

8.3.3 Acceleration of electrons

Establishing a potential difference (high voltage) between the cathode and the anode plays a key role in our experimental setup. This potential difference facilitates the acceleration of the electrons emitted by the tungsten cathode, allowing them to travel at high speed and in a straight line towards the central hole of the anode. By applying this high voltage, we create an electric field that attracts the electrons towards the anode, propelling them with significant kinetic energy. This ensures that the electrons follow a precise and controlled path towards the anode hole, promoting optimal interaction with the target for the desired X-ray production.

8.3.3.1 Acceleration zone

An accelerating voltage creates an electric field: $E = \frac{Ub}{d}$

The electrons released by heating the tungsten experience a force F in the electric field : $F = Ee = \frac{Ub.e}{d}$.

The electron undergoes work between the cathode and the anode: $W = Fd = \frac{Ub.e.d}{d} = U_b.e$

This work increases the kinetic energy of the electron.

The kinetic energy E_c of an electron is : $E_c = \frac{1}{2}mv^2$

This equality with work gives: $\frac{1}{2}mv^2 = eU_b$

The final speed is then: $v_f = \sqrt{\frac{2 \cdot e \cdot U_b}{m}}$

8.3.3.2 Comparison between classical and relativistic calculations

At accelerating voltages of 2.7 kV and above, the speed of electrons reaches 10% of the speed of light, so it is recommended to opt for relativistic calculations.

Relativistic calculation of electron speed:

Kinetic energy is equal to total energy minus remaining energy:

$$E_c = m_r \cdot c^2 - mc^2$$

This equality with work gives:

$$U_b \cdot e = m_r \cdot c^2 - mc^2$$

m_r is related to m by the Lorentz factor γ :

$$m_r = \gamma \cdot m = \frac{m}{\sqrt{1 - \frac{v^2}{c^2}}}$$

Substituting, factoring and dividing by mc^2 , we get:

$$\frac{U_b \cdot e}{m \cdot c^2} = \frac{1}{\sqrt{1 - \frac{v^2}{c^2}}} - 1$$

Then add 1 and take the square:

$$\left(1 + \frac{U_b \cdot e}{m \cdot c^2}\right)^2 = \frac{1}{1 - \frac{v^2}{c^2}}$$

Inverting the equation, multiplying by (-1) and adding (1), we obtain:

$$\frac{v^2}{c^2} = 1 - \frac{1}{\left(1 + \frac{U_b \cdot e}{m \cdot c^2}\right)^2}$$

Multiplying by c^2 and taking the square root, we finally obtain:

$$v_r = c \cdot \sqrt{1 - \frac{1}{\left(1 + \frac{U_b \cdot e}{m \cdot c^2}\right)^2}}$$

Comparison between classical and relativistic calculations :

$U_b = 10 \text{ kV}$ (here 1.3.5. *Electron-matter interaction zone*)

Classic calculation of final speed:

$$v_c = \sqrt{\frac{2 \cdot e \cdot U_b}{m}} = 0.198 \text{ C} \text{ [19.8\% of the speed of light].}$$

Relativistic calculation of the final velocity:

$$v_r = c \cdot \sqrt{1 - \frac{1}{\left(1 + \frac{U_b \cdot e}{m \cdot c^2}\right)^2}} = 0.194 \text{ C} \text{ [19.4\% of the speed of light].}$$

Absolute difference:

$$v_c - v_r = 0.198 \text{ C} - 0.194 \text{ C} = 12 \cdot 10^5 \text{ m/s} = 432 \cdot 10^4 \text{ Km/h.}$$

Relative difference:

$$1 - \left(\frac{v_r}{v_c}\right) = 1 - \frac{0.194 \text{ C}}{0.198 \text{ C}} = 0.02 = 2\%$$

This difference increases if the acceleration voltage also increases:

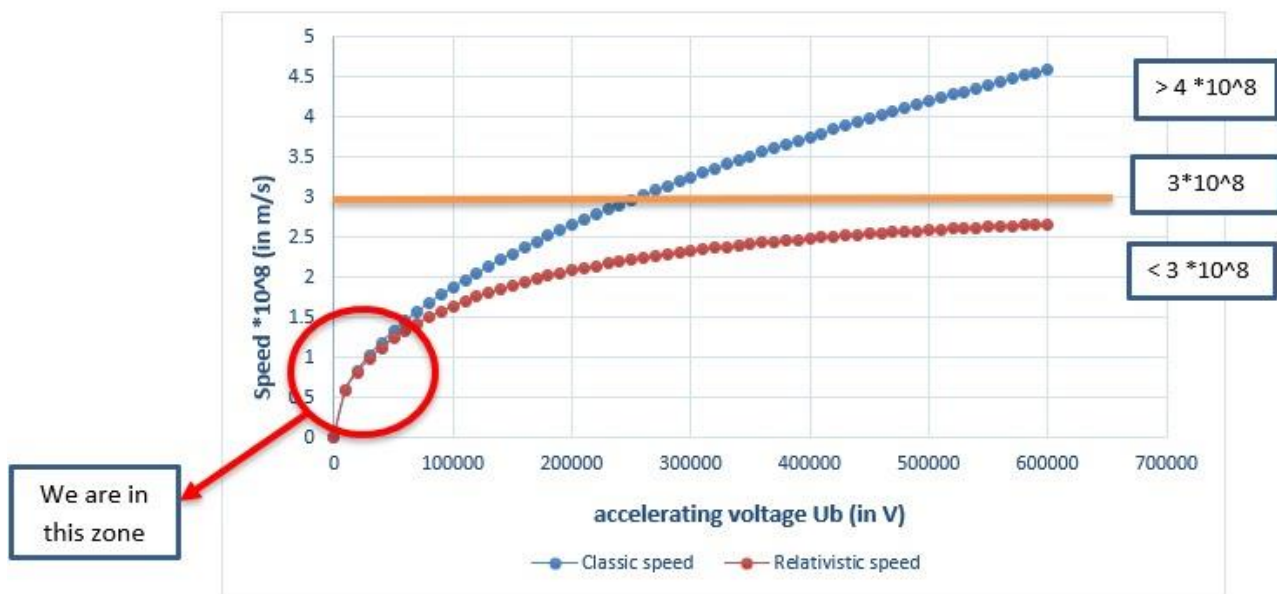


Figure I. 3: Comparison between classical speed and relative speed

8.3.3.3 Passage area

After passing through the hole in the disk, the electrons continue their path in a straight line with uniform rectilinear motion, thus leaving the initial accelerating electric field. Therefore, they no

longer experience acceleration. At this stage, we apply the principles of uniform rectilinear motion to describe their trajectory:

$$X(t) = v_f \cdot t.$$

$$v(t) = v_f.$$

$$a(t) = 0.$$

The electrons now move at the speed acquired during their passage through the acceleration zone, evolving in a constant uniform rectilinear motion.

8.3.3.4 Deflection zone

Once the electrons have crossed the inside of the lines, due to the complexity of our prototype's path, they begin the deflection stage before colliding with the target. To this end, the electrons will be subjected to a magnetic field that induces this deflection. This magnetic field must be oriented perpendicular to the electrons' trajectory. This controlled deflection will allow the electrons to follow a specific path towards the target for the desired collision.

Using the equation $R = \sqrt{\frac{2mUb}{qB^2}}$, we can calculate the radius of the circular trajectory of electrons in the magnetic field (B) when subjected to an accelerating voltage (Ub) in an X-ray tube device:

In our case, we have $B = 0.01 \text{ T}$; $U_b = 10 \text{ Kv}$; $m = 9.11 \cdot 10^{-31} \text{ Kg}$; $q = 1.6 \cdot 10^{-19} \text{ C}$.

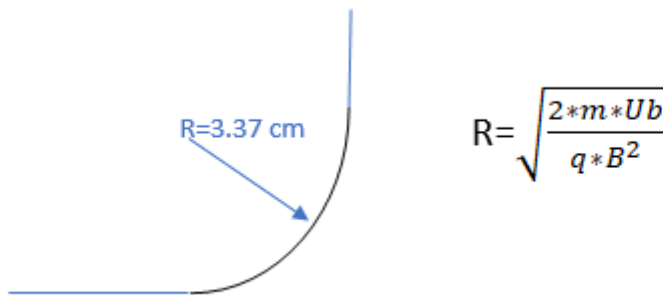


Figure I. 4: Deviation of the trajectory of electrons under the effect of the magnetic field

8.3.3.5 Electron-matter interaction zone

After undergoing the deflection due to the magnetic field, the electrons follow their trajectory towards the target, where they collide with it, thus giving rise to obtaining an X-ray. In most cases, the target used is usually made of materials such as tungsten or copper, which play an essential role in the production of X-rays.

Target	Tungsten	Copper
K-shell binding energy	69.5 Kev	8.98 Kev

Table I. 1: Comparison between the binding energy of the k-layer of copper and tungsten

As we know, the generation of X-rays requires sufficient kinetic energy of electrons, exceeding the binding energy of the K-shell. However, due to the lack of a safe high voltage above 70 kilovolts, we will opt for the use of copper instead of tungsten.

8.4 Vacuum Pump

8.4.1 The fundamentals of vacuum theory

Pressure range	pressure, mbar	pressure, engine
Low vacuum	1 bar – 1 mbar	750 torr-750 mtorr
Medium vacuum	1 – 10^{-3}	750 – 0.75
High vacuum	10^{-3} – 10^{-7}	$0.75 - 7.5 * 10^{-5}$
Ultra-high vacuum	$< 10^{-7}$	$< 7.5 * 10^{-5}$

Table I. 2: Pressure ranges in vacuum technology

8.4.2 Basic vacuum system for our prototype

In an X-ray tube, maintaining a vacuum environment is imperative for several critical reasons. First, it is essential to prevent the absorption of X-rays by gas molecules, as their presence could significantly reduce the intensity of the X-ray beam before it reaches the tube's target (the anode). Second, a vacuum is necessary to prevent X-ray scattering by gas molecules, as such scattering would result in beam dispersion and energy loss. In addition, the vacuum ensures uninterrupted and precise movement of X-rays from the anode to the focal point, where the sample to be analyzed is positioned, thus allowing for precise beam focusing. Finally, the absence of gas inside the tube reduces the risk of interaction with the anode, limiting potential damage caused by molecular collisions. As a result, a high vacuum level, typically between 10^{-6} and 10^{-7} torr, is maintained inside the X-ray tube to ensure optimal operation and reliable results when analyzing samples.

In order to achieve the required vacuum level, we considered several options, including the use of a high-performance vacuum pump or the combination of several pumps in series. After a thorough evaluation, we opted for the combination of a turbo molecular pump with a rotary pump. However, due to constraints such as the unavailability of this configuration in our center and its high cost, we decided to turn to the pump already present on site, of the Arnocanali type .



Figure I. 5 : Arnocanali Bistadium high pressure pump 421/H

However, it is essential to note that this pump does not fully meet the needs of our prototype, particularly for applications involving X-ray tubes and mass spectrometers. Its use could lead to a

variety of significant problems, including inadequate vacuum performance, risk of contamination due to the presence of oil, less favorable noise and vibration levels, limited durability, and the need for substantial modifications to adapt it to our specific application.

8.5 Electron gun Glass Tube LINAC Testing

8.5.1 System requirements

The LINAC must be able to produce electrons and accelerate them.

The LINAC tube must allow observation of the trajectory of electrons.

8.5.2 Mechanical requirements

The cathode must be able to withstand thermal and electrical stress.

The cathode must be tungsten. The anode must be made of copper.

The tube must be made of glass.

The vacuum pump used to create the vacuum in the glass tube.

8.5.3 Electrical requirements

The power supply must be able to supply tungsten with 6V.

Tungsten must be able to release electrons.

The power supply must be capable of providing a voltage between 5Kv and 60 kv .

8.5.4 Safety requirements

8.5.4.1 Electrical safety:

Insulation must be placed around the anode, so that it does not remain exposed and dangerous.

All electrical connections must be coated with the appropriate insulation depending on the current and voltage flowing through the connections.

6V cables and connections must be insulated with...

Cables and connections [5 Kv ;60kV] must be insulated with...

8.5.4.2 Radiological safety :

For X-ray protection, a metal box with a lead plate inside must be placed at the point of X-ray emission.

8.5.4.3 Chemical safety:

The lead must be completely enclosed to ensure that no toxic gases are emitted.

8.5.5 System test specification

00001: Ensure complete air evacuation

Stage	Description of the stage	Expected result
-------	--------------------------	-----------------

Electron Source, LINAC (with glass tube), electromagnetic deflection of electrons and X-Ray Generation

Precondition	The system is off	
Turn on the system	Turn on the pump	95% empty
Presence of a leak	We found a leak near the anode, the cathode and the junction between the cathode and the pump pipe.	Seal leak locations
Turn off the system	Turn off the pump	The pump stops extracting air.
Use of silicone	Apply silicone to areas where there are air leaks	Stop the leaks and get a 95% vacuum when we restart the pump.
Postcondition	The system is off.	

00002: Power supply

Stage	Description of the stage	Expected result
Precondition	The system is off	
Turn on the system	Turn on the cathode (tungsten) power supply	Obtain a continuous power supply (6 V)
Turn off the system	Turn off the cathode power supply	Continuous power supply stops
Postcondition	The system is off	

00003: Obtain electrons

Stage	Description of the stage	Expected result
Precondition	The system is off	
Turn on the pump	Turn on the pump	95% empty
Turn on the power supply	Turn on the cathode power supply	Obtain a continuous power supply (6 V)

Electron Source, LINAC (with glass tube), electromagnetic deflection of electrons and X-Ray Generation

Heat the tungsten	Heat the tungsten by supplying it with a 6 V power supply	Get electrons around the tungsten (the lamp will light up)
Turn off the power supply	Turn off the power supply	The lamp will go out
Turn off the pump	Turn off the pump	The pump stops extracting air
Postcondition	The system is off	

00004: High voltage

Stage	Description of the stage	Expected result
Precondition	The system is off	
Turn on the system	Turn on the high voltage (HV)	Obtain a continuous power supply (between 5 kV and 60 kV)
Turn off the system	Turn off high voltage (HV)	Continuous power supply stops
Postcondition	The system is off	

00005: Acceleration of electrons

Stage	Description of the stage	Expected result
Precondition	The system is off	
Turn on the pump	Turn on the pump	95% empty
Turn on the power supply	Turn on the cathode power supply	Obtain a continuous power supply (6 V)
Turn on the high voltage	Turn on the high voltage (HV) power supply	Obtain a continuous power supply (between 5 kV and 60 kV).
Acceleration of electrons	Connect the high voltage to the anode and cathode (while	

Electron Source, LINAC (with glass tube), electromagnetic deflection of electrons and X-Ray Generation

	monitoring the change in intensity until we observe the passage of electrons and their acceleration).	Electrons leave the anode and accelerate towards the cathode, colliding with it.
Turn off the high voltage (HV)	Turn off the high voltage (HV) power supply	Stopping the acceleration of electrons
Turn off the power supply	Turn off the power supply	The lamp will go out
Turn off the pump	Turn off the pump	The pump stops extracting air
Postcondition	The system is off	

8.5.6 System Test and Results

A LINAC, or linear accelerator, is a device used to increase the speed of individual particles using electromagnetic fields. It is capable of generating high-energy particle beams for various applications.

In a previous experiment conducted by our colleagues, a device consisted of a glass tube containing an anode (tungsten) and a cathode (a copper rod). By heating the tungsten and applying a potential difference, electrons were accelerated through the tube to reach the cathode and anode. Although this work was designated a LINAC, it is important to note that the specifications of this experiment do not match those of a conventionally recognized LINAC.

Our colleagues conducted a single experiment using tungsten found in an incandescent lamp. They accelerated the electrons using a 12.5 kV transformer and a circuit (diode + capacitor) to quadruple the voltage. However, they encountered a problem: the current was practically zero.

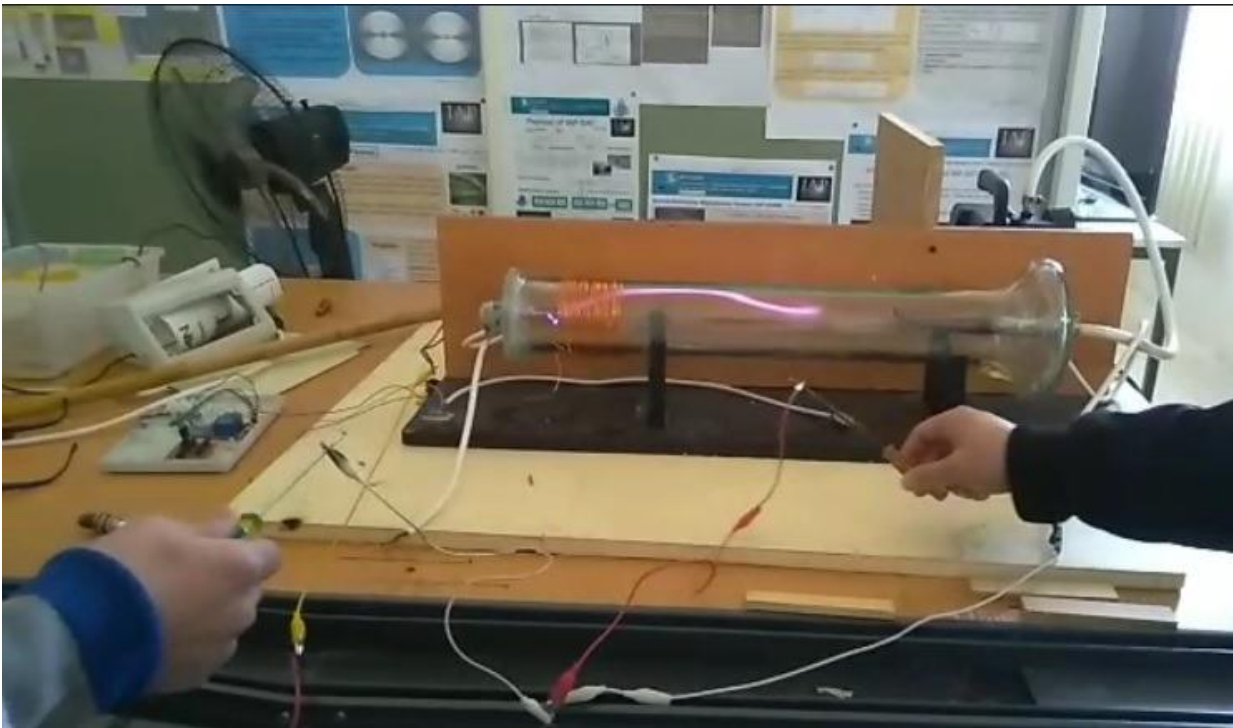


Figure III. 15: Previous experience of colleagues in generating electron beams

Based on the data from this experiment, we conducted several experiments aimed at improving the results.

8.5.6.1 LINAC Test 01/16/23

Test Analysis: When we turned on the pump, we found that the vacuum had not yet been completely achieved, and we knew where the air leak was coming from.

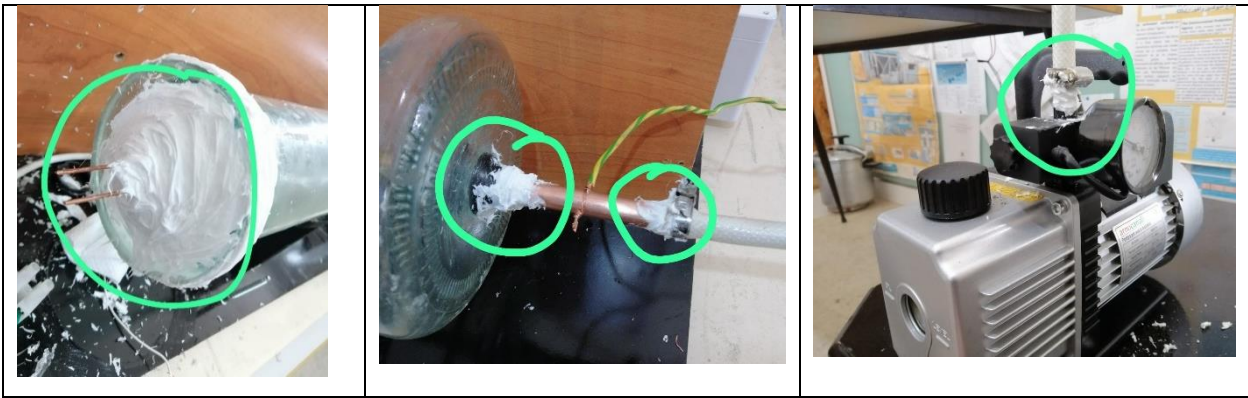


Figure III. 16: Air leak locations

What we did: So we sealed the leaks with silicone.

8.5.6.2 LINAC Test 01/16/23

Analysis of test results: In this test, we used a neon lamp with its tungsten as anode.

When we powered the lamp with 6 volts, it lit up and there was no problem (lighting up --> this means we should get electrons).

However, the problem arose when the anode was connected to a high voltage: the lamp burned out due to the thinness of the tungsten filament.



Figure III. 17: a neon lamp

What we need to do: We should use a lamp with a thicker tungsten filament to withstand the higher voltage.

8.5.6.3 LINAC Test 28-01-23

Analysis of test results: In this test, we used an ordinary lamp, but we replaced its tungsten with another thicker tungsten, which can withstand high voltage.

However, when we powered the lamp with 6V, it quickly burned out, as the tungsten used draws more amperage than expected, causing the tungsten rods in the lamp to melt.

So we didn't get any electrons, and of course we couldn't accelerate them because there were no electrons.

These are the filaments that could not withstand the current and melted:

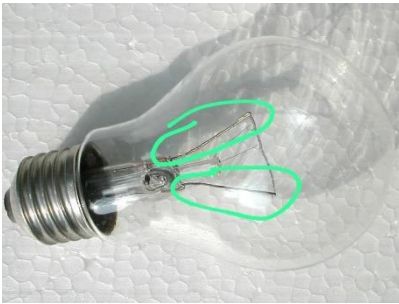


Figure III. 18: an ordinary lamp

Here is our tungsten (the tungsten from the lamp was removed and replaced with this):



What we need to **Figure III. 19: tungstène plus épais** do: It is necessary to use another lamp, because its filaments are thicker (~2 mm) to support the amperage.

8.5.6.4 LINAC Test 30_01_23

Analysis of test results: In this test, we used a lamp with filaments of a good thickness (~2 mm) and we attached tungsten to these filaments.

Then we supplied the lamp with a voltage of 6 V, and it lit up, indicating that we got electrons.

After this step, we turned on the high voltage, and we observed a violet light path, which indicates that the electrons are moving quickly between the anode and the cathode.

However, the problem was that the light path was winding and not straight.

Before turning on the high voltage:



Figure III. 20: The tungsten lamp is lit



Figure III. 21: At the first instant of high voltage ignition

After turning on the high voltage:

Moments later, the electronic path appeared:

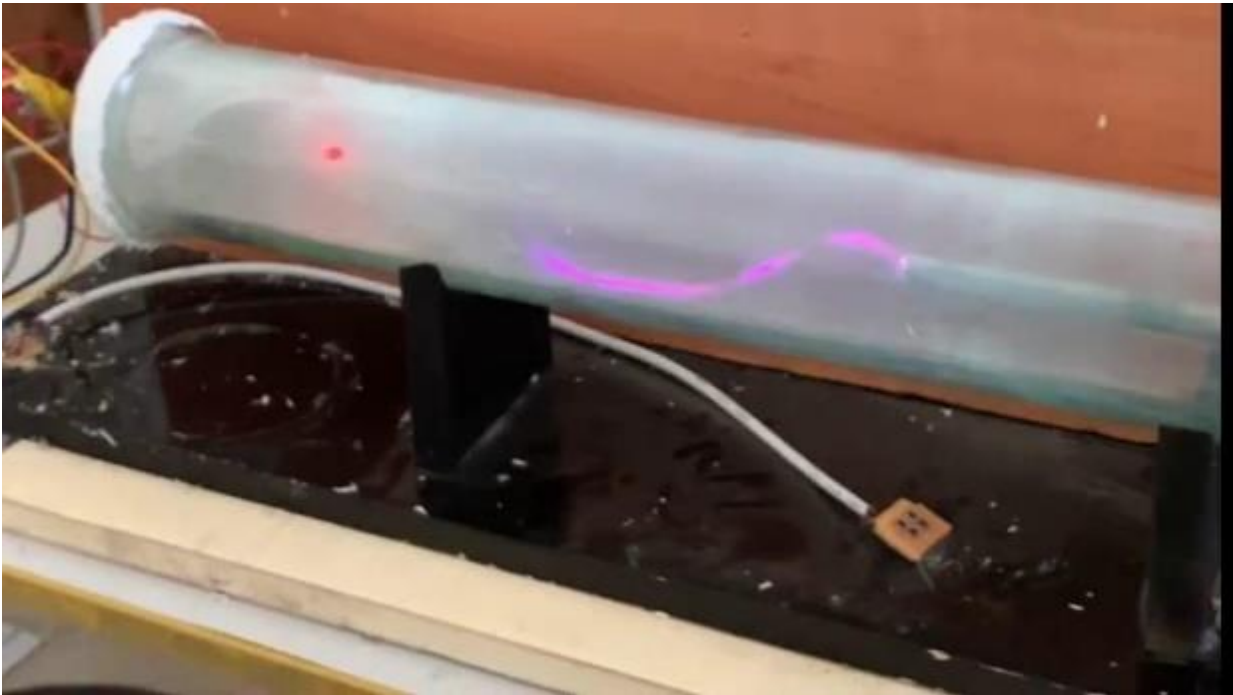


Figure III. 22: Electron beams appear

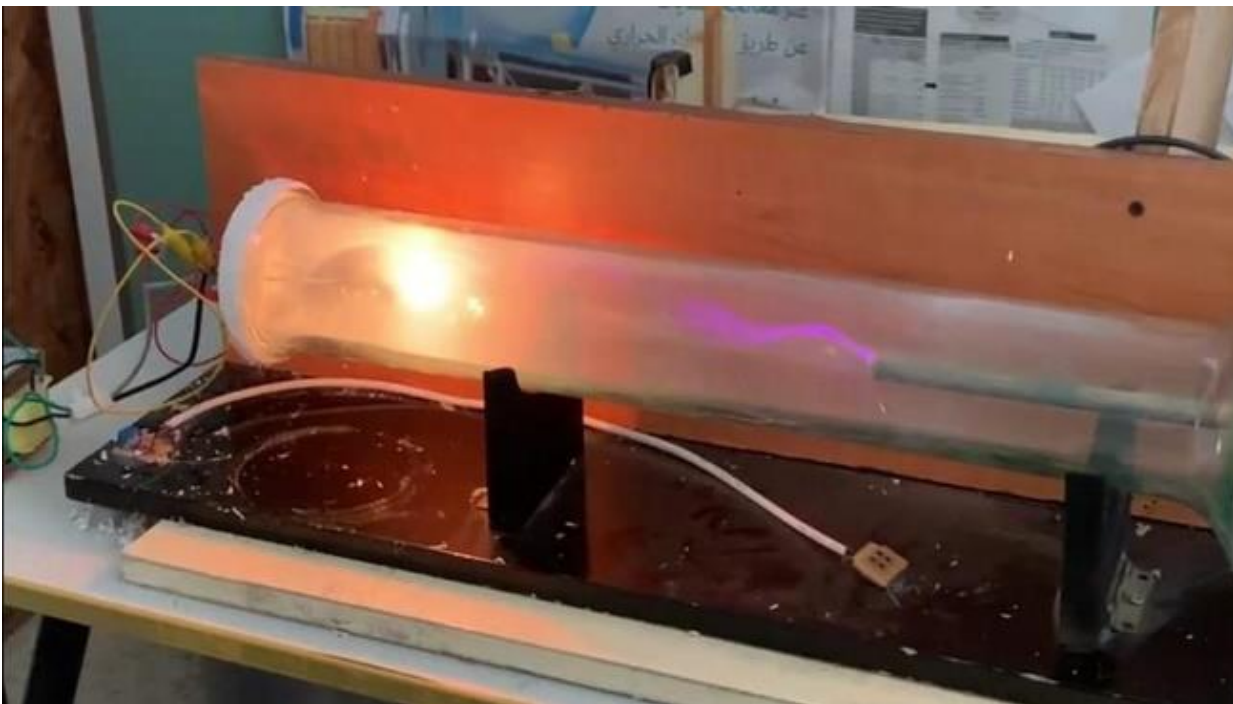


Figure III. 23: Electron beams appear with high voltage ~ 60 kV

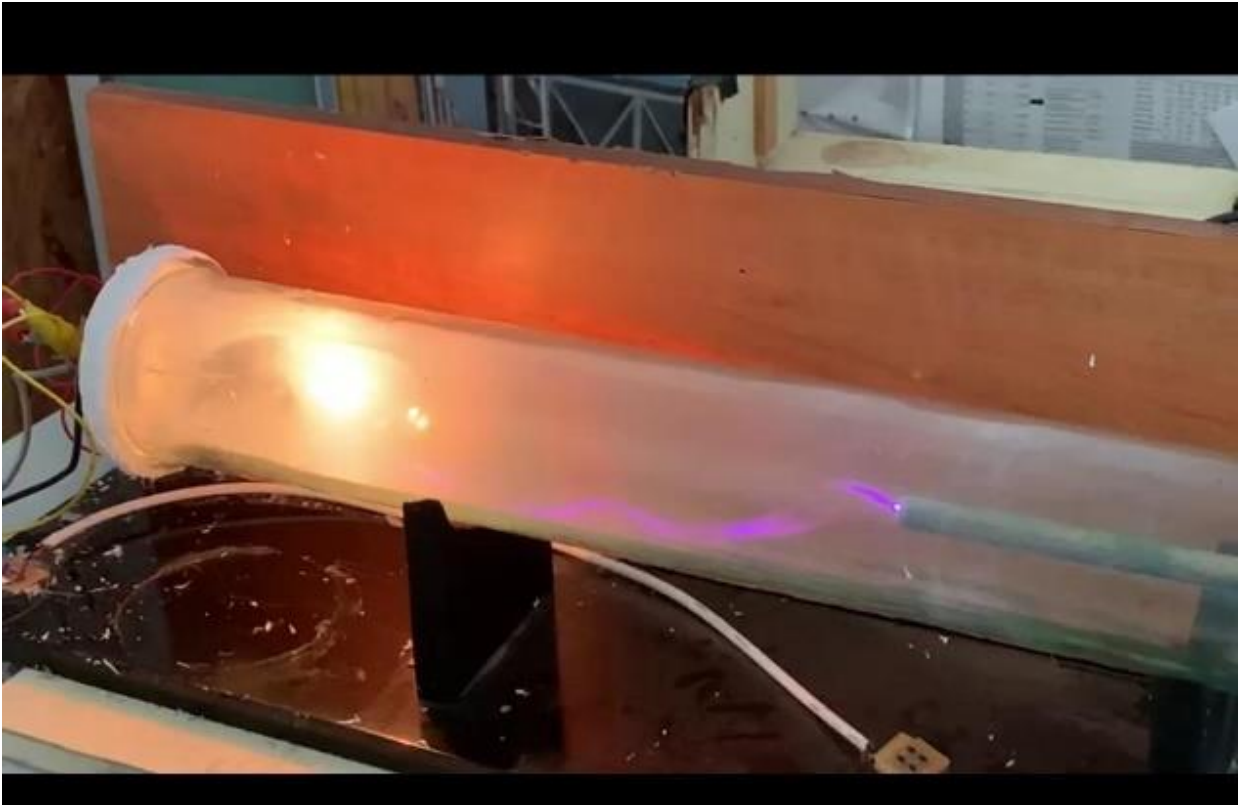


Figure III. 24: Electron beams appear with high voltage ~ 30-40 kV

What we need to do:

We will move the cathode slightly backward, thus increasing the distance between the anode and the cathode, and observe the changes.

We will perform the test while leaving the pump running.

8.5.6.5 LINAC Test 01/31/23

In previous tests we achieved vacuum and then turned off the pump.

Here we will try to leave the pump running.

This test also differs from the previous one because we moved the cathode slightly backward.

Analysis of test results: In this test, we used a lamp with filaments of a good thickness, and we attached tungsten to these filaments.

Then we supplied the lamp with a voltage of 6 V, and it lit up, indicating that we got electrons.

After this step, we turned on the high voltage, and we observed a violet light path, which indicates that the electrons are moving quickly between the anode and the cathode.

However, the problem was that the light path was winding and not straight. In addition, the tungsten burned due to the air ingress, which led to the appearance of a white powder inside the tube.

Despite the tungsten burning, we still had electrons (due to the presence of high voltage) and they continued to flow across the path.

When we turned on and kept the pump running, the electron path began to stabilize and became almost straight.

After a while, the purple color began to fade, as the electrons continued to flow through their path while the pump was still running.

Turn on 6V and high voltage:

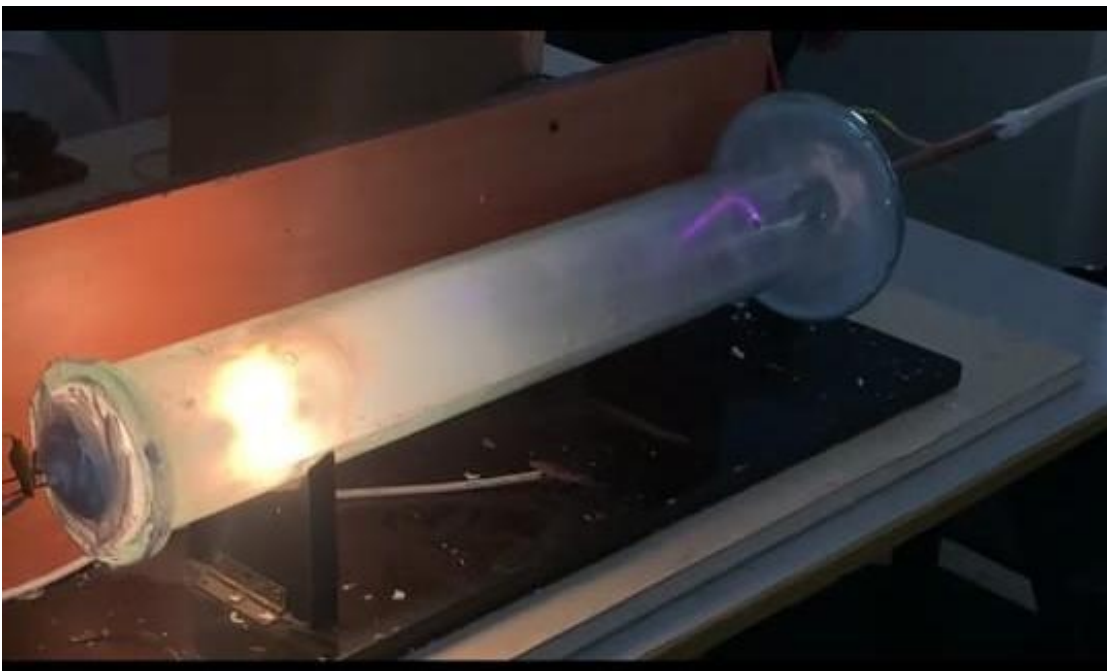


Figure III. 25: Lighting of the lamp and appearance of the electron trajectory

After a while, the tungsten burned out, but the electrons continued to flow:

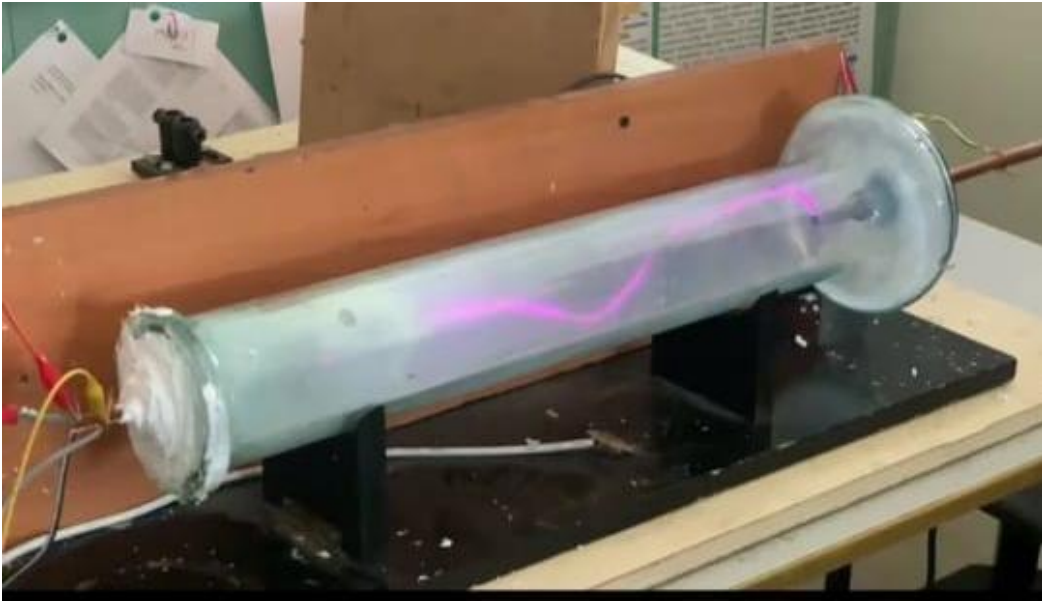


Figure III. 26: The tungsten has burned out



Figure III. 27: Trajectory of electrons while keeping the pump running

Here we started to run the pump continuously:

With the pump running, the color began to gradually fade, as the path became straighter:

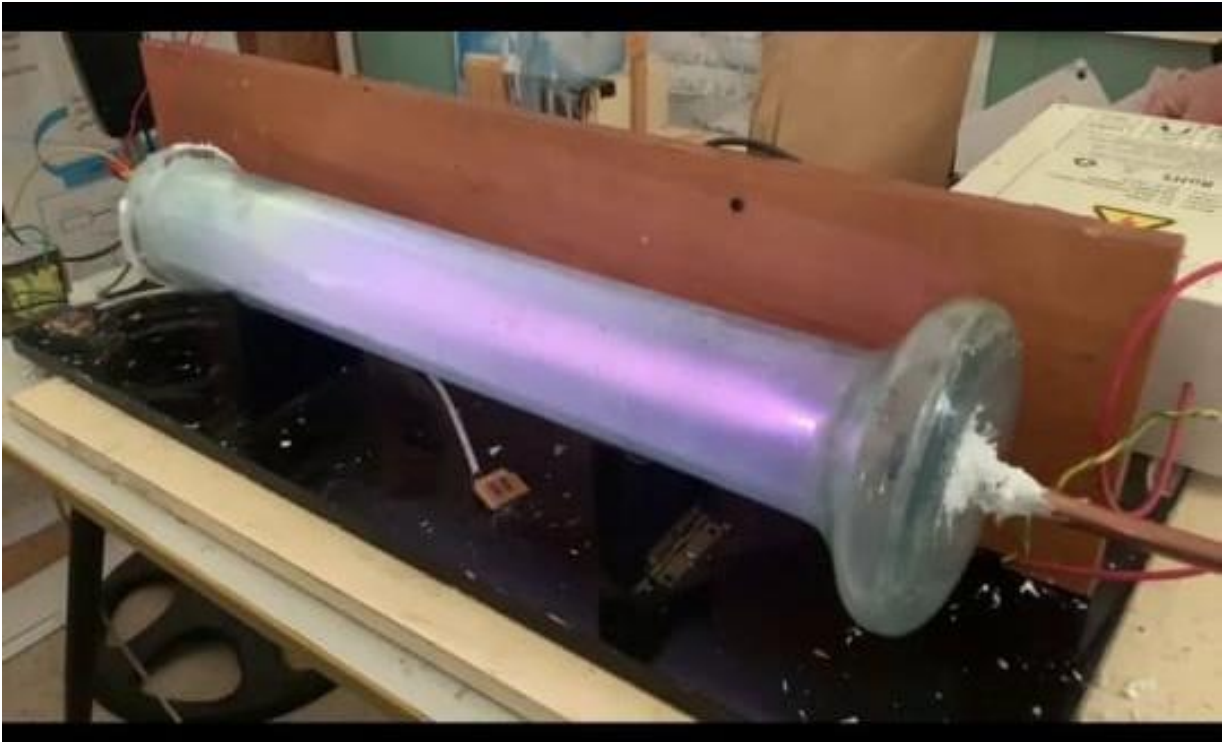


Figure III. 28: Beginning of the discoloration of the electron trajectory

Here we turned off the pump, the color reappeared and the path began to zigzag:

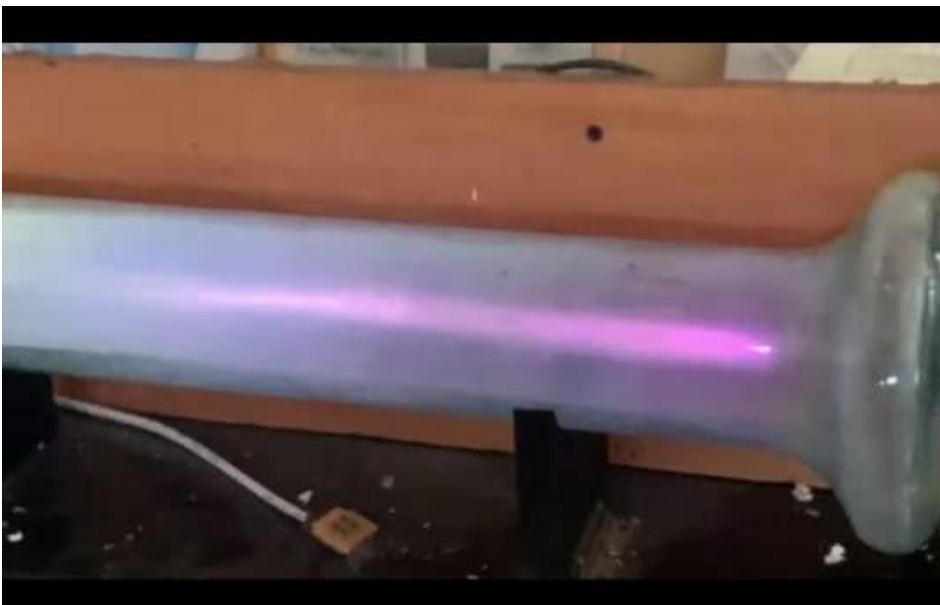


Figure III. 29: after turning off the pump



Figure III. 30: Combustion of tungsten

This white powder that appeared after the combustion of tungsten:



Figure III. 31: white powder

What we need to do:

We will run the pump from the beginning of the test until its end, to ensure that the combustion of the lamp and the appearance of powder are due to the entry of air.

Experiment with high voltage without supplying the lamp with another power supply (6 V).

8.5.6.6 LINAC Test 08/02/23

Analysis of test results:

With the pump running: we used a lamp with filaments of a good thickness, and we attached tungsten to these filaments.

Then we supplied the lamp with a voltage of 6 V, and it lit up, indicating that we got electrons.

After this step, we turned on the high voltage, and we observed a violet light path, which indicates that the electrons are moving quickly between the anode and the cathode.

Since the pump was still running, the electrons followed a nearly straight path.

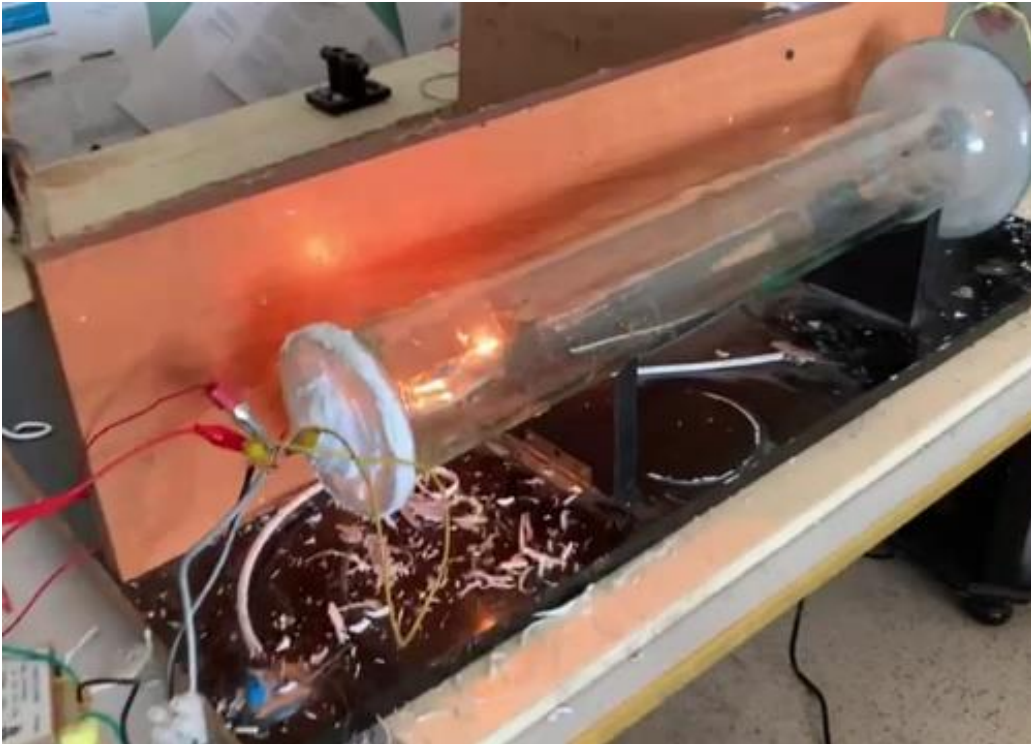




Figure III. 32: ignition of the tungsten lamp and appearance of the electron trajectory

When we turned off the tungsten power supply, the purple color remained. This indicates that the electrons generated by the presence of the high voltage continue to flow.





Figure III. 33: After turning off the tungsten power supply

What we need to do:

We will replace the tungsten used previously with the tungsten contained in the television lamp to obtain a thin electron beam.

8.5.6.7 LINAC Test 10/02/23

Analysis of test results:

With the pump running: We used a television lamp containing tungsten.

Then we supplied the lamp with a voltage of 6 V; it lit up briefly and then burned out, indicating that we are not getting a continuous output of electrons through the heater (6 V).

After this step, we turned on the high voltage, and we observed a violet light path, which indicates that we are getting electrons from the high voltage, and these electrons are moving quickly between the anode and the cathode.

Since the pump was still running, the electrons followed a nearly straight path.

However, this path was not thin because the electrons were coming out of all sides of the lamp (because the lamp was present without the bulb covering it).

The lamp we used for this test:



Figure III. 34: Television lamp

The route we got:



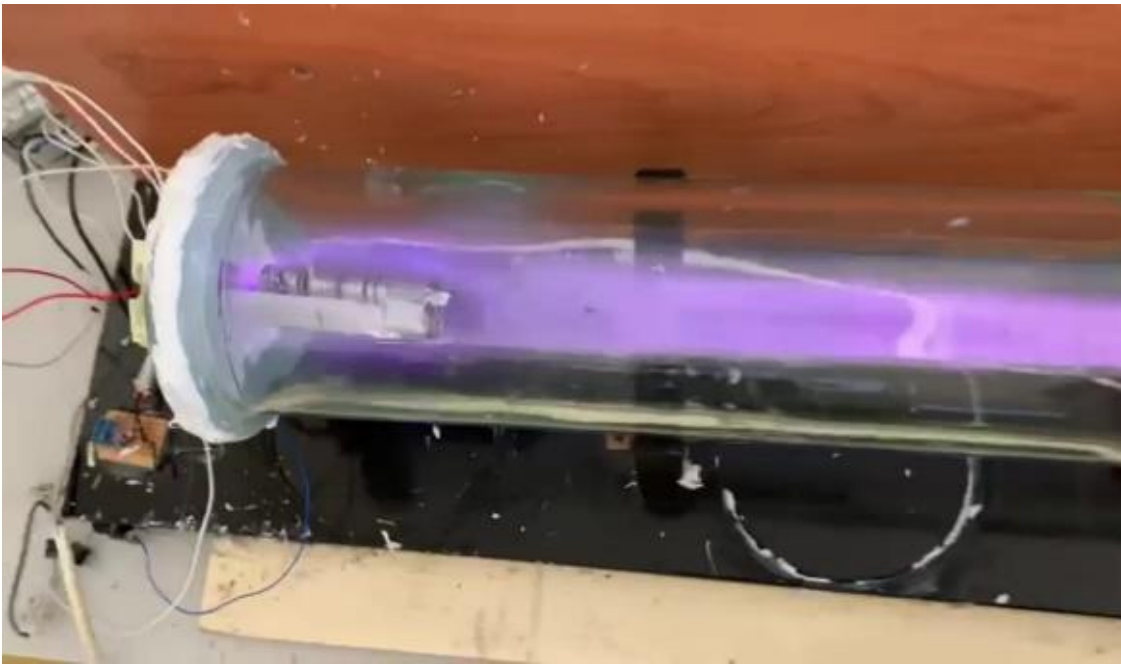


Figure III. 35: Path of electrons using the television lamp

What we need to do:

We are going to use a lamp that has glass surrounding it.

We're going to put a cylinder across the path of the electrons to center them.

8.5.6.8 LINAC Test 03.03.23

Analysis of test results:

With the pump running:

We used a lamp wrapped in glass.

Then we supplied the lamp with a voltage of 6 V; it lit up briefly and then burned out, indicating that we are not getting a continuous output of electrons through the heater (6 V).

After this step, we turned on the high voltage, and we observed a violet light path, which indicates that we are getting electrons through the high voltage (HV), and these electrons are moving.

However, this path did not complete until the anode, it stopped at the cylinder. Sometimes it touches the cylinder opening, and sometimes it crosses the cylinder from its beginning, then it deviates and touches the outer part of the cylinder.



Figure III. 36: Television lamp with its envelope



Figure III. 37: Cylinder to center the trajectory of the electrons



Figure III. 38: Safety rod





Figure III. 39: The outer part of the cylinder





Figure III. 40: Path of the electrons that we obtained

8.5.6.9 Summary of our experiments :

LINAC tests	Issue	Solution	Result
Test 16.01.23	We found a leak near the anode, the cathode and the junction between the cathode and the pump pipe.	Seal the leak areas by adding silicone	Positive
Test 16.01.23	The high voltage connection between the anode and the cathode burned out the lamp due to the thinness of the tungsten filament	Use a lamp with a thicker tungsten filament to withstand the higher voltage.	Negative
Test 01/28/23	Even with the use of thicker tungsten,	Use another tungsten lamp	Negative

	it burned out quickly due to the melting of the tungsten rods in the lamp.	with thicker filaments to handle the amperage (~2mm)	
Test 01/30/23	The path of the violet light was winding and not straight (in the shape of a standing wave)	Increase the distance between the anode and the cathode	Positive
Test 01/31/23	Burning tungsten and appearance of white powder inside the tube due to turning off the pump during the experiment	Operate the pump from the start of the test to the end	Positive
Test 08.02.23	No problem (We get an almost straight purple path)	Replace old tungsten with TV lamp tungsten to get a fine electron beam	Positive
Test 10.02.23	The path was not thin because the electrons came out of all sides of the lamp (Because the lamp was present without the bulb covering it)	Use a lamp that has a glass frame around it, And put a cylinder across the path of the electrons to center them.	Negative
Test 03.03.23	The lamp went out, but we got electrons thanks to the high voltage	The choice of this lamp was not appropriate. We will return to using	Negative

	(HV)+ the purple path did not complete to the anode, it stopped at the cylinder.	the previous tungsten lamp because it produced better results.	
--	--	--	--

8.6 Basics concerning X-ray production (by collision of accelerated electrons on heavy metals)

When electrons impact the target, this results in the production of X-rays. This X-ray emission can be classified into two distinct types: characteristic radiation and bremsstrahlung radiation .

8.6.1 The characteristic radiation

When an electron from the cathode collides with an electron in the K-shell of the target atom, it can knock that electron off, causing an electron to transition from a higher shell (e.g., the L-shell) to fill the vacancy in the K-shell. During this transition, energy is released in the form of characteristic X-ray radiation. If the electron falls from the L-shell to the K-shell, the characteristic K-Alpha X-ray radiation is obtained. And if the electron comes from the M-shell to fill the vacancy in the K-shell, the characteristic K-Beta X-ray radiation is obtained. These characteristic radiations are specific to each chemical element, which makes them suitable for use in X-ray analysis to identify the elements present in a material.

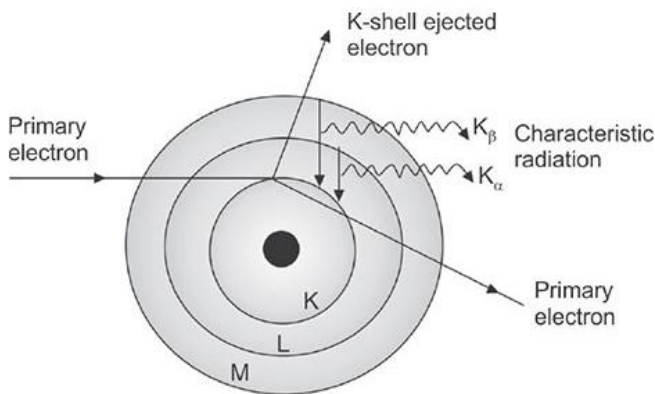


Figure I. 6: explanatory diagram of the production of characteristic radiations

8.6.1.1 Braking radiation (Bremsstrahlung):

When an electron moves quickly and interacts with the Coulomb field of the atomic nucleus, it can be deflected from its original path. This deflection causes the electron to lose kinetic energy, and this lost energy is emitted as a bremsstrahlung X-ray.

8.6.1.2 X-ray spectrum:

When electrons interact with the target, their kinetic energy can be dissipated in different ways, depending on the precise location of their interaction with the target's atoms. Some electrons may interact with atoms on the surface of the target and then interact with other atoms deeper inside. Other electrons may interact directly with deep atoms as soon as they enter the target. Because of these different interactions, the amount of energy of the X-rays produced can vary, leading to a different energy spectrum. This is a normal characteristic of X-ray production processes. As shown in the figure below:

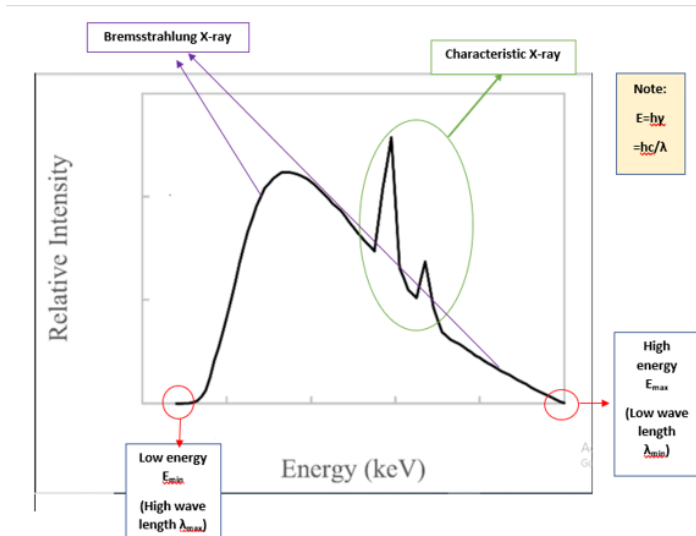


Fig. I.7: Graph representing the X-ray spectrum

8.6.2 The target (copper)

As mentioned earlier, we have chosen copper as our target. We will therefore conduct a detailed study of the energy required for electrons to collide with copper and produce X-rays. We will also analyze the X-ray spectrum resulting from this electron-copper interaction.

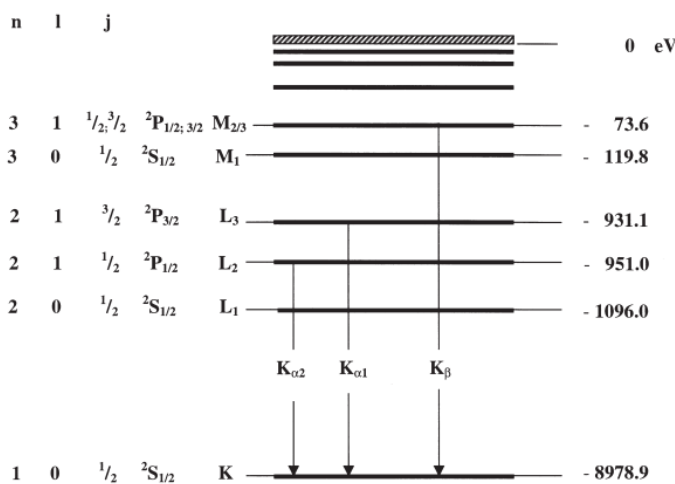


Figure I. 8: Energy levels of copper

- $E_K = 8.979 \text{ KeV}$; therefore the applied voltage must be greater than or equal to this energy.

For this we take $U_b = 10 \text{ Kv}$.

- $E_{k\alpha} = E_k - E_L = 8.979 - 0.951 = 8.028 \text{ KeV}$.
- $E_{k\beta} = E_k - E_M = 8.979 - 0.073 = 8.906 \text{ KeV}$.
- X-ray spectrum for the copper atom:

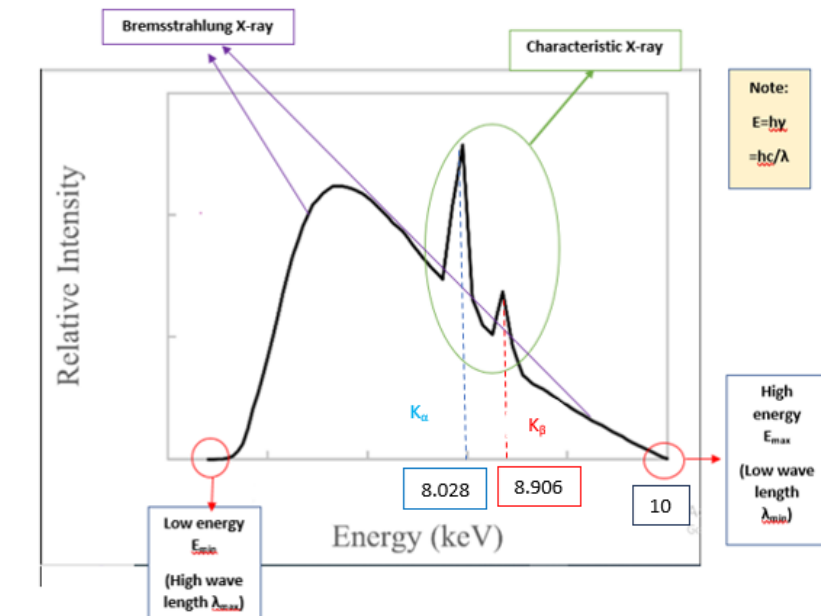


Figure I. 9: Graph representing the X-ray spectrum for the copper atom

8.7 Detection of X-rays with Geiger Muller counter

It should be noted that among the multitude of specialized detectors for capturing X-rays, we have the "XR1 Pro" type detector.

The XR1 Pro is a portable device designed specifically for the detection of nuclear radiation, such as gamma rays and ionizing X-rays. It is primarily used in areas such as radioactivity detection, radioactive contamination monitoring, and radiation dose measurement in various radiation protection applications.

It should be noted that the XR1 Pro is not specifically designed for detecting X-rays used in applications such as radiography or materials analysis. While it may be capable of detecting some X-rays, its primary purpose is to detect nuclear radiation, particularly gamma rays.



Figure I. 10: Détecteur du rayon x de type "XR1 Pro"

- R = Alarm Value Setting (Alarm): This function allows you to set an alarm value for radiation detection.
- M = AVG Reset (Average): This function allows you to reset the average of the values recorded by the detector.
- L= mute or sound.
- L+R = ACC Reset (Accumulation): This function resets the accumulation of radiation values recorded by the detector.
- REAL: This indication means that the detector displays the current radiation value in real time.
- AVG (Average): This indication means that the detector displays the average of the radiation values recorded over a given period of time.
- Prompt: Means that the detector takes radiation measurements in real time or almost immediately after radiation has been detected.

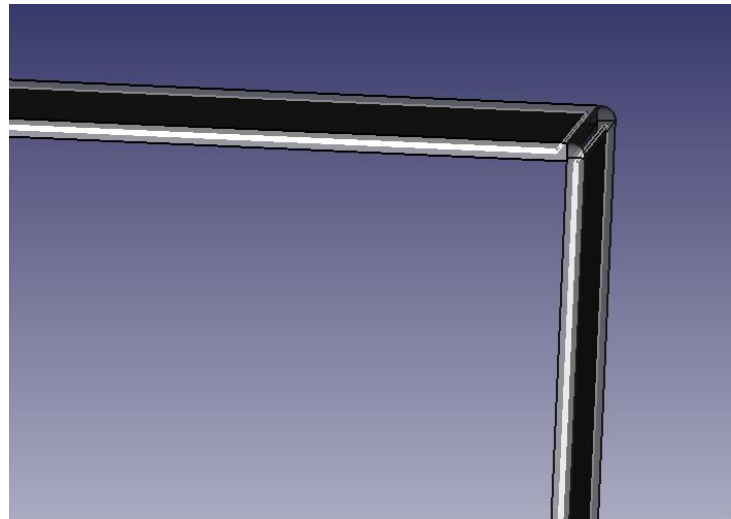
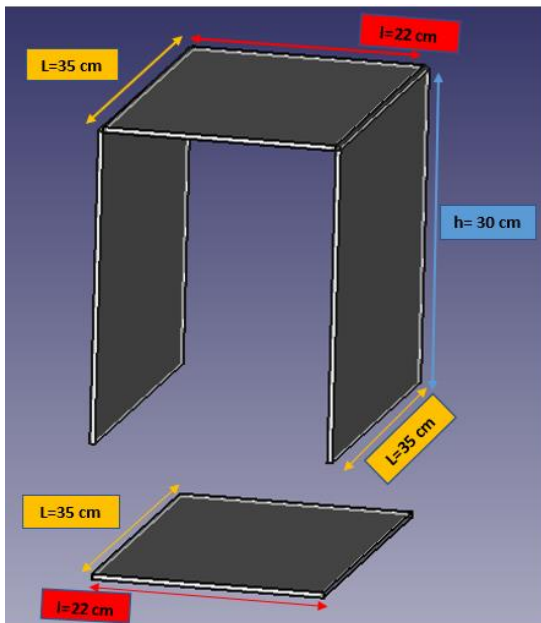
8.8 Safety with X-rays working

X-rays are a type of electromagnetic radiation characterized by their high energy and ability to penetrate body tissues. Prolonged or repeated exposure to this type of radiation can induce alterations at the cellular and tissue level, increasing the potential for genetic mutations and the incidence of malignant pathologies. To mitigate these potential risks, it is common to resort to shielding methods involving the use of materials with high X-ray absorption capacity, among which lead is a common shielding method. Lead has the ability to block a large portion of X-rays, acting as an effective shield to reduce radiation exposure.

8.9 X-Ray Protection Lead box design & Realization

As you know, lead plays a crucial role in X-ray protection due to its ability to effectively reduce the ionizing radiation emitted by these rays. Lead is a dense material that can block or significantly reduce the penetration of X-rays through objects. This is why its use in the design and manufacture of X-ray protective equipment is essential.

Based on this understanding, we decided to create a lead box that will protect us from these rays effectively.



8.9.1 Computer Aided Design (CAD)

The box we use consists of two iron plates with a 1 mm thick lead plate positioned between them. The dimensions were selected proportionally to the area from which the X-rays will be emitted.



14022023-IAP-lead
box for safety.FCStd

Figure II. 6: les mesures associées à la boîte du plomb

Figure II. 5: l'emplacement de la feuille de plomb



Being aware of the toxicity of lead, it is not possible to make a box using only this substance. Therefore, we placed it between two sheets of iron and soldered them together.

8.9.2 Realization



In this paragraph, we will present you with several images describing the box manufacturing process

Figure II. 7: Soldering during the manufacture of the lead box

Figure II. 8: The final design of the lead box

8.10 Basics concerning electron beam deflection by Helmholtz coil

In our design process, we identified the imperative need to create a magnetic field to deflect the electrons along the path determined for the production of X-rays. This magnetic field had to meet certain essential characteristics, including its uniformity, its perpendicularity to the electron speed and its upward orientation. In accordance with these requirements, we set out to find a suitable magnet to generate this magnetic field.

Among the commonly used magnet types, we considered flat coils, solenoid coils, and U-shaped magnets. However, after careful analysis, we concluded that these types of magnets were not suitable for our device due to certain specific limitations. The reasons for our decision are outlined in the table below:



Types of magnets	Flat coil	Solenoid coil	U-shaped magnet
	Absence of a uniform magnetic	Difficulty in manufacturing a	Inability to manufacture and

Disadvantages	field at a certain distance from this coil	large solenoid coil with a large number of turns and inability to place the device within these turns	control the intensity of the magnetic field
----------------------	--	---	---

Table I. 3: Disadvantages of some types of magnets

This evaluation guided us towards other options for securing the magnetic field required for our X-ray production device, which led us to the design of the Helmholtz coil.

8.10.1 Definition

Helmholtz coils are an electromagnetic device consisting of two identical circular coils placed in parallel, facing each other, at a distance equal to their own radius. They are used to generate a relatively uniform magnetic field in the space between the coils, making them useful in many scientific and experimental applications requiring a controlled and stable magnetic field.

8.10.2 Features

The main characteristics of Helmholtz coils are:

- **Specific geometry** : Helmholtz coils have a well-defined geometry with two identical circular coils, aligned in parallel and placed at a distance equal to their radius.
- **Uniform Magnetic Field**: They are designed to create a relatively uniform and predictable magnetic field in the central area between the two coils.
- **Low Amount of Material**: Helmholtz coils are designed to operate with a relatively small amount of magnetic material, making them economical and practical.
- **Magnetic Field Control**: By adjusting the electric current flowing through the coils and the number of turns, the strength of the magnetic field generated can be precisely controlled.
- **Various uses** : They are commonly used in experimental physics, materials research, geophysics, and electronics to eliminate the Earth's magnetic field, study high-frequency phenomena, and perform experiments requiring a controlled magnetic field .

8.10.3 Mathematical formula

The formula for calculating the magnetic field at the center of the gap between the two Helmholtz coils is given by the equation:

$$B = \frac{\mu_0 I N R^2}{2(R^2 + \left(x - \left(\frac{d}{2}\right)^2\right)^{\frac{3}{2}}}$$

This formula is derived from the Biot-Savart law and allows the calculation of the magnetic field at any point on the central axis of the coils as a function of the physical parameters of the configuration.

8.10.4 Manufacturing conditions

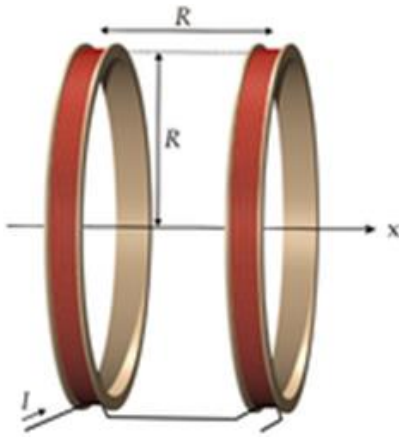


Figure I. 11: Schéma représentant d'une bobine de Helmholtz

Precise manufacturing of Helmholtz coils is essential to ensure a uniform magnetic field. The coils must be designed with identical geometric specifications, including the number of turns and the current flowing through them. Using materials with high conductivity and low resistance helps minimize energy losses and ensure optimal performance. Precise coil alignment and spacing equal to the radius are key factors in achieving a uniform magnetic field at the center of the gap between them. Finally, careful coil insulation is necessary to prevent current leakage and unwanted electromagnetic interference.

8.11 Helmholtz Coil Design

8.11.1 Fundamental Precepts

The proper development of Helmholtz coils requires strict adherence to various imperative conditions, which define the essential basis of their design. This section examines the fundamentals of Helmholtz coil design, highlighting the principles inherent in their optimal manufacture and ensuring superior performance.

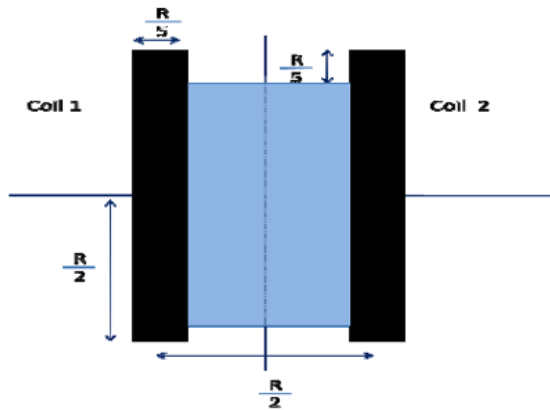
- Consistent Twin Coil Characteristics

The geometric cohesion, the number of turns, and the intensity of the current flowing through the two coils must be strictly identical. This strict uniformity ensures the harmonization of the generated magnetic field, thus contributing to the achievement of optimal performance.

- Alignment and Spacing Accuracy

Careful parallel alignment, combined with spacing identical to the radius, is essential to achieve a uniform distribution of the magnetic field at the heart of the device. This rigorous arrangement eliminates any unwanted asymmetry.

Figure II. 9: Quelques conditions de fabrication de la bobine de Helmholtz



- Sizing of the Rolled Section

For optimum performance, the dimensions of the wound section, in terms of width and depth, should not exceed one tenth of the coil diameter ($D/10$). This criterion ensures consistent winding and helps avoid unwanted distortions of the magnetic field.

- Selection of good conductive materials

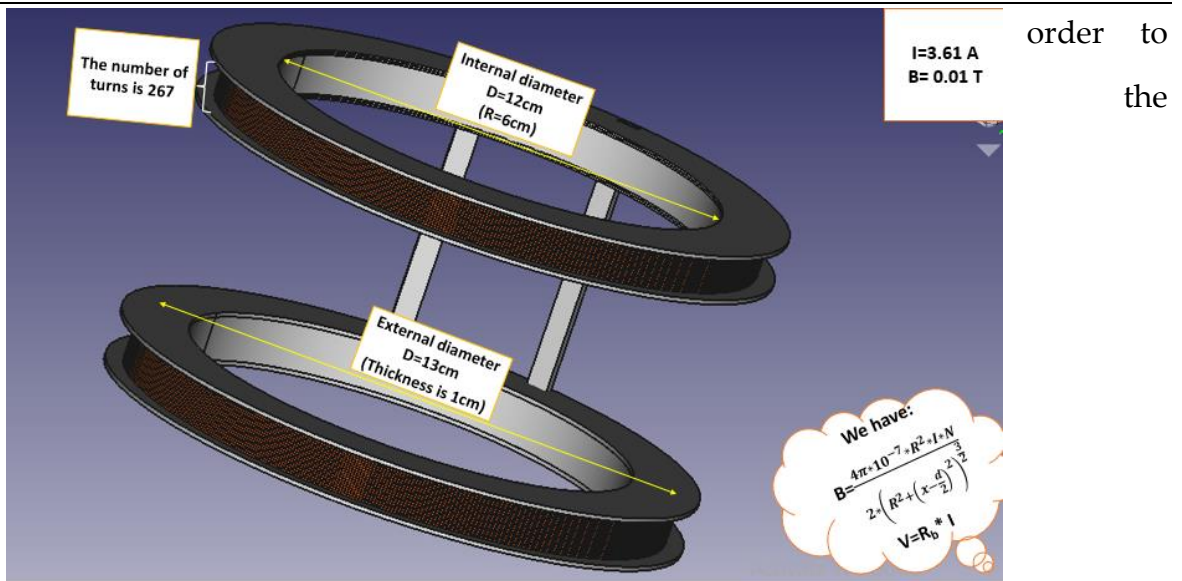
Choosing the right materials for the coils is very important. Using materials (in our case, we'll use 1 mm thick copper wire) that allow current to flow well and don't resist too much is crucial to avoid losing energy and for the coils to work optimally. It also makes the entire coil more efficient.

- Careful insulation

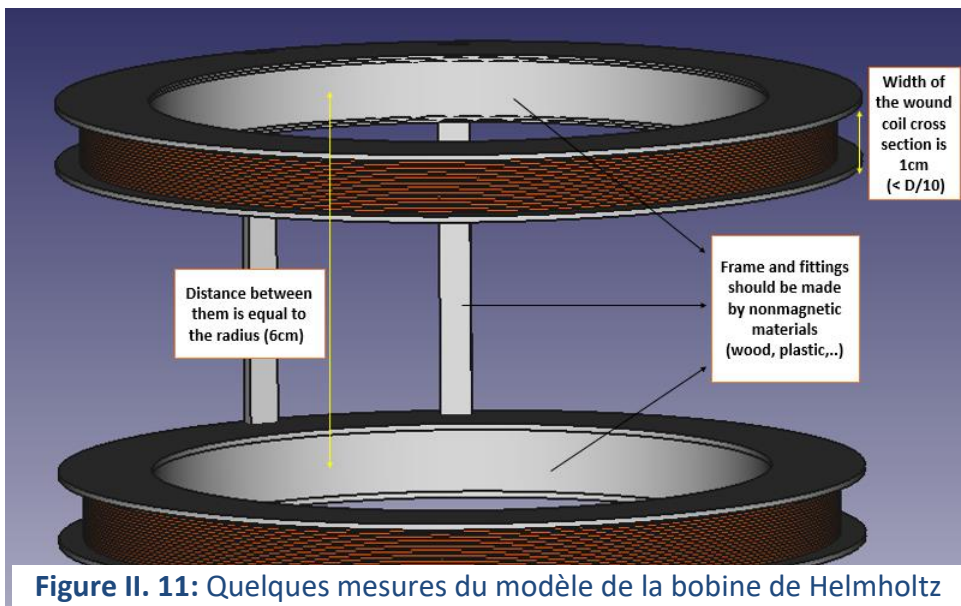
Properly insulating the coils is very important to prevent current leakage and prevent annoying electromagnetic interference. Good insulation allows the coils to operate independently and prevents unwanted external influences; that's why we'll use a specific type of plastic.

8.11.2 Computer Aided Design (CAD)

In design



Helmholtz coil model, we used " FreeCad ".




 221122_IAP_Helmoh
 ltz coil design.FCStd

8.11.3 Realization

We have:

Figure II. 12: Quelques caractéristiques du modèle de la bobine de Helmholtz

- $B=0.01$ T
- $I=3.6$ A
- $R' = 6$ cm
- $d' = 6$ cm
- $x=3$ cm

Using the following formula: $B = \frac{\mu_0 I N R^2}{2(R^2 + (x - \frac{d}{2})^2)^{\frac{3}{2}}}$, we determine the number of turns $N=267$ turns.

A tube with a diameter of 6 cm will be positioned at the center of the Helmholtz coil arrangement. Based on this characteristic, we designed the Helmholtz coil with a radius of 6 cm.



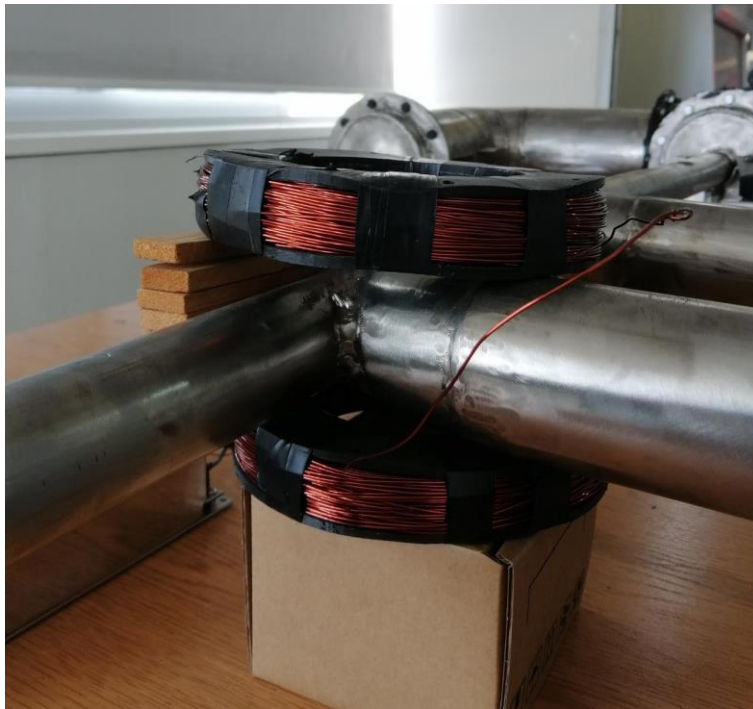
Figure II. 13: Le tube courbé où la bobine de Helmholtz est positionnée'

In accordance with the conditions of production of the coil was carried out as follows:



Figure II. 14: Position de la bobine de Helmholtz dans le prototype

with the stated above, the the Helmholtz



8.12 Helmholtz coil test

8.12.1 Requirements

- System Requirements:

The Helmholtz coil is to be made from two pieces of plastic on which a copper strip is wound (Each piece is wound with 267 turns).

- Electrical requirements:

A power supply must be capable of supplying a voltage of 21.7 V and a current of 3.61 A to the Helmholtz coil.

- Magnetic requirements:

The Helmholtz coil must be able to generate the magnetic field necessary to deflect the electrons.

The Helmholtz coil must be able to generate a magnetic field of 0.01 T.

- Safety requirements:

Electrical safety:

21.7V cables and connections must be insulated with...

8.12.2 System test specification

Stage	Description of the stage	Expected result
Precondition	The system is off	
Turn on the system	Turn on the Helmholtz coil by supplying it with a supply of 21.7 V.	Obtain a magnetic field ($B = 0.01 \text{ T}$)
Turn off the system	Turn off the Helmholtz coil.	Stopping the magnetic field
Postcondition	The system is off	

8.12.3 System Test and Results

- Magnetic field test 03.05.23

Stage	Description of the stage	Expected result	Result
Precondition	The system is off		
Turn on the system	Turn on the Helmholtz coil by supplying it with a supply of 21.7 V.	Obtain a magnetic field ($B = 0.01 \text{ T}$)	Positive
Turn off the system	Turn off the Helmholtz coil.	Stopping the magnetic field	Positive
Postcondition	The system is off		

Analysis of test results:

Electron Source, LINAC (with glass tube), electromagnetic deflection of electrons and X-Ray Generation

First, we place the magnetic field meter in the appropriate position (with its head in the middle between the two coils, and perpendicular to the direction of the magnetic field).

Then we started changing the voltage at each step, which changes the current I and the magnetic field B.

We continue increasing U until we reach the required current I, which gives us B = 0.01 T.

Experimentally:

U(V)	4.55	5	6	7	8	9	9.47	10.05	12	14.33	17.46	21.7	
I(A)	0.8	0.88	1.05	1.24	1.42	1.6	1.75	1.79	2.13	2.5	3	3.61	
B(mT)	2.3	2.5	3	3.5	4	4.5	4.8	5.02	5.96	7.01	8.45	10	
R(Ω)	5.69	5.68	5.71	5.65	5.63	5.62	5.41	5.61	5.63	5.73	5.82	6.01	R _m =5.68

Theoretically:

I(A)	0.8	0.88	1.05	1.24	1.42	1.6	1.75	1.79	2.13	2.5	3	3.61
B(mT)	2.24	2.46	2.94	3.46	3.97	4.47	4.89	5.01	5.96	6.99	8.38	10.09

The formula for the magnetic field in a Helmholtz coil is given by:

$$B = (\mu_0 * I * N * R^2) / (2 * (R^2 + (x - d/2)^2)^{3/2})$$

Or :

B is the magnetic field in Tesla (T).

μ₀ is the magnetic permeability of vacuum, equal to $4\pi \times 10^{-7}$ T m/A.

I is the electric current flowing through the coil in amperes (A).

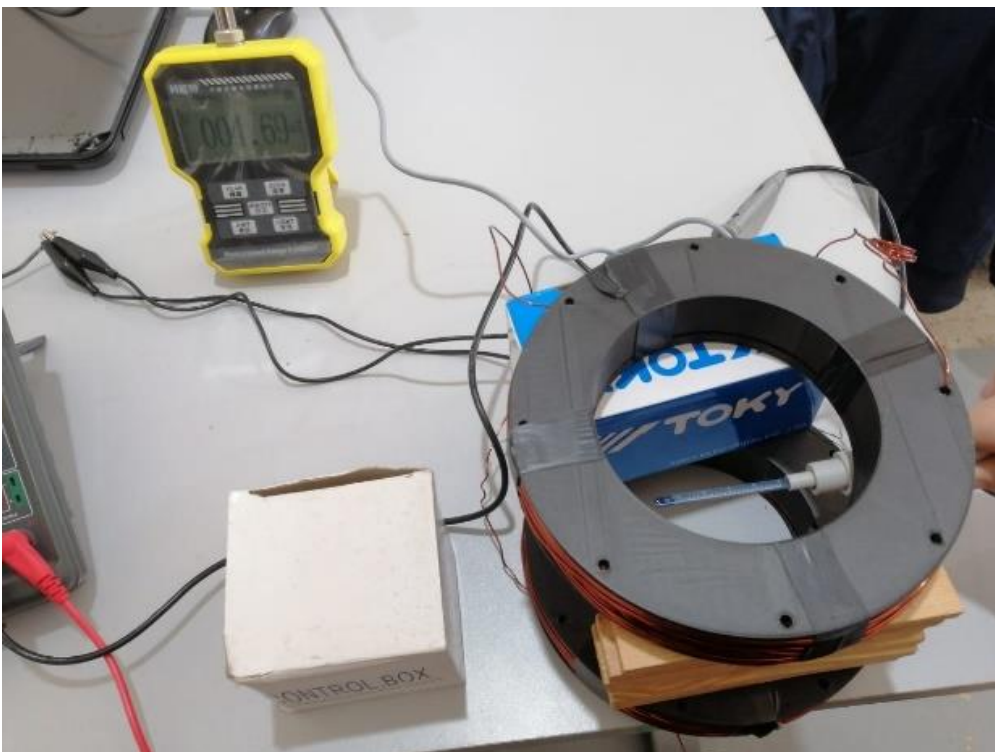
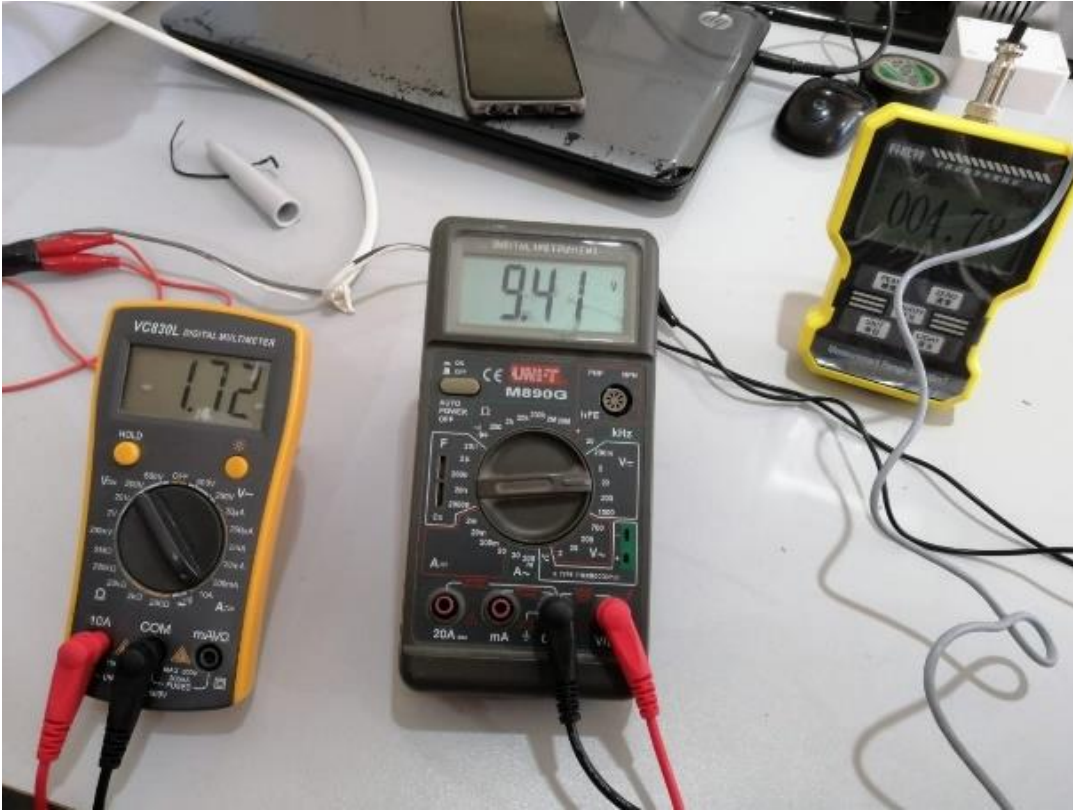
N is the number of turns in each coil.

R is the radius of each coil in meters (m).

d is the distance between the two coils in meters (m).

x is the distance along the central axis of the coils in meters (m).

In our case: $N= 267$; $R=6*10^{-2}$ m; $x=3*10^{-2}$ m; $d=6*10^{-2}$ m.



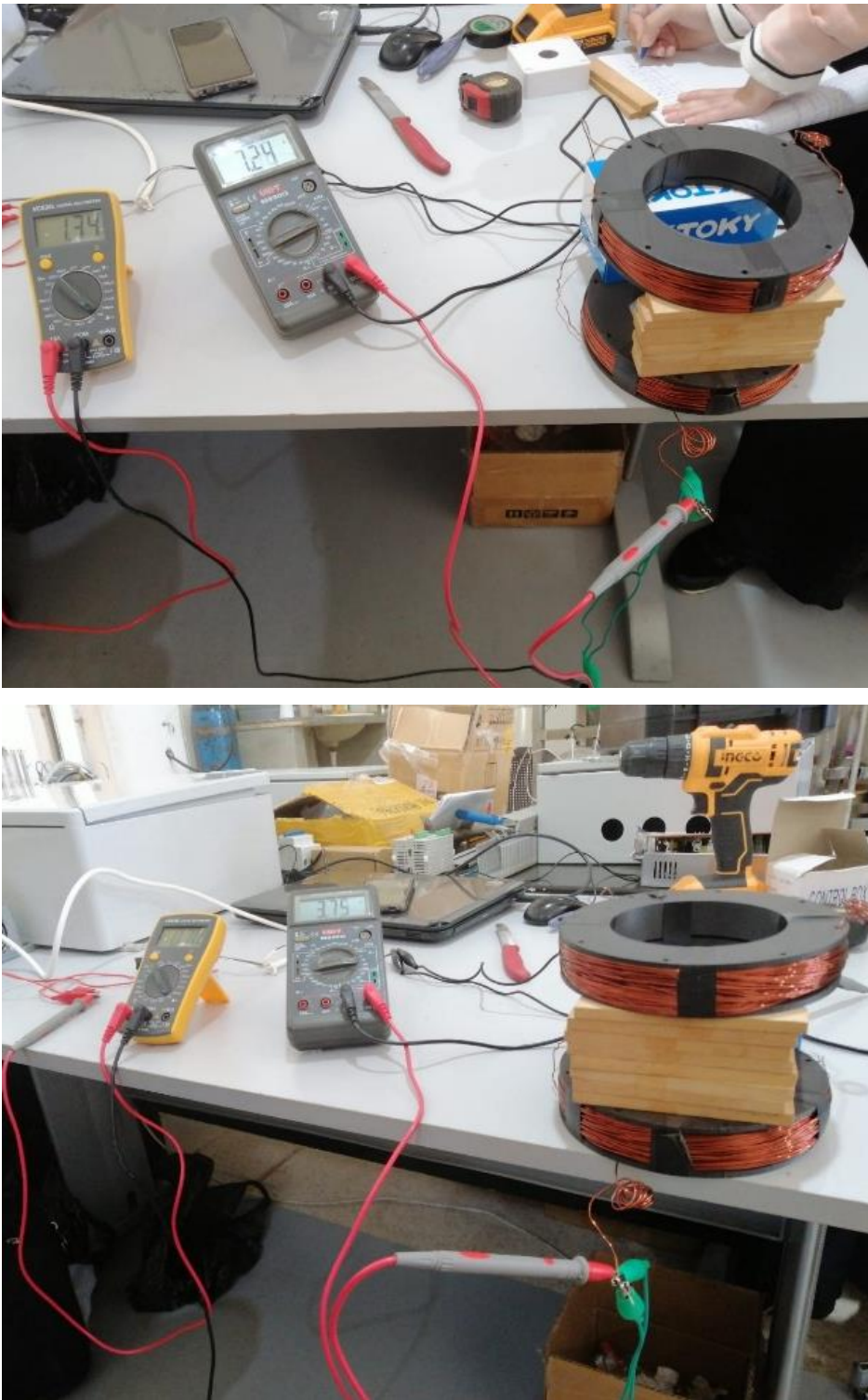


Figure III. 41: During our various measurements of the magnetic field

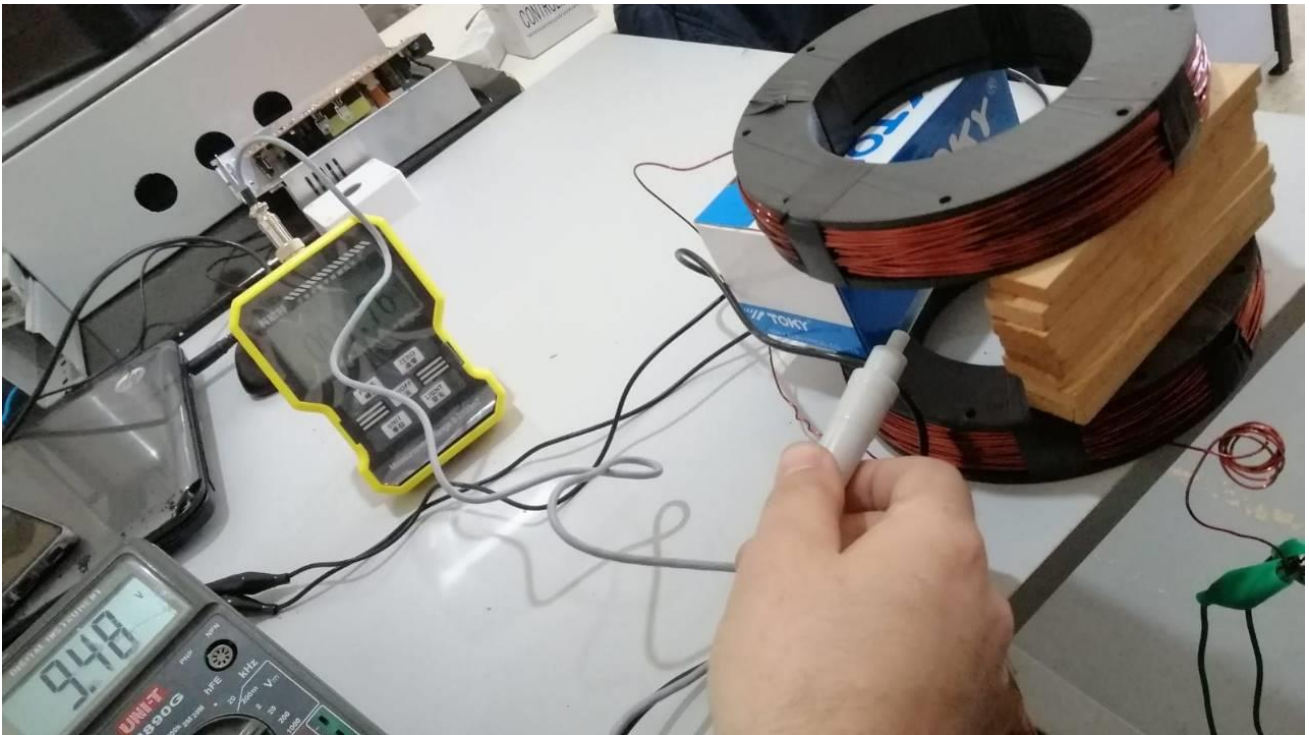


Figure III. 42: Magnetic field measurement protocol

We confirmed that the direction of the magnetic field is uniform by positioning the gauge in the same direction as the expected magnetic field; and the result was positive ($B=0$).

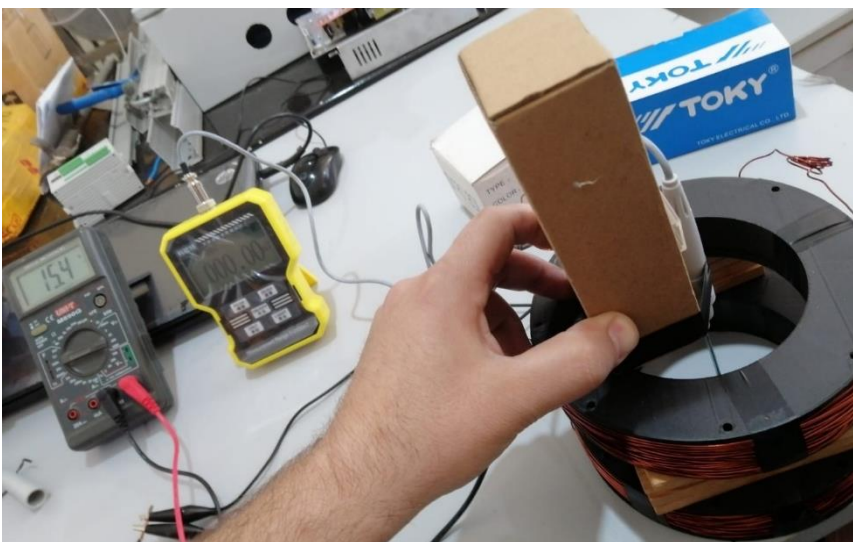


Figure III. 43: The case of zero magnetic field

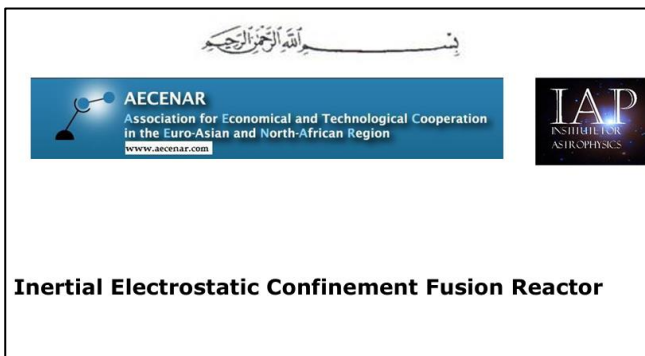
9 IECF (Inertial Electrostatic Confinement Fusion)

9.1 On www.aecenar.com

IAP	IAP Physics L	IAP Physics Lab Initial	
ICS	IAP Observat	Mechanical Realization	
ICPT	IAP Planning	PhysicsLab Initial PCS	
INT	2024	IECF	
ICP			IECF System Concept/
ICPT Lab		IAP-XRAMS	Design
AECENAR Technology Center		Laser Based	IECF Realization
تطبيقية		Detection	/Implementation
MEGBI-VPP / APP		Flue Gas Ana	IECF System Test
IAP-SAT		Mass Spectro	Specification
AECENAR Buildings Complex		Vacuum pump	IECF System Testing

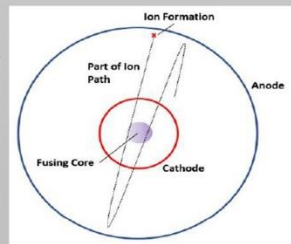
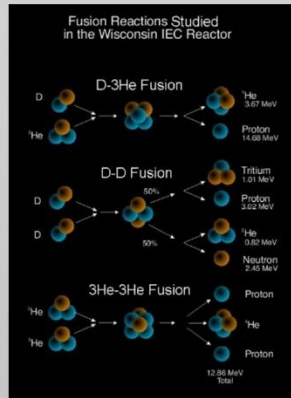
9.2 IAP-IECF Device Concept and Design

This section is from this report:

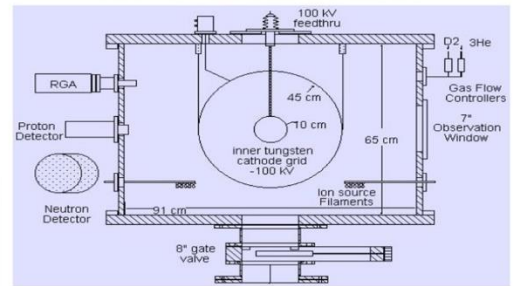


Principles

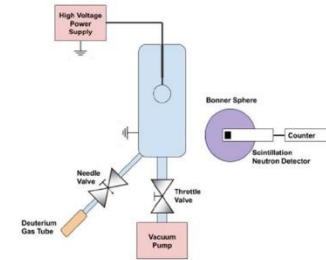
Inertial electrostatic confinement fusion does not rely on any magnetic field, and instead uses an electric field to perform the plasma confinement. The device is formed by arranging two spherical metal meshes concentrically and putting an extremely large voltage across them, typically 10 to 100 kV in vacuum. The meshes are supported by a high-voltage stalk. Fusion fuel, in this case deuterium, is then released into the chamber where the large voltage ionizes a portion of the gas. These positively charged ions are accelerated by the electric field toward the center of the device, where most will pass straight through the cathode at the center and out the other side due to the large gaps in the metal mesh. Once on the other side, the electric field slows the ions and eventually turns them back towards the center, setting up a recirculation. The ion density in the center increases, and eventually fusion occurs. This does not require nearly as large a machine as the tokamak: typical IEC devices comfortably sit on tabletops.



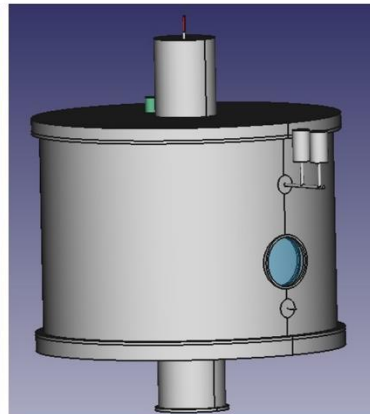
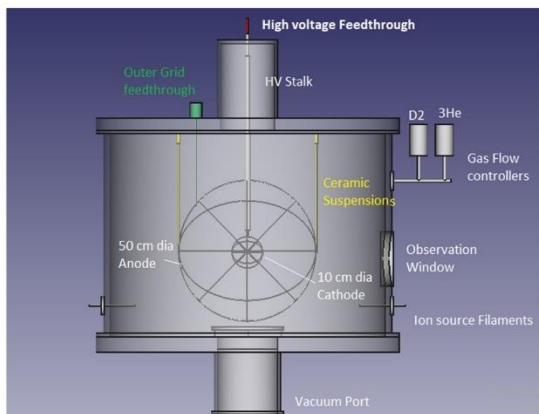
Inertial Electrostatic Confinement Fusor



University of Wisconsin-Madison IEC Device



Part	Description	Material	Size
Anode wire	grounded,	stainless steel	45 cm diameter grid of stainless-steel wire
Cathode wire	-100KV DC, supported on a 200 kV vacuum feed-through. input power levels exceeding 8.5 kW at voltages ranging from -25 kV to -185 kV and at currents from 30-75 mA.	tungsten	10 cm diameter coarse-grid sphere of 0.8 mm tungsten wire
stalk (will hold the cathode)	stainless steel tubing Quartz tubing non-porous high alumina ceramic (Alumina ceramic (Aluminum Oxide or Al2O3) is an excellent electrical insulator)	stainless steel, quartz, alumina	0.64 cm dia stanless 70 cm 1.28 cm dia quartz 55 cm 0.95 cm dia quartz 60 cm 1.91 cm dia Alumina 31 cm
Vacuum chamber	cylindric, base pressure of 2×10^{-7} torr, Experiments run steady-state within the limitations of chamber heating	Aluminum	91 cm diameter, 65 cm tall
Deuterium/ He gas tube	Electronically controlled gas flow regulators adjust the fuel flow ratio and amount into the system.		
Ion Source Filaments	2 filaments a discharge voltage and current of 80V and 200-500 mA is maintained	thoriated tungsten filaments	
vacuum pump	450l/s turbo pump		
high voltage supply	provides up to 200 kV at 75 mA		
neutron detector	helium proportional counter neutron detector, placed 60 cm from the center		



FreeCAD

Maryam Abdel-karim
@AECENAR / July 2021

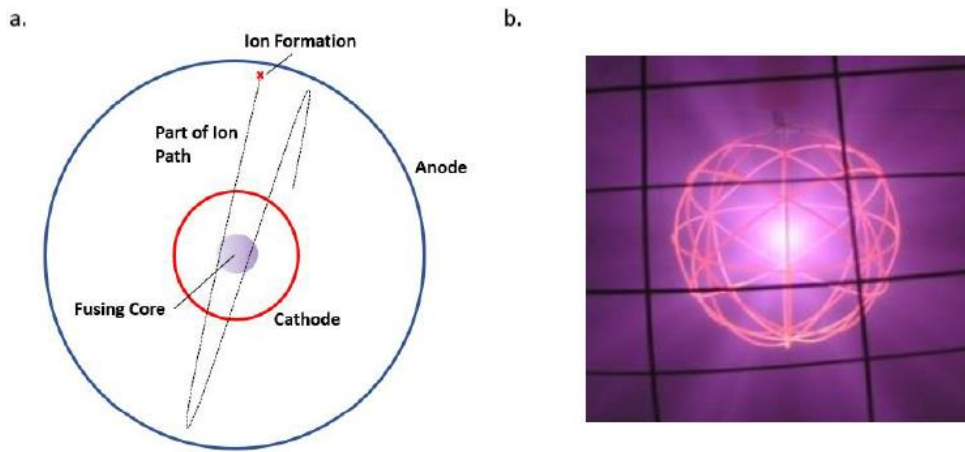


Figure 1.2 a) A general schematic of an idealized IEC fusion device. The red spherical cathode has a large negative voltage, while the larger blue sphere is a grounded anode. Deuterium is ionized near the anode, and these positive ions are accelerated by the radial electric field toward the center. The ions pass through the center and out the other side, where the electric field slows and turns them back. A high-density core sets up due to the presence of recirculating ions, and fusion occurs. b) A photo of an IEC device in operation at the University of Wisconsin-Madison [3]. The cathode grid glows orange from heat, while the anode (foreground) does not. Reproduced with permission.

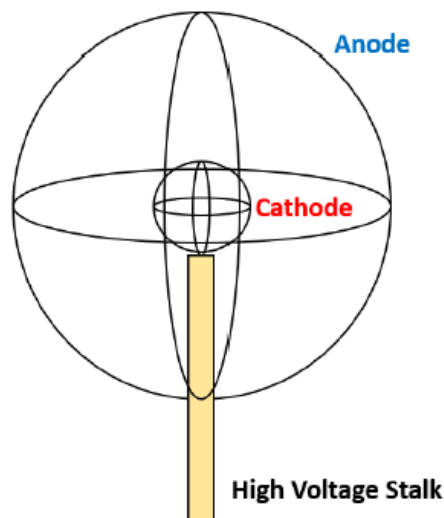


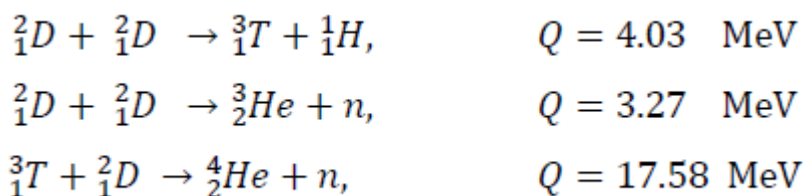
Figure 1.3 Realistic schematic of IEC device. The high voltage stalk supports the anode and cathode. The anode and cathode are far from being an ideal spherical surface, and are instead constructed from several wires. The stalk and wires are loss channels for ions recirculating within the device and inhibit ideal IEC operation.

1

9.2.1.1 Nuclear fusion

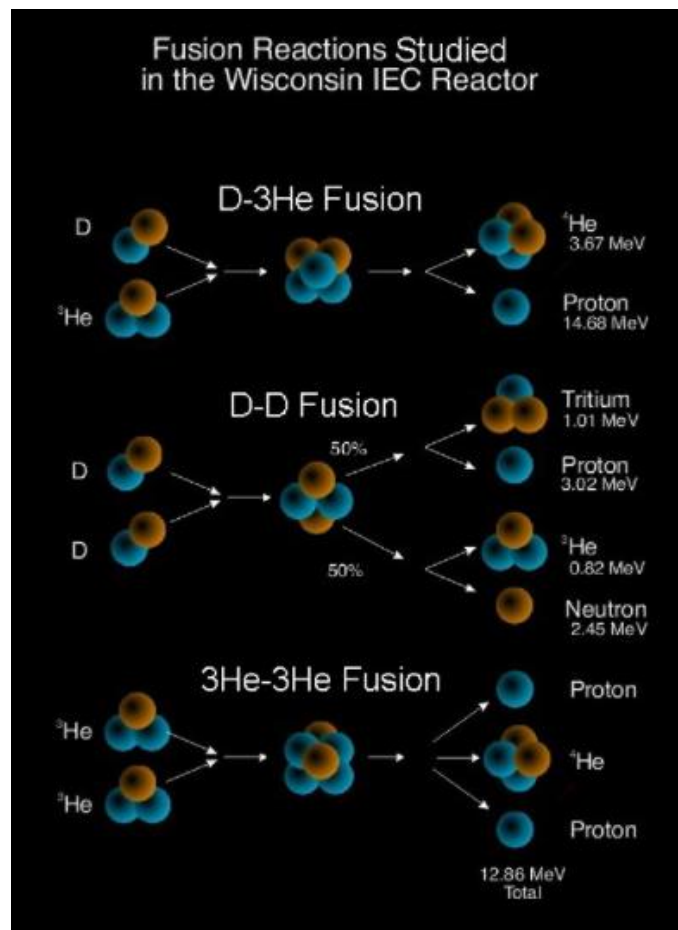
Nuclear fusion is the process by which small elements and isotopes can combine into heavier isotopes. The fusion reaction products will have a net mass that is lower than the reactants that entered the fusion reaction, called the mass defect. This mass defect Δm is exactly the amount of kinetic energy gained by the products of the fusion reaction. This kinetic energy gain can be

solved for using Einstein's famous equation $Q = \Delta mc^2$, where Q is the kinetic energy gained by the products and c is the speed of light in vacuum. Fusion reactions occur between two positively charged nuclei only when the two reactants come close enough for the strong force to fuse the two reactants. The two reactant nuclei must overcome the powerful Coulomb repulsion between the two positive nuclei for the fusion reaction to occur. The energy to overcome this Coulomb barrier can be supplied by the temperature of the products. If the thermal motion of the reactants where Q is the kinetic energy gained by the products and c is the speed of light in vacuum. Fusion reactions occur between two positively charged nuclei only when the two reactants come close enough for the strong force to fuse the two reactants. The two reactant nuclei must overcome the powerful Coulomb repulsion between the two positive nuclei for the fusion reaction to occur. The energy to overcome this Coulomb barrier can be supplied by the temperature of the products. If the thermal motion of the reactants is high enough, then the reactants will have enough kinetic energy to overcome the Coulomb barrier and initiate the fusion reaction. It is the high temperature requirements of fusion reactants that necessitate the merging of fusion science and plasma physics: most common fusion reactants, deuterium and tritium, exist in a plasma state at the temperatures required for fusion. The fusion reaction occurring in the device proposed here is D-D (deuterium-deuterium) fusion. An extremely small amount of D-T (deuterium-tritium) fusion could occur as tritium is a product of the D-D reaction. However, D-T fusion is likely not occurring at appreciable rates due to the low amount of D-D fusion occurring in the device and the short operating times. The branching ratio, defined as the probability of a certain set of products emerging from the same fusion reaction, is 50% for D-D products The two D-D reactions and the D-T reaction are



Where n is a neutron. The kinetic energy gain Q is shared between the products of the fusion reaction, with the lighter product particle receiving a larger proportion of the energy. The neutron produced by the D-D reaction has an energy of 2.45 MeV, and the proton produced by the D-D reaction has an energy of 3.02 MeV. These energy values are important for particle detection, which is discussed in Section 2.4. The neutron produced by the D-T reaction has an energy of 14.1 MeV. It is the 2.45 MeV neutron that can be measured to validate that fusion is occurring

in the proposed device. The number of 2.45 MeV neutrons detected per second can be used to predict the total fusion rate occurring in the device.²



9.2.1.2 Applications

Depending on the fuel, fusion produces several unique and potentially useful products: high-energy neutrons (2-14 MeV), thermal neutrons, high-energy protons (3-15 MeV), and electromagnetic radiation (microwave to x-ray to gamma-rays). These fusion products have many potential commercial applications, including but not limited to:

- production of radioisotopes for medical applications and research, including isotopes for positron emission tomography (PET)
- detection of specific elements or isotopes in complex environments, including explosives in the form of improvised explosive devices (IEDs), landmines, fissile material, and concealed nuclear weapons
- radiotherapy
- alteration of the electrical, optical, or mechanical properties of solids

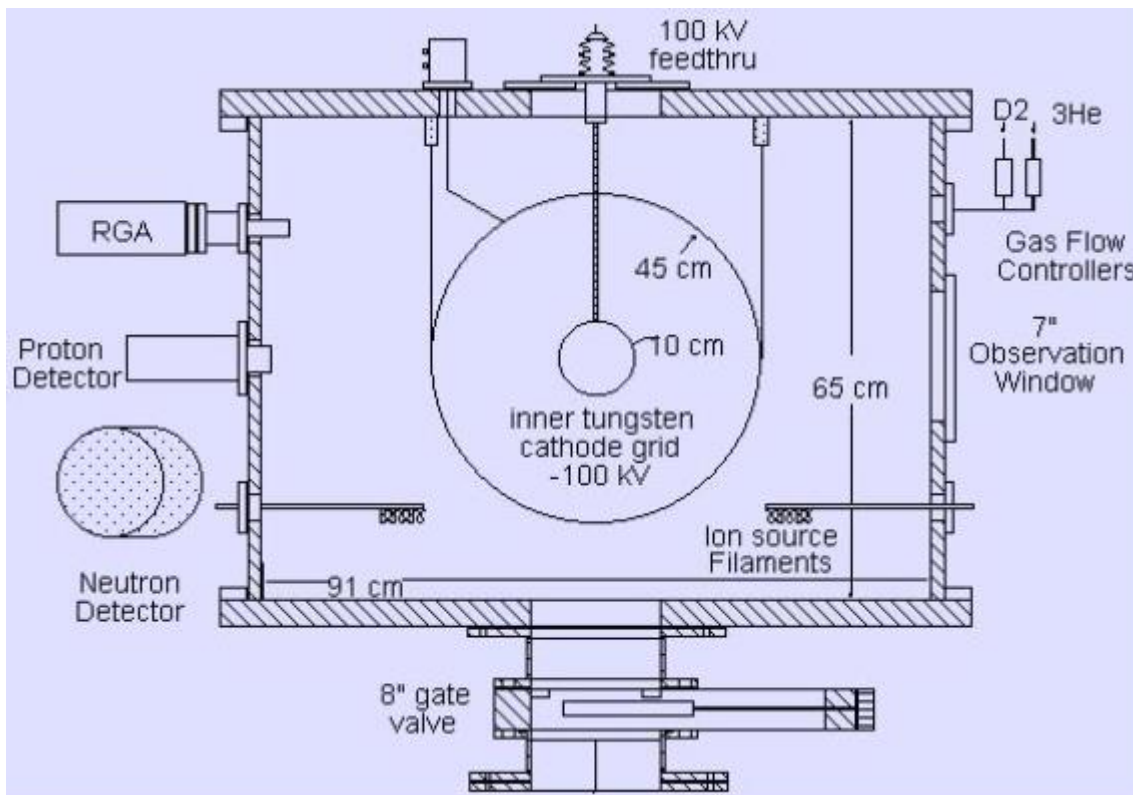
² Modeling the Fusion Reaction in an Inertial Electrostatic Confinement Reactor with the Particle-in-Cell Method - Jacob van de Lindt - 2020

- destruction of long-lived radioactive waste
- destruction of fissile material from nuclear warheads
- production of tritium for military and civilian applications
- food and equipment sterilization
- pulsed x-ray sources

9.2.1.3 University of Wisconsin-Madison Device

Design

The IEC reactor is a vacuum chamber filled with a fuel gas such as deuterium at low pressure. There are inner and outer spherical or cylindrical grids centered inside the chamber. The outer grid is held at nearly zero potential, and the inner, 90-99% transparent grid is held at a high negative potential, typically -100 kV. The potential difference between the grids accelerates ions inward to velocities of fusion relevance.



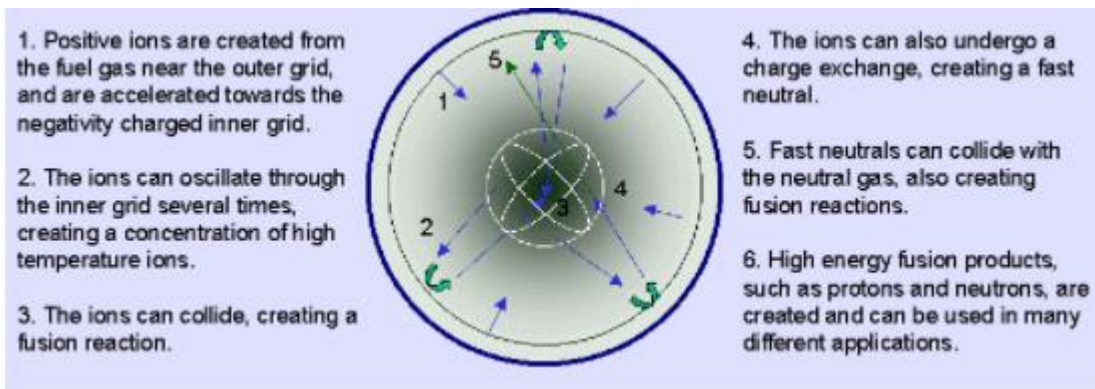
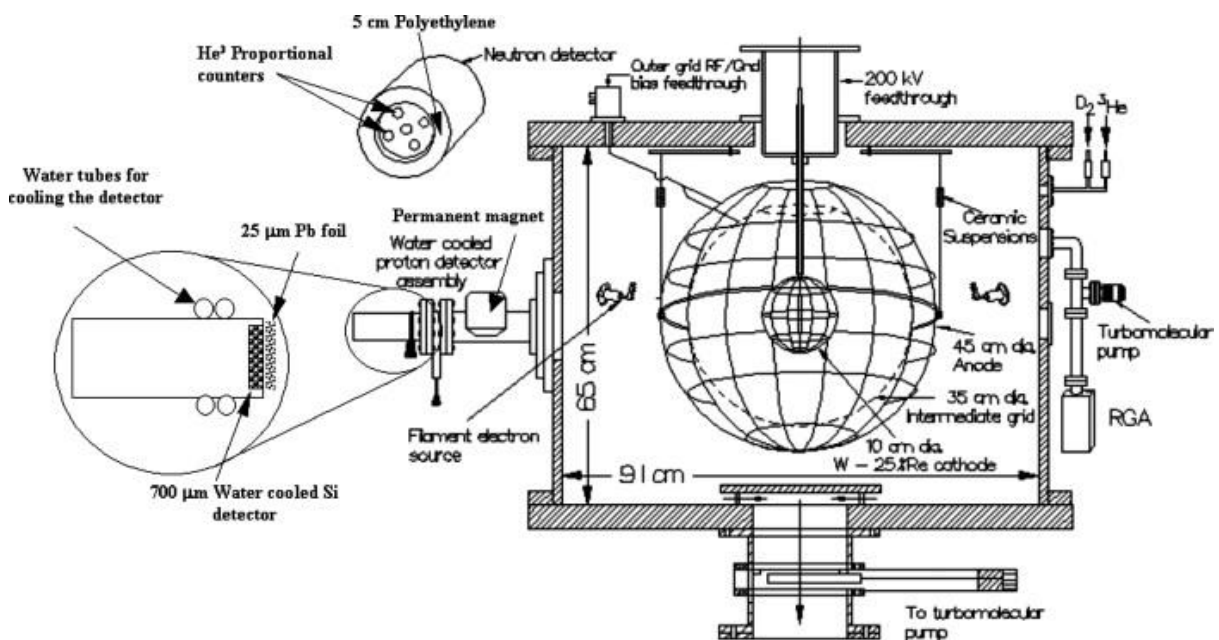
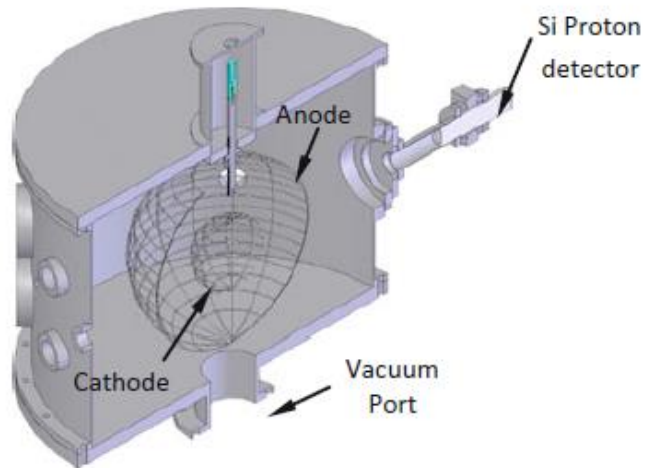


Fig. 1.6 Schematic of the IEC device (named Homer) at UW Madison. The cathode, anode, and the various detector ports are shown in the cross-sectional diagram [38]



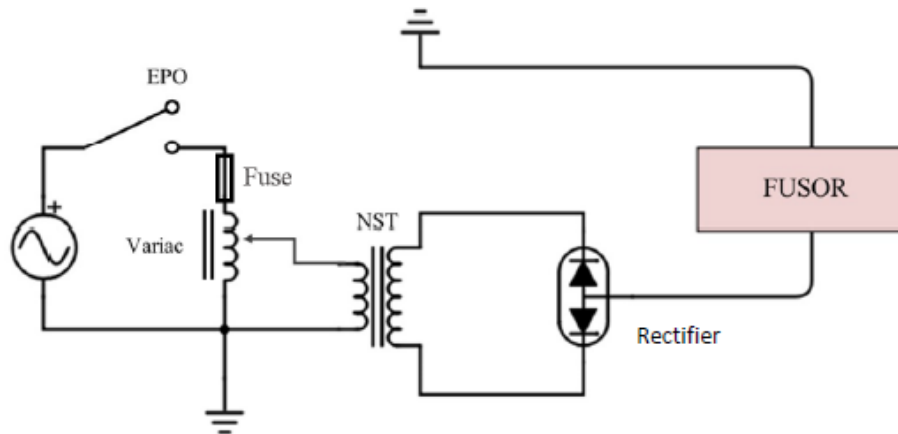


Figure 2.11 The general schematic of the proposed electrical system, which includes an emergency power off (EPO) switch and a fuse. The Variac and NST step up the wall voltage. The high voltage rectifier converts AC to DC [10].

High-Voltage Stalk Design for IEC

At the University of Wisconsin, Madison, the construction of the inner-grid stalk support was done to ensure the structural integrity and minimize the electrostatic stresses that are imparted to the stalk. Figure 4.7 shows the schematic of the side view of the high-voltage stalk assembly. Concentric tubes of aluminum and quartz were selected for the bulk stalk materials based on their rigidity and high voltage insulation properties. The ceramics are cut to size from the stalk using a diamond-bladed saw, and they are sealed together using ceramic cement and Torr-seal vacuum epoxy. The vacuum end of the stalk is also rounded using diamond files in order to minimize the electric stresses in that region.

The inner grids are tack-welded to rounded screws that then thread into the end of the stainless steel center tube.

The inner spherical grid hangs from a special ceramic stalk structure that is held in place by a ½" Cajon fitting atop a 100-kV isolation feedthrough. This independent attachment allows the inner cathode to be raised, lowered, and rotated with respect to the fixed outer grids and chamber walls. This arrangement provides external alignment of the cathode and further experimental flexibility (even under vacuum).

Fig. 4.7 Cross section of the complete stalk, along with the inner cathode grid, previously used at University of Wisconsin (UW), Madison [9]

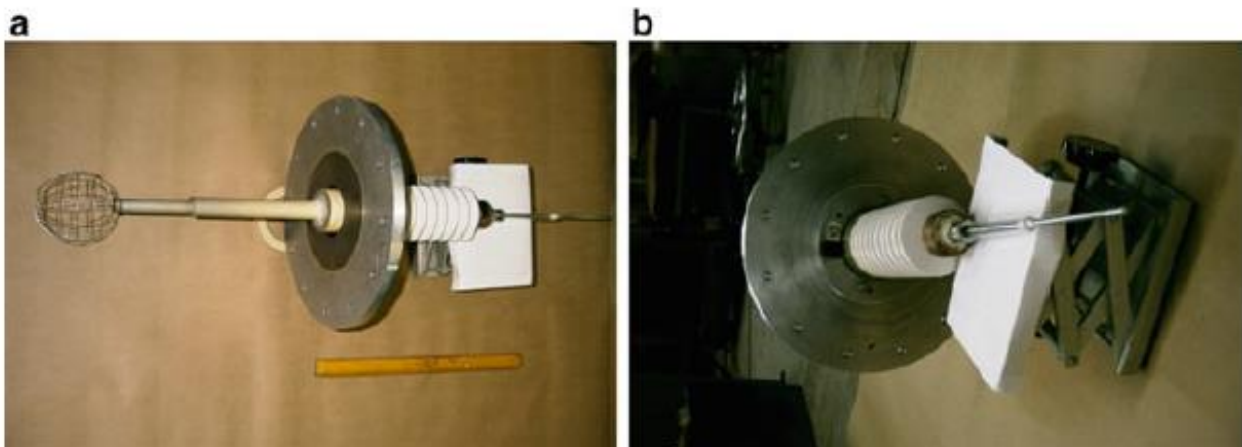
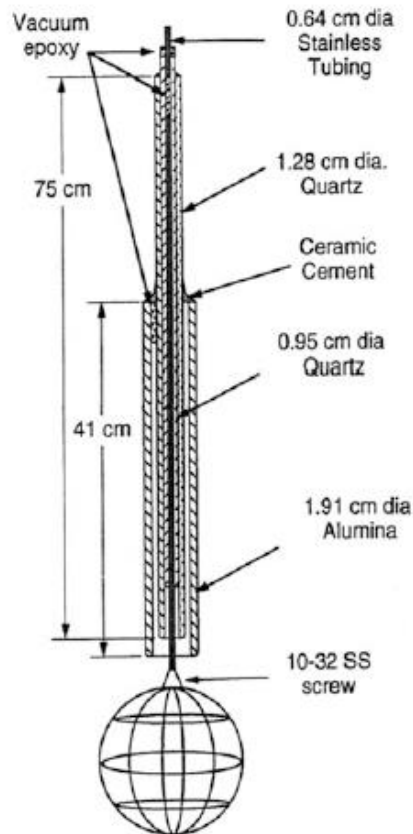


Fig. 4.8 Top view (a) and side view (b) of the stalk assembly [3]

Construction of grids

Prior to standardized grid manufacturing, most groups resorted to manual grid construction. Wires were typically made of stainless steel or tantalum. These wires were turned into loops using a spot welder prior to arranging them in the form of a grid and securing these loops together, once again using a spot welder. A "mold" cut from wood or other material was often used to hold wires in place while spot welding them. It was realized early on that despite its low

cost and ease of use, stainless steel is not ideal, as it sputters profusely and melts at a relatively low temperature. Thus, varieties of other materials have been used in some IECs. Though tungsten was a preferable alternative, it was not widely used due to the lack of accessible welding techniques. Attempts were made to use intermediate materials like nickel foil, placed between the two tungsten wires that needed spot welding. The nickel melted and secured the tungsten wires. However, the melting point of the nickel fundamentally limited these grids so the advantages of tungsten wires could not be fully exploited. As previously discussed, the University of Wisconsin group selected W-25 %Re for grid construction and testing. Experience with this alloy has been very encouraging. For example, the stainless steel wires previously used by Murali lasted for under a week depending on the power load. In contrast, with the W-25 %Re alloy, the grid lasted for over 2 years. It was eventually replaced when a cleaning attempt (using a sand blaster) unfortunately turned the smooth surface texture into a rough surface, rendering the grid useless (Ashley RP, 2002, University of Wisconsin, Madison, private communication). Otherwise the grid could have continued in use for some time.

A very successful rapid prototyping technique was developed at the University of Wisconsin, Madison. The technique is illustrated in Table 5.2 along with the description of the grid construction procedure. This procedure produces a reproducible, uniform grid, but unlike the NASA work, it still requires spot welding.

Another commonly used design for the cathode grid uses a series of plates/disks (such as shown in Fig. 5.14). The idea of using such disks for the construction of cathode grids was first suggested by P. T. Farnsworth in his original patents. The major advantage of using such grids is that while the grid transparency is maintained constant, the surface area for radiating the heat away from the grid increases. These disks are cut using lasers, though powerful water jets can also be used. One of the principal considerations while building a grid is to improve the grid transparency. As we explained earlier, operation in the "Star" mode (microchannel) depends more on the "effective" transparency versus the geometric transparency.

However, operation in other modes is very dependent on the geometric value, so improvements in the geometric transparency are very desirable. One such technique that was developed by Murali and colleagues at Los Alamos National lab for this purpose used a combination of several wires with different diameters to accomplish the desired grid transparency. Thicker wires were used to construct a strong skeleton structure, while thinner gauge wires were used to fill in the gaps to obtain the desired spacing. The grid constructed in this way is shown in Fig. 5.15. The geometric transparency achieved with this technique was 95%. With the large openings in these grids, microchannel form, providing an even higher effective transparency. Still, many ions eventually scatter out of the microchannel and hit grid wires. That factor in turn depends on the

geometric transparency. The high geometric transparency is valuable in the sense of reducing those collisions, increasing ion recirculation times.³

Table 5.2 Standardized grid construction procedures developed at the University of Wisconsin, Madison [10]

Figure	Procedure
1. 	Plastic model created using rapid prototyping
2. 	Rubber mold created using the plastic template
3. 	Wax is poured into the rubber mold and is left there until it solidifies
4. 	A wax template is created using the rubber mold
5. 	The wax template is used to keep the wires positioned until it is spot-welded
6. 	After spot welding the wires, the wax template is melted away using a hot air gun. The wax can then be reused
7. 	The grid is cleaned in an ultrasonic cleaner to remove any residual wax from the grid surface. The grid is now ready for use

³ Inertial electrostatic confinement (IEC) fusion fundamentals and applications – George H. Miley S. Krupakar Murali

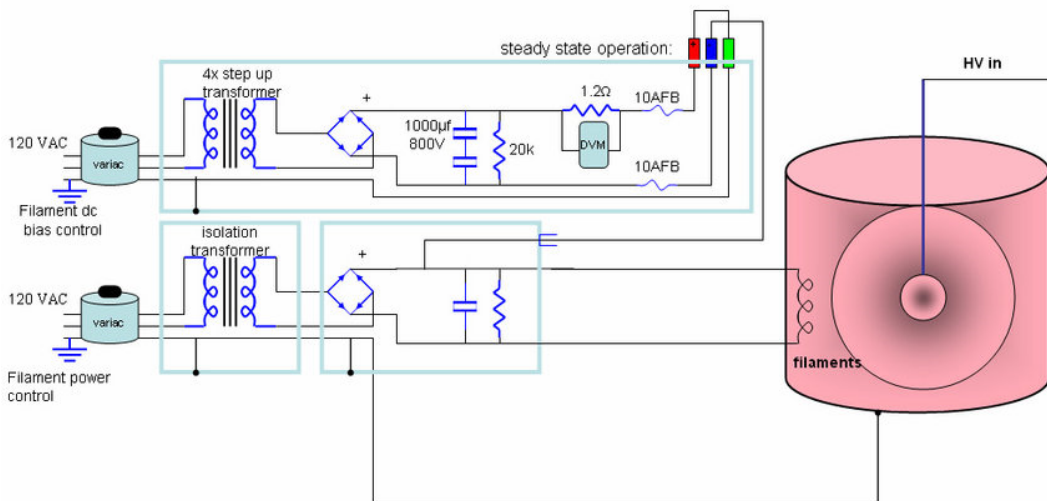
Operation⁴

It consists of a 91 cm diameter, 65 cm tall cylindrical aluminum vacuum chamber. Experiments run steady-state within the limitations of chamber heating. Partly to circumvent this constraint, a spherical, stainless-steel, water-cooled chamber has recently been brought into operation.

A 450 l/s turbo pump pumps the chamber down to a base pressure of 2×10^{-7} torr. The inner tungsten-rhenium (W-Re) cathode is a 10 cm diameter coarse-grid sphere of 0.8 mm tungsten wire supported on a 200 kV vacuum feed-through. It has operated at input power levels exceeding 8.5 kW at voltages ranging from -25 kV to -185 kV and at currents from 30-75 mA. A power supply provides up to 200 kV at 75 mA. The outer anode is typically a 50 cm diameter grid of stainless-steel wire.

The wire can be biased with variable amplitude AC and DC voltages. Electronically controlled gas flow regulators adjust the fuel flow ratio and amount into the system. A remote controlled throttle on the turbo pump is used to control the operating pressure of the gas mix.

{The deuterium plasma is created by adopting hot cathode discharge (i.e. filamentary discharge) method in which two thoriated tungsten filaments are placed at two diagonally opposite positions and at 10 cm away from the wall of the chamber. The filaments are heated to produce thermionic electrons and a discharge voltage and current of 80 V and 200–500 mA is maintained, respectively, at a working pressure of $\sim 10^{-3}$ Torr. Then, negative voltage is applied to the cathode through the feedthrough}



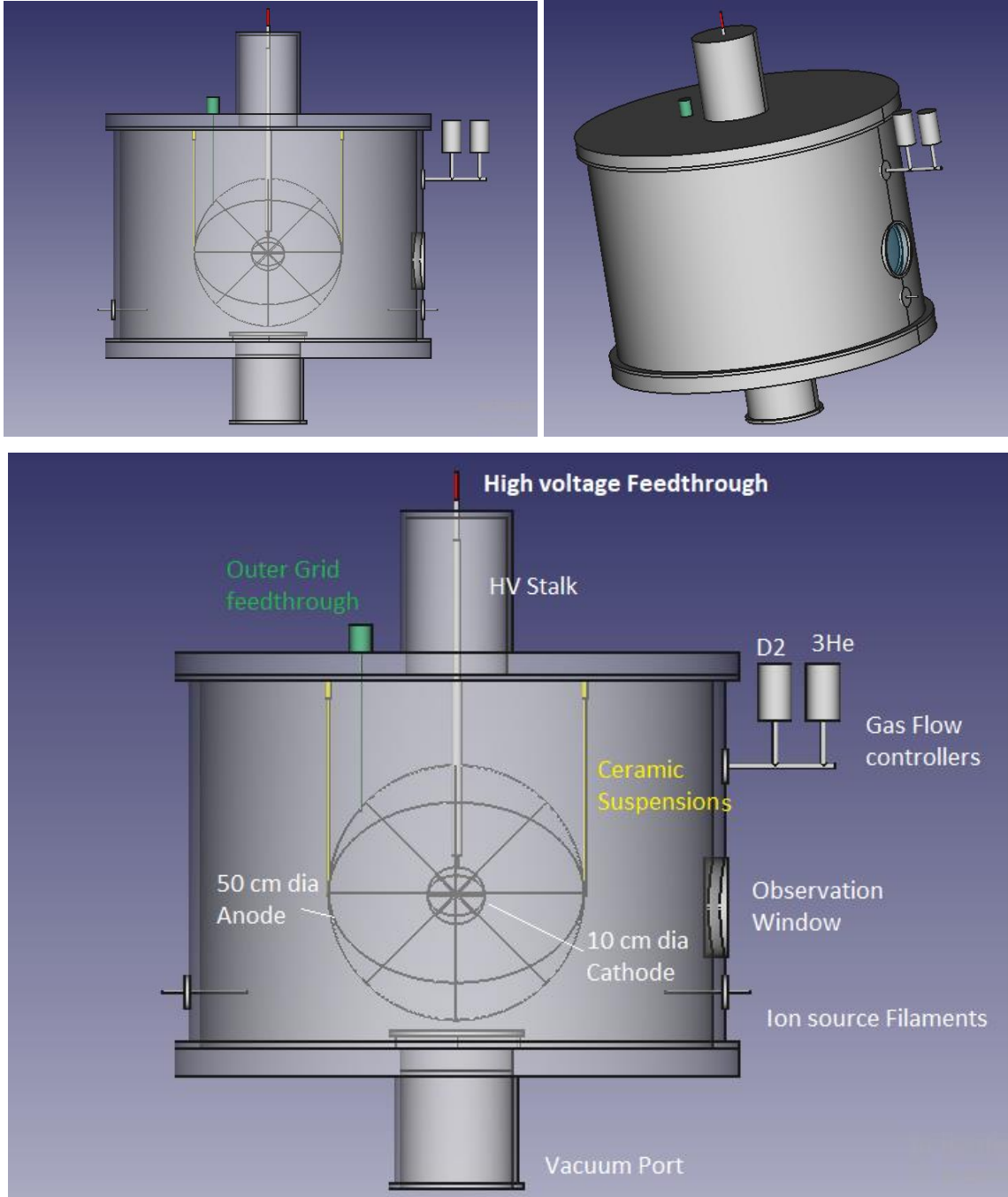
IEC source region filament control circuit.


The fusion reactions in the IEC chambers produce neutrons, protons, electrons, helium-4, tritium, γ -rays, and x-rays, depending on the fuel. The present diagnostic set detects 2.45 MeV D-D neutrons, 3.02 MeV D-D protons, and 14.7 MeV D-3He protons. The proton detector is an EG&G Ortec Ultra solid-state detector, has an active area of 1200 mm², and has a depletion region thickness of 700 μ m.

⁴ Fusion Science and Technology - Overview of University of Wisconsin Inertial Electrostatic Confinement Fusion Research

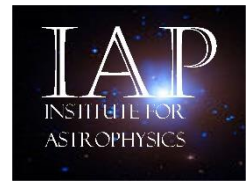
This thickness allows both the 3 MeV protons and the 14.7 MeV protons to be detected simultaneously. A helium proportional counter neutron detector, placed 60 cm from the center, is used to detect the 2.45 MeV DD neutrons. A residual gas analyzer (RGA) assesses neutral gas components.

9.2.2 Our Device



IAP-IECF Device	 18082021-IECDevice.F CStd
-----------------	---

بِسْمِ اللَّهِ الرَّحْمَنِ الرَّحِيمِ



Inertial Electrostatic Confinement Fusion Reactor

Author: Maryam ABDEL-KARIM

Last Update: 15.04.2025 15:55

Contents

1	IEC Device.....	5
1.1	Introduction.....	5
1.2	Inertial Electrostatic Confinement Fusion Principle.....	5
1.3	Nuclear fusion.....	7
1.4	Applications	8
1.5	University of Wisconsin-Madison Device	9
1.5.1	Design	9
1.5.2	High-Voltage Stalk Design for IEC.....	11
1.5.3	Construction of grids.....	12
1.5.4	Operation.....	15
2	Our Device	18
3	Simulation.....	20
3.1	Computational Domain.....	20
3.1.1	Defining the Geometric Mesh	20
3.1.2	Initial Conditions and Boundary Conditions.....	21
3.1.3	Particle-in-cell Technique.....	21
3.2	Particle-in-Cell Python Code	24

9.2.3 IEC Device

9.2.3.1 Introduction

Historically, most fusion research has focused on energy production in two basic configurations: magnetic confinement (magnetic fusion energy or MFE), and inertial confinement (inertial fusion energy or IFE). Each of these may lead eventually to a viable fusion reactor, yet they tend to be large, complicated, and expensive. This generates many physics and engineering difficulties, so the time frame for their development remains uncertain. The present note describes a fundamentally different fusion concept based on electrostatic focusing of ions into a dense core. Generically, such systems are called *inertial-electrostatic confinement* (IEC) fusion systems. In the 1950's, research was done on one form of IEC, purely electrostatic confinement, in which a voltage difference on concentric grids focuses charged particles. Ions accelerate down the electrostatic potential in spherical geometry, and convergence at the origin gives high density⁵.

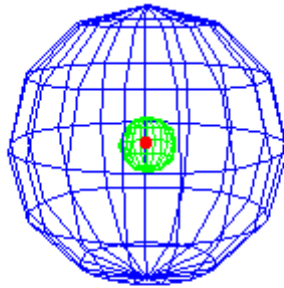
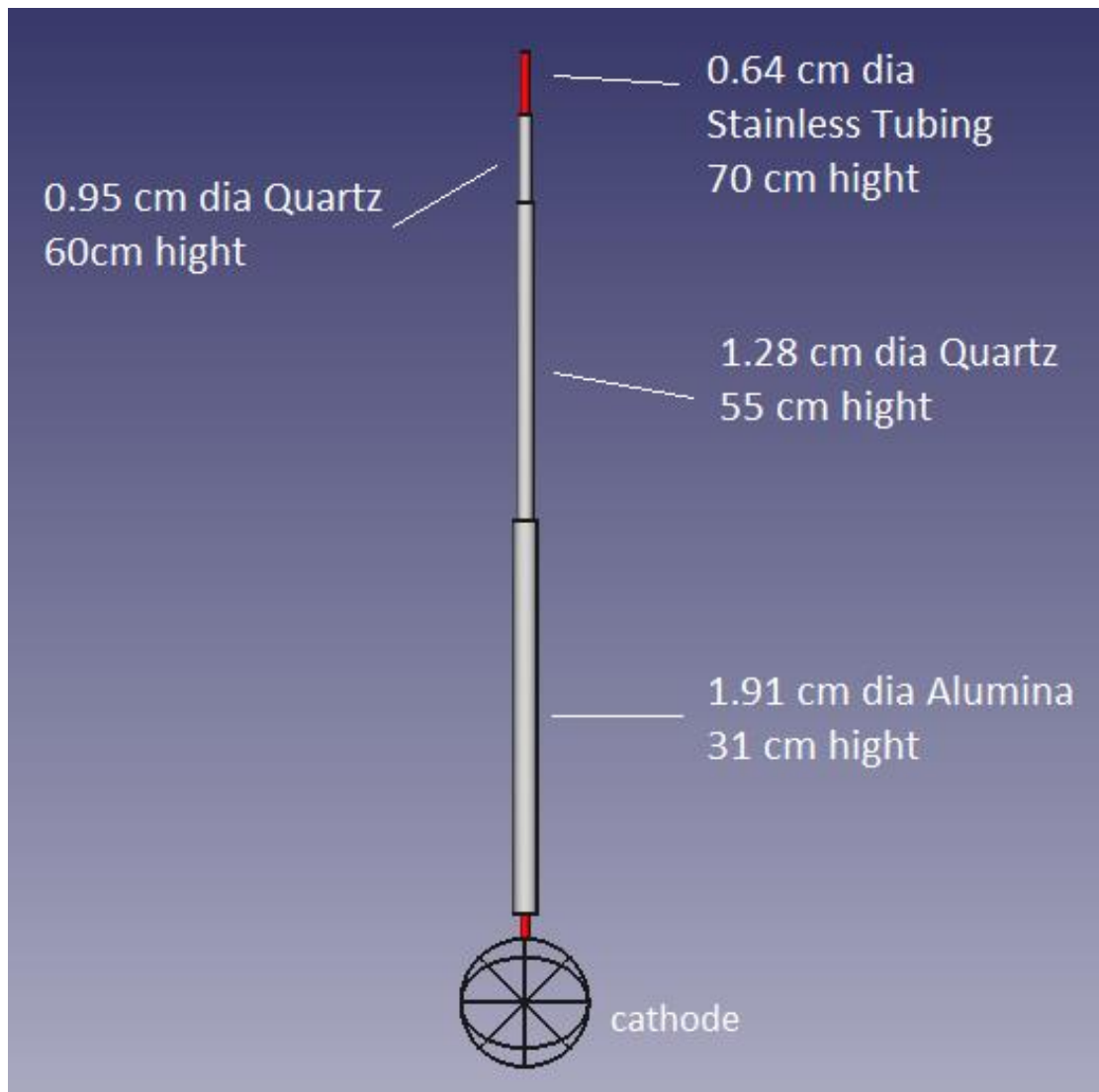


Figure 1: Grids plus energetic plasma core of the simplest IEC configuration.

9.2.3.2 Inertial Electrostatic Confinement Fusion Principle

Inertial electrostatic confinement fusion does not rely on any magnetic field, and instead uses an electric field to perform the plasma confinement. The device is formed by arranging two spherical metal meshes concentrically and putting an extremely large voltage across them, typically 10 to 100 kV in vacuum (Figure 1.2). The meshes are supported by a high-voltage stalk (Figure 1.3). Fusion fuel, in this case deuterium, is then released into the chamber where the large voltage ionizes a portion of the gas. These positively charged ions are accelerated by the electric field toward the center of the device, where most will pass straight through the cathode at the center and out the other side due to the large gaps in the metal mesh. Once on the other side, the electric field slows the ions and eventually turns them back towards the center, setting up a recirculation. The ion density in the center increases, and eventually fusion occurs. This does not require nearly as large a machine as the tokamak: typical IEC devices comfortably sit on tabletops.

⁵ <https://iec.neep.wisc.edu/overview.php>



9.2.4 Simulation⁶

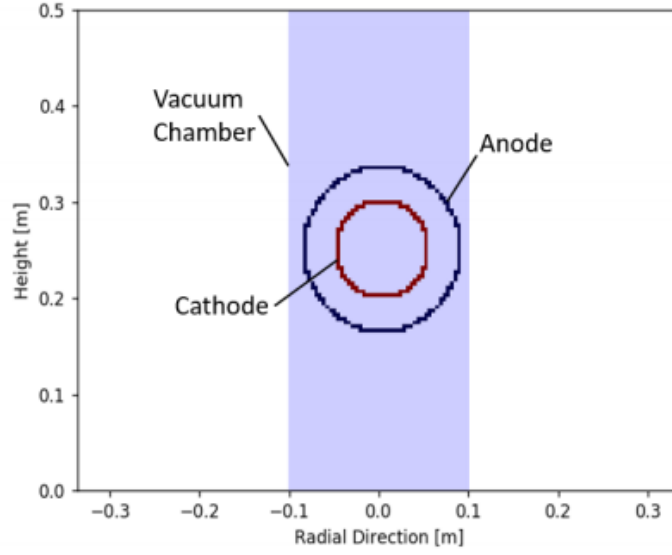
9.2.4.1 Computational Domain

- ◇ The computational domain was meshed using a regular Euclidian mesh with equal cell dimensions in x and y , despite the spherical geometry of the device.
- ◇ The computational model of the IEC device replaces the physical wire grids with two circular equipotential of the same radii.
- ◇ The potential of these circles is equal to the grid voltage.
- ◇ The computational domain is two-dimensional.
- ◇ The domain's outer-most boundary is the cylindrical vacuum chamber
- ◇ Assuming the anode and cathodes are closed circles, assigning a geometric transparency.

⁶ Modeling the Fusion Reaction in an Inertial Electrostatic Confinement Reactor with the Particle-in-Cell Method - Jacob van de Lindt - 2020

◇ The stalk was ignored in this study.

The computational domain used in this model is visualized in Figure 2.1.



Defining the Geometric Mesh

The regular Euclidian mesh making up the computational domain was extended over a region with N_x cells in x direction, and N_y cells in y direction. This domain can be translated into a set of $N_x N_y$ equations, one for each cell corner by using the discretized Poisson's Equation:

$$\nabla^2 \phi = -\frac{\rho}{\epsilon_0}.$$

Here ρ is the net charge density, given by $q(n_{ion} - n_e)$, the number density of ions minus the number density of electrons times q , the charge of a proton. ϕ is the electric potential, and ϵ_0 is the permittivity of free space. This equation can be discretized in a finite difference form in three dimensions:

$$\frac{\phi_{i-1,j,k} - 2\phi_{i,j,k} + \phi_{i+1,j,k}}{(\Delta x)^2} + \frac{\phi_{i,j-1,k} - 2\phi_{i,j,k} + \phi_{i,j+1,k}}{(\Delta y)^2} + \frac{\phi_{i,j,k-1} - 2\phi_{i,j,k} + \phi_{i,j,k+1}}{(\Delta z)^2} = q \frac{n_e - n_i}{\epsilon_0}. \quad (2.2)$$

Equation 2.2 in two dimensions is the basis for the computational simulation carried out in this work.

Initial Conditions and Boundary Conditions

At the radius of the cathode (red cells in Figure 2.1), an equipotential circle is defined with a Dirichlet boundary condition equal to the grid voltage imparted to the device. A similar condition is applied to the anode (dark blue cells), which is set to 0 V. The vacuum chamber walls are simulated as an open boundary: any particle that collides with this surface passes through and is lost from the computational domain. The domain is initiated with zero ions present, with a particle source near the anode. Particles are assumed to have no net initial velocity beyond thermal motion sampled from a Maxwellian distribution of initial ion velocities.

Particle-in-cell Technique

The PIC algorithm in this study utilizes the following steps in the main loop:

1. Determine the Charge Density
2. Determine the Electric Potential
3. Determine the Electric Field
4. Move the Macro particles and Check for Fusion
5. Sample Sources and Determine Losses
6. Repeat until Maximum Number of Time Steps is reached.

Determine the Charge Density

$$q_G = q \frac{(h_y)(h_x)}{\Delta x \Delta y} . \quad (2.4)$$

Here q_G is the charge contribution the green node receives from the grey macroparticle, h_x is the grey macroparticle position from the left of the cell, and h_y is the grey macroparticle position from the bottom of the cell.

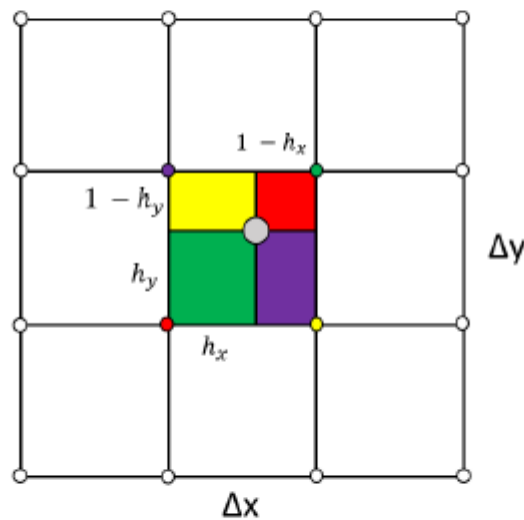


Figure 2.2 Visualizing the charge weighting to nearby numerical grid intersections. The grey macroparticle's charge is distributed to the nodes of the cell it is in. The proportion of charge that is received by the nodes is found by the area ratio using the particle's position in the cell as shown by Equation 2.4. This is visualized by the colored rectangles within the cell. The green node, for example, receives the green rectangle's proportion of the grey macroparticle's charge. Figure based on a discussion in [5].

Determine the Electric Potential

An important assumption that will be used in this study is that the electrons in the IEC plasma move instantly relative to the ions. In an electromagnetic field a particle's acceleration is proportional to the charge to mass ratio qm . The deuterium mass is nearly 4,000 times larger than the electron mass, and hence to the ion the electron moves nearly instantly. The electrons are assumed to be a fluid with a temperature T_e . The electron density is assumed to maintain a Boltzmann distribution given by

$$n_e = n_o e^{\frac{q(\phi - \phi_o)}{k_B T_e}},$$

where ϕ_o is the reference ground potential, 0 V. Equation 2.5 can be substituted into Equation 2.2 for the electron number density in two dimensions with the cell length in the x and y direction equaling the Debye length, yielding Equation 2.6:

$$\frac{\phi_{l-1,j} - 2\phi_{l,j} + \phi_{l+1,j}}{(\lambda_D)^2} + \frac{\phi_{l,j-1} - 2\phi_{l,j} + \phi_{l,j+1}}{(\lambda_D)^2} = \frac{q}{\epsilon_o} \left[n_o e^{\frac{q(\phi_{l,j} - \phi_o)}{k_B T_e}} - n_{ion} \right].$$

Equation 2.6 is no longer linear due to the exponential on the RHS containing the potential ϕ_i , so a simple matrix inversion by gaussian elimination cannot solve this system of equations. The potential ϕ_i is solved for by setting the domain boundary conditions: the vacuum chamber walls and the anode are set to a potential of 0 V. The cathode is set to the cathode voltage (between -10 and -200 kV).

Next, the interior cells of the domain (excluding the vacuum chamber walls) are looped over and the potential at each cell is updated. The update formula is found by rearranging Equation 2.6:

$$\phi_{l,j}^k = \frac{\phi_{l-1,j}^k + \phi_{l+1,j}^k + \phi_{l,j-1}^k + \phi_{l,j+1}^k}{4} - \frac{\lambda_D^2 q}{4\epsilon_o} \left[n_o e^{\frac{q(\phi_{l,j}^{k-1} - \phi_o)}{k_B T_e}} - n_{ion} \right].$$

Determine the Electric Field

$$E_{x,lj} = -\frac{\phi_{l+1,j} - \phi_{l,j}}{\Delta x},$$

$$E_{y,lj} = -\frac{\phi_{l,j+1} - \phi_{l,j}}{\Delta y},$$

$$E_{x,lj} = -\frac{\phi_{l+1,j} - \phi_{l-1,j}}{2\Delta x},$$

$$E_{y,lj} = -\frac{\phi_{l,j+1} - \phi_{l,j-1}}{2\Delta y}.$$

Move the Macroparticles and Check for Fusion

The macroparticles are moved using Newton's Second Law according to Equation 2.13:

$$\mathbf{v}^{s+0.5} = \mathbf{v}^{s-0.5} + \frac{q}{m_m} \mathbf{E} \Delta t.$$

Here the superscript s refers to the s^{th} timestep iteration. The particle position \mathbf{r} at the next timestep is determined from the s^{th} timestep iteration as

$$\mathbf{r}^{s+1} = \mathbf{r}^s + \mathbf{v}^{s+0.5} \Delta t. \quad (2.14)$$

The probability P that a macroparticle moving from \mathbf{r}_s to \mathbf{r}_{s+1} will undergo a fusion reaction is given by

$$P = w_s |\mathbf{v}^{s+0.5} \Delta t| \sigma_f(\mathbf{v}) n_{ion}.$$

9.2.4.2 Particle-in-Cell Python Code

```
import numpy as np
import matplotlib.pyplot as plt

#setup constants
EPS0 = 8.854e-12      #permittivity of free space
QE = 1.602e-19       #elementary charge
kb = 1               #boltzmann constant
AMU = 1.661e-27      #atomic mass unit
m_ion = 2*AMU        #ion mass (deuterium)

# Physical Grid Dimensions
R1 = 0.05            # Cathode [m]
GEO_C = .95          # Geometric transparency cathode (manual for now)
R2 = .085            # Anode [m]
GEO_A = .95          # Geometric transparency anode (manual for now)
#Physical Chamber Dimensions
R_Chamber = .1       # [m]
H_Chamber = 0.5      # [m]
r_wire = .80*1e-3 / 2 # Radius of 20 guage wire in m
#Source Dimension and Distrobution
R_Source_min = .08   # smallest radius a source particle can appear at
source_spread = .0025 # largest radius a source particle can appear minus the minimum

#input settings
# n0 = 4.6e13
n0 = 1e16            #electron background density in #/m^3
```

```

phi_Cathode = -210000      #cathode potential
phi0 = 0
# Te = np.abs(phi_Cathode)#reference potential
Te = 600      #electron temperature in eV
Ti = 0.1      #ion velocity in eV (not used yet)
vth = np.sqrt(2*QE*Ti/m_ion)  #thermal velocity with Ti in eV
Operating_Pressure = 7      # Pa (Not used yet)
#calculate plasma parameters
#lD = np.sqrt(EPS0*Te/(n0*QE))      #Debye length (not used yet)
vth = np.sqrt(2*QE*Ti/m_ion)      #Thermal velocity with Ti in eV (not used yet)
lD = 0.004      # MANUAL SETTING FOR TESTING
dx = lD      #x cell size
dy = lD      #y cell size
#set simulation domain in the x dimension
nx = np.floor((2*R_Chamber)/dx).astype(int) #number of nodes in x direction, with a physical
                                             #domain +/- R_Chamber
#set simulation domain in the y dimension
ny = np.floor((H_Chamber)/dy).astype(int)  #number of nodes in y direction, with a physical
                                             #domain +/- H_Chamber / 2
ts = 800      #number of time steps

#calculate maximum expected velocity and timestep
E_av = (np.abs(phi_Cathode) - 0) / (R2 - R1)
a_av = E_av*QE / m_ion
v_max = np.sqrt(2*a_av*R2)
dt = 1e-10      #time step size, at vmax move 0.10dx

# Domain length in the x direction
Lx = (nx-1)*dx
# Domain length in the y direction
Ly = (ny-1)*dy
# SET UP THE POINTS REPRESENTING THE GRIDS
def get_discrete_Value(y, dy):
    # Takes in an array y and a grid spacing dy and returns an array
    # with the same physical dimensions as y but with a spacing of dy.
    actual = y / dy
    index = np.round(actual)
    return index*dy

```

```
# CATHODE SETUP
Thetav = np.arange(0, 2*np.pi, np.pi/1000)
x_cathode = R1*np.cos(Thetav)
y_cathode = R1*np.sin(Thetav)
X_cathode = get_discrete_Value(x_cathode, dx)
Y_cathode = get_discrete_Value(y_cathode, dy)

INDEX_X_Cathode = (X_cathode/dx).astype(int)
INDEX_Y_Cathode = (Y_cathode/dx).astype(int)

# ANODE SETUP
x_anode = R2*np.cos(Thetav)
y_anode = R2*np.sin(Thetav)
X_anode = get_discrete_Value(x_anode, dx)
Y_anode = get_discrete_Value(y_anode, dy)

INDEX_X_Anode = (X_anode/dx).astype(int)
INDEX_Y_Anode = (Y_anode/dy).astype(int)

# LEFT WALL SETUP
y_left_wall = np.arange(-H_Chamber/2, H_Chamber/2, dy)
x_left_wall = np.ones(y_left_wall.shape[0]) * (-R_Chamber)
INDEX_X_left_wall = (x_left_wall/dx).astype(int)
INDEX_Y_left_wall = (y_left_wall/dy).astype(int)

# RIGHT WALL SETUP
y_right_wall = np.arange(-H_Chamber/2, H_Chamber/2, dy)
x_right_wall = np.ones(y_right_wall.shape[0]) * (R_Chamber - dx)
INDEX_X_right_wall = (x_right_wall/dx).astype(int)
INDEX_Y_right_wall = (y_right_wall/dy).astype(int)

# BOTTOM WALL SETUP
x_bottom_wall = np.arange(-R_Chamber, R_Chamber, dx)
y_bottom_wall = np.ones(x_bottom_wall.shape[0]) * (-H_Chamber/2)
INDEX_X_bottom_wall = (x_bottom_wall/dx).astype(int)
INDEX_Y_bottom_wall = (y_bottom_wall/dy).astype(int)

# TOP WALL SETUP
x_top_wall = np.arange(-R_Chamber, R_Chamber, dx)
y_top_wall = np.ones(x_bottom_wall.shape[0]) * (H_Chamber/2 - dy)
```



```

INDEX_X_top_wall = (x_top_wall/dx).astype(int)
INDEX_Y_top_wall = (y_top_wall/dy).astype(int)

# Delete repeate XY Pairs
Cathode_Id1 = np.zeros([2, INDEX_X_Cathode.shape[0]])
Cathode_Id1[0, :] = INDEX_X_Cathode
Cathode_Id1[1, :] = INDEX_Y_Cathode
Cathode_Id2 = np.unique(Cathode_Id1, axis=1)
INDEX_X_Cathode = Cathode_Id2[0, :].astype(int)
INDEX_Y_Cathode = Cathode_Id2[1, :].astype(int)

# Calculate specific weight and prepair to insert particles
np_insert = 400                #insert 2 particles per anode cell.
#flux = 4.6e22
flux = 1.6e21*np.abs(phi_Cathode)/100000    #Flux of entering ions [ions per second]
npt = flux*dt
spwt = npt/np_insert          #specific weight, real particles per macroparticle
mp_q = 1                      #macroparticle charge
max_part = 200000            #buffer size

#allocate particle array
part_x = np.zeros([max_part,2]) #particle positions
part_v = np.zeros([max_part,2]) #particle velocities
source_storage = np.zeros([max_part,2]) #particle sources
# Define the potential solver function

PHI_B = np.zeros([nx, ny])
idx = np.round(nx/2).astype(int)
idy = np.round(ny/2).astype(int)

#Potential Solver

def get_Potential(PHI_B, den, nx, ny, iters):
    for k in range(iters):
        PHI_OLD = PHI_B
        for i in range(1,nx-2):
            for j in range(1, ny-2):
                ni = den[i,j]
                rho = QE*(ni - n0*np.exp((PHI_OLD[i,j] - phi0)/(kb*Te))) / EPS0

```

```

        chrg = -rho*dx**2
        PHI_B[i,j] = (chrg - PHI_B[i+1, j] - PHI_B[i-1, j] - PHI_B[i, j+1] - PHI_B[i, j-
1])/(-4)
        PHI_B[INDEX_X_Cathode + idx, INDEX_Y_Cathode + idy] = phi_Cathode
        PHI_B[INDEX_X_Anode + idx, INDEX_Y_Anode + idy] = phi0
    return PHI_B

# Ion Source
def sample_Source(nump, R_Sl, r_spread):
    # Updated to generate particles randomly in theta and in R.
    xv = np.zeros([nump])
    yv = np.zeros([nump])
    for i in range(nump):
        R_S = R_Sl + np.random.rand()*r_spread
        theta = np.random.rand(1)*2*np.pi # Generate random polar angle
        x = R_S*np.cos(theta) # Get x position
        y = R_S*np.sin(theta) # Get y position
        xv[i] = x
        yv[i] = y
    return np.array([xv, yv])

# D-D Cross Section from 5 parameter fit
def fusion_Cross_Section(vx, vy):
    # Takes in velocity components in m/s and returns a cross section in barns
    E = .5*m_ion*(vx**2 + vy**2)
    E = E*6.242e15 # convert J to KeV
    A1 = 46.097
    A2 = 372
    A3 = 4.36e-4
    A4 = 1.22
    A5 = 0
    AA1 = 47.88
    AA2 = 482
    AA3 = 3.08e-4
    AA4 = 1.177
    AA5 = 0
    term1 = A5 + A2/((A4 - A3*E)**2 + 1)
    term2 = E*(np.exp(A1/np.sqrt(E)) - 1)

```

```
term3 = AA5 + AA2/((AA4 - AA3*E)**2 + 1)
term4 = E*(np.exp(AA1/np.sqrt(E)) - 1)
sig1 = term1/term2
sig2 = term3/term4
return sig1 + sig2

#####
# MAIN LOOP
#####

#INITIALIZE
PHI_M = np.zeros([nx, ny])
idx = np.round(nx/2).astype(int)
idy = np.round(ny/2).astype(int)
PHI_M[INDEX_X_Cathode + idx, INDEX_Y_Cathode + idy] = phi_Cathode
PHI_M[INDEX_X_Anode + idx, INDEX_Y_Anode + idy] = phi0
fuse_pos_x = np.array([])
fuse_pos_y = np.array([])
fuse_time = np.array([])
col_counter = 0
```

```
top_counter = 0
bot_counter = 0
left_counter = 0
right_counter = 0
anode_counter = 0
cathode_counter = 0
fuse_counter = 0
num_p = 0 #Clear number of particles
iters = 600 #Number of iterations used in the potential solver
P_FUS = 0 # set a checker to report max fusion probability
print('Beginning Main Loop. This could take a while. \n')

for it in range(ts):
    P_FUS = 0
    print('Time Step ', it, 'Particles ', num_p)
    #reset field quantities
    den = np.zeros([nx,ny]) #number density
```

```

efx = np.zeros([nx,ny])           #electric field, x-component
efy = np.zeros([nx,ny])           #electric field, y-component
chg = np.zeros([nx,ny])           #charge distribution
col_counter = 0

# *** 1. Calculate Charge Density ***
# deposit charge to nodes
for p in range(num_p):             #loop over particles
    fi = (part_x[p, 0] + R_Chamber-dx)/dx #real i index of particle's cell
    i = np.floor(fi).astype(int)         #integral part
    hx = fi - i                        #the remainder
    fj = (part_x[p,1] + (H_Chamber/2)-dx)/dx #real i index of particle's cell
    j = np.floor(fj).astype(int)         #integral part
    hy = fj - j                        #the remainder
    #interpolate charge to nodes
    chg[i, j] = chg[i, j] + (1-hx)*(1-hy)
    chg[i+1, j] = chg[i+1, j] + hx*(1-hy)
    chg[i, j+1] = chg[i, j+1] + (1-hx)*hy
    chg[i+1, j+1] = chg[i+1, j+1] + hx*hy

# Calculate the Density
den = spwt*mp_q*chg / (dx**2)
den[0,:] = 2*den[0,:]               # Double density since only half volume contributing
den[nx-1,:] = 2*den[nx-1,:]
den[:,0] = 2*den[:,0]
den[:,ny-1] = 2*den[:,ny-1]
den = den + 1e3                      # Add density floor to help the solver

# *** 2. Calculate the Potential
PHI_M = get_Potential(PHI_M, den, nx, ny, iters)
print('Potential Solution Complete.')

# *** 3. Calculate the Electric Field ***
efx[1:nx-2,:] = PHI_M[0:nx-3,:] - PHI_M[2:nx-1,:] #central difference on internal nodes
efy[:,1:ny-2] = PHI_M[:,0:ny-3] - PHI_M[:,2:ny-1] #central difference on internal nodes
efx[0,:] = 2*(PHI_M[0,:] - PHI_M[1,:])             #forward difference on x=0
efx[nx-1,:] = 2*(PHI_M[nx-2,:] - PHI_M[nx-1,:])   #backward difference on x=Lx
efy[:,0] = 2*(PHI_M[:,0] - PHI_M[:,1])             #forward difference on y=0
efy[:,ny-1] = 2*(PHI_M[:,ny-2] - PHI_M[:,ny-1])   #forward difference on y=Ly

```

```

efx = efx / (dx**2)          #divide by denominator
efy = efy / (dx**2)

# *** 4. Generate New Particles
print('Generating Particles')
#insert particles randomly distributed and within the source region
Posv = sample_Source(np_insert, R_Source_min, source_spread)
part_x[num_p:num_p+np_insert, 0] = Posv[0,:]  #x position
part_x[num_p:num_p+np_insert, 1] = Posv[1,:]  #y position
#source_storage[num_p:num_p+np_insert, 0] = Posv[0,:]
#source_storage[num_p:num_p+np_insert, 1] = Posv[1,:]
#sample maxwellian in x and y
pt1 = np.random.rand(np_insert)
pt2 = np.random.rand(np_insert)
pt3 = np.random.rand(np_insert)
pt11 = np.random.rand(np_insert)
pt12 = np.random.rand(np_insert)
pt13 = np.random.rand(np_insert)
part_v[num_p:num_p+np_insert,0] = (-1.5 + pt1 + pt2 + pt3)*vth  # x velocity
part_v[num_p:num_p+np_insert,1] = (-1.5 + pt11 + pt12 + pt13)*vth # y velcoity
num_p = num_p + np_insert          #increment particle counter

# *** Move Particles ***
print('Moving Particles... DO NOT INTERRUPT')
p=0
while p < num_p:          # Loop over particles
    fi = (part_x[p, 0] + R_Chamber-dx)/dx  # i index of particle's cell. Taking into account
    i = np.floor(fi).astype(int)          # that the physical domain is centered at (0,0)
    hx = fi - i
    fj = (part_x[p,1] + (H_Chamber/2)-dx)/dx
    j = np.floor(fj).astype(int)
    hy = fj-j
    #print('Fi: ', fi, 'Fj: ', fj)
    # gather electric field
    E = np.array([0,0])
    E = np.array([efx[i,j], efy[i,j]])*(1-hx)*(1-hy)          #contribution from (i,j)
    E = E + np.array([efx[i+1,j], efy[i+1,j]])*hx*(1-hy)          #(i+1,j)
    E = E + np.array([efx[i,j+1], efy[i,j+1]])*(1-hx)*hy          #(i,j+1)
    E = E + np.array([efx[i+1,j+1], efy[i+1,j+1]])*hx*hy          #(i+1,j+1)

```

```

#print('E:', E)
# Update Velocity and Position
F = QE*E      # Lorenz force F = qE
a = F/m_ion   # Acceleration
part_v[p,:] = part_v[p,:] + a*dt
part_x[p,:] = part_x[p,:] + part_v[p,:]*dt
#print(part_v[p,:])
#print(part_x[p,:])
# Get Fusion probability
vx = part_v[p, 0]
vy = part_v[p, 1]
delx = vx * dt * 1e4
dely = vy * dt * 1e4
path_len = np.sqrt(delx**2 + dely**2)
sigma = fusion_Cross_Section(vx, vy)*1e-28 # microscopic cross section [m^2]

# gather density at particle position
Rho = den[i,j]*(1-hx)*(1-hy)      #contribution from (i,j)
Rho = Rho + den[i+1,j]*hx*(1-hy)  # (i+1,j)
Rho = Rho + den[i,j+1]*(1-hx)*hy  # (i,j+1)
Rho = Rho + den[i+1,j+1]*hx*hy    # (i+1,j+1)

# Calculate macroscopic cross section
SIGMA = Rho * sigma
Prob_fusion = SIGMA * path_len * spwt
# Store
if Prob_fusion > P_FUS:
    P_FUS = Prob_fusion
# Prepare to check for fusion
random = np.random.rand(1)

# Process Boundries and Sinks
R = np.sqrt(part_x[p,0]**2 + part_x[p,1]**2)
#print('Finished Position and Velocity Update')
#print('Checking Top Wall')
# Top Wall
if part_x[p,1] > H_Chamber/2:
    part_x[p,:] = part_x[num_p-1,:] # Kill particle by replacing with last particle

```

```
part_v[p,:] = part_v[num_p-1,:]
part_x[num_p-1,:] = np.array([0,0]) # Reset last particle to 0
part_v[num_p-1,:] = np.array([0,0])
num_p = num_p - 1          # Reduce particle count
p = p - 1                 # Reduce particle index
col_counter = col_counter + 1
top_counter = top_counter + 1

# Bottom Wall
elif part_x[p,1] < -H_Chamber/2:
    #print('Checking Bottom Wall')
    part_x[p,:] = part_x[num_p-1,:] # Kill particle by replacing with last particle
    part_v[p,:] = part_v[num_p-1,:]
    part_x[num_p-1,:] = np.array([0,0]) # Reset last particle to 0
    part_v[num_p-1,:] = np.array([0,0])
    num_p = num_p - 1          # Reduce particle count
    p = p - 1                 # Reduce particle index
    col_counter = col_counter + 1
    bot_counter = bot_counter + 1

# Right Wall
elif part_x[p,0] > R_Chamber:
    #print('Checking Right Wall')
    part_x[p,:] = part_x[num_p-1,:] # Kill particle by replacing with last particle
    part_v[p,:] = part_v[num_p-1,:]
    part_x[num_p-1,:] = np.array([0,0]) # Reset last particle to 0
    part_v[num_p-1,:] = np.array([0,0])
    num_p = num_p - 1          # Reduce particle count
    p = p - 1                 # Reduce particle index
    col_counter = col_counter + 1
    right_counter = right_counter + 1

# Left Wall
elif part_x[p,0] < -R_Chamber:
    #print('Checking Left Wall')
    part_x[p,:] = part_x[num_p-1,:] # Kill particle by replacing with last particle
    part_v[p,:] = part_v[num_p-1,:]
    part_x[num_p-1,:] = np.array([0,0]) # Reset last particle to 0
```

```

part_v[num_p-1,:] = np.array([0,0])
num_p = num_p - 1          # Reduce particle count
p = p - 1                  # Reduce particle index
col_counter = col_counter + 1
left_counter = left_counter + 1

# Process grids

# Anode
elif (R < R2 + r_wire) and (R > R2 - r_wire):
    #print('Check Anode')
    prob = np.random.rand(1)
    if prob > GEO_A:
        # Delete particle if it collides with the grid
        part_x[p,:] = part_x[num_p-1,:] # Kill particle by replacing with last particle
        part_v[p,:] = part_v[num_p-1,:]
        part_x[num_p-1,:] = np.array([0,0]) # Reset last particle to 0
        part_v[num_p-1,:] = np.array([0,0])
        num_p = num_p - 1          # Reduce particle count
        p = p - 1                  # Reduce particle index
        col_counter = col_counter + 1
        anode_counter = anode_counter + 1

```

```

# Cathode
elif (R < R1 + r_wire) and (R > R1 - r_wire):
    #print('Check Cathode')
    prob = np.random.rand(1)
    if prob > GEO_A:
        # Delete particle if it collides with the grid
        part_x[p,:] = part_x[num_p-1,:] # Kill particle by replacing with last particle
        part_v[p,:] = part_v[num_p-1,:]
        part_x[num_p-1,:] = np.array([0,0]) # Reset last particle to 0
        part_v[num_p-1,:] = np.array([0,0])
        num_p = num_p - 1          # Reduce particle count
        p = p - 1                  # Reduce particle index
        col_counter = col_counter + 1
        cathode_counter = cathode_counter + 1

```

```

elif random <= Probab_fusion:
    print('FUSION!\n')
    fuse_pos_x = np.append(fuse_pos_x, part_x[p, 0])
    fuse_pos_y = np.append(fuse_pos_y, part_x[p, 1])
    fuse_time = np.append(fuse_time, dt*it)
    fuse_counter = fuse_counter + 1
    # Delete particle if it fused
    part_x[p,:] = part_x[num_p-1,:] # Kill particle by replacing with last particle
    part_v[p,:] = part_v[num_p-1,:]
    part_x[num_p-1,:] = np.array([0,0]) # Reset last particle to 0
    part_v[num_p-1,:] = np.array([0,0])
    num_p = num_p - 1 # Reduce particle count
    p = p - 1 # Reduce particle index

    p = p + 1 # Move to the next particle
print('Finished Moving Particles.')
print('Net Change in Ion Population: ', np_insert - col_counter)
print(col_counter, ' particles lost.')
print('Max probability of fusion: ', P_FUS, '\n')

# Replace voltage with Phi_Cathode
np.savetxt('Density_210kV_1.csv', den, delimiter=',')
np.savetxt('Potential_210kV_1.csv', PHI_M, delimiter=',')
np.savetxt('fus_time_210kV_1.csv', fuse_time, delimiter=',')
np.savetxt('fus_pos_x_210kv_1.csv', fuse_pos_x, delimiter=',')
np.savetxt('fus_pos_y_210kV_1.csv', fuse_pos_y, delimiter=',')
np.savetxt('part_x_210kV_1.csv', part_x, delimiter=',')
np.savetxt('part_v_210kV_1.csv', part_v, delimiter=',')

av_fusion_rate = (fuse_counter / (dt*ts)) / 1e4
print('Field Properties and Fusion Data Saved to File.\n')
print('Average Fusion Rate: %.6f Fusions per Second\n' % av_fusion_rate)

```

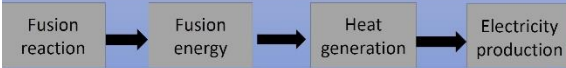
9.3 IAP-IECF Device Realization



IECF realisation

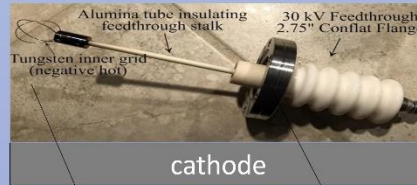
Introduction:

Fusion takes place only when the average kinetic energy of nuclei is sufficiently raised (to overcome the coulomb barrier) by accelerating their speed and increasing the density of nuclei in the center of the Inertial Electrostatic Confinement (IEC) reactor. This is achieved by creating a potential between electrodes, i.e. a sufficiently high voltage is created between cathode and the external sphere (anode).



Measurement of fusion event is done through measurement of neutrons created by fusion

- To operate the fusor, it requires fuel particles to be accelerated which are introduced into the fusor in the form of a gas (deuterium gas) injected into the vacuum chamber through a precisely regulated valve, which will become ionized in a strong electric field.
- In our case, the avalanche of electrons causes through high voltage.
- The 2nd stage of ionized gas is a formation of quasi-neutral plasma, concentrated in the center of the hollow cathode (poisor), and this is observed by a sudden increase in the current between the electrode followed by a drop in voltage.
- Our cathode (concentric in the chamber) consists of a 30 kV crosshead with a 2.75" stainless steel flange, an insulating aluminum tube crosshead rod and the negative hot inner grid of the tungsten filament with its stainless steel base that connects the inner grid with the crossing pin. This grid is a combination of 3 rings forming a sphere with a diameter 20% of that of the external sphere (anode).



Cylindrical shape :

This is the most common shape for vacuum chambers.

Allowable external pressure:

If $D0/t \geq 10$

Eq.1: $P_a = 4B/3(D0/t)$

Eq.2: $P_a = 2AE/3(D0/t)$

If $D0/t < 10$

Eq.1: $P_a = B/(R0/t)$

Eq.2: $P_a = 0.0625E/(R0/t)^2$

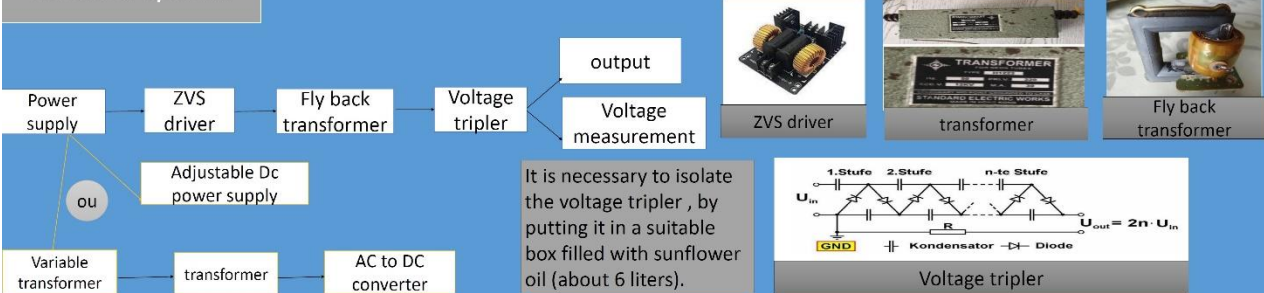
Allowable stress:

- It is the amount of force exerted on an object, divided by its cross section $\sigma = F/A$.
- Deformation, due to applied forces, is of two types : elastic and plastic ; $\epsilon = \Delta L/L$
- Elastic limit : corresponds to the point where the material begins to deform plastically.
- Safety factor : $r = (\text{Elastic limit}) / (\text{Work or design constraint})$.

- The conditions of pressure, high voltage between electrodes and electrodes distance should be such that voltage breakdown in the plasma\electron cloud will be prevented, i.e. electric discharges between the electrodes are unwanted.

- Plasma turns into poison if a mean free path of ions has been reached : $l = K_b T / (\sqrt{2} \pi d^2 p)$.
- For $l > 2R$; recirculation occurs.
- The fusion rate (D-D) : $F = (1/2)n^2 (\sigma V)$

Electrical system:



It is necessary to isolate the voltage tripler , by putting it in a suitable box filled with sunflower oil (about 6 liters).

Results of tests:

So far our test results have achieved an 80% reduction in air leakage and the pressure gauge indicates that the vacuum pump has extracted 900 mbar from the chamber. The desired result is to reach approximately 95% vacuum for a good fusion reaction.



This section is from this report:

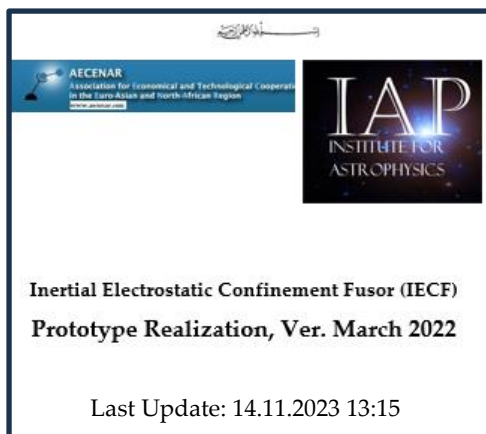


Table of Contents

Open Tasks Status Apr 22 / Nov 23 for IECP	5
1 Introduction	6
1.1 Overview	6
1.2 Electrostatic Nuclear Fusion Reactor	6
1.3 Concept Summary (Maryam Abdelkarim article)	7
2 Physics.....	9
2.1 Vacuum Chamber	9
2.1.1 Boundary conditions:	9
2.1.2 Materials	9
2.2 Design	9
2.2.1 Basics	9
2.2.2 Tube shape.....	10
2.3 Calculation Steps for Pipe Thickness Verification	12
2.3.1 Step 1: Calculate D_o/t	12
2.3.2 Step 2: Calculate L/D_o , this will help to find the value of factor A	12
2.3.3 Step 3: Find the Factor 'A' from Figure 'G' of ASME Section II, Subpart 3, Part D	12
2.3.4 Step 4: Now, Find The Factor 'B'	13
2.3.5 Step5: Calculate Maximum Allowable External Pressure (Pa).....	14
2.3.6 Quast-rectangular shape approximated by beam.....	15
2.4 Allowable Stress (Strength).....	17
2.4.1 What Is Stress?	17
2.4.2 What Is Strain?	18
2.4.3 What is yield strength or yselid stress?.....	18
2.4.4 Safety factor:.....	18
2.5 Grid Design.....	20
3 Fuel of Fusor reactor.....	24
3.1 Deuterium Gas	24
3.2 Deuterium Oxide	25
3.3 Traditional Electrolysis	26
3.4 PEM Electrolysis	26
3.5 Ionization of fuel Atoms	28
3.6 Choice of Energy	32
3.7 Radiation Hazards	37
4 Electrical System	42
4.1 High voltage Power supply.....	42
4.1.1 General System Diagram.....	42

4.1.2	The High voltage power supply	43
4.1.3	Equipment.....	48
4.1.4	Power supply.....	59
4.1.5	Voltage Tripler Isolation	61
4.1.6	Cable and isolation.....	61
4.1.7	Measurement	61
4.1.8	Remote control.....	63
4.1.9	Vacuum System.....	63
5	Mechanical system	65
5.1	Vacuum system.....	65
5.1.1	Mechanical pump.....	65
5.1.2	Diffusion pump	67
5.1.3	Efficiency of Arnocanal NPAV72(Present at AECENAR)	69
6	Detectors.....	70
6.1	Helium-3 Proportional Counters and Alternatives for Neutron Detection:.....	70
6.1.1	Identification of Special Nuclear Material by Neutron Detection	70
6.1.2	Helium-3 Gas-Filled Proportional Counters and the Helium-3 Shortage.....	70
6.1.3	Alternative Neutron Detection Materials	71
6.2	Conclusions	71
7	Vacuum tests.....	72
7.1	Test 1:.....	72
7.1.1	Assembling and pieces:	74
7.1.2	Result:.....	74
7.2	Test 2:.....	76
7.2.1	Result.....	78
7.3	Test 3:.....	79
7.3.1	Result.....	80
7.4	Test 4.....	80
7.4.1	Result.....	82
7.4.2	Result.....	83
7.5	Test 5:.....	83
8	Searching for materials.....	88
8.1	chamber glass window:.....	88
8.2	stainless steel wire	90
8.3	cathode inner grid assembling	94
8.4	Power supplies.....	99
8.4.1	Ac to Dc converter:.....	99
8.4.2	Cockcroft waltan voltage multiplier test	105
8.4.3	System Test.....	106
8.4.4	1 stage voltage multiplier test.....	113
9	Procurements	114
10	References	116

9.3.1 Introduction

9.3.1.1 Overview

Fusion power is a form of power generation in which energy is generated by using fusion reactions to produce heat for electricity generation. In contrast to fission, fusion creates energy by combining lighter elements into heavier elements. The advantages for fusion are (1) abundant fuels, (2) no radioactive waste produced and (3) controlled side reaction. The potential of fusion to create clean energy has attracted many scientists over several decades. One idea for a safe and efficient reactor for fusion is called the "Fusor". But unfortunately, no Fusor designs have yet achieved a positive energy gain, due to the difficulty of controlling the fusion reaction. In other words, the energy needed to initiate the reaction is more than the energy produced by the reaction. The Fusor employs inertial electrostatic confinement - the use of an electric field to confine the plasma.

9.3.1.2 Electrostatic Nuclear Fusion Reactor

The Fusor device typically consists of two wire cages called grids. The inner cage holds a negative voltage compared to the outer cage. When the fusion fuel is introduced (ionized gas: Deuterium gas), the voltage will ignite the fuel. The huge electric field accelerates the ions into fusion conditions.

9.3.2 Physics

9.3.2.1 Vacuum Chamber

Explaining Vacuum

Vacuum can be defined as a space that is empty of matter; however, achieving such an empty space is essentially impossible on earth. Instead, vacuum is best described as a space with gaseous pressure much less than atmospheric pressure. Physicists and vacuum scientists describe this lack of a "perfect vacuum" in manmade chambers, such as production furnaces, as partial pressure or partial vacuum. ¹

The quality of a vacuum is indicated by the amount of matter remaining in the system, so that a high quality vacuum is one with very little matter left in it. Vacuum is primarily measured by its absolute pressure.

At room temperature and normal atmospheric pressure, one cubic foot (0.03 cubic m) of air contains approximately 7×10^{23} molecules moving in random directions and at speeds of around 1,000 miles per hour. ² The momentum exchange imparted to the walls is equal to a force of 14.7 (psia) pounds for every square inch of wall area. ² This atmospheric pressure can be expressed in a number of units, but until relatively recently it was commonly expressed in terms of weight of a column of mercury 760 mm high. ² Thus, one standard atmosphere equals 760 mm Hg.

Boundary conditions:

- *Pressure and forces*

The differential pressure on a vacuum chamber is obviously one bar during operation but it is recommended to check what all the intermediate steps are like, for example, an over-pressure test for qualification. In the presence of a closed end, the resulting forces could be large and the design should take into account the transmission of these forces to the fixing points through the vacuum chamber wall.

- **Temperature**

Specifying operating temperature (usually room temperature), bake-out temperature (usually between 150°C and 300°C), and exceptional temperature in the case of an incident (like a cool-down due to cryogen losses) together with all the transients is a must. The effects of temperature are dilatations, stresses and changes of material properties and they may have destructive effects if badly mastered. Slow temperature transients allow the resulting stresses to be minimized but it becomes an operational constraint that is not necessarily acceptable.

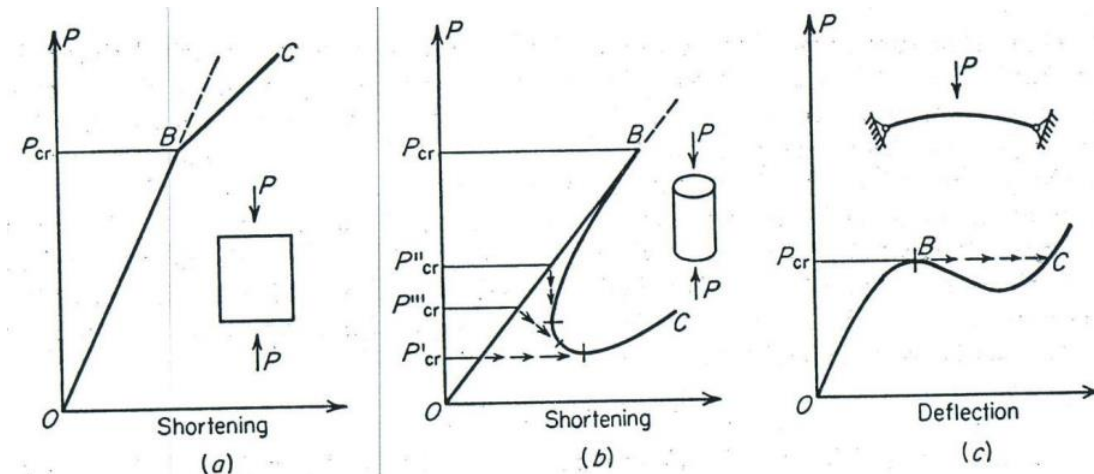
Materials

The material parameters design are only three main ones: the modulus of rigidity (Young’s modulus: E), the elastic ($\sigma_{0.2}$) and rupture (σ_r) limits.

9.3.2.2 Design

Basics

Stresses generated by the loads enumerated before should usually remain in the elastic range. This means that the equivalent stress shouldn’t exceed the elastic limit ($\sigma_{0.2}$) anywhere in the structure.



Tensile strength	115-234	σ_b /MPa
Yield Strength	23	$\sigma_{0.2} \geq$ /MPa
Elongation	65	$\delta_5 \geq$ (%)
ψ	-	$\psi \geq$ (%)
Akv	-	Akv \geq /J
HBS	123-321	-
HRC	30	-

Physical proprieties of stainless steel 306

https://www.steelss.com/Materials/Stainless-Steels/YB-306_31_804.pdf

Steel Alloys		
Metal	Modulus of Elasticity	
	GPa	10 ⁶ psi
Carbon and Low Alloy Steel	200	29
Stainless Steel	193	28
Cold Drawn Wire Steel	210	30.5
Tool Steel	210	30.5

The first step of the analysis is the linear elastic one which gives all the information on a structure: displacements, strains, and stresses.

Tube shape

Cylindrical shape:

Tubes are obviously the most common shape for vacuum chambers.

Condition 1: Pipes having D_o/t values ≥ 10

Where,

D_o = Outside Diameter of Pipe

t = Minimum required thickness (means t = selected thickness – mill tolerance – corrosion allowance)

If the above condition met, Allowable External Pressure P_a can be calculated using the two equations below as per their conditions:

If the value of factor 'B' is determined, use below equation

$$P_a = \frac{4B}{3(D_o/t)} \quad \text{Eq. (1)}$$

If the value of factor 'A' falls to the left of material or temperature curve and because of that value of factor 'B' cannot be determined, then go for the second equation below

$$P_a = \frac{2AE}{3(D_o/t)} \quad \text{Eq. (2)}$$

Where,

P_a = Allowable external pressure

A = Factor determined from Figure 'G' in a sub-part of ASME Section II, Part D

B = Factor determined from the applicable [material chart in sub-part 3 of ASME Section II, Part D](#)

E = Modulus of elasticity of the material at design temperature interpolation may be made between the lines for intermediate temperature.

Condition 2: Pipes having Do/t values < 10

If the above condition met, Allowable External Pressure P_a can be calculated using the two equations below as per their conditions: **If the value of factor 'B' is determined, use below equation**

$$P_a = \frac{B}{(R_o/t)} \quad \text{Eq. (3)}$$

If the value of factor 'A' falls to the left of material or temperature curve and because of that value of factor 'B' cannot be determined, then go for the another equation below

$$P_a = \frac{0.0625E}{(R_o/t)^2} \quad \text{Eq. (4)}$$

Where,

$$A = \frac{0.125}{(R_o/t)}$$

B = Factor B will be the same as the first condition, per UG-20(c)

R_o = Outer Radius of the Pipe

E = Modulus of Elasticity

Note: The second condition “Do/t values < 10” is very rare, in most of case we need to verify pipe wall thickness calculation for external pressure under the first condition “Do/t values ≥ 10”.

9.3.2.3 Calculation Steps for Pipe Thickness Verification

cylinder (D₀=30cm. L=35cm) E= 193 GPa

assume a thickness t=1.5 mm. P_{ext}=14.7 psi.

Step 1: Calculate Do/t

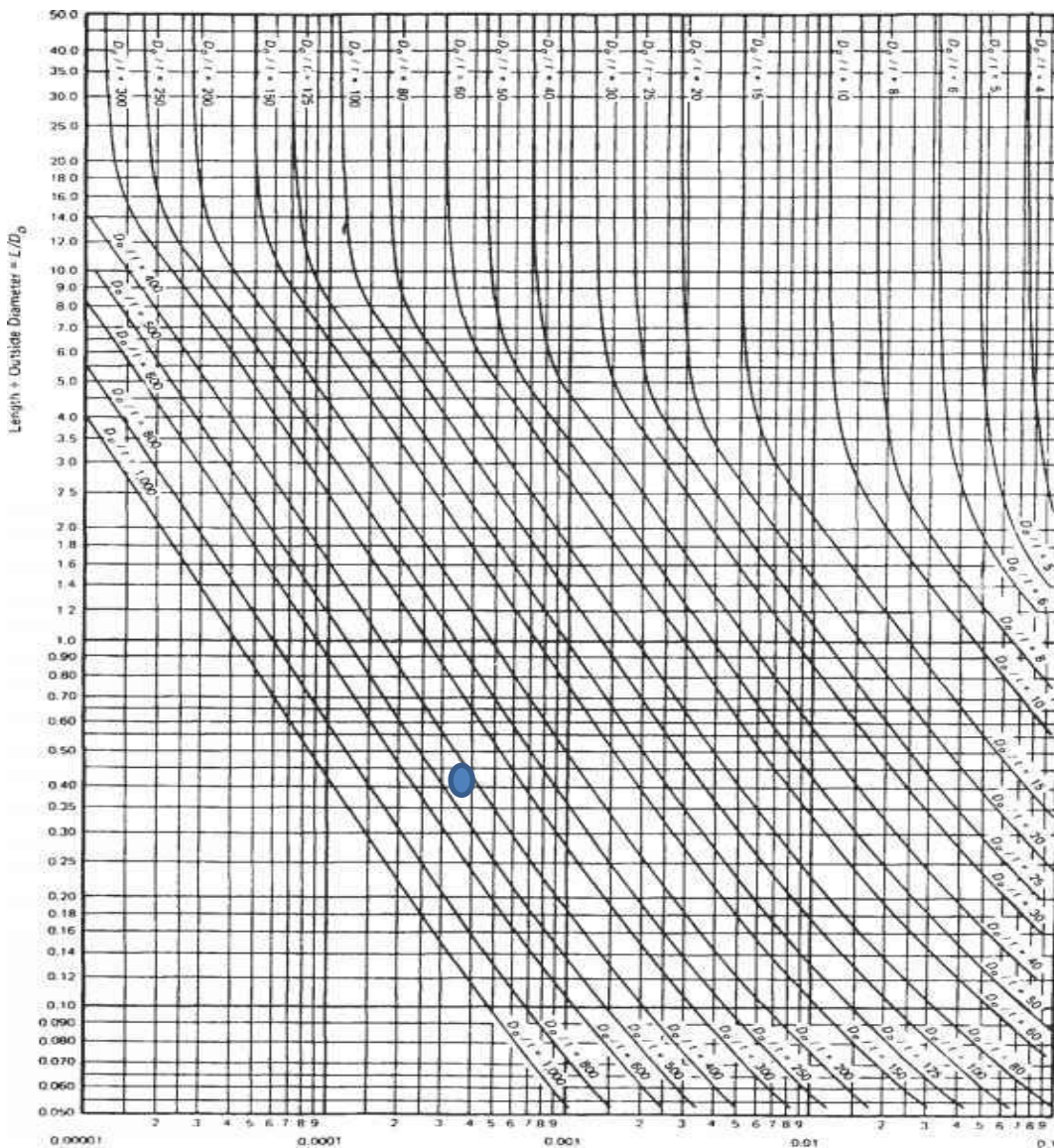
$$D_0/t=200 \gg 10$$

Step 2: Calculate L/D₀, this will help to find the value of factor A

$$L/D_0=1.67$$

Step 3: Find the Factor 'A' from Figure 'G' of ASME Section II, Subpart 3, Part D

To find factor 'A' open the (Charts and tables for determining shell thickness of components under external pressure)



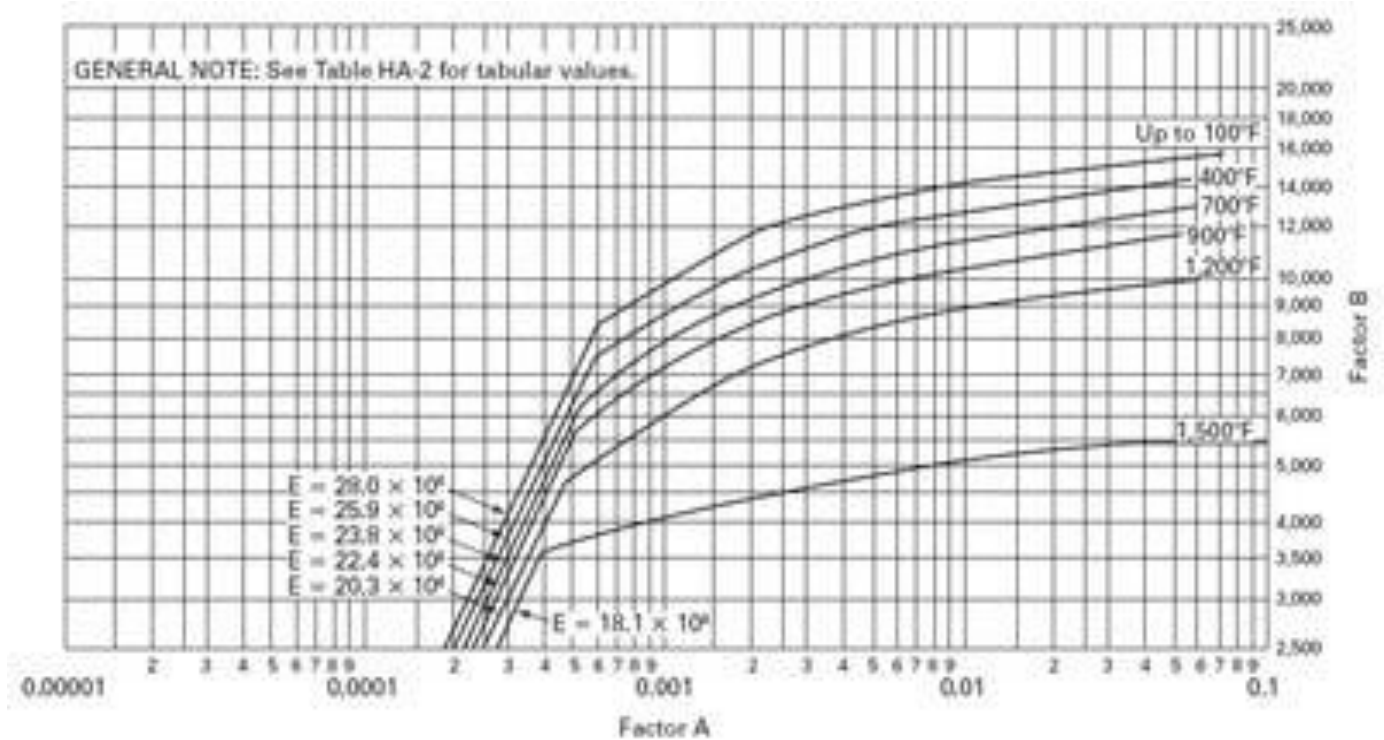
In subpart 3, go to Figure G, move vertically to see the value of L/Do , and move horizontally to see the value of Do/t . As per the calculated value match the both lines.

$A=0.0003$

Step 4: Now, Find The Factor 'B'

Using the value of factor A (for our case $A = 0.0003$) and design temperature (300°C), we need to find the value of factor B.

Open the applicable material chart. As for our case pipe material is SS (stainless steel). So according to the pipe material and their SMYS value select the appropriate chart, for our case, we have to refer **Figure HA-2** (refer the fig below).



B=3800

Fig. 2: Chart for Determining Shell Thickness of Components under External Pressure For stainless Steel

Here from the figure, we can see that the value of factor A is on the right side of the material or temperature curve. So, it is clear that we will use Eq. (1) for calculating Allowable External Pressure.

Important Note: If the value of factor A would be at the left side of the curve then we will have to calculate allowable external pressure using Eq. 2 and Modulus of Elasticity (E) would be utilized in the equation.

Now, move horizontally to see the value of Factor A, select the curve according to design temperature (for our case it 300°C), and then match the lines. We can get the value of factor B on the right side of the chart (refer above fig. 2).

Step5: Calculate Maximum Allowable External Pressure (Pa)

Now, using the value of factor B, calculate the maximum allowable external working pressure (Pa) using the below equation:

$$P_a = \frac{4B}{3(D_o/t)} \quad \text{Eq. (1)}$$

Pa= 25.33psi t=1.5mm is safe thickness as Pa> Pext= 14.7psi .

If $P_a < P$, then need to increase the selected pipe wall thickness and follow the all steps again to verify the selected pipe thickness. This practice will be repeated until and unless the condition met $P_a > P$.

According to ASME CODE SECTION VIII- DIVISION – I - UG-16 (b)- minimum thickness permitted for shells and heads holding components shall be 1.6mm exclusive of any corrosion. Therefore, minimum thickness of cylindrical shell = 1.6mm.

reference: * <https://www.youtube.com/watch?v=0J6ci3IxUkc>

*<https://www.youtube.com/watch?v=CJSaAjJMK5w>

*

The most stable ones are circular ones for which a quick analysis is quite straightforward. The circumferential stress under external pressure p is simply:

$$\sigma_o = PR/t$$

R and t being, respectively, the radius and the thickness of the circular tube. If the tube is closed and subjected to an axial force F , the axial stress is

$$\sigma_z = \frac{PR}{2t} + \frac{F}{2\pi Rt}$$

And the Von Mises equivalent stress to be compared to the material maximum allowable stress is

$$\sigma_e = \frac{1}{2} \left[3 \left(\frac{PR}{t} \right)^2 + \left(\frac{F}{2\pi Rt} \right)^2 \right]^{\frac{1}{2}}$$

The buckling pressure can also be computed through analytical formulas, depending upon the Geometrical parameters of the tube and the Young's modulus of the material. The most conservative One is for an infinite length of the tube:

$$P_{cr} = \frac{0.25E}{1 - \mu^2} \left(\frac{t}{R} \right)^3$$

For stainless steel and aluminum $\mu=0.3$.

Calculation example:

alfa 8:28 PM 65%

★ **desertfox** (Mechanical) 28 Dec 10 09:26

hi Superslinky

The cylinder a thin walled vessel so the hoop stress in the cylinder can be found by:-

$$\sigma = P \cdot D / (2 \cdot t)$$

for your case if the vessel internal pressure was 10psi then:-

$$P = 10 - 14.7 \text{ psi} = 4.7 \text{ psi}$$

$$\sigma = 4.7 \cdot 20 / (2 \cdot 0.25) = 188 \text{ psi}$$

because the end of the vessels are capped there will be a longitudinal stress this is typically half the hoop stress.

This of course is not the full story because the end caps need stressing and I am not familiar with the Lexan material, the stressing in the end caps will depend on the shape whether flat or spherical etc. You would be wise to look at ASME 8 or PD5500 which are both pressure vessel codes and should cover vessels under vacuum.

desertfox

Superslinky (Automotive) (OP) 28 Dec 10 12:06

I'm having a hard time grasping the issue with $P = 10 - 14.7 \text{ psi} = 4.7 \text{ psi}$, if my application is a vacuum then does that change? For example, I will be applying around 12psi internally or I should say negatively to the outside atmosphere to create a "suction".

Also if I follow your calculation (assuming it's still simply 12psi wether + or -) then my calculation would be:

eng-tips.com

Quasi-rectangular shape approximated by beam

If approximated by a beam, the maximum deflection (w_{\max}) and stress (σ_{\max}) (upper and lower bounds) are

$$\frac{1}{32} \frac{pl^4}{Et^3} < w_{\max} < \frac{5}{32} \frac{pl^4}{Et^3} \quad (5)$$

$$\frac{1}{2} p \left(\frac{l}{t} \right)^2 < \sigma_{\max} < \frac{3}{4} p \left(\frac{l}{t} \right)^2 \quad (\text{not at the same location}), \quad (6)$$

l and t being, respectively, the span and the thickness of the tube.

Windows

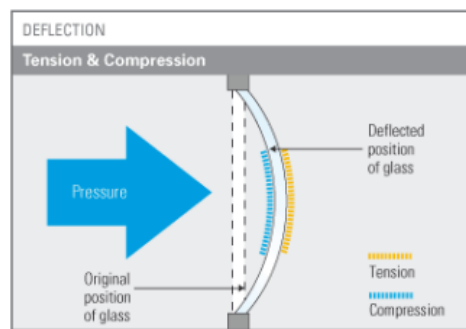
Special care is required for these critical items. Designed to allow particle beams to escape the vacuum Chambers without interaction, windows are thin and often manufactured with a special material. **The best shape** for resisting external pressure is a **spherical dome** but the **manufacture is difficult**. And the external ring must be quite rigid. If the window is oriented in such way that it can buckle, the Classical buckling pressure is

$$P_{CL} = \frac{2E}{\sqrt{3(1-\nu^2)}} \left(\frac{t}{R} \right)^2,$$

R and t being, respectively, the radius of curvature and the thickness of the spherical dome. **A flat window is the other common option** but, when put under pressure, the deflection (w_{max}) is Not negligible.

R and t being, respectively, the radius and the thickness of the **circular window**.

$$w_{max} = \frac{3}{16} \frac{p}{E(1-\nu^2)} \frac{R^4}{t^3},$$



Properties

Density	25 kN/m ³
Young's modulus	70 000 MPa
Shear modulus	28 000 MPa
Poisson's ratio	0,23
Hardness (Mohs scale)	6
Coefficient of thermal expansion	9·10 ⁻⁶ K ⁻¹
tensile strength	45 MPa
compressive strength	800 MPa

*Mechanical proprieties of Glass. reference: [*https://www.slideshare.net/ARGHASAHA4/vacuum-chamber-design](https://www.slideshare.net/ARGHASAHA4/vacuum-chamber-design)*

Density

The density of glass is 2.5, which gives flat glass a mass of 2.5 kg per m² per mm of thickness, or 2500 kg per m³.

Compressive strength

The compression strength of glass is extremely high: 1000 N/mm² = 1000 MPa. This means that to shatter a 1 cm cube of glass, it requires a load of some 10 tonnes.

Tensile strength

When glass is deflected, it has one face under compression and the other in tension. Whilst the resistance of glass to compression stress is extremely high, its resistance to tensile stress is significantly lower. The resistance to breakage on deflection is in the order of: - 40 MPa (N/mm²) for annealed glass - 120 to 200 MPa for toughened glass (depending on thickness, edgework, holes, notches etc.).

Elasticity

Glass is a perfectly elastic material: it does not exhibit permanent deformation, until breakage. However it is fragile, and will break without warning if subjected to excessive stress.

Young's modulus, E

This modulus expresses the tensile force that would theoretically have to be applied to a glass sample to stretch it by an amount equal to its original length. It is expressed as a force per unit area. For glass, in accordance with European standards: $E = 7 \times 10^{10} \text{ Pa} = 70 \text{ GPA}$

Poisson's ratio, μ (lateral contraction coefficient)

When a sample is stretched under mechanical stress a decrease in its cross-section is observed. Poisson's ratio (μ) is the relation between the unit decrease in the direction perpendicular to the axis of the effort and the unit strain in the direction of the effort. For glass in buildings, the value of coefficient μ is 0.22.

9.3.2.4 Allowable Stress (Strength)

The **allowable stress** or allowable strength is the maximum **stress** (tensile, compressive or bending) that is allowed to be applied on a structural material. The allowable stresses are generally defined by building codes, and for steel, and aluminum is a fraction of their **yield stress** (strength):

$$F_{\alpha} = \frac{F_y}{F.S.}$$

In the above equation, F_{α} is the *allowable stress*, F_y is the *yield stress*, and $F.S.$ is the *factor of Safety* or *factor*. This factor is generally defined by the building codes based on particular condition under consideration.

What Is Stress?

Before looking at what causes these changes, there are a few concepts that need to be looked at first. **Stress** is the amount of forces (strength or energy) that is being exerted on an object, divided by its cross-sectional area to account for size. Larger objects are able to withstand higher forces. By using stress instead of just force, we are able to use the same yield stress for the same material, regardless of how large the object actually is. To compute the amount of stress acting on the object, use the equation:

$$\sigma = \frac{F}{A}$$

Where:

σ is stress

F is force

A is cross sectional area

What Is Strain?

Another important concept is **strain**, or how much an object deforms when forces are applied to it. Most of the time this deformation will either cause the object to elongate or shorten, depending on how forces are applied. To compute strain, this change is divided by the object's original length, again to account for size.

Larger objects will have a greater change in length than smaller objects, even though they experience the same forces acting on them. To compute the amount of strain on an object, use the equation:

$$\varepsilon = \frac{\Delta L}{L}$$

Where:

ε is the strain

ΔL is the change in length

L is the original length

There are two different types of deformation: elastic and plastic.

- **Elastic deformation** will automatically reverse itself when external forces are removed. Imagine a rubber band - no matter how you stretch it, once you let go of one end it will 'snap' back to its original shape.
- **Plastic deformation** is a permanent deformation. To reverse it, an additional external force needs to be applied to return the object to its original shape. When you squeeze the middle of a plastic bottle, it compresses and stays deformed even when you let go. You'd have to add pressure to the inside or squeeze the opposite direction to return it to normal.

What is yield strength or yield stress?

The yield strength or yield stress is a material property and is the stress corresponding to the yield point at which the material begins to deform plastically.

Safety factor:

The definition of the safety factor is simple. It is defined as the ratio between the strength of the material and the maximum stress in the part.

$$n = \frac{\text{strength}}{\text{stress max}}$$

When the stress in a specific position becomes superior to the strength of the material, the safety factor ratio becomes inferior to 1, this when there is danger

What it tells us basically is that in a specific area of the model, the stress is higher than the strength the material can bear.

When the stress in the model remains much inferior to the strength of the material, the safety factor stays superior to 1 and the model is « safe ».

Keep in mind that if the safety factor is way superior to 1 everywhere in your model, this is also indicating that your part may be over-engineered. In this case, this is not desirable either, because you are just wasting material resources and increasing the cost.

Safety factor must be applied to any computed buckling value: pressure vessel codes like CODAP use (3.0) but EN 13458-2 quotes only (2.0) for outer jackets.

Mathematically,

$$\text{Factor of safety} = \frac{\text{Maximum stress}}{\text{Working stress or design stress}}$$

For Brittle : It is the ratio of the Ultimate stress to the working or design stress

$$\text{Factor of safety} = \frac{\text{Ultimate stress}}{\text{Working stress or design stress}}$$

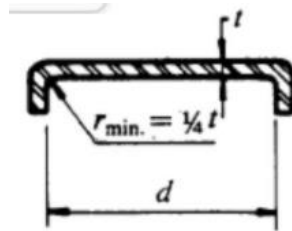
For Ductile: It is the ratio of the Yield stress to the working stress

$$\text{Factor of safety} = \frac{\text{Yield stress}}{\text{Working stress or design stress}}$$

Note: we will take 3 as a safety factor

Faces of cylinder:

Circular flat face of stainless steel:



Equation applies when:

- when d does not exceed 24 in.
- th/d is not less than 0.05 or greater than 0.25.
- Head thickness, this is not less than the shell thickness, ts.

Required minimum wall thickness:

$$t = d \left(\frac{0.13P}{S \times E} \right)^{0.5}$$

Where:

P= Design pressure or max allowable working pressure, psi.

d=Inside diameter of vessel of the material.

t=Minimum thickness of shell (wall) exclusive of corrosion, inches.

S= Maximum Allowable Stress

th= Actual thickness used in actual design, inches.

t_r = Minimum required thickness of seamless shell for pressure, inches.

t_s = Actual thickness of shell, exclusive of corrosion allowance, inches.

E = Weld joint efficiency=0.85

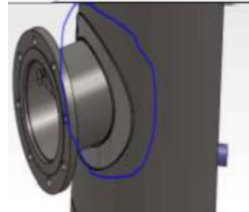
https://www.engineersedge.com/pressure_vessels_menu.shtml

Conflat Flanges:

The standard design method uses an increased wall thickness plate at the equator line of vessel to support the additional stresses caused by the attachment of the legs. The formula for calculation the wall thickness of a segmented plate of to be welded in a vessel or spherical shells is:

$$t = \frac{PL}{2SE - 0.2P} + C$$

$$L = D_i/2$$



t =Minimum design wall thickness (in);

P =Design Pressure (psi);

D_i =Inside Diameter of sphere (in);

L =Sphere Radius (in);

E =Tube welding factor (1 for seamless pipe, 0.85 for welded pipe)

C = Weld Corrosion Allowance (0 for no corrosion, 0.0625 in commonly used, 0.125in maximum);

S = Maximum Allowable Stress.



9.3.2.5 Grid Design

A grid consists of a sphere wire structure and is connected to the high voltage feedthrough. The diameter size of the grid is usually about 20% of the diameter of the outer sphere (anode). Should we have an anode sphere with a diameter of 20 cm than the diameter of the grid should be 4 cm. The material for the grid can be stainless steel wire because it permits welding but in order to resist the high temperatures that can occur in the grid also tungsten or tantalum wire is used.



This particular jig is suitable for winding a grid with a diameter of 1.5" or 38 mm. It requires two 14" or 360 mm lengths of wire (tungsten or tantalum). The crossing intersections can be spot welded for a better rigidity.

Experiments in IEC research have demonstrated that fusion efficiency increases when the grid transparency is greater than 92%.

The grid transparency can be calculated as follows:

$$((\text{Grid Surface Area} - \text{Wire Cross-section Area}) / \text{Grid Surface Area}) \times 100\% = \% \text{Transparency}$$

For which, assuming that the grid is a perfect sphere:

$$\text{Wire Cross-section Area} = \text{Total Length of Wire per Loop} \times \text{Diameter Wire} \times \text{Number of Wire Loops} = \text{Grid Circumference} \times \text{Diam. Wire} \times \text{Number of Wire Loops} = 2\pi r n d$$

And

$$\text{Grid Surface Area} = 4\pi r^2$$

Transparency = $((4\pi r^2 - 2\pi r n d) / 4\pi r^2) \times 100\%$, which can be reduced to

$$\text{Transparency} = ((r - \frac{1}{2} n d) / r) \times 100\%$$

In which: r = radius of the grid

n = number of wire loops

d = diameter of wire

Example: The grid in image 10 has a diameter of 38 mm (a radius of 19 mm), is made of wire with a diameter of 0.23 mm and has 3 loops. The transparency is according to the formula:

$$(19 - \frac{1}{2} \times 3 \times 0.23) / 19 \times 100\% = 98.2\%$$

Based on the available materials in our country, we found the best choice is stainless steel wire (diameter d=1.6mm). n=3 d=1.6mm radius of loop r= 3.5cm

$$\text{transparency} = 93.14\% > 92\%$$

verify.

The grid transparency can be enhanced effectively to exceed the geometrical transparency by focusing the grid carefully inside the vacuum chamber, i.e. by placing the grid precisely concentric with the outer vacuum chamber sphere. Precise focusing can result in the Fusor operating in "star mode" which causes channelization of the ions into distinct rays converging from the center of the

grid. The rays (ion paths) go through the grid openings and stay clear from the grid wires. As a result the ion recirculation factor may increase to 100 or higher.

The material for the grid wire can be stainless steel but should preferably be tungsten or tantalum. During operation of the Fusor the grid wire becomes hot and stainless steel will not keep its shape but will start sagging. Tungsten is the best choice because of its low vapor pressure, its great tensile strength and its high melting point of 3422°C. However, it is not very suitable for spot welding and therefore an alloy of tungsten and rhenium can be used or tantalum wire.

The grid transparency calculation shows that a thin wire contributes to a high transparency. It should however be noted that too thin a wire might cause a problem. In a Fusor with a relatively high vacuum and a high voltage potential of 25 kV on the Tungsten wire nothing will happen as long as a plasma short cut (from grid to Fusor wall) does not occur.

The resistivity of Tungsten is $5.6 \times 10^{-8} \Omega/\text{m}$ and the resistance of a wire is calculated according to:

$$R = (\rho \cdot l) / w$$

For which

R = resistance

ρ = resistivity

l = length

w = width

The formula shows that the width (diameter) of the wire is inversely proportional to the resistance, or with other words; a thinner wire has a larger resistance. In case of a plasma short cut our very thin wire might probably light up in a flash to white hot and burn away. Or maybe not?? In a hypothetical example we assume that a plasma short cut occurs at a quarter length of one of the wires (360 mm long) that make our grid, i.e. the path length for the current is 90 mm, the width of the wire is 0.23 mm, the resistivity of the Tungsten wire is $5.6 \times 10^{-8} \Omega/\text{m}$ and the Fusor is operated at 25 kV. We also assume that the plasma has no resistance (which is incorrect but we have no data for a deuterium plasma at given pressures). The formula yields a resistance of the wire path length of $2.2 \times 10^{-5} \Omega$, which at 25 kV theoretically might draw a current of about 10^9 A. This high amount of current has the effect of a true short cut. Fortunately, the Fusor is not capable of supplying such an extreme current as the power supply is limited at 15 mA before it cuts out. In fact, our tungsten wire of 90 mm length and a diameter of 0.23 mm will be emitting maximally a power of 25 kV at 15 mA which equals 375 W. The surface area of the wire is $2\pi r l$ or $2 \times 3.14 \times 0.115 \times 90 = 65.031 \text{ mm}^2$ or $6.5 \times 10^{-5} \text{ m}^2$

According to the Stefan Boltzmann law for the power per unit area:

$$I = \sigma T^4$$

Where σ = the Boltzmann constant, $5.670373 \times 10^{-8} \text{ W m}^{-2} \text{ T}^{-4}$, the temperature of the wire will be

$$T = \sqrt[4]{\frac{375}{(6.5 \times 10^{-5}) \times (5.670373 \times 10^{-8})}} \text{ K}$$

Or $T = 3176 \text{ K}$ which equals $2903 \text{ }^\circ\text{C}$. This calculation is an approximation as several parameters have not been taken into account, such as the true effective area, heat loss through conduction into the feedthrough and heat loss to gas molecules around the wire, etc. Nevertheless the result is below the melting point of Tungsten ($3422 \text{ }^\circ\text{C}$) and therefore the grid will probably become white hot when the maximum current flows through it during a short cut, but the grid will probably not be destroyed.

Our example clearly demonstrates that for developing a grid we should take into account the diameter of the wire and the type of material to be chosen. With materials such as tungsten it will be possible to apply a thinner wire and this will improve the grid transparency.

In this prototype:

$$\text{Voltage } V=12\text{kv} \quad \text{current } I=30\text{mA}$$

$$L=2\pi r=0,2198 \text{ m}$$

$$P= UI= 360 \text{ watts.}$$

$$\pi dL= 1,104 \times 10^{-3}$$

$$T= 1548.49 \text{ k}= 1275.49 \text{ }^\circ\text{C} < 1400^\circ\text{C melting Point of stainless steel(1400 to 1530).}$$

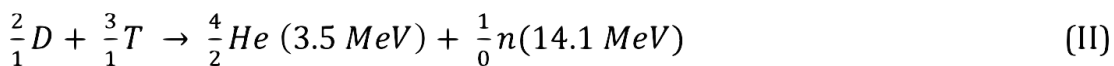
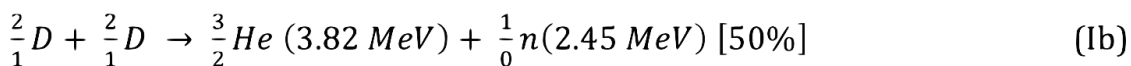
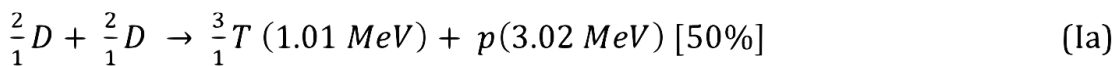
Verify

[Reference: http://fusor.eu/theory.html](http://fusor.eu/theory.html)

9.3.3 Fuel of Fusor reactor

The fuel for the Fusor is Deuterium gas, which is injected into the vacuum chamber through a precision regulated valve. Injected means here that the precision valve is slightly opened and the high vacuum in the vacuum chamber (reactor) draws Deuterium gas into the vacuum reactor. The applied high voltage in the reactor ionizes Deuterium to Deuterium ions (Deuterons).

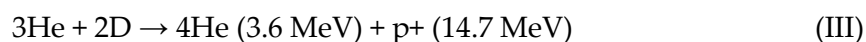
For obtaining a maximally fusion rate a direct relationship exists between the pressure of Deuterium in the reactor (Deuteron density) the applied potential difference and the current. The higher each one of these three parameters, the higher the fusion rate, though an optimum appears to exist for these parameters. When the parameters have been optimized, fusion for D-D occurs according to the following reactions:



The first stage reactions! a and! b have equal opportunities to occur and yield Tritium (as Tritons), Helium-3 (as a Helium-3 nucleus), a proton, a fast neutron and energy.

The second stage reaction is between Deuterons present in the reactor and Tritons formed in reaction Ia and yields Helium-4 (as nucleus) and a fast neutron. The neutron formed in reaction II has such a high energy that is carries away 80% of the energy formed in this reaction.

The second stage reaction has also the probability for fusion between Deuterons present in the reactor and Helium-3 nuclei formed in reaction Ib:



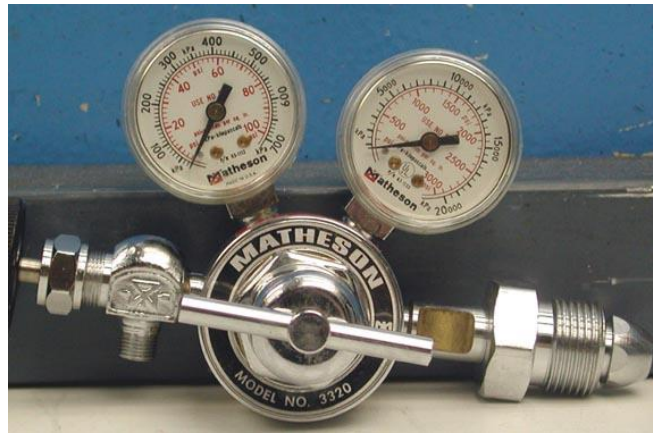
This reaction yields Helium-4 nuclei and a high energy proton, but the reaction is less likely to occur because the peak energy required for this reaction is much higher than for the D-D reactions.

In practice we usually deal with the reactions! a, Ib and II.

Deuterium can be obtained as gas in lecture bottles and as Deuterium oxide (heavy water). When obtained as heavy water, Deuterium needs to be liberated as gas by electrolysis of heavy water.

9.3.3.1 Deuterium Gas

Deuterium gas is available in lecture bottles, typically e.g. 38 liters at a pressure of 100 kgf/m² (atm). It is a highly flammable gas and air shipment of Deuterium cylinders is not allowed. This limits the possibility of buying Deuterium gas and it explains why Deuterium oxide is quite popular amongst fusioners, despite the fact that an electrolysis unit will have to be built. The costs of an electrolysis unit, however, is more or less comparable with the costs of the pressure regulator that will have to be applied to extract the gas from the high pressure lecture bottle and convert it to a low pressure



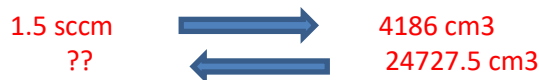
The pressure regulator should preferably be of the two stage type, intended for Hydrogen and produce an output pressure as low as possible. When operating a spherical Fusor with a diameter in the range between 160 and 200 mm, a volume of Deuterium will be used of approximately 1 to 1.5 sccm, i.e 1 - 1.5 milliliter per minute at normal pressure and ambient temperature. A single bottle of Deuterium will therefore last for many years of Fusor operation experiments.

In our fusor we use an autoclave cylinder (D0=30cm. L=35cm):

$$\text{Volume} = \pi R^2 * L = 24727.5 \text{ cm}^3$$

Sccm unit (standard cubic centimeters per minutes)

$$\text{Sphere } D= 200 \text{ mm} \quad V_s = \frac{4}{3} \pi R^3 = 4186 \text{ cm}^3$$



So in our reactor we will use a volume of Deuterium approximately 8.8 Sccm
8,8 ml/minute.

9.3.3.2 Deuterium Oxide

When obtained as heavy water (image 2), Deuterium gas needs to be produced by electrolysis to make it suitable for feeding into the reactor.

The density of heavy water is 1.107 g per ml and the molar mass of heavy water is 20.0276 g per mole. One mole of Deuterium oxide will yield two Deuterium ions or one Deuterium gas molecule. From a commercial volume of 100 ml of heavy water therefore almost 101 liters of Deuterium gas, at standard pressure and temperature, can be electrolyzed as calculated below.

Calculation:

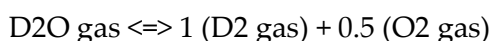
$$\text{Mass D}_2\text{O} = 100 \text{ ml} \times 1.107 \text{ g/ml} = 110.7 \text{ gram}$$

$$\text{Molar mass D}_2\text{O} = 20.0276 \text{ g/mole}$$

$$\text{Moles D}_2\text{O} = 110.7 \text{ g} / 20.0276 \text{ g/mole} = 5.52 \text{ moles}$$

One mole D₂O is equivalent with a volume of 22.4 liter D₂O vapour

$$5.52 \text{ Moles equal } 5.52 \times 22.4 = 123.8 \text{ liters of D}_2\text{O vapour}$$



$$1 \text{ mole gas} \rightleftharpoons 1.5 \text{ mole gas}$$

mole ratio = 1.5

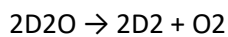
The volume of the elemental gases is: Volume D₂O gas x mole ratio = 123.8 liter x 1.5 = 185.7 liter or approximately 186 liter D₂ gas and 93 liter O₂ gas are formed by electrolysis.

The average price of 100 ml heavy water 99% is about 120 USD, hence one liter of Deuterium gas (after electrolysis) for amateur fusioner use costs about 0.65 USD.

Under similar conditions as described in the paragraph about Deuterium gas, a volume of 100 ml of heavy water (when electrolyzed without losses and transferred into the Fusor) will enable continuous Fusor operation during more than 70 days.

9.3.3.3 Traditional Electrolysis

A method to extract Deuterium from heavy water is by means of electrolysis: an electrical current is passed through heavy water by using two inert metal electrodes, preferably made of platinum. Deuterium will appear at the negatively charged electrode, the cathode, and Oxygen will appear at the positively charged electrode, the anode, conform the overall chemical reaction:



The theoretical voltage to be applied is for starting electrolysis is 1.48V, but usually higher voltages will be used. As an electrolyte a solution of Sodium hydrogen carbonate (NaHCO₃ [baking soda] analytical grade) needs to be added.

Do not add Sodium chloride as this will produce Chlorine gas together with Deuterium gas from your electrolysis cathode.

The highest production of Deuterium gas will be obtained when performing electrolysis in a 0.4M solution of NaHCO₃ in heavy water, i.e. at pH 8.2 of the solution (reference 1). A 0.4M solution of NaHCO₃ (molar mass is 84.00661 g/mol) will be obtained by dissolving 3.36 gram of NaHCO₃ in 100 ml of heavy water. From a strictly theoretical point of view adding (highly pure) baking soda to heavy water introduces Hydrogen atoms into the solution, which will join Deuterium at the cathode as an impurity in Deuterium gas. To avoid this, we could add NaDCO₃, which is not commercially available and needs to be synthesized by leading CO₂ gas through a Sodium carbonate (soda, Na₂CO₃) solution, consisting of Na₂CO₃ dissolved in heavy water. A method to do this could be performed by dissolving a molar equivalent amount of Na₂CO₃ (i.e. equivalent to 0.4M NaHCO₃) in a chosen volume of Deuterium oxide (heavy water) and bubbling CO₂ gas through the solution (by means of an aquarium air diffusor) until more or less a pH of 8.2 will be obtained. This is apparently quite a lot of work and it remains the question whether the created H₂ impurity in Deuterium gas is of importance in the overall process of fusion in our Fusor.

Similarly to the H₂ impurity in Deuterium, CO₂ gas will join Oxygen gas as an impurity at the cathode, when we use either NaHCO₃ or NaDCO₃, but that is of no concern to us as gases at the anode are of no use for the Fusor and are allowed to escape in the air.

A more important disadvantage of the classical electrolysis process is that in the gas line following the electrolysis cell a (rather large capacity) gas dryer needs to be installed because the electrolysis produces moist Deuterium gas (saturated with heavy water). This occurs because the Deuterium gas bubbles up from the cathode through heavy water before it arrives in the output gas line. This is a very efficient way to saturate gas with heavy water.

9.3.3.4 PEM Electrolysis

Electrolysis with a polymer electrolyte membrane (PEM), also called proton exchange membrane (PEM), is electrolysis of (heavy) water in a cell with a solid polymer electrolyte that is responsible for conduction of Protons (for heavy water read "Deuterons"), separation of product gases and

electrical insulation of the electrodes (reference 3). The cell material is Nafion, a sulfonated tetrafluoroethylene based fluoropolymer-copolymer, with a thickness of 100-200 μm (reference 4).

The PEM cell is a highly efficient way to produce Deuterium gas with a very high purity (99.999%) with no cross over of oxygen. There is some doubt about the statement that the cell produces dry gas because the membrane itself is hydrated and therefore it is believed that the Deuterium gas produced in the cell can be saturated with (heavy) water and in that case it would not harm to add a Drierite column in the Deuterium gas line. It is a fact, however, that heavy water resides at the anode side of the (wet) membrane, where Oxygen is produced. There are therefore no doubts that the Oxygen gas is saturated with heavy water and it might be worthwhile to consider a cold trap in the Oxygen line in order to retain heavy water from the Oxygen gas outlet. A nice calculator to calculate how much heavy water is contained in a volume of saturated Deuterium gas can be found in reference 5.

Advantages of the PEM cell are further that it can operate at elevated temperatures (50-80°C), it has a high current density (0.6-2.0 mA/cm²), a cell operating voltage of 1.75-2.20V and it can produce gas at a high pressure (stack pressure < 30 bar). The latter is not possible with the cell from images 4 and 5 because the housing is made of plastic and will burst when subjected to high pressures.

For the production of Deuterium gas for a Fusor one single cell is usually sufficient because a (Nafion) cell surface of 10 cm² produces about 2 liter Deuterium per hour at ambient temperature and pressure. The commercial PEM cell as shown in images 4 and 5 has a Deuterium production of 5 ml per minute when operated at 2.0 V DC at 700 mA current. That is a production rate of five times the required Deuterium input for a Fusor! In order to regulate the flow rate from the cell to the intake rate of the Fusor, a (preferably automatic) system needs to be developed for a PEM cell Deuterium line.

Fortunately for the fusioner, PEM cells are easily available either as a single cell (approx. 40 - 45 EUR) or as part of an educational kit (approx. 55 EUR) as shown in image 3:

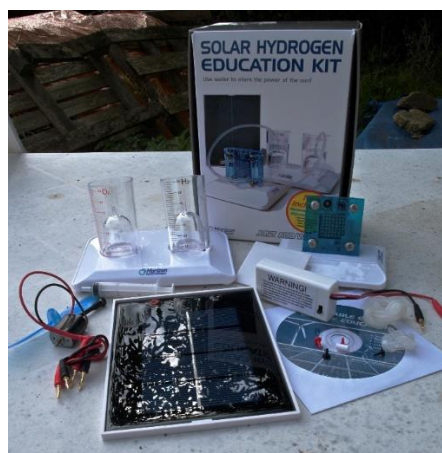


Image 3

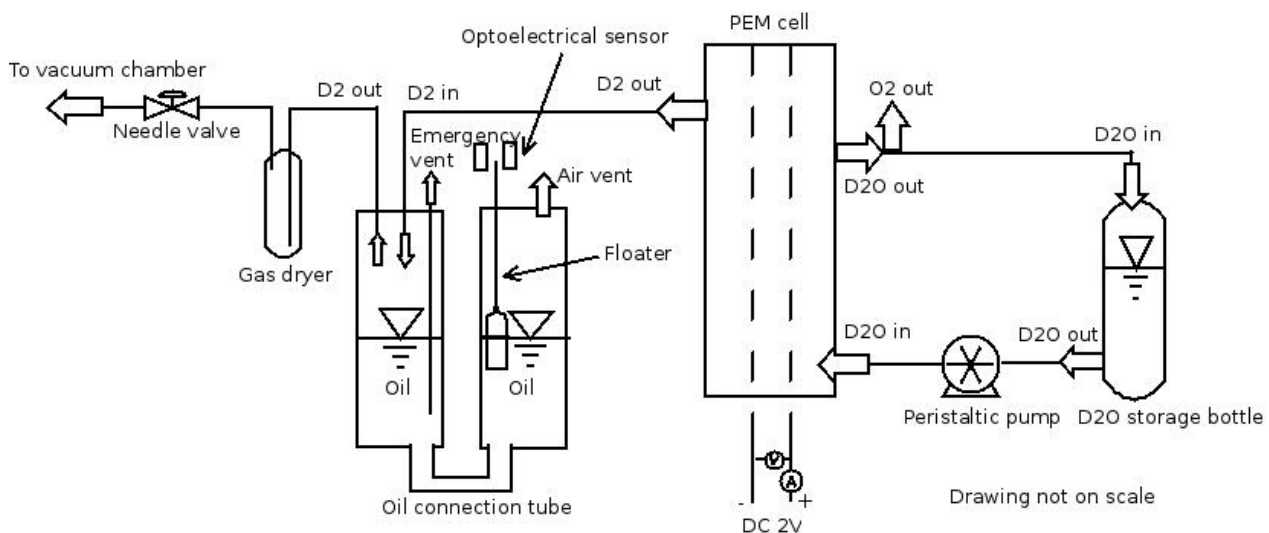
The Horizon Solar Hydrogen Educational Kit contains the PEM cell, a solar panel, an electric motor, a propellor, reservoirs for collecting Hydrogen and Oxygen, a battery holder for two 1.5V AA batteries (useless, because the cell eats a lot of power and the batteries will not last long), wires and plugs, tubing, stands for the reservoirs and the cell and a CD-ROM with information and

experiments. The dimensions of this PEM cell are 65x65x20 mm and it has a weight of 87 grams (empty). More about this and similar kits can be found in reference 6.

For the Fusor we are only interested in the PEM cell (images 4 and 5) , the wiring and the tubing.



For those who want to construct their own PEM cell, the membrane is available at a price of approx. 16 EUR for a square piece of 10 cm² (sides of 3.3.cm). The power requirements are 1 A per cm² at 0.6V. The reason for constructing a PEM cell might be for producing Deuterium at high pressure or at a higher capacity by stacking cells. In that case the housing(s) of the cell(s) must be made of SS (stainless steel or inox or rostfrei) steel.



Layout of PEM cell electrolyser

9.3.3.5 Ionization of fuel Atoms

In order to operate the Fusor it needs a supply of nuclei to be accelerated, a fuel, which is fed into the Fusor as a gas that will become ionized. Because the Fusor operates under a high vacuum, the fuel gas is "leaked" into the vacuum chamber (reactor) by means of a precision regulated valve.

The ionization of gas molecules, e.g. Deuterium gas, occurs in a sufficiently strong electrical field which is created between the outer wall of the vacuum chamber, the anode, and the inner grid, the cathode. When a sufficient amount of energy is transferred to a bound electron, i.e. when the threshold of the ionization potential is exceeded, a free electron is created which will drift towards the anode leaving a positively charged ion which will drift towards the cathode. In a sufficiently strong electric field the liberated electron will gain sufficient energy to liberate a further electron when it collides with another molecule and the process of gaining energy now proceeds for two

electrons which will liberate each another electron, and so on. Free electrons not only originate directly from ionized gas but are also generated by cosmic rays colliding with gas molecules and thus exciting them to higher energy states. The free electrons originating from cosmic rays interaction are called "seeding electrons" because they are at the basis of the process of generation of secondary free electrons. Another source of free electrons is the cathode (grid) in the Fusor, which releases electrons when under high voltage. This chain reaction of electron generation is called a Townsend avalanche. It depends on the free electrons gaining sufficient energy between collisions to sustain the avalanche. The final state of the Townsend avalanche is the Townsend breakdown, which is the situation when the gas suddenly changes from being a dielectric to a conductor by clouds of free electrons conducting the current between cathode and anode.

The next step in the ionized gas process is formation of a plasma, another fundamental state of matter next to solid, liquid and gas. A plasma has similar conductive properties to that of metals and this can be observed by a sudden raise in current between the electrodes once the state of plasma has occurred, possibly followed by plummeting of the voltage (depending on the type of HV power supply).

Characteristics of a plasma are the high electrical conductivity and the response to magnetic fields. Plasma is usually quasineutral, i.e. positive and negative particles are more or less in equilibrium. However, plasma of monocharged particles do exist but the density must generally be very low, or it must be very small, otherwise it will be dissipated by repulsive electrostatic force. For plasma to exist, ionization is required and the degree of ionization is the proportion of atoms that have lost or gained electrons and is controlled by the temperature of the plasma. An inert electrostatic confinement plasma can have a particle density of 10^{32} per m^3 and the temperature of the same plasma can reach 10^8 Kelvin. In an IEC device the plasma concentrates in the center of the hollow cathode, the Poisor, basically a spherical focus diode. When pressure in the vacuum chamber and high voltage have the right conditions the ion density in the Poisor increases until a glowing ball of plasma will be formed. When the plasma is fed with a higher grid voltage with a correspondingly higher current a dense plasma focus will result and a plasma-magnetic entity will be formed in the Poisor: a plasmoid. The plasmoid goes through different shapes when the power is further raised: bugle mode, jet mode and star mode. In bugle mode the ball shaped plasmoid has a trumpet-shaped ion blow-out, in jet mode the ion blow-out is a sharp line and in star mode brilliant rays are ejected from each aperture of the inner grid.

At higher pressures and at a too high starting potential electric discharges may occur before the Fusor comes into glow discharge mode: Depending on the pressure of the gas in the vacuum chamber, the voltage applied between cathode and anode and the distance between these electrodes, an electric discharge through the plasma and the avalanching free electrons cloud may occur. An electric discharge is however not what we want in an operating Fusor and it is therefore desirable to know the conditions under which discharges may develop.

The voltage necessary to start a discharge or electric arc, between two electrodes in a gas as a function of pressure and gap length is called the breakdown voltage (as described above) and can be defined by an equation known as Paschen's Law:

$$V = \frac{apd}{\ln(pd) + b}$$

in which:

V = breakdown voltage in volts

p = pressure in bar

d = gap distance in meters (i.e. distance between anode and cathode in the Fusor)

a and b are constants depending on the composition of the gas

The breakdown voltage depends on the mean free path (MFP) of the particles which increases with decreasing pressure. The MFP is the average distance a particle travels before colliding with another particle. The relationship between pressure and voltage is flat at higher pressures, goes through a minimum voltage, and then asymptotically rises as the mean free path exceeds the electrode spacing.

A graph based on the equation is the Paschen curve, as shown in image 5 for a number of gases.

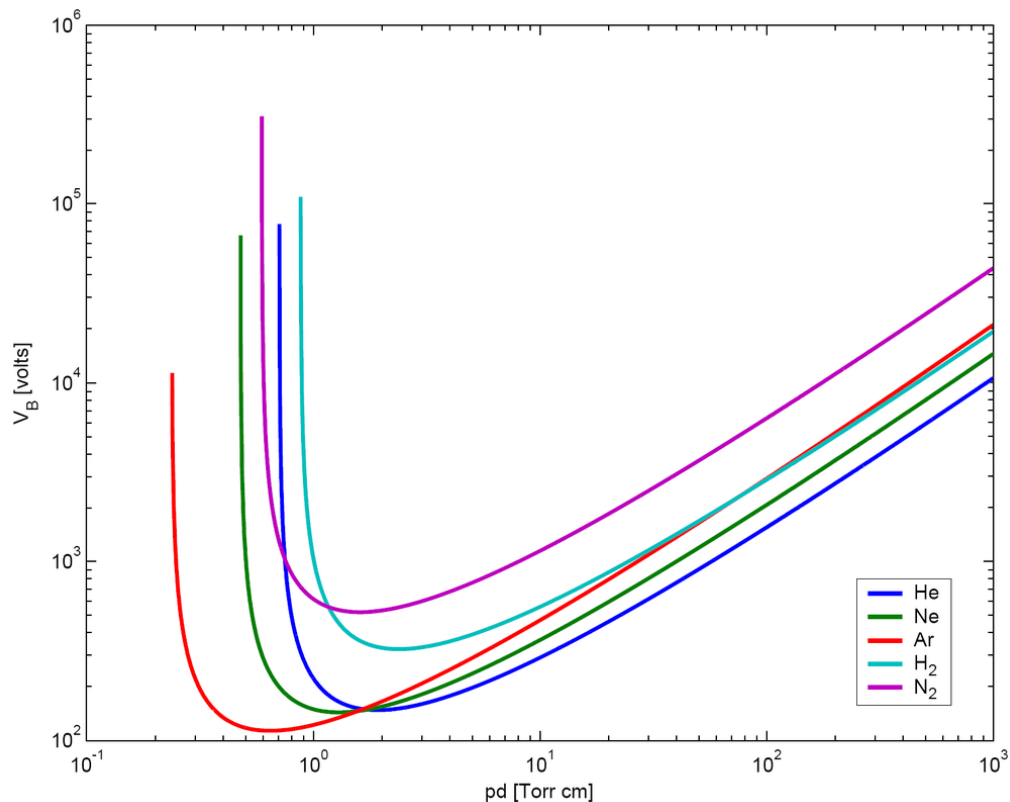
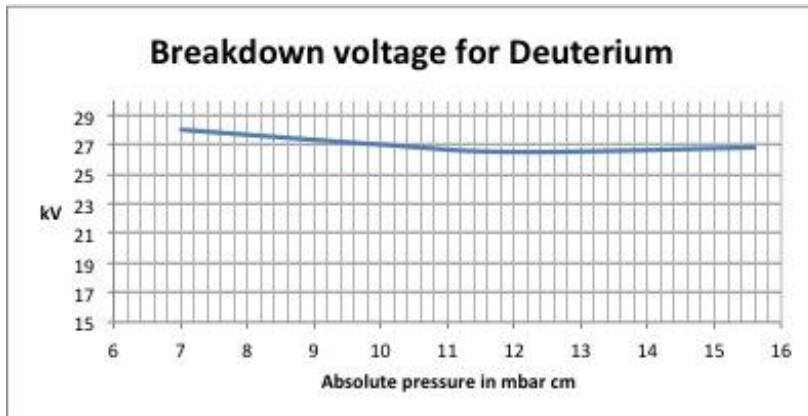


Image 5: Paschen curves obtained for helium, neon, argon, hydrogen and nitrogen, using the expression for the breakdown voltage as a function of the parameters A,B that interpolate the first Townsend coefficient.

The breakdown voltages in the curve from image 5 have been drawn for gases that are not of interest for use as fuel in a Fusor. We have collected some data for Deuterium and plotted a graph as shown in image 6:



Breakdown voltage for Deuterium.

The graph of image 6 shows that for the high voltage region of interest (ROI) for a Fusor, 26 to 30 kV, the voltage breakdown for Deuterium occurs at absolute pressures ranging from 7 to 16 mbar cm.

It is difficult to draw conclusions from these data because not much has been published on the relationships between voltage, current and pressure in IEC devices. The graphs relating to Paschen's Law are based on measurements with flat plate electrodes but in an IEC reactor the cathode is spherical and hollow. It is, however, known that the geometry of the electrodes have a significant effect on the results (streamer discharge concept).

The Townsend breakdown mechanism is only valid for slowly rising voltages and low pressures. The resulting discharge is diffuse of shape. At fast rising voltages and when the product between pressure and anode/cathode distance is sufficiently large, a distortion of the electrical field may occur yielding a filamentary channel (or streamer) bridging the anode/cathode gap.

When we summarize our findings from these first two chapters it becomes clear that:

- Fusion takes place only when the average kinetic energy of nuclei is sufficiently raised (to overcome the Coulomb barrier) by accelerating their speed and increasing the density of nuclei in the center of the IEC reactor;
- This is achieved by creating a potential well between electrodes, i.e. a sufficiently high voltage is created between cathode and anode;
- A vacuum inside the IEC reactor is required to maintain the high voltage potential field which 'powers' the fusion reaction, to eliminate contamination of the fusion process with unwanted and unsuitable nuclei, to prevent heat damage to the fusion reactor and -most important of all- to enable formation of plasma;
- A suitable 'fuel' will be required that gets ionized and creates a plasma; nuclei (ions) of the fuel are accelerated and may fuse;

- The conditions of pressure, high voltage between electrodes and electrodes distance should be such that voltage breakdown in the plasma/electron cloud will be prevented, i.e. electric discharges between the electrodes are unwanted.

9.3.3.6 Choice of Energy

The fusion process in the Fusor is thermonuclear fusion, or hot fusion, not to be confused with cold fusion processes or low energy nuclear fusion (LENR).

In our Fusor we apply a voltage of (e.g.) 25 kV and an electrostatically accelerated Deuteron (an ion with a charge +1) which passes through the grid has gained a kinetic energy of 25,000 electronvolts (25 keV).

When multiplied with 11,604 to obtain Kelvin we find that in the heart of our Fusor a temperature exists of more than 290 million degrees Kelvin.

Somewhat surprisingly it is not heat that is the key to achieve fusion but it is velocity caused by electrostatic acceleration. From the Maxwell–Boltzmann distribution (or Maxwell speed distribution) for particle speeds in idealized gases the following equation for velocity v of a particle was developed:

Equation I

$$v=(2KT/m)^{1/2}$$

Where:

v is velocity of a particle

K is the Boltzmann constant= 1.4×10^{-23} JK⁻¹

m is the mass in kg

T is the temperature in K.

The equation shows that a direct relationship exists for the velocity of a particle and temperature and also that heat is a means to achieve speed (and vice versa as shown in our 25 keV Fusor example above).

It appears that this is a very crucial point because large governmental institutions are struggling for decades now to achieve fusion by heating gas with conventional means in tokamaks (e.g. ITER) and high power lasers (e.g. HiPER), whereas the answer may be found in using a more simple and direct way to obtain high velocity by using electrostatic acceleration.

At fusion energies (> 10 keV) the fusion reactants exist in a plasma state because the ionization energy for Deuterium of 15.47 eV is highly exceeded. The plasma in a Fusor turns into a Poisor (a plasma focus, plasmoid) when a mean free path for particles (ions) has been reached comparable to the vacuum chamber radius. In general, extending the mean free path of particles is achieved by lowering the pressure in the vacuum chamber as can be derived from equation II, the equation for calculating the mean free path of a particle:

$$\ell = \frac{k_B T}{\sqrt{2} \pi d^2 p}$$

where:

ℓ is the mean free part for particles k_B is the Boltzmann constant in Joule per Kelvin ($1.3806488(13) \times 10^{-23}$ JK⁻¹)

T is the temperature in Kelvin

d is the diameter of gas particles in meters

p is the pressure in Pascal

some mean free path values for air at room temperature at different pressures, which have been listed in table 1:

Vacuum range	Pressure in mbar	Molecules per cm ³	Mean free path
Ambient pressure	1013	2.7×10^{19}	68 nm
Low vacuum	300 - 1	$10^{19} - 10^{16}$	0.1 - 100 μ m
Medium vacuum	$1 - 10^{-3}$	$10^{16} - 10^{13}$	0.1 - 100 mm
High vacuum	$10^{-3} - 10^{-7}$	$10^{13} - 10^9$	10 cm - 1 km
Ultra high vacuum	$10^{-7} - 10^{-12}$	$10^9 - 10^4$	1 km - 10^5 km
Extremely high vacuum	$> 10^{-12}$	$< 10^4$	$> 10^5$ km

When the mean free path of a particle in a sphere shaped Fusor exceeds approximately three radii, the particle will start recirculation and when the pressure is further lowered (i.e. the mean free path further enlarged) the particle will start to oscillate back and forth through the plasma focus until the mean free path has been reached or until a (negatively charged) cathode wire of the grid is met and the (positively charged) particle ceases to exist .

the recirculation of ions occurs when the mean free path of the ions exceed the diameter of the vacuum chamber; after all the particles cannot escape from the vacuum chamber to accomplish their mean free path. Therefore, particles which have passed the plasma focus will decelerate, reverse their direction and accelerate again towards the plasma focus, taking another opportunity to collide and fuse or to end their existence as an ion when caught by a grid wire. In a Farnsworth-Hirsch Fusor an ion generally makes about five recirculation passes before it ends against the grid. In an ideal situation a grid wire should be infinitely thin, which is impossible, and the concept of grid transparency has been developed for constructing a grid with the best possible open structure for the Fusor.

The general rule of five recirculation passes proved to be incorrect when the grid is geometrically good designed and accurately placed in the vacuum chamber. Very precisely adjusted Fusors may show the George Miley effect, where the plasma turns into the "star" mode. Apparently this is a phenomenon where ions seem to avoid hitting the grid and will travel through void places in the grid and form star-like rays, which named this plasma mode.

The equation that defines fusion rate for a plasma with a constant particle density is:

$$\text{Equation III} \quad f = n_1 n_2 \sigma v$$

or, when taking into account that particle velocity in general has a Maxwellian distribution it makes sense to average σv over the integral region of the relative velocity:

$$\text{Equation IV} \quad f = n_1 n_2 \langle \sigma v \rangle$$

where:

f is the fusion rate or reaction rate (fusions per volume per time, i.e. per cm³ per second)

n_1 and n_2 are the densities of two colliding ion species in particles per cm³

σ (sigma) is the reaction cross section in *barns*

v is the relative particle velocity in cm/sec

It should be noted here that nowhere in the equation (II or III) temperature appears because the fusion process deals only with densities, dimensions and velocity.

The term (σv) is called the reactivity, the appropriate average of the fusion cross section σ over the relative velocities v , expressed in units of cm^3/sec . A plot of reaction rates versus kinetic temperature is shown in image 10, similar to images 8 and 9. The plot clearly shows that D-D fusion rates increase with increasing energies (temperatures): at 10 keV just over $10^{-24} \text{ m}^3/\text{sec}$ and at 30 keV approximately $10^{-23} \text{ m}^3/\text{sec}$.

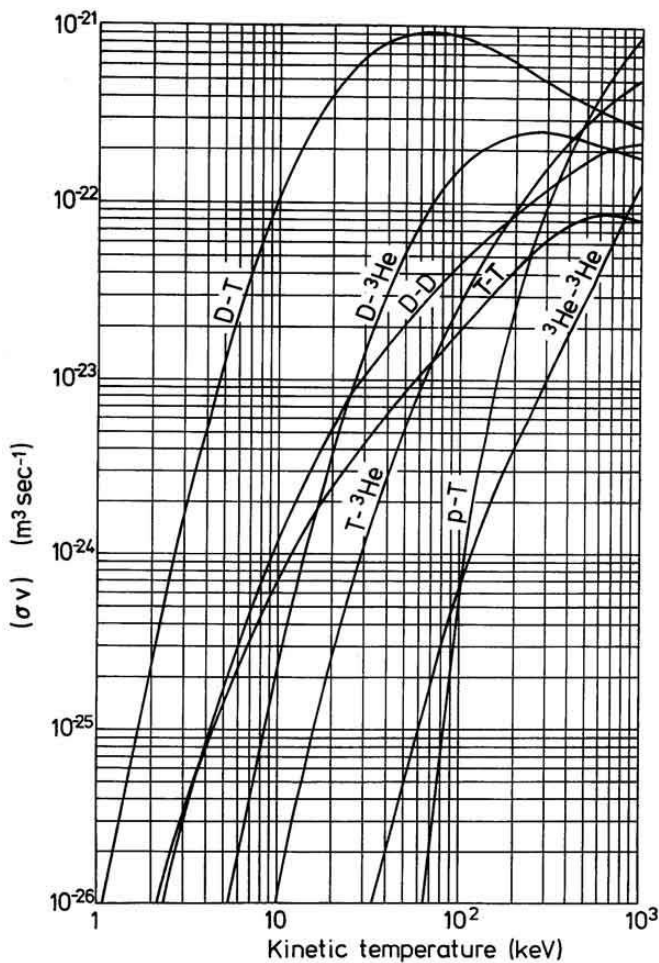


Image 10: Fusion rates for some fusion reactions

The reaction cross section σ is a measure of the probability of a fusion reaction as the function of the relative velocity of two reactant nuclei. The cross section is expressed in *barns*, a surface unit with the approximate dimensions of the nucleus of an atom, where 1 *barn* is 10^{-24} cm^2 .

When nuclei are reacting with itself (as in our D-D fusion reaction), the product $n_1 n_2$ becomes $\frac{1}{2}n^2$:

Equation V

$$f = \frac{1}{2}n^2(\sigma v)$$

At first sight equation V seems quite logical apart maybe from the factor $\frac{1}{2}$, which of course obviously is explained by the fact that when nuclei react with itself the given density of nuclei (i.e. number of particles per unit volume) is reduced to half that nucleus density or with other words, the factor $\frac{1}{2}$ has been introduced into the formula to avoid counting the same interaction twice.

The value v may require frame-shifting assuming that one particle is moving and the other is stationary because that is how cross sections were measured in experiments with linear accelerators ([reference 23](#)). Fusors are ion accelerators but certainly not linear accelerators with a stationary target and this has nasty consequences for finding a mathematical model as shown in the next paragraph.

Equation V should enable to calculate the fusion rate of a Fusor but unfortunately fusion reactions in a Fusor are far from predictable and are difficult to catch in mathematical equations. The reason for this complexity is that particles in a Fusor do not have a fixed kinetic energy and the paths they follow are not straight beams. Particles may be orbiting in circular or elliptical orbits. The kinetic energy of a particle in a Fusor depends on its location in the Fusor, except for those particles orbiting in circular paths, etc. Furthermore, fusion reactions in a Fusor do not occur only in the plasma focus inside the grid but also just outside the grid and possibly also with non-ionized Deuterium gas near the walls of the Fusor.

Any attempt to calculate a reaction rate in a Fusor is therefore a simplistic approximation of real values for which different calculation models are available for such an approximation, usually based on different theoretical approaches. One of those methods is shown in the next paragraphs.

The velocity v of the colliding nucleus is non-relativistic and can be calculated with the classical formula from equation I, which is mentioned here as:

$$\text{Equation VI} \quad v = \sqrt{2 \frac{E_k}{m}}$$

(derived from equation I: kinetic energy = $\frac{1}{2} mv^2$) in which

v = particle velocity in meters per second (m/s)

E_k = kinetic energy converted from eV to joules (J)

m = mass of the nucleus in kg

The cross section for D-D reactions at 10 keV ranges from 2E-4 barn (center collisions) to 1E-3 barn (head-on collisions). A (one) barn is 1E-28 m² or 1E-24 cm² as mentioned earlier.

Knowing v (converted from m/s to cm/s) and the cross section σ (in cm²) we can calculate the reactivity (σv) expressed in cm³/s.

The remaining term of the equation to be calculated is the density of particles (nuclei) per cm³.

A simplified method is by assuming that all or at least the majority of the current through the grid is due to ion flow with a charge of +1. We know that one Ampère equals one Coulomb per second, or 6.24E18 charges per second. We need to compensate for losses caused by the grid by multiplying the charges with the "ion recirculation factor". Assuming that we have a grid transparency (see [below](#)) of 98% then 2% of the ions will be blocked by the grid. This means that an ion will be neutralized by the grid one pass in fifty and therefore the ion recirculation factor would be 50. Another approximation of the recirculation factor can be found by calculating the mean free path of the ions [as shown below](#).

The result of multiplying the charges with the ion recirculation factor yields an estimation of the number of ions passing the grid per second.

Because we know the diameter of the grid and because we have calculated the velocity of the ions, we can calculate now the the amount of time that an ion is actually in the grid.

The overall density in the grid can then be calculated from the time that an ion is in the grid and the amount of ions that pass per second through the grid. The results is expressed as particles per cm³. The calculation rules out time because we multiply

Duration in seconds (t) × number per second (n/t) × volume (cm³) = n/cm³

For a more accurate estimation of the density it is advised to break up the grid sphere volume in two or more concentric spheres (or shells) with in the central region a sphere with the (estimated) dimensions of the Poisor (the visible bright spot), where the ion density is progressively higher. For those who have forgotten their geometry equations to calculate the volume of a sphere:

$$V_s = \frac{4}{3} \pi r^3$$

When the radius of the grid sphere is r_g and the radius of the Poisor sphere is r_p we find the following equations for calculation of the volumes of the shells:

Equation (Poisor sphere)	VII	$V_p = \frac{4}{3} \pi r_p^3$
-----------------------------	-----	-------------------------------

Equation (Grid shell)	VIII	$V_g = \frac{4}{3} \pi (r_g^3 - r_p^3)$
--------------------------	------	---

Next is to calculate for each shell the fusion rate as the product of half the particle density squared and the sigma v values. For the inner shell use the cross section value for the center collisions; for the outer shell(s) use the cross section value for the head-on collisions.

Summarize the fusion rates for each shell.

Example:

for a Fusor operates at 10 kV at a current of 10 mA; it has a grid diameter of 6 cm and the Poisor has an estimated diameter of 4 cm; the cross sections σ for Deuterium at 10 kV are 2E-4 barn for center collisions and 1E-3 barn for head-on collisions. The mass of a deuteron is 3.43583719E-27 kg and the conversion factor from eV to J is 1.60217657E-19. The ion recirculation factor based upon the mean free path is calculated in the next paragraph and found to be 41. This well in line with the rule of thumb calculation based upon the grid transparency which yields 50 recirculations.

An estimated calculation of the recirculation factor was done by applying equation II with a deuteron radius of 2.1413E-15 m, a Fusor pressure of 1E-5 Torr (equals 1.333223684E-3 Pascal), a plasma temperature of 10 keV for which 1eV equals 11604.45 K yielding a plasma temperature of 1.16E8 K, a Boltzmann constant of 1.3806488(13)×10⁻²³ JK⁻¹. With these parameters equation II yields

a mean free path length of 8.1719 m, which results in 41 recirculations in a Fusor with a diameter of 20 cm (mean free path length divided by diameter is approximate number of passes or recirculations).

In this system the velocity v of the colliding ions is the square root ($2 \times ((41 \times 1.60217657E-19)/3.43583719E-27)) = 61836.633572$ m/s or 6183663.3572 cm/s.

The factor σv for center collisions is 6183663.3572 cm/s $\times 2E-4$ barn $\times 1E-24$ cm² = $1.2367E-21$ cm³/s and for head on collisions 6183663.3572 cm/s $\times 1E-3$ barn $\times 1E-24$ cm² = $6.1837E-21$ cm³/s.

The amount of time that an ion is in the grid is diameter grid divided by the velocity or 6 cm $\div 6183663.3572$ cm/s = $9.7030E-7$ s.

The number of ions per second equals 10 mA for which 1 A $6.24E18$ charges per second times the ion recirculation factor or $1E-3 \times 6.24E18 \times 41 = 2.558E19$ ions/s.

The overall density in the grid is amount of time that the ion is in the grid times number of ions per second or $9.7030E-7$ s $\times 2.558E19$ ions/s \times volume = $2.4820E13$ ions in the total volume of the grid.

For the poison shell we find a volume of ($r = 2$ cm) $4/3 \times \pi \times 2^3 = 33.5$ cm³. The ion density in this shell is $2.4820E13 \div 33.5 = 7.41E11$ ions/cm³.

The fusion rate for the poison shell equals $1/2 \times n^2 \times (\sigma v)$ is $1/2 \times (7.41E11)^2$ n/cm³ $\times 6.1837E-21$ cm³/s = 1698 reactions per second.

Similarly, for the grid shell we find a volume of ($r = 3$ cm) $4/3 \times \pi \times (3^3 - 2^3) = 79.6$ cm³. The ion density in this shell is $2.4820E13 \div 79.6 = 3.27E12$ ions/cm³.

The fusion rate for the grid shell equals $1/2 \times n^2 \times (\sigma v)$ is $1/2 \times (3.27E12)^2$ n/cm³ $\times 1.2367E-21$ cm³/s = 6595 reactions per second.

The total fusion rate in the fusor (grid) equals $1698 + 6595 = 8293$ reactions per second.

Above mentioned method(s) for calculating the fusion rate are very rough estimations and a total reaction rate of just over 8000 reactions per second is considered quite sufficient for detection by a neutron detector. A large number of reactions is required here because the number of reactions should exceed the detection limit of the detector sufficiently but it should also be noted that the neutrons from the fusion reactions are randomly emitting from the Fusor in all directions and our detector is just on one fixed spot at a distance from the Fusor. Therefore the majority of these neutrons will not be "seen" by the detector.

From the calculations it should be clear that a higher voltage (is more velocity) and a higher current (is more ions) will increase the reaction rate.

9.3.3.7 Radiation Hazards

Röntgen (γ) Radiation

Operating a Fusor means applying a high voltage to a cathode in a medium or high vacuum environment, which produces thermionically emitted electrons directed outward from the cathode and by colliding with the vacuum envelope generate Bremsstrahlung röntgen radiation. Because we

use Deuterium as "fuel", which becomes ionized in Deuterons with a single positive charge, the γ -energy of the röntgen radiation in eV is directly related to the potential differential applied. For example a potential difference of 30 kV emits röntgen radiation with an energy up to 30 keV.

Generally, it is said that up to a voltage of 25 - 30 kV no röntgen radiation of importance will pass through the (metal) walls of the vacuum chamber. For information about calculating the amount of röntgen radiation that will penetrate the vacuum chamber wall and we shall use that info for the following calculation.

The mass attenuation coefficient for steel is at 30 keV 8.2 cm²/g and at 10 keV 170 cm²/g.

De Beer-Lambert's Law of exponential attenuation is used for calculation of the penetrating flux:

$$\text{Equation IX} \quad I(x) = e^{(-mx)}$$

where

m = mass attenuation coefficient

x = thickness expressed as mass per unit area (g/cm²)

The mass density for steel is $\rho_m = 8.0 \text{ g/cm}^3$

For a vacuum chamber with a wall thickness of 2 mm: $x = \rho_m \times t$, where t is the wall thickness,

$$x = 8.0 \text{ g/cm}^3 \times 0.2 \text{ cm} = 1.6 \text{ g/cm}^2$$

For 30 keV röntgen radiation we find: $\exp(-8.2 \times 1.6) = 2\text{E-6}$ or 0.0002% of the radiation will penetrate the vacuum chamber walls, which is indeed of no importance. At 10 kV potential difference or 10 keV röntgen radiation energy we will find even considerably less: $7.4 \times \text{E-117}\%$!

For calculating what this means as a biological radiation dose we assume that our Fusor runs at 30 keV and 10 mA or an energy of 300 Watt = 300 J/s. suppose that we have no losses in the system and the röntgen radiation (Bremsstrahlung) is generated by two entities:

- electrons emitted from the grid
- ions colliding in the plasma focus

Which absorb the 300 J/s kinetic energy.

For a Fusor 30kV, each Deuterium has one single charged ion (30 keV) and one electron (30 keV) and therefore the kinetic energy for each is 50% of 300 J/s = 150 J/s. The efficiency for generating röntgen radiation is about 1E-9 and thus we have $150 \text{ J/s} \times \text{E-9} = 1.5\text{E-7} \text{ J/s}$ keV X-rays emitting from the plasma focus, of which 0.0002% exits the vacuum chamber = $3\text{E-13} \text{ J/s}$.

For an average body mass of 70 kg (see [method 1](#) under Neutron Radiation below) we find an absorbed energy dose of $3\text{E-13} \text{ J/s} \div 70 \text{ kg} = 4.3\text{E-15} \text{ J/kg/s}$ or $1.5\text{E-11} \text{ J/kg/h}$. This equals (conversion: 1 J/kg = 1 Gray) $1.5\text{E-5} \mu\text{Gy/h}$ which converts with a weighting factor of 1 for gamma's to an equivalent tissue dose of $1.5\text{E-5} \mu\text{Sv/h}$. Compared to the annual limit for professional workers of $20\mu\text{Sv/h}$ (>250 h/y) this is indeed neglectable.

Neutron Radiation

It is difficult to measure accurately the total amount of neutrons produced by the fusion reaction as the efficiency for the neutron detector should be known, i.e. taking into account the distance from the detector to the core of the reactor and the factor describing the amount of neutrons hitting the detector in relation to the total amount of neutrons emitted randomly in all directions, etc. Therefore we propose to tackle the problem of calculating the radiation dose from neutrons by two different ways.

Method 1

One method is to use the maximum allowable limit for radiation exposure and to calculate the corresponding maximum production rate of reactions in the Fusor. Knowing that maximum production rate enables to calculate more or less up to what high voltage and current the Fusor can safely be operated.

As a starting point we take the EU dose limit for professional nuclear workers, which is an absorbed dose of 20 $\mu\text{Sv/h}$ (< 250 h/year). To compensate for stochastic radiation effects, an energy dependent weighting factor W_r connects the absorbed dose in Gray (Gy to the equivalent tissue dose in Sievert (Sv).

For neutrons the following equations as a continuous function of the neutron energy:

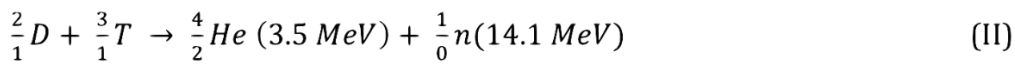
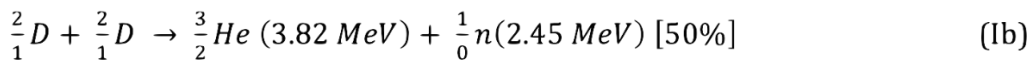
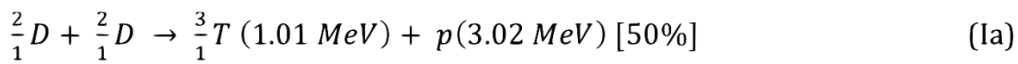
$$w_R = \begin{cases} 2.5 + 18.2e^{-|\ln(E_n)|^2/6}, & E_n < 1 \text{ MeV} \\ 5.0 + 17.0e^{-|\ln(2E_n)|^2/6}, & 1 \text{ MeV} \leq E_n \leq 50 \text{ MeV} \\ 2.5 + 3.25e^{-|\ln(0.04E_n)|^2/6}, & E_n > 50 \text{ MeV} \end{cases}$$

When we substitute the neutron energies of respectively 2.45 MeV and 14.1 MeV in the appropriate equation (for the relevant energy) we find respectively $W_{2.45} = 12.5$ and $W_{14.1} = 7.7$. The sum of both weighting factors is about 20.

Therefore the Fusor is allowed to produce maximally an absorbed dose of 1 $\mu\text{Gy/h}$ and this is equivalent with an energy deposition of E-6 J/kg/h. The average body mass of an adult in Europe is just over 70 kg and when we take a body mass of 70 kg as the norm we find that a Fusor energy output of 7E-5 J/h or 1.9E-8 J/s should be considered as acceptable.

Neutrons emitted from the Fusor have an energy of respectively 2.45 MeV and 14.1 MeV, which equals respectively 3.93E-13 J and 2.26E-12 J. We divide the maximum allowable fusor output of 1.9E-8 J/s by the neutrons energy and find respectively a maximum allowable fusion rate (# = number of fusions or reactions) of 48500 #/s and 8400 #/s.

The outcome may be confusing because we find for one neutron energy a "safe" fusion rate of almost 50,000 fusions per second and for the other neutron energy a "safe" fusion rate of almost 8,500 fusions per second. We should however realize ourselves that both reactions possibly may occur simultaneously. The equations Ia, Ib and II show the D-D reactions that may occur in the Fusor:



The probability that reactions Ia and Ib occur is 50% for each, therefore the emission of neutrons with an energy of 2.45 MeV is realistic. The Tritium formed in reaction Ia will may further react with Deuterons present in the Fusor because the minimum energy required for the D-T reaction is lower than for the D-D reaction and therefore this reaction might also occur. However, the assumption that reactions (Ia,II) and (Ib) occur equally is taken here as a worst case assumption. Worst case because neutrons emitted with an energy of 14.1 MeV are more harmful because of depositing more kinetic energy in tissue. In reality we probably may expect in majority to produce neutrons with an energy of 2.45 MeV because it is expected that most of the formed Tritium decays before being burnt-up by the D-T reaction.

With respect to the biological radiation burden the total amount of allowable fusions per time unit is therefore worst case $48,500/s + 8,400/s = \text{approx. } 57,000/s$.

This calculation is valid for an exposure to neutrons directly at the source, i.e. like the Fusor operator was present inside the vacuum chamber during exposure to neutrons produced. Distance reduces the effect of exposure to neutrons but despite such a reduction in neutron flux caused by distance it is not good for your health to be exposed to neutrons. Water contained in the body will moderate (slow down) the neutrons but once an atomic nucleus inside the body is hit, a reaction will occur which produces radioisotopes and reactive free radicals, which stay inside your body until decayed. However, prior to full decay they may be harmful to your health.

Method 2

Another method can be used when the neutron flux form the Fusor is known by converting the neutron flux rate to neutron dose rate for which the calculation is

$$\text{Dose rate (rem/h)} = \text{conversion factor (rem/h/ [neut/cm}^2\text{s}^{-1}\text{])} \times \text{neutron flux (neutrons per cm}^2\text{/s)}$$

The conversion factors

for converting from the rem unit to the currently used unit of Gray: $1 \text{ rem/h} = 0.01 \text{ Gy/h} = 10 \text{ mGy/h}$.

For our D-D reactions yielding neutrons with energies of 2.45 MeV and 14.1 MeV we find respectively conversion factors of about $1.25\text{E-}4$ and $2.08\text{E-}4$. The same argument about a worst case calculation is equally valid here as in method 1.

When measured with the neutron detector and calculated for the distance from the detector to the Fusor operator we find an (assumed) neutron flux of $1000 \text{ neutrons/cm}^2\text{/s}$ at operator level. Because the neutron detector is inside a moderator to slow down fast neutrons to thermic neutrons, which are counted by our detector, our neutron flux consists of (assumed) 50% neutrons with an energy of 2.45 MeV and 50% neutrons with an energy of 14.2 MeV.

IECF (Inertial Electrostatic Confinement Fusion)

The dose rate for 2.45 MeV neutrons is calculated as dose rate (mGy/h) = 1.25×10^{-4} (conversion factor) $\times 500$ (50% of neutron flux) $\times 0.01$ (from mrem/h to mGy/h = 0.00104 mGy/h = 1.04 μ Gy/h).

The dose rate for 14.2 MeV neutrons is calculated as dose rate (mGy/h) = 2.08×10^{-4} (conversion factor) $\times 500$ (50% of neutron flux) $\times 0.01$ (from mrem/h to mGy/h = 0.000073 mGy/h = 0.073 μ Gy/h).

The weighting factors for neutrons in order to obtain an equivalent dose in Sv is mentioned before in method 1. By applying the weighting factors $W_{2.45}$ and $W_{14.1}$ the total equivalent neutron dose rate is $(0.625 \times 12.5) + (1.04 \times 7.7) = 15.8 \mu\text{Sv/h}$.

This equivalent dose is at a safe level, i.e. below the allowable limit for professional workers of $20 \mu\text{Sv/h}$ (>250 h/y).

9.3.4 Electrical System

9.3.4.1 High voltage Power supply

The high voltage power supply needed is 35Kv at up to 5 mA. The system is divided to four main Phases: the power supply, ZVS Driver, fly back transformer, and the Voltage tripler.

General System Diagram

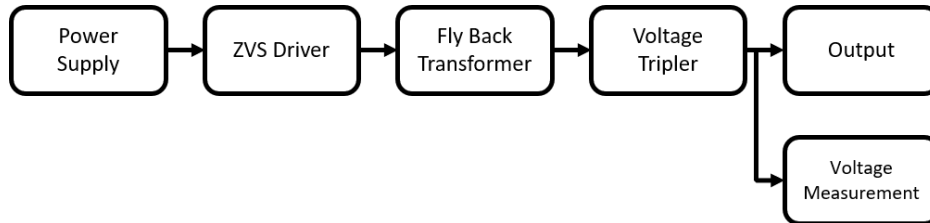


Figure 9-1. High Level High Voltage Power Supply Diagram

To obtain a power 35kV at up to 5 mA at the output. the normal power, as shown is 220 Volts with alternating current (AC), should go through mutli-diverse phases. phase 1, the current will be converted from AC or Alternating current (where it changes the direction periodically), to DC or direct current (where it only flows in one direction). In addition to ensure the needed power for the next phase. Phase 2, the DC power is an input for a zero-voltage switching driver (ZVS) which is a self-oscillator (push-pull oscillator). The ZVS driver provide a high frequency (KHz) oscillator for the fly back transformer in the phase 3. Phase 4 is a volatge tripler, that multiply the voltage through utilizing cockroft-waltan voltage multipler stages. All theses mentioned above is illustrated in figure 3-1 above.

Therefore, There are 3 kind of systems that can be adopted:

Detailed System 1 diagram

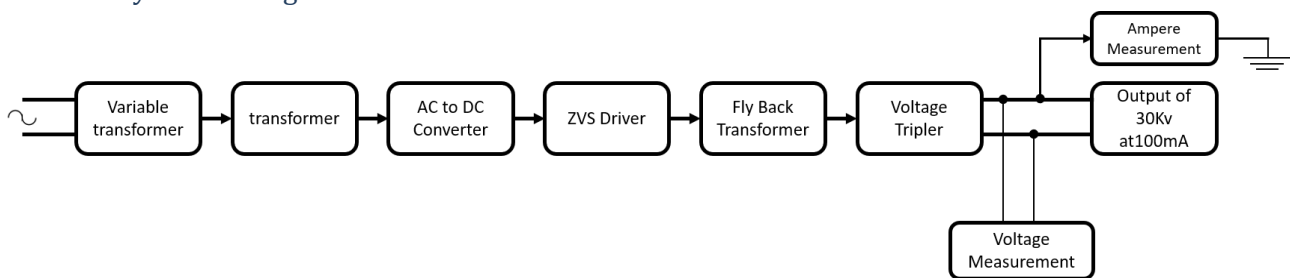


Figure 9-2. Detailed system 1 diagram

Starting from the left, The variable transformer is for controlling the intensity of plasma inside the vacuum chamber. Then, a step up transformer is needed, before converting the power from AC to DC that is required as an input for the zero voltage switch driver (ZVS). After that, a fly back transformer and voltage tripler generats arround 30 Kv at 100 mA from the magnetic feild coming from ZVS driver. Finally, there are the voltage, and current circuit measurement to measure the arrived voltage and current to the vacuum chamber (connected to the output).

Detailed System 2 diagram

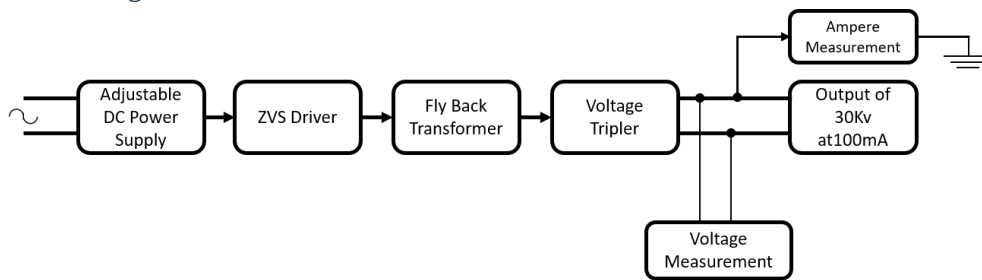


Figure 9-3. detailed system diagram 2

In this system, the power needed for the ZVS Driver is fed by a custom adjustable DC Power Supply.

Detailed System 3 Diagram

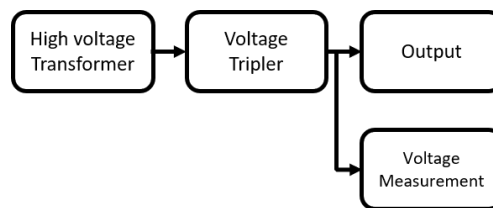


Figure 9-4. Detailed system diagram 3

In this system, a high voltage transformer of 12KV at 30 mA will feed a voltage Tripler circuit, in order to step up the voltage at the output. Note that the output voltage will depend on the number of stages of voltage Tripler as well be mentioned later. This method gives a fix amount of voltage. In other word, it cannot adjust the voltage in order to optimize the voltage according to fusor sensor and measurement.

Detailed System 4 Diagram:

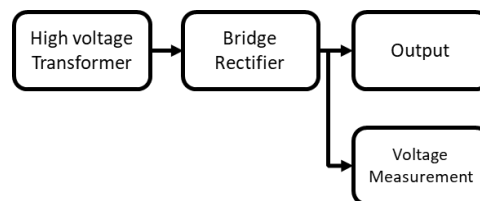
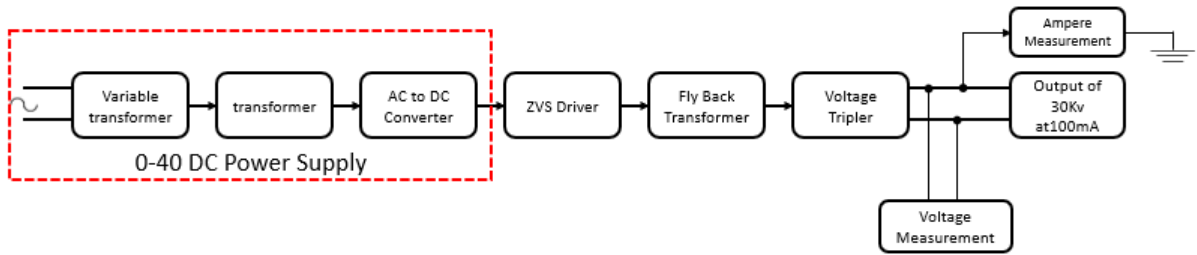


Figure 9-5. detailed System Diagram 4

Similar to the last method, but in order to keep the current at 30 mA, the voltage Tripler will be replaced by a bridge rectifier, just for converting the Alternative current to a Direct Current. This method gives a fix amount of voltage. In other word, it cannot adjust the voltage in order to optimize the voltage according to fusor sensor and measurement. Therefore, the output will be fed by a power of ~12kv at 30mA.

The High voltage power supply

The power supply will be composed to some step. The first step is presented as shoun figure below.



System 1 DC Power Supply

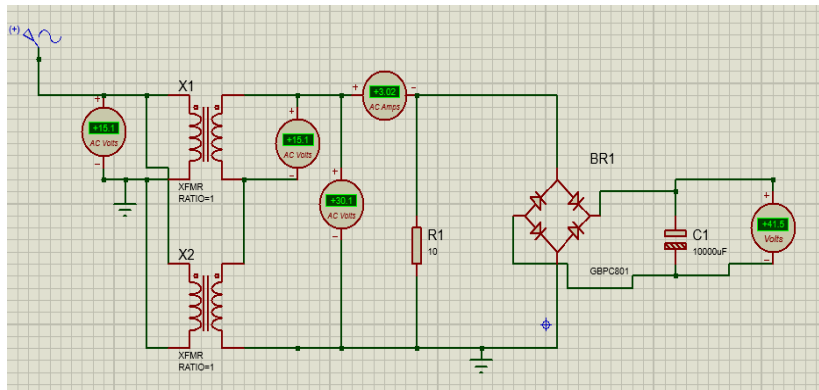


Figure 9-6. Step1 circuit simulation

As shown above, a Ac power source of 15 VAC feeds two transformer of ratio equal to 1, for insulation and safety reasons. Then, the two transformer provides a power of 30 VAC (the transformer are connected in series). After that, a Ac to DC converter (rectifier) transform the AC voltage to DC, with the presence of capacitor of 10,000 uF to eliminate voltage ripple.

System 2 DC Power Supply

This system is as simple as it is, an adjustable DC Power supply of 0 – 30v 20A can be sufficient, such as this one in figure 3-4, below:



Figure 9-7. Adjustable DC Power Supply

System 3 and 4 high voltage Power Supply

...

Zero voltage Switching (ZVS)

The ZVS Driver circuit (Royer converter) is a Royer-type push-pull oscillator with a resonated primary that is implemented with FETs. This type of oscillator can be used to drive the ferrite core of a flyback transformer to generate high voltage. It can also drive a high-current air-core "work" coil for an induction heater.

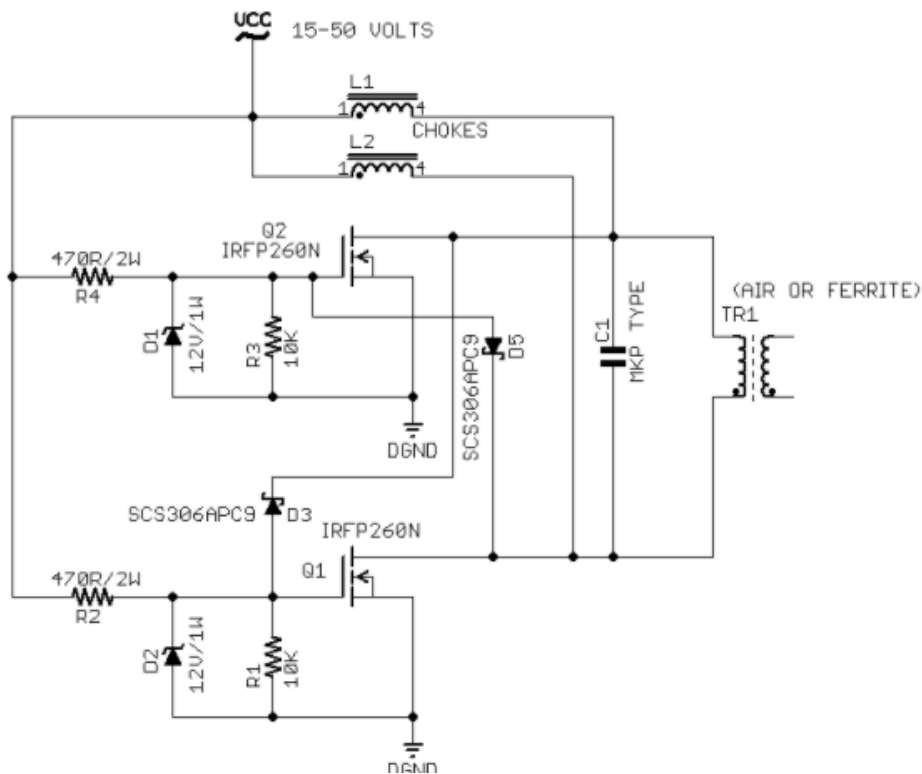


Figure 9-8 Basic ZVS Driver circuit

The ignoring the power supply chokes and resonating capacitor(s), the ZVS circuit is simply a push-pull FET-based oscillator where the drain of each FET is cross-coupled to the gate of the opposite (out of phase) FET. It is worth to mention, that The FET(Field Effect Transistor) is a three-terminal electronic device used to control the flow of current by the voltage applied to its gate terminal.

The operation of this kind of driver for the primary of a transformer is very straightforward and need not be discussed here. The circuit is fed from the power supply through a center-tapped primary coil and a single choke or from two separate chokes connected to the FET drains (as shown in figure 3.2).

Note1: it is not recommended to use a center-tapped coil cause of the ability of "lock-up" if the supply voltage is not applied fast enough to kick it into operation. These phenomena appear when you slowly increase the input voltage. So, in order to avoid it, it much better to apply the input voltage abruptly. You can use a remote-control relay to operate the ZVS circuit.

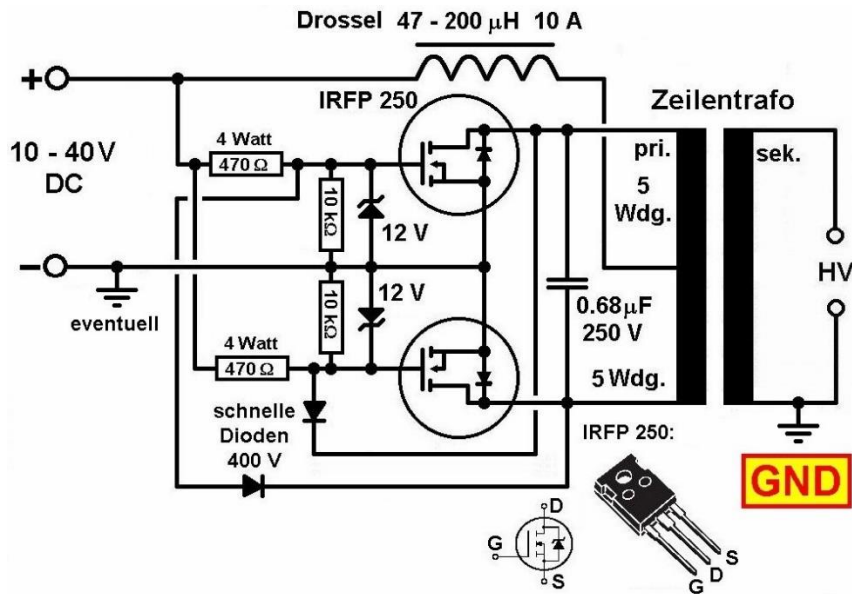
With the two (47uH-200 uH) choke coils (L1, L2) and the resonating capacitance across the primary, the circuit operates as a "Royer" type inverter where the primary is resonated with the capacitance and where the chokes keep the power supply from reducing the resonant action of the primary. These chokes also keep the primary oscillations from feeding back to the power supply.

Zener diodes are connected across the FET gates so that the maximum gate to drain voltage is not exceeded. **NOTE2: Use of a Zener voltage higher than the minimum gate to source turn-on voltage ensures that the FETs are conducting at a high level. Plus, the diode should be a fast diode**

Note 3: the capacitor C1, and the two MOSFET should be cool. Otherwise, the signal will be shifted, until the circuit broke, and the MOSFET will be burned down.

NOTE4: TAKE CARE TO THE GROUND, THE GROUND SHOULD BE CONNECTED WITH THE NEGATIVE OF THE POWER SUPPLY.

ZVS MAZZILLI Circuit



This kind of ZVS driver needs an input voltage abruptly, cause of the high probability of “lock-up” phenomena, aforementioned. the main difference between typical ZVS MAZZILLI Circuit and circuit above are the center-tapped coil, and the larger capacitor between Drain-Drain. In this application this kind of ZVS driver will not work properly. **It is not recommended to use this ZVS MAZZILLI.**

ZVS Simulation

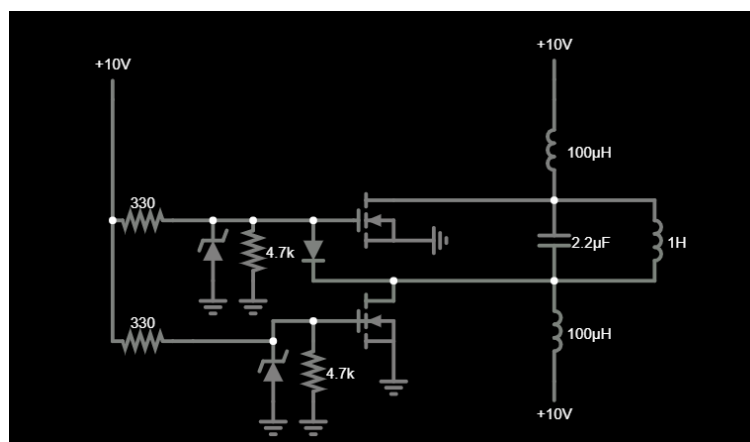


Figure 9-9. ZVS circuit in the stop Mode

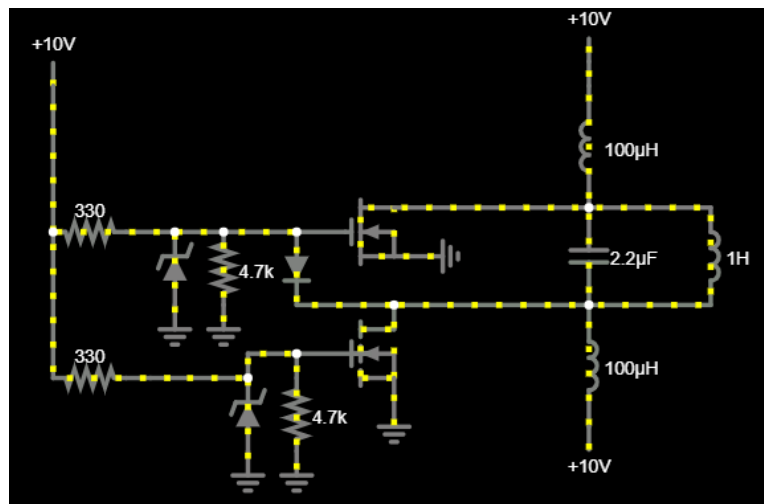


Figure 9-10. ZVS circuit in the RUN Mode

In the figure 3-3 and 3-4 above, a center-Tapped inductor has been avoided and place a simple inductor o 100uH. The capacitor (2.2uF) and inductor (1000mH) is selected via trial and error for a soft sine wave (as shown in the figure)

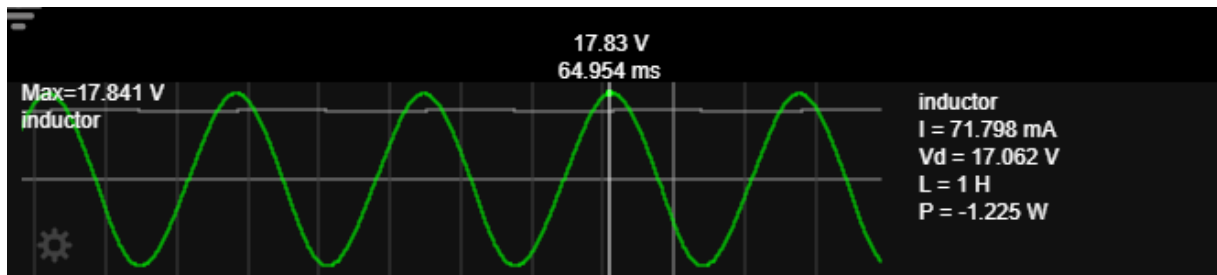


Figure 9-11. AC output Voltage

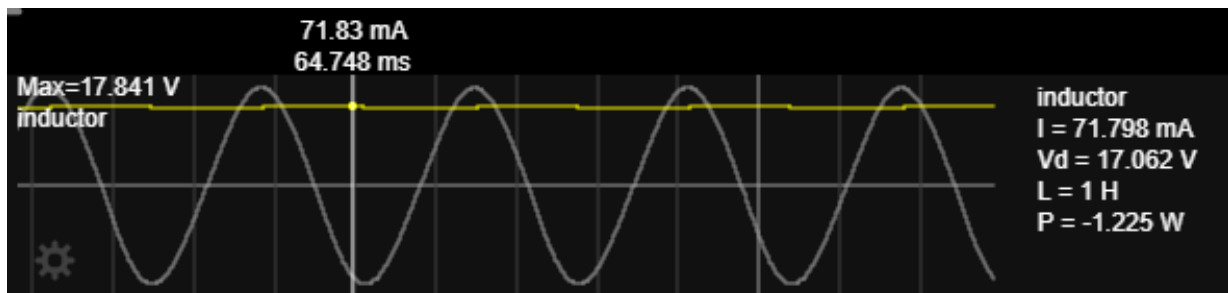


Figure 9-12. Output Current

ZVS with flyback and cockroft-waltan voltage multiplier circuit

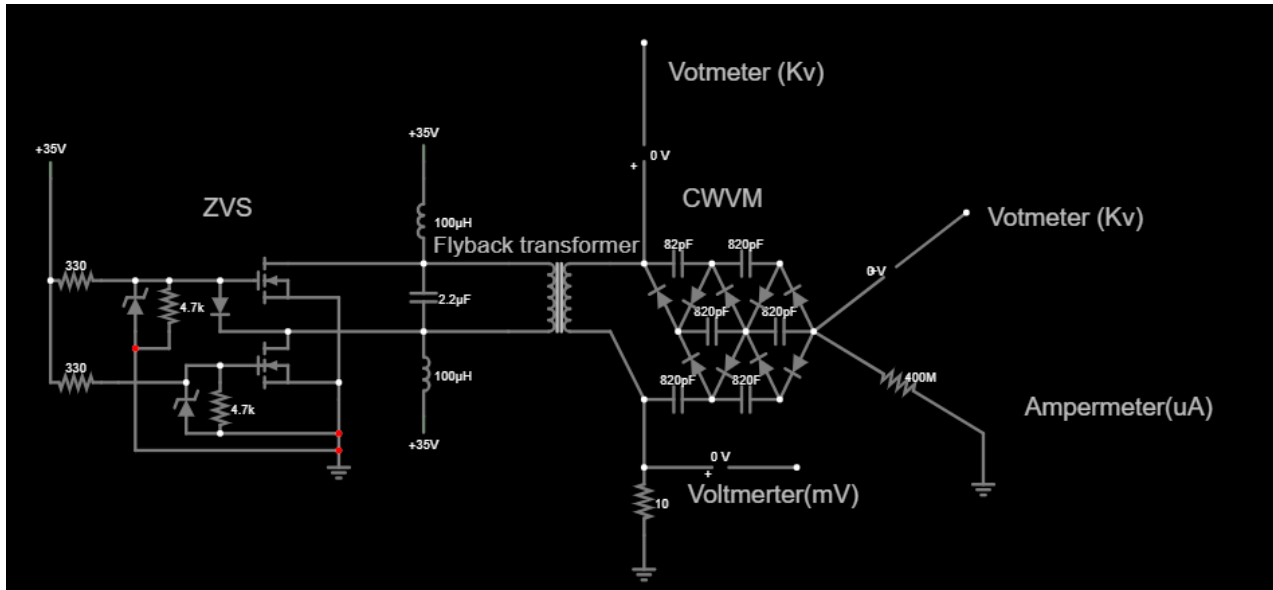


Figure 9-13. ZVS with flyback and voltage Tripler simulation

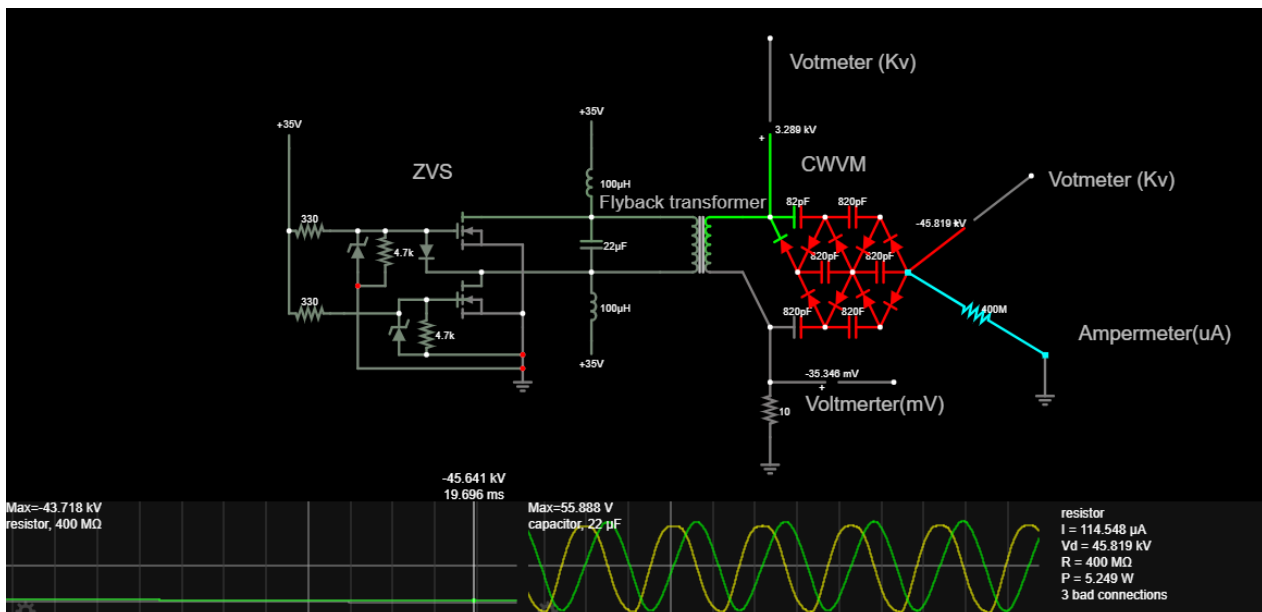


Figure 9-14 Output voltage and current

The output voltage at the end of voltage Tripler is -45Kv at 114.54 uA . With the presence of a soft sign wave in the ZVS self-oscillator.

Equipment

Cathode

The cathode, shown in figure 3.13, consists of 30kV feedthrough with $2.75''$ stainless steel flange (figure 3.14), alumina tube insulating feedthrough stalk (figure 3.15), and the negative hot inner grid of tungsten filament with its base of stainless steel that connect the inner grid with the pin of feedthrough (figure 3.16). The power about -35 kv at $0\sim 5\text{ mA}$ cross the cathode in this application.

Note 1: This feedthrough needs to be rated for the cathode voltage that will be used

Note 2: it is recommended to buy the feedthrough flange, not DIY. The ceramic isolation should be molded on the flange correctly for many reasons such as the isolation, high vacuum, conductivity.

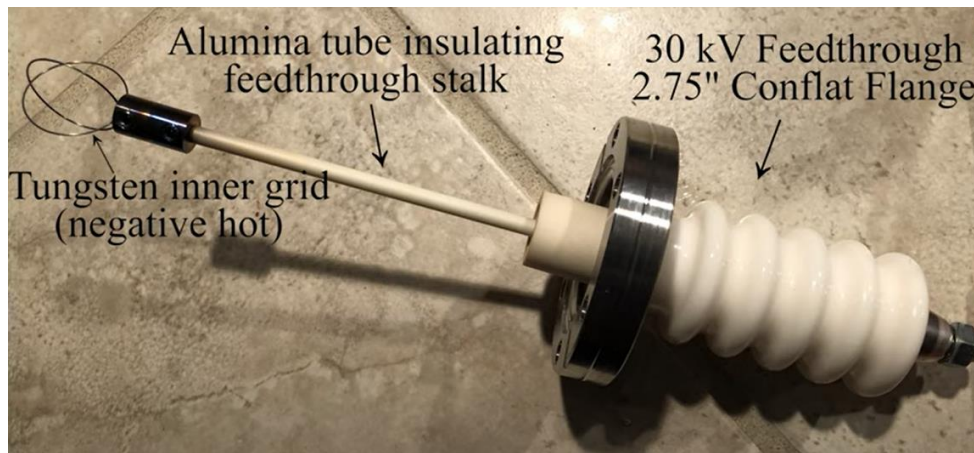


Figure 9-15. Fusor Reactor Cathode



Figure 9-16. feedthrough flange



Figure 9-17. alumina tube insulating feedthrough stalk

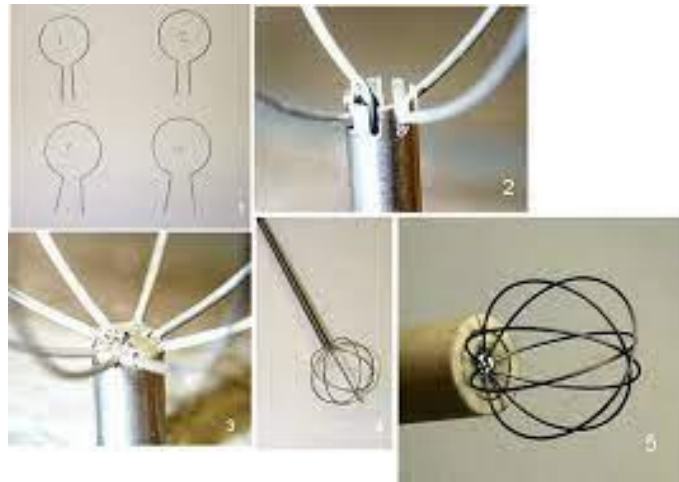


Figure 9-18. Tungsten grid

The cathode inner grid material can be one of the following materials: tungsten, tantalum, Rhenium, molybdenum, Titanium, and stainless steel. But a demo fusor can use stainless steel wire as they are not stressed to the degree encountered in a real fusing fusor. The best suitable for real fusor is tungsten.

According to available material in the local market, a 1.6mm diameter of stainless-steel wire has been used in this project.

The cathode inner grid has been built in the following steps:

Step 1:

Get three stainless steel rods (2 x diameter: 1.6mm, 1 x diameter: 2 mm). the 1.6mm rods are used for the spherical inner grid. This thickness is compatible for the transparency (<92%), as mentioned before.

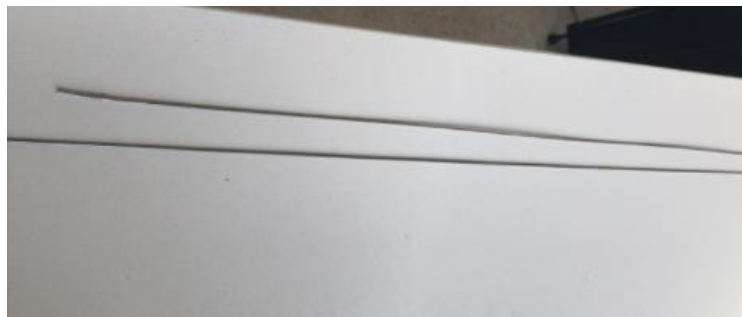


Figure 9-19. stainless steel wire

Step 2:

Build the spherical inner grid according to its characteristic calculated before.

(The spherical diameter: 7cm, the wire thickness: 1.6mm, and the wire loop number: 3).

In order to build the three loops (circle) of diameter equal to 7 cm, an available gas tank of diameter equals to 7cm has been used.

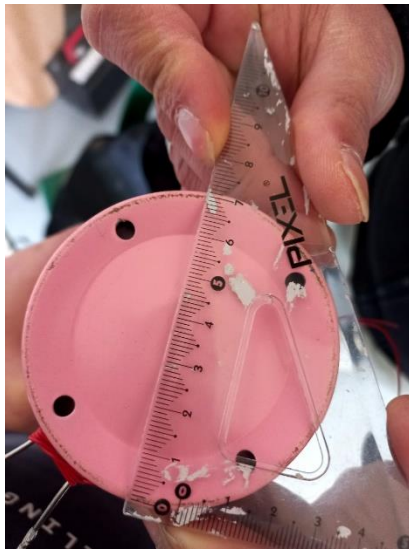


Figure 9-20. gas tank of 7 cm diameter

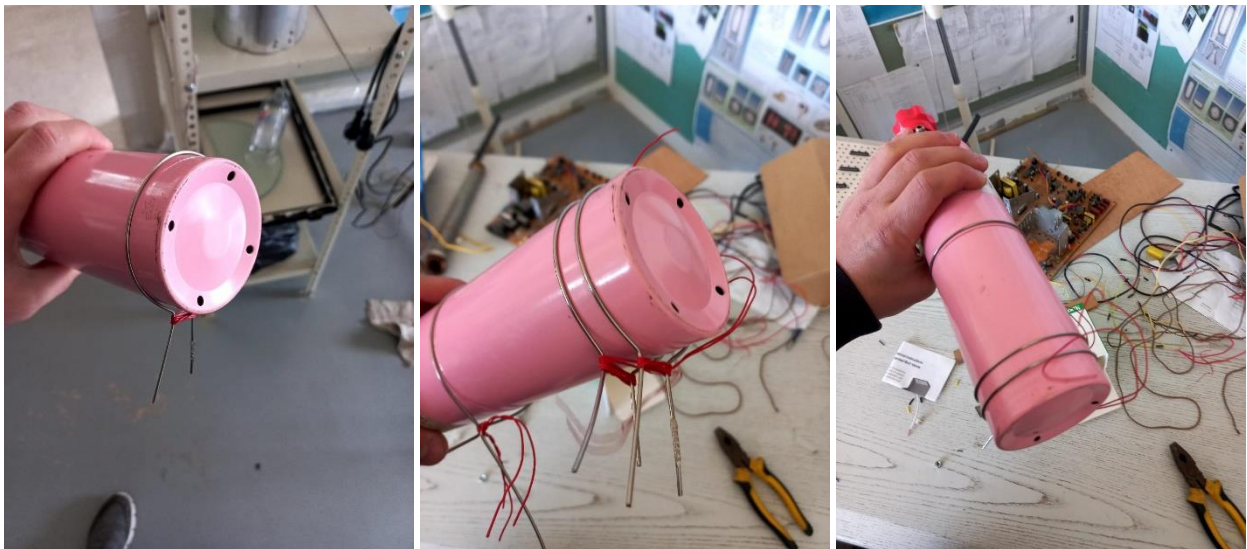


Figure 9-21. stainless steel reshaping

NOTE: each loop has two pins, that is needed to fix the inner grid sphere on its base, as will be mentioned later.

Check each circle reshaped by using the pink gas tube, with a red wire (as shown in figure 3-20 above), the two pins have been tied by a red wire to keep the stainless steel in its circular shape. After two days, the requires shape of stainless-steel wire was achieved. Hence, the three stainless circle has been extracted from the pink gas tank, as shown in figure 3-21.



Figure 9-22. stainless steel with circular shape

Step 3:

Gather three stainless circles in order to obtain a spherical shape, as figure below.



Figure 9-23. stainless steel inner grid

Step 4:

Choose the base of spherical inner grid

As shown in figure 3-22, there are 4 pins of thickness equals to 1.6mm, in total of 6.4mm. according to that, the inner grid base should have an inner diameter greater than 6.4 mm. according to local market, a stainless pipe of inner diameter of 7 mm and outer diameter of 10 mm, a length of 10 cm is suitable for this project.



Figure 9-24. stainless pipe tube

Step 5:

Fix all components via argon soldering electrical machine.

NOTE: the soldering needs an expert person, and it is more preferable to use a non-electrical argon soldering machine, cause of the complexity and the accuracy needed of the soldering position.



Figure 9-25. argon soldering electrical machine

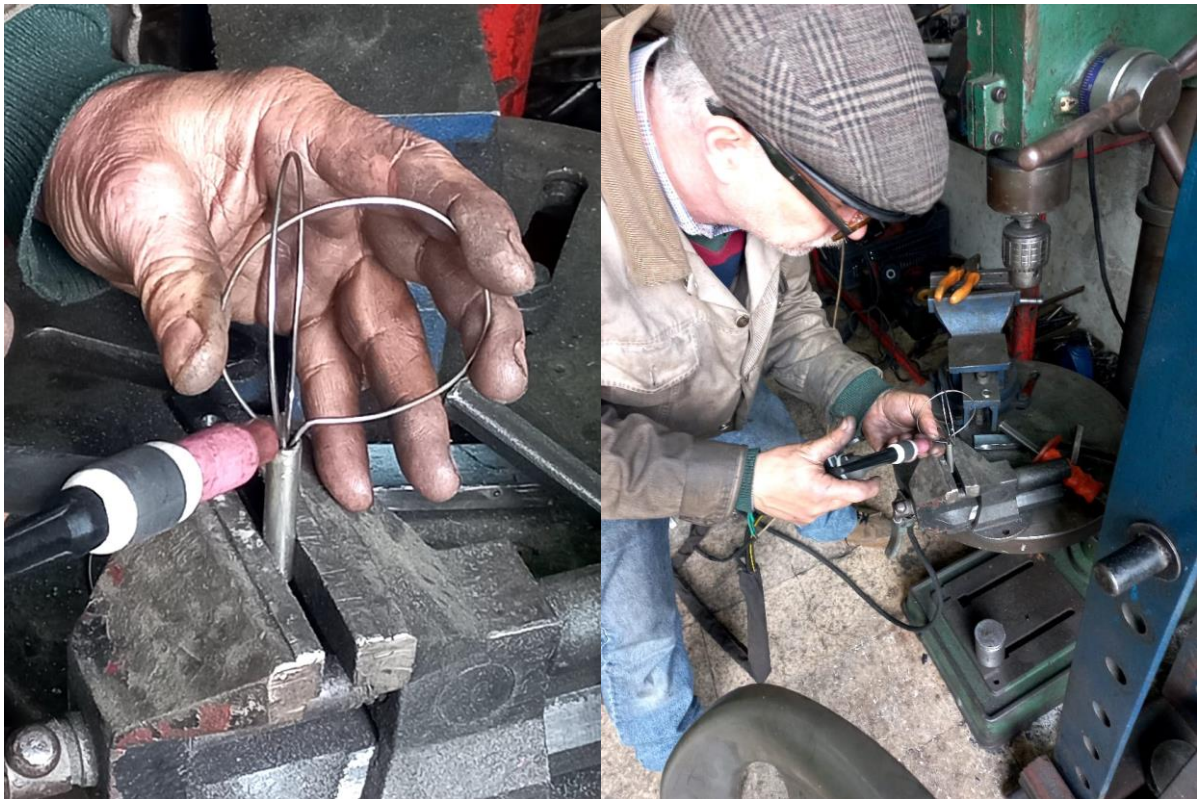
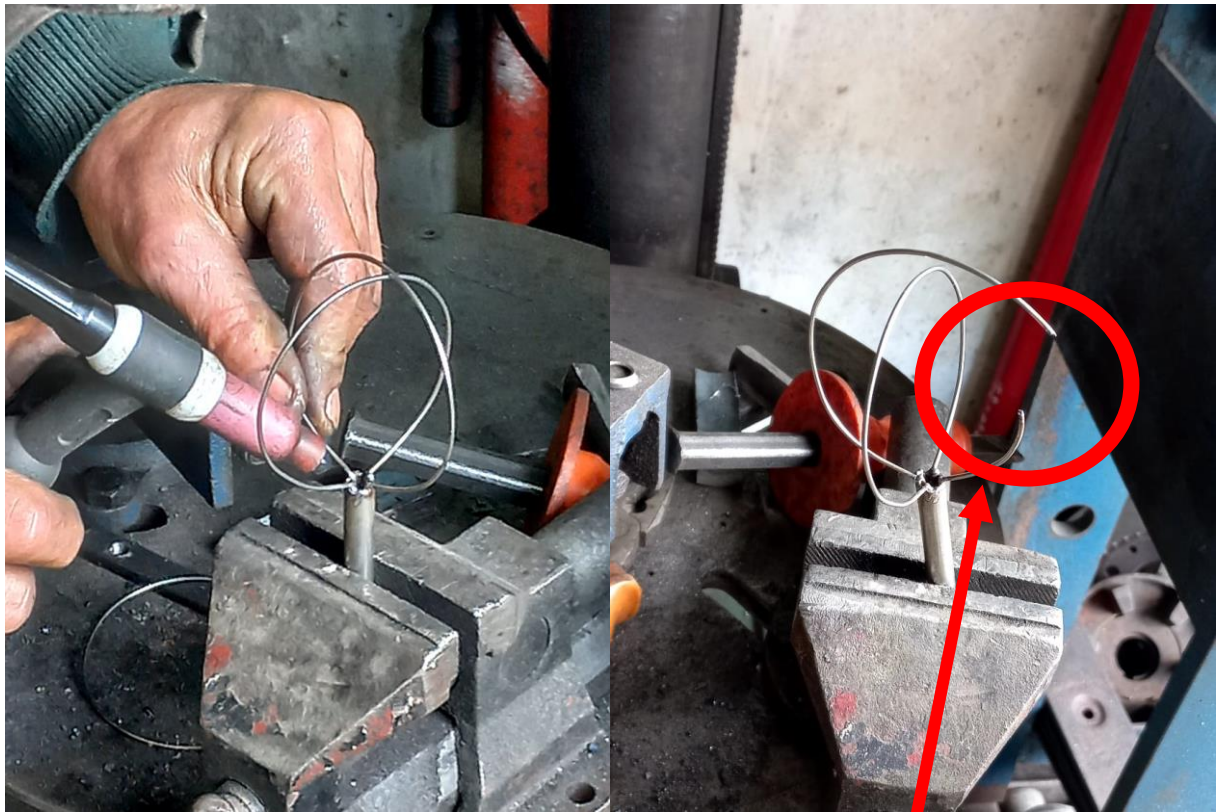
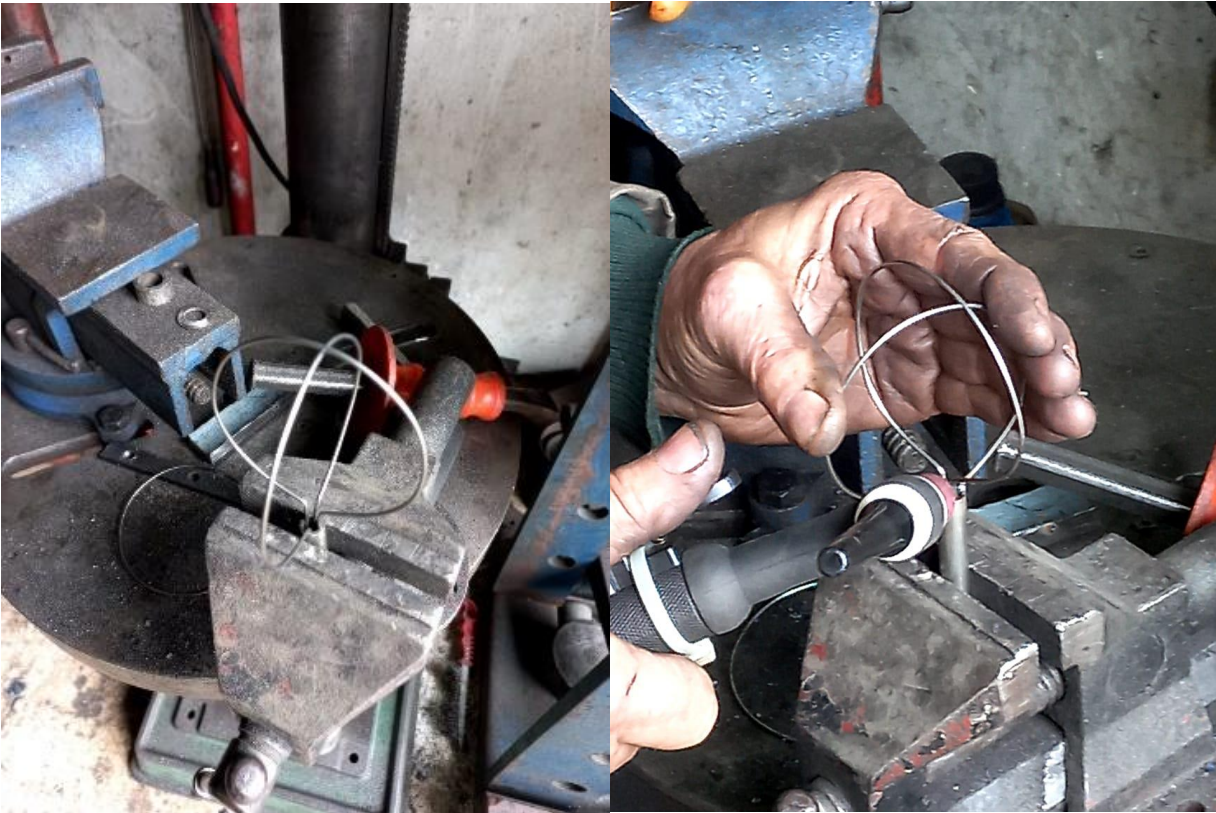


Figure 9-26. inner grid assembling



The wire chopped off cause of high sensitivity of wire

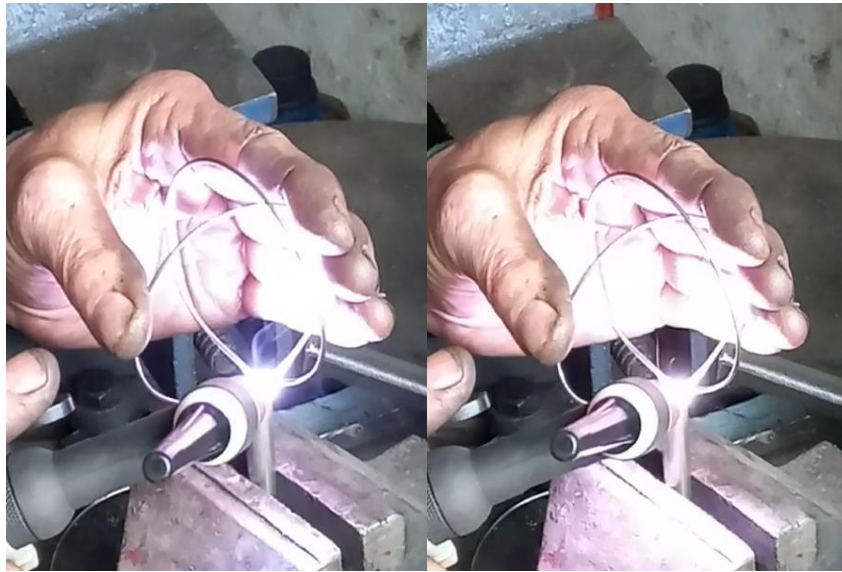


Figure 9-27. Stainless steel Inner Grid argon Soldering

Step 6:

After gathering the stainless sphere with its base, the 2 mm stainless wire has been soldered in other side of stainless pipe (sphere base). the



Figure 9-28. final form of stainless inner grid

ZVS Driver

The ZVS needed for this project should has the following specification shown in the table below:

Specification	description
Input Voltage	DC 12-30V
Power	1000W
Working Frequency	30-50KHz
Input current	>5A (under 12V) >10A (under 15V)

NOTE1: **THE POWER SUPPLY SHOULD AT LEAST 12V AT 5A.** otherwise, this will lead to low power input, thus, the Two MOS will connect at the same time, this will damage it.

NOTE2: **DO NOT TURN ON THE MODULE AT NO LOAD,** because it will lead to produce a high frequency noise that damage the mosfet.

NOTE3: **DO NOT EXCEED 30V.**



Figure 9-29. ZVS Driver

The ZVS driver will generate as an output power 800 times the input Voltage. So, for 20V at 10~15A the output power is 16KV

Estimated cost: 20\$

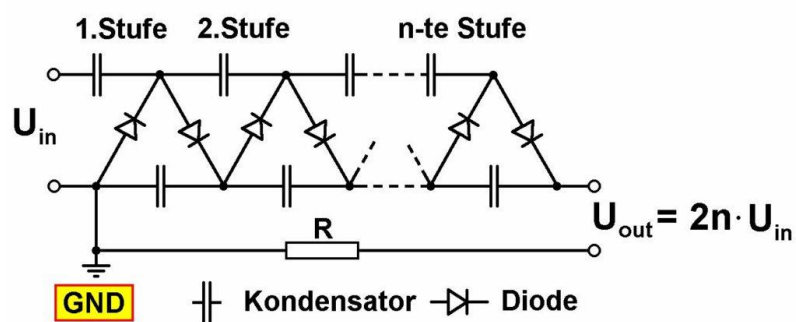
AC flyback transformer



This combination delivers an output voltage of around 27 kV peak to peak at an input voltage of 24V using 4x4 windings on the primary side of the flyback transformer.

Estimated cost: 35\$

Voltage Tripler (Cockroft-Waltan Voltage multiplier)



for 16kv as input, and in order to reach the 200kV. Approximately, 6 stage is needed

$$200Kv \div 2 \div 16 Kv = 6.25 \text{ stages}$$

Each stage needs two diodes, and two capacitors. The following components specification is compatible for this project.

Diode: High Voltage diode 2CL20Kv 20mA (48pcs, each two in series, and well isolated)

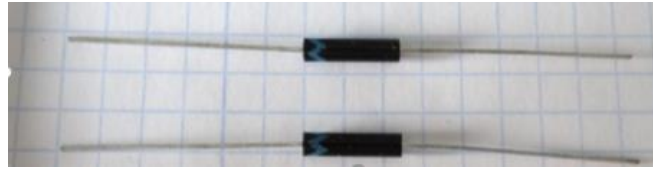


Figure 9-30. 20Kv 20mA high voltage diode

Capacitor: High Voltage capacitor 30Kv 1000pF (1nF) (24pcs, each one should be well isolated at its pin connections)

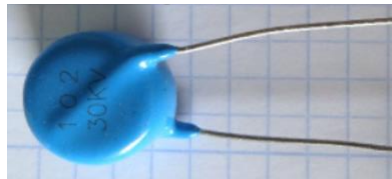


Figure 9-31. 30Kv 1nF capacitor

NOTE: this part of circuit should be in a suitable box filled of sunflower-oil, 6 liters of it is enough for isolation.

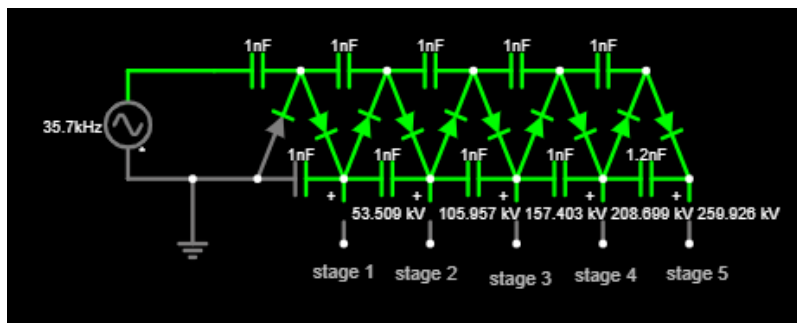


Figure 9-32. Voltage Tripler circuit simulation

Power supply

The power supply is acquired to feed the ZVS driver. This purpose can be achieved in two Methods.

Method 1:

The power supply is composed to 3 parts: variable transformer, to control the voltage existed at the input of ZVS driver. Hence, the power delivered to the fusor reactor cathode. Then, a two-transformer (1:1) connected in parallel at the primary, and series at the secondary side, to isolate the variable transformer form the whole system. Finally, the AC voltage produced by these two transformers must be converted from AC to DC voltage, which is compatible with the ZVS inputs.



Figure 9-33. Power Supply Method 1

Items	Quantity	specification	Estimated cost
-------	----------	---------------	----------------

Variable transformer	1		150\$
Power transformer	2	473-9101-B Rev15 Class: 180(H) R333H E154515 Type: LEI-4	40\$
Bridge rectifier	1	Single phase Diode Bridge rectifier Module: 60A 1600V High power 4 terminals current conversion module	20\$
Capacitor	1	10,000uf 50V	2\$

Remark: the bridge rectifier is not the best size for the project

Method 2:

The power supply is simple as it is, an adjustable switch power supply drive can ensure the needed power input of the ZVS driver (12v at +5A / 15v at + 15A)

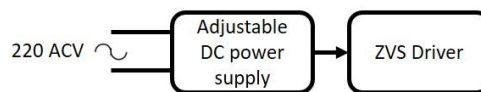


Figure 9-34. Power supply Method 2

Items	Quantity	specification	Estimated cost
adjustable switch power supply drive	1	0-30V DC 20A	25\$



Figure 9-35. Adjustable DC power supply

Method 1 vs Method 2:

The two methods can feed the ZVS driver. Method 1 is more expensive than method 2 (about 8 times method 2). Method 1 is more complex than 2, need more maintenance, etc.

Voltage Tripler Isolation

The voltage Tripler part should be in a suitable box felled by sunflower-oil (about 6 Liter). plus, the capacitor pins isolator

Estimated cost: Box 2\$

Sunflower-oil 12\$

Capacitor isolator 1\$

Cable and isolation

Cathode cable

The cable needed to connect the output of high voltage power system with the vacuum chamber must be a Tinning Tesla Coil Laser Wire 40KV High Voltage Cable High Pressure 22AWG 40 KV, as shown in figure 3.18



Figure 9-36. Tinning Tesla Coil Laser Wire 40KV High Voltage Cable High Pressure 22AWG

Heat shrinks tube wire wrap

The heat shrinks tube wire wrap is used isolate the capacitor pins from each other, cause of the sparks excited at it at high voltage. Otherwise, it is needed for the resistors of the negative output power side.



Figure 9-37. heat shrink tube wire

Measurement

For voltage measuring, two resistors are acquired (1x 20M Ohm 10W and 1x 20K Ohm 1W) for 1:1000 voltage divider reason. The 20Mohm resistor should be similar to figure 3-20 below. Plus, the 20K Ohm resistor should be similar to figure 3-21.



Figure 9-38. high voltage resistor of 500Mj

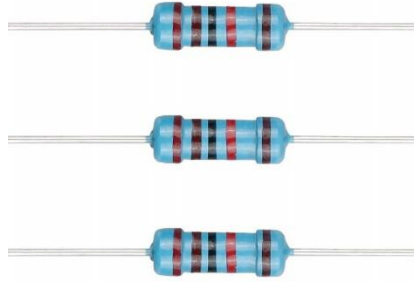


Figure 9-39. 20K ohm resistor of 1-2% tolerance

In addition, 4 resistors of 100Mohm 5-watt 1% resistor (MAXI-MOX series) are needed with an ammeter of 0-100 μ A for 0-40Kv.



Figure 9-40. 100M Ohm Maxi-Mox Series

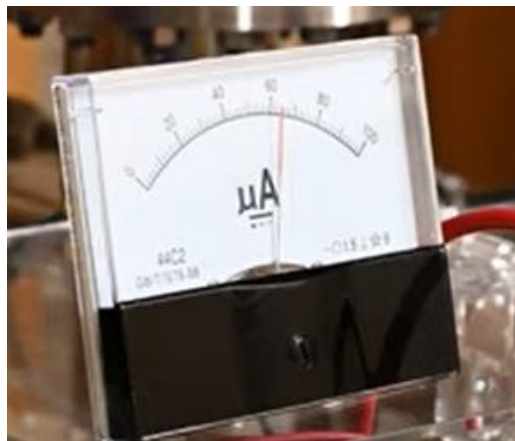


Figure 9-41. amperemeter (μ A)

Finally, a 10-ohm 20watt is required for fly back transformer voltage measurement (mV voltmeter)

And 14 pcs of 20Kohm/10W for the anode side of chamber (connected together in series)



Figure 9-42. 10-Ohm 20w resistor

Remote control

For security reason a remote control should be connected to switch ON/OFF the power.



Figure 9-43. Wireless Remote-Control Receiver

Vacuum System

items	description
Diffusion pump	EDWARDS DIFFSTAK 63/150
Mechanical pump	Arnocanali NPAV72
stalk	
Vacuum pipe	

9.3.5 Mechanical system

The mechanical system is composed to tow subsystems: vacuum system, and the vacuum chamber system.

9.3.5.1 Vacuum system

The vacuum system should vaccumed the fusor reactor chamber approximetly to 2×10^{-7} tor (apporximatly 99% vaccumed), where $1 \text{ atm} = 760 \text{ tor}$ or $1 \text{ atm} = 760 \text{ mmhg}$. The system consists of two pumps: diffusion, and mechanical pump.

Mechanical pump

The following pumps are compatible for this project (or any pumps alternative for it).

Edwards Rotary Vacuum pump Model 5:



Figure 9-44. Edwards Two Stage 5 Rotary Vane Vacuum Pump E2M5 1/2 HP 115/208-230 VAC 1 Phase:

Description:

This is a Used well maintained E2M5 Rotary Dual Stage Vacuum Pump. Tested and Quite Serial Number Of Pump 53503.

- The Edwards 5 E2M5 dual stage rotary vane mechanical vacuum pump offers an excellent ultimate pumping speed.
- The Edwards 5 E2M5 has superior vapor handling capabilities, while operating quietly.
- They are very reliable and have accessories to match any application.
- Applications Include use with
 - Refrigeration dehydration
 - Brake line evacuation
 - Epoxy degassing
 - Sterilization
 - Mass spectrometry
 - Vacuum ovens
 - Lasers
 - Backing combinations
 - Thin film coating
 - Vacuum distillation
 - Freeze drying
 - Space research and other vacuum processes.
- The Edwards 5 E2M5 vacuum pumps have a pumping speed displacement at 60Hz of 3.75 CFM and an ultimate pressure of 7.5×10^{-4} Torr.

Technical data:

- Peak Pumping Speed 3.75 CFM @ 60 HZ
- Ultimate Pressure 7.5×10^{-4} TORR (1×10^{-3} MBAR)
- Noise Level 52 DB (A)
- Connection Inlet NW25
- Connection Exhaust NW25
- Maximum Water Vapor Inlet Pressure 10 TORR (15 MBAR)
- Maximum Water Vapor capacity 60 Grams / HR
- Physical Data 43 Lbs. 17.5 Length x 5.9 Inches Wide x 8.6 Inches High
- Electrical Supply 115 / 208-230 VAC Wired Set For 115 VAC with cord & plug
- Operating Range 12- 40 C
- Oil Capacity 0.6 L
- Oil Type Ultragrade 19

[Click here](#) to go to the website.

Edwards Rotary Vacuum pump Model 2:



Figure 9-45. Edwards E2M2 Rotary Vane Vacuum Pump

Description:

Edwards E2M2 rotary vane pumps have a peak pumping velocity of 1.5 cfm and a ultimate pressure of 7.5×10^{-4} Torr. The E2M2 is a dual stage rotary vane mechanical vacuum pump with a 1 phase or 3 phase electrical supply. It is reliable and operates quietly at 52 dB(A).It has excellent vapor handling capabilities and can be used in many applications. [Click here](#) to go to website. Comparison between Model 2 and 5:

Vacuum Pump Model		E2M2	E2M5
Nominal Displacement	<i>cfm</i>	2	4
Nominal Displacement	<i>l/m</i>	57	113
Stage		2	2
Motor HP	<i>hp</i>	1/3	1/2
Oil Capacity	<i>ltr</i>	.6	.6
Weight	<i>kg</i>	18.2	19.6
Noise Level	<i>dBA</i>	52	52

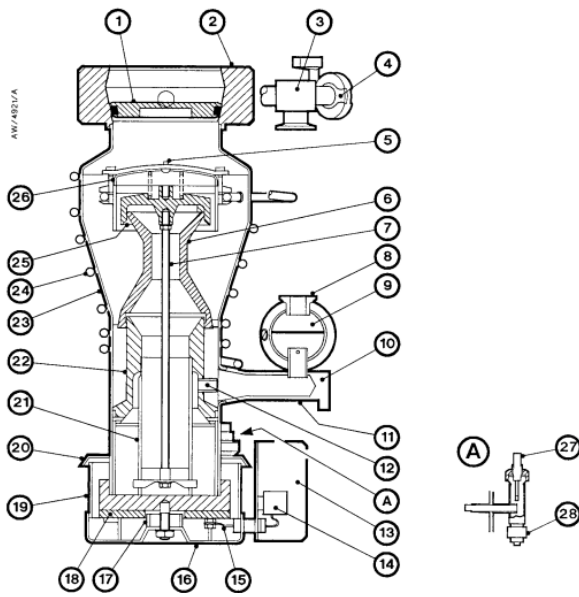
Arnocanali NPAV72

Description:
 Nominal displacement: 71l/min
 Motor Hp: 0.3HP
 Voltage: 220V
 Oil load: 300 ml
 Final vacuum: 0.2



Diffusion pump

Figure 1 - Sectional view of valved Diffstak 63/150 pump



- | | | |
|--------------------------------------|-----------------------|--|
| 1. High-vacuum isolation-valve | 11. Backing spout | 22. 3rd-stage jet assembly |
| 2. Inlet-flange | 12. Ejector jet | 23. Pump-body |
| 3. Roughing connection | 13. Terminal-box | 24. Water-cooling coil |
| 4. Gauge connection (NW10) | 14. Terminal-block | 25. Top-jet assembly |
| 5. Retainer strap | 15. Electrical cables | 26. Baffle-cap |
| 6. 2nd-stage jet assembly | 16. Heater assembly | 27. Fluid filler and dipstick assembly |
| 7. Tie-rod | 17. Spacer | 28. Fluid drain |
| 8. Backing connection | 18. Heater | |
| 9. Backing condenser | 19. Pump-boiler | |
| 10. Pump-ready switch mounting plate | 20. Radiation shield | |
| | 21. Vapour-tube | |

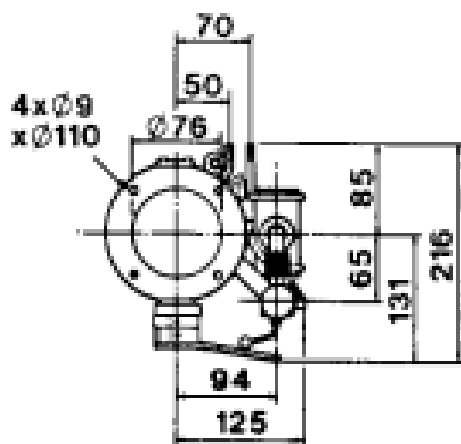
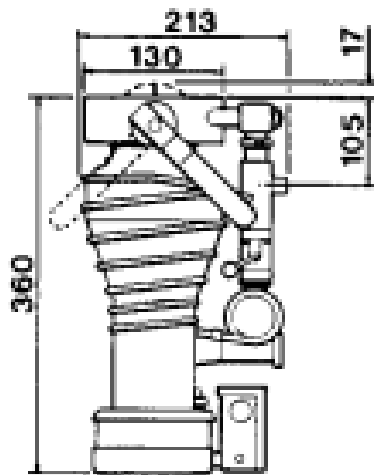
	63/150M 63/150P	100/300M 100/300P	160/700M 160/700P	250/2000M 250/2000P
Pumping speed				
nitrogen	135 l s ⁻¹	280 l s ⁻¹	700 l s ⁻¹	2000 l s ⁻¹
hydrogen	200 l s ⁻¹	500 l s ⁻¹	1300 l s ⁻¹	3000 l s ⁻¹
Minimum backing pump displacement for maximum throughput	5 m ³ h ⁻¹	5 m ³ h ⁻¹	12 m ³ h ⁻¹	40 m ³ h ⁻¹
Recommended backing pump	RV3* or RV5	RV5 or RV8	RV12 or E2M18	E2M40
Maximum pump pressure	1300 mbar 1.3 x 10 ⁵ Pa	1300 mbar 1.3 x 10 ⁵ Pa	1300 mbar 1.3 x 10 ⁵ Pa	1300 mbar 1.3 x 10 ⁵ Pa
Recommended pump fluid	Santovac 5	Santovac 5	Santovac 5	Santovac 5
Fluid charge (dry)	60 ml	125 ml	250 ml	500 ml
Inlet connection, compatible with	ISO63	ISO100	ISO160	ISO250
Backing connection	NW10	NW25	NW25	NW40
Cooling water connection	6 mm compression couplings		10 mm compression couplings	
Minimum cooling-water flow at 20 °C	42 l h ⁻¹	60 l h ⁻¹	115 l h ⁻¹	180 l h ⁻¹
Heater power	0.45 kW	0.65 kW	1.35 kW	2.25 kW
Pneumatic connections †	6 mm couplings x 1/4 BSP male stud			
Pneumatic actuating pressure †	2.4 to 6.9 bar (35 to 100 psi, 2.4 x 10 ⁵ to 6.9 x 10 ⁵ Pa)			
Mass				
M-model	8 kg	12 kg	26 kg	59 kg
P-model	9 kg	13 kg	27 kg	60 kg
Dimensions	See Figures 5 and 6			
Position indicators †				
Maximum voltage	48 V a.c.	48 V a.c.	48 V a.c.	48 V a.c.
Maximum current	380 mA	380 mA	5 A	5 A
Enclosure protection	IP67	IP67	IP22	IP22

2.2 Pump fluid data

Note: Edwards Material Safety Data Sheets for the following fluids are available on request.

Fluid type	Critical backing pressure		Ultimate vacuum	
Santovac 5	0.6 mbar	6.0 x 10 ¹ Pa	3 x 10 ⁻⁸ mbar	3 x 10 ⁻⁶ Pa
DC702	1.2 mbar	1.2 x 10 ² Pa	7 x 10 ⁻⁶ mbar	7 x 10 ⁻⁴ Pa
DC704EU	0.8 mbar	8.0 x 10 ¹ Pa	7 x 10 ⁻⁸ mbar	7 x 10 ⁻⁶ Pa
DC705	0.6 mbar	6.0 x 10 ¹ Pa	3 x 10 ⁻⁸ mbar	3 x 10 ⁻⁶ Pa
Edwards L9	0.6 mbar	6.0 x 10 ¹ Pa	3 x 10 ⁻⁸ mbar	3 x 10 ⁻⁶ Pa
Apiezon C	0.7 mbar	7.0 x 10 ¹ Pa	7 x 10 ⁻⁸ mbar	7 x 10 ⁻⁶ Pa

Fluid Type	Flash point °C	Auto-ignition point °C	Molecular weight
Santovac 5	288	590	446
DC702	193	500	530
DC704EU	221	500	484
DC705	243	500	546
Edwards L9	241	370	407
Apiezon C	246	420	479



reference: https://www.lesker.com/newweb/vacuum_pumps/diffusionpump_boceowards_diffstak.cfm

Efficiency of Arnocanali NPAV72(Present at AECENAR)

The diffusion pump does not work if the pressure in the chamber is greater than 50 microns.

$$1\text{micron}=0.001\text{ torr}$$

$$50\text{ microns}=5*10^{-2}\text{ Torr}=6.6\text{ Pa}$$

For this reason we use a mechanical pump to decrease the pressure below 6.6 Pa.

Arnocanali NPAV72 can decrease the pressure in the chamber to 0.2 Pa < 6.6 Pa,

Therefore this pump works well.

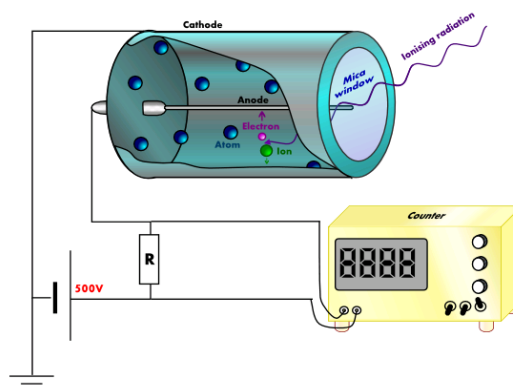
9.3.6 Detectors

9.3.6.1 Helium-3 Proportional Counters and Alternatives for Neutron Detection:



Identification of Special Nuclear Material by Neutron Detection

Special nuclear material (SNM) such as plutonium-239, uranium-233, or uranium-235 is used in the creation of nuclear explosives and atomic bombs due to its fissile nature, or capability to self-sustain a chain reaction with neutrons. As such, the detection and control of SNM is essential to global nuclear threat reduction. One method used to identify SNM is through the sensing of fast and slow neutrons, which have energies above and below 0.5-1.0 Kev, respectively. This approach is attractive for several reasons. First, since the ambient background of neutrons is fairly low (0.005-0.02 neutrons/(s cm²)), any measured neutron levels above the background value is a strong indicator that SNM is present. Moreover, neutrons cannot be easily concealed or shielded from detection since they can penetrate several meters with only 1 MeV in energy. These particles also have unique fission signatures (i.e. release of gamma-rays and neutrons) that depend on their specific interaction with the detection material. Together, these characteristics make SNM identification via neutron detection an appealing approach



Helium-3 Gas-Filled Proportional Counters and the Helium-3 Shortage

Neutrons can be detected using helium-3-filled gas proportional counters. A typical counter consists of a gas-filled tube with a high voltage applied across the anode and cathode. A neutron passing

through the tube will interact with a helium-3 atom to produce tritium (hydrogen-3) and a proton. The proton ionizes the surrounding gas atoms to create charges, which in turn ionize other gas atoms in an avalanche-like multiplication process. The resulting charges are collected as measurable electrical pulses with the amplitudes proportional to the neutron energy. The pulses are compiled to form a pulse-height energy spectrum that serves as a "fingerprint" for the identification and quantification of the neutrons and their energies. However, one significant concern regarding the use of helium-3 gas proportional detectors is the global shortage of helium-3. This isotope is rarely found in nature but exists as a decay product of tritium, which is primarily produced in nuclear reactors. A recent estimate by GE Reuter Stokes estimates that the United States' demand for helium-3 is approximately 65 kliters per year while the total supply is only 10-20 kliters per year. As a result, there has been a rising and urgent demand for the development of new strategies for neutron detection.

Alternative Neutron Detection Materials

There are several alternatives for neutron detection that are currently in use or under development. Boron trifluoride (BF₃) is one of the most widely-used fill gases for proportional counters. In this case, each neutron interacts with BF₃ to create lithium-7 and an alpha particle, the latter of which serves as the ionizing charge in the gas proportional counter. However, BF₃'s toxicity makes it undesirable to handle, especially in applications that utilize larger detectors.

Other boron-related detectors employ powdered boron-10. Recent work at Los Alamos National Laboratory has demonstrated that boron-10 detectors can achieve neutron detection efficiencies comparable to those of helium-3 detectors. Boron-10 is also non-toxic, in abundant supply, and offers excellent discrimination between neutrons and gamma-rays. This material is used as wall-lining in gas-filled proportional counters, as thin films coupled to the surface of semiconductor detectors, and in scintillators (materials that interact with ionizing radiation to produce detectable light). Lithium-6 is another material that is being used for neutron detection. It is used in crystal scintillator compounds like Cs₂LiYCl₆, Cs₂LiLaCl₆, and LiI, as well as liquid scintillators and glass fibers. However, one main drawback of lithium-6 is its lower detection sensitivity. Additional options for neutrons under development include liquid argon detectors, scintillating-dye-loaded polymers, and graphene field effect transistors.

9.3.6.2 Conclusions

It is clear that no material for neutron detection can meet all of the demands for high efficiency, high abundance, good discrimination, low cost, low toxicity, and ease of scalability. Many of the future solutions will likely rely on the improvement and modification of existing methods and will be designed to be application-specific. Although it is uncertain when the next major breakthrough in neutron detection will occur, shortcomings in certain detection methods can be overcome by coupling complementary and multiple techniques for a more comprehensive analysis.

Reference: <http://web.mit.edu/8.13/www/JLExperiments/38/tgm-neutron-detectors.pdf>

9.3.7 Vacuum tests

9.3.7.1 Test 1:

In this test we will try to vacuum an Aluminum pressure sterilizer model 1925X by arnocanali pump.



Calculation of minimum thickness wall of this chamber:

$D_0=32.1 \text{ cm}$ $L= 42.5 \text{ cm}$ $P_{ext}= 14,7 \text{ psi}$.

Young modulus of Aluminum $E = 69 \text{ GPa} = 1.008 * 10^7 \text{ psi}$

Thickness $t= 3.5 \text{ mm}$.

$D_0/t= 91.71$

$L/D_0= 1.32$

A= 0.001

$$Pa = 2A E/3(D0/t)$$

Pa= 72.75 psi >> Pext

Pa/Pext= 4.94. 5 is a safety factor.

Calculation minimum thickness of chamber faces:

Yield stress of aluminum= 530 MPa

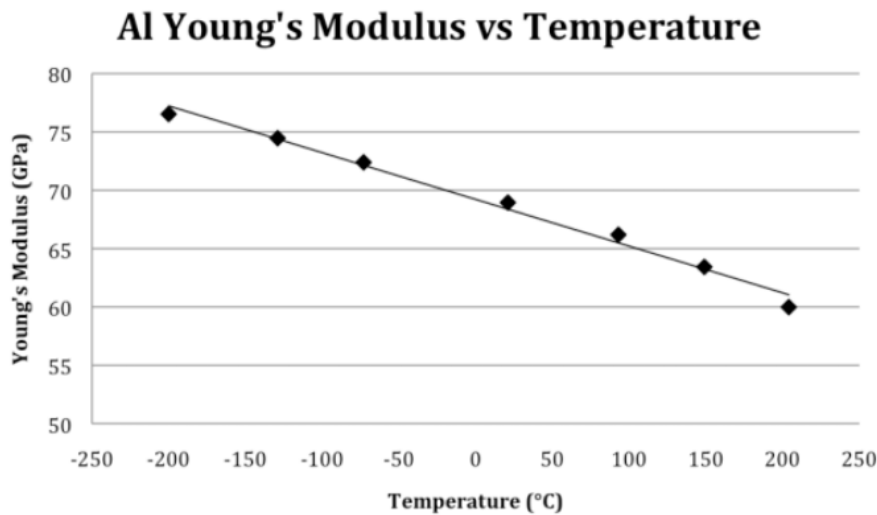
Max allowable stress S =530/5= 106 MPa 5 safety factor.

$$t = D0(0.13P/SE)^{0.5}$$

➔ **t= 0.4 cm= 4 mm**

thickness of this chamber is equal 8mm. This chamber is Safe

Aluminum young s modulus vs Temperature:



$$E = aT + 69 \quad a = 60 - \frac{63}{200} - 150 = -0.06$$

maximum temperature strenght of chamber:

if t= 3.5 mm and Pa= 14.7 psi= Pext E= 15 Gpa

$$T_{max} = 675^{\circ}C$$

so we have do not exceed 675°C on the wall of chamber

Assembling and pieces:



Result:



The pressure in the vessel reach around 100 mbar.

This value is bigger than required.

The required pressure for work a diffusion pump to work is 50 *microns* = $1.333 \cdot 10^{-3} \text{ mbar}$

The specifications of this pump shows that the pressure can reach $0.2 \text{ Pa} = 0.002 \text{ mbar}$.

Test failed.

Possible reasons:

- The pump does not work well. (Check the oil level in the pump).
- Air leakage into the chamber and connectors.

Solutions:

- Test the pump by connecting it directly to a pressure Microns gauge



- If the pump work well, we have to check the leakage in the chamber and the connectors by a **helium leak testing**.



Helium leak testing:

Helium tracer gas is used for several leak testing applications. It has a small atomic size that allows the gas to pass through incredibly small leaks and is also non-toxic and non-flammable. One common method of tracer gas leak detection is the hard vacuum test, which involves the use of vacuum chambers and tracer gas to detect microleaks.

9.3.7.2 Test 2:

in order to know where is the air leakage, a water evaporation test had been done. The chamber was filled to its middle, as shown in figure 7-1. The vacuum chamber was filled at the top of viewport, in

other word, water had burial the viewport in order to know if the air leakage was from the viewport, which it will be know if there is any water leakage from the view port, or the air leakge was from the pot cover, that itwill known if there is any steam leakage from the pot cover.



Figure 9-46. Vacuum chamber in water evaporation test

After that, vacuum chamber has been closed tightly and heated by fire for 10-15 min.

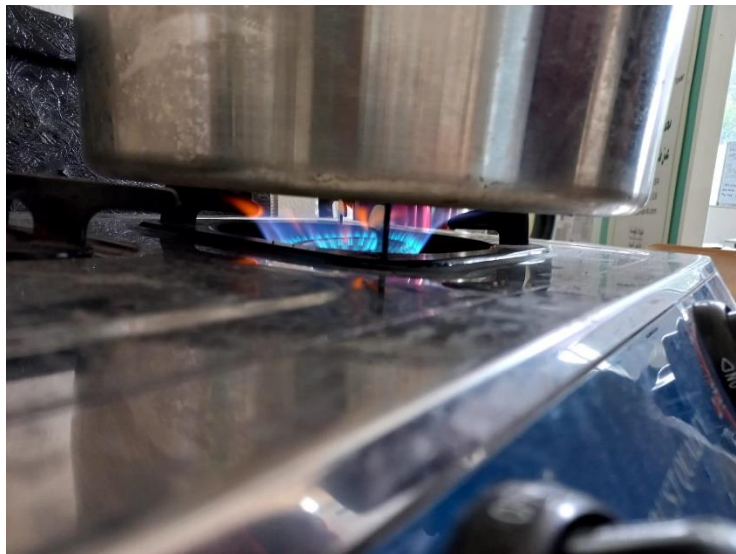


Figure 9-47. vacuum chamber heating operation

The pressure and temperature sensor were monitored by a gauge fixed on the top of the vacuum chamber pot.

IECF (Inertial Electrostatic Confinement Fusion)



The following figure, below, shows where the air leakage take place, the air leakage place is the same place of steam leakage, that is described by a white steam. In figure 7-3 below, the blue zone shows the steam out of chamber, plus, the red zone shows the water bubble exited from the chamber.



Figure 9-48. steam leakage

After some analysis, the pot position has been change as shown in figure 7-4.



Figure 9-49. pot position

The same test was performed again, and the results shows that no noticeable steam leakage.

Result

TEST SUCCESSFUL

9.3.7.3 Test 3:

After checking in the level of oil in the pump we saw that is under the minimum level. We added oil in the pump and we retried.



In order to be sure that the pump can reach its maximum, a thumb was putted where the pump is connected to the chamber.

We got a successful result, the pump reached around 0.002 mbar in the chamber, to make sure of this we will use a Microns gauge.

After each test, the pressure is eliminated by opening the safety valve manually, as shown in figure below.



Figure 9-50 safety valve opened



Figure 9-51. safety valve closed

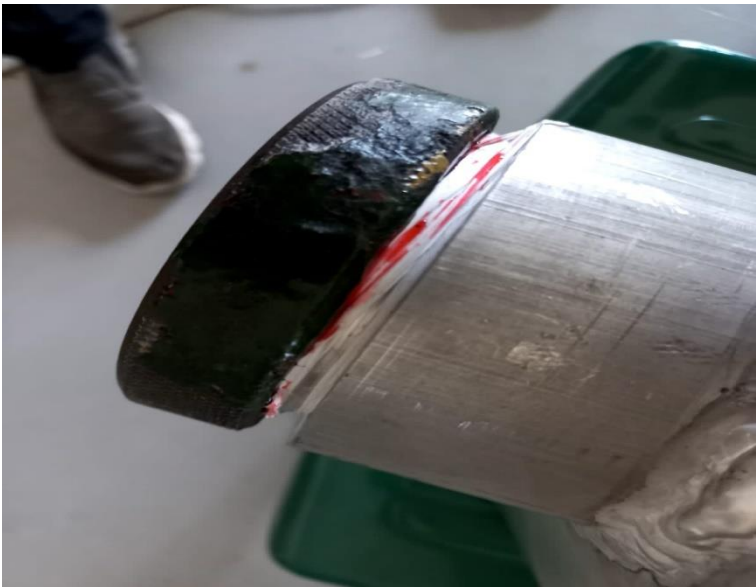
Result

Test successful

9.3.7.4 Test 4

After welding the glass support and assembling pieces we retried to vacuum the chamber



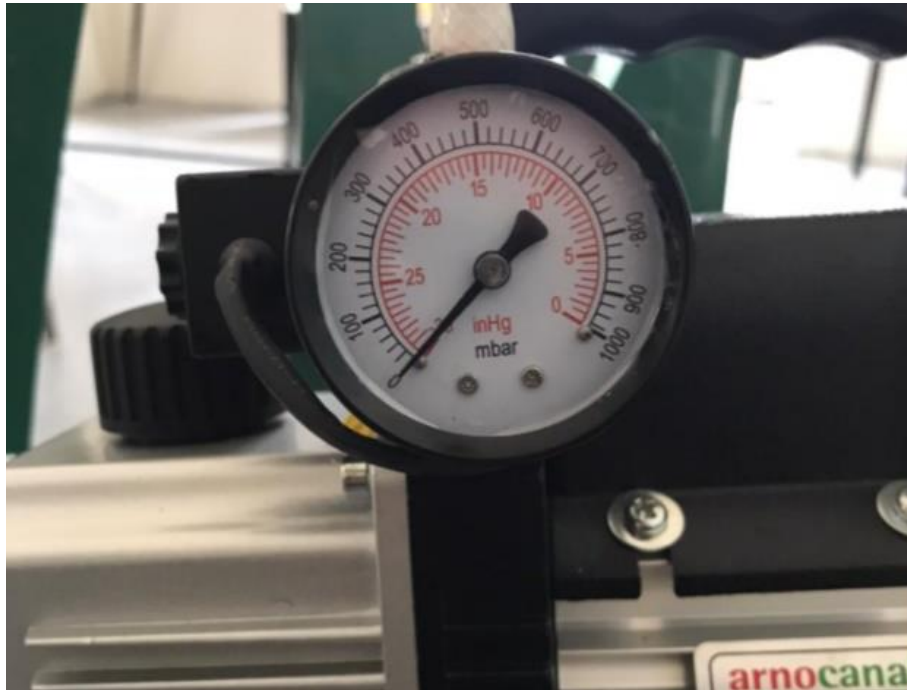


Result

The test failed due to leaking in the red circle on top.



To stop air leaking we put silicon on the red circle, and we vacuumed the chamber



Result

Test successful

9.3.7.5 Test 5:

After aforementioned water evaporating test, air starts leak from another place, where just 400 mBar has been extracted by vacuum pump, as shown in figure 7-7 below.



Figure 9-52. Pressure value in mBar

In order to find where the air leakage take place, one medical clove was putted at the viewport. Figure 7-8 illustrates how the clove was putted at the viewport. Where, if the clove shrinks through vacuum operation, hence, the air leakage could be from the viewport. If no so, this estimated place will be eliminated.



Figure 9-53. clove test

There is no air leakage from the viewport side.

Otherwise, in order to ensure that the chamber pot was totally closed tightly. The wall surface that faced the pot has been anointed through an oil submerged tissue.



Figure 9-54. chamber edges lubrication

The same result has been gotten, **no air Leakage from chamber edges.**

After that, another place had been tested. Where, a hand has been putted on the safety valve at the top of pot chamber, as illustrated bellow, and vacuum pump was turned ON.



A pull force has been sensed by the hand, which describes the place where the air leaks. And the pressure gauge shows the following value.

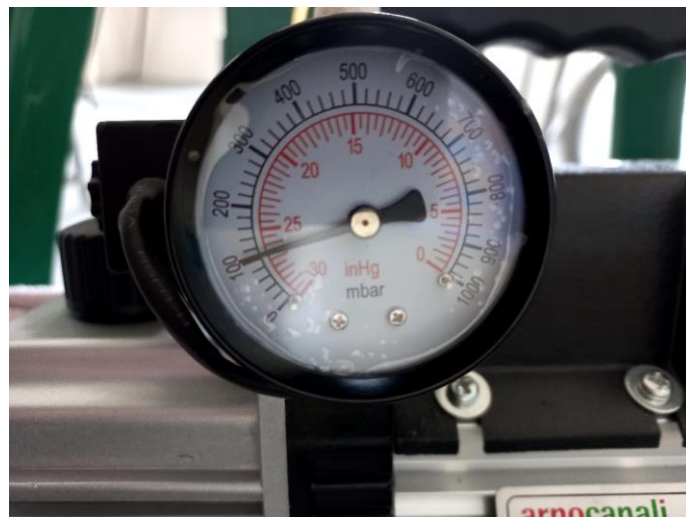


For air leakage blocking, a melted wax has been added on the safety valve.





The air leakage was decreased 80 percent, where the pressure gauge shows that vacuum pump extracted 900 mBar from chamber.



For this reason, and for safety valve hole benefits, the safety valve will be eliminated, and it will be replaced by the input of deuterium gas.

9.3.8 Searching for materials

9.3.8.1 chamber glass window:

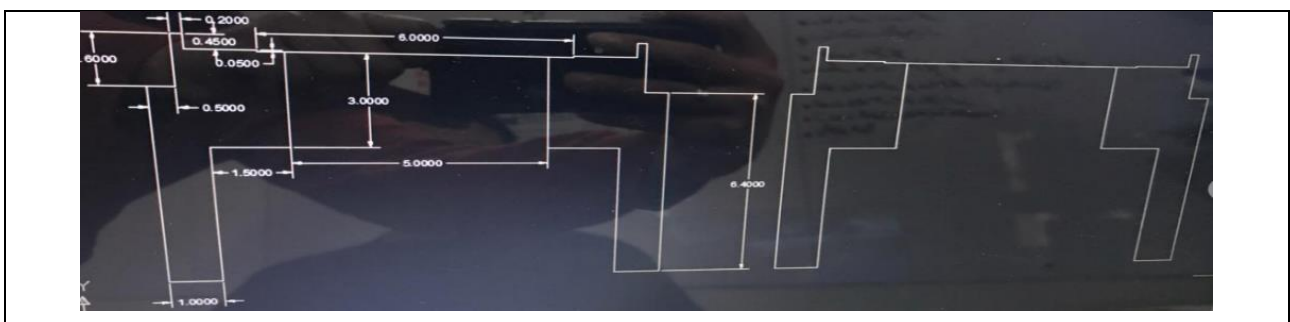
We found a thermal glass window that had been used in a submarine.



We will weld a Glass support on the Chamber.

The support is not available in Tripoli so we are going to make one.

We bought an aluminum mold and we cut it this way:



IECF (Inertial Electrostatic Confinement Fusion)



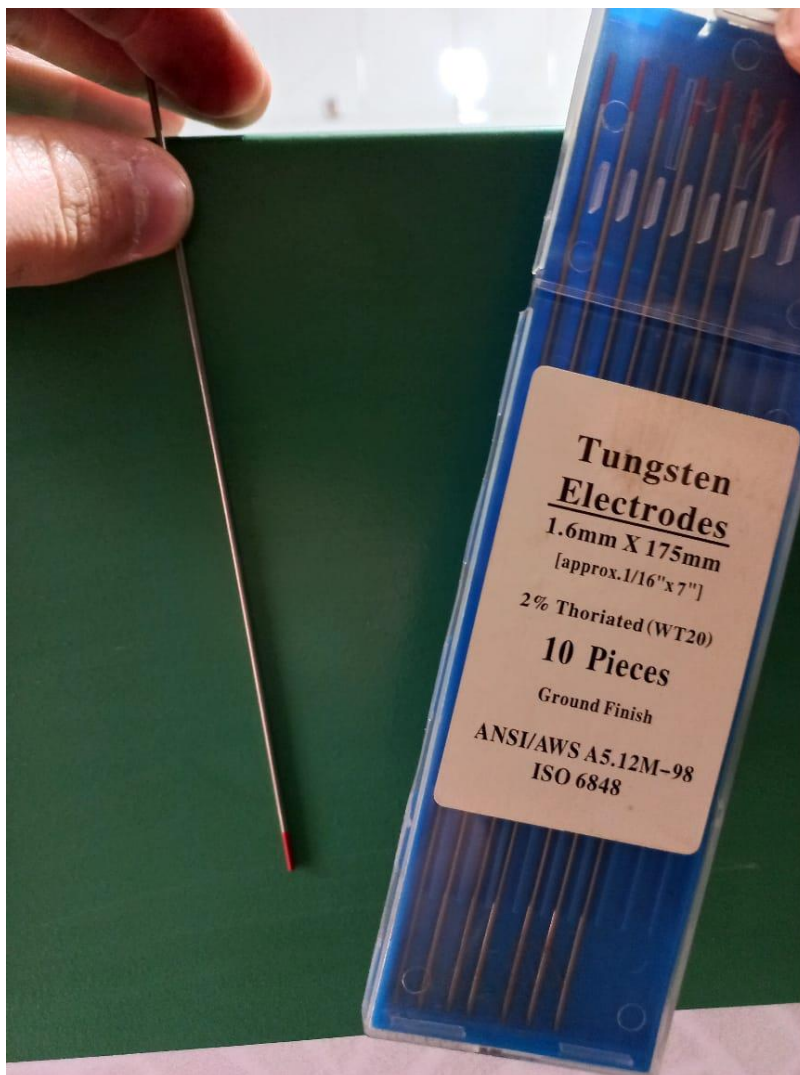


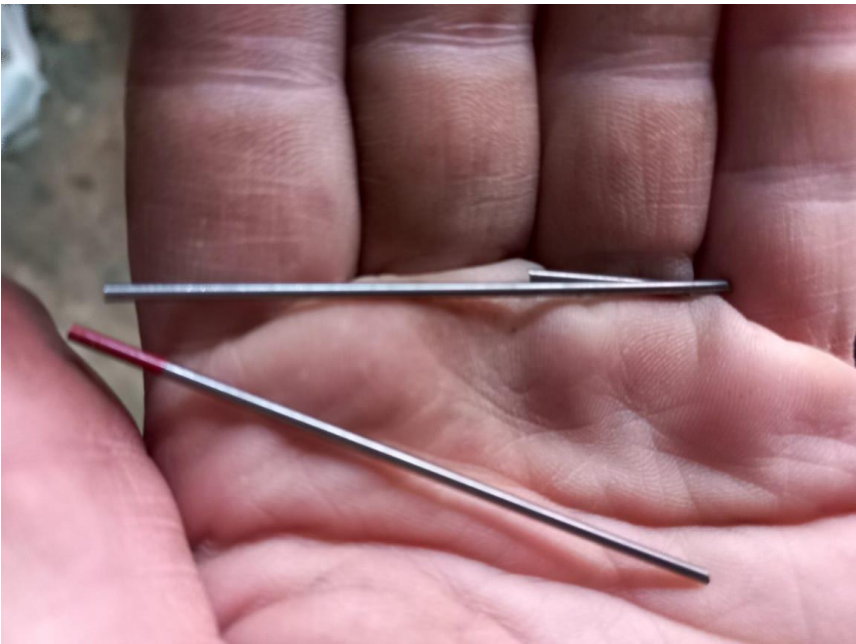
9.3.8.2 stainless steel wire

The best choice we found in our country is a stainless-steel wire in (1.6mm diameter of wire).



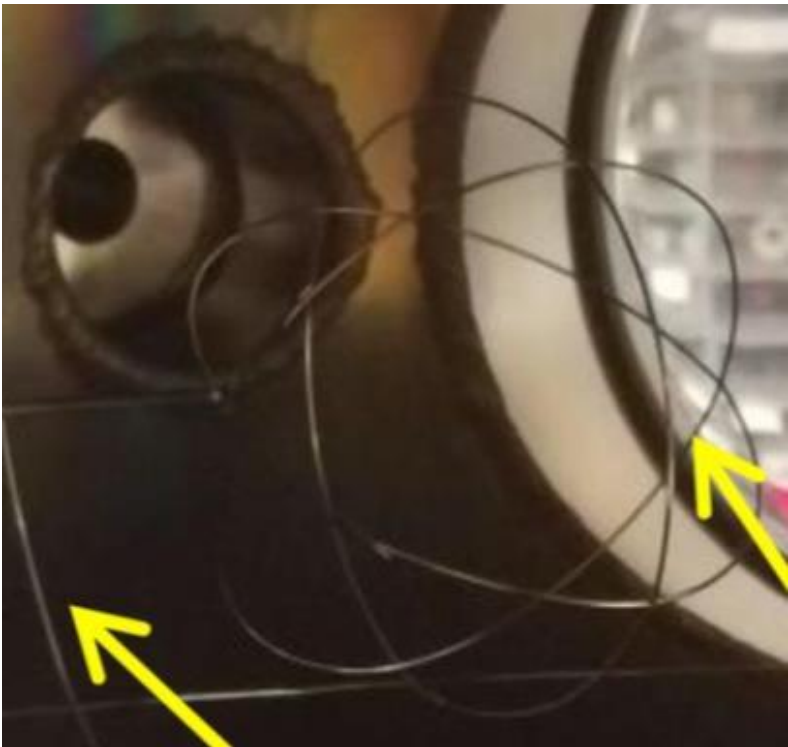
Note: a tungsten filament had been found, but it can be reshaped. The next figures show how the tungsten electrode broke while we trying to reshape its.





The cathode is a 7 cm diameter grid and consists of three 7 cm diameter rings that have been welded together, each ring is arranged such that the three rings form a spherical grid.





9.3.8.3 cathode inner grid assembling

The cathode inner grid has been built in the following steps:

Step 1:

Get three stainless steel rods (2 x diameter: 1.6mm, 1 x diameter:2 mm). the 1.6mm rods are used for the spherical inner grid. This thickness is compatible for the transparency (<92%), as mentioned before.

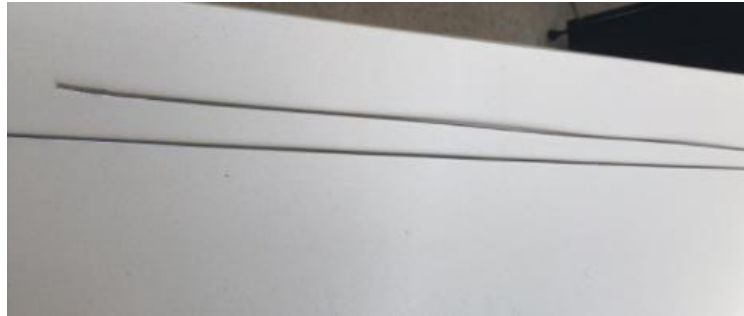


Figure 9-55. stainless steel wire

Step 2:

Build the spherical inner grid according to its characteristic calculated before.

(The spherical diameter: 7cm, the wire thickness: 1.6mm, and the wire loop number: 3).

In order to build the three loops (circle) of diameter equal to 7 cm, an available gas tank of diameter equals to 7cm has been used.

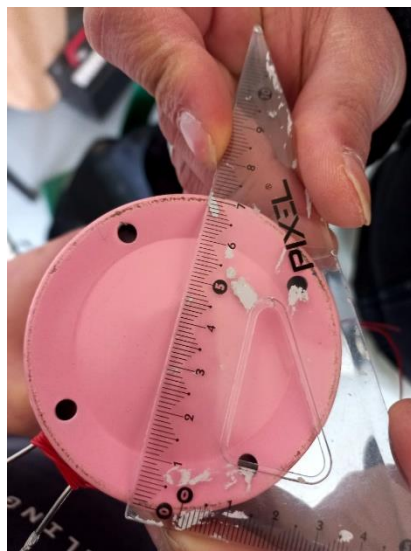


Figure 9-56. gas tank of 7 cm diameter

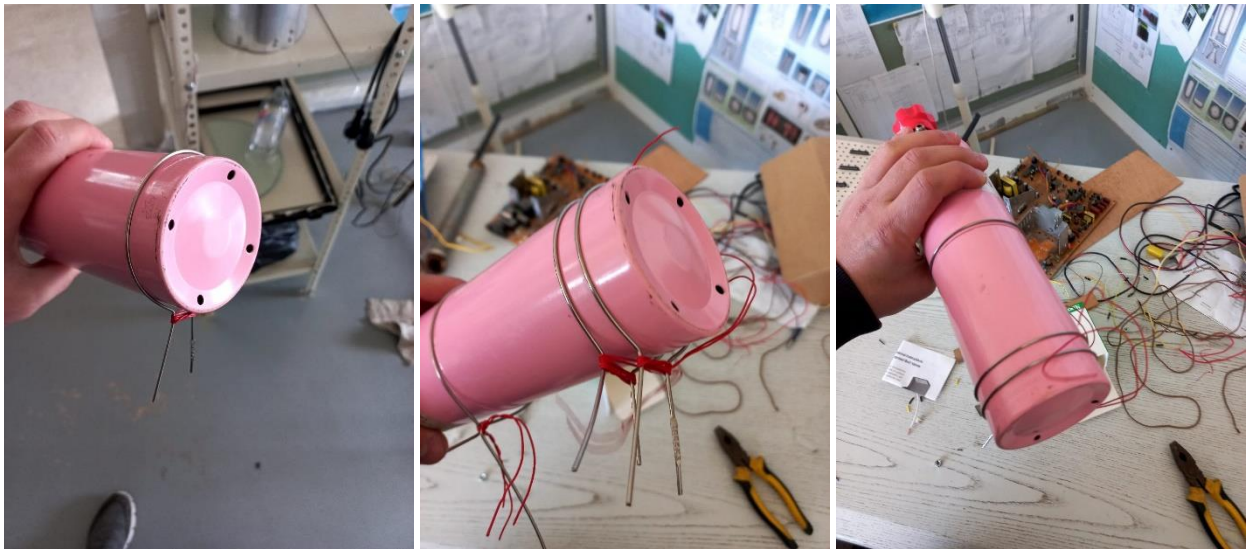


Figure 9-57. stainless steel reshaping

NOTE: each loop has two pins, that is needed to fix the inner grid sphere on its base, as will be mentioned later.

Check each circle reshaped by using the pink gas tube, with a red wire (as shown in figure 3-20 above), the two pins have been tied by a red wire to keep the stainless steel in its circular shape. After two days, the requires shape of stainless-steel wire was achieved. Hence, the three stainless circle has been extracted from the pink gas tank, as shown in figure 3-21.



Figure 9-58. stainless steel with circular shape

Step 3:

Gather three stainless circles in order to obtain a spherical shape, as figure below.



Figure 9-59. stainless steel inner grid

Step 4:

Choose the base of spherical inner grid

As shown in figure 3-22, there are 4 pins of thickness equals to 1.6mm, in total of 6.4mm. according to that, the inner grid base should have an inner diameter greater than 6.4 mm. according to local market, a stainless pipe of inner diameter of 7 mm and outer diameter of 10 mm, a length of 10 cm is suitable for this project.



Figure 9-60. stainless pipe tube

Step 5:

Fix all components via argon soldering electrical machine.

NOTE: the soldering needs an expert person, and it is more preferable to use a non-electrical argon soldering machine, cause of the complexity and the accuracy needed of the soldering position.



Figure 9-61. argon soldering electrical machine

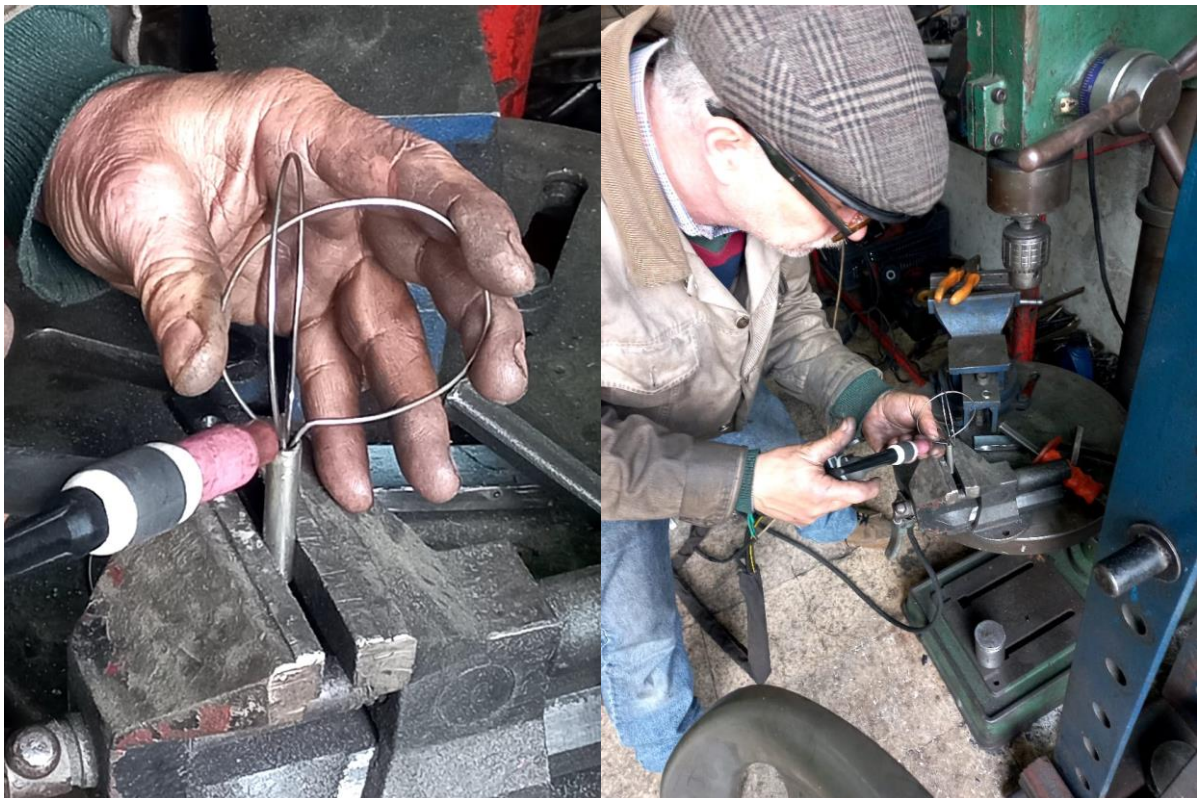
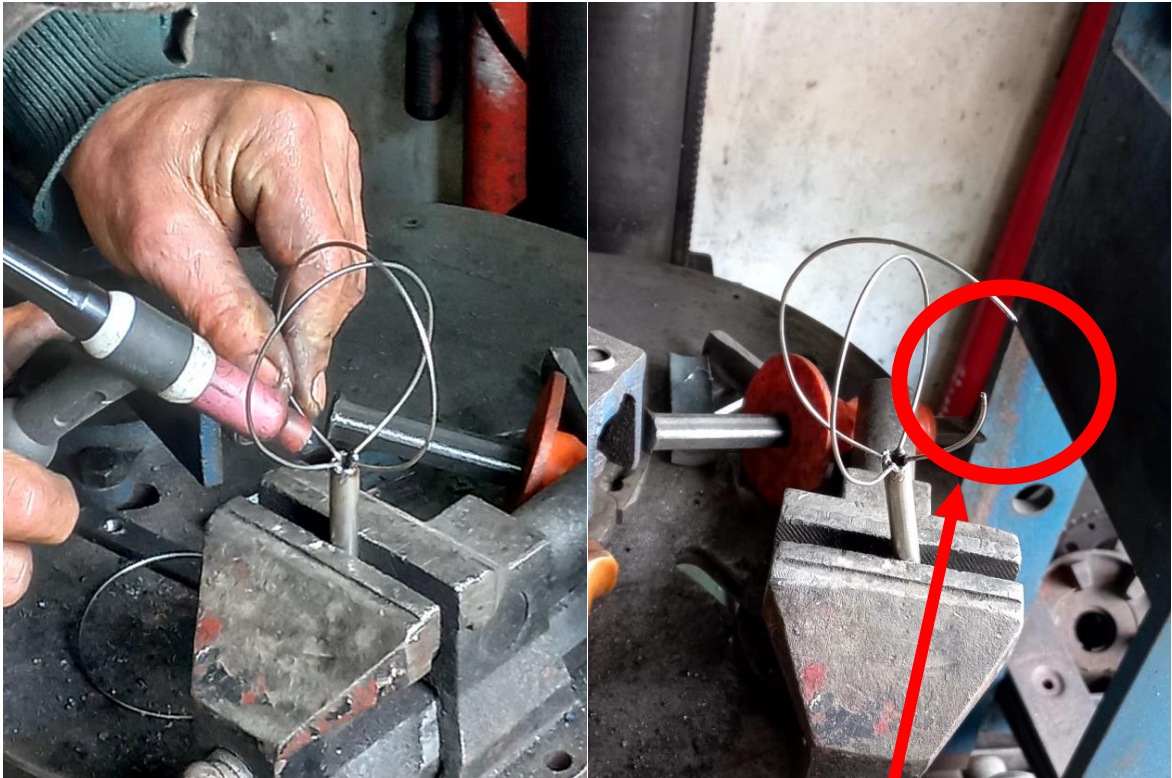
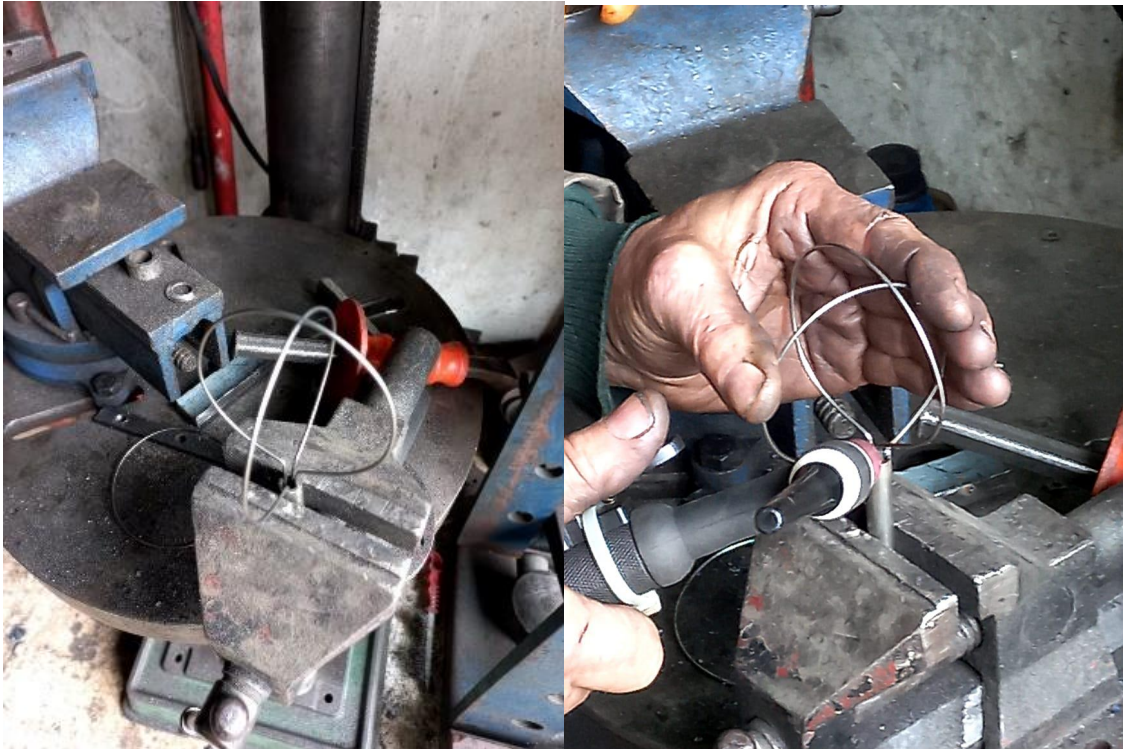


Figure 9-62. inner grid assembling



The wire chopped off cause of high sensitivity of wire

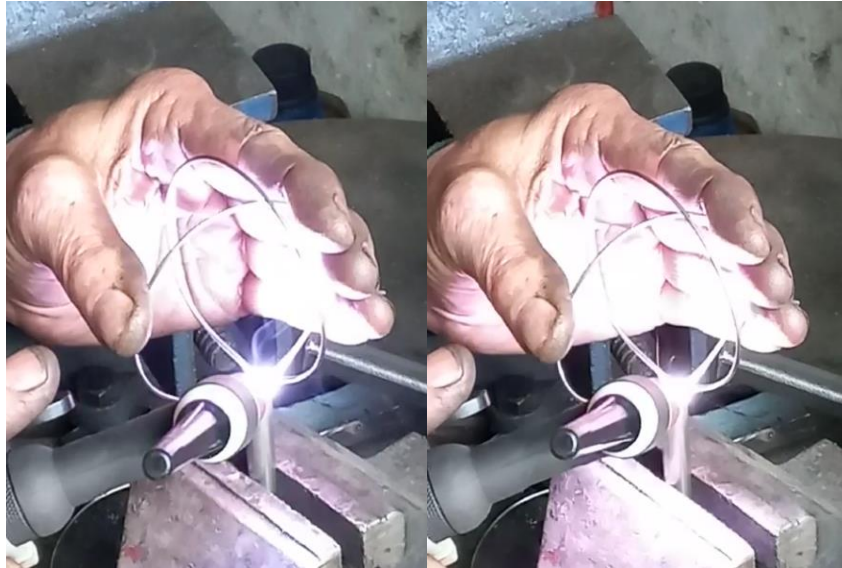


Figure 9-63. Stainless steel Inner Grid argon Soldering

Step 6:

After gathering the stainless sphere with its base, the 2 mm stainless wire has been soldered in other side of stainless pipe (sphere base). the



Figure 9-64. final form of stainless inner grid

9.3.8.4 Power supplies

Ac to Dc converter:

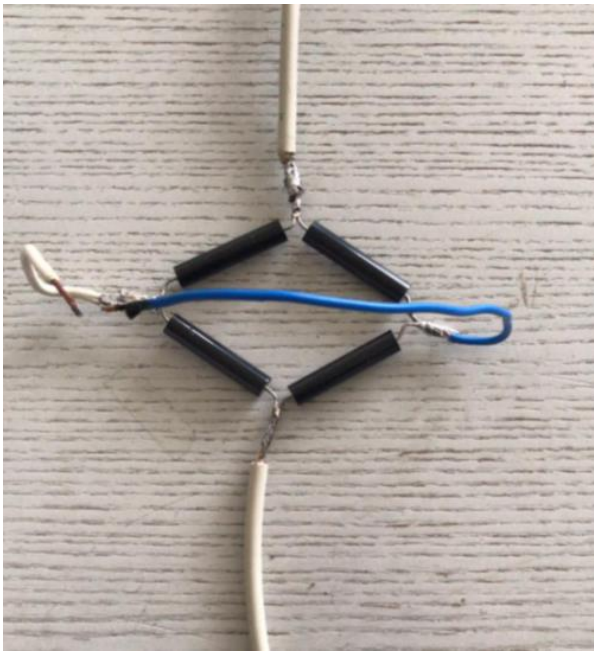
To apply 12kv we use transformer:



This transformer is an AC mode output, to convert to DC mode we use 4 diodes (30KV.0.5A)



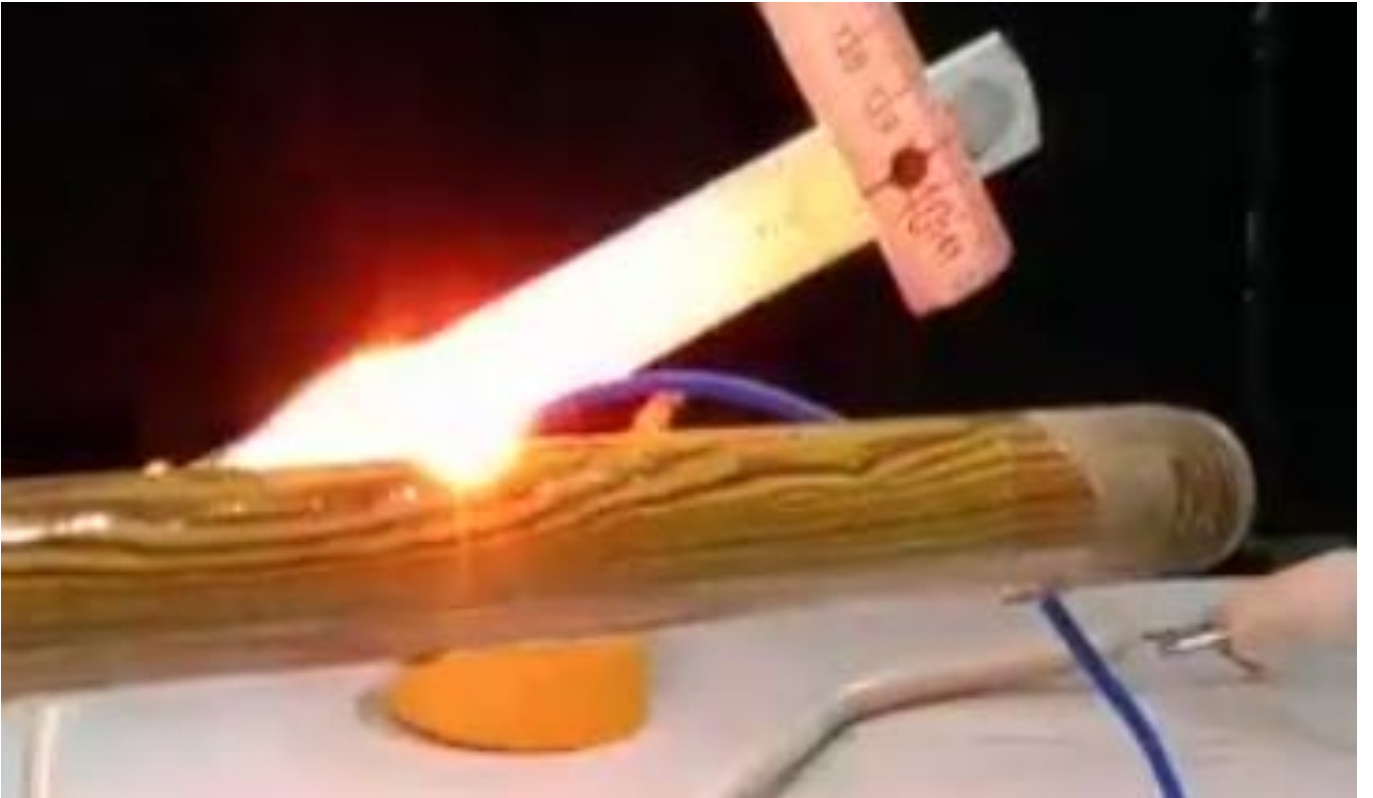








~ 1.3cm a spark length



Cockroft waltan voltage multiplier test

The high voltage transformer has been connected to a voltage multiplier circuit of two stage, which provides an total voltage of 48kv ($2 \times \text{number of stages} \times \text{input volatge}$).

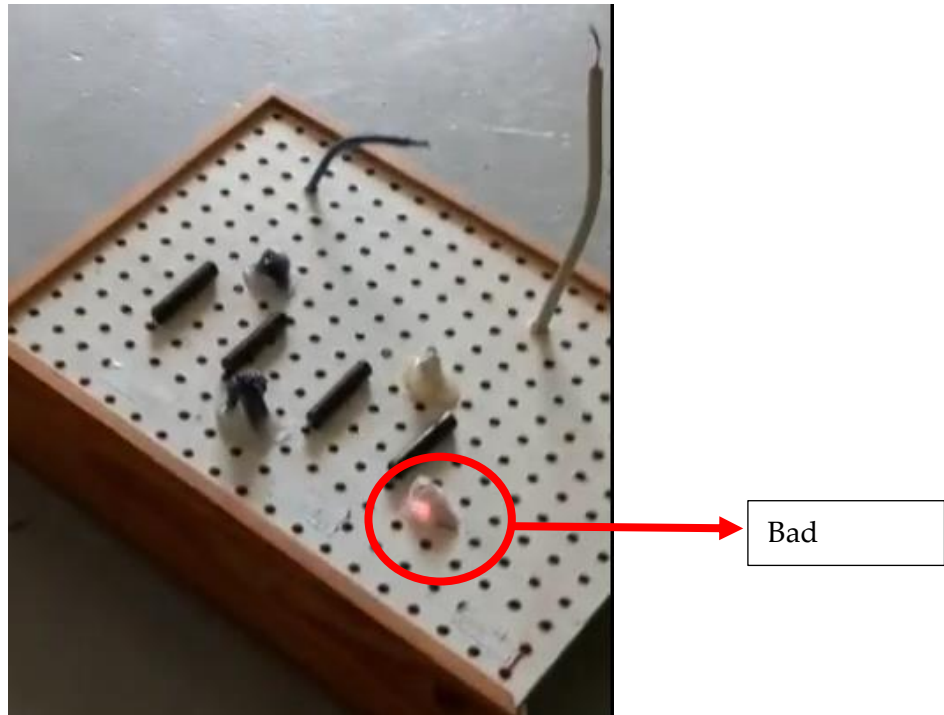


Figure 9-65voltage multiplier test 1

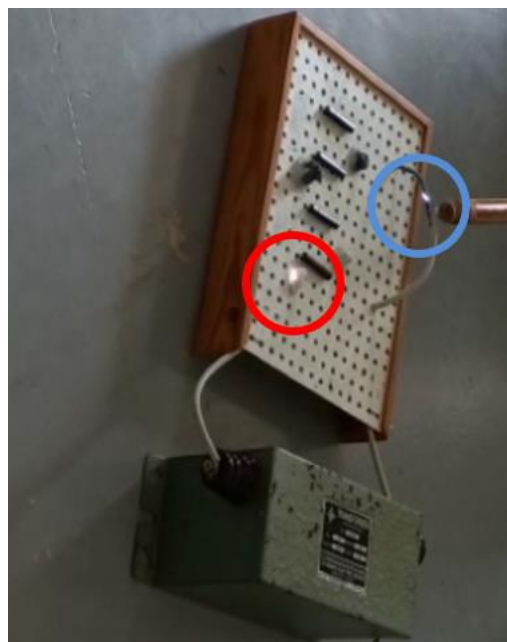


Figure 9-66. voltage multiplier test 2

TEST FAILED

Due to the bas isolation, the voltage jumped form a capacitor pin to another.

Even while, the cathode and anode were close to each other, an electric spark take place in two places, as shown in figure 8-11.

To improve the isolation, the voltage multiplier circuit has been putted in an oil pool.



In this way, voltage multiplier circuit worked correctly.

System Test

The anode side of voltage multiplier has been connected to the chamber. as the red arrow indicates. And the cathode has been connected to the inner grid (the stainless-steel filament), as the orange arrow indicates.



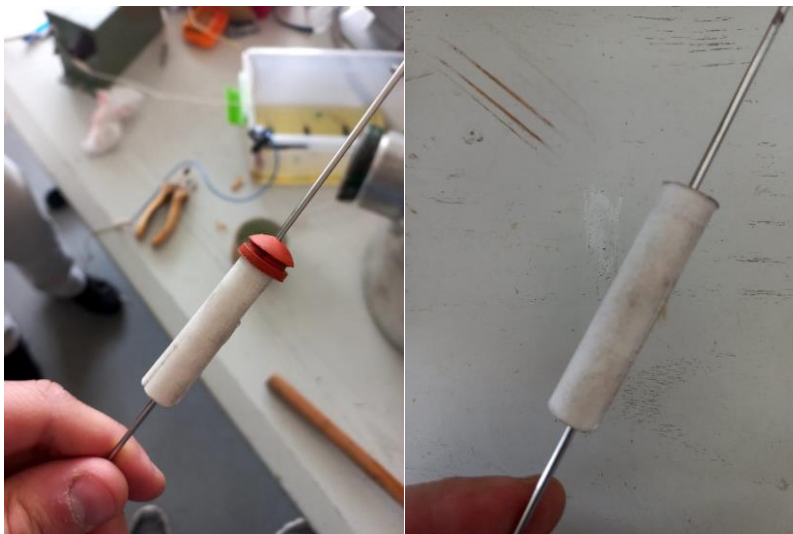
IECF (Inertial Electrostatic Confinement Fusion)

Then, the vacuum pump has been ON.

NOTE: Keep vacuum pump turned ON during the whole procedure.



The following figure illustrates how the cathodes has been isolated from the chamber. The cathode stainless steel has been covered by an TEFLON cylinder, at the nearest place between the cathode rod and chamber, and supported by the red safety valve to cover its hole.



Then, a layer of milted wax has been added on it, for air leakage reason.



The following figure, shows that electric sparks has crossed TEFLON, and other isolation.

BAD ISOLATION





The electric spark milts the TEFLON.

In the figures below, illustrate where sparks take place, plus, the light provided in the chamber







1 stage voltage multiplier test

In this test, a car spark plug has been connected at the negative side of the output voltage multiplier (consisted of 1 stage), in order to compare spark length with older test. In this test, the spark was orange, while its color was near the white color.



Helium

Diffusion pump

Micron gauge

Fuel cell for deteruim

.detiruim oxide 25-100ml

Pump oil

Accesorioes for deteruim

High voltage 60kv 10mA

9.3.10 References

<http://aecenar.com/index.php/downloads/send/3-meae-institute/731-iecfc-prototype-concept-pdf>

https://www.steelss.com/Materials/Stainless-Steels/YB-306_31_804.pdf

<https://www.youtube.com/watch?v=0J6ci3IxUkc>

<https://www.youtube.com/watch?v=CJSaAjMK5w>

<https://www.slideshare.net/ARGHASAHA4/vacuum-chamber-design>

https://www.engineersedge.com/pressure_vessels_menu.shtml

9.4 Open Tasks Status Apr 22 / Nov 23 for IECF

- cathode assembly: 40\$

- ▣ base design
- ▣ equipment purchasing
- ▣ assembling + soldering
- ▣ testing
- ▣ report

- Fuel inlet (D2) 40\$

- ▣ base design
- ▣ equipment purchasing
- ▣ خراطة + soldering

- sensor system (neutron, x-ray...) 40\$

- ▣ x-ray sensor
- ▣ monitoring system
- ▣ pressure sensor
- ▣ assembling + testing

- vacuum system (available or buy defusing pump) 40\$

- ▣ design
- ▣ خراطة + soldering
- ▣ vacuum and diffusion pumps gathering
- ▣ cooling system
- ▣ Testing
- ▣ report

- control system 40\$

- ▣ sensors
- ▣ coding
- ▣ GUI
- ▣ equipment purchasing
- ▣ assembling
- ▣ testing
- ▣ report

- poster 20\$

+ 50\$ on task successfully done

Related Sites/Items on aecenar.com

System Specification

[IAP - IECF](#)

Mechanical Design

[IECF Mechanical Design](#)

Process Control System Spec./Design

[PCS Design](#)

Mechanical Realization

IECF Mechanical Realization

Process Control System Realization
(PLC+GUI)

PCS Implementation

System Test Specification

Test Specification

System Testing

System Testing

<http://fusor.eu/theory.html>

9.5 Neutron Production at FRANZ proton thruster in Frankfurt/Germany

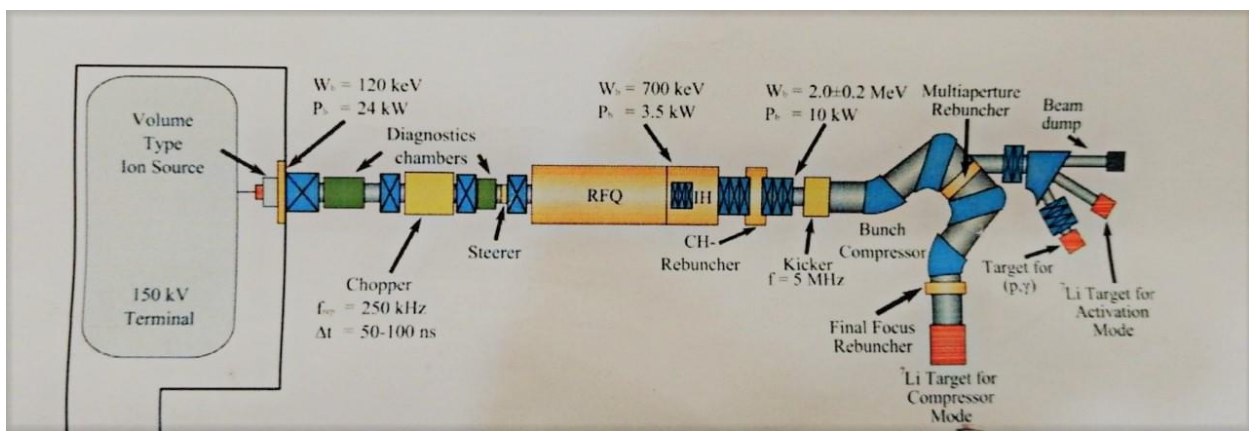


Figure II. 1: Schematic diagram of the FRANZ proton thruster with four target stations for neutron production

The image shown is from a study titled "FRANZ-Frankfurt neutron source," in which an ion source produces a continuous stream of protons. These protons are then accelerated and can follow one of four specific trajectories. Each trajectory offers distinct opportunities for research and various applications. Interactions with different targets and the resulting nuclear reactions provide important information on nuclear structure, isotope creation, neutron production, and other areas of nuclear physics and related scientific disciplines.

10 Mass Spectrometer Concept

بِسْمِ اللَّهِ الرَّحْمَنِ الرَّحِيمِ



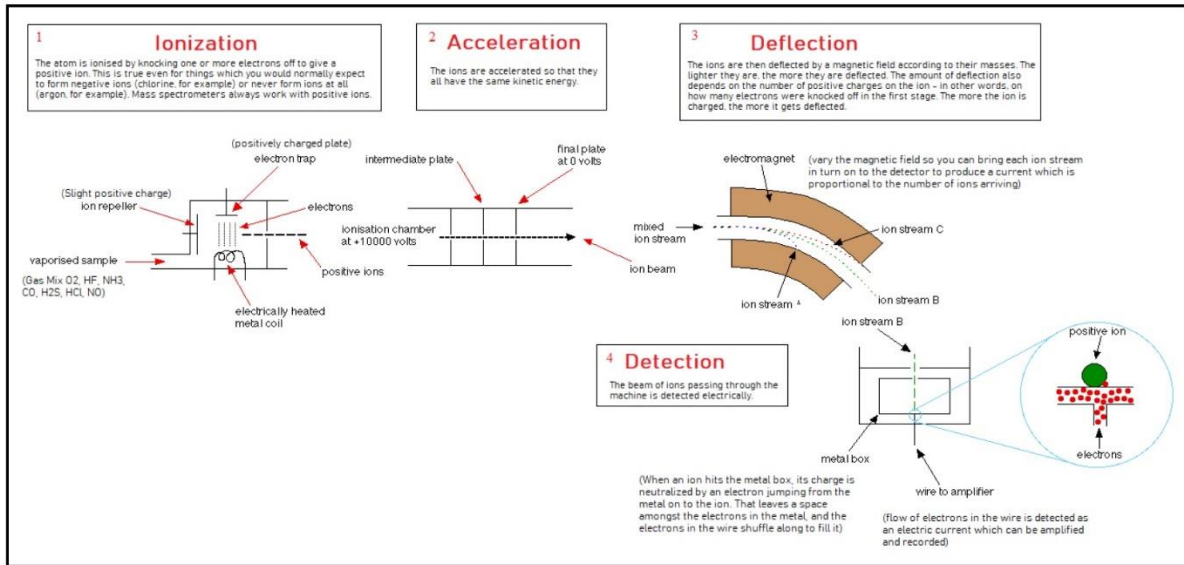
Magnetic Sector Mass Spectrometry

Author: Maryam Abdel-Karim

Last Update: 22.12.21

Principles

Magnetic Mass Spectrometer



Parts

Overview

Parts	Qty	Description
Metal Plate	2	slight positive charge
Slits	4	2 acceleration slits (slight negative potential) 1 Focusing Slit (extremely high voltage) 1 Detecting Slit
* metal coil	1	Tungsten filament
electromagnet	1	strong magnetic field is applied perpendicular to the motional direction of the ions
Vacuum pump	1	10 ⁻⁷ mbar
Faraday cup	1	
Amplifier	1	
Metal Tube	3	2 horizontale tubes 1 curved tube 60°

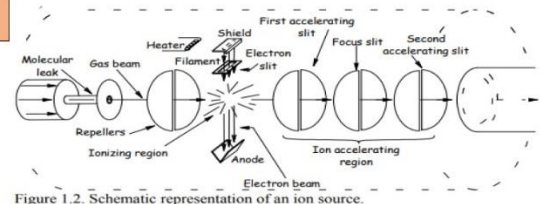


Figure 1.2. Schematic representation of an ion source.

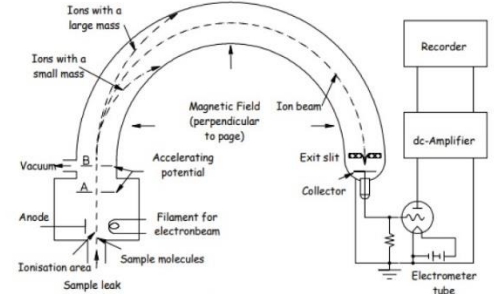
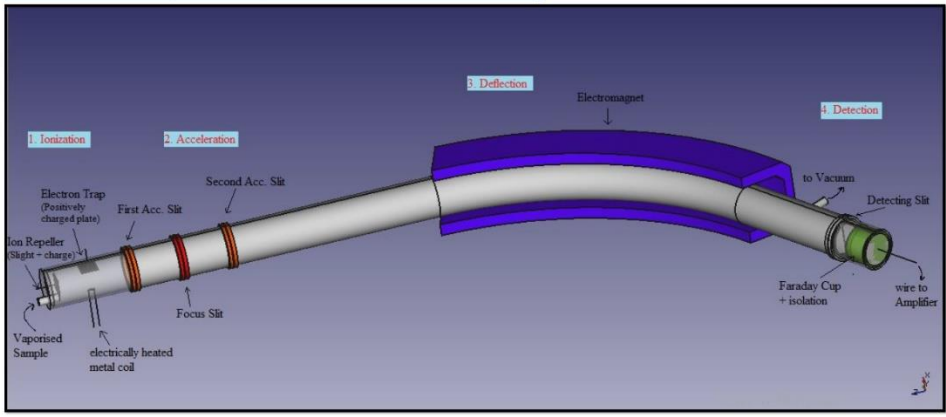


Figure 1.1. Schematic representation of a mass spectrometer



FreeCAD

Maryam Abdel-karim
@AECENAR / July 2021

بِسْمِ اللَّهِ الرَّحْمَنِ الرَّحِيمِ



Magnetic Sector Mass Spectrometry

Author: Maryam Abdel-Karim

Last Update: 22.12.21

Contents

1	Basic Principles.....	391
1.1	Introduction	391
1.2	Measurement principles.....	392
1.3	Sampling.....	393
1.4	The Ion source	393
1.5	Magnetic Mass Analyser	394
1.6	Detectors.....	395
1.6.1	Faraday Cup	396
1.6.2	Electron Multipliers.....	397
1.7	Mass Spectrometry / Gas Chromatography	399
1.8	VG-70S Magnetic Sector Mass Spectrometer	400
2	Our Device.....	401
2.1	Overview	401
2.2	Parts.....	404
2.3	Acceleration Slits	404
2.4	Magnet.....	405
2.5	Detector	405
2.6	FreeCad.....	407

10.1 Basic Principles⁷

10.1.1 Introduction

In mass spectrometry, one generates ions from a sample to be analyzed. These ions are then separated and quantitatively detected. Separation is achieved on the basis of different trajectories of moving ions with different mass/charge (m/z) ratios in electrical and/or magnetic fields.

Though the principles of a modern analytical mass-spectrometer are easily understood this is not necessarily true for the apparatus. A mass spectrometer especially a multi-sector instrument is one of the most complex electronic and mechanical devices one encounters as a

⁷ Mass Spectrometry Peter M. van Galen and Martin C. Feiters Department of Organic Chemistry

chemist. Therefore this means high costs at purchase and maintenance besides a specialized training for the operator(s).

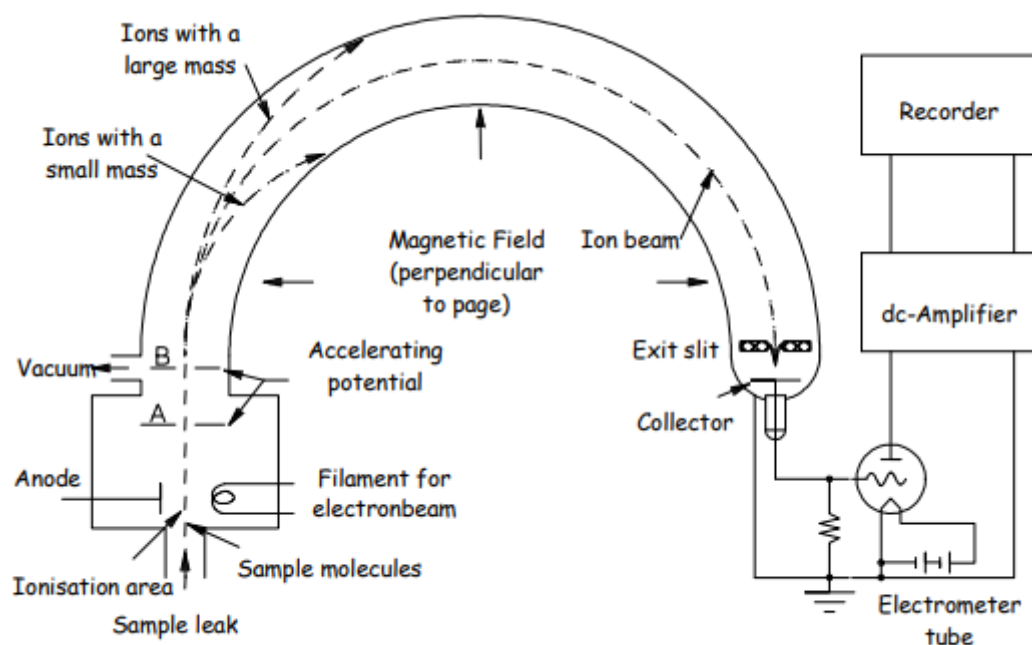


Figure 1.1. Schematic representation of a mass spectrometer

10.1.2 Measurement principles

In Figure 1.1, the essential parts of an analytical mass spectrometer are depicted. Its procedure is as follows:

1. A small amount of a compound, typically one micromole or less is evaporated. The vapor is leaking into the ionization chamber where a pressure is maintained of about 10^{-7} mbar.
2. The vapor molecules are now ionized by an electron-beam. A heated cathode, the filament, produces this beam. Ionization is achieved by inductive effects rather than strict collision. By loss of valence electrons, mainly positive ions are produced.
3. The positive ions are forced out of the ionization chamber by a small positive charge (several Volts) applied to the repeller opposing the exit-slit (A). After the ions have left the ionization chamber, they are accelerated by an electrostatic field ($A > B$) of several hundreds to thousands of volts before they enter the analyzer.
4. The separation of ions takes place in the analyzer, in this example a magnetic sector, at a pressure of about 10^{-8} mbar. A strong magnetic field is applied perpendicular to the motional direction of the ions. The fast moving ions then will follow a circular trajectory, due to the Lorentz acceleration, whose radius is determined by the mass/charge ratio of the ion and the strength of the magnetic field. Ions with different mass/charge ratios are forced through the exit-slit by variation of the accelerating voltage ($A > B$) or by changing the magnetic-field force.

5. After the ions have passed the exit-slit, they collide on a collector-electrode. The resulting current is amplified and registered as a function of the magnetic-field force or the accelerating voltage.

The applicability of mass-spectrometry to the identification of compounds comes from the fact that after the interaction of electrons with a given molecule an excess of energy results in the formation of a wide range of positive ions. The resulting mass distribution is characteristic (a fingerprint) for that given molecule. Here there are certain parallels with IR and NMR. Mass-spectrograms in some ways are easier to interpret because information is presented in terms of masses of structure-components.

10.1.3 Sampling

As already indicated a compound normally is supplied to a mass-spectrometer as a vapor from a reservoir. In that reservoir, the prevailing pressure is about 10 to 20 times as high as in the ionization chamber. In this way, a regular flow of vapor-molecules from the reservoir into the mass spectrometer is achieved. For fluids that boil below about 150C the necessary amount evaporates at room temperature. For less volatile compounds, if they are thermally stable, the reservoir can be heated. If in this way, sampling cannot be achieved one passes onto to direct insertion of the sample.

10.1.4 The Ion source

In Figure 1.2, the scheme of an ionization chamber, ion-source, typically electron impact, is presented. In this chamber in several ways, ions of the compound to be investigated can be produced. The most common way is to bombard vapor-molecules of the sample with electrons of about 70 eV. These electrons are generated by heating a metal wire (filament), commonly used are tungsten or rhenium. A voltage of about 70 Volts (from 5 to 100) accelerates these electrons towards the anode.

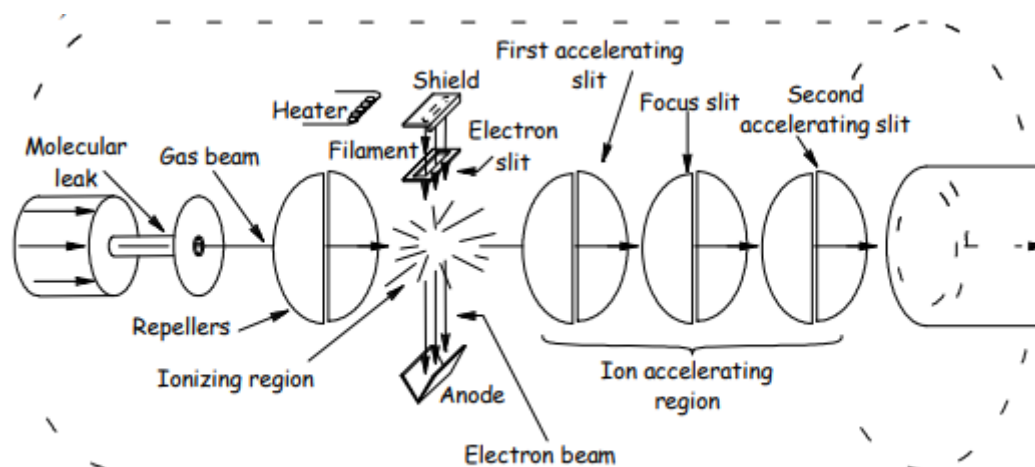


Figure 1.2. Schematic representation of an ion source.

During the bombardment, one or more electron can be removed from the neutral molecule thus producing positively charged molecular radical-ions. Only about one in 10³ of the

molecules present in the source are ionized. The ionization probability differs among substances, but it is found that the cross-section for most molecules is a maximum for electron energies from approximately 50 to 100 eV. Most existing compilations of electron impact spectra are based on spectra recorded with approximately 70 eV electrons, since sensitivity is here close to a maximum and fragmentation is unaffected by small changes in electron energy around this value. During this ionization, the radical-ions on average gain an excess energy enough to break one or more bonds hence producing fragment-ions. In Figure 1.3 the possible fragmentation of a molecule ABCD is presented. It should be stated here that this is a simplified presentation and that in real life a multitude of possible ways to form fragments even via re-arrangement reactions exists. Fragmentation of a molecular radical cation to give a neutral molecule and a new fragment radical cation is also possible.

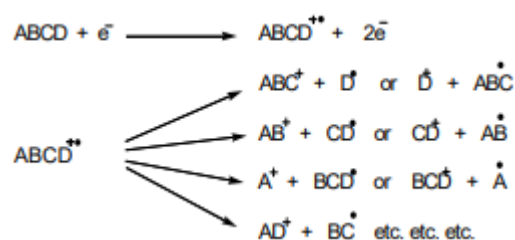


Figure 1.3. Possible fragmentation of a 'molecule' ABCD.

10.1.5 Magnetic Mass Analyser

Consider an ion of mass m and charge q , accelerated in the source by a potential difference V_s . At the source outlet, its kinetic energy is

$$E_k = \frac{mv^2}{2} = qV_s$$

If the magnetic field has a direction that is perpendicular to the velocity of the ion, the latter is submitted to a force F_M as described in Figure 2.48. Its magnitude is given by

$$F_M = qvB$$

The ion follows a circular trajectory with a radius r so that the centrifugal force equilibrates the magnetic force

$$qvB = \frac{mv^2}{r} \quad \text{or} \quad mv = qBr$$

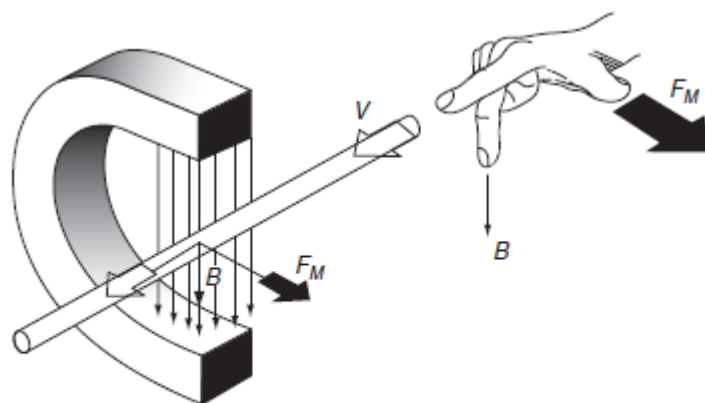


Figure 2.48
Orientation of the magnetic force on a moving ion.

8

Ions at the source outlet leads to

$$mv^2 = 2qV_s$$

Hence

$$\frac{m}{q} = \frac{r^2 B^2}{2V_s}$$

(bending magnet)

10.1.6 Detectors²

The ions pass through the mass analyzer and are then detected and transformed into a usable signal by a detector. Detectors are able to generate from the incident ions an electric current that is proportional to their abundance.

Several types of detectors presently exist. The choice of detector depends on the design of the instrument and the analytical applications that will be performed. Varieties of approaches are used to detect ions. However, detection of ions is always based on their charge, their mass or their velocity. Some detectors (Faraday cup) are based on the measurement of direct charge current that is produced when an ion hits a surface and is neutralized. Others (electron multipliers or electro-optical ion detectors) are based on the kinetic energy transfer of incident ions by collision with a surface that in turn generates secondary electrons, which are further amplified to give an electronic current. Because the number of ions leaving the mass analyzer at a particular instant is generally quite small, significant amplification is often necessary to obtain a usable signal. Indeed, 10 incident ions per second at the detector corresponds to an electric current of 1.6×10^{-18} A. In consequence, subsequent amplification by a conventional

⁸ Mass Spectrometry Principles and Applications Edmond de Hoffmann
Universite Catholique de Louvain, Belgium & Ludwig Institute for Cancer Research, Brussels,
Belgium

electronic amplifier is required. Furthermore, with the exception of Faraday cup and image current detection, the other detectors multiply the intensity of the signal by a cascade effect.

Ion detectors can be divided into two classes. Some detectors are made to count ions of a single mass at a time and therefore they detect the arrival of all ions sequentially at one point (point ion collectors). Others detectors, such as photographic plates, image current detectors or array detectors, have the ability to count multiple masses and detect the arrival of all ions simultaneously along a plane (array collectors). These detectors are effective for most of the applications in mass spectrometry. Nevertheless,

if a detector must ideally be free of any discrimination effect, its efficiency generally decreases when the mass of the ion increases. This induces limitations for the detection of high-mass ions and can compromise a quantitative analysis from these data because the signal decreases exponentially with increasing mass. On the other hand, progress in mass spectrometry has led to the advent of entirely new ionization sources and analyzers that allow the study of analytes with very high molecular mass. For these reasons, the development of new detectors, which eliminate these limitations, is required. These new classes of detectors such as the charge or inductive detector [2] or cryogenic detector [3] are under development. They are based on physical principles that differ from those used for the current detectors and their efficiencies are the same for all the detected ions and are unrelated to their masses. They have near 100% efficiency for very large slow ions.

Indeed, the inductive detector simply produces a signal by inducing a current on a plate generated by a moving charged ion. Its efficiency is related to the charge of the ion but is independent of its mass and its kinetic energy. In the same way, the cryogenic detector is a kinetic energy sensitive calorimetric detector operating at low temperatures.

10.1.6.1 Faraday Cup

A Faraday cup is made of a metal cup or cylinder with a small orifice. It is connected to the ground through a resistor, as illustrated in Figure 3.1. Ions reach the inside of the cylinder and are neutralized by either accepting or donating electrons as they strike the walls. This leads to a current through the resistor. The discharge current is then amplified and detected. It provides a measure of ion abundance.

Because the charge associated with an electron leaving the wall of the detector is identical to the arrival of a positive ion at this detector, secondary electrons that are emitted when an ion strikes the wall of the detector are an important source of errors if they are not suppressed. In consequence, the accuracy of this detector can be improved by preventing the escape of reflected ions and ejected secondary electrons. Various devices have been used to capture ions efficiently and to minimize secondary electron losses. For instance, the cup is coated with carbon because it produces few secondary ions. The shape of the cup and the use of a weak magnetic field prevent also any secondary electrons produced inside to exit.

The disadvantages of this simple and robust detector are its low sensitivity and its slow response time. Indeed, the sensitivity of such detectors is limited by the noise of the amplifiers. Furthermore, this detector is not well adapted to ion currents that are not stable in the same time as during the scanning of the analyzer because of its slow response time. These detectors are nevertheless very precise because the charge on the cylinder is independent of the mass, the speed and the energy of the detected ions. The Faraday cup was widely used in the beginning of mass spectrometry but all the characteristics of this detector mean that it is now generally used in the measurement of highly precise ratios of specific ion species as in isotopic ratio mass spectrometry (IRMS) or in accelerator mass spectrometry (AMS). To obtain a highly accurate ratio in such relative abundance measurements, the intensities of the two stable beams of specific ions are measured simultaneously with two Faraday cups.

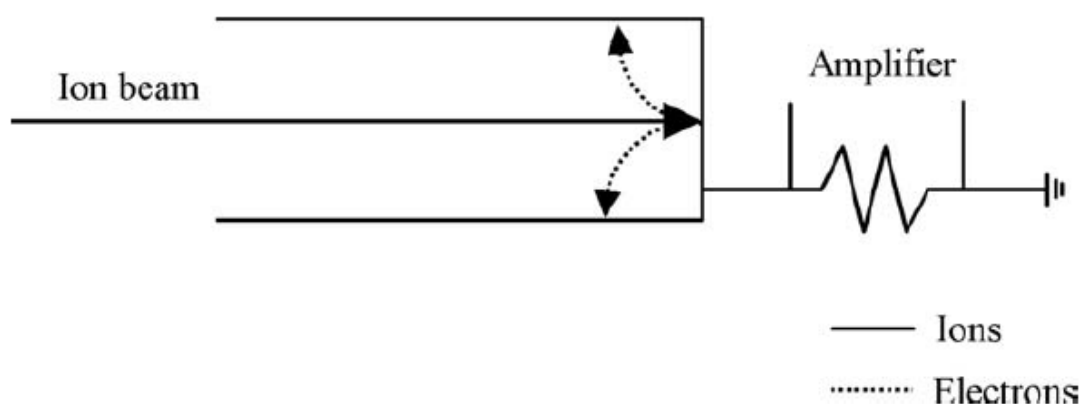


Figure 3.1
Schematic diagram of a Faraday cup.

10.1.6.2 Electron Multipliers

At present (2006), the most widely used ion detector in mass spectrometry is the electron multiplier (EM). In this detector, ions from the analyzer are accelerated to a high velocity in order to enhance detection efficiency. This is achieved by holding an electrode called a conversion dynode at a high potential from ± 3 to ± 30 kV, opposite to the charge on the detected ions. A positive or negative ion striking the conversion dynode causes the emission of several secondary particles. These secondary particles can include positive ions, negative ions, electrons and neutrals. When positive ions strike the negative high-voltage conversion dynode, the secondary particles of interest are negative ions and electrons. When negative ions strike the positive high-voltage conversion dynode, the secondary particles of interest are positive ions. These secondary particles are converted to electrons at the first dynode.

These are then amplified by a cascade effect in the electron multiplier to produce a current. The electron multipliers may be of either the discrete dynode or the continuous dynode type (channeltron, microchannel plate or microsphere plate). The discrete dynode electron multiplier is made up of a series of 12 to 20 dynodes that have good secondary emission

properties. As shown in Figure 3.2, these dynodes are held at decreasing negative potentials by a chain of resistors. The first dynode is held at a high negative potential from -1 to -5 kV, whereas the output of the multiplier remains at ground potential. Secondary particles generated from the conversion dynode strike the first dynode surface causing an emission of secondary electrons. These electrons are then accelerated to the next dynode because it is held at a lower potential. They strike the second dynode causing the emission of more electrons. This process continues as the secondary electrons travel towards the ground potential. Thus, a cascade of electrons is created and the final flow of electrons provides an electric current at the end of the electron multiplier that is then increased by conventional electronic amplification.

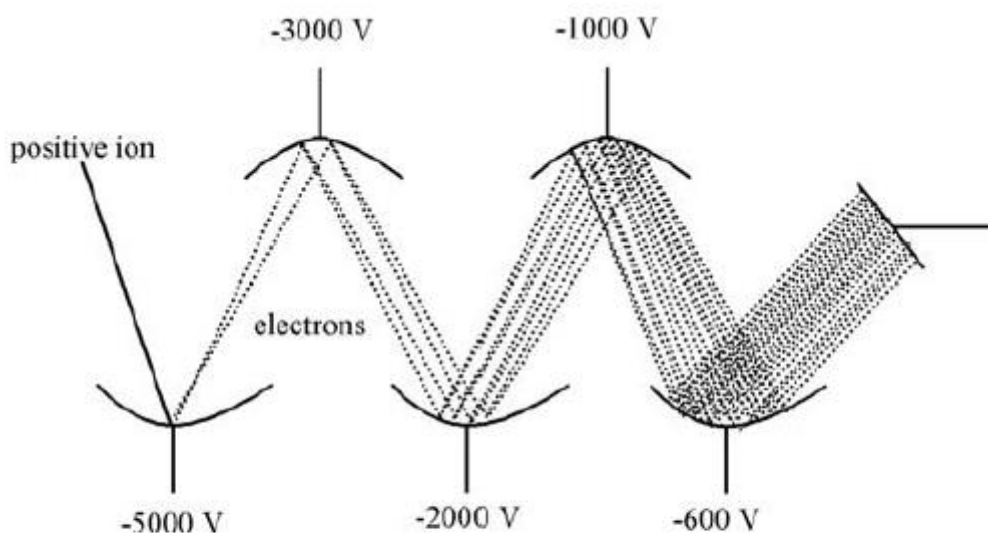


Figure 3.2
Schematic diagram of electron multiplier. The first dynode is a conversion dynode to convert ions into electrons.

There is another design of electron multiplier for which the discrete dynodes are replaced by one continuous dynode. A type of continuous-dynode electron multipliers (CDEM), which is called a channeltron, is made from a lead-doped glass with a curved tube shape that has good secondary emission properties (Figure 3.3). As the walls of the tube have a uniform electric resistance, a voltage applied between the two extremities of the tube will therefore produce a continuous accelerating field along its length. Secondary particles from the conversion dynode collide with the curved inner wall at the detector entrance and produce secondary electrons, which are then accelerated by the field towards the exit of the tube. These electrons pass further into the electron multiplier, again striking the wall, causing the emission of more and more electrons. Thus a cascade of electrons is created and finally a metal anode collects the stream of secondary electrons at the detector exit and the current is measured.

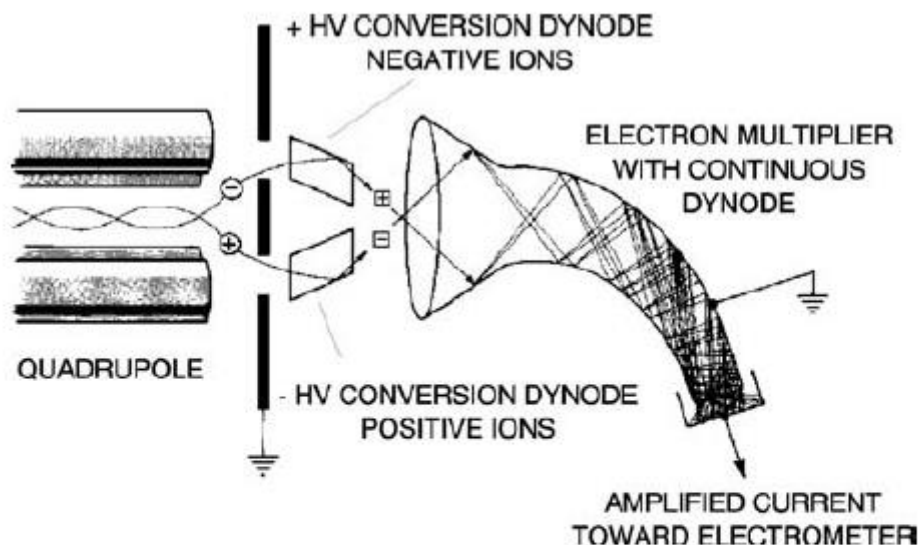


Figure 3.3
 Continuous dynode electron multiplier, also known as the channeltron. ○, incident ions; □, secondary particles. Reproduced (modified) from Finnigan MAT documentation, with permission.

The amplifying power is the product of the conversion factor (number of secondary particles emitted by the conversion dynode for one incoming ion) and the multiplying factor of the continuous dynode electron multiplier. It can reach 10^7 with a wide linear dynamic range (10^4 – 10^6). Their lifetime is limited to 1 or 2 years because of surface contamination from the ions or from a relatively poor vacuum. Their high amplification and their fast response time allow their use with rapid scanning of the analyzer. The conversion factor is highly dependent on the impact velocity of the detected ions and on their nature (mass, charge and structure), so these detectors are not as precise as Faraday cups. Since the detection efficiency on all electron multipliers is highly dependent on ion velocity, they are characterized by the mass discrimination effect for ions with constant energy. Because of their slower velocity, large ions produce fewer secondary electrons and thus the efficiency decreases when the mass of the ion increases. However, as already mentioned, the conversion dynodes at high voltages reduce the mass discrimination effect and serve to increase signal intensity and therefore sensitivity because they accelerate ions to a high velocity in order to enhance detection efficiency. Conversion dynodes are thus very useful for detecting high-mass ions, especially with analyzers delivering ions at low kinetic energy, such as quadrupoles or ion traps.

10.1.7 Mass Spectrometry / Gas Chromatography

In order to analyse a complex mixture, for example natural products, a separation technique – gas chromatography (GC), liquid chromatography (LC) or capillary electrophoresis (CE) – is coupled with the mass spectrometer. The separated products must be introduced one after the other into the spectrometer, either in the gaseous state for GC/MS or in solution for LC/MS

and CE/MS. This can occur in two ways: the eluting compound is collected and analysed off-line; or the chromatograph is connected directly to the mass spectrometer and the mass spectra are acquired while the compounds of the mixture are eluted. The latter method operates on-line.

10.1.8 VG-70S Magnetic Sector Mass Spectrometer

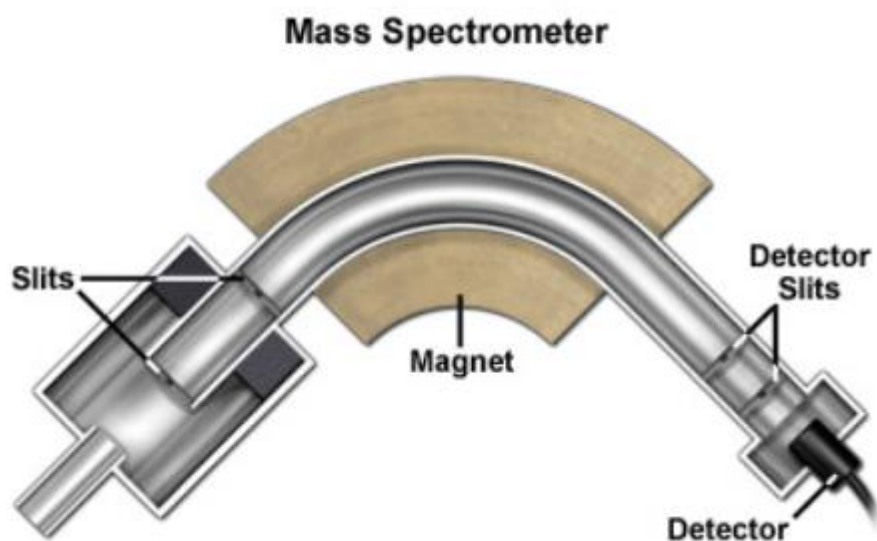
Check this magnetic mass spectrometer at JHONS HOPKINS Krieger school of arts and sciences

<https://sites.krieger.jhu.edu/mass-spec/facility-instrumentation/vg-70s-magnetic-sector-mass-spectrometer/>

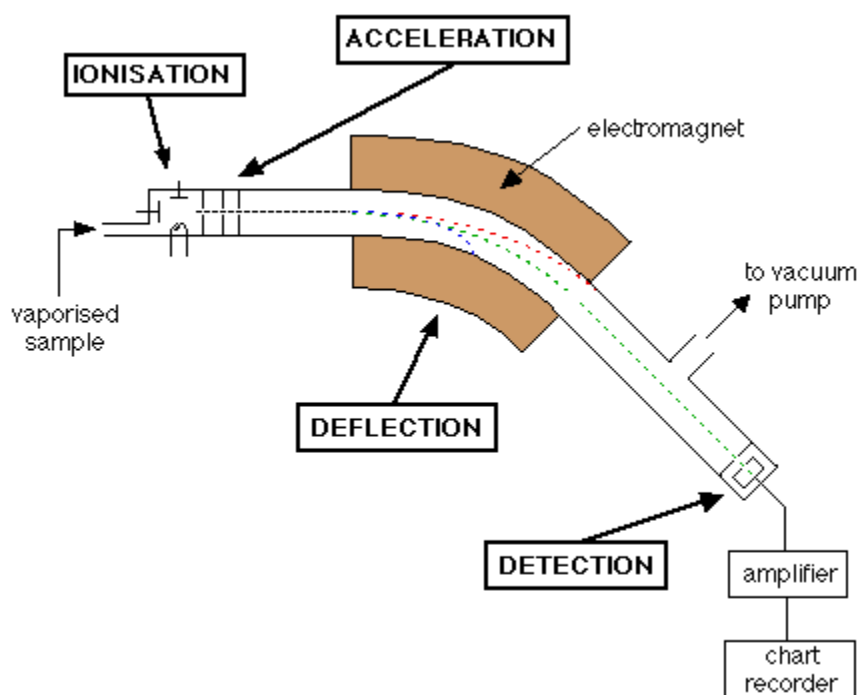


10.2 Our Device

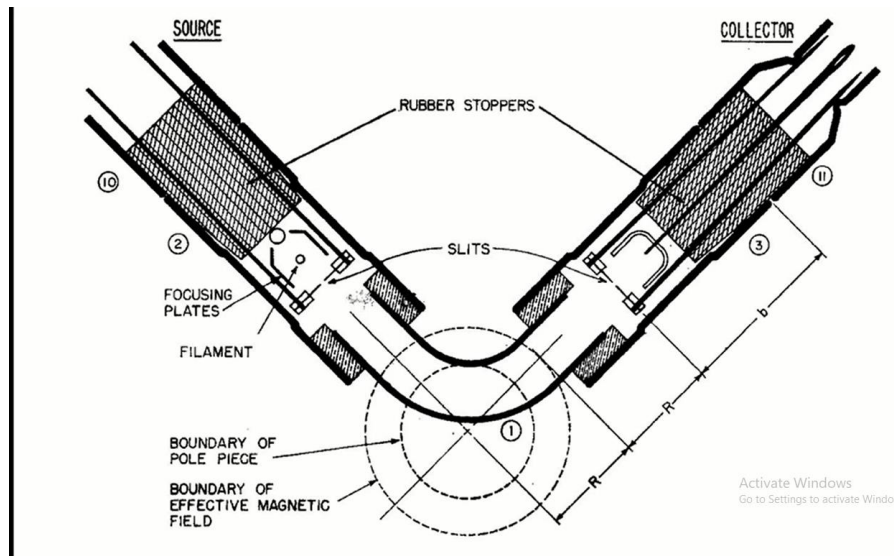
10.2.1 Overview



<https://nationalmaglab.org/education/magnet-academy/learn-the-basics/stories/mass-spectrometry>



[https://chem.libretexts.org/Bookshelves/Analytical_Chemistry/Supplemental Modules \(Analytical Chemistry\)/Instrumental Analysis/Mass Spectrometry/How the Mass Spectrometer Works](https://chem.libretexts.org/Bookshelves/Analytical_Chemistry/Supplemental_Modules_(Analytical_Chemistry)/Instrumental_Analysis/Mass_Spectrometry/How_the_Mass_Spectrometer_Works)



https://www.youtube.com/watch?v=nIKhUizkXxA&ab_channel=AppliedScience

1 Ionization

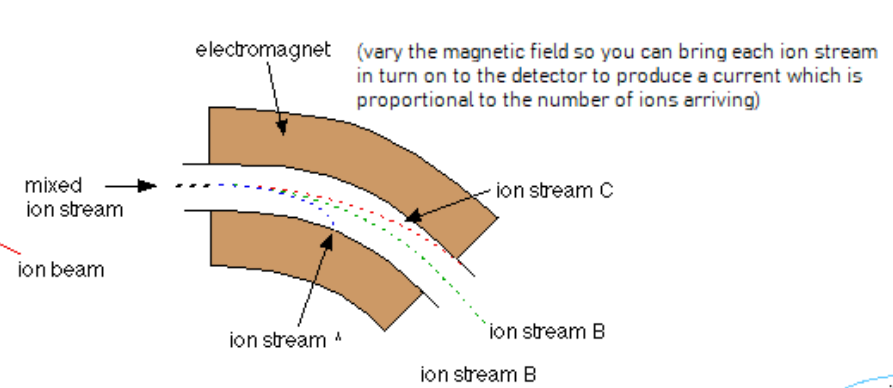
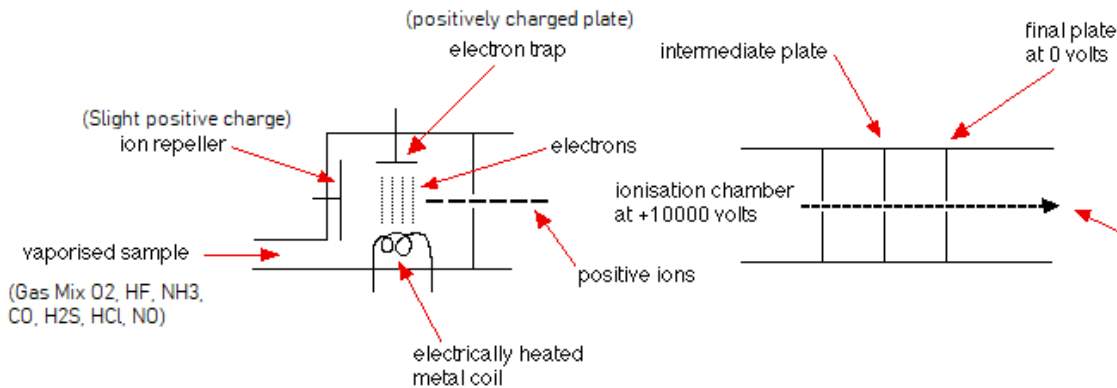
The atom is ionised by knocking one or more electrons off to give a positive ion. This is true even for things which you would normally expect to form negative ions (chlorine, for example) or never form ions at all (argon, for example). Mass spectrometers always work with positive ions.

2 Acceleration

The ions are accelerated so that they all have the same kinetic energy.

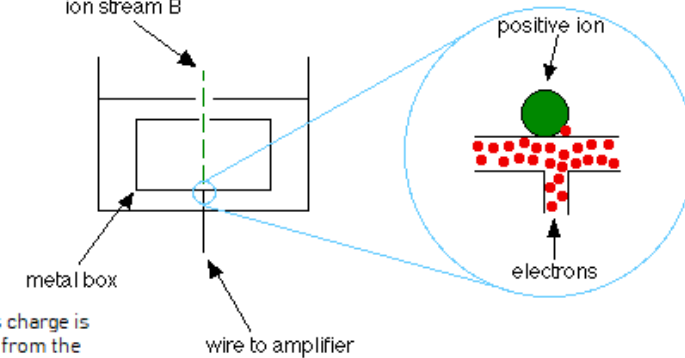
3 Deflection

The ions are then deflected by a magnetic field according to their masses. The lighter they are, the more they are deflected. The amount of deflection also depends on the number of positive charges on the ion - in other words, on how many electrons were knocked off in the first stage. The more the ion is charged, the more it gets deflected.



4 Detection

The beam of ions passing through the machine is detected electrically.



(When an ion hits the metal box, its charge is neutralized by an electron jumping from the metal on to the ion. That leaves a space amongst the electrons in the metal, and the electrons in the wire shuffle along to fill it)

(flow of electrons in the wire is detected as an electric current which can be amplified and recorded)

10.2.2 Parts

Parts	Qty	Description
Metal Plate	2	slight positive charge
Slits	4	2 acceleration slits (slight negative potential) 1 Focusing Slit (extremely high voltage) 1 Detecting Slit
* metal coil	1	Tungsten filament
electromagnet	1	strong magnetic field is applied perpendicular to the motional direction of the ions
Vacuum pump	1	10^{-7} mbar
Faraday cup	1	
Amplifier	1	
Metal Tube	3	2 horizontale tubes 1 curved tube 60°



10.2.3 Acceleration Slits

The simplest way to accelerate ions is to place them between a set of charged parallel plates. The ions are repelled by one plate, attracted to the other, and if we cut a hole in the second plate, the ions emerge with a kinetic energy determined by the potential difference between the plates.

$$K = q | \Delta V |$$

Definition of acceleration slits

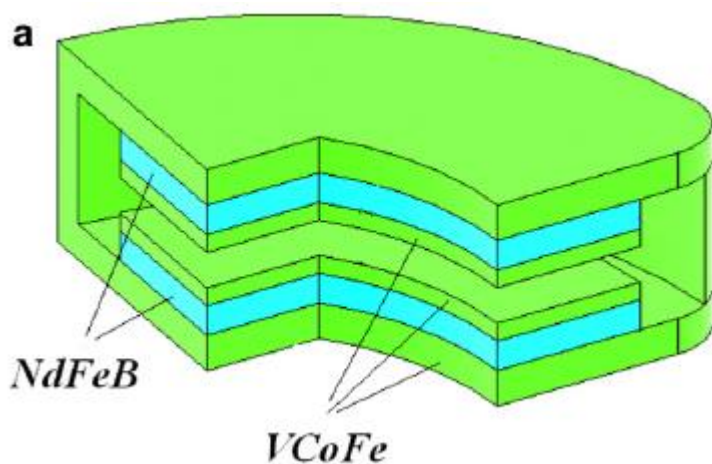
Positively charged ions produced in an ionization chamber of a mass spectrometer are passed into the analyzer by the acceleration slits. Generally, two acceleration slits are used; one has a slight negative potential with respect to the ionization chamber in order to attract the positive ions, and the other slit has an extremely high voltage, which accelerates that ions to up to half the speed of light.

How can I give a metal surface a static negative or positive charge?

By adding or subtracting electrons.

Here is one approach. Rest the object on foam polystyrene sheet (very high resistivity). Charge a capacitor with several hundred volts DC. Ground the cap's negative lead. Touch the positive lead to the metal plate. This extracts electrons. Recharge the capacitor. Ground the cap's positive lead. Touch the negative cap lead to the plate. This adds electrons.

10.2.4 Magnet



Iron Cobalt Vanadium Alloy (VCoFe)

A neodymium magnet (also known as *NdFeB*, NIB or Neo magnet) is the most widely used type of rare-earth magnet.⁹

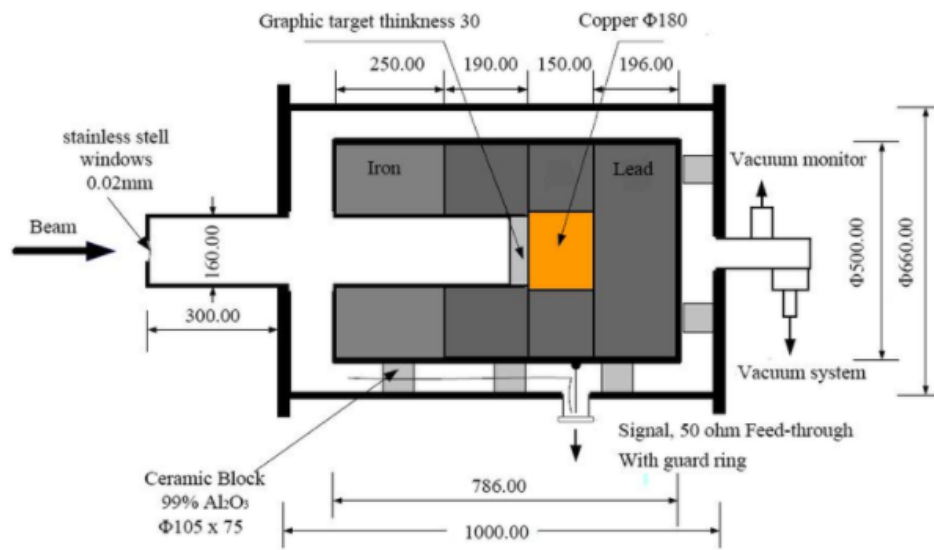
10.2.5 Detector

Dyanode detector



<https://www.photonis.com/products/discrete-dynode-detector>

⁹ Development of a miniature magnetic sector mass spectrometer Detian Li, Meiru Guo, Yuhua Xiao*, Yide Zhao, Liang Wang

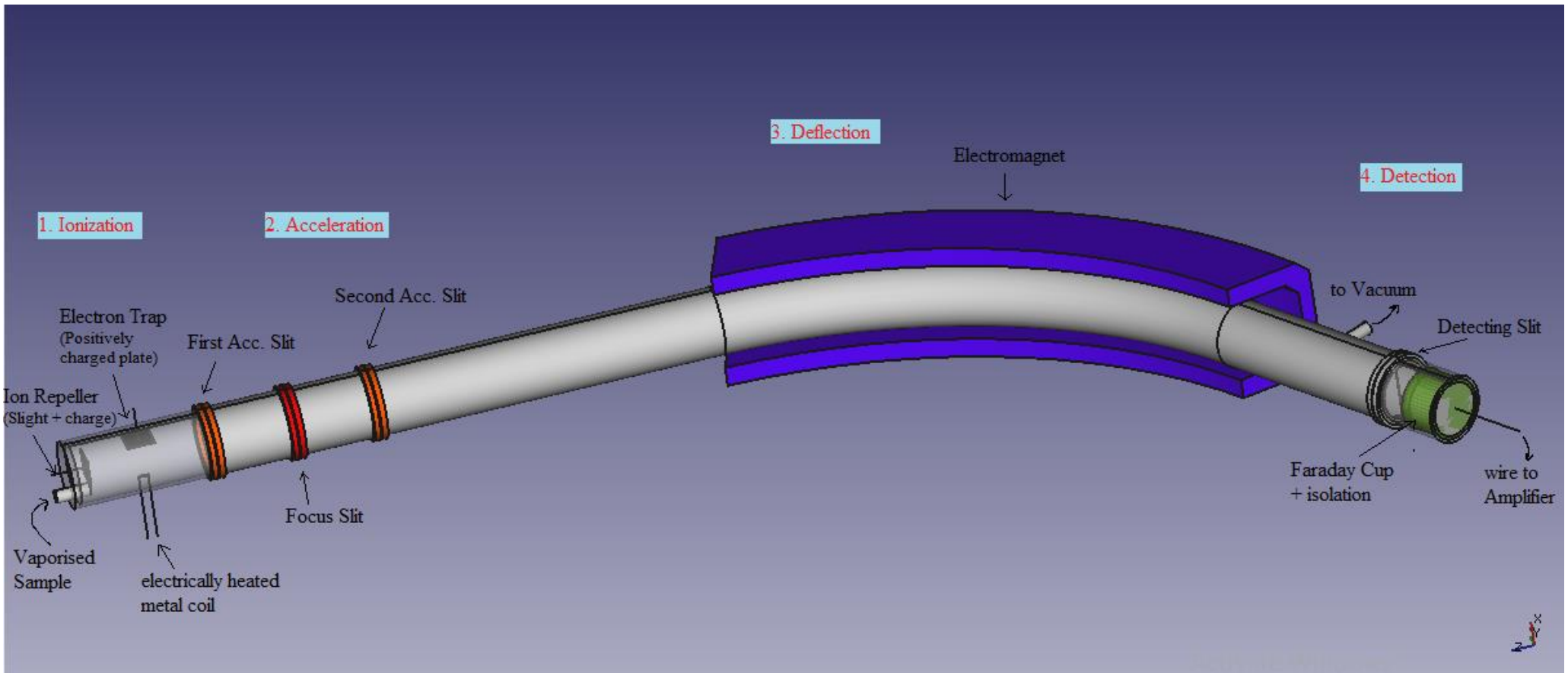


design structure of Faraday Cup at E2 line

https://www.researchgate.net/figure/The-design-structure-of-Faraday-Cup-at-E2-line_fig1_283762179

10.2.6

10.2.7 FreeCad



MassSpectro.FCStd

11 Mass Spectrometer Detector¹⁰

Mass spectrometer detector

Electron multiplier

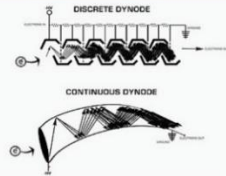
Various approaches are used to detect ions. However, the detection of ions is always based on their charge, mass or velocity. Electron multipliers are perhaps the most common detectors in modern mass spectrometers due to their exceptionally high gain and low noise. A single ion entering the front of the multiplier can result in upwards of one million electrons exiting the back.

Principle of operation

The operation of electron multipliers is fundamentally based on the concepts of "dynodes" and "secondary emission". A "dynode" is simply an electrode in vacuum that emits electrons when an ion or electron with sufficient kinetic energy slams into it. This process of emitting electrons is termed "secondary emission". Electron multipliers essentially string together a series of dynodes so that the process of secondary emission happens repeatedly, amplifying the number of electrons exponentially at each step along the way. There are two common geometries for electron multiplier: the "continuous dynode" and the "discrete dynode"...

Discrete dynode

The "discrete dynode" geometry utilizes a series of dynodes that are chained together by resistors. A relatively large negative voltage is applied to the "front" dynode where the ions enter the detector. Meanwhile, the "back" dynode is held at ground. The voltage difference between the front and back of the dynode chain along with the resistors between each dynode results in a gradual voltage drop down the line. Each dynode is typically 100-200V more positive (less negative) than the preceding dynode.



Continuous dynode

The "continuous dynode" geometry has very similar characteristics to the discrete dynode geometry, with a high negative voltage at the front end and ground at the back end. As with the discrete geometry, an ion is accelerated into the front of the dynode by the high negative potential. The chief difference is that the continuous dynode geometry has one continuous electrode that has sufficient resistance to make the voltage gradually drop from front to back.

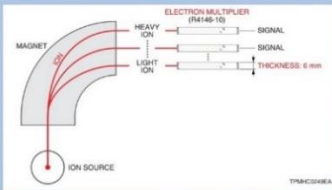
Hamamatsu electron multipliers

Electron multipliers are mainly used as positive/negative ion detectors. They are also useful for detecting and measuring vacuum UV rays and soft X-rays. Hamamatsu electron multipliers have a high gain (multiplication factor) yet low dark current, allowing operation in photon counting mode to detect and measure extremely small incoming particles and their energy. This means our Hamamatsu electron multipliers are ideal for electron spectroscopy, vacuum UV spectroscopy such as ESCA (electron spectroscopy for chemical analysis) and Auger electron spectroscopy as well as mass spectroscopy and field-ion microscopy.

Type No.	Structure	Dynode		Characteristics							
		Number of stages	Material	Input aperture size (mm)	Supply voltage (V)	Gain Typ.	Rise time (ns)	Dark current Typ. (pA)	Total resistance (MΩ)	Detection ion polarity	Anode to all other electrode capacitance (pF)
R4146-10	Linear-focused	18	Cu-BeO	8 × 1	-1800	1 × 10 ⁶	3.5	0.1	21	Positive	4.0
R6985-80	Box-and-line	19	Al ₂ O ₃	φ11	-1900	1 × 10 ⁶	4.5	0.1	17.15	Positive	1.8
R5811	Circular-edge	13	Al ₂ O ₃	φ3	-1500	1 × 10 ⁶	1.6	0.1	13	Positive	0.8
R2362	Coarse mesh	23	Cu-BeO	φ20	-2700	1 × 10 ⁶	3.5	1	23	Positive	23
R5150-10	Box-and-line	17	Cu-BeO	φ8	-1800	1 × 10 ⁶	1.7	0.1	19.5	Positive	4.0
R1474	Box-and-grid	16	Cu-BeO	8 × 6	-1500	1 × 10 ⁶	11.8	0.1	16	Positive	5.0
R5115	Box-and-grid	19	Cu-BeO	8 × 6	-1500	1 × 10 ⁶	11.8	0.1	19	Positive	4.0
R596	Box-and-grid	16	Cu-BeO	12 × 10	-1500	2 × 10 ⁶	12.6	0.1	16	Positive	9.0
R595	Box-and-grid	20	Cu-BeO	12 × 10	-1500	4 × 10 ⁶	14.4	0.1	20	Positive	9.0

We choose R4146-10 :

The linear-focused type exhibits fast time response and has a thin configuration that is easy to design and use. Because of these advantages the linear-focused type is frequently used in magnetic field deflection mass spectrometers where multiple detector need to be installed side-by-side.



Maximum ratings

Operating gain	Anode to first dynode voltage (V)	Conversion voltage (kV)	Faraday cup voltage (V)	Average anode current (μA)	Bake-out temperature 1.10 ⁻¹ Pa (°C)	Operating vacuum level (Pa)
1 × 10 ⁸	2500	—	—	10	350	1 × 10 ⁻²
1 × 10 ⁸	3000	±10 ^②	—	10	350	1 × 10 ⁻²
5 × 10 ⁶	2000	—	-200	10	350	1 × 10 ⁻²
1 × 10 ⁸	4000	—	—	10	350	1 × 10 ⁻²
1 × 10 ⁸	3500	—	—	10	350	1 × 10 ⁻²
1 × 10 ⁸	4000	—	-100	10	350	1 × 10 ⁻²
1 × 10 ⁸	4000	—	-100	10	350	1 × 10 ⁻²
1 × 10 ⁸	4000	—	—	10	350	1 × 10 ⁻²
1 × 10 ⁸	5000	—	—	10	350	1 × 10 ⁻²

③ Do not perform baking on the R6985-80.
④ Use a supply voltage that does not cause the operating gain to exceed its maximum rating.

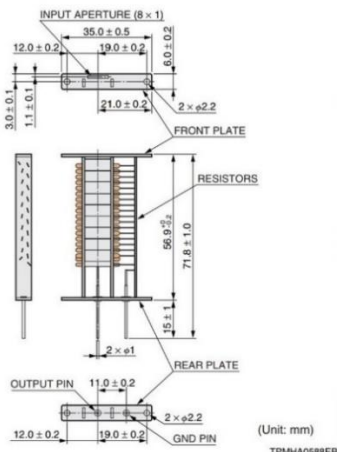
R4146-10

Features

- Thin configuration
- Can be stacked side-by-side

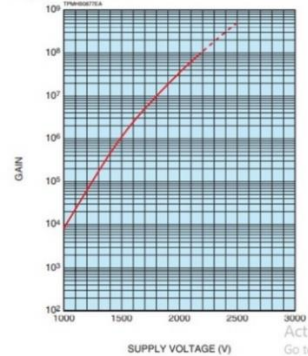
Mounting plate potential

- Front plate: -HV
- Rear plate: GND



Note: we need 4 pieces of this detector for our project.

Figure 1: Typical Gain



Note:

The vacuum level affects the generation of noise in an electron multiplier. The noise is usually low at a vacuum level for example of 10⁻⁴ Pa, but increases as the vacuum level drops for example to 0.1 Pa. We recommend operating the electron multiplier at a vacuum level higher than about 10⁻⁴ Pa although the level may depend on the operating gain and the type of detector.

¹⁰ See <https://aecenar.com/index.php/institutes/institute-for-astronomy-and-astrophysics/physics-lab/flue-gas-analysis-with-mass-spectrometry/mass-spectrometry-detector>

Mass Spectrometer Detector

Mass spectrometer sensor

Introduction:

A mass spectrometer is a device that can detect charged particles such as ions, protons, and electrons by separating them according to their mass-to-charge ratio using a magnetic field. Followed by a detector that receives these particles and transforms them into an electric signal. This signal is amplified by an amplifier circuit so that it can be recorded.

Objective:

To make a mass spectrometer to identify the composition of any gas for these molecules: HCl, HF, SO₂, and Hg, with their respective quantities.

Structure and roles

1. Analyzer:

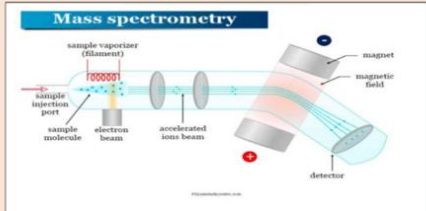


Fig. 1.1: The analyzer of the spectrometer

The analyzer is one of the three main parts of the mass spectrometer that has **three essential stages**:

Ionization, Acceleration, and Separation.

- **Ionization:** the sample of gas that needs a study is injected into a chamber that has a heat filament and electron gun that allow the gas to become charged (ionized).

- **Acceleration:** the sample is then accelerated using a magnetic field due to its charge.

- **Separation:** the accelerated ions go through another magnetic field parallel to their direction but this time to change their direction, since all ions have the same charge, they will experience the same moving force. However, due to the different masses of each ion, they will move in a different directory i.e., the heavier the ion the longer the arc will take.

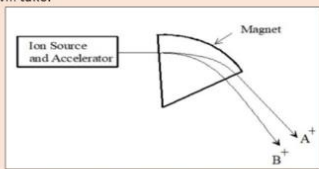


Fig.1.2: ion A+ and B+ separated using a magnet.

For the wanted sample:

1.4 Measurement of physical quantities

We have $R = \frac{1}{4\pi\epsilon_0} \frac{q_1 q_2}{r^2}$, and $v = \frac{1}{4\pi\epsilon_0} \frac{q_1 q_2}{r^2}$. For a magnetic field $B = 20 \times 10^{-3}$ T, and a potential difference $U = 300$ v, we obtain the values of the radius and the velocity as follow:

Gas type	Masses m (kg)	Radius R (m)	Velocity v (cm/s)
HCl	5.76×10^{-26}	0.073	408
HF	3.2×10^{-26}	0.056	547
SO ₂	10.24×10^{-26}	0.098	306
Hg	32×10^{-26}	0.173	173

3. Amplification circuit:

The electric charge is a property that is constant for all electrons and protons. In the mass spectrometer currently being worked on, the particles of interest are ionized so that all molecules become ions with one less electron which makes them positively charged thus for large ion currents, 1 ion (+1) has: 1.6×10^{-19} Coulombs and that means 1 ion/second is 1.6×10^{-19} A or 1.6×10^{-4} fA.

Even with the ability to collect charge efficiently, the need to amplify the current input of Faraday's cups so it can be measured and recorded vital.

In that sense, an amplification circuit is introduced to solve these problems.

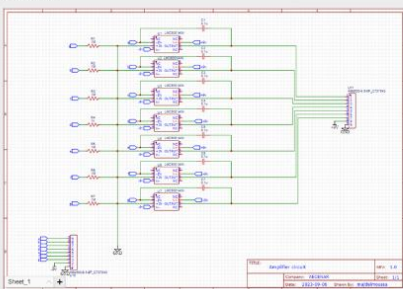


Fig.4: Schematic of the amplifier circuit for faraday's cup

2. Detector:

The detector is the second main part of the mass spectrometer that allows us to know the location of ions when they exit the analyzer and thus know their masses. There are several types of detectors out there, but it was chosen to use "Faraday's Cup" as a detector.

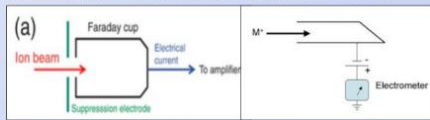


Fig. 2.1: Faraday's Cup

The Faraday's cup works based on the principles of electrochemistry and the conservation of electric charge.

Electrochemical process is the core principle behind Faraday's cup. When charged particles, such as ions or electrons, encounter a conductive surface (the collection surface of the cup), they can transfer their charge to that surface. This transfer of charge is facilitated by an electrochemical reaction between the charged particles and the conductive material of the cup's electrode.

This reaction creates a potential difference between the electrodes and the current integrator circuit which induce electric current that flows through an external circuit connected to the cup. This current is proportional to the number of charged particles that have been collected by the cup. By measuring this electric current, the number of charged particles that have impacted the cup's surface.

When the ions collide with the plate it induces a current equal to its charge, therefore the more ions the higher the current and thus the bigger the signal allowing us to know the quantity.

When designing a Faraday's Cup, a few considerations should be considered:

1. Material Selection:

A conductive material with high thermal and electrical conductivity. Commonly used materials are stainless steel and brass.

2. Cup Geometry:

The cup's geometry is critical for efficient ion collection and minimizing losses due to scattering.

3. Aperture Size:

The aperture size should be optimized to allow ions of interest to pass through while minimizing the passage of unwanted neutral particles or larger molecular clusters.

4. Electric Isolation:

The Cup must be electrically isolated from the analyzer to prevent interference with the magnetic fields used in it.

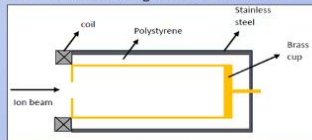


Fig.2.2: model #1 of Faraday's cup module #1

In the above fig., the brass cup is the collector; Polystyrene is not only an electric insulator, but also a shield against outside noise. The stainless steel is a protective casing, and finally, the coil, when electrified is going to induce a magnetic field that will prevent unwanted charged particles from interfering with the signal (protecting from potential inside noise).

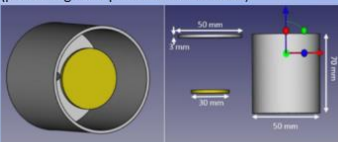


Fig.3: Module 2 made and ready to test.

As it is observed, each electrode signal of the faraday's cup must be amplified individually as it is too low and vulnerable to noise, thus the use of a mechanism that transfers the signal to the amplifier in series format instead of parallel (like a multiplexer) is unlikely due to noise.

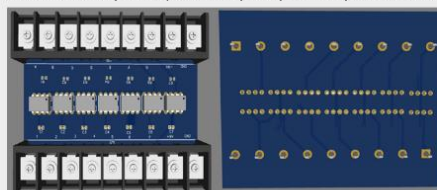


Fig.5: The front-back image of the amplifier circuit (3D)

About the LMC 6001 Op-Amp:

Input bias current (max) = 25 fA

Vos (offset voltage at 25°C) (max) = 0.35 mV

Total supply voltage (+5 V = 5, ±5 V = 10) (max) = 15.5 V

Total supply voltage (+5 V = 5, ±5 V = 10) (min) = 4.5 V

Large signal voltage gain (A) = 1400V/mV or 1400000 times the input.

So, if the input is 1nV the output will be 1.4 mV.

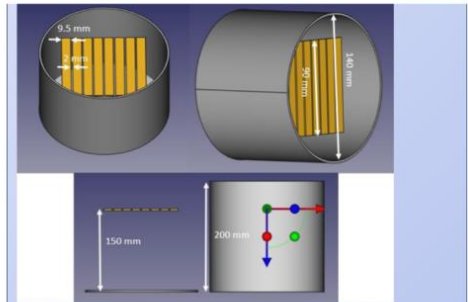
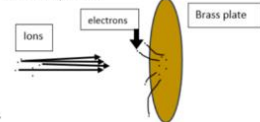
Yellow is brass, gray is stainless.

When the ion beam collide with the plate electrochemical reaction between them will transfer the charge to the plate that will generate current through the wire into the electrometer.

It is important to note that this design is not efficient as module 1 due to the possibility of the ion to bounce off electrons off the surface is a process called "electron scattering" which involves the interaction of atoms or particles with the electrons in the material of the conductive plate. This interaction can lead to changes in the direction and energy of the electrons as they bounce off other charged particle off the plate's surface when they collide.

This will prevent an accurate measurement as these electrons carry charge that will be lost and thus current change.

However, this problem can be solved by implementing a tiny change that will be mentioned later.



In this module the "electron scattering is not yet solved; however, the introduction of rectangular brass plates is to make this detector an array one.

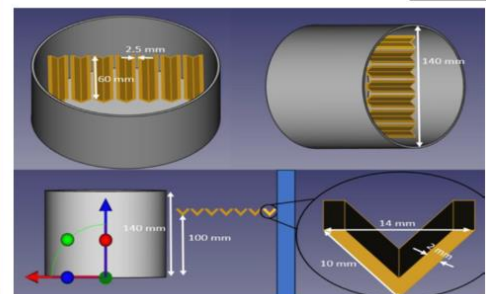
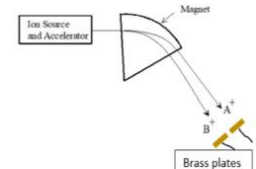
The problem with faraday's cup is that it can only be used detect only one type of ions in the mass spectrometer unless a flight time analysis was implemented which is not.

An array of faraday's cup can solve the problem as each plate can detect one type of ions according to their position (masses).

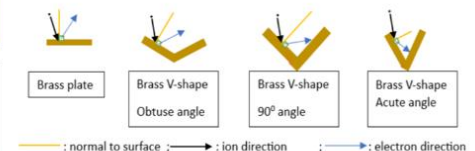
The accelerated ions go through a magnetic field which change their direction, since all ions in the experiment have the same charge, they will experience the same moving force. However, due to the different masses of each ion, they will move in a different directory i.e., the heavier the ion the longer the arc will take.

Looking at the diagram, it can be concluded that the more plates implemented the larger the ion type range that can be detected.

Which will directly affect module 4 the detector.

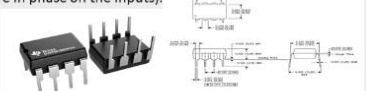


The final module reflects modules 5, but with replacing the plate-like brass into V-like shape. This will reduce the effect of "electron scattering" since when it happens the shot electrons will go in the direction of ion trajectory. This will leave the following cases:



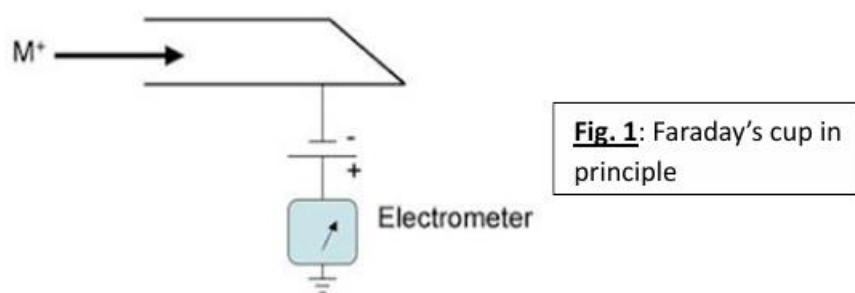
What this shows is that the electrode shape actually matters because as the angle of the V-shaped is 180° (plate) or is obtuse the scattered electrons will leave; however, when it is 90° the electrons are more likely to hit the plate, but when it is acute angle the electrons are guaranteed to hit more than once which will drop the loss to minimum.

The LMC 6001 A1 Op-Amp was chosen for this application due to its high sensitivity and its low noise amplification process, since its Common-Mode Rejection Ratio (CMRR) is 83 dB, it means that the op-amp can effectively reject common-mode signals (inside noise). This is a desirable value for precision and sensitive applications. It means that the op-amp can amplify differential signals (signals that are in anti-phase on the inputs) while attenuating common-mode signals (signals that are in phase on the inputs).



11.1.1 Introduction

A Faraday's Cup is a detector that detects the presence of charged particles, by accumulating on the surface of the detector. Statement The Faraday's cup works based on the principles of electrochemistry and the conservation of electric charge. Electrochemical process is the core principle behind Faraday's cup. When charged particles, such as ions or electrons, encounter a conductive surface (the collection surface of the cup), they can transfer their charge to that surface. This transfer of charge is facilitated by an electrochemical reaction between the charged particles and the conductive material of the cup's electrode. This reaction creates a potential difference between the electrodes and the current integrator circuit which induce electric current that flows through an external circuit connected to the cup. This current is proportional to the number of charged particles that have been collected by the cup. By measuring this electric current, the number of charged particles that have impacted the cup's surface.



The design of the faraday's cup is one of the factors that will decide whether it will work as wanted. This report will discuss the modules that have been studied so far.

11.1.2 Faraday's cup (test module)



11.1.3 Fundamental Precepts

A Faraday Cup is a detector that detects the presence of charged particles by accumulating them on the surface of the detector.

The Faraday Cup operates based on the principles of electrochemistry and the conservation of electric charge. The electrochemical process is the fundamental principle behind the Faraday Cup. When charged particles, such as ions or electrons, encounter a conductive surface (the cup's collection surface), they can transfer their charge to that surface. This charge transfer is facilitated by an electrochemical reaction between the charged particles and the conductive material of the cup's electrode. This reaction creates a potential difference between the electrodes and the current-integrating circuit, which induces an electric current that flows through an external circuit connected to the cup. This current is proportional to the number of charged particles collected by the cup. By measuring this electric current, the number of charged particles that impacted the cup's surface can be determined. [18]

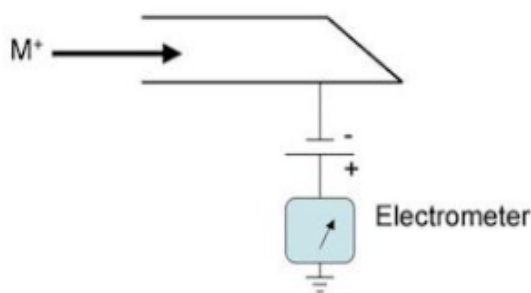


Figure II. 15: Principle of the Faraday cup

The design of the Faraday Cup is one of the factors that will determine whether it will function as intended. This report will discuss the modules that have been studied so far.

11.1.4 Computer Aided Design (CAD)

In this section, we will examine the development of the Faraday dish model. This may be motivated by constraints related to the availability of materials required for its manufacture, or to meet the specific requirements of our project, thus requiring adjustments to the model.

11.1.4.1 Model #1

The original model is renowned for its notoriety in the field of Faraday cups. It is distinguished by a cylindrical brass cup, optimized to minimize electron losses during reflection within the cup. [20]

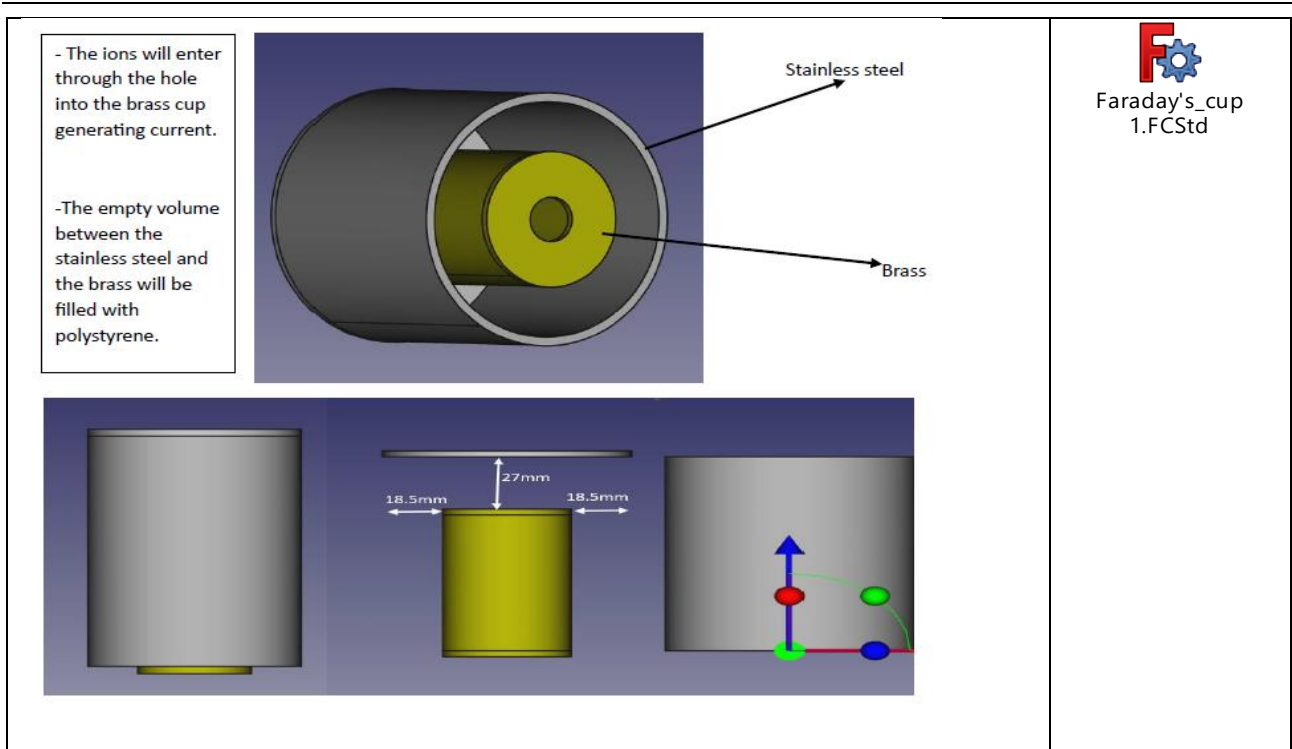


Figure II. 19: First design proposal [18]

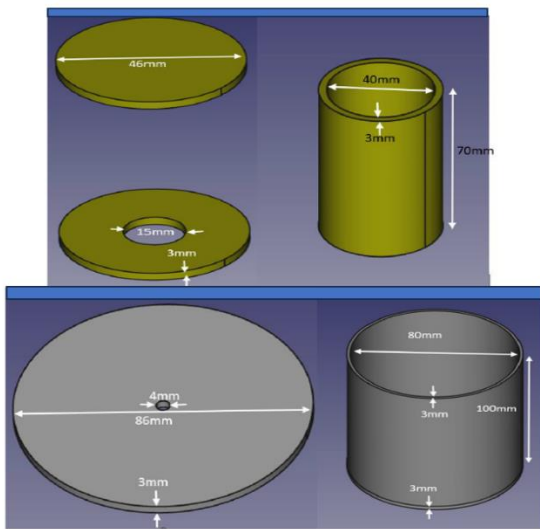


Figure II. 20: Measurements of the first model

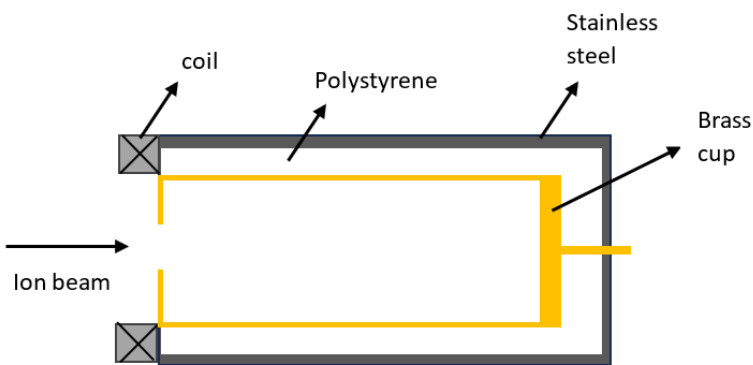


Figure II. 21: Cross section of module 1

The challenge we faced in creating this prototype was the complexity of adjusting the brass cylinder to the necessary size, in addition to the delicacy required when soldering the brass components,

given that it does not withstand the high temperatures inherent in the soldering process. Therefore, we chose to focus on the second model.

11.1.4.2 Model #2

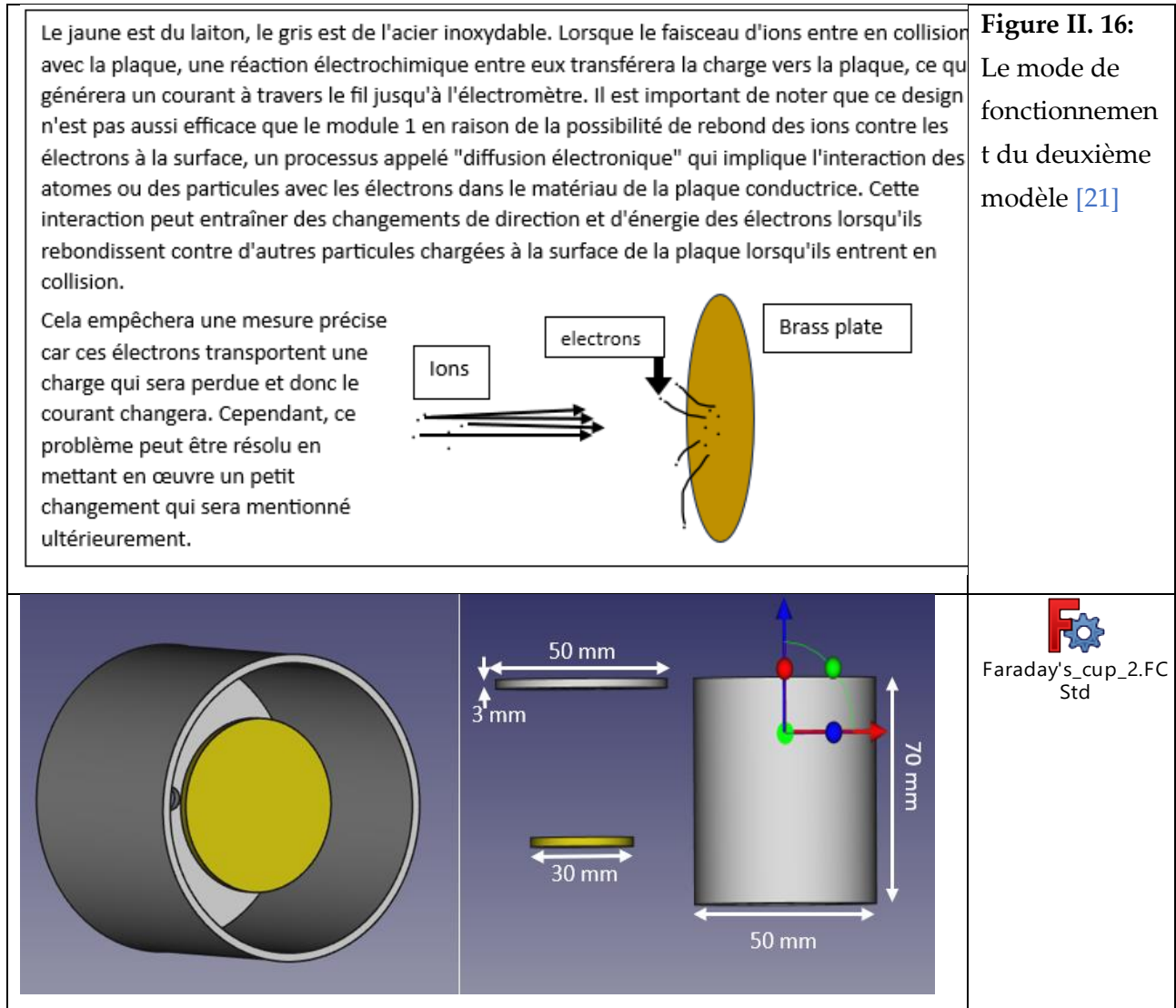


Figure II. 23: Measurements of the second model

11.1.4.3 Model #3

Les ions accélérés passent à travers un champ magnétique qui modifie leur direction. Étant donné que tous les ions dans l'expérience ont la même charge, ils subiront la même force de déplacement. Cependant, en raison des masses différentes de chaque ion, ils se déplaceront dans une direction différente, c'est-à-dire que plus l'ion est lourd, plus l'arc prendra du temps.

En examinant le schéma, on peut conclure que plus on implémente de plaques, plus grande sera la gamme de types d'ions pouvant être détectée. Cela aura un impact direct sur le module 4, le détecteur.

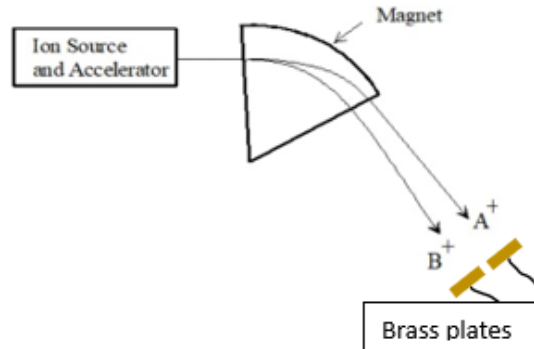
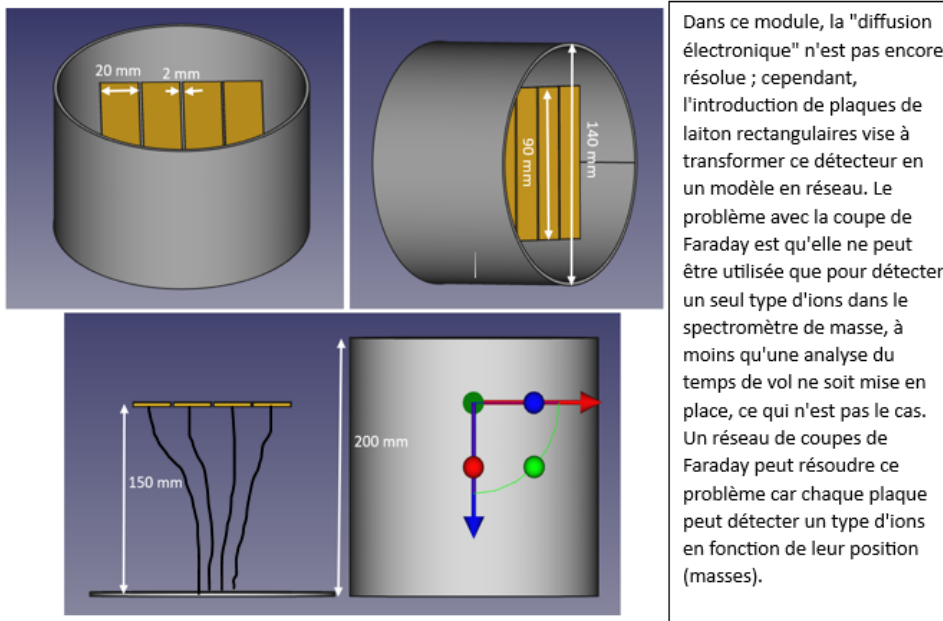


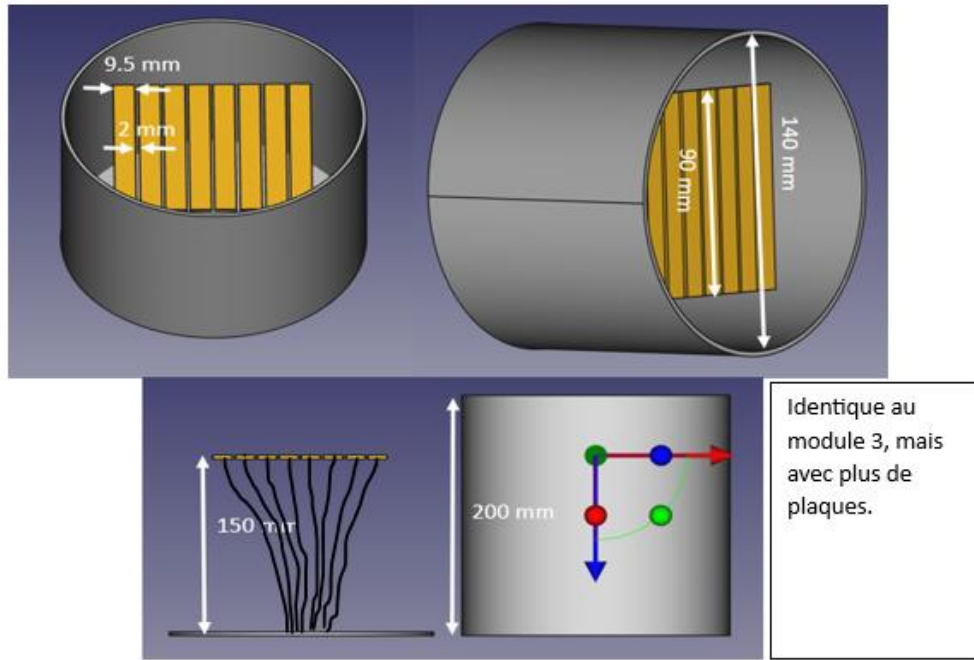
Figure II. 24: The Operation of the Second Model [20]




Faraday's cup
3.FCStd

Figure II. 25: Measurements of the third model

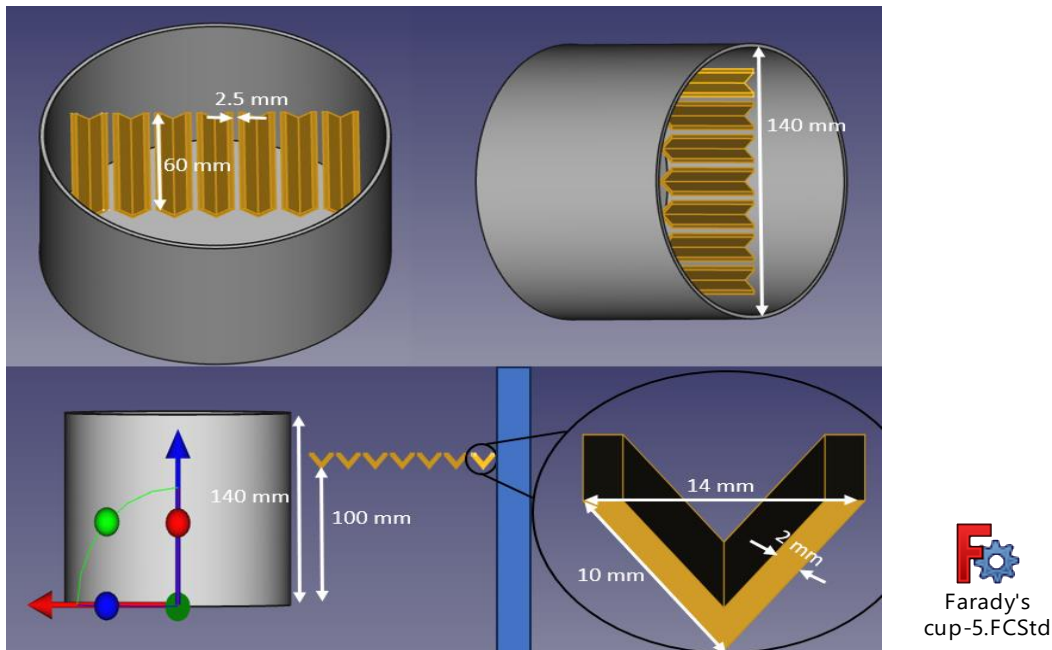
11.1.4.4 Model #4




 Faraday's cup
 4.FCStd

Figure II. 26: Measurements of the fourth model

11.1.4.5 Model #5




 Faraday's
 cup-5.FCStd

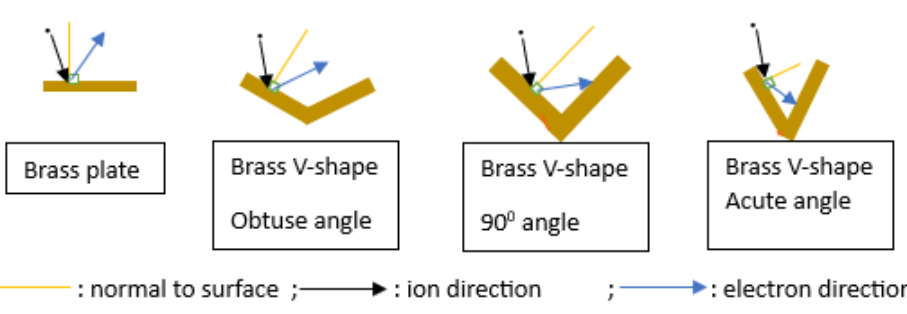
Figure II. 27: Measurements of the fifth model

11.1.5 Realization

The attached photograph illustrates the making of the second model of the Faraday dish. Starting with the simplest to make, we first ensure that it can capture charges, before proceeding to the manufacture of the model most suited to our project. This Faraday dish consists of a stainless steel

cylinder, with a brass plate placed in the center and an insulating material between the two to ensure fixation.

Le module final reflète les modules 5, mais en remplaçant les plaques de laiton en forme de plaque par une forme en V. Cela réduira l'effet de la "diffusion électronique", car lorsqu'elle se produit, les électrons émis iront dans la direction de la trajectoire de l'ion. Cela entraînera les cas suivants:



— : normal to surface ; — : ion direction ; — : electron direction

Ce que cela montre, c'est que la forme de l'électrode compte en réalité, car lorsque l'angle du V est de 180 degrés (plaque) ou est obtus, les électrons dispersés partiront. Cependant, lorsqu'il est de 90 degrés, il est plus probable que les électrons frappent la plaque. Mais lorsque l'angle est aigu, les électrons sont assurés de frapper plus d'une fois, ce qui réduira les pertes au minimum.

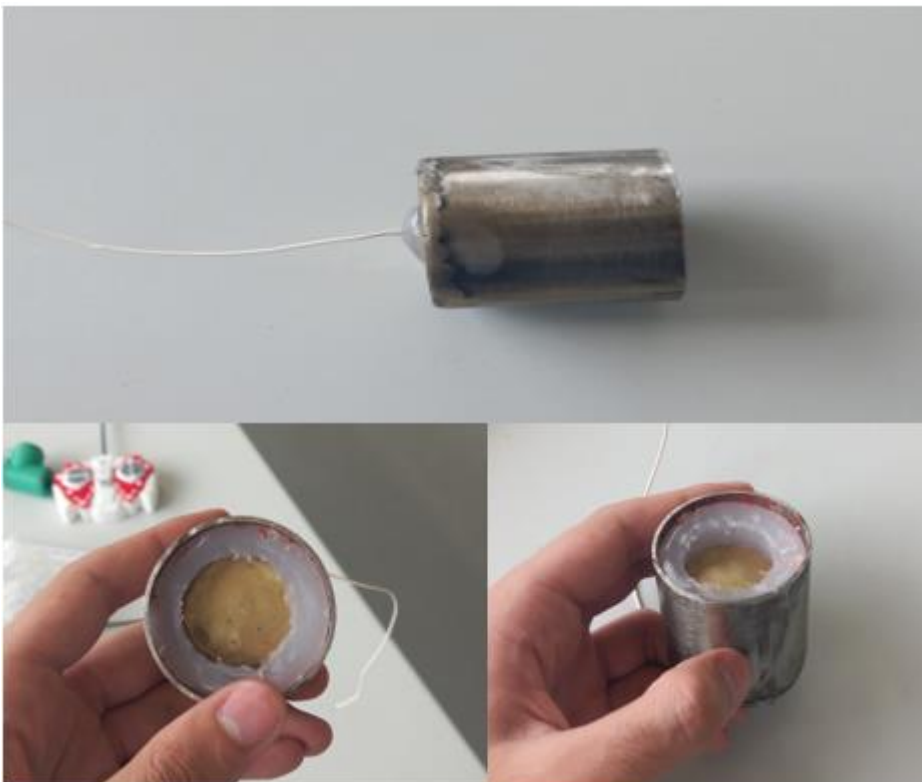
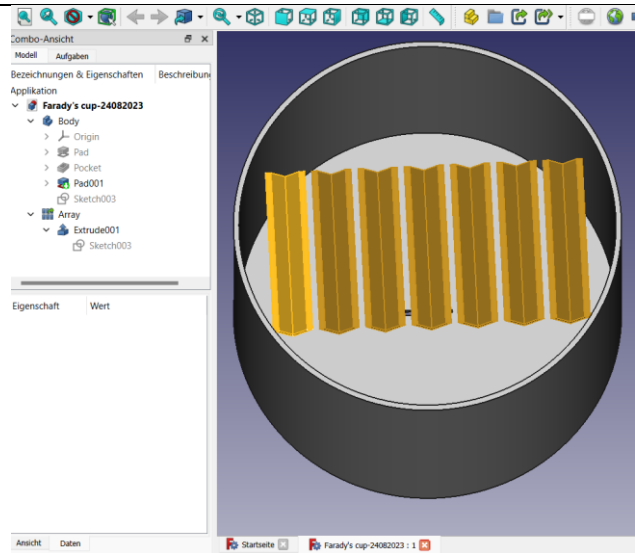


Figure II. 29: Miniaturized Design of the Second Model

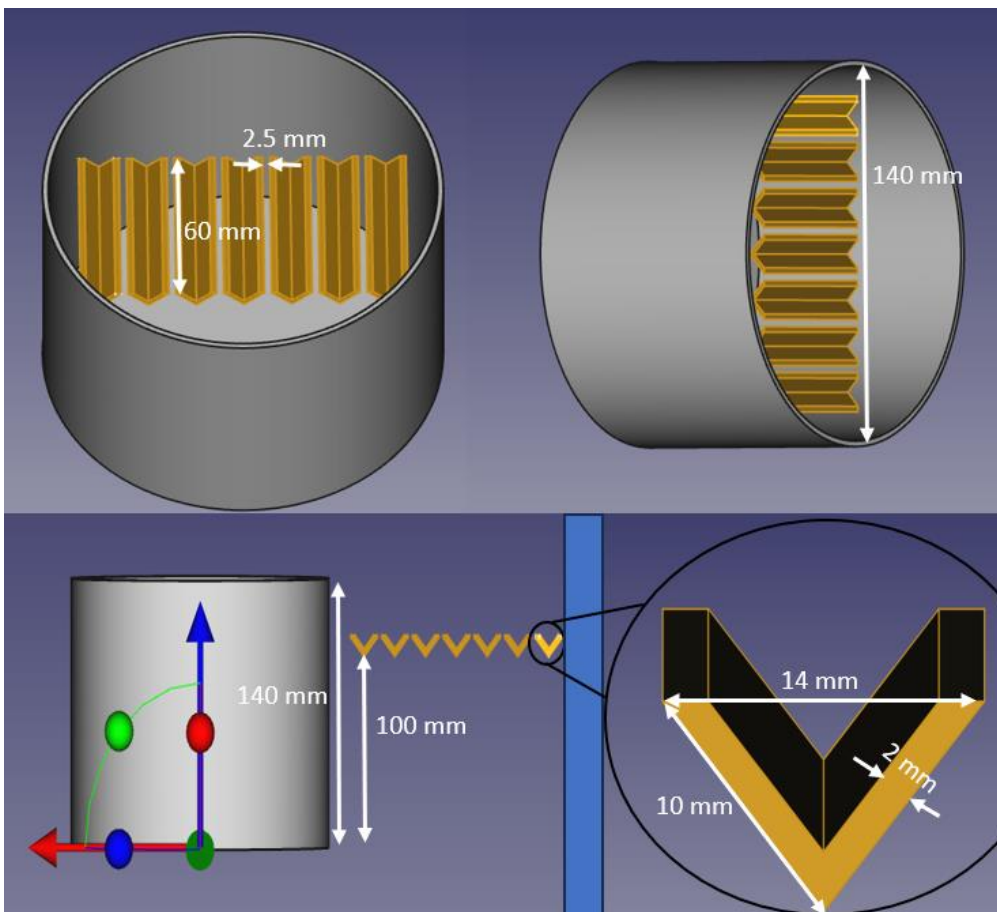


Farady's
cup-24082023.FCStd



Faraday's cup (total detector)





Faraday's cup final design (details in <https://aecenar.com/index.php/downloads/summary/10-iap/1365-design>)

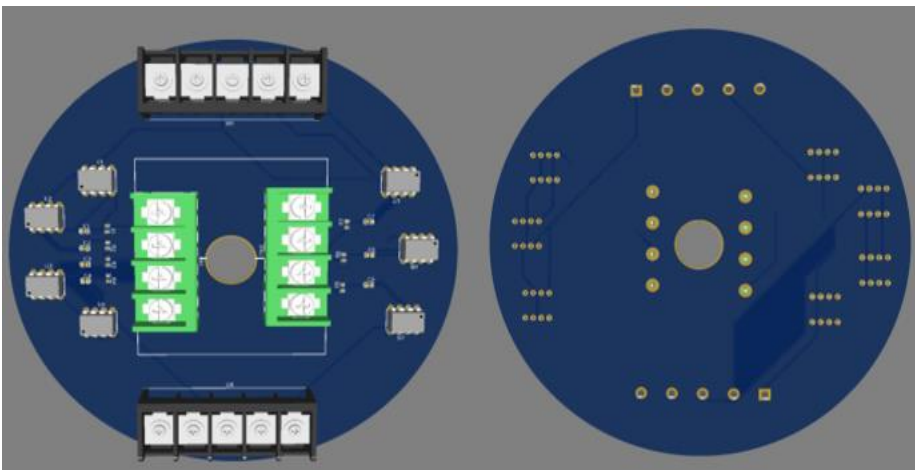
11.1.5.1 Realization of Faraday cups (last update: 14.2.24)

cutting copper for Faraday cups:

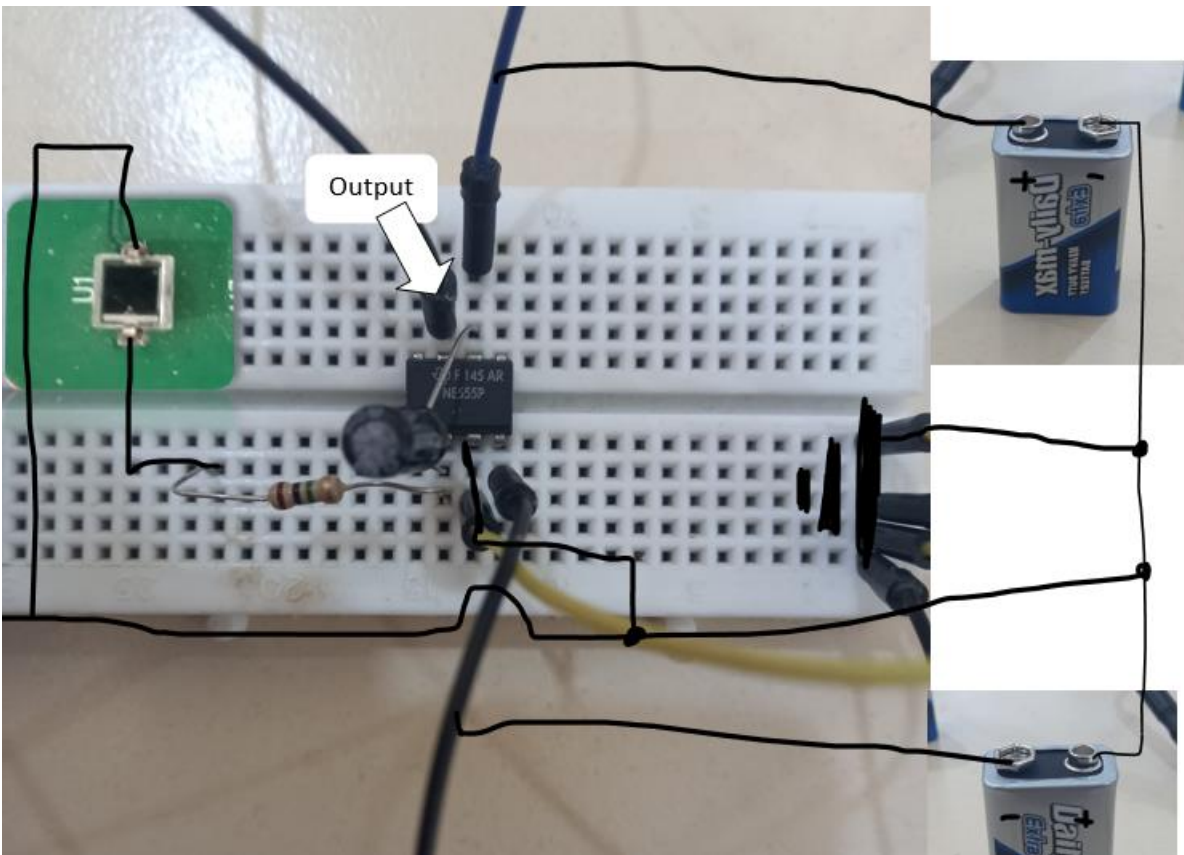




11.1.6 Electronics and Amplification Process:
[Amplifier circuit of FC \(PDF\)](#)



PCB version of the amplifier circuit.



Amplifier circuit of FC module on a bread board

11.1.7 In summary

Faraday's cup operations are based on the principles of electrochemical deposition and charge conservation. It provides a way to measure the intensity of charged particle beams by collecting the particles on a conductive surface and quantifying the resulting electric current. And the design of the Faraday cup has an effective factor on the performance of the detector.

11.1.8 Faraday Cut Detector Amplification Circuit

11.1.8.1 Introduction

By opting for the Faraday cup design, we anticipate an extremely low current at the cup output. This underlines the need to integrate an amplification circuit to increase this signal to a detectable and usable level. In the mass spectrometer under development, the particles of interest undergo ionization, thus transforming each molecule into a positively charged ion, having lost an electron. Therefore, for significant ion currents, an ion (+1) carries a charge of 1.6×10^{-19} Coulombs. This means that one ion per second is equivalent to 1.6×10^{-19} A, or 1.6×10^{-4} fA.

11.1.8.2 Equipment and roles

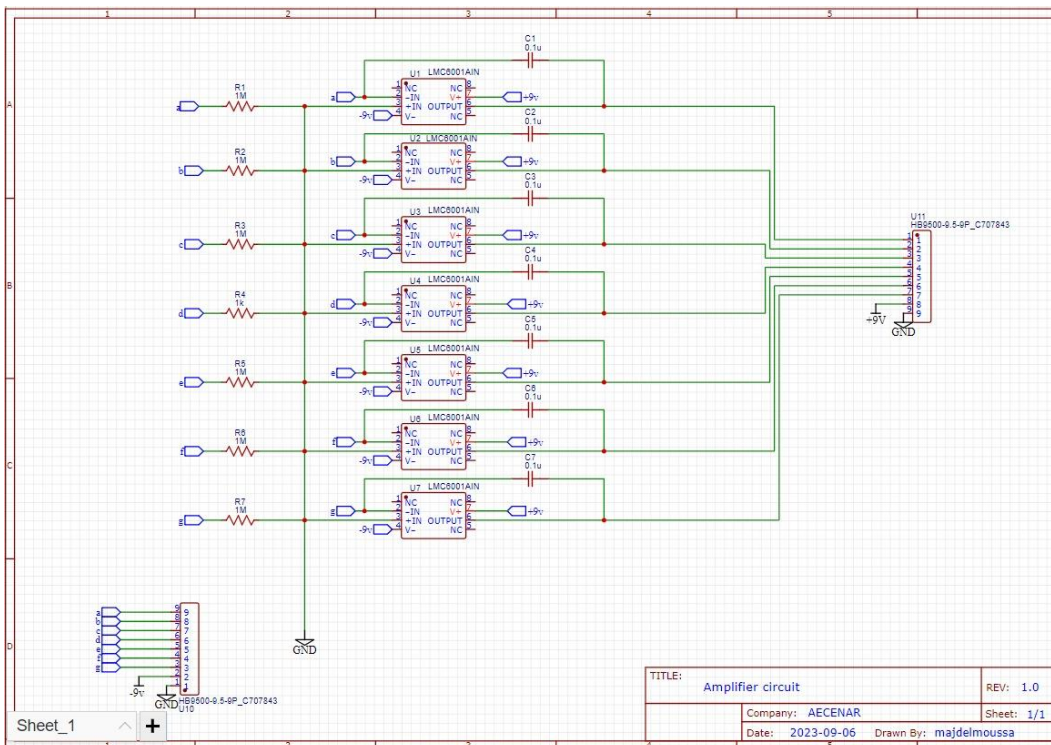
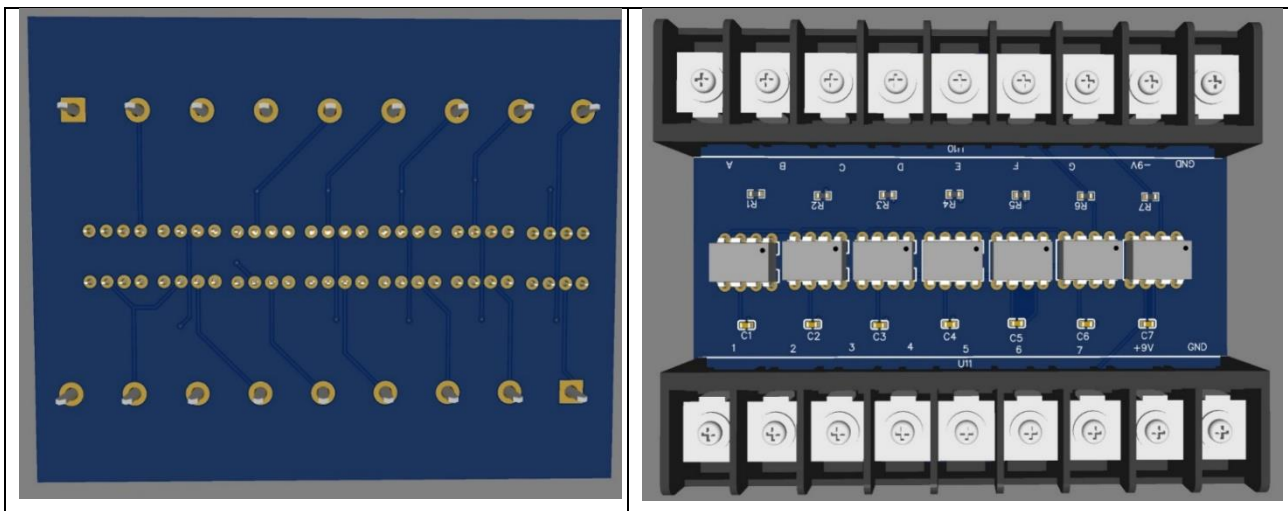


Figure II. 30: Circuit diagram of the amplifier for the Faraday cup

11.1.8.3 Printed Circuit Board (PCB) Design



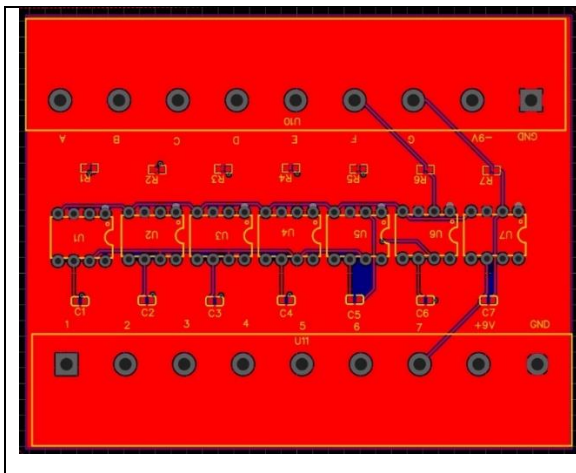


Figure II. 17: The front-back image of the amplifier circuit (3D)

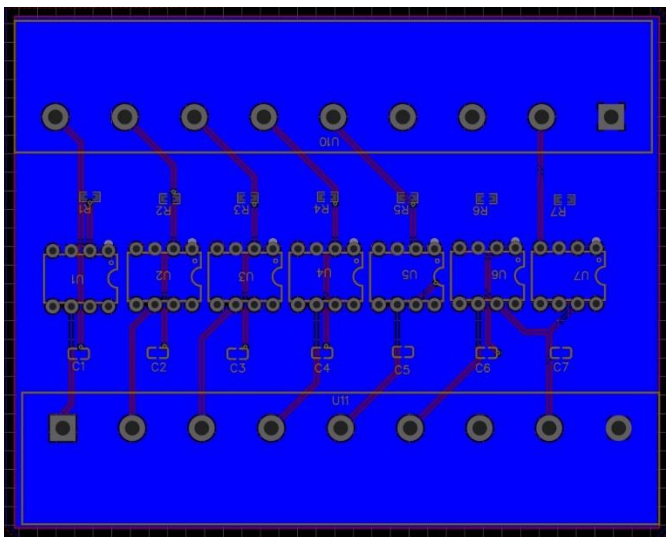


Figure II. 18: The front-back image of the amplifier circuit with the copper layers

11.1.8.4 Amplifier circuit

Operational Amplifiers U_{1-7} : Operational amplifiers, or op-amps, are circuit elements that can be used for several tasks. Here, they amplify voltage signals from Faraday cups so that they can be recorded and stored.

Resistors R_{1-7} : The current created by the Faraday cups will induce a potential difference across these resistors, which will then be amplified by the op-amps.

Capacitors C_{1-7} : Capacitors are used to reduce the effect of external noise on the signal from the cuts.

Port U_{10-11} : Input/output port of the amplification circuit.

11.1.8.5 Calculations and figures

About the LMC 6001 Operational Amplifier:

Input bias current (max) = 25 fA

Your (voltage offset at 25°C) (max) = 0.35 mV

Total supply voltage (+5 V = 5, ±5 V = 10) (max) = 15.5 V

Total supply voltage (+5 V = 5, ±5 V = 10) (min) = 4.5 V

Voltage gain for strong signals (A) = 1400V/mV or 1400000 times the input.

So if the input is 1nV, the output will be 1.4mV.

The LMC 6001 A1 operational amplifier was chosen for this application due to its high sensitivity and low amplifier noise. Its common mode rejection ratio (CMRR) is 83 dB, which means that the op-amp can effectively reject common mode signals (internal noise).

This is a desirable value for precision and sensitive applications. It means that the op-amp can amplify differential signals (out-of-phase signals on the inputs) while attenuating common-mode signals (in-phase signals on the inputs).

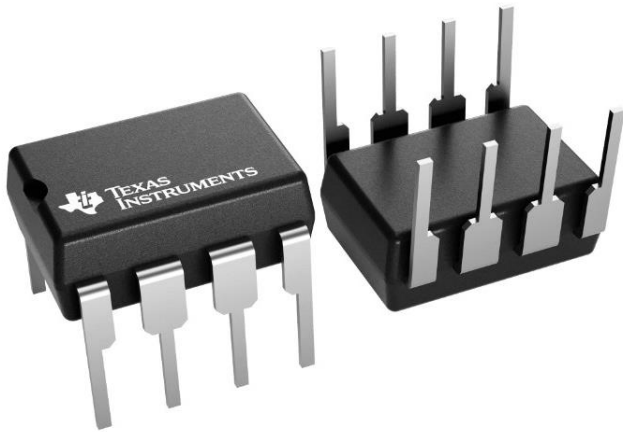


Figure II. 33: Operational amplifier

12 Mass Spectrometer Design and Realization based on Helmholtz Coils

From the following master thesis:



MEMORY

In order to obtain the

RESEARCH

In

PIRM: Physics of Radiation-Matter Interaction

Presented and Supported by:

Asmaa Ahmad El Mir

Jan 2023

Title

**Evolution of mass spectrometer device for the detection of combustion gases
from municipal waste**

Supervisor

Prof. Ahmad Osman

Readers

Dr. Hamed Khatib

Dr. Adnan Naja

Lebanese University-Faculty of sciences

12.1 SUMMARY

The mass spectrometer represents an intriguing field for researchers. It finds a wide range of applications, particularly in detecting toxic gases emitted during waste combustion. This process involves the passage of these gases through several stages, starting with their ionization, followed by their acceleration and deflection, ultimately reaching the detector to identify the type and quantity of gases present. The design and improvement of this device were accompanied by numerous experiments, the results of which underwent thorough analysis and discussions.

12.2 Introduction

In light of the waste crisis in Lebanon and the state's inability to find solutions to this problem, as well as the economic collapse that hinders the securing of electricity for the population, the AECENAR Scientific Research Center, based in Tripoli, mobilized one of its departments, the "ENERGY Department", to look into the production of electricity by burning municipal waste. However, being aware that this combustion produces toxic gases requiring elimination in order to preserve the health of the population, the use of a mass spectrometer is essential. The latter will play a key role in ensuring the detection of these gases prior to filtration, as well as confirming their elimination after the filtration process. This master's thesis in physics therefore focuses on the evolution of the mass spectrometer device for the detection of gases emitted during the combustion of municipal waste.

12.3 Mass Spectrometer Requirements

12.3.1 System requirements:

The mass spectrometer must be able to provide electrons to collide with the atoms of the introduced gas, thus obtaining ions.

The mass spectrometer must be able to accelerate ions by exposing them to a high voltage.

The mass spectrometer must be able to separate the ions from each other and change their trajectory by exposing them to a magnetic field coming from the Helmholtz coil.

The detector must be able to capture ions based on their (mass/charge) after deflection.

12.3.2 Mechanical requirements:

The cathode must be able to withstand thermal and electrical stress.

The cathode must be tungsten.

The anode must be made of stainless steel.

The tube must be made of stainless steel (ionization chamber + 2 horizontal tubes + 1 curved tube).

The vacuum pump must be able to create a vacuum in the stainless steel tube.

The plate that pushes the ions out of the ionization chamber should be made of stainless steel (slight positive charge).

The three plates that accelerate the ions must be made of stainless steel.

The Helmholtz coil should be made of two plastic pieces, with iron inside, and copper strips wrapped around it.

12.3.3 Physical requirements:

A stainless steel plate (slightly positive charge) should be able to push the ions out of the ionization chamber.

Three stainless steel plates should be able to accelerate the ions.

The detector must be able to capture the ions and transmit a signal to the computer.

12.3.4 Electrical requirements:

A power supply must be capable of supplying 17V to the tungsten.

A power supply must be capable of gradually supplying -300V, -150V and zero to the accelerator plates.

The anode and all stainless steel plates must be insulated from the tube to prevent voltage from propagating and passing through the tube.

12.3.5 Magnetic requirements:

The Helmholtz coil must be able to generate the magnetic field on the bent tube.

The Helmholtz coil must be able to generate a magnetic field of 0.2 T.

12.3.6 Safety requirements:

Electrical safety

All electrical connections must be coated with the correct insulation based on the current and voltage flowing through the connections.

12.4 Mass spectrometer Design

12.4.1 Fundamental Concepts

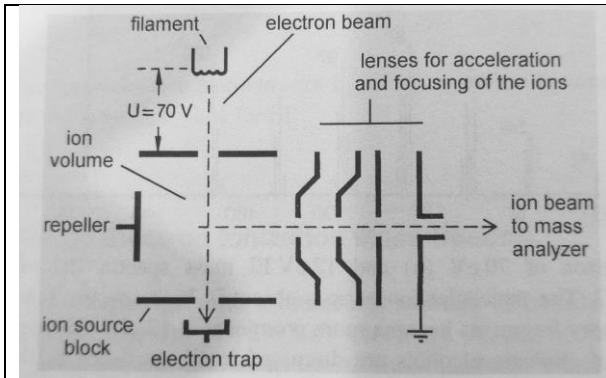


Figure II. 19: Typical schematic arrangement of an ion source

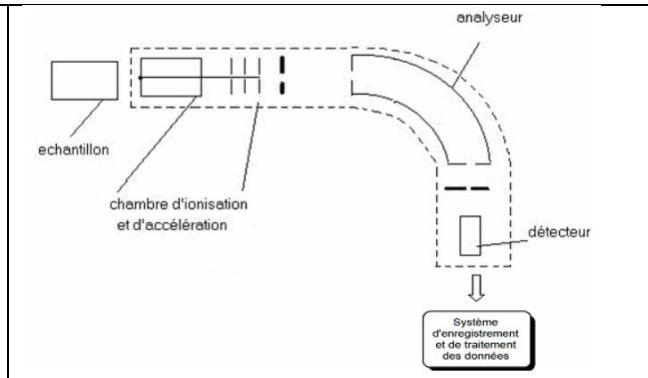


Figure II. 20: Sequence of steps in a mass spectrometer

The two aforementioned illustrations illustrate the trajectory of ions through different stages, starting with the gas ionization phase inside the ionization chamber. The ions then progress to the acceleration zone before entering the deflection section, and finally end up in the detection zone. Based on this principle, a similar design was developed, encompassing these four crucial phases.

Within the ionization chamber, a sample of residual gas containing harmful compounds such as HCl, HF, SO₂ and Hg is introduced. There, this gas is positively ionized by a collision with electrons emanating from a tungsten filament, carrying a kinetic energy of 17 eV. Following this ionization process, the ions are repelled by an ion repellent plate, prompting them to enter the acceleration phase.

At this stage, the ions wait in front of three negative potential plates – 300, 150 and 0 volts respectively – before progressing to the deflection phase. There, they are subjected to a 0.2 T magnetic field created by an inverted coil. This magnetic field causes the ion trajectories to deviate, so that each ion follows a specific path based on the m/z (mass/charge) ratio. Subsequently, the ions are captured by a "Faraday cup" type detector during the detection phase.

12.4.2 Computer Aided Design (CAD)

To develop the mass spectrometer model, we used "FreeCAD" software.

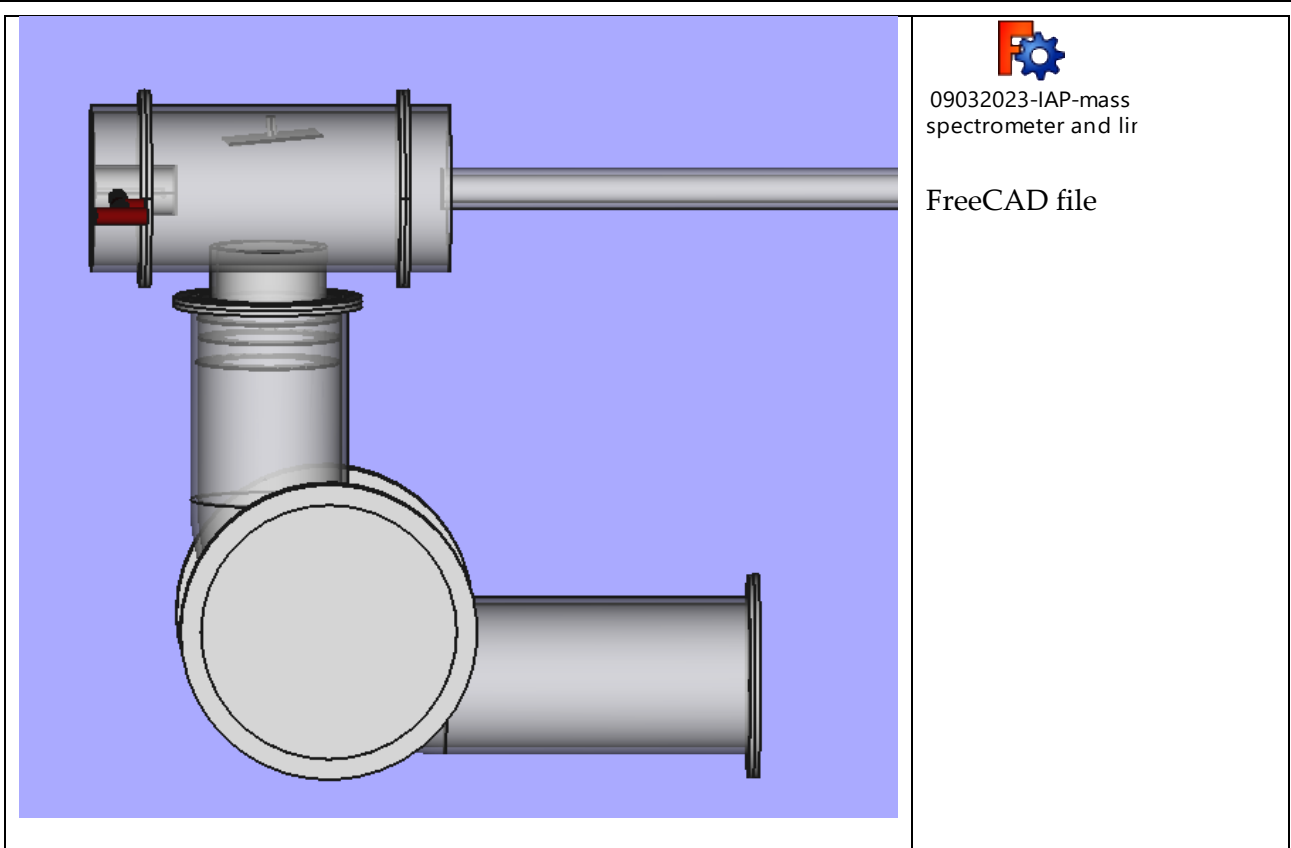


Figure II. 21: Design of the mass spectrometer model

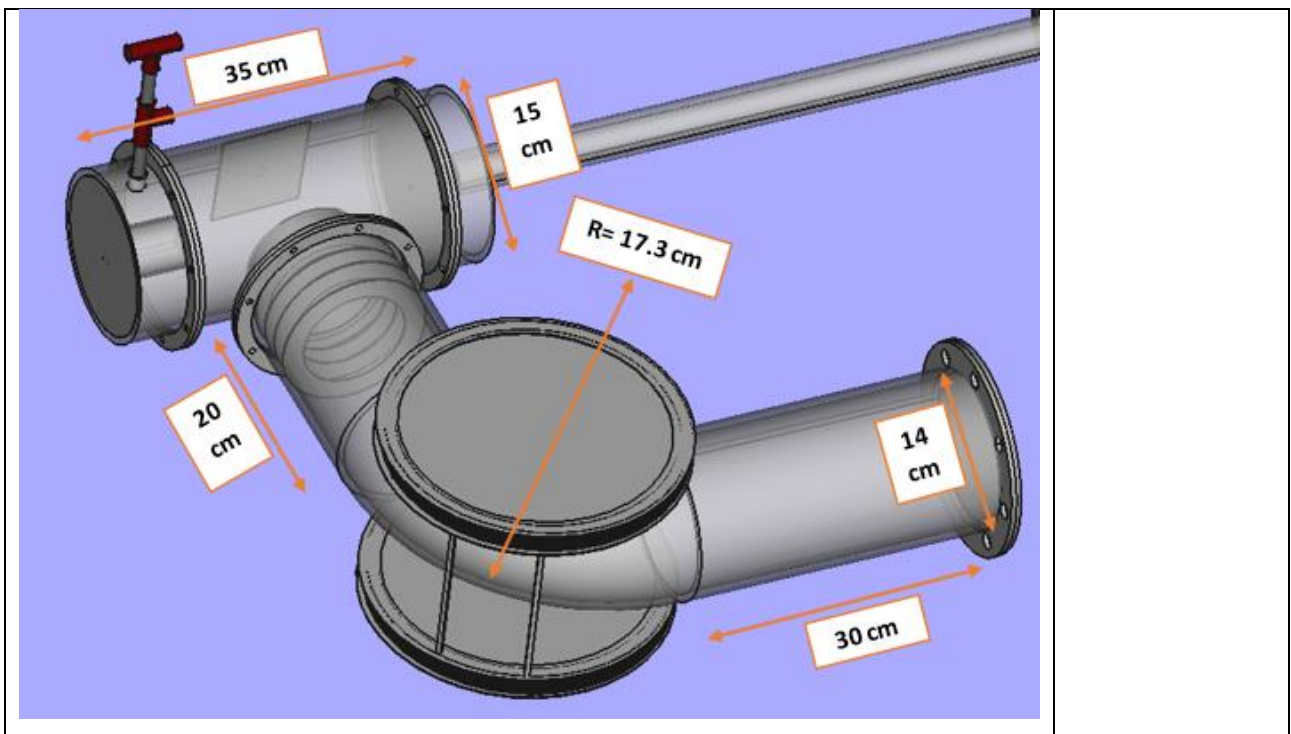


Figure II. 22: Mass spectrometer model-specific measurements

12.4.2.1 Ionization chamber

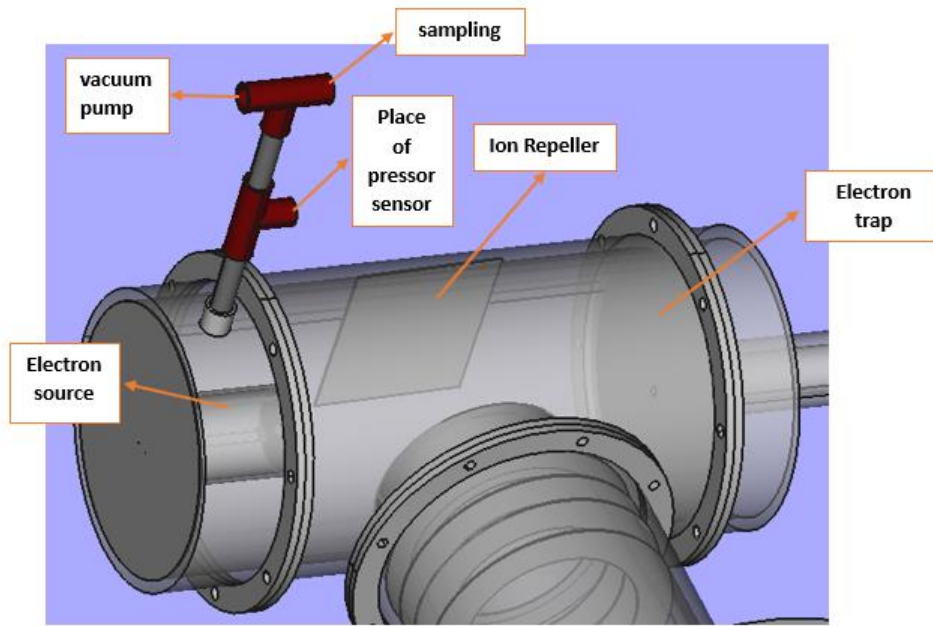


Figure II. 23: The components of the ionization chamber

12.4.2.2 Acceleration zone

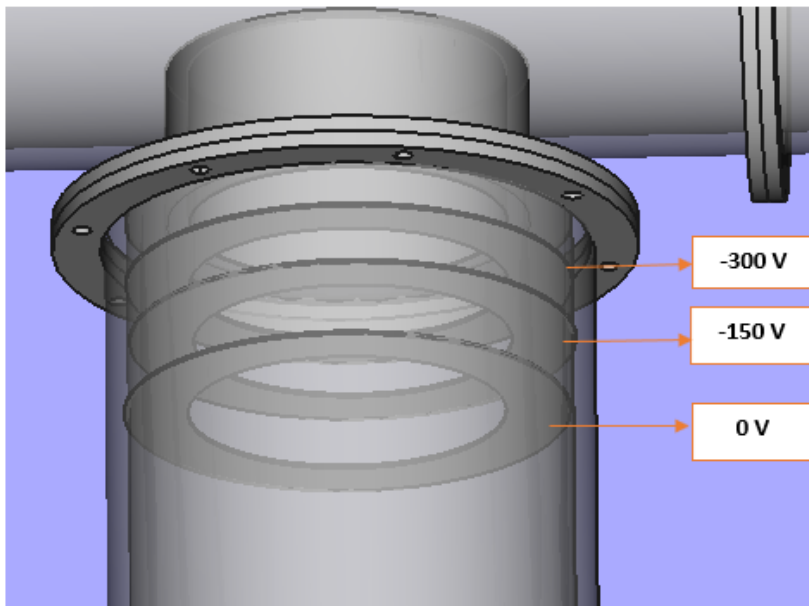


Figure II. 24: Distribution of tension on the acceleration plates

12.4.2.3 Deflection zone

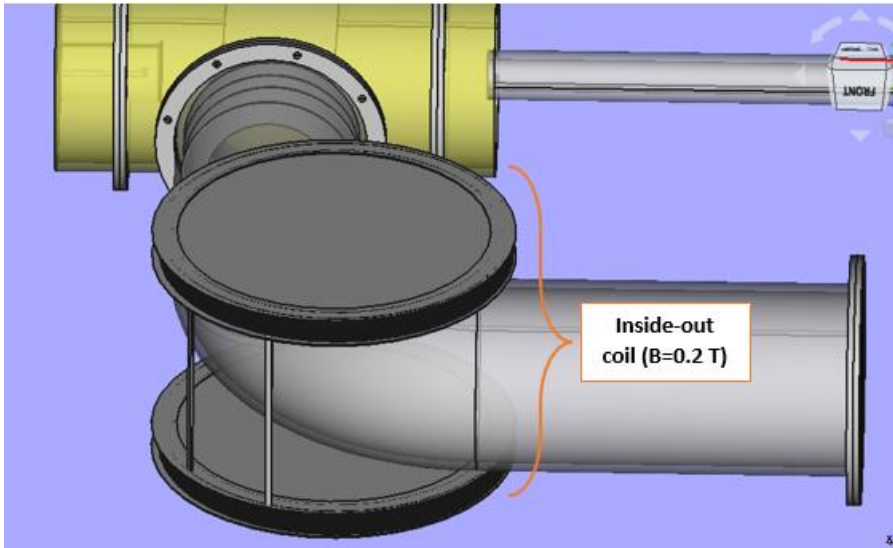


Figure II. 25: The presence of the Helmholtz coil in the deflection zone

12.4.2.4 Detection zone

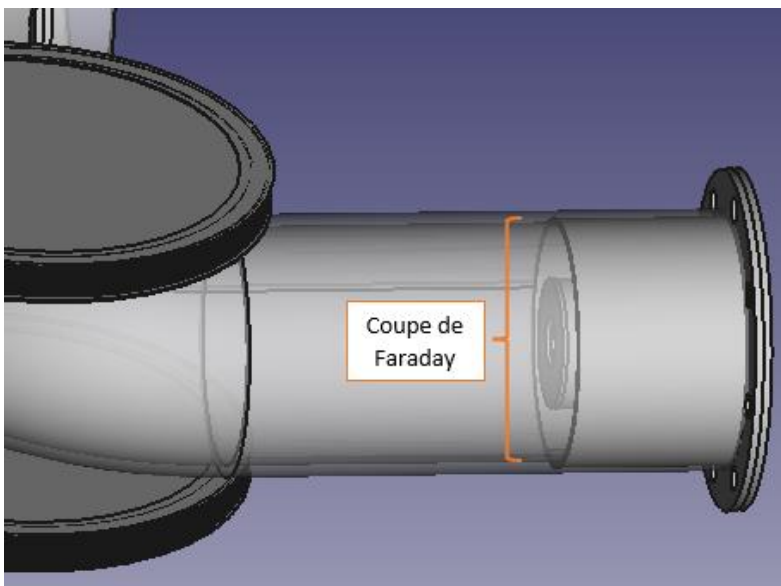


Figure II. 26: Position of the Faraday Cup type detector in the deflection zone

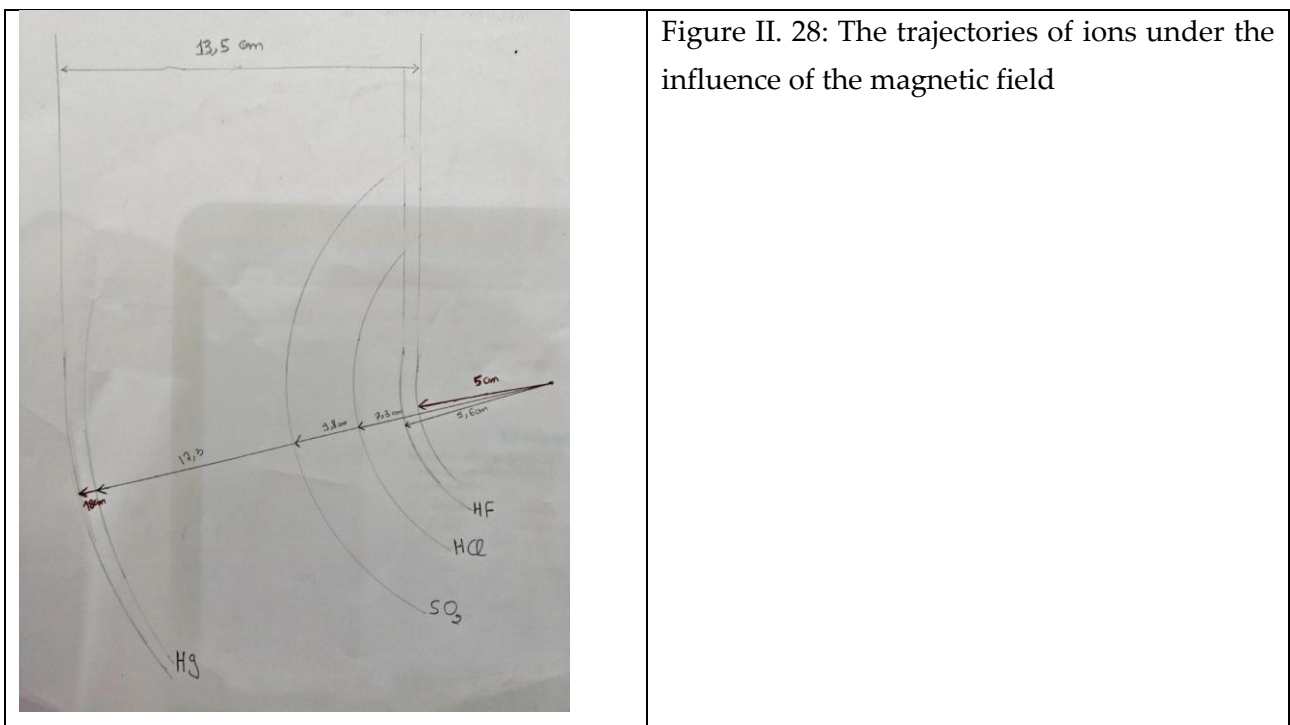
12.5 Mass Spectrometer Realization

Due to its advantageous properties, such as resistance to corrosion, heat, ease of maintenance and shaping, as well as its long durability, stainless steel proves to be an optimal choice [13]. In addition, it has low reactivity with gases, such as HCl, HF, SO₂, Hg, compared to other materials. Considering the easy availability of this type of metal within the center, we made the decision to manufacture our mass spectrometer from stainless steel. This option fits perfectly with our objective of ensuring the quality and durability of our equipment.

The elbow shown below, which will act as the deflection zone in the mass spectrometer, was designed taking into account all the trajectories that the ions will follow when subjected to the magnetic field. This ensures that all ions will follow their path without risk of collision or loss.



Figure II. 27: The curved tube where the magnetic field is applied



Section (1.5. Deflection) specified the radii of each ion. Using this data, we calculated the difference between the largest and smallest radius. As a result, we made an elbow with a diameter greater than this difference, and with a curvature of 17.3 cm, thus ensuring the inclusion of all possible trajectories.

The component in question, made available by the AECENAR Centre, was used and adapted to ensure the function of ionization chamber within the mass spectrometer.

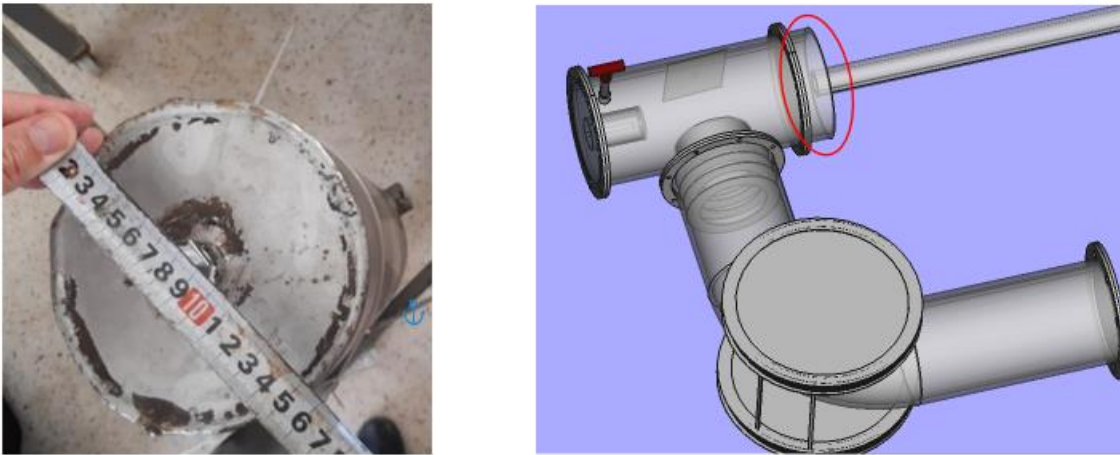


Figure II. 29: Length of the ionization chamber (~35 cm)

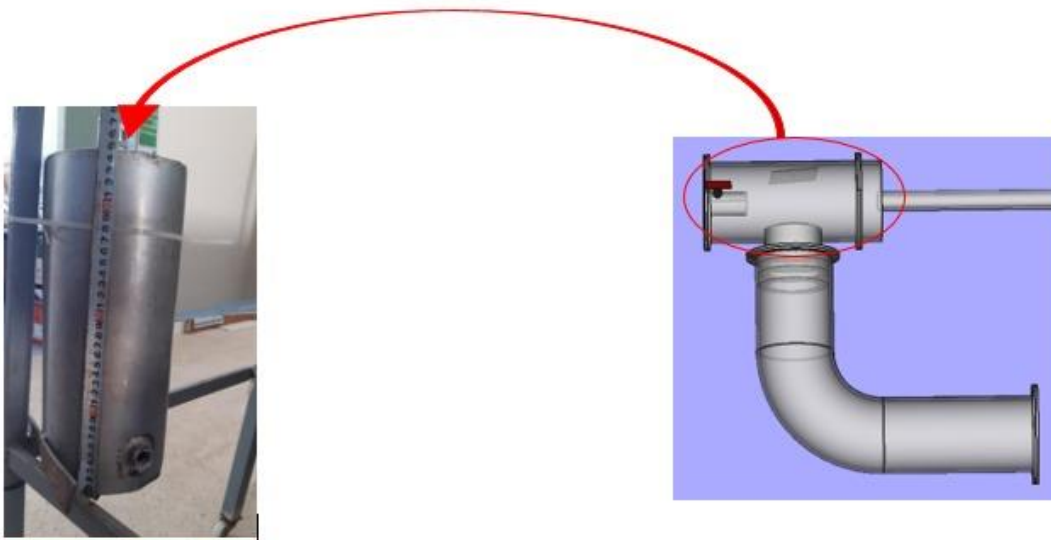


Figure II. 30: Cross-sectional diameter of the ionization chamber (~15 cm)



Figure II. 31: Cross-sectional diameter of two horizontal tubes (~14 cm)

In the diagrams shown below, flanges play a fundamental role in ensuring a secure connection between two components. They provide easy assembly and disassembly, ensuring a robust connection. They also allow for the isolation of specific sections if necessary. In terms of importance, flanges contribute significantly to the structural integrity, safety, and flexibility and adaptability of systems. [13]



Figure II. 19: Fabrication of flanges for the various mass spectrometer components



Figure II. 33: Mass spectrometer manufacturing and assembly steps



Figure II. 34: Welding during mass spectrometer manufacturing

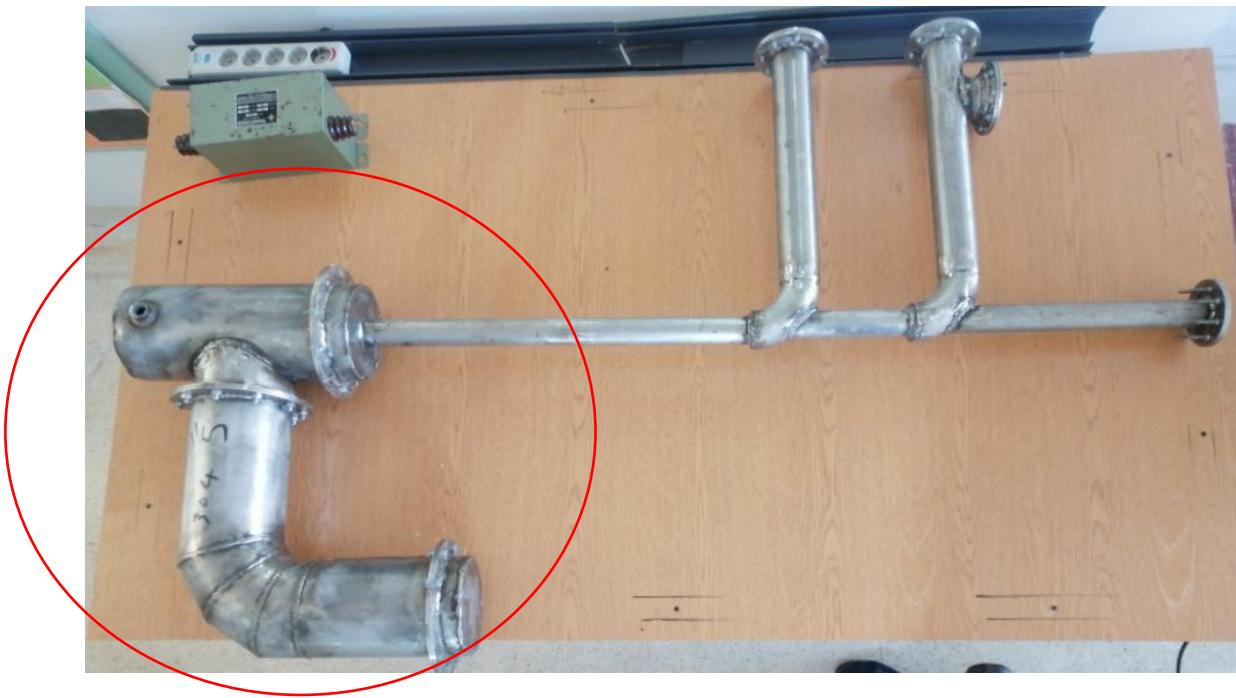


Figure II. 17: The assembled prototype, where the mass spectrometer is integrated

12.6 Helmholtz coil with soft iron

To distinguish between gas types, a crucial preliminary step is to subject them to deflection. This procedure directs each gas in a specific direction, giving them distinct trajectories. To accomplish this, the use of a magnetic field is imperative. The choice of magnet, particularly in terms of uniformity, perpendicular alignment relative to the ion velocity, and downward orientation, led us to favor the use of a Helmholtz coil equipped with soft iron.

12.6.1 Definition

The Helmholtz coil with soft iron is a device used in physics to create a uniform and constant magnetic field in a specific area of space. It consists of two identical circular coils, positioned

symmetrically on either side of a central axis, at a distance equivalent to their own radius [16] . The key element of this type of coil is the integration of soft iron cores inside the coils. The presence of this material is crucial to enhance the intensity of the magnetic field [17] . Soft iron has a great ability to effectively concentrate and guide magnetic field lines through itself due to its high magnetic permeability. By incorporating it into the winding, it reduces field losses to the outside and improves field uniformity, thus ensuring an even distribution of magnetic forces. In addition, it helps maintain the stability of the magnetic field by minimizing external disturbances.

12.6.2 Features

The main characteristics of Helmholtz coils with soft iron are:

- Two identical coils: A Helmholtz coil usually consists of two identical coils, usually circular in shape, each having the same number of turns and the same radius.
- Fixed Distance: The two coils are spaced a specific distance apart, called the intercoil distance, so that the resulting magnetic field is uniform in a specific area between the two coils.
- Uniform magnetic field: The main purpose of a Helmholtz coil is to create a uniform magnetic field in the region between the two coils. This allows experiments or measurements to be performed in a constant magnetic environment.
- Series Configuration: Helmholtz coils are usually wired in series, so that the electric current flows in the same direction through both coils, thus producing a strengthened magnetic field in the central region.
- Precise control: By adjusting the electric current flowing through the coils and the inter-coil distance, it is possible to precisely control the intensity and direction of the magnetic field in the central area.
- Magnetic field amplification: Soft iron increases the magnetic permeability of the system, meaning it makes it easier for magnetic field lines to pass through the material. This has the effect of amplifying the magnetic field in the central region between the coils.

-
- Magnetic field concentration: Soft iron can channel magnetic field lines, "steering" them more through the central region between the coils. This can potentially lead to an increase in magnetic flux density in this region. [16] .

12.6.3 Mathematical formula

The formula for calculating the magnetic field at the center of the gap between the two Helmholtz coils is given by the equation:

$$B = \frac{\mu_0 I N R^2}{2(R^2 + \left(x - \frac{d}{2}\right)^2)^{\frac{3}{2}}} \quad [16]$$

This formula is derived from the Biot-Savart law and allows the calculation of the magnetic field at any point on the central axis of the coils as a function of the physical parameters of the configuration.

The integration of soft iron cores into the Helmholtz coil requires consideration of the relative permeability coefficient of this material. Thus, we will complete the previously stated rule with μ_r [17] :

$$B = \frac{\mu I N R^2}{2(R^2 + \left(x - \frac{d}{2}\right)^2)^{\frac{3}{2}}}$$

With $\mu = \mu_r \mu_0$.

12.6.4 Manufacturing conditions

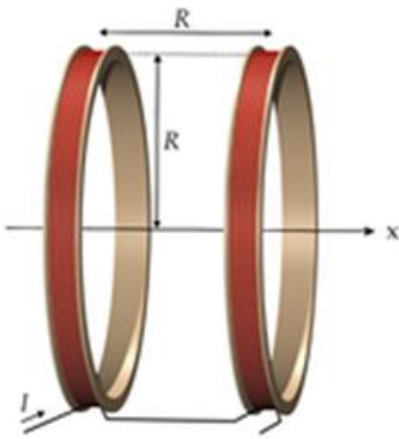


Figure I. 12: Schéma représentant d'une bobine de Helmholtz

Precision in the manufacture of Helmholtz coils is crucial to ensuring a uniform magnetic field. It is essential that the coils have identical geometric specifications, such as the number of turns and the current flowing through them. The use of highly conductive materials with low resistance helps minimize energy losses and ensure optimal performance. Precise coil alignment and spacing equivalent to the radius are determining factors for achieving a uniform magnetic field between them. In addition, meticulous coil insulation is necessary to prevent current leakage and unwanted electromagnetic interference. [16]

The addition of soft iron cores introduces additional considerations into the manufacturing process. It is essential to select a high-quality soft ferromagnetic material, such as mild steel, with high magnetic permeability and low coercivity. The cores must be precisely integrated into the coil structure, ensuring they are properly aligned to maximize their impact on magnetic permeability. They must also be securely fixed in place to prevent movement during coil use. In addition, it is imperative to ensure adequate electrical insulation between the soft iron cores and the coils to prevent short circuits. [17]

12.7 Requirements for Helmholtz coils

12.7.1 Mechanical requirements:

The Helmholtz coil should be made of two plastic pieces, with iron inside, and copper strips wrapped around it.

12.7.2 Electrical requirements:

The power supply will be variable until we achieve the desired result .

12.7.3 Magnetic requirements:

The Helmholtz coil must be able to generate the magnetic field on the bent tube.

The Helmholtz coil must be able to generate a magnetic field of 0.2 T.

12.8 Design of Helmholtz coil with soft iron

12.8.1 Fundamental Precepts

Proper design of Helmholtz coils requires strict adherence to essential conditions that form the basis of their development. This section focuses on the fundamental principles of Helmholtz coil design, highlighting the crucial elements for optimal manufacturing and ensuring superior performance.

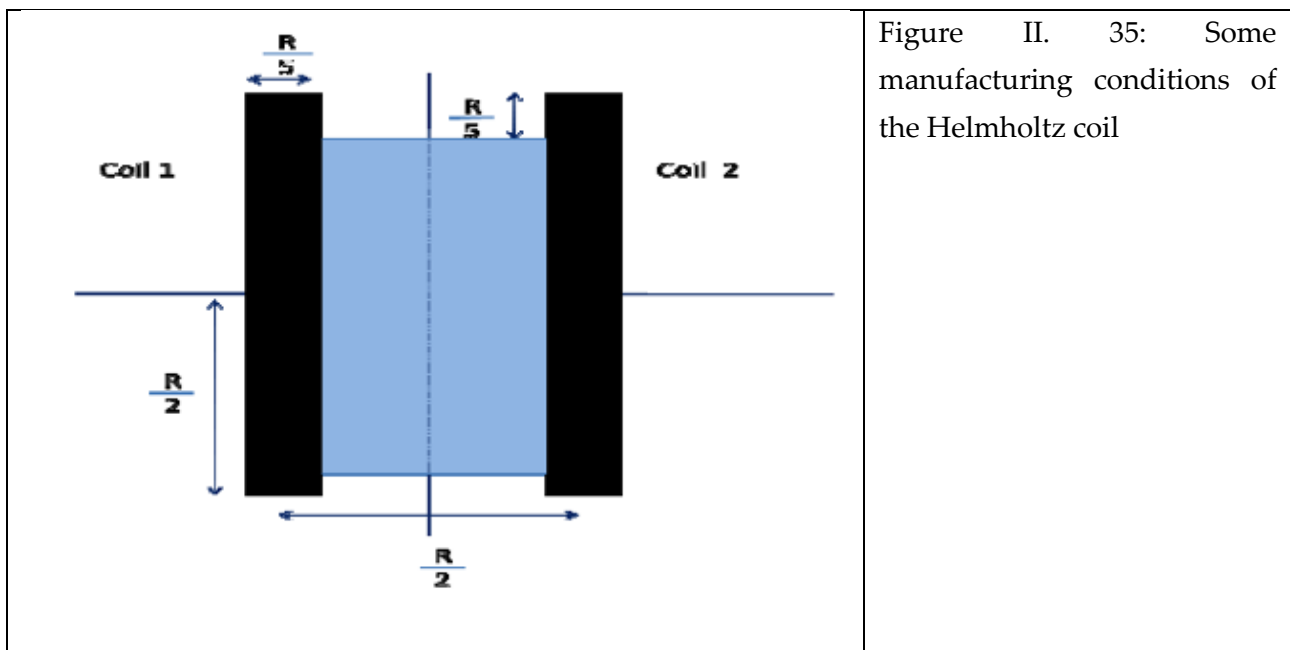


Figure II. 35: Some manufacturing conditions of the Helmholtz coil

12.8.1.1 Consistent Twin Coil Characteristics

It is imperative that the coils have identical geometric characteristics, number of turns, and electrical current. This strict uniformity ensures the harmonious alignment of the generated magnetic field, thus contributing to optimal performance.

12.8.1.2 Alignment and Spacing Accuracy

Precise parallel alignment, combined with radius-equivalent spacing, is essential to achieve uniform magnetic field distribution across the core of the device. This rigorous arrangement eliminates any unwanted asymmetry.

12.8.1.3 Sizing of the Coiled Section

For optimum performance, the dimensions of the wound section in terms of width and depth should not exceed one tenth of the coil diameter ($D/10$). This measurement ensures consistent winding and prevents unwanted distortions of the magnetic field.

12.8.1.4 Selection of Good Conductive Materials

The choice of materials for the coils is crucial. Using materials such as 1 mm thick copper wire, which allows good current flow and has low resistance, is essential to minimize energy losses and optimize coil operation.

12.8.1.5 Careful Insulation

Proper coil insulation is essential to prevent current leakage and unwanted electromagnetic interference. Good insulation allows the coils to operate independently and prevents unwanted external influences. Therefore, the use of a specific type of plastic is recommended.

12.8.1.6 Adding Iron

The incorporation of iron into the Helmholtz coil significantly contributes to increasing the magnetic field, thus avoiding the need to excessively increase the number of turns. This helps to optimize the efficiency of the device.

12.8.2 CAD

To develop the model of the Helmholtz coil, we used the software "FreeCad".

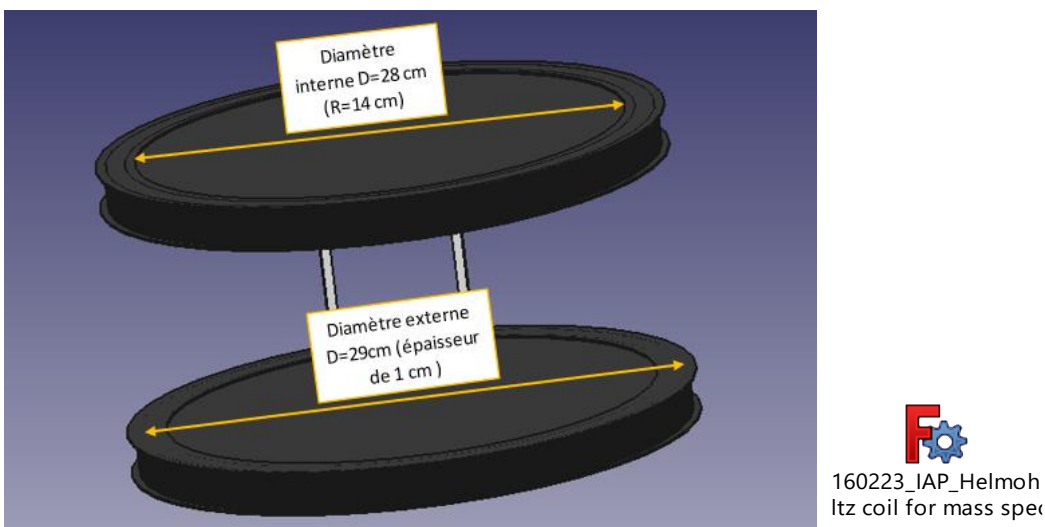
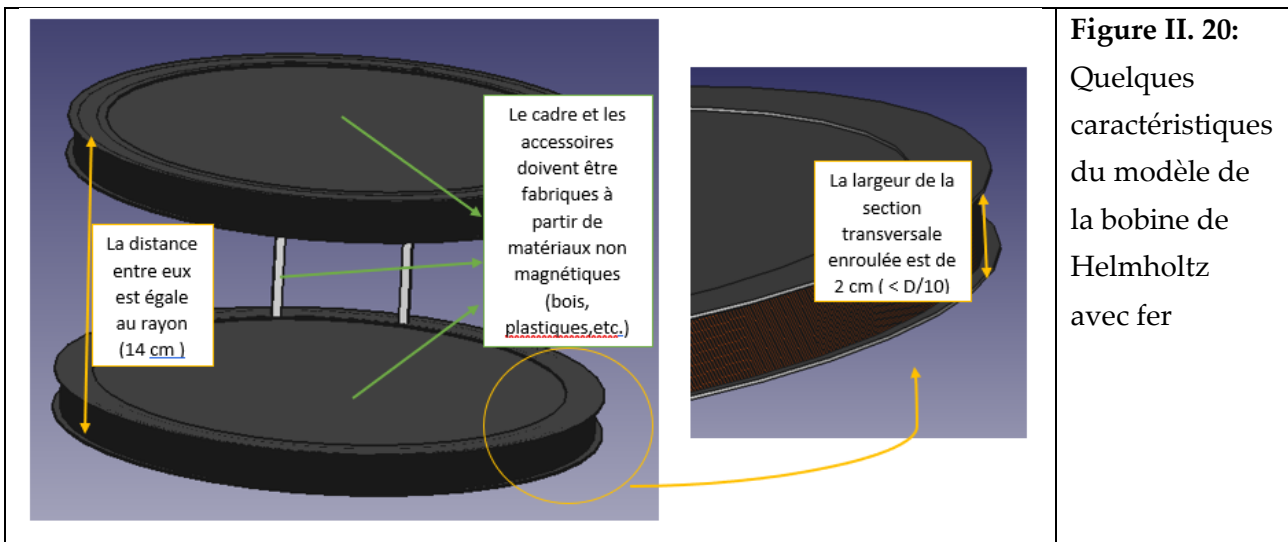


Figure II. 36: Some measurements of the Helmholtz coil model with iron



12.9 Realization of Helmholtz Coils

To exploit the Helmholtz coil formula while ensuring the required diameter and meeting our need for a significant magnetic field, it is important to consider the constraint related to the electric current that can be supplied to the coil. This implies a high number of turns, exceeding 4000, which can be difficult to achieve. In order to reduce this number, we opted for the addition of ferrous material inside the coil. This approach increases the magnetic field while requiring a lower number of turns. It should be noted that soft iron is the preferred material in such projects, but due to its limited availability, we undertook an experiment comparing two commonly available types of iron: ordinary iron, accessible to all, and the type used in transformers, known for its beneficial effect on the magnetic field.

We have: $B = \frac{\mu I N R^2}{2(R^2 + (x - \frac{d'}{2})^2)^{\frac{3}{2}}}$ with $R'=14$ cm, $x=7.5$ cm, $d'=14$ cm.

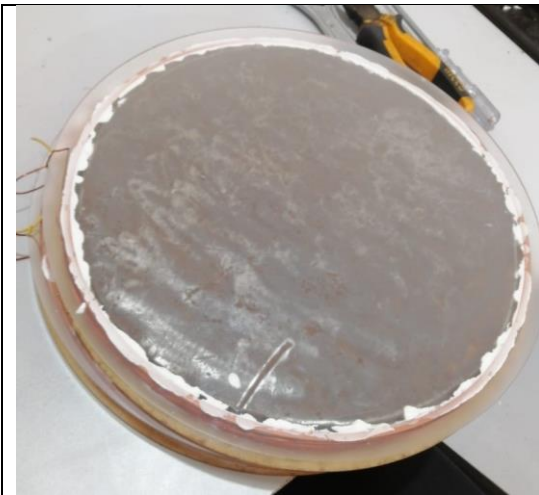


Figure II. 21: l'emplacement du fer ordinaire dans la bobine de Helmholtz

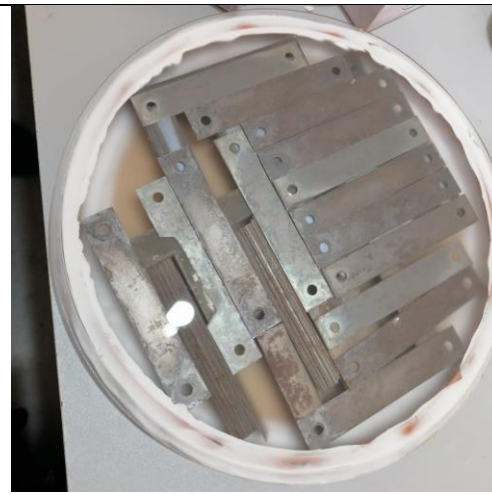


Figure II. 22: L'emplacement du fer spécifique des transformateurs dans la bobine de Helmholtz

The permeability of iron will be determined from the experiment. The parameters I and N will be adjusted until a magnetic field of 0.2 Tesla is obtained.

12.10 Helmholtz Coils System Test Specification

Stage	Description of the stage	Expected result
Precondition	The system is off	
Turn on the system	Turn on the Helmholtz coil by supplying it with a corresponding power supply	Obtain a magnetic field ($B = 0.2$ T)
Turn off the system	Turn off the Helmholtz coil	The magnetic field stops
Postcondition	The system is off	

12.11 Helmholtz Coils System Tests and Results

12.11.1 Test 22.09.23

Stage	Description of the stage	Expected result	Result
Precondition	The system is off		
Turn on the system	Turn on the Helmholtz coil by supplying it with a corresponding power supply	Obtain a magnetic field ($B = 0.2 \text{ T}$)	Negative
Turn off the system	Turn off the Helmholtz coil	The magnetic field stops	Positive
Postcondition	The system is off		

12.11.1.1 Analysis of test results:

In this experiment, we used iron similar to that found in transformers. We connected them optimally and inserted them inside each flat coil. We set the number of turns to $N = 10$. At each step, we gradually increased the voltage, which caused an increase in the current as well as the magnetic field. This process was repeated until the value $B = 0.6 \text{ mT} \ll 200 \text{ mT}$ was reached.

I (A)	0.58	1.14	1.72	2.32	2.88	3.41	3.98	4.53	5.63	6.13	6.62	7.15	7.62	8.62
U (v)	0.25	0.5	0.75	1	1.25	1.5	1.76	2	2.5	2.75	3	3.26	3.51	4
B (mT)	---	---	---	0.2	0.25	0.28	0.31	0.34	0.42	0.45	0.48	0.51	0.53	0.6

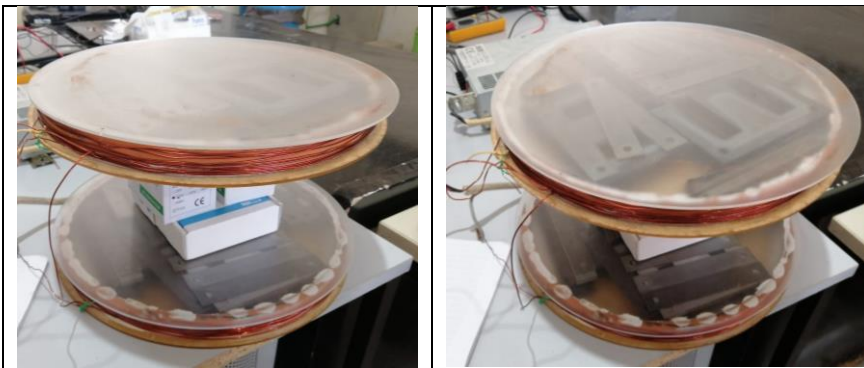


Figure III. 44: Arrangement of the transformer iron at a distance of 14 cm in each of the flat coils

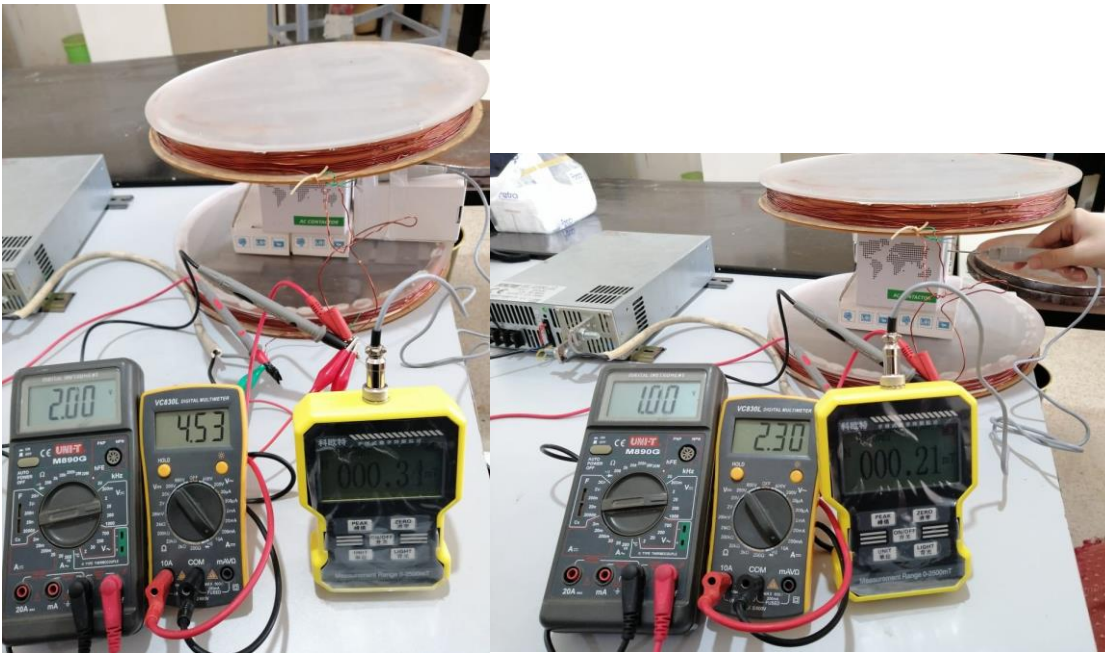


Figure III. 45: Measurement of the magnetic field at the center of the Helmholtz coil using the transformer iron

What we need to do:

- We will change the type of iron.
- We will change the location of the iron each time.

12.11.2 Test 09.10.23

In this study, variations were made to the type of ferrous material used and its location, while maintaining a constant number of turns, $N = 10$.

- a) In the first phase of the experiment, an ordinary iron plate with a diameter of 28 cm and a thickness of 1.5 cm was used. Only one of these plates was positioned in each flat coil. By modulating the voltage at each iteration, results similar to those obtained in the previous experiment regarding the value of magnetic induction (B) were observed. The maximum value reached was $B = 0.6 \text{ mT} \ll 200 \text{ mT}$.

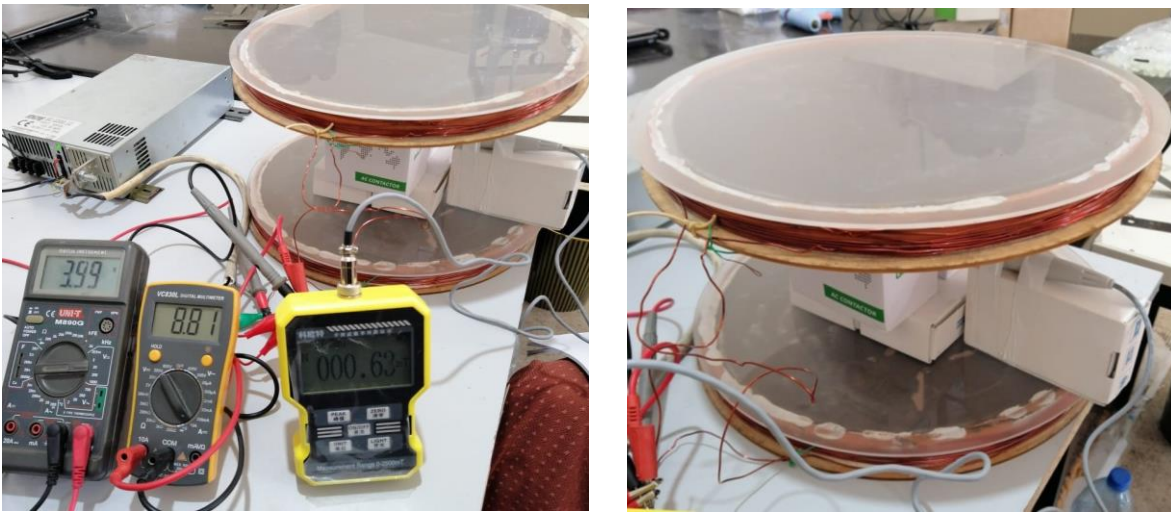


Figure III. 46: Measurement of the magnetic field using two ordinary iron plates 28 cm in diameter and 1.5 cm thick

b) In order to study the influence of iron on the magnetic field, a second experiment was conducted using Helmholtz coils without having iron inside the flat coils. We will then proceed to a comparison with the results obtained in the previous experiment.

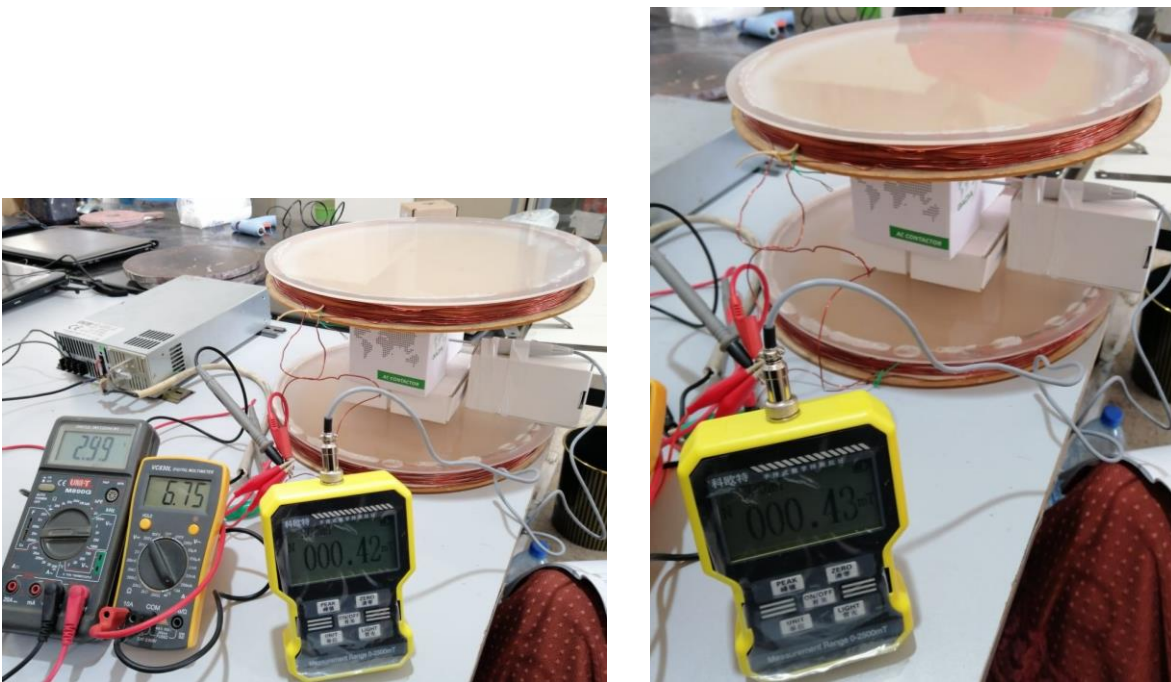


Figure III. 47: Evaluation of the magnetic field in the absence of ferromagnetic material

In this comparison, we have chosen only two voltage values:

For $V = 3 \text{ v}$, $I = 6.72 \text{ A}$, we obtain $B = 0.42 \text{ mT}$.

For $V = 4 \text{ v}$, $I = 8.69 \text{ A}$, we obtain $B = 0.53 \text{ mT}$.

The observed difference between the experiment with and without iron amounts to approximately 0.06 mT , thus demonstrating that the influence of iron is extremely low.

c) At this point we adjusted the iron layout according to the diagrams shown below.

Despite the change in the position of the iron, the result remains almost unchanged.

We were unable to increase the intensity of the magnetic field.

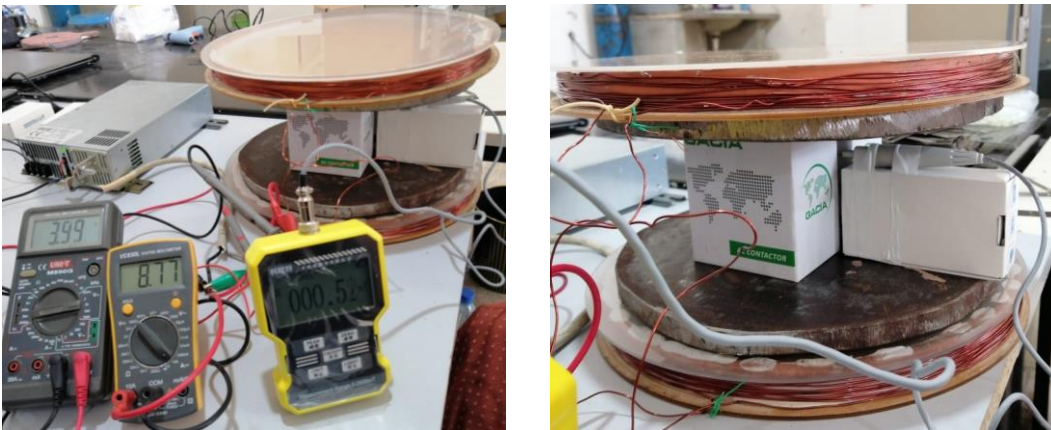


Figure III. 48: Evaluation of the magnetic field when inserting two ordinary iron plates inside the space separating the flat coils of the Helmholtz coil

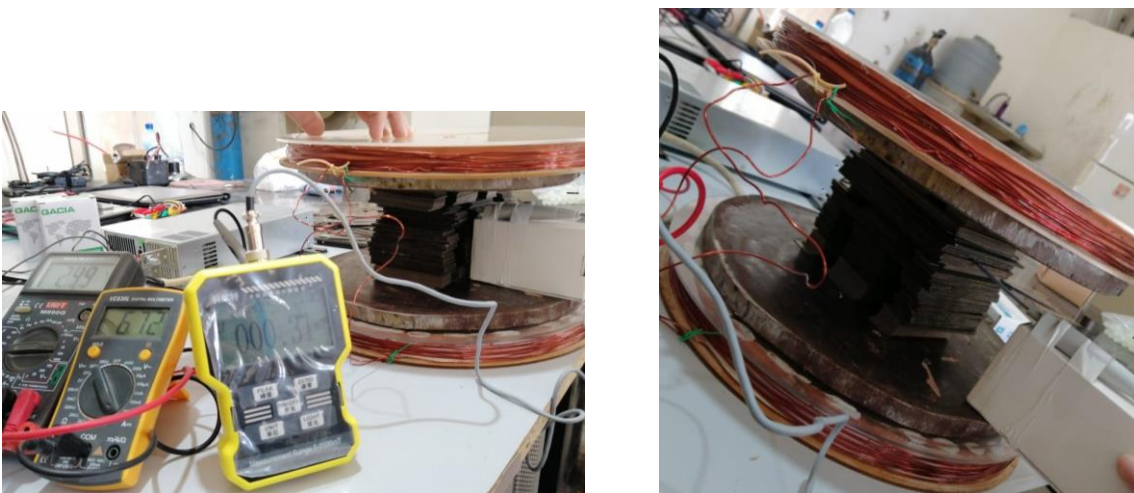


Figure III. 49: Evaluation of the magnetic field when ordinary iron and transformer iron are simultaneously installed in the center of the Helmholtz coil.



Figure III. 50: Evaluation of the magnetic field when inserting two ordinary iron plates in the center of the Helmholtz coil

12.11.2.1 Conclusion

From previous experiences we have drawn the following conclusions:

- The use of iron in the transformer did not bring any significant improvement. This can be attributed to the space between the pieces of iron and their uneven distribution inside the flat coil.
- Replacing the iron used in the transformer with another disc-shaped piece of iron placed inside the flat coil also did not bring any significant improvement. When we revisited this issue and researched the principle of using iron cores inside the coil to improve the magnetic field, we found that it was usually better to use iron where the radius \ll the width. Thus, the lack of increase in the magnetic field could be attributed to the fact that the thickness of the iron \ll the radius.
- Changing the position of the iron and placing it in the middle of the Helmholtz coil also did not bring any significant improvement.

12.11.3 Test 20.10.23

The choice of iron volume in the Helmholtz coil design, where the radius is considerably larger than the thickness, presented an inefficiency in amplifying the magnetic field. This observation prompted consideration of an alternative iron configuration to optimize the magnetic field. Thus, we favored the use of an iron cylinder, where the thickness \gg the radius, while wrapping the cylinder with copper coils. This approach was guided by maintaining the fundamental principles of the Helmholtz coil.

In our experiments, solenoids were positioned opposite each other, respecting a distance of 14 cm between them, as detailed in the experiments below.

- a) In the case where two solenoids have been arranged face to face: For $N=42$ turns, $I= 6.02$ A, $d= 14$ cm; we have $B= 0.23$ mT.



Figure III. 51: Évaluation du champ magnétique lors du positionnement de deux solénoïdes en face l'un de l'autre

- b) In the case where three solenoids, placed at equal distances from each other, were arranged face to face:

For $N=42$ turns, $I= 3.5$ A, $d= 14$ cm; we have $B= 0.28$ mT.

- c) In the case where three solenoids, glued to each other, were arranged face to face:

For $N=42$ turns, $I= 6$ A, $d= 14$ cm; we have $B= 0.5$ mT.

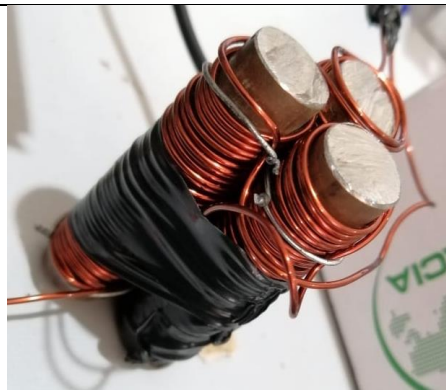


Figure III. 52: Évaluation du champ magnétique avec l'installation de trois solénoïdes, espacés de manière égale les uns des autres, en configuration face à face



Figure III. 53: Evaluation of the magnetic field when positioning three solenoids, back to back, in a face-to-face configuration

d) In the case where three solenoids, glued to each other, were arranged face to face. However, in this situation we replaced the copper wires with wires with a higher thickness (2.25 mm).

For $N=90$ turns, $I= 9.5$ A, $d= 14$ cm; we have $B= 2.54$ mT.

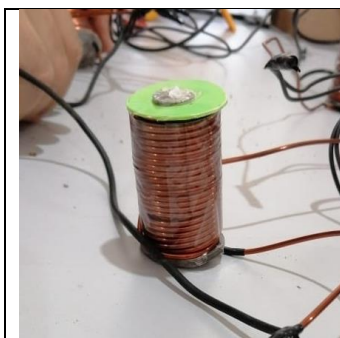


Figure III. 54: Evaluation of the magnetic field when installing three juxtaposed solenoids, using 2.25 mm thick copper wires

12.12 Mass Spectrometer System Test Specification

12.12.1 00001: Ensure complete air evacuation

Stage	Description of the stage	Expected result
Precondition	The system is off	
Turn on the system	Turn on the pump	95% empty
Presence of a leak	Risk of air leakage at the following locations: welds, flanges, anode, cathode, plates, tungsten windows, detector	Seal leak locations
Turn off the system	Turn off the pump	The pump stops extracting air

Use of silicon	Apply silicone to the areas where air is leaking.	Stop the leak and achieve 95% vacuum when we restart the pump
Postcondition	The system is off	

12.12.2 00002: Tungsten power supply

Stage	Description of the stage	Expected result
Precondition	The system is off	
Turn on the system	Turn on the power supply	Obtain a continuous power supply (8 V)
Turn off the system	Turn off the power supply	Continuous power supply stops
Postcondition	The system is off	

12.12.3 00003: First positively charged plate (trap) electron)

Stage	Description of the stage	Expected result
Precondition	The system is off	
Turn on the system	Turn on the power between the tungsten and the plate	Obtain a continuous power supply (17 V)
Turn off the system	Turn off the power supply	Continuous power supply stops
Postcondition	The system is off	

12.12.4 00004: Second positively charged plate (ion repellent)

Stage	Description of the stage	Expected result
Precondition	The system is off	
Turn on the system	Turn on the power supply	Obtain continuous power (determine experimentally)

Turn off the system	Turn off the power supply	Continuous power supply stops
Postcondition	The system is off	

12.12.5 00005: Obtain electrons

Stage	Description of the stage	Expected result
Precondition	The system is off	
Turn on the specific pump valve	Turn on the valve	The valve is open
Turn on the pump	Turn on the pump	95% empty
Turn on the tungsten power supply	Turn on the power supply	Obtain a continuous power supply (8 V)
Turn on the power between the tungsten and the plate	Turn on the power supply	Obtain a continuous power supply (17 V)
Burning tungsten	Burn the tungsten by supplying it with 8V power	Get electrons around the tungsten (the lamp will light up).
Electron trap	The 17v power supply is connected to the first board	The first positively charged plate attracts electrons towards it (moving electrons)
Turn off the power to the electron trap	Turn off the power supply	Electrons are not in motion
Turn off the tungsten power supply	Turn off the power supply	The lamp will go out
Turn off the pump	Turn off the pump	The pump stops extracting air
Turn off the specific pump valve	Turn off the valve	The valve is closed
Postcondition	The system is off	

12.12.6 00006: Detector

Stage	Description of the stage	Expected result
Precondition	The system is off	
Turn on the system	Turn on the detector	The detector emits a signal when it receives ions
Turn off the system	Turn off the detector	The detector is not working
Postcondition	The system is off	

00007: Ionization

Stage	Description of the stage	Expected result
Precondition	The system is off	
Turn on the specific pump valve	Turn on the valve	The valve is open
Turn on the pump	Turn on the pump	95% empty
Turn on the tungsten power supply	Turn on the power supply	Obtain a continuous power supply (8 V)
electron trap " plate	Turn on the power supply	Obtain a continuous power supply (17 V)
Burning tungsten	Burn the tungsten by supplying it with 8V power	Get electrons around the tungsten (the lamp will light up)
Electron trap	The 17V power supply is connected to the first board	The first positively charged plate attracts electrons towards it (moving electrons)
Turn off the pump	Turn off the pump	The pump stops extracting air
Turn off the specific pump valve	Turn off the valve	The valve is closed
Turn on the detector	Turn on the detector	The detector is working

Turn on the specific gas valve	Open the valve, introduce the steam, then, after a few minutes, turn off the valve	The electrons will collide with the atoms in the vapor sample (obtaining ions with a (+1) charge)
Turn on the power supply to the "ion repellent" plate	Turn on the power supply	Obtain continuous power (determine experimentally)
Ion repellent	The power supply is connected to the second plate	The detector emits a signal (indicating that the second positively charged plate has repelled the ions out of the ionization chamber, and the ions have entered the tube)
Turn off the detector	Turn off the detector	The detector is not working
Turn off the power to the "ion repellent" plate	Turn off the power supply	The second plate is no longer loaded
electron trap plate	Turn off the power supply	The first plate is no longer loaded
Turn off the tungsten power supply	Turn off the power supply	The lamp will go out
Postcondition	The system is off	

12.12.7 00008: Power supply to the three plates (Acceleration zone)

Stage	Description of the stage	Expected result
Precondition	The system is off	
Turn on the system	Turn on the power supply	Obtain a continuous power supply (-300 V, -150, 0)
Turn off the system	Turn off the power supply	Continuous power supply stops
Postcondition	The system is off.	

12.12.8 00009: Helmholtz coil

Stage	Description of the stage	Expected result
Precondition	The system is off	
Turn on the system	Turn on the Helmholtz coil by supplying it with power (determine experimentally)	Obtain a magnetic field ($B = 0.2 \text{ T}$)
Turn off the system	Turn off the Helmholtz coil	The magnetic field stops
Postcondition	The system is off	

12.12.9 00010: Acceleration and Deviation

Stage	Description of the stage	Expected result
Precondition	The system is off	
Turn on the specific pump valve	Open the valve	The valve is open
Turn on the pump	Turn on the pump	95% empty
Turn on the tungsten power supply	Turn on the power supply	Provide continuous power (8V)
electron trap " plate	Turn on the power supply	Provide 17V DC power
Burning tungsten	Burn the tungsten by supplying it with 8V power	Generate electrons around the tungsten (the lamp will light up)
Electron trap	The power supply is connected to the first plate	The first positively charged plate attracts electrons towards it (moving electrons)
Turn off the pump	Turn off the pump	The pump stops extracting air
Turn off the specific pump valve	Close the valve	The valve is closed
Turn on the detector	Turn on the detector	The detector is on

Turn on the specific gas valve	Turn on the valve, let the steam in, then after a few minutes turn the valve off	The electrons will collide with the atoms in the vapor sample (creating ions with a +1 charge)
Turn on the specific power supply for the "ion repellent" plate	Turn on the power supply	Obtain continuous power (determine experimentally)
Turn on the specific power supply for three plates	Turn on the power supply	Get a continuous power supply of (-300V, -150V, 0)
Turn on the Helmholtz coil	Turn on the Helmholtz coil on the bent tube	Obtain a magnetic field ($B = 0.2 \text{ T}$)
Ion repellent	The power supply is connected to the second plate	The second positively charged plate repels the ions out of the ionization chamber, and the ions enter the tube
Acceleration of ions	Connect the power supply to the three plates at the beginning of the tube	Ions entering the tube will be accelerated
Ion deflection	The ions will be subjected to a magnetic field of $B = 0.2 \text{ T}$ as they pass through the curve	The detector emits a signal (indicating that the ions have left the ionization chamber, entered the tube, been accelerated by the plates, deflected by the magnetic field and have been detected)
Turn off the power to the three-plate stove	Turn off the power	Ion acceleration stops, no signal will appear
Turn off the detector	Turn off the detector	The detector is not working
Turn off the Helmholtz Coil	Turn off the Helmholtz coil	The magnetic field stops

Turn off the power supply (ion repellent)	Turn off the power	The second plate is no longer loaded
Turn off the power supply (electron trap)	Turn off the power	The first plate is no longer loaded
Turn off the tungsten power supply	Turn off the power	The lamp will go out
Postcondition	The system is off	

12.13 Conclusion and Perspectives for using Helmholtz Coils for Mass Spectrometer

In conclusion, the project to manufacture a mass spectrometer to detect toxic gases from waste combustion presented several challenges, particularly in the design of the Helmholtz coil to ensure a magnetic field of 0.2 T in the deflection zone. Optimization attempts, whether using iron from the transformer or ordinary iron, faced limitations related to the material thickness. Adjustments, such as increasing the iron thickness and using thicker copper coils, improved the magnetic field, although the target value was not reached.

Looking ahead, promising solutions include exploring the use of soft iron cores, known for their high relativistic permeability, or fabricating iron cylinders by melting transformer material with a thickness greater than the radius. These approaches will need to adhere to the principles of the Helmholtz coil to ensure the spectrometer's efficiency.

Additionally, potential challenges in spectrometer operation have been identified, such as vacuum issues. Addressing this will require the adoption of a pump that can achieve high vacuum up to 10^{-7} torr, such as a turbomolecular pump in series with a rotary pump. Concerns regarding the insulation and fabrication of the Faraday cup detector are also raised, but further research could help address these potential issues.

In summary, these proposed improvements and solutions pave the way for future developments aimed at optimizing the mass spectrometer for more efficient detection of toxic gases.

12.14 Bibliography

- [1] E. Garg and M. Zubair, "Mass Spectrometer," *In StatPearls [Internet]*, 2023.
- [2] W. Barthelemy, "Thermionic Emission Isotope Mass Spectrometry," 2009.
- [3] G. Bouchoux and M. Sablier, "Mass spectrometry: principle and apparatus," *Engineering Techniques*, 2005.
- [4] "Mass Spectrometry Basics," [Online]. Available: <https://www.jeolusa.com/RESOURCES/Analytical-Instruments/Mass-Spectrometry-Basics>.

-
- [5] P. Noriega, G. Gortaire and E. Osorio, "Mass Spectrometry and Its Importance for the Analysis and Discovery of Active Molecules in Natural Products," *Natural Drugs from Plants*, 2021.
- [6] S. Harper, P. Calandra and S. Price, "Electron-impact ionization of hydrogen chloride," *Physical Chemistry Chemical Physics*, vol. 3, no. 5, pp. 741-749, 2001.
- [7] J. Fletcher, M. Parkes and S. Price, "Electron ionization of sulfur dioxide," *The Journal of Chemical Physics*, vol. 138, no. 18, 2013.
- [8] J. Johns and R. Barrow, "Ionization Potentials of Hydrogen Fluoride and the Ground-State of the HF⁺ Ion," *Nature*, vol. 179, no. 4571, p. 1186-1186, 1957.
- [9] M. Alagia and et al., "The double photoionization of hydrogen iodide molecules," *The Journal of Chemical Physics*, vol. 124, no. 20, 2006.
- [10] D. Lide, "Ionization potentials of atoms and atomic ions," *Handbook of Chemistry and Physics*, vol. 10, p. 211, 1992.
- [11] P. Redhead and S. Feser, "Multiple ionization of mercury by successive electron impacts," *Canadian Journal of Physics*, vol. 46, no. 17, pp. 1905-1913, 1968.
- [12] V. Bellosta, "Identification of organic compounds by mass spectrometry," 2005.
- [13] C. Cassagnol, Y. Ortel and J. Taieb, "A mass spectrometer for the rapid analysis of gaseous mixtures; Mass spectrometer for the rapid analysis of gaseous mixtures," 1950.
- [14] J. Beynon and L. Brown, "Mass Spectrometry," *Encyclopedia Britannica*, Nov 3, 2023.
- [15] J. Gross, *Mass spectrometry: a textbook*, Springer Science & Business Media, 2006.
- [16] V. Bhatt, R. Rautela, P. Sharma, D. Tiwari and S. Khushu, "Design & Development of Helmholtz Coil for Hyperpolarized MRI," *In Proceedings of the COMSOL Conference*, pp. 1-6, 2010.
- [17] M. Ashby, H. Shercliff and D. Cebon, "Materials: engineering, science, processing and design," 2018.
- [18] "Faraday Cup," [Online]. Available: <https://www.electricity-magnetism.org/faraday-cup/>.
- [19] E. Hoffmann and V. Stroobant, "Mass spectrometry: principles and applications," 2007.
- [20] K. Busch, "Detecting ions in mass spectrometers with the Faraday cup," *Spectroscopy*, vol. 26, no. 11, pp. 12-18, 2011.
- [21] S. Sabbah, "A Solid-State Ion Detector for Use in Portable Mass Spectrometry," *Brigham Young University*, 2014.

12.15 LIST OF FIGURES

Figure I. 1: Schematic representation of a mass spectrometer **Error! Bookmark not defined.**

Figure I. 2: Ionization chamber of the mass spectrometer **Error! Bookmark not defined.**

Figure I. 3: Ion acceleration zone of a mass spectrometer **Error! Bookmark not defined.**

Figure I. 4: Deflection zone of a mass spectrometer	Error! Bookmark not defined.
Figure I. 5: Orientation of the magnetic force on a moving ion	Error! Bookmark not defined.
Figure I. 6: Deflection of the trajectory of ions under the effect of the magnetic field	Error! Bookmark not defined.
Figure I. 7: The detection process at the microscopic level	Error! Bookmark not defined.
Figure I. 8: Arnocanali 20 type pump	Error! Bookmark not defined.
Figure III. 1: Arrangement of the transformer iron at a distance of 14 cm in each of the flat coils	443
Figure III. 2: Measurement of the magnetic field at the center of the Helmholtz coil using the iron of transformer	444
Figure III. 3: Measurement of the magnetic field using two ordinary iron plates 28 cm in diameter and 1.5 cm thick	445
Figure III. 4: Evaluation of the magnetic field in the absence of ferromagnetic material	445
Figure III. 5: Evaluation of the magnetic field when inserting two ordinary iron plates inside the space separating the flat coils of the Helmholtz coil	446
Figure III. 6: Evaluation of the magnetic field when ordinary iron and transformer iron are simultaneously installed in the center of the Helmholtz coil	446
Figure III. 7: Evaluation of the magnetic field when inserting two ordinary iron plates into the center of the Helmholtz coil	447
Figure III. 8: Evaluation of the magnetic field when positioning two solenoids opposite each other	448
Figure III. 9: Magnetic field evaluation with the installation of three solenoids, equally spaced from each other, in face-to-face configuration	448
Figure III. 10: Evaluation of the magnetic field when positioning three solenoids, back to back, in a face-to-face configuration	449
Figure III. 11: Evaluation of the magnetic field when installing three juxtaposed solenoids, using 2.25 mm thick copper wires	449
Figure III. 12: Instruments used to locate air leaks	Error! Bookmark not defined.
Figure III. 13: Air leak points	Error! Bookmark not defined.
Figure III. 14: During the cleaning process of the stainless steel tube	Error! Bookmark not defined.
Figure III. 15: Preparation in progress of the device to improve the welding process	Error! Bookmark not defined.
Figure III. 16: Performing a new air leak check	Error! Bookmark not defined.
Figure III. 17: Air leak locations	Error! Bookmark not defined.

12.16 LIST OF TABLES

Table I. 1: Ionization energy of certain types of gas	Error! Bookmark not defined.
--	-------------------------------------

Table I. 2: Characteristics of some types of gases **Error! Bookmark not defined.**
Table I. 3: Pressure ranges in vacuum technology **Error! Bookmark not defined.**



MASTER THESIS

In order to obtain the

PROFESSIONAL MASTER

Energetics

Insured by:

Faculty of Sciences of the Lebanese University

Presented and defended by:

Omar Ali Zreika

On October, 2024

Title

**Mass Spectrometer for Detection of Toxic Metals in Municipal Waste
Incineration Flue Gas**

Supervisor

Dr. Samir Mourad

Reviewers

Dr. Ahmad El Mol

Dr. Wassim Shmaysem

13.1 ABSTRACT

The mass spectrometer is a critical tool in research, with numerous applications, particularly in detecting toxic gases emitted during waste combustion. This analytical process consists of several stages, beginning with the ionization of the gases, followed by their acceleration and subsequent deflection, ultimately leading to their detection to ascertain both the type and mass of the gases present. The design and optimization of the electromagnet within the deflection zone are essential for facilitating this deflection. The findings of this research have been subjected to comprehensive analysis and discussion concerning the principles of electromagnetism.

13.2 CHAPTER 0: INTRODUCTION

In Lebanon, we are currently facing a crisis in energy generation.

Therefore, one of AECENAR's most significant projects was the construction of a power generation facility, specifically an incinerator, designed to generate energy through the combustion of waste.

Burning waste produces emissions of toxic and carcinogenic gases, making it essential to purify these gases to prevent the release of harmful substances into the atmosphere.

AECENAR has installed an electrostatic filter to purify the gases emitted during incineration; however, the Municipality requires evidence that no toxic emissions are present. This is where the mass spectrometer detector plays a crucial role.

This system can detect and identify the types and quantities of gases produced based on their mass.

This project was initiated two years ago by students Asmaa El Mir and Rouwayda El Sakka. However, it remains incomplete, particularly the magnetic sector, which is essential for gas detection.

The structure of this thesis is outlined below:

In the first chapter, we introduced the fundamental principles of mass spectrometry and its critical role in gas detection. Furthermore, we discussed magnetic permeability and presented various methods to enhance it. Additionally, we explained the simulation of the magnetic field and the effects of ferromagnetic cores on it.

In the second chapter, we explored electromagnetic concepts and conducted a simulation, along with a straightforward comparison between two systems: the multi-solenoid and the C-shaped coil. Based on the simulation results, we drew our conclusions.

In the third chapter, we began the realization of the electromagnetic system through a series of processes. Ultimately, we constructed the system and conducted tests on it.

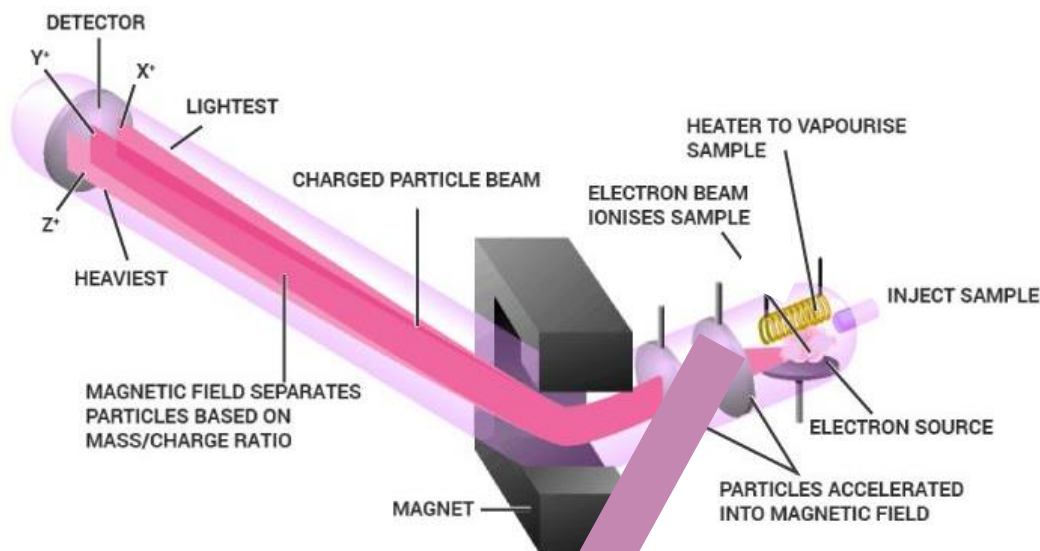
Finally, we reached our conclusion in the last chapter.

13.3 CHAPTER I: BASICS

13.3.1 Mass Spectrometer Principle

Mass spectrometers analyze the distinct fragments or ions produced by organic molecules by bombarding the compound with electrons to create positively charged ions.

The resulting mass spectrum displays each ion as a peak. [1]



MS

consists of four main parts: the ionization source where the molecules get ionized, the acceleration zone where ions gain higher velocity, the deflection determined by the mass-to-charge ratio (m/z), and finally, the detection part which is proportional to the abundance of ions (see Figure 1).

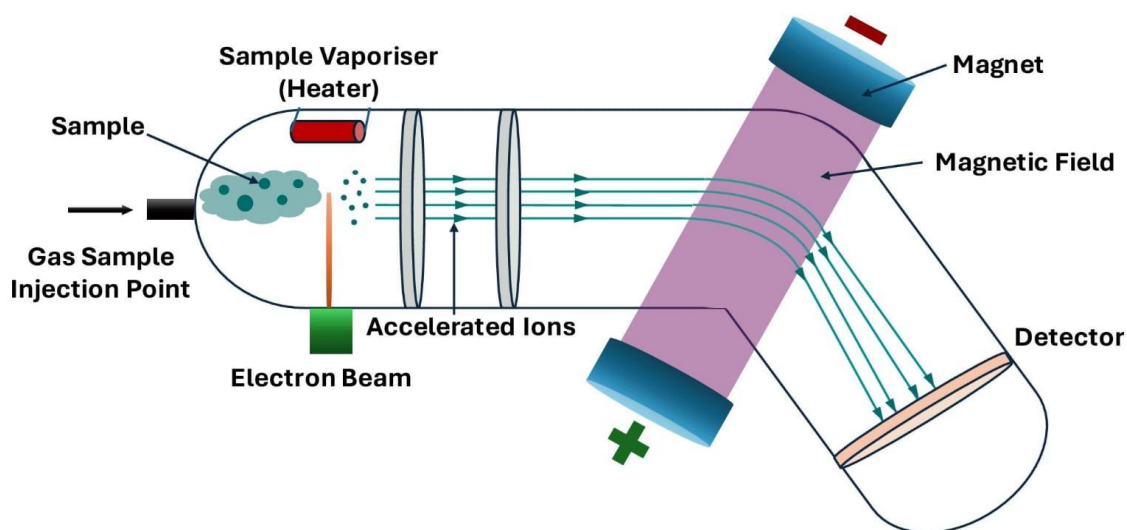
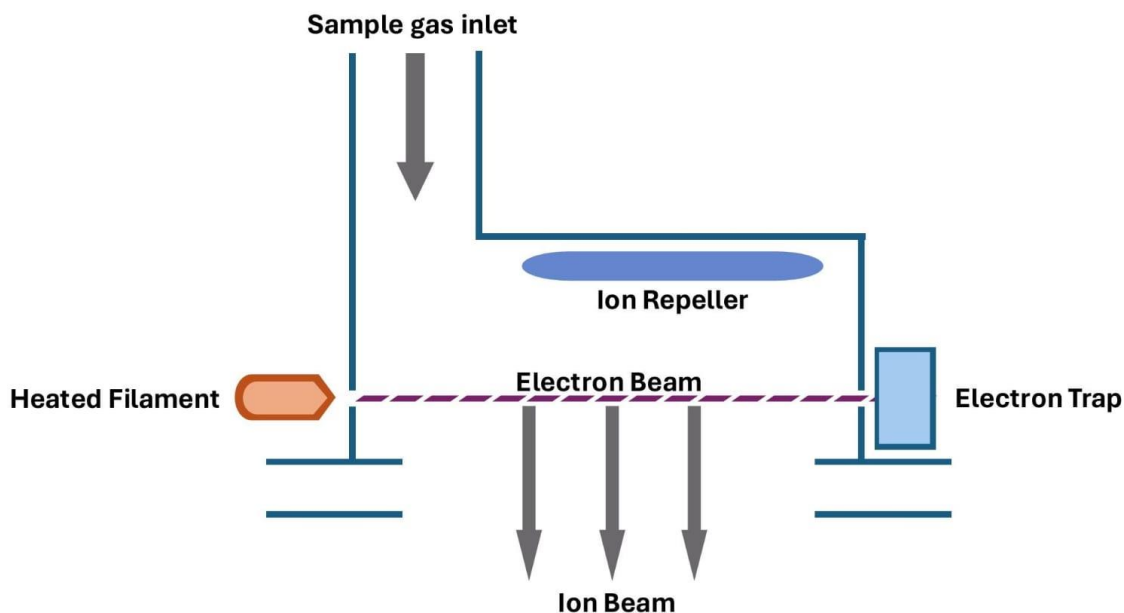


Figure 1: Schematic representation of the principle of mass spectrometry

13.3.1.1 Ionization Source

The ionization source is a device that can be used in several methods and techniques to ionize molecules. The method chosen depends on the type of the sample, such as gas, liquid, or solid. Since our project focuses on toxic gases, electron impact ionization [2] is the suitable method in our case (see Figure 2). The sample should be in a gaseous phase to enter the ion source. In this situation, we use a heated filament made of tungsten to collide with the gaseous sample molecules and generate positive ions. Since it is much more difficult to remove more than one electron, most of the ions will have a charge of +1.

It is important to note that the ion source must be evacuated to prevent contact with air molecules.



[3]

Figure 2: Schematic representation of the ionization chamber

13.3.1.2 Acceleration Zone

The positive ions are pushed out by the ion repeller, which is a positively charged plate (see Figure 2). Subsequently, they pass through the acceleration zone, where they are subjected to an intense electric field specifically designed to accelerate them and increase their kinetic energy.

The acceleration zone is created by three plates that are gradually charged negatively, with the first disc being strongly negative (300 V), generating a powerful electric field that propels the positive ions towards the last disc.

As the ions progress towards the subsequent discs, they continue to be accelerated by the electric field until they reach the final disc, which is neutral and acts as a ground (see Figure 3).

The precise control of the electric field between the discs ensures optimal focusing of the positive ions, preventing any undesired dispersion or deflection. An intermediate disc, also negatively charged (150 V) but at a reduced intensity compared to the first disc, ensures a gradual acceleration of the positive ions. This stabilization in their trajectory allows them to pass to the third disc, which acts as a final barrier, enabling the positive ions to reach the region of the mass spectrometer dedicated to their analysis.

We should note that all positive ions will have the same kinetic energy after acceleration. [4]

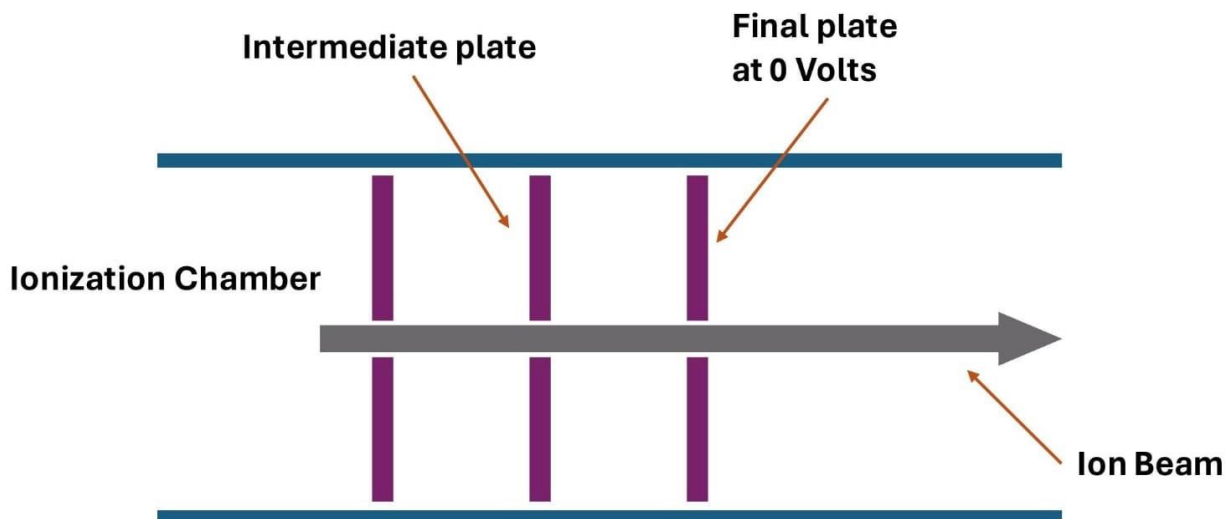


Figure 3: Schematic representation of the acceleration plates

13.3.1.3 Deflection Zone

The deflection zone in a mass spectrometer is a crucial step for separating ions based on the mass-to-charge ratio (m/z), allowing us to identify each chemical species in our sample.

The ions emerging from the ionization source enter a region with a uniform magnetic field, causing them to experience a magnetic force that deviates them from their initial trajectory.

Ions with higher m/z ratios will experience less deflection compared to ions with lower m/z ratios. This difference enables us to separate ions based on their masses. Since most ions carry the same charge of +1, the extent of deflection will be determined by the mass of the ions. [5]

The path of the ions is typically curved with a radius R . This trajectory is governed by either Biot-Savart's law or the Lorentz force. [6]

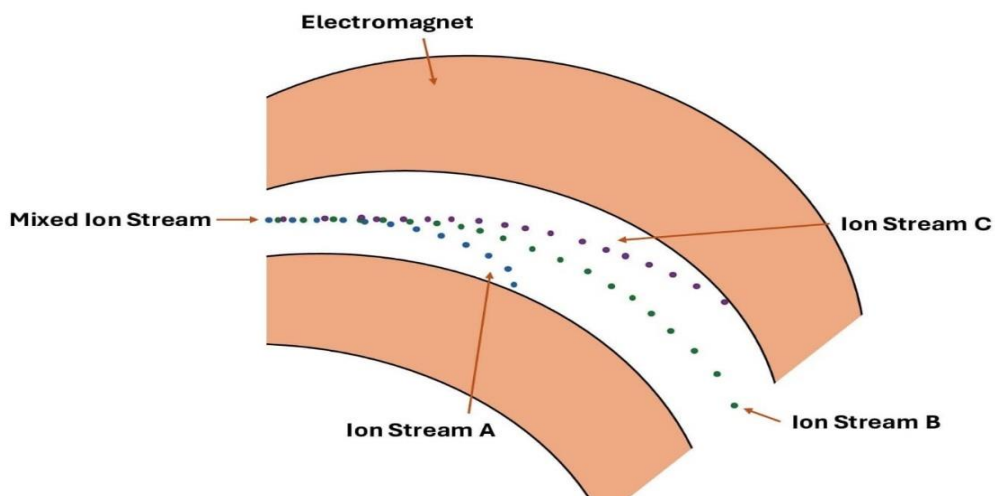


Figure 4: Deflection of a mixed ion stream under magnetic field

In other words, the heavier the ions, the less they deflect. Furthermore, they will require a stronger magnetic field to deflect them. For example, we recognize that ion stream C is heavier than B, which is heavier than A. (see Figure 4).

13.3.1.4 Detection of Ions

In the realm of mass spectrometry, the detection stage holds significant importance as it pertains to the identification of ions that have traversed the mass analyzer's pathway.

The detector plays an essential role in converting ions into a detectable and usable signal.

Once sorted by the mass analyzer, the ions enter the detection zone where the detector is located. This component is designed to capture the physical characteristics of the ions, including their kinetic energy, electric charge, and mass. Mass spectrometers utilize a variety of detector types, each with unique advantages tailored to the specific requirements of the analytical application. Furthermore, the selection of the detector is influenced by the design of the instrument itself. [7]

When an ion reaches the collector, its charge is neutralized by an electron transferring from the metal to the ion. The flow of electrons generated in the wire is identified as an electric current, which can be amplified and recorded. The level of detected current increases with the increasing number of arriving ions.

We should announce that the Faraday cup detector design is complete and ready for testing. [4](see Figure 5).

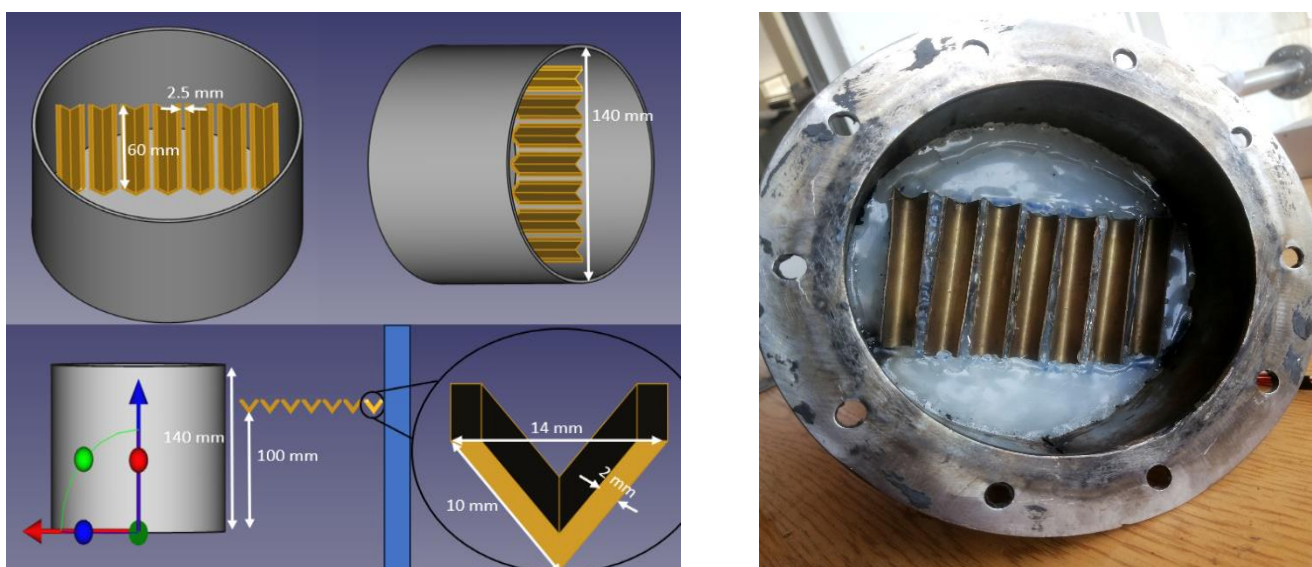


Figure 5: Module 5 of the Faraday cup

13.3.2 Electromagnetism

As mentioned earlier, we cannot deflect ions without a magnetic field, and it must be strong enough to deflect the heavy ions emitted from the toxic gases.

The previous tests indicate that the Helmholtz coil is not effective in generating a strong magnetic field (0.2 T). [4]

Based on the famous formula of the magnetic field:

$$B = \mu n I$$

In the equation, B represents the magnetic flux density in Tesla, μ stands for the permeability in Henry per meter, n denotes the number of turns per meter, and I represents the electrical current in Amperes.

We have the ability to manipulate these elements to achieve the magnetic flux density we desire. The challenge lies in the variability of permeability among different ferromagnetic cores. Conversely, achieving high permeability would reduce the need for high levels of other factors such as the number of turns (n) and current (I).

13.3.2.1 Magnetic Permeability

In electromagnetism, permeability refers to a material's ability to concentrate magnetic fields, indicating how easily a material can become magnetized (see Figure 6).

We denote μ_r as the relative permeability compared to free space ($\mu_0 = 4\pi \times 10^{-7}$ Henry/meter).

$$\mu_r = \mu / \mu_0 \quad (\text{The relative permeability of free space is } \mu_r = 1)$$

Different types of permeability can be identified based on the characteristics of changes in B and H , where H represents the magnetic field strength in amperes per meter. The relationship between magnetic permeability and this change is described by a formula:

$$\mu = \Delta B / \Delta H$$

The relative permeability (μ_{ferro}) of magnetic materials (ferromagnets) is significantly greater than that of non-magnetic materials such as vacuum (μ_{vac}), diamagnets (μ_{dia}), paramagnets (μ_{para}), and superconductors (μ_{sup}) (see Figure 7). [8]

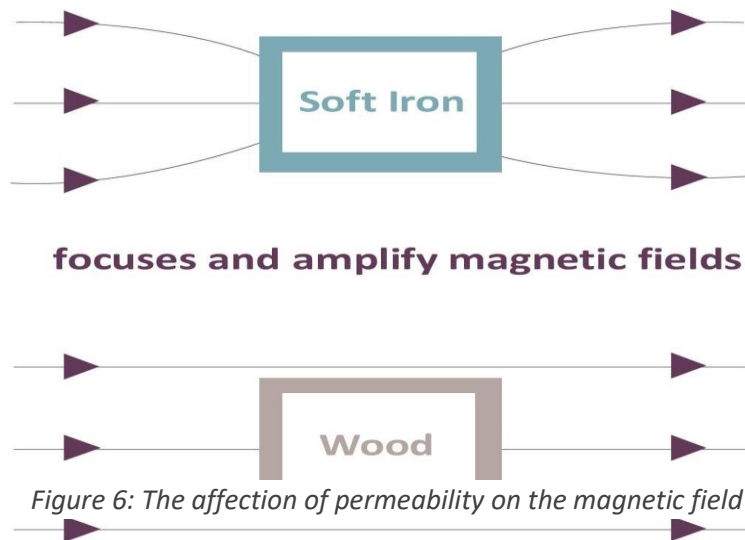


Figure 6: The affection of permeability on the magnetic field

$$B = \mu \cdot H \quad (\text{T})$$

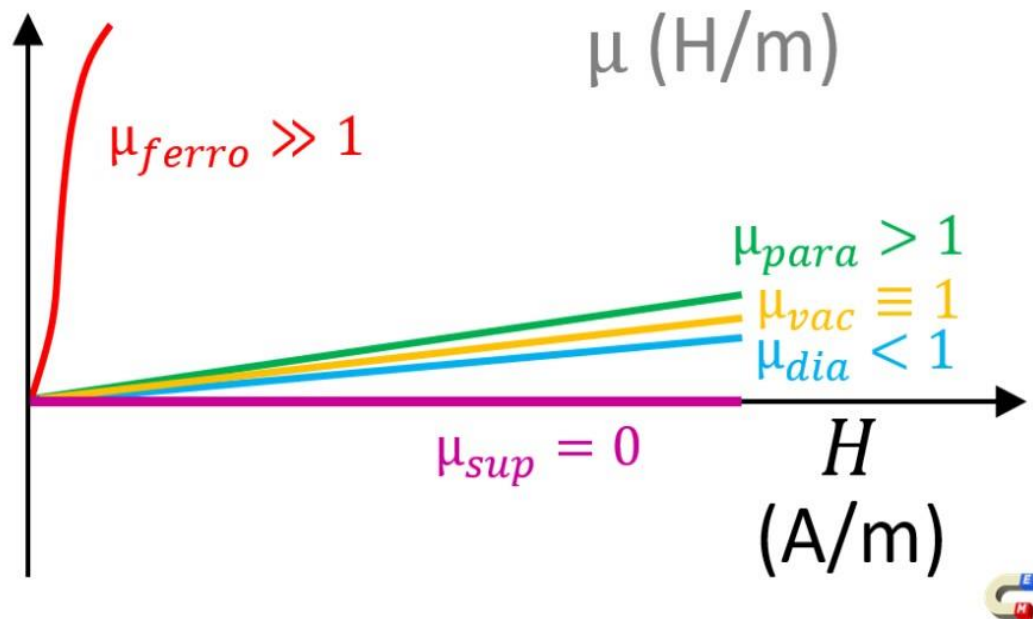


Figure 7: B-H curve illustrating the varying permeability of different materials

In simpler terms, ferromagnetic materials are ideal for constructing an electromagnet.

This works best when they are operating below the saturation point, where the relative permeability is at its peak (see Figure 8).

We can observe that the permeability of ferromagnetic materials decreases as they approach saturation, and this relationship is non-linear with the applied excitation.

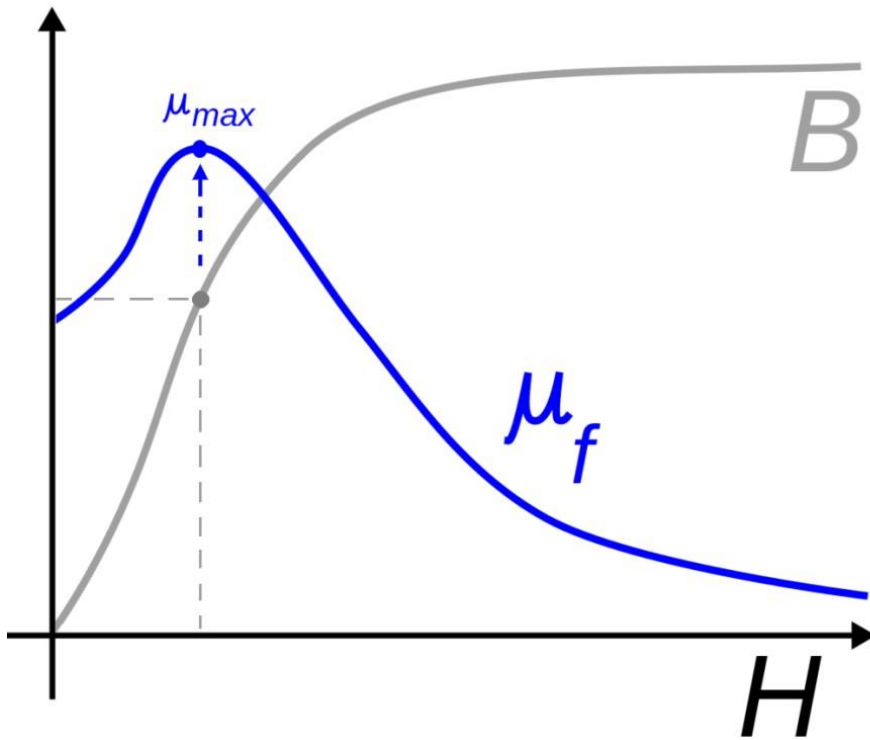


Figure 8: B-H curve showing the saturation point of magnetic permeability

13.3.2.2 Calculations and Discussion

The previous calculation shows that we need a magnetic flux density of 0.2 Tesla [4] based on the following formulas:

$$r = \sqrt{2mU} / qB^2$$

$$v = \sqrt{2qU / m}$$

Where r is the radius of curvature and v is the velocity. We have found that for $B = 0.2$ Tesla and $U = 300$ V, the velocity will be provided in the following table:

Type of gas	Mass m (Kg)	Radius r (m)	Velocity v (m/s)
HCL	5.76×10^{-26}	0.073	40.8×10^3
HF	3.2×10^{-26}	0.056	54.7×10^3
SO ₂	10.24×10^{-26}	0.098	30.6×10^3
Hg	32×10^{-26}	0.173	17.3×10^3

Table 5: Mass, radius of curvature and velocity for different ions

Since our project focuses on toxic gases, a heavy ion such as lead (Pb), which has a mass of 34×10^{-26} Kg, will have a radius of 17.8 cm, exceeding the range (see Figure 9).



Figure 9: The maximum radius in the deflection zone for the mass spectrometer

Therefore, we must repeat the calculation to find the ideal solution for the system.

In general, reducing the potential difference and magnetic flux density will enhance the economic benefits of the project.

Furthermore, decreasing the magnetic flux density will make the manufacturing of the electromagnet easier and less expensive.

To reduce the magnetic flux density, we need to decrease the velocity of the ions, which implies reducing the voltage in the acceleration plates.

Taking, for example, $U = 20$ V and $B = 0.06$ Tesla, the table will be as follows:

Type of gas	Mass m (Kg)	Radius r (m)	Velocity v (m/s)
HCL	5.76×10^{-26}	0.063	10.5×10^3
HF	3.2×10^{-26}	0.047	14.1×10^3

SO₂	10.24 x 10⁻²⁶	0.084	7.9 x 10³
Hg	32 x 10⁻²⁶	0.149	4.4 x 10³
Pb	34 x 10⁻²⁶	0.153	4.3 x 10³

Table 6: Mass, radius of curvature and velocity for different ions included Pb

Reducing the potential difference will decrease the velocity of the ions in the acceleration zone, but the velocity is still sufficient, as we can observe.

13.3.2.3 Single Solenoid Coil

A solenoid is essentially a coil of wire, typically made of copper. When an electrical current flows through the wire, it generates a magnetic field, similar to how a magnet works (see Figure 10).

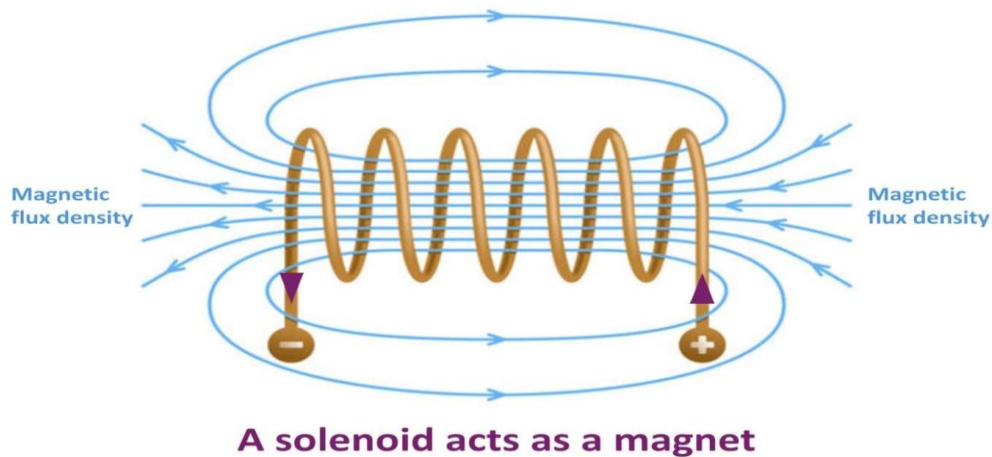


Figure 10: Magnetic Flux in a Solenoid

The solenoid often has a cylindrical shape, which helps to create strong and uniform magnetic field. Despite this, there may be variations in design. Solenoids have the potential to feature a D-shaped frame customized for specific applications. However, the prevailing perception of a solenoid usually corresponds to that of an elongated, cylindrical coil. [9]

13.3.2.4 Simple Simulation

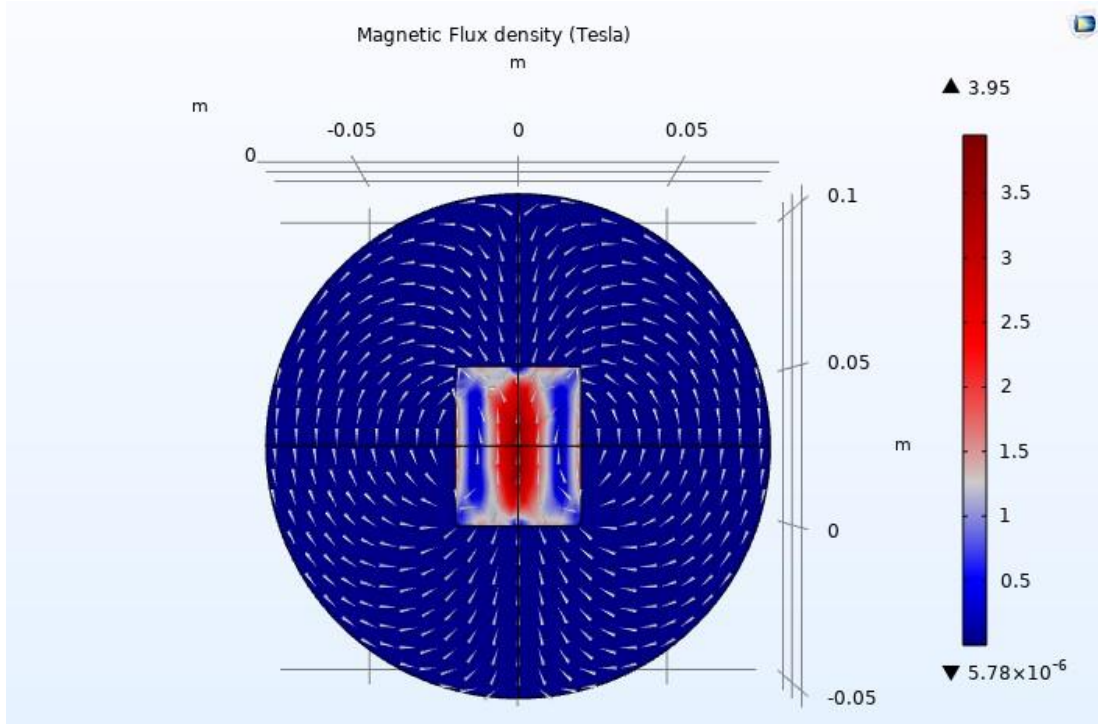


Figure 671: A Simulation of a Single Solenoid

We used COMSOL Multiphysics to simulate a simple design consisting of a single solenoid with a cylindrical shape (4 cm in diameter and 5 cm in height).

We used 200 turns, a relative permeability of 200, and 6 amperes, and that was the result for the 2D plane (see Figure 11).

The white arrows represent the flow of the magnetic field to determine its direction and uniformity. We can observe that the maximum magnetic flux density is depicted in red in the center, gradually decreasing in intensity towards blue.

The simulation was conducted again with two solenoids positioned 15.8 cm apart to analyze the magnetic field between them (see Figure 12).

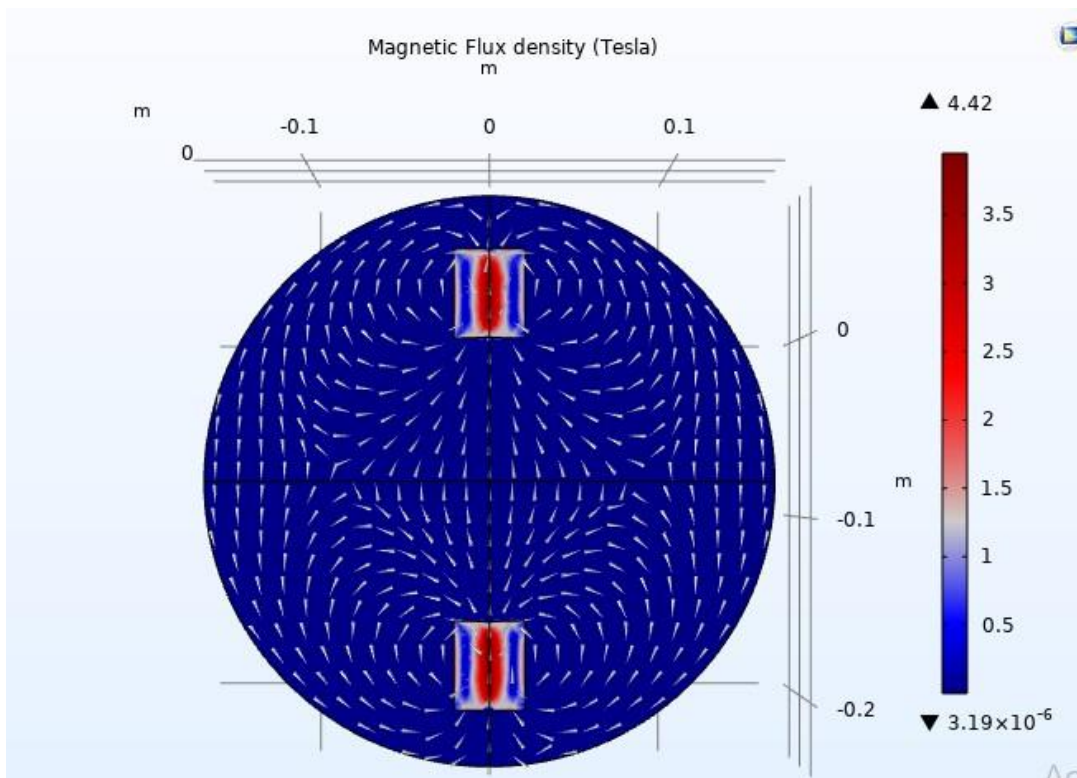


Figure 12: A Simulation of Two Solenoids

As we can see, the magnetic field is uniform only in the middle, which is insufficient for our application. By employing additional solenoids, we can attain an even more uniform magnetic field. The simulation indicates that the magnetic field density is insufficient to achieve a 60 mT (0.06 Tesla) strength between the two solenoids.

When we increase the relative permeability to 3000, we observe that the maximum magnetic flux density also increases (4.42 Tesla to 65.9 Tesla) (see Figure 13).

But how can we determine the effect of permeability outside the coils where the relative permeability is one? This will be known after the following simulation.

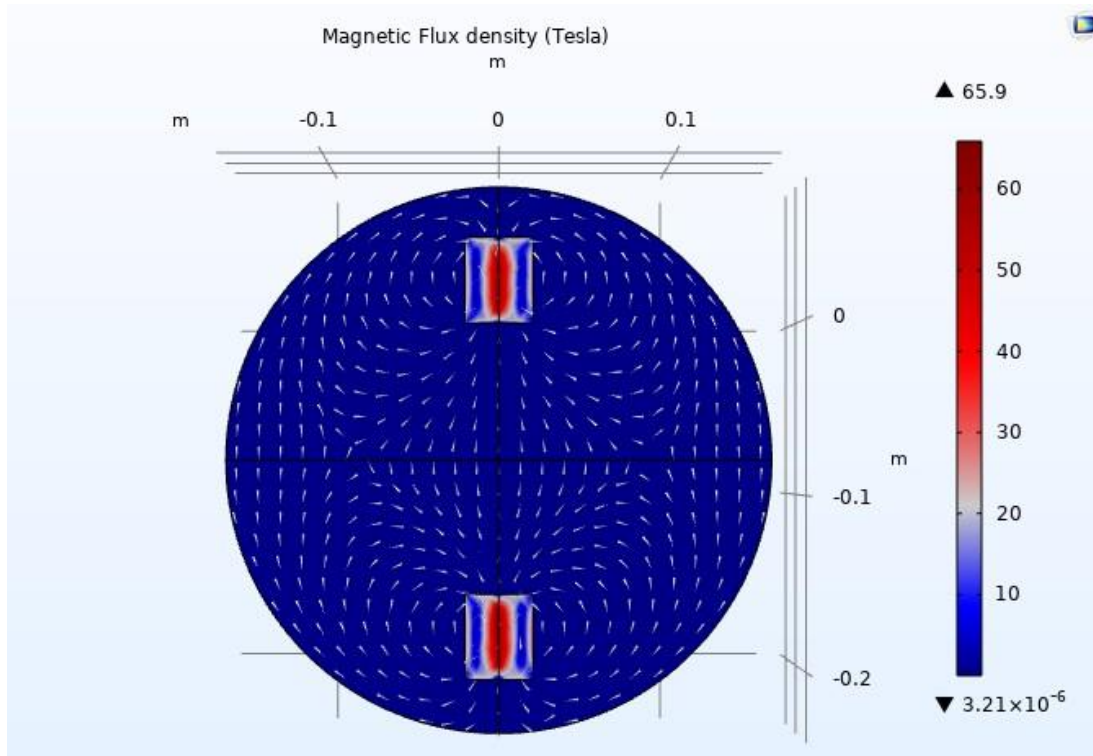


Figure 13: A 2D Simulation of Two Solenoids with 3000 relative permeability

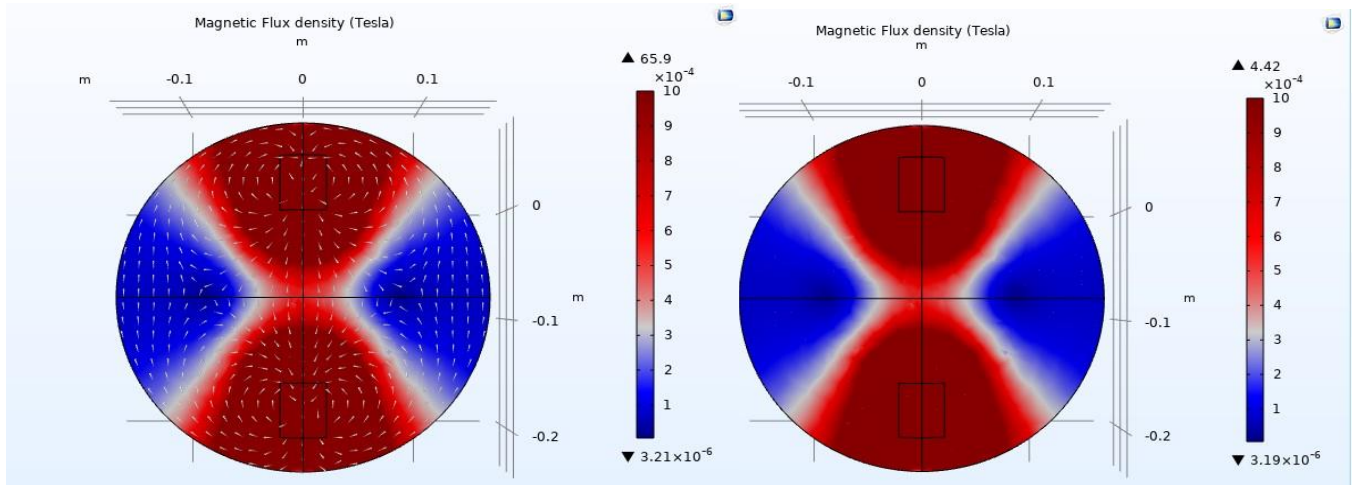


Figure 14: Relative permeability is 3000

Figure 15: Relative permeability is 200

We adjusted the scale to a maximum magnetic flux density of one milliTesla (1 mT) to illustrate the color distribution outside the coils (see Figure 14). When we reduced the relative permeability to 200, the arrow volumes representing the magnetic fields nearly disappeared, indicating a loss of uniformity; however, there was no change in the magnetic flux outside the solenoids, where the color remained consistent (see Figure 15). Nevertheless, we were able to observe the arrow volumes again by readjusting the arrow scale.

13.3.2.5 Biot-Savart Law

According to Biot-Savart's law, the magnetic field density at point P, which is on the axis of the center of the solenoid (see Figure16), is equal to:

$$B = NI\mu (\cos \theta_1 + \cos \theta_2) / 2L$$

As

we

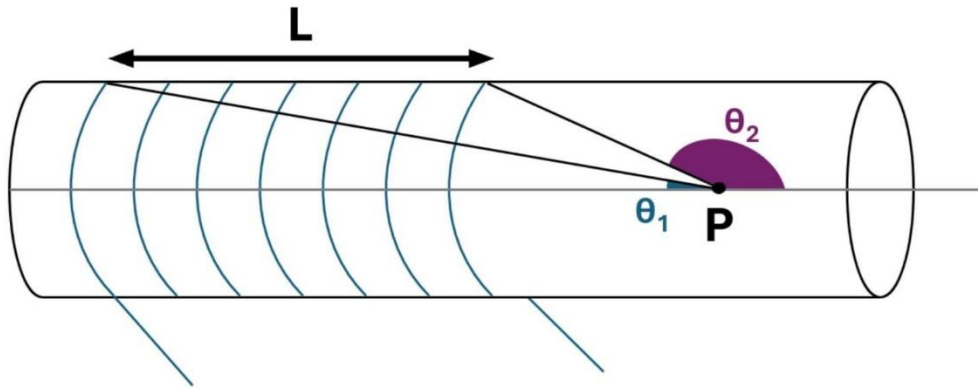


Figure 16: The two angles formed by a point P located outside the solenoid.

observe, $\cos\theta_2$ is always negative outside the solenoid since θ_2 is greater than 90 degrees, while $\cos\theta_1$ is always positive.

In general, when θ belongs to $[0, \pi]$, if θ increases, $\cos\theta$ decreases. Therefore, increasing the radius of the solenoid will decrease the difference between $\cos\theta_1$ and $\cos\theta_2$, thus increasing the overall magnetic field.

But the effect of increasing the radius will be negligible for a point far away from the solenoid and at the center of the solenoid since $B = NI\mu$.

13.3.3 Purification of Iron

The purity of iron is an important factor to consider because pure iron is more effective in magnetic fields due to its high permeability.

So, in order to remove impurities from iron, there are several methods, each with its own advantages and disadvantages, to produce pure iron. [10]

We chose to use the electrolytic refining method, which involves an electrolysis cell. The impure iron serves as the anode, while on the cathode side, we use another iron that will be purified. [11]

13.3.3.1 Needed Materials

1.1.1. Electrolysis Cell

To purify iron, we use an electrolysis cell, which is a container capable of handling the electrolyte solution and separating the anode from the cathode. The container is often made of acrylic.

1.1.2. Power Source

We will need a DC power supply to deliver a constant current with sufficient voltage to drive the electrolysis process. The specific voltage and current requirements will depend on the cell setup and the desired purity of iron.

1.1.3. Impure Iron Anode

The iron you want to purify acts as the anode. The size and shape of the iron will depend on the amount you wish to purify.

1.1.4. Iron Electrolyte Solution

This is a crucial component in the process. Iron(II) chloride (FeCl_2) is a popular choice due to its good solubility and availability.

1.1.5. The Cathode

The cathode is where the purified iron will deposit. It is typically made of a thin sheet of iron, which is commercially available as high-purity iron.

13.3.3.2 The Electrolytic Refining Process

1.1.6. Preparing the Electrolysis Cell

We fill the cell with an ionic electrolyte solution, such as FeCl_2 in this case. Next, we submerge the impure iron anode and the cathode into the solution, ensuring that they remain separated. To minimize the dissolution of anode material into the cathode compartment, a diaphragm can be employed.

1.1.7. Applying a DC Current

We must connect the power source to the electrodes. The anode will be connected to the positive terminal, while the cathode will be connected to the negative terminal.

1.1.8. Electrolysis

When the current is applied to the cell, chemical reactions occur.

At the anode side, oxidation takes place: $\text{Fe} \rightarrow \text{Fe}^{2+} + 2\text{e}^-$.

The iron atoms from the impure iron anode lose electrons and dissolve into the solution as Fe^{2+} ions.

At the cathode, reduction occurs: $\text{Fe}^{2+} + 2\text{e}^- \rightarrow \text{Fe}$.

The Fe^{2+} ions from the electrolyte solution gain electrons and deposit on the cathode as pure iron atoms (see Figure 17).

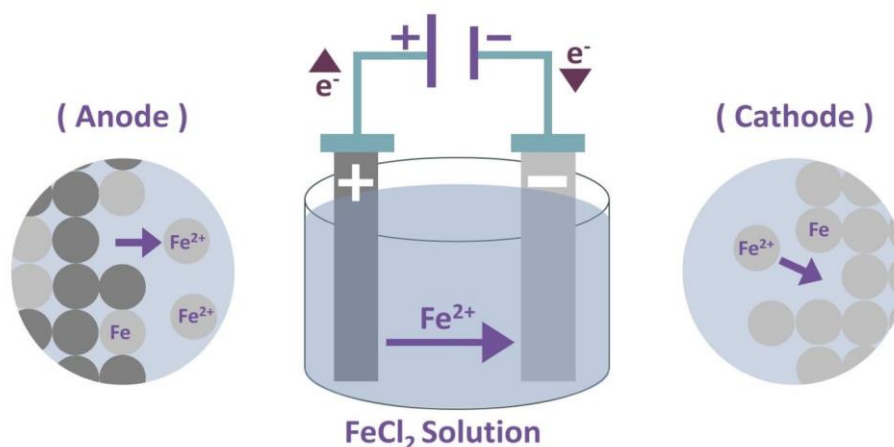


Figure 17: The Electrorefining Method of Iron

13.3.3.3 Drawbacks

Electrorefining is technically feasible for small-scale iron purification; however, it is not the most practical option for several reasons. Its efficiency is relatively low compared to other methods, and it requires significant energy consumption to transport the iron ions. In this context, we must either employ an alternative purification method or purchase high-purity iron (99.5%) and undergo the electrolytic refining process to achieve even higher purity (99.9%).

13.3.4 Annealing

The annealing process is a heat treatment method used to reduce the hardness and enhance the ductility and toughness of various steels, cast iron, and alloys. This technique involves heating the material above its recrystallization temperature, which promotes the formation of new grains and enables the reorientation of existing grain structures. [12]

13.3.4.1 History of Annealing

Annealing involves heating to a specific temperature and then cooling at a controlled rate. Historically, annealing was discovered around the 12th century when the word originated from the Middle English term "anelen," which means to set on fire or bake. In Europe, it was discovered through advances in blacksmithing that annealing alters the properties of steel and iron. [13]

Blacksmiths discovered that by heating iron to a specific temperature and then rapidly cooling it, the iron would become stronger and more durable.

The metal heat treatment techniques were developed in the Middle Ages when medieval blacksmiths discovered a process that involved reheating quenched metal to a lower temperature and then cooling it slowly. This enhancement made weapons and armor more effective in wars.

The Industrial Revolution in the 18th and 19th centuries led to the development of the annealing process as we know it today. This process involves heating metal to a high temperature and then allowing it to cool slowly. Subsequently, heat treatment methods have continued to evolve up to the present day. [14]

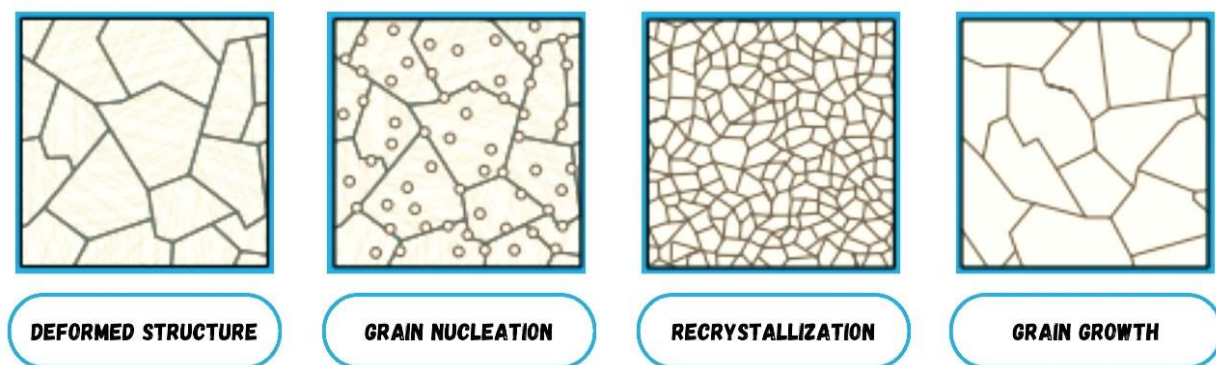
13.3.4.2 Annealing Process

The annealing process consists of three distinct stages: an initial recovery phase, a subsequent recrystallization phase, and a final grain growth phase. [12]

During the recovery phase, a metal is heated to a specific temperature below its melting point using a programmable furnace or oven to regulate the temperature. Typically, nitrogen is purged as an inert gas to prevent the oxidation of the metal. [15]

During the recrystallization phase, the metal is heated to the desired temperature and held for a specific duration, which varies based on the desired properties.

This phase involves the reorganization of the crystal structure and the initiation of new grain structures. During the grain growth stage, the size of both newly formed and existing grains increases once the cooling process commences. The phase composition, crystal grain size, and growth are determined by factors such as the cooling rate, atmosphere, and material grade (see Figure 18).



STAGES *Of* ANNEALING

Figure 18: The Different Stages of the Annealing Process

1.2. Annealing & Permeability

Annealing can enhance the initial magnetic permeability of metals. By subjecting the metals to high temperatures during annealing, the permeability can be significantly increased. The extent of this increase is influenced by various factors, including the temperature applied, the rate of cooling, and the duration of soaking.

Typically, metal permeability increases with higher temperatures, as evidenced by superior results at 1180°C compared to 1093°C. Additionally, longer soaking times contribute to enhanced permeability, with a six-hour hydrogen annealing process yielding higher permeability levels than a two-hour anneal. [16]

13.4 CHAPTER II: ELECTROMAGNETIC CONCEPTIONS

1. Multi-solenoid Unit

Multi-solenoid unit is an electromagnet specifically designed to produce a more uniform magnetic field across a large air gap and throughout a relatively extensive volume.

1.1. Prototype Design

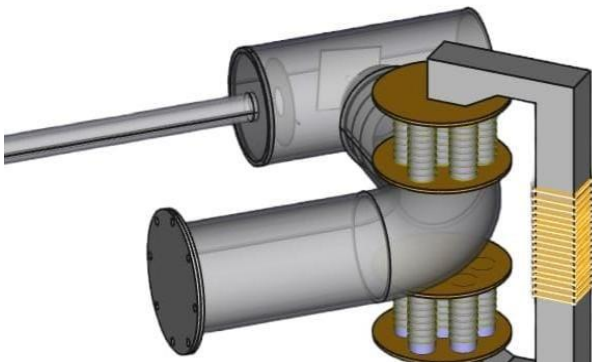


Figure 19.3: Electromagnet view 3

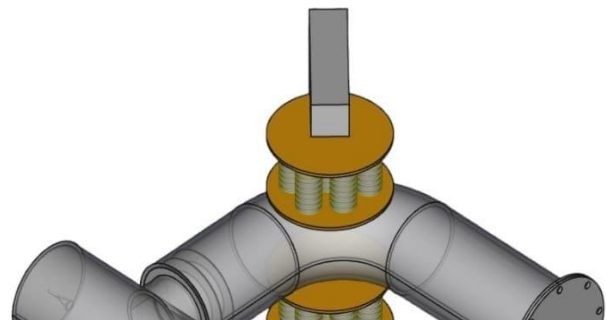


Figure 19.2: Electromagnet view 2

We used Computer-Aided Design (CAD) to construct a basic prototype of an electromagnet that utilizes a multi-solenoid unit (see list of Figures 19).

In this design, the overall magnetic field magnitude depends on the strength of each individual solenoid. Adding more solenoids does not increase the magnetic flux magnitude but increases its volume while maintaining uniformity.

Each solenoid must induce a magnetic field in the same direction.

1.2. Simulation Part

The magnetic field must fill the entire area inside the vacuum tube. To determine this, we conducted a simulation for a multi-solenoid system. We used two cylindrical coils with a radius of 6.25 cm and 500 turns each, with a relative permeability of 200 and an electrical current of 6 amperes. The coils were positioned 15.8 cm apart (see Figure 20). As we can observe, the magnetic field is almost uniform but less than 5 mT.

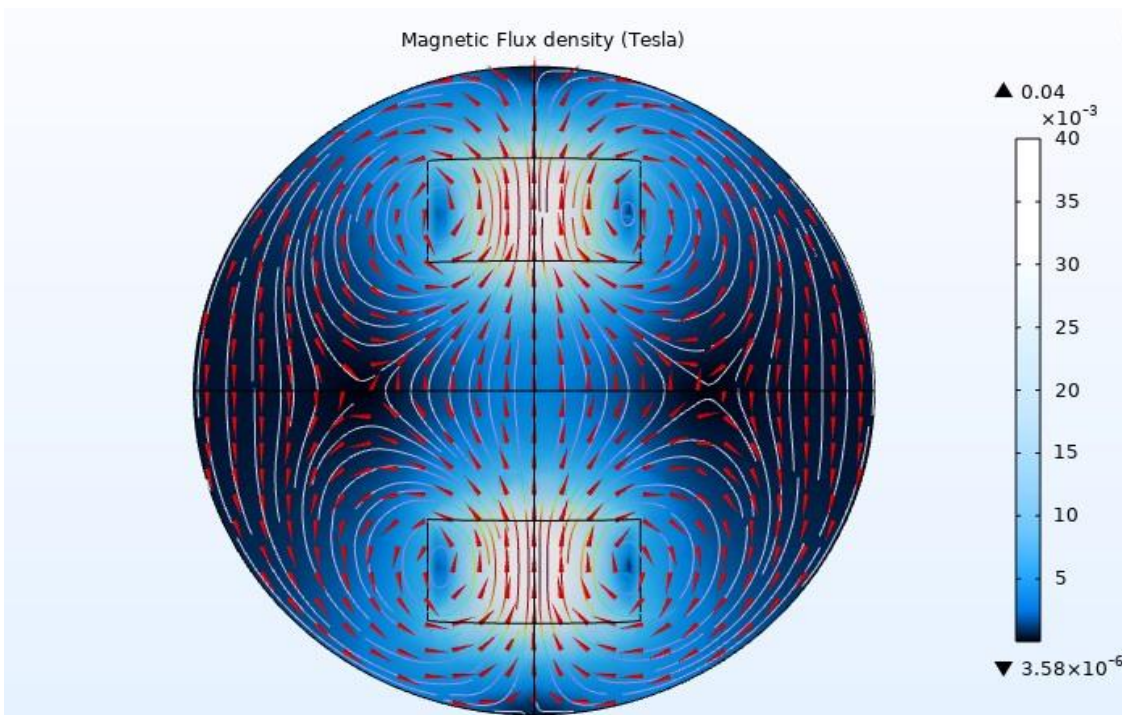


Figure 680: A 2D simulation of two solenoids with a diameter of 12.5 cm.

To clearly observe the effects of the multi-solenoid system, we utilized ten solenoids instead of two (see Figure 21).

Each solenoid has a radius of 1.75 cm, with a distance of 1 cm between each pair of solenoids, creating a 12.5 cm diameter, which matches the diameter of the previous simulation and with the same conditions.

However, we observe that the magnetic field inside the vacuum tube is now almost uniformly distributed compared to before, with a slight increase in strength (see Figure 22).

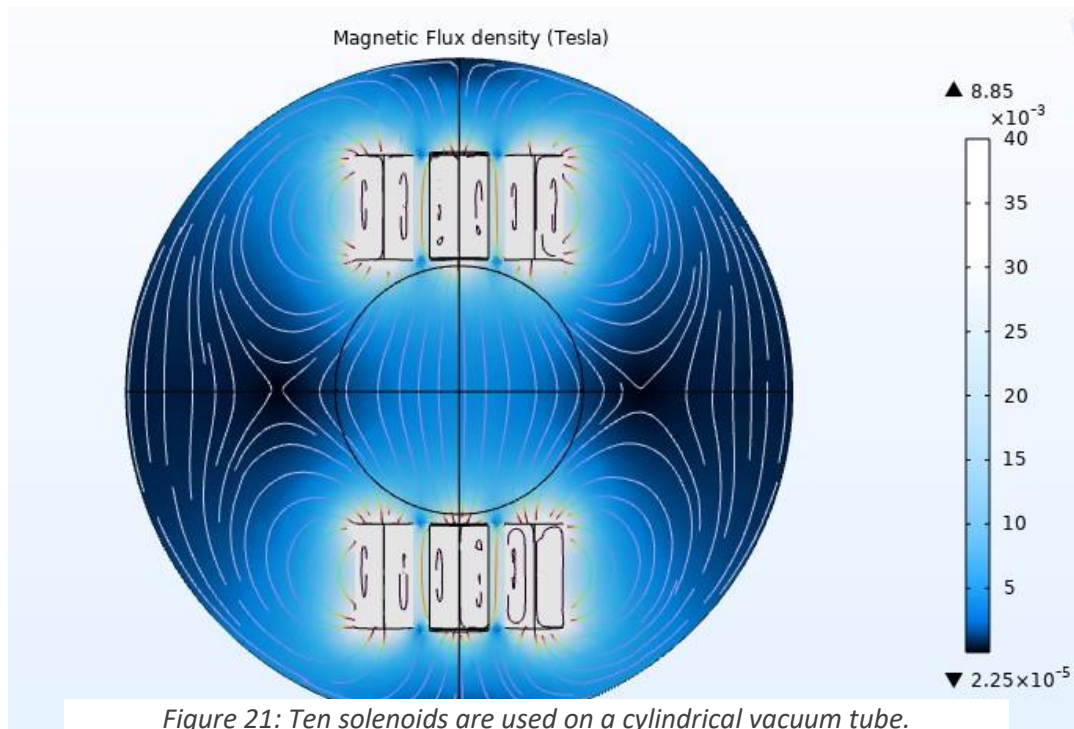


Figure 21: Ten solenoids are used on a cylindrical vacuum tube.
Figure 23: The 2D Simulation without arrow volumes

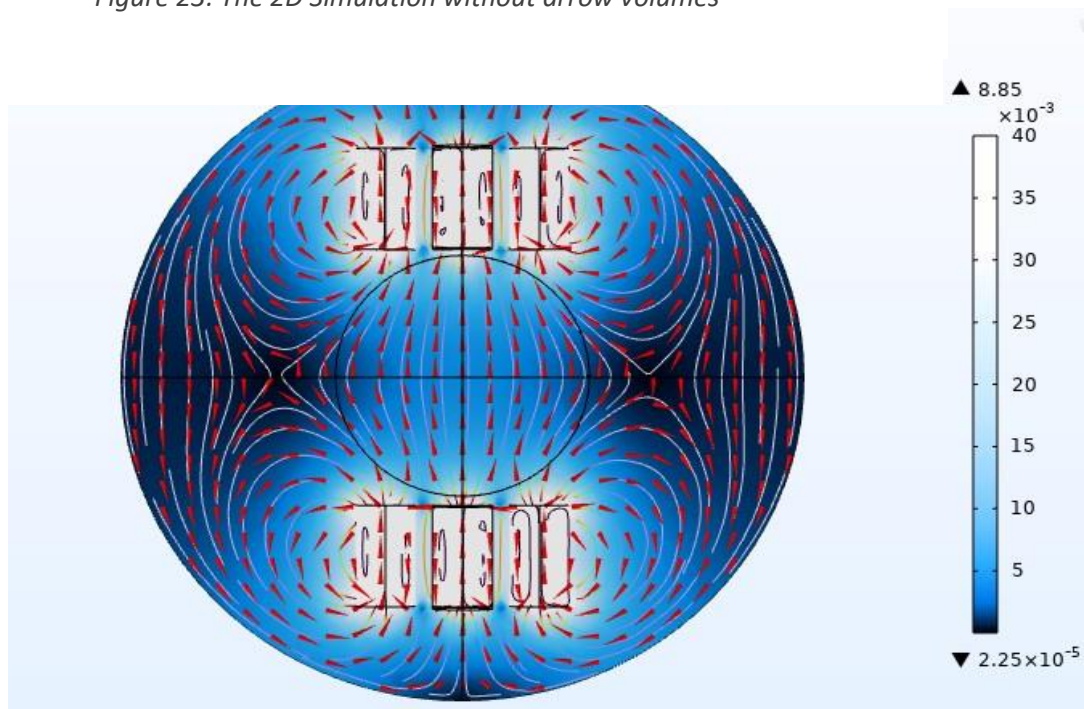


Figure 22: The 2D simulation utilizing arrow volumes

The color inside the vacuum tube is nearly uniform, light blue, indicating a consistent magnetic flux density in the Tesla simulation measurement (see Figure 23).

In conclusion, the multi-solenoid system can generate a uniform magnetic field, but it is too weak, which poses challenges in achieving 60 mT.

2. C-shaped Unit

One of the most common components in the magnetic sector is the C-shaped coil, an electromagnet that focuses the magnetic field within the gap area based on an electromagnetic circuit.

2.1. Fundamental Principles of Electromagnetism

It can be observed that the air gap volume is the region where we aim to achieve the desired magnetic field (see Figure 24).

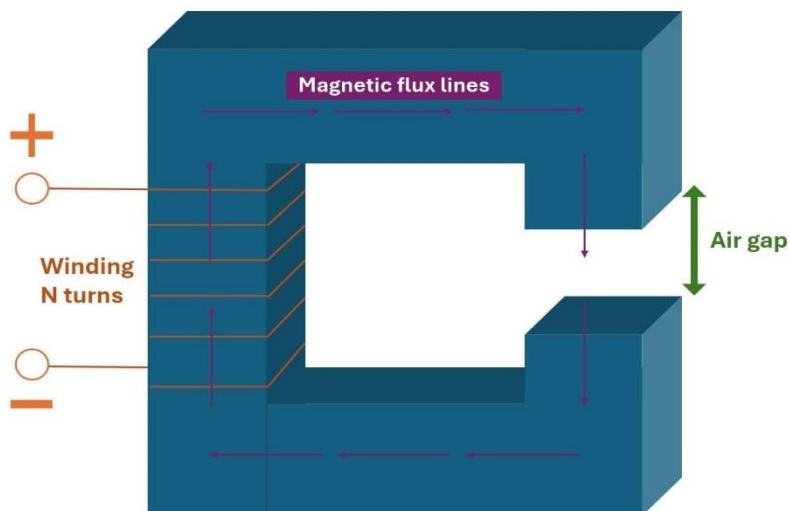


Figure 24: The C-shaped core was taken from one side of the transformer.

The equation for magnetic flux density, denoted as (B), can be derived from the fundamental principles of electromagnetism:

$$\Phi = BA$$

Φ : magnetic flux (Weber)

A : surface area that the flux going through (m^2)

B : magnetic flux density (T)

Now, we have another equation that is directly related to the fundamental characteristics:

$$Ni = \Phi (\mathcal{R}_g + \mathcal{R}_c)$$

N: number of coil turns (turn)

i: current going through the coil (A)

\mathcal{R}_c : Reluctance of the core (A.turn/Wb)

\mathcal{R}_g : Reluctance of the air gap (A.turn/Wb)

The magnetic system can be transformed into a magnetic circuit (see Figure 25), and the equations used are analogous to Ohm's Law.

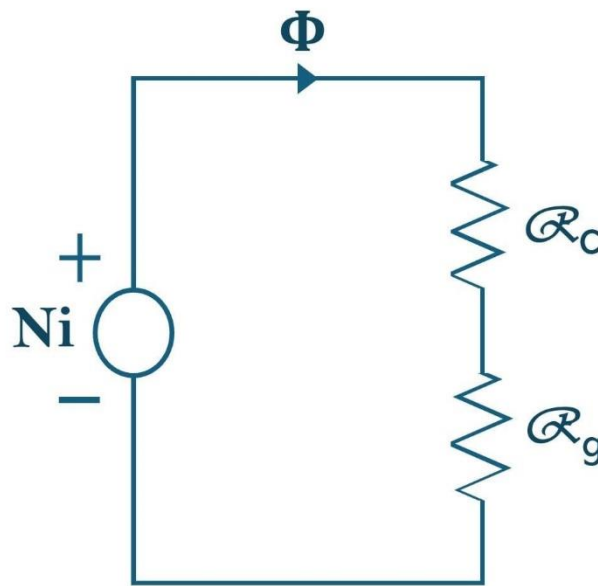


Figure 25: The magnetic circuit of a C-shaped core

We can deduce from the equations that reducing the total reluctance ($\mathcal{R}_c + \mathcal{R}_g$) will increase the magnetic flux (Φ), which, in turn, will enhance the strength of the magnetic flux density.

$$\mathcal{R}_c = L_c / A_c \mu_c$$

$$\mathcal{R}_g = L_g / A_g \mu_g$$

L_c represents the mean length of the core, while A_c denotes its cross-sectional area. Additionally, L_g indicates the length of the air gap in meters, and A_g represents the cross-sectional area with a 5% correction applied (see Figure 26).

μ_c represents the core permeability, while μ_g denotes the permeability of free space (μ_0).

From these equations, we can conclude that reducing the lengths of both the core and the air gap will lead to a decrease in reluctance (see Figure 27).

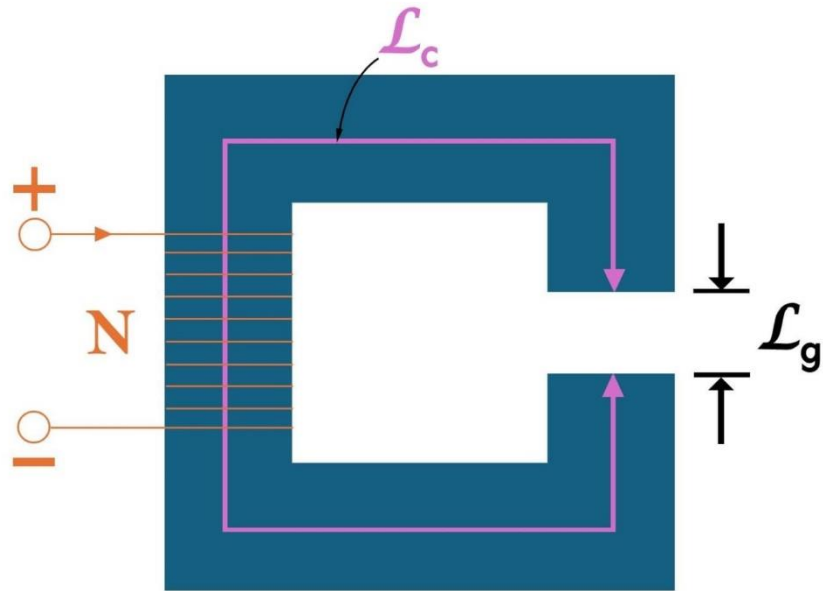


Figure 26: The C-shaped core showing the mean core length

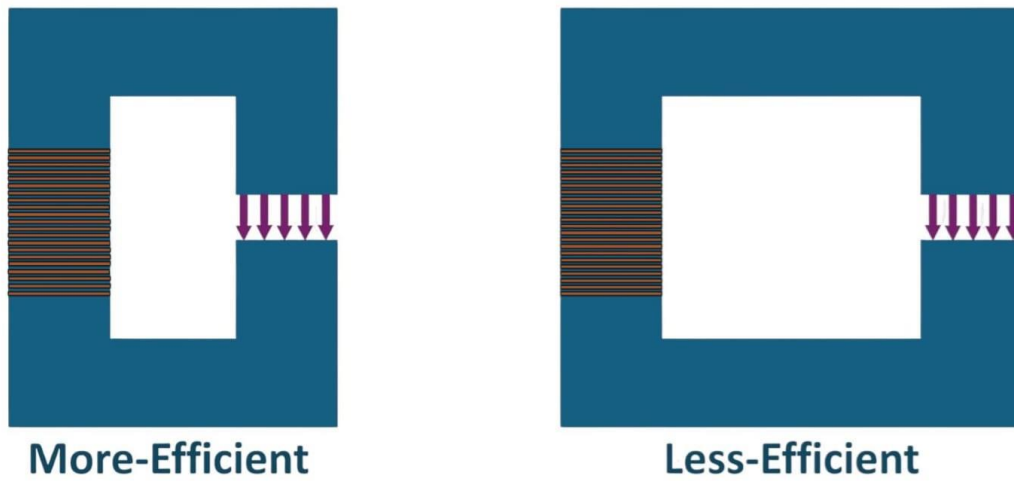


Figure 27: The efficiency comparison of two C-Shaped modules

By combining the equations, we obtain the following result:

$$Ni = BA (\mathcal{R}_g + \mathcal{R}_c)$$

Substituting \mathcal{R}_g and \mathcal{R}_c with their respective values:

$$Ni = BA ((L_g/A_g\mu_g) + (L_c/A_c\mu_c))$$

or

$$N = BA ((L_g/A_g\mu_g) + (L_c/A_c\mu_c)) / i$$

In the air gap, the useful magnetic flux tends to bulge outward, resulting in a slight increase in area—approximately 5%, depending on the size of the gap and the geometry of the core. This phenomenon is known as fringing.

This implies that $A_g = A_c + 5\%$ of A_c , which can be expressed as $A_g = 1.05A_c$.

Therefore, we will have:

$$N = B ((1.05L_c/\mu_c) + (L_g/\mu_g)) / i$$

adding in account that $\mu_c = \mu_r\mu_0 = \mu_r\mu_a$

then the equation will be:

$$N = B (1.05L_c + \mu_r L_g) / \mu_c i$$

At a very high permeability (μ_r), the minimum number of turns required is as follows:

$$N = BL_g / \mu_0 i$$

For a magnetic field strength (B) of 0.06 Tesla, with a length (L_g) of 15.8 cm, and a current of 6 A, the minimum number of turns required is 1,258.

2.2. Design Assembling

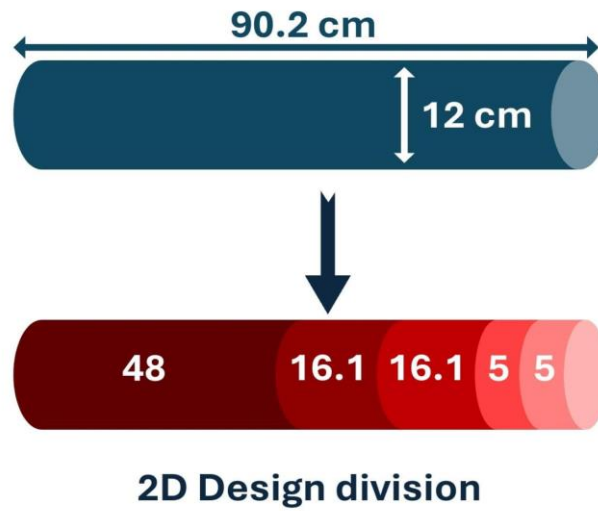


Figure 28: The cutting plan for the iron bar

Since we do not have a cubic iron core, we will utilize a cylindrical core with precise dimensions to construct our assembly (see Figure 28), we will purchase an iron bar with 12 cm diameter and a length of 90.2 cm, and then we will cut it to five sections, the biggest one with 48 cm, two sections with 16.1 cm and the last two sections with 5 cm each.

Finally, we will assemble the iron into a C-shape (see Figure 29), as specified in the plan with an air gap of 15.8 cm.

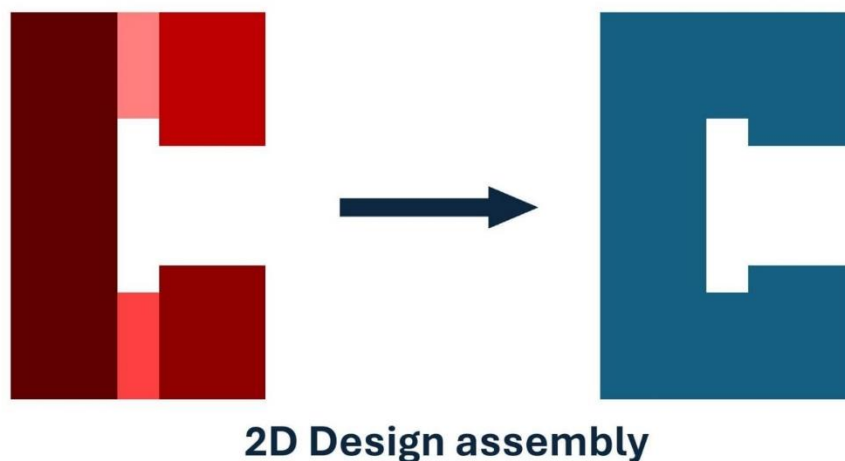


Figure 29: The assembling plan for the C-shape core

2.3. The Simulation Conditions of the Iron Core

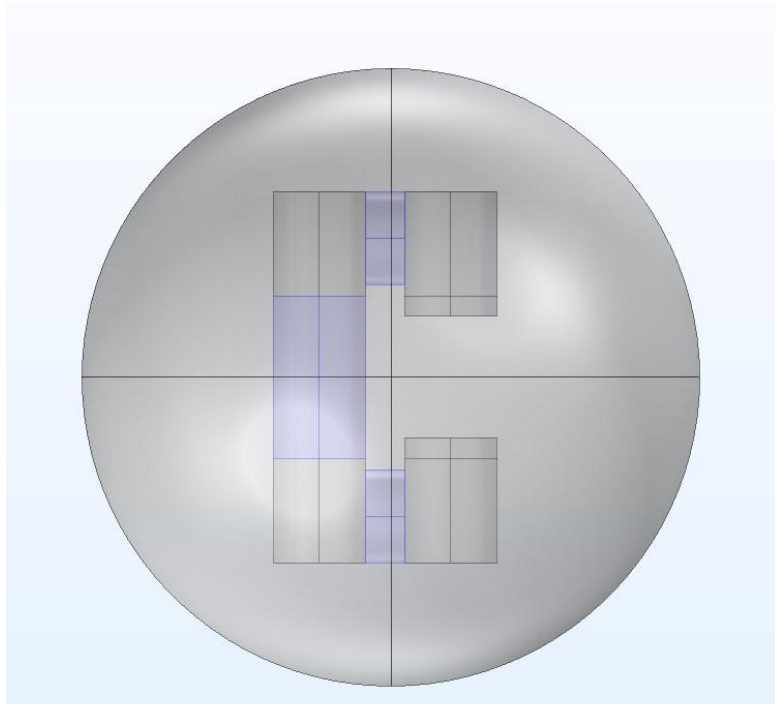


Figure 1090: The C-shaped core illustrates the region where we wrap the copper

First and foremost, we developed a simulation of our C-shaped iron core. The colored sections indicate the locations of the coils (see Figure 30). Subsequently, we conducted the meshing process, which is a software-based simulation for Finite Element Analysis (FEA) (see Figure 31).

The properties of iron are presented in the table below:

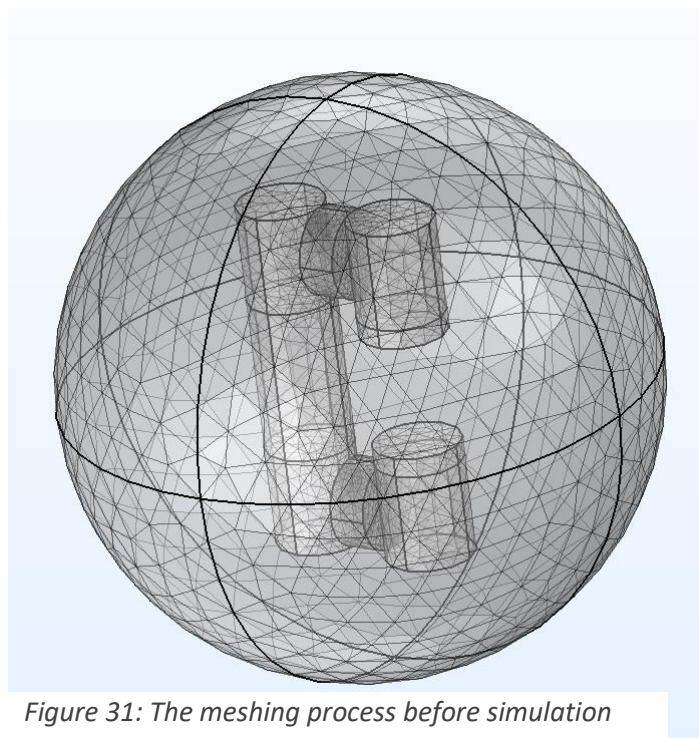


Figure 31: The meshing process before simulation

Property	Variable	Value	Unit	Property group
<input checked="" type="checkbox"/> Relative permeability	mur_i...	200	1	Basic
<input checked="" type="checkbox"/> Electrical conductivity	sigma...	1.12e7[S...	S/m	Basic
<input checked="" type="checkbox"/> Relative permittivity	epsilo...	1	1	Basic
Coefficient of thermal expans...	alpha...	12.2e-6[...	1/K	Basic
Heat capacity at constant pre...	Cp	440[J/(k...	J/(kg·K)	Basic
Density	rho	7870[kg...	kg/m ³	Basic
Thermal conductivity	k_iso ;...	76.2[W/...	W/(m...	Basic
Young's modulus	E	200e9[Pa]	Pa	Young's modulus and...
Poisson's ratio	nu	0.29	1	Young's modulus and...

Table 7: Properties of the Iron Core: Establishing Permeability

The total number of turns required to achieve a magnetic field strength of 0.06 T at the air gap, using a 9 A electric current, is 3,500 turns. The largest coil on the left side contains 1,500 turns, while each of the two coils located above and below contains 1,000 turns.

We conducted simulations using a variety of permeabilities (see list of Figures 32).

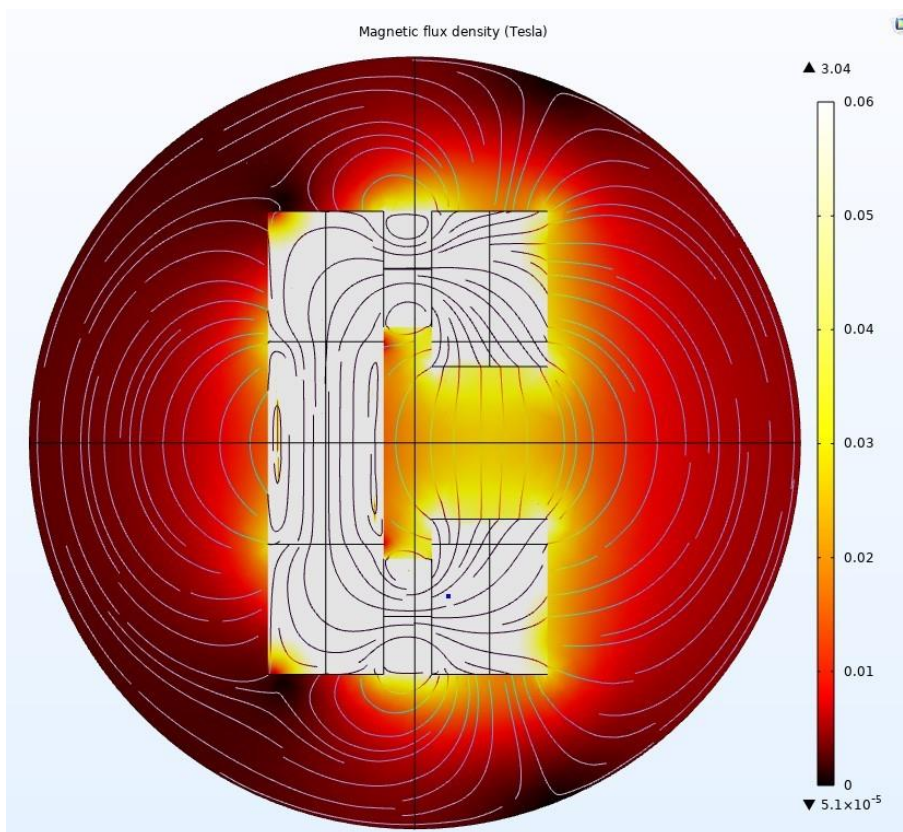


Figure 32.1: Relative permeability is 20

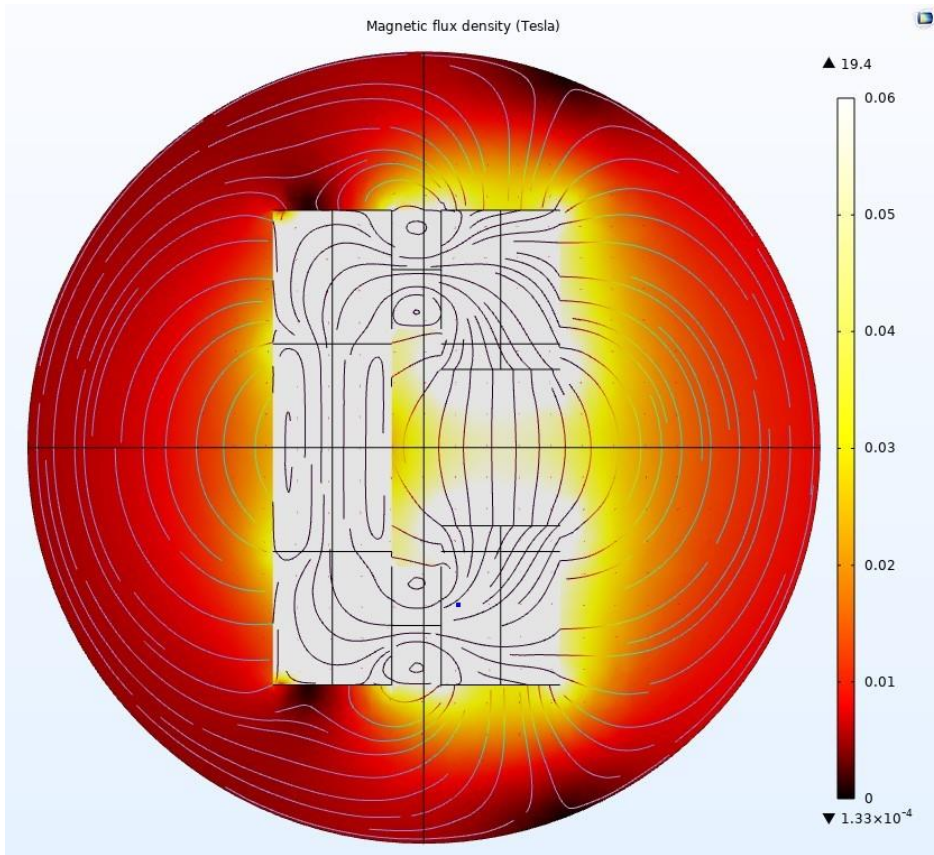


Figure 32.2: Relative permeability is 100

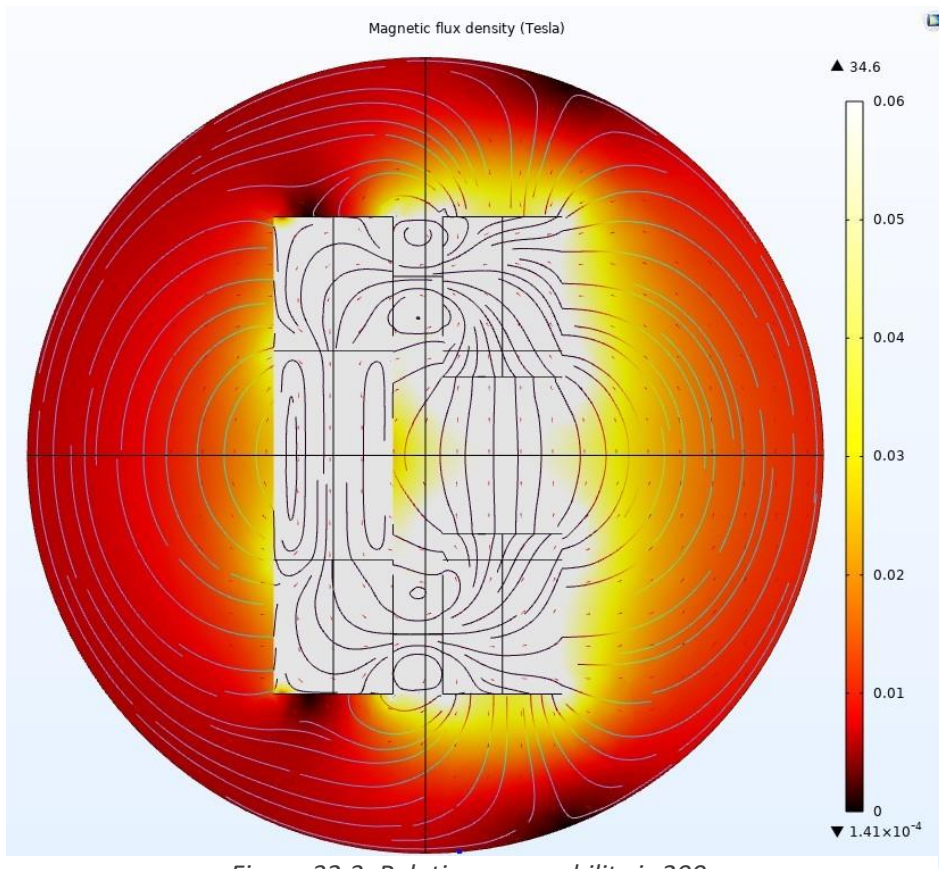


Figure 32.3: Relative permeability is 200

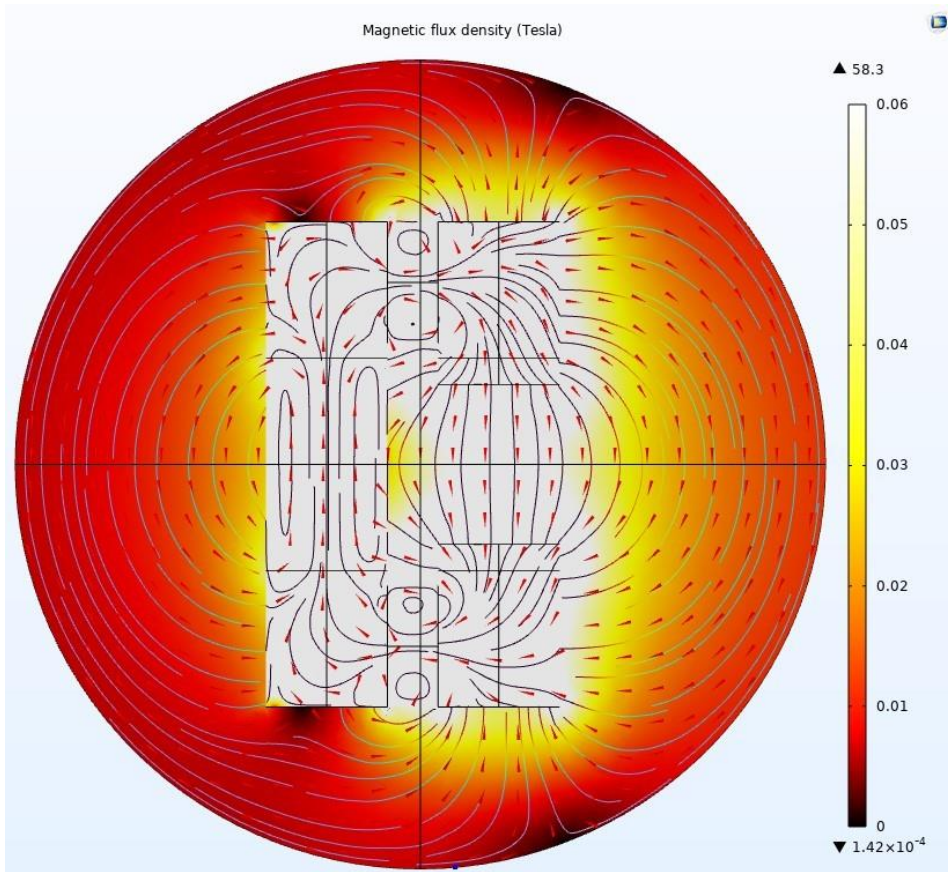


Figure 32.4: Relative permeability is 500

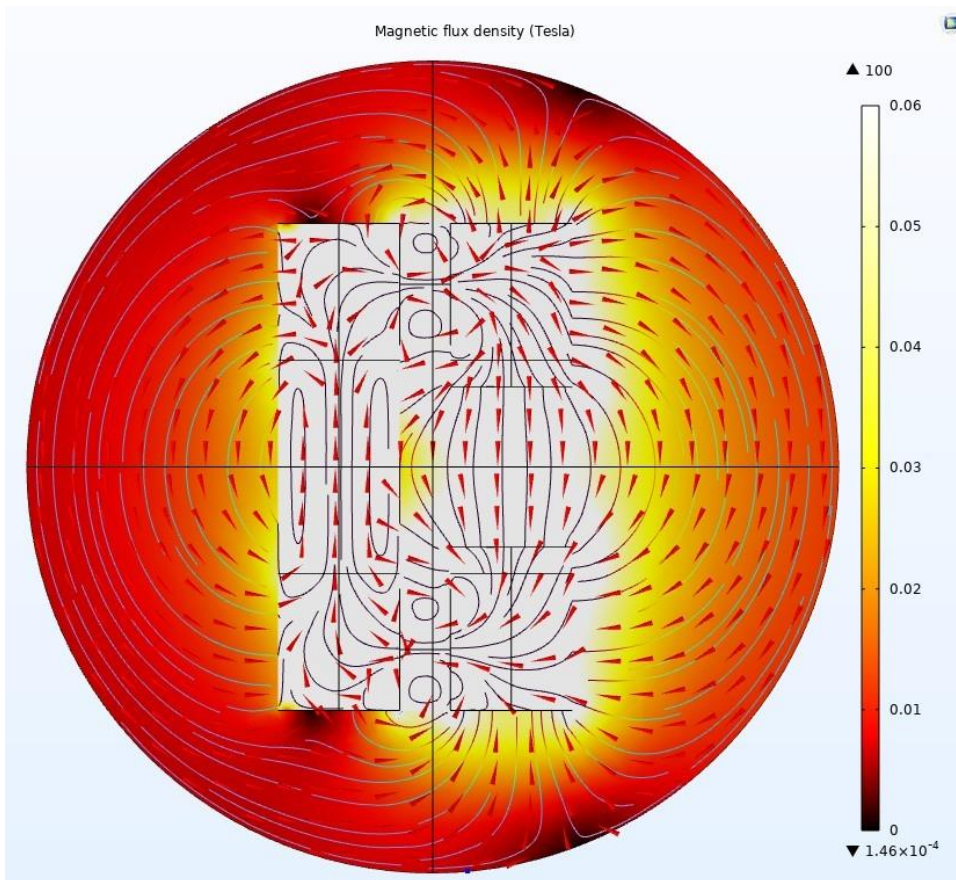


Figure 32.5: Relative permeability is 1000

The simulation results indicate a significant magnetic field density, denoted as "B" (measured in Tesla), within the core. The density increases from a maximum of 3.04 Tesla at a relative permeability of 20 to a maximum of 100 Tesla at a relative permeability of 1,000. Additionally, we observed a variation in the volume of the magnetic field vectors.

However, in the air gap, the magnetic field density varies from 0.02 Tesla to 0.06 Tesla, which may seem like a significant decrease.

Nevertheless, this variation is quite normal, as the permeability of iron is x times greater than that of air, so it is essential to maintain a high flux density in the core to achieve the desired flux density in the air gap.

In conclusion, the C-shaped module is more user-friendly because it effectively generates a stronger magnetic field while ensuring a uniform distribution of that field, which is more beneficial for our project.

2.4. Calculation of the Mass of Copper

The equations used to measure the mass of copper are:

$$m_c = \rho_c \times V_c$$

$$V_c = A_c \times L_c$$

m_c is the mass of copper

ρ_c is the density of copper

V_c is the volume of copper

A_c is the cross-sectional area of copper

L_c is the length of wire of copper

ρ_c is given by 8960 kg/m³

for a diameter of 12cm L_c will be $12 \times \pi \times 10^{-2}$ m

For a wire with $A_c = 2\text{mm}^2$

$$V_c = 2 \times 10^{-6} \times 12 \times \pi \times 10^{-2} = 0.754 \times 10^{-6} \text{ m}^3$$

$$m_c = 8960 \times 0.754 \times 10^{-6} = 0.006755 \text{ kg}$$

for 2000 turns:

Total mass = $2000 \times 0.006755 = 13.51 \text{ kg}$

for 1500 turns:

Total mass = $1500 \times 0.006755 = 10.1325 \text{ kg}$

This calculation seems to contain an error. We made 25 turns using a copper wire with a cross-sectional area of 2 mm^2 , and the weight was 0.3 kg.

For 1,500 turns, this is equivalent to 60 sets of 25 turns each. Therefore, 0.3 multiplied by 60 equals 18 kg.

This value is significantly greater than 10.1325 kg.

2.5. CAD Design

Here is a CAD design we created for the C-shaped coil (see Figure 33).

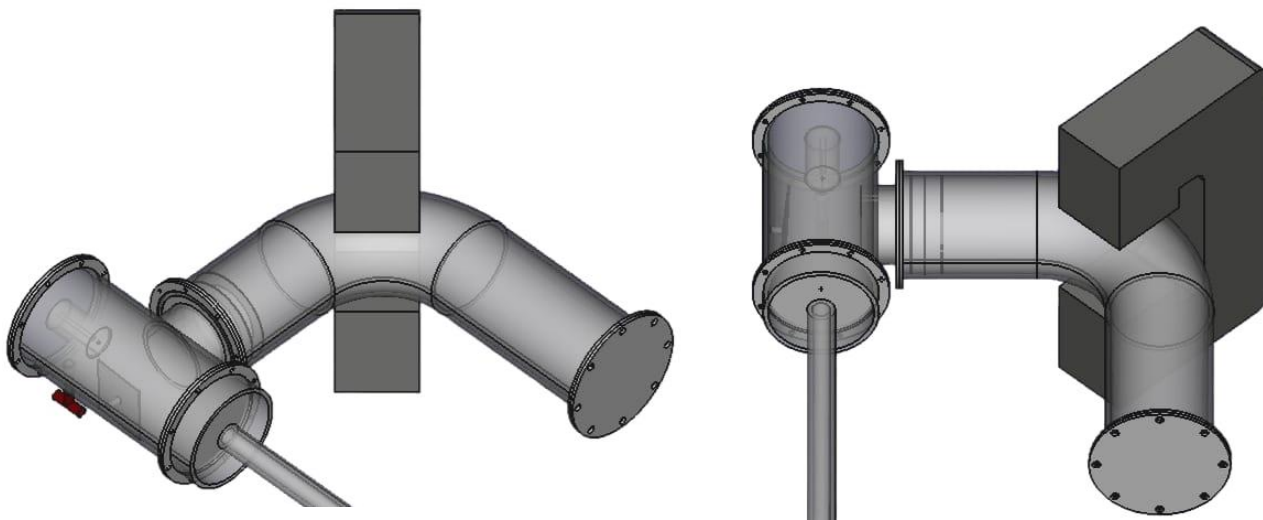


Figure 33: CAD design of the C-shaped coil from two perspectives

13.5 CHAPTER III: REALIZATION, TESTS & DISCUSSION

13.5.1 Realization

We purchased an iron bar weighing 84 kilograms from "Nawfal and Khawli" and proceeded with the cutting process according to the specified dimensions. The liquid is used to prevent the iron from overheating and to facilitate easier cutting (see Figure 34).



Figure 34: The cutting process for the iron

1.1. Annealing Process

Once the iron is prepared, we proceed with the annealing process to enhance its permeability. We utilize a muffle furnace, which allows us to achieve extremely high temperatures using a temperature sensor (see Figure 36).

We have confirmed that the furnace is completely sealed and ready to proceed with the annealing process (see Figure 35).



Figure 36: The temperature sensor



Figure 35: The iron bars inside the furnace

We purged the nitrogen from the furnace using an inert gas to prevent the oxidation of iron by air. The gauge on the left side indicates the amount of nitrogen in the bottle, while the gauge on the right displays the volume of gas that has been purged, which is slightly smaller (see Figure 37). We must continue purging throughout the entire annealing process.

We began heating the iron in the furnace. It took approximately one and a half hours to reach the



Figure 37: The nitrogen bottle filled with 150 bar

desired temperature of 870 degrees Celsius which is logical, as the optimal temperature depends on the material's structure [17]. The green number indicates the target temperature, while the red number represents the actual temperature

(see Figure 38).

We left it there for approximately one hour before turning off the furnace and keeping it closed to allow the iron to cool slowly and uniformly.



Figure 38: Numerical panel shows the temperature inside the furnace

We observed that we consumed approximately 100 bars of nitrogen gas throughout the entire annealing process (see Figure 40), leaving the iron in the furnace until the following day.

The outer shell of iron must be cleaned before beginning the construction of our C-shaped core.

We observed that the iron exhibited some burnt impurities resulting from the heating process it underwent. The taller iron bar took a longer time to cool, which is expected due to its size and the amount of heat it absorbed (see Figure 39).



Figure 40: Comparison between of nitrogen amount before and after annealing



Figure 41: Polishing the iron from the black impurities from smaller to larger parts

1.2. Iron Cleaning

The first step after annealing was to clean the outer shell of the iron, removing any burnt remnants and polishing it until it was completely free of black impurities. We began with the smaller sections before advancing to the larger ones (see Figure 41).

The difference can be observed in the accompanying figures (see Figure 42).

Cleaning the iron is essential for the successful construction of the C-shaped core, as impurities can hinder the construction process.



Figure 42: The difference steps of cleaning the heated iron

1.3. Core Construction

After ensuring that the iron was thoroughly cleaned, we commenced the welding process to fabricate our C-shaped iron core.

We placed the larger section of iron on two concrete blocks and began welding the smaller components to it (see Figure 43).



Figure 43: A factor was welding the iron

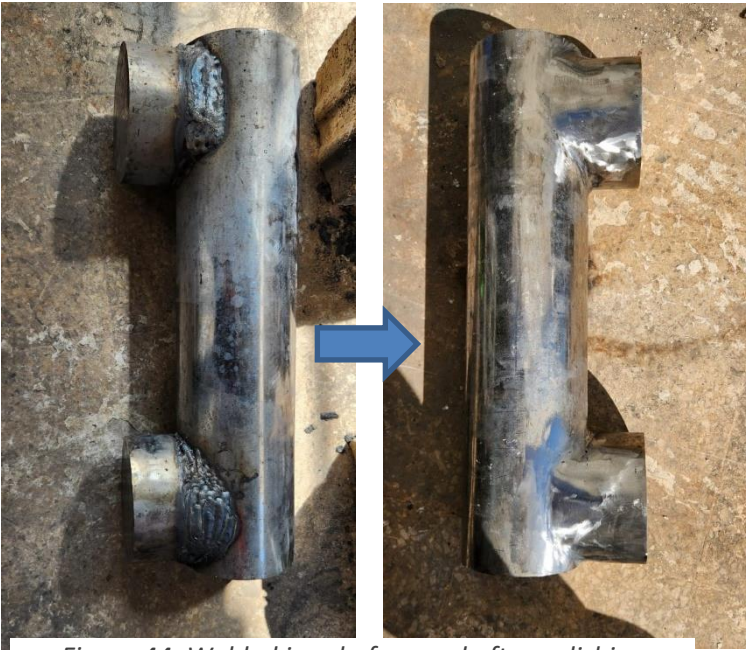


Figure 44: Welded iron before and after polishing

After completing the welding process, we began polishing to remove the burnt impurities that resulted from welding. Consequently, the three sections now appear as a single cohesive unit (see Figure 44).

The iron core was shaped according to the design specifications. We welded four small iron bars to facilitate handling the core (see Figure 45), which weighed approximately 84 kilograms.

When we completed the welding, the iron core was prepared to proceed with winding the copper.

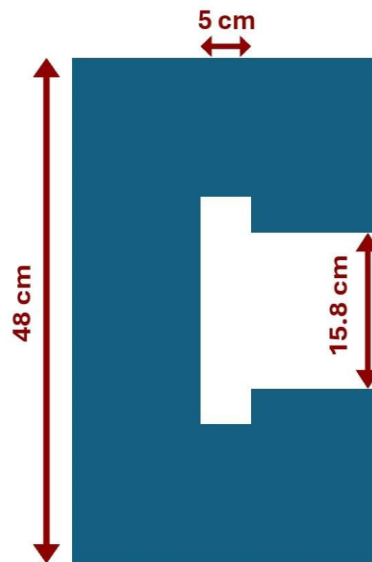


Figure 45: C-shaped iron core and its 2D ch

13.5.1.1 1.4. Winding the Coil

We began winding the core with copper wire that has a cross-sectional area of 2 mm². First, we covered the core with insulating paper, and then we continued winding the wire on top of it.

The winding process was challenging; it was performed manually (see Figure 46) and required a significant amount of time due to the heavy weight of our core, which made the winding machine impractical.



Figure 46: Factors that wind the copper around our C-shaped core

We calculated the required number of turns using the equation:

$$N = B (1.05L_c + \mu_r L_g) / \mu_0 i$$

We found for a $B = 0.06$ Tesla, $L_c = 90.2$ cm, $L_g = 15.8$ cm, $i = 6$ A and for $\mu_r = 25$

We require 1,558 turns; however, we have observed that this figure does not align with the simulation results, which indicate that a greater number of turns and a significantly higher relative permeability are necessary. This discrepancy arises from the fact that the iron is circular rather than rectangular, as is the case with transformers.

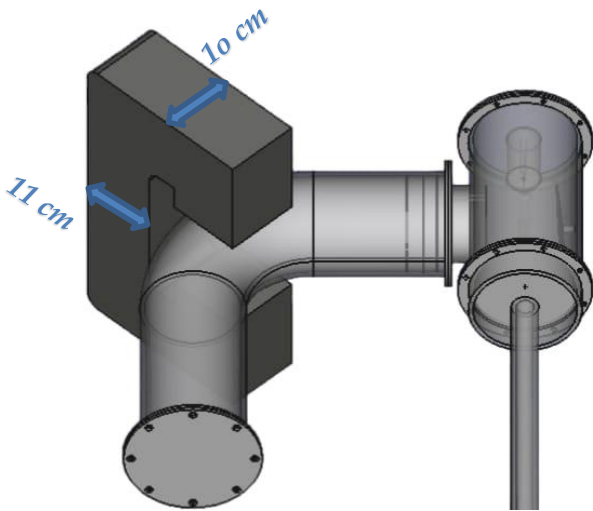
As a result, this equation is applicable only for very small air gaps.

Finally, we have completed winding our electromagnet, achieving a total of 1,530 turns. Due to the dimensions of the deflection zone tube, there is no capacity for additional turns.

Considering the weight of the electromagnet, which is approximately 104 kilograms (with the copper component weighing around 20 kilograms), we constructed a specialized stand to support it (see Figure 47).



Figure 1107: The C-shaped Electromagnet



The

primary difference between the CAD

Figure 48: Comparison between the real and CAD designs

design and our

electromagnet is the cross-sectional area, which is circular. Although we were unable to use a rectangular iron core due to its unavailability in the market, the air gap and overall dimensions are nearly identical, as can be observed (see Figure 48).

$$A_{\text{rectangle}} = 11 \times 10 = 110 \text{ cm}^2$$

$$A_{\text{circle}} = \pi \times 6^2 = 113 \text{ cm}^2$$

13.5.2 Tests and Results

1.4. Single Solenoid Testing

We took a small piece of iron measuring 16.1 cm in length and 2 cm in diameter to investigate the strength of the magnetic field both with and without the iron core. To conduct this experiment, we constructed a coil consisting of 115 turns of copper wire, supported by two holders, one at each end (see Figure 49).



We required a power supply, a



multimeter,

Figure 49: The small iron section with 5cm, before and after winding the copper

and a teslameter to initiate the testing process. After preparing the necessary equipment (see Figure 50), we began measuring the current in the wire, which was 3.5 amps. The results indicated that for a 2.7 cm segment of iron, we achieved a magnetic field strength of 8.4 mT (see Figure 51).

In contrast, when measuring a 2.7 cm air gap, the teslameter recorded only 2.3 mT.

This difference is logical, given the relative permeability of iron compared to that of air.

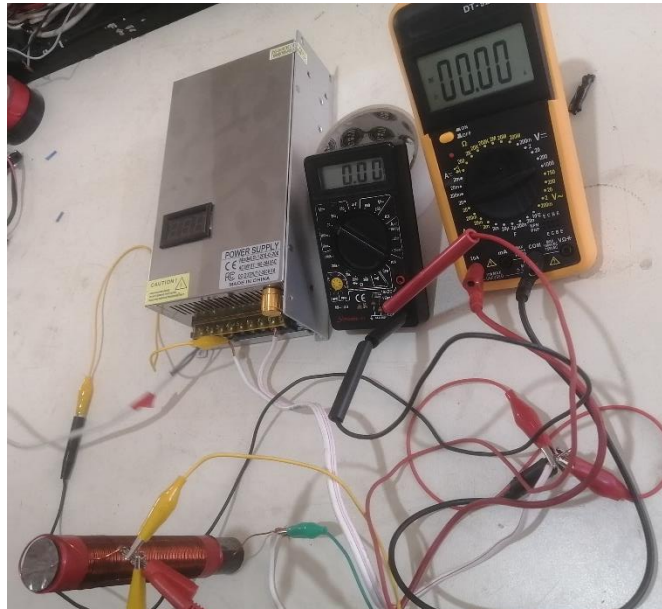


Figure 1110: The system is ready for testing

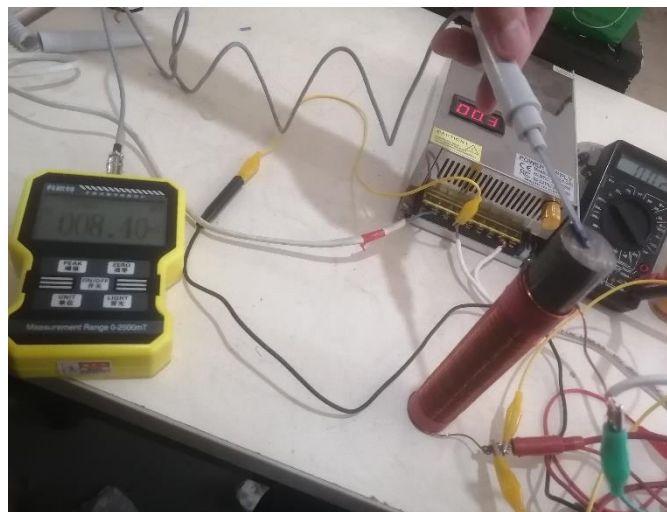


Figure 51: The teslameter indicates a magnetic field strength of 8.4 milliteslas.

We can simply see the difference in the following table:

	Current I	Magnetic Field B
2.7 cm of iron	3.5 A	8.4 mT
2.7 cm of air gap	3.5 A	2.3 mT

Table 51: Comparison between air gap and on iron core effect on the magnetic field

1.5. Electromagnet C-shaped Testing

Once we completed the construction of the C-shaped electromagnet, it was ready to be tested for its magnetic field in the air gap.



Figure 52.3: C-shaped electromagnet along the mass sector tube in the mass spectrometer



Figure 52.2: Fitting the mass sector tube in the air gap



Figure 52.1: C-shaped electromagnet along the mass sector tube

1.5.1. Magnetic Field without Pipe Test

Requirements:

- *Mechanical Requirements:*

The C-shaped electromagnet is constructed from iron shaped into a C configuration, wound with copper wire, and includes an air gap specifically designed to accommodate the mass sector tube (see

list of Figures 52).

- *Electrical Requirements:*

The electrical supply must be adjustable until the desired outcome is achieved.

- *Magnetic Requirements:*

The C-shaped electromagnet must produce a magnetic field within the mass sector tube.

The C-shaped electromagnet must produce a magnetic field of 0.06 Tesla.

Test Specification:

Step	Step description	Desired result
Pre-Condition	The system is powered off	
Turning on the system	Activating the C-shaped electromagnet using a power supply	Achieving a magnetic field (B = 0.06 Tesla)
Turning off the system	Deactivating the C-shaped electromagnet	The magnetic field has ceased.
Post-Condition	The system is powered off	

System Test and Results:

Test 1:

Step	Step description	Desired result	Result
Pre-Condition	The system is powered off		
Turning on the system	Activating the C-shaped electromagnet using a power supply	Achieving a magnetic field (B = 0.06 Tesla)	Negative
Turning off the system	Deactivating the C-shaped electromagnet	The magnetic field has ceased.	Positive
Post-Condition	The system is powered off		

Analyzing the results of the test:

We measured the magnetic field at the center of the air gap, where the ions are expected to move. We observed that applying a current of 6 amperes results in a teslameter reading of 50 millitesla (see Figure 53), which is insufficient for our project. However, this serves as a solid starting point, as we need to achieve a magnetic field of 60 millitesla, necessitating an additional 10 millitesla.

So, all we can do is enhance the current situation; in this manner, we can attain the desired result.



Figure 53: The teslameter displays a reading of 50 millitesla

Test 2:

Step	Step description	Desired result	Result
Pre-Condition	The system is powered off		
Turning on the system	Activating the C-shaped electromagnet using a power supply	Achieving a magnetic field (B = 0.06 Tesla)	Positive
Turning off the system	Deactivating the C-shaped electromagnet	The magnetic field has ceased.	Positive
Post-Condition	The system is powered off		

Analyzing the results of the test:

We successfully achieved our target of 60 millitesla (see Figure 55) by increasing the current to 7.5 amperes (see Figure 54). Fortunately, the copper wire can safely handle approximately 9 amperes before reaching a critical threshold. However, at 7.5 amperes, the results were optimal.

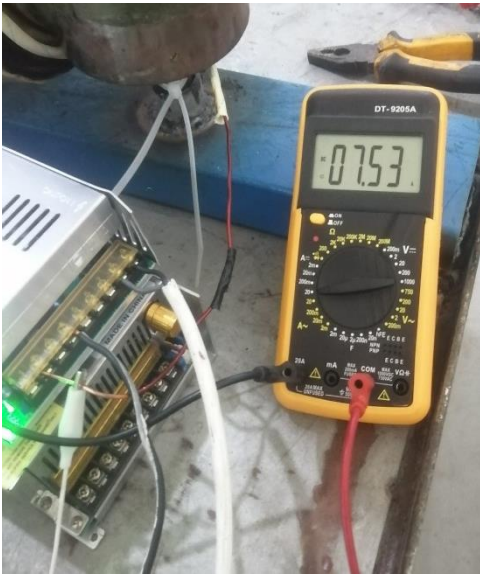


Figure 54: The multimeter displays a reading of 7.5 amperes



Figure 55: The teslameter displays a reading of 60 millitesla

All ferromagnetic materials exhibit the phenomenon of hysteresis. [18]

We observe a small residual magnetic field of approximately 1 millitesla (see Figure 56).

Consequently, our C-shaped core becomes magnetized, indicating that its permeability has increased even further.



Figure 572: System is off and the teslameter displays a reading of 1 millitesla

1.5.2. Magnetic Field in Open Pipe Test

This test is identical to the previous one; however, the key difference is that the mass sector curve tube is now positioned within the air gap of the electromagnet, enabling us to take measurements.

13.5.3 Calibrating Mass Spectrometer with Known Material Probes

13.5.3.1 Process Control System

It is important to identify the sensors and actuators that will be connected to the PLC (see Figure 57); therefore, we will install them in the control panel. Program the PLC using “DELTA WLPSOFT” software.

Create the graphical user interface (GUI) using C#.NET. we should note that the addresses in the Programmable Logic Controller (PLC) program differ from those in the C# code.

Reason: Improved clarity and technical accuracy by expanding the acronym.

Graphical user interface



Modbus RS 485 Network

Control Panel



Electrical Cables

Sensor & Actuator



Vacuum Pump

Power Supply
For Tungsten

Power Supply
HV

Power Supply
for Helmholtz Coil

Pressure Sensor

Power Supply
for Inside-out Coil

Solenoid valve 1

Solenoid valve 2

Power Supply
150VDC
300VDC

Figure 57: The required sensors and elements in the process control system

13.5.3.2 3.2. System Test Specification

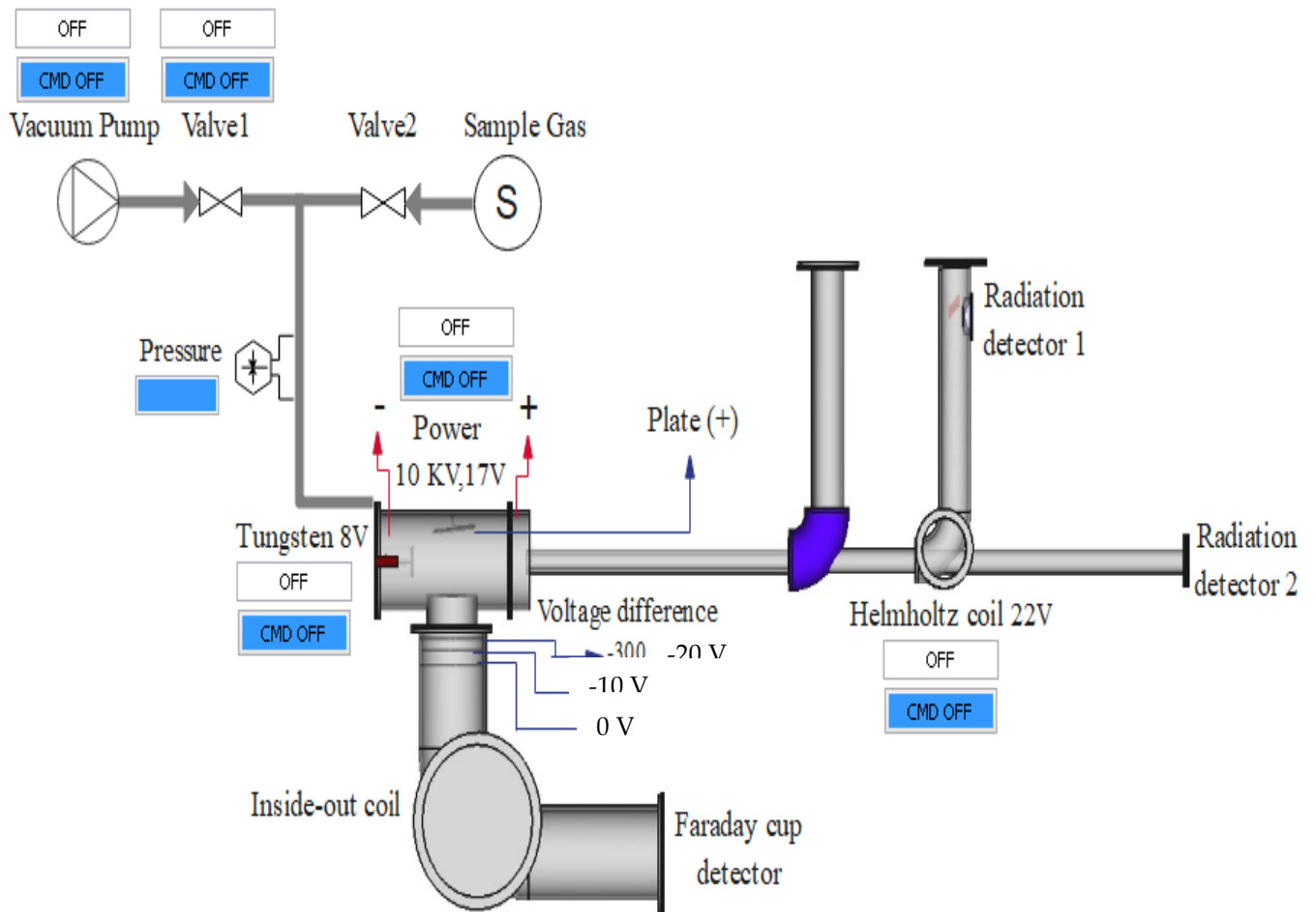


Figure 58: System specification

This test will not be conducted due to time constraints; however, we would like to present the test specifications. To enhance understanding, we provide a description of the current process control system:

Action	Expected result
--------	-----------------

Turn on the valve V1 and the pump	V1 is open, 95% Vacuum
Turn on the Power Supply P4 and P9	Continuous Power (17V)
Burn the Tungsten by supplying it with P9	Get electrons around the Tungsten (the lamp will light)
Connect the power supply P9 to the first plate	The first plate positively charged attracts the electrons towards it
Turn off the pump and the valve V1	The air stopped and V1 is closed
Turn on the detector	Detector is running
Turn on the valve (V2) for a few minutes	The electrons will collide with the atoms of the vapour sample (Get ions with charge (+1))
Turn on P8 and P5	Continuous power (20 V)
Turn on the electromagnetic Coil	Get magnetic field ($B=0.06$ T)
Connect the power supply P8 (10V) to the second plate	The second plate positively charged repulses the ions out of the ionization chamber, and the ions enter the tube
Connect the power supply P5 to the three plates in the tube	The ions that entered the tube will be accelerated
Ions will be subjected to a magnetic field of $B= 0.06$ T when they pass through the curve	The detector gives a signal (this indicates that the ions left the ionization chamber, entered the tube, accelerated by the plates, deflected by the magnetic field, and were detected)

Turn off P5, the detector and the electromagnetic Coil

Ions acceleration stops, no signal will appear. Detector is not running.

Magnetic field stops

Turn off P8, P9 and P4

The second and the first plates are no longer charged and the lamp will turn off

13.6 CHAPTER IV: CONCLUSION & PERSPECTIVES

We successfully constructed our electromagnet while taking economic factors into account. Initially, we aimed for a more ambitious target of 0.2 T across an air gap of approximately 15 cm; however, this goal proved to be both challenging and costly.

Consequently, we established a more affordable and achievable target of 0.06 T across the same air gap, which is ideal for our purposes, at the same time the acceleration zone will require a lower voltage of 20 V, compared to 300 V.

Although the process control system developed by AECENAR is ready for testing, a computer software program must be employed for gas detection.

Additionally, we need to utilize a high-performance pump capable of achieving an ultra-high vacuum of 10^{-7} bar to facilitate the ionization of ions and ensure that the volume inside the mass spectrometer is thoroughly evacuated, we can achieve this by using multiple high-vacuum pumps in series, and then the mass spectrometer will be completed and ready for the detection of toxic gases.

13.7 List of References

- [1] J. & A. F. & S. M. & A. J. & N. L. Ahamad, "Ahamad, Javed & Ali, Faraat & Sayed, Manjoor & Ah Basic Principles and Fundamental Aspects of Mass Spectrometry," 2022.
- [2] S. Medhe, "Ionization Techniques in Mass Spectrometry: A Review," 23 6 2018.
- [3] P. M. V. R. & A. R. Barron, "Principles of Mass Spectrometry and Modern Applications".s licensed CC BY 4.0.
- [4] A. E. MIR, "Asmaa EL MIR, Évolution de dispositif de spectromètre de masse pour la détection des gaz de combustion des déchets municipaux," 2022-2023.
- [5] W. Harris, "How Mass Spectrometry Works," 1 January 1970. [Online]. Available: HowStuffWorks.com. [Accessed 22 May 2024].
- [6] "Mass spectroscopy Chapter 13," University of Calgary.
- [7] S. Medhe, "Mass Spectrometry: Detectors Review. Annual Review of Chemical and Biomolecular Engineering," 2018.
- [8] S. Zurek, "Magnetic permeability," Encyclopedia Magnetica.
- [9] "Linear Solenoid - Classic Line LCL-D. Kendrion Solenoids Impulse Automation Ltd."
- [10] M. Uchikoshi, "Metal purification method and metal refinement method," 21 May 2002.
- [11] T. K. M. a. M. I. Kekesi, ". "Ultra-high purification of iron by anion exchange in hydrochloric acid solutions."Hydrometallurgy," 13 January 2002.
- [12] S. Sild, " Annealing Explained – Definition, Process and Benefits. Fractory," 2024 January 26.
- [13] "Annealing: Definition, Purpose, How It Works, and Stages".
- [14] "A Historical Journey Through the Evolution of Metal Heat Treating".
- [15] "What Gases Work Best for Annealing?," nexAir, 16 March 2022.
- [16] Lin, "Controlling annealing and magnetic treatment parameters to achieve high permeabilities in 55 Ni-Fe toroid cores," July 2001.
- [17] Y. Z. R. Z. T. He, "Effect of Annealing Temperature and Time on the Magnetic Properties and Magnetic Anisotropy of a Temper-Rolled, Semi-processed Non-oriented Electrical Steel," 2024.
- [18] .. K. S. I. Altpeter, "Materials Characterization Using Nondestructive Evaluation (NDE) Methods," 2016.

13.8 List of Figures

Figure 1: Schematic representation of the principle of mass spectrometry	463
Figure 2: Schematic representation of the ionization chamber	464
Figure 3: Schematic representation of the acceleration plates	465
Figure 4: Deflection of a mixed ion stream under magnetic field	465
Figure 5: Module 5 of the Faraday cup	466
Figure 6: The affection of permeability on the magnetic field	467
Figure 7: B-H curve illustrating the varying permeability of different materials	468
Figure 8: B-H curve showing the saturation point of magnetic permeability	469
Figure 9: The maximum radius in the deflection zone for the mass spectrometer	470
Figure 10: Magnetic Flux in a Solenoid	471
Figure 11: A Simulation of a Single Solenoid	472
Figure 12: A Simulation of Two Solenoids	473
Figure 13: A 2D Simulation of Two Solenoids with 3000 relative permeability	474
Figure 14: Relative permeability is 3000	474
Figure 15: Relative permeability is 200	474
Figure 16: The two angles formed by a point P located outside the solenoid.	475
Figure 17: The Electrorefining Method of Iron	477
Figure 18: The Different Stages of the Annealing Process	478
Figure 19.3: Electromagnet view 3	479
Figure 19.2: Electromagnet view 2	479
Figure 19.1: Electromagnet view 1	479
Figure 20: A 2D simulation of two solenoids with a diameter of 12.5 cm.	480
Figure 21: Ten solenoids are used on a cylindrical vacuum tube.	481
Figure 22: The 2D simulation utilizing arrow volumes	481
Figure 23: The 2D Simulation without arrow volumes	481
Figure 24: The C-shaped core was taken from one side of the transformer.	482
Figure 25: The magnetic circuit of a C-shaped core	483
Figure 26: The C-shaped core showing the mean core length	484
Figure 27: The efficiency comparison of two C-Shaped modules	484
Figure 28: The cutting plan for the iron bar	486
Figure 29: The assembling plan for the C-shape core	486
Figure 30: The C-shaped core illustrates the region where we wrap the copper	487
Figure 31: The meshing process before simulation	487
Figure 32.1: Relative permeability is 20	488
Figure 32.3: Relative permeability is 200	489
Figure 32.2: Relative permeability is 100	489

Figure 32.5: Relative permeability is 1000-----	490
Figure 32.4: Relative permeability is 500 -----	490
Figure 33: CAD design of the C-shaped coil from two perspectives-----	492
Figure 34: The cutting process for the iron-----	493
Figure 35: The iron bars inside the furnace -----	494
Figure 36: The temperature sensor-----	494
Figure 37: The nitrogen bottle filled with 150 bar -----	494
Figure 38: Numerical panel shows the temperature inside the furnace-----	495
Figure 39: The iron bars depending on the cutting plan after the annealing process -----	496
Figure 40: Comparison between of nitrogen amount before and after annealing -----	496
Figure 41: Polishing the iron from the black impurities from smaller to larger parts-----	496
Figure 42: The difference steps of cleaning the heated iron-----	497
Figure 43: A factor was welding the iron-----	497
Figure 44: Welded iron before and after polishing-----	498
Figure 45: C-shaped iron core and its 2D characteristics -----	498
Figure 46: Factors that wind the copper around our C-shaped core-----	499
Figure 47: The C-shaped Electromagnet-----	500
Figure 48: Comparison between the real and CAD designs -----	501
Figure 49: The small iron section with 5cm, before and after winding the copper -----	501
Figure 50: The system is ready for testing-----	502
Figure 51: The teslameter indicates a magnetic field strength of 8.4 milliteslas. -----	502
Figure 52.1: C-shaped electromagnet along the mass sector tube -----	503
Figure 52.2: Fitting the mass sector tube in the air gap -----	503
Figure 52.3: C-shaped electromagnet along the mass sector tube in the mass spectrometer	503
Figure 53: The teslameter displays a reading of 50 millitesla-----	505
Figure 54: The multimeter displays a reading of 7.5 amperes-----	506
Figure 55: The teslameter displays a reading of 60 millitesla-----	506
Figure 56: System is off and the teslameter displays a reading of 1 millitesla -----	507
Figure 57: The required sensors and elements in the process control system-----	508
Figure 58: System specification -----	509

13.9 List of Tables

Table 1: Mass, radius of curvature and velocity for different ions -----	469
Table 2: Mass, radius of curvature and velocity for different ions included Pb -----	471
Table 3: Properties of the Iron Core: Establishing Permeability-----	488
Table 4: A comparison between air gap and an iron core effect on the magnetic field -----	502



14 Electron Gun for Mass Spectrometer¹¹

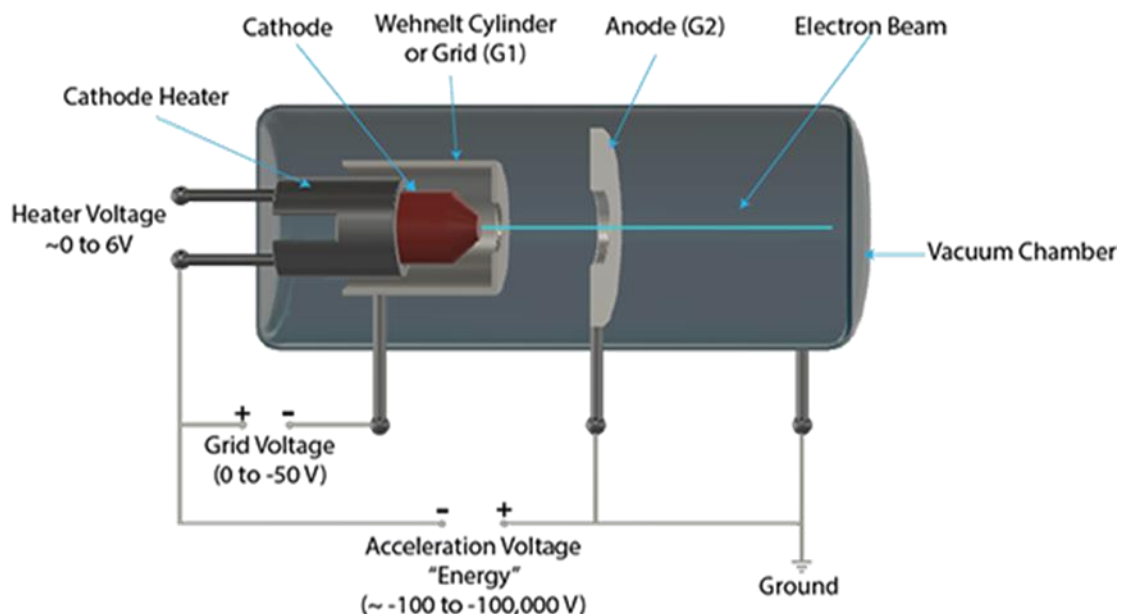
14.1 Introduction

Electron guns are fundamental components in many scientific instruments, including, cathode ray tubes, particle accelerators, and mass spectrometer. An electron gun's core components—a cathode, anode, and Wehnelt grid—work together to emit and focus electrons. Through thermionic emission and controlled electric fields, electrons are accelerated and formed into a coherent beam.

14.1.1 Structure and Function of an Electron Gun

An electron gun is composed of several primary elements: the "cathode", which emits electrons; the "anode", which accelerates the electrons; and the "Wehnelt grid" for electron flow control. The structure is often enclosed in a high vacuum environment to ensure minimal interference.

Cathode: The cathode in an electron gun is typically made of tungsten due to its high melting point and low work function, which makes it efficient for thermionic emission. When heated (by current or another heating source), the cathode releases electrons.



14.1.2 Electric Fields and Electron Acceleration

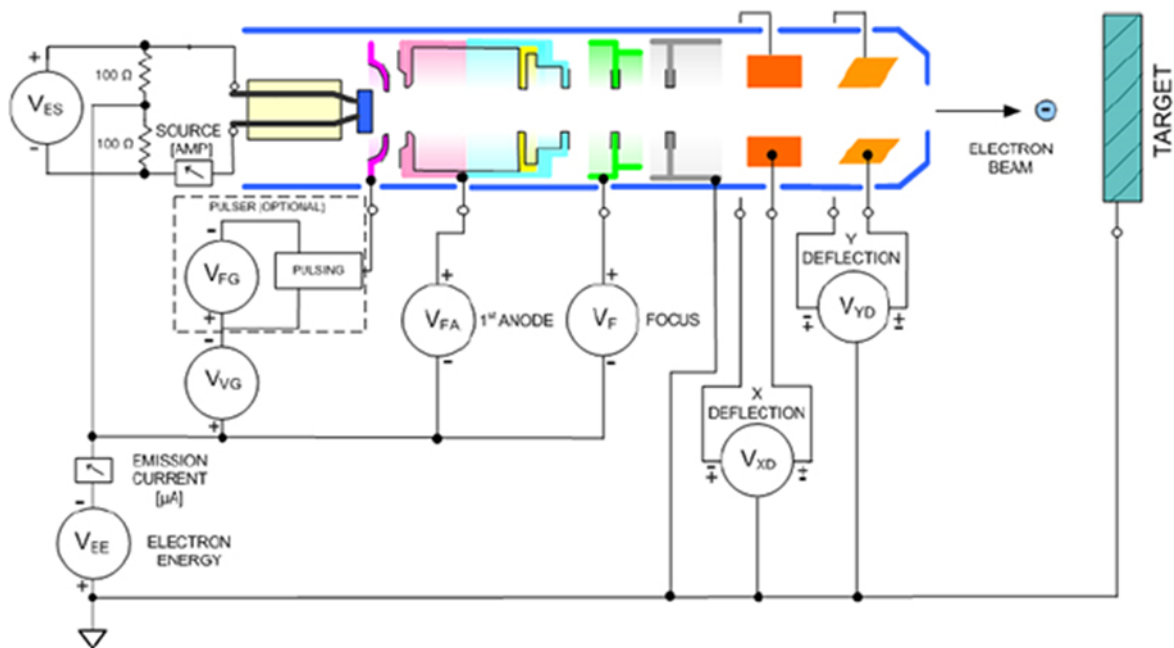
Once electrons are emitted from the cathode, the anode (often set at ground or 0 V) attracts them by creating an electric field. The potential difference between the cathode and anode accelerates the electrons toward the anode.

¹¹ From <https://aecenar.com/index.php/institutes/institute-for-astronomy-and-astrophysics/physics-lab/flue-gas-analysis-with-mass-spectrometry/electron-gun-for-mass-spectrometer>

14.1.3 Role of the Wehnelt Grid

The Wehnelt grid, positioned between the cathode and anode, helps shape and control the electron beam. By applying a voltage slightly more negative than the cathode's, the Wehnelt grid forms a localized electric field that can focus or suppress electron emission.

This field helps concentrate the electrons along the beam's longitudinal axis, creating a more collimated flow.



Voltage Ranges	
V _{EE} ENERGY (HIGH)	up to -2 keV
(LO)	up to -200 eV
V _{VG} GRID	0 to -50 V
V _{FA} 1 ST ANODE	0 to 200 V
V _F FOCUS	0 to 2000 V
V _{ES} SOURCE	0 to 3V @ 3A
V _{XD} DEFLECTION	-150 V to +150 V
V _{YD} DEFLECTION	-150 V to +150 V
FIXED GRID (OPTIONAL)	-50V

14.1.4 High Vacuum (HV) Requirements and Materials

To maintain optimal electron flow and prevent scattering, electron guns operate in high vacuum (HV) conditions. Commonly used materials for HV are metals like stainless steel and ceramics due to their low outgassing rates and resistance to vacuum pressure.

This helps prevent electron collision with gas molecules, which would otherwise disrupt the beam.

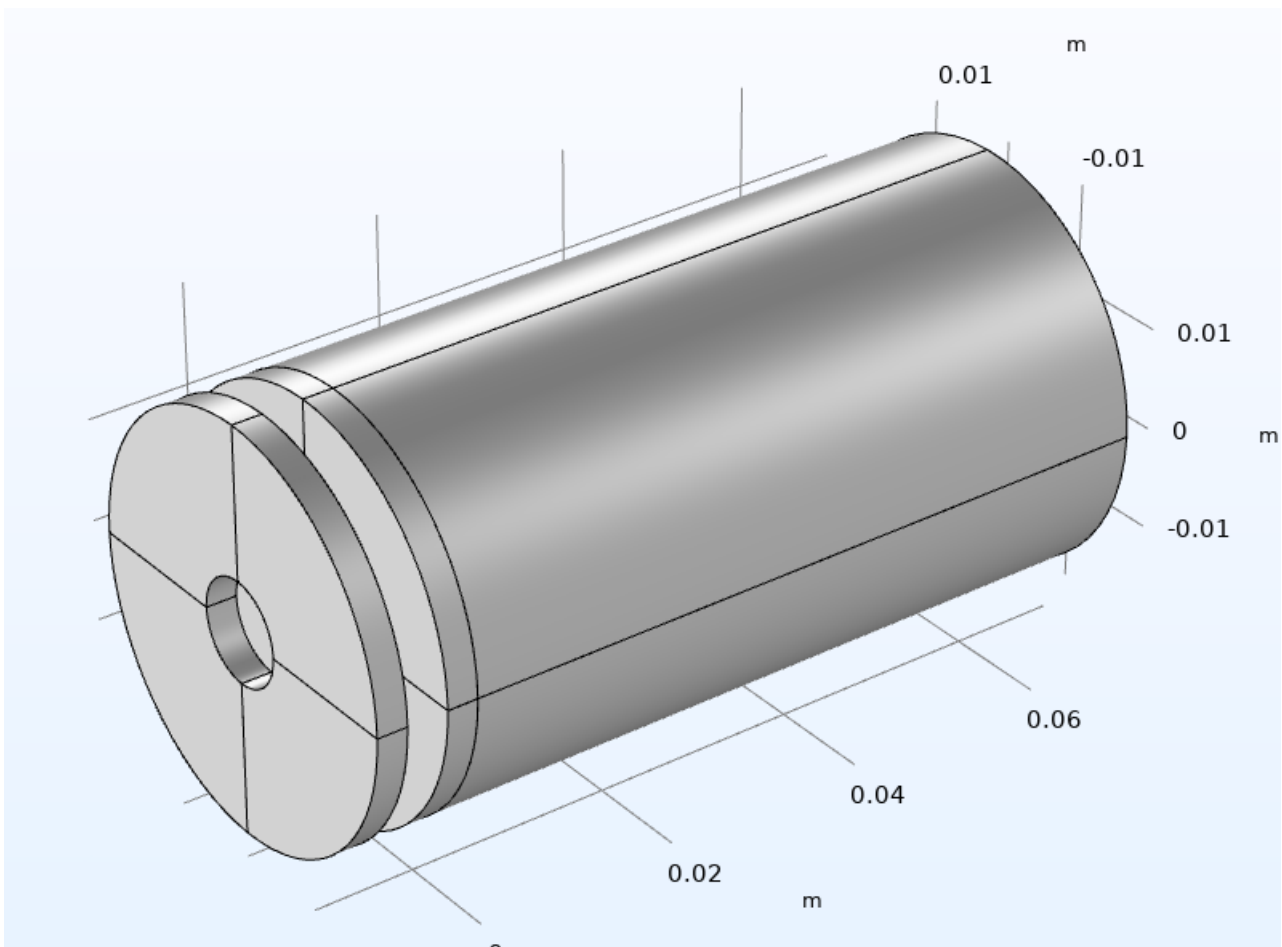
Vacuum Range	Pressure (mmHg, torr)	Molecules/cm ³	Mean free path
Ambient pressure	759.8 (~1.0 atm)	2.7×10^{19}	68 nm
Medium vacuum	$8 \times 10^{-1} - 8 \times 10^{-4}$	$10^{16} - 10^{13}$	100 mm
High vacuum	$8 \times 10^{-4} - 8 \times 10^{-8}$	$10^{13} - 10^9$	10 cm - 1 km
Ultra-high vacuum	$8 \times 10^{-8} - 8 \times 10^{-13}$	$10^9 - 10^4$	$1 - 10^5$ km

Notes: torr x 133 = Pascal, torr /51.715 = PSI. 10^{-9} torr ~ 10^{-7} pascal, 10^{-7} torr ~ 10^{-5} pascal
 Data adapted from: <https://en.wikipedia.org/wiki/Vacuum>

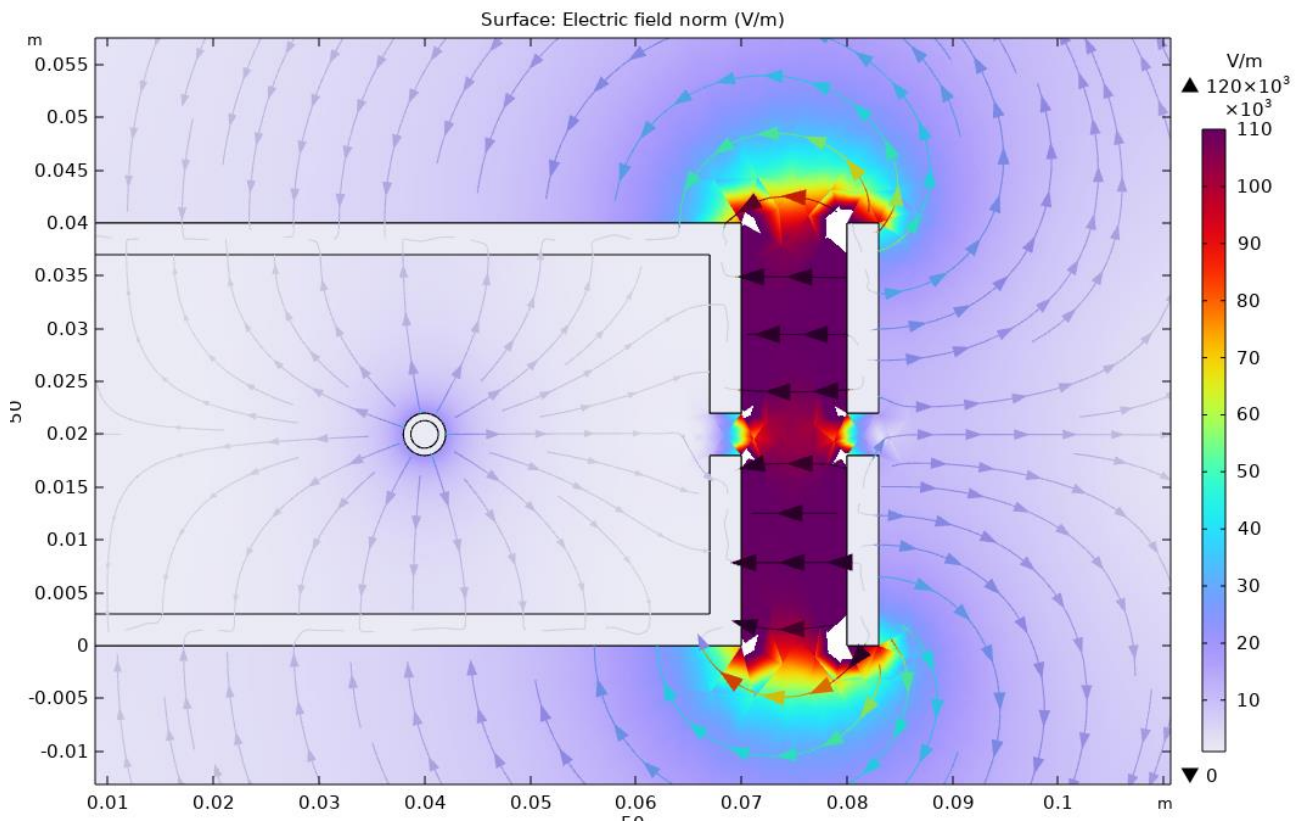
14.1.5 Magnetic Lenses and Electron Optics

Electron optics use magnetic or electric fields to further control the electron beam. Magnetic coils (lenses) focus electrons by bending their path. The field strength of these lenses can be calculated to match the focal length needed for the beam.

14.2 Simulation



cross sectional view:

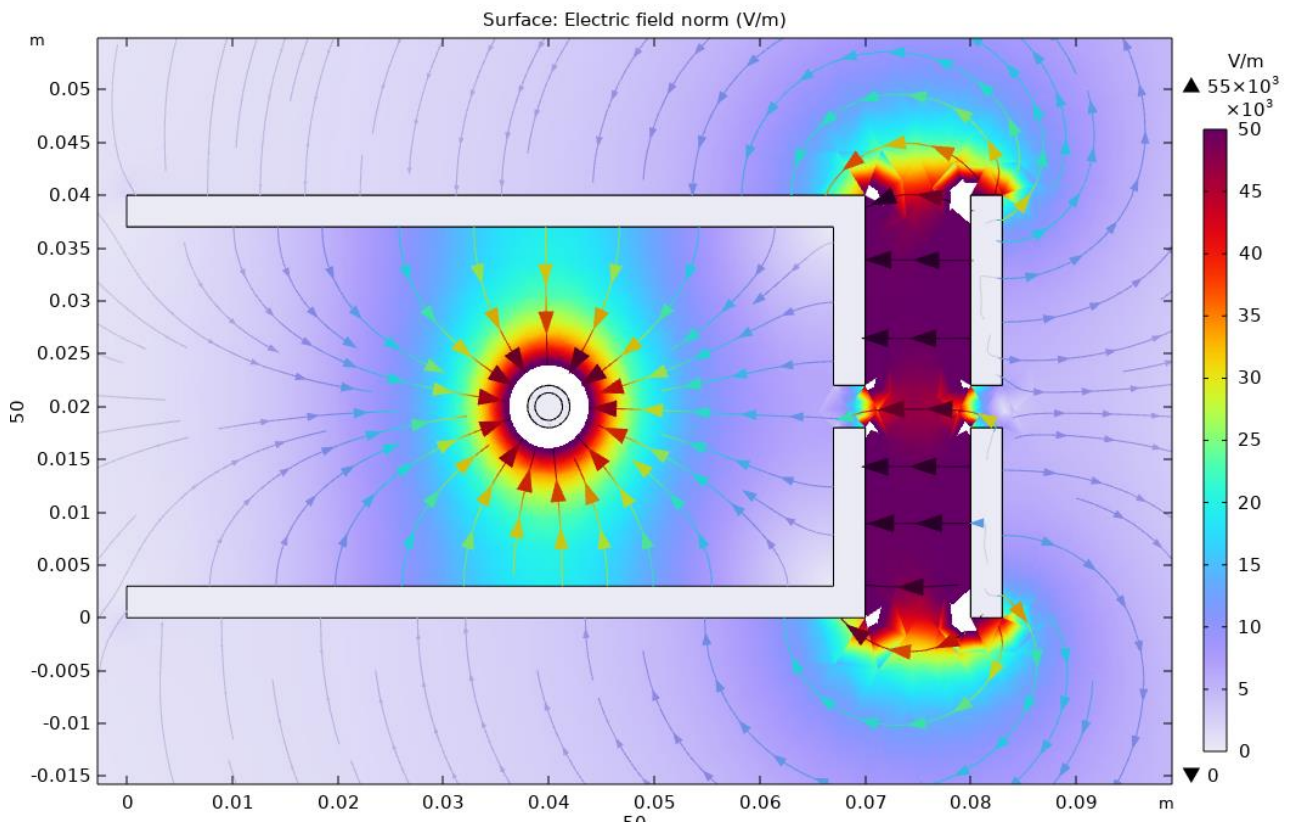


The Voltage on each part:

Tungestun = -1000 V

Wehnelt grid = -1100 V

anode = 0 V



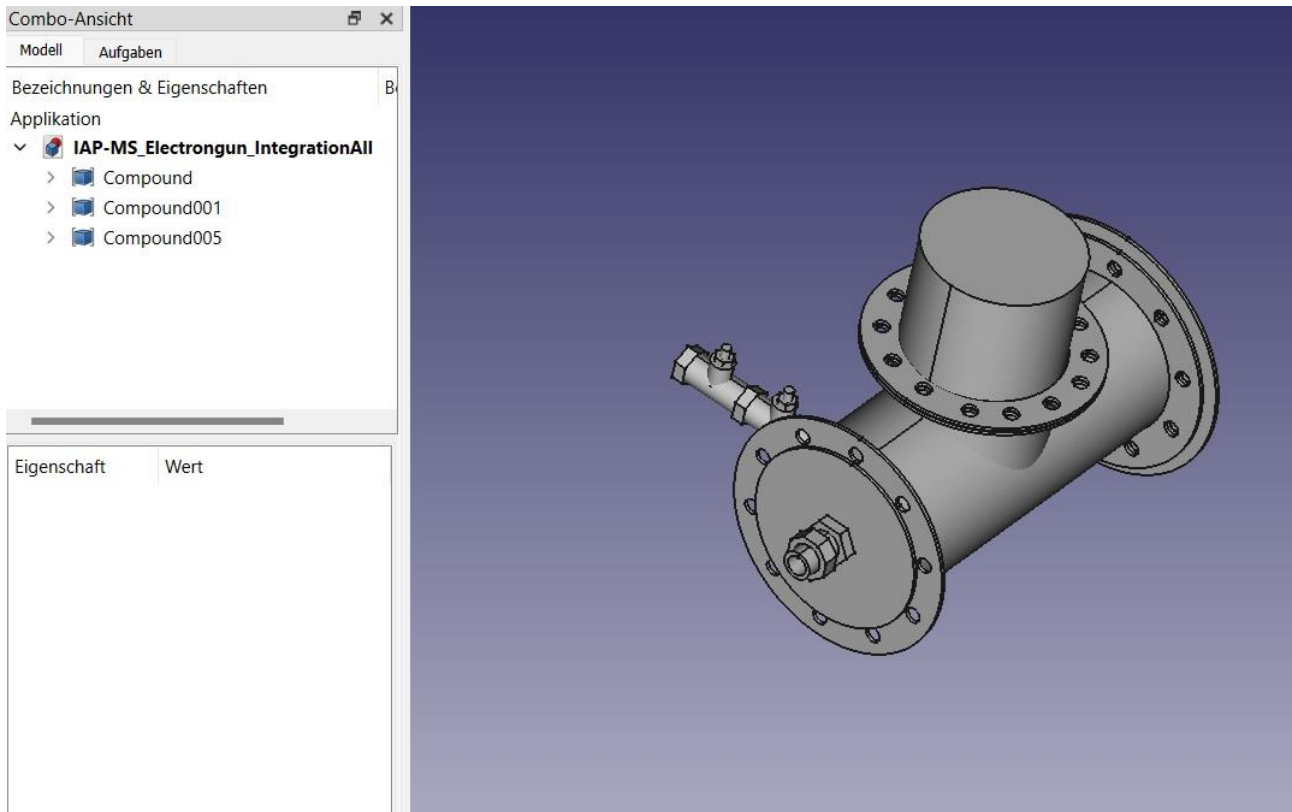
The Voltage on each part:

Tungestun = -500 V

Wehnelt grid = 0 V

anode = 500 V

14.2.1 ElectronGun Outer Cover Design (Dec24/25)



14.2.2 Electron Entrance Realization Concept (4.1.25)

14.3 System Test Specification

Pre-Start requirement	Role	Condition	Starting Process of the Mass Spectrometer
Vacuum pump	To get a high vacuum (below 0.8 mmHg) for electron mean free path of 100 mm. In addition, not to burn the tungsten heating filament.	The system should be completely air sealed from the outside. Silicon paste was used to seal off any potential leak holes.	First step: Turning on the vacuum pump and reaching the specified pressure.
Heating Filamint power supply	To heat up the cathode,	12V DC power soures	Second step:

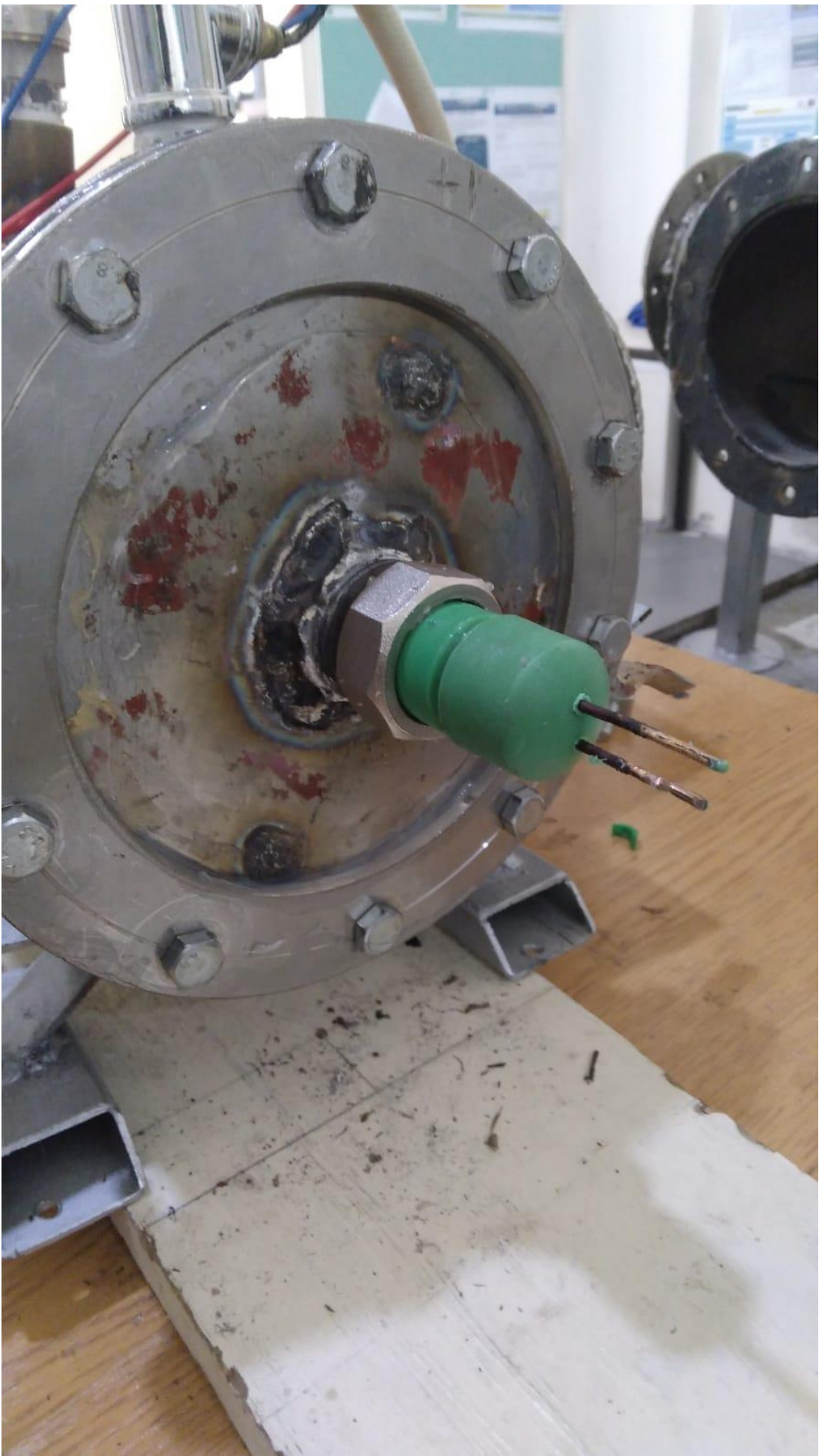
	<p>which will allow for an easier way for electrons to bounce off the cathode's surface.</p> <p>This will allow the use of a relatively low voltage (300V to 1000V) for the anode and cathode</p>		Turning on the heating filament power supply.
High-voltage power supply	To create a high potential difference between the anode's electrode and the cathode's electrode (about 500V)	500V DC power source	Third step: Turning the high voltage supply while watching the multimeter to know that there is a flow of current.
Low-voltage power supply	To create an electric field that will trap the positive charged ions	30V DC power source	Fourth step: Turning on the power supply of the ion trap while watching the multimeter connected to it.
Ammeter 1	To measure the current flowing through the FC detector	A multimeter will be connected in series with the 30V DC source	The presence of a reading on this multimeter marks the success of this test. Which implies the presence of an electron beam in the system and the ability to ionize gases in the body of the mass spectrometer.

			In addition this will prove that the Faradays cup detector is capable of detecting charged particles
Ammeter 2	To measure the electron beam current generated by the cathode	A multimeter will be connected in series with 500V DC power source	





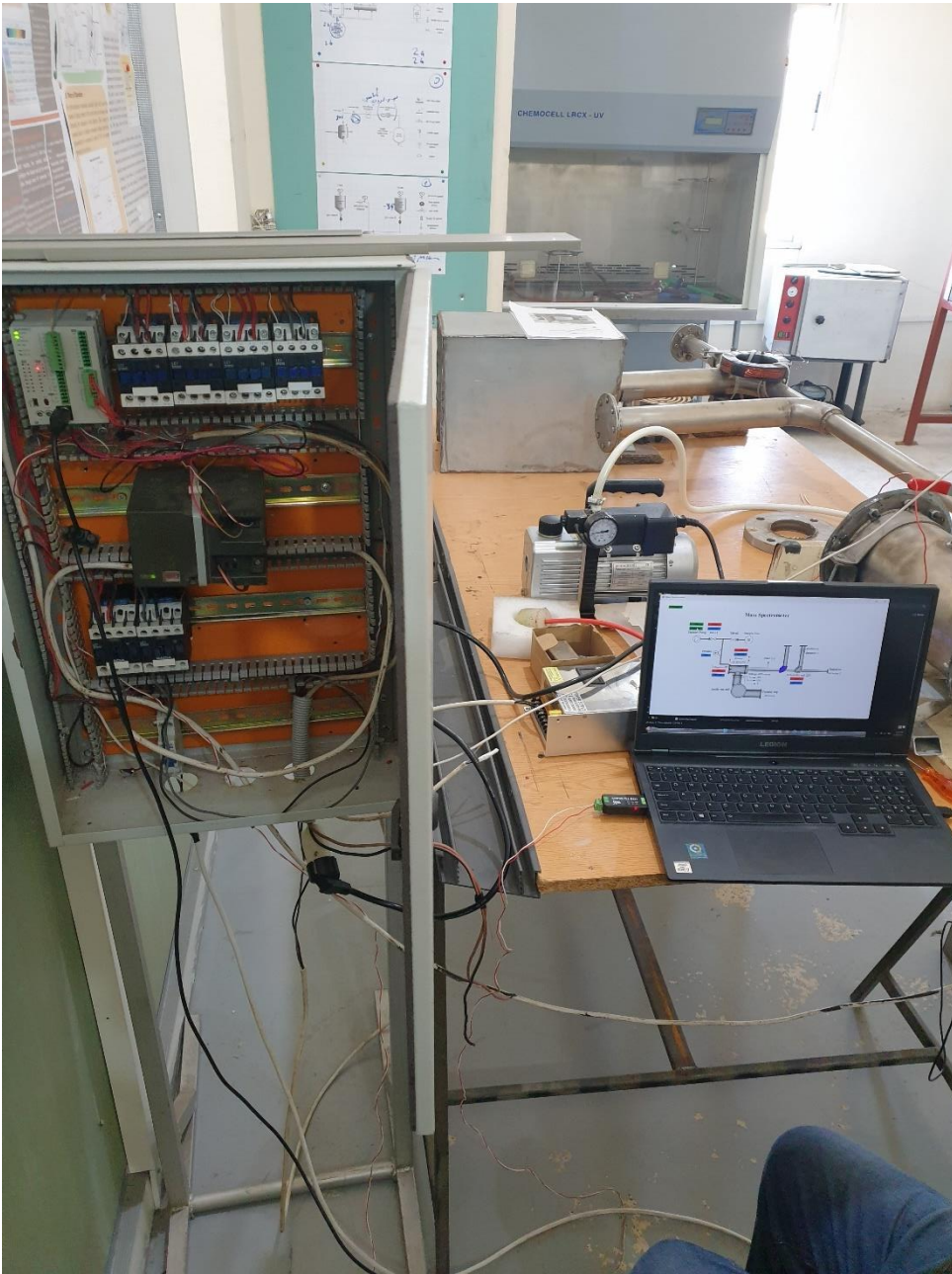








Conducting test 2 for vacuum:

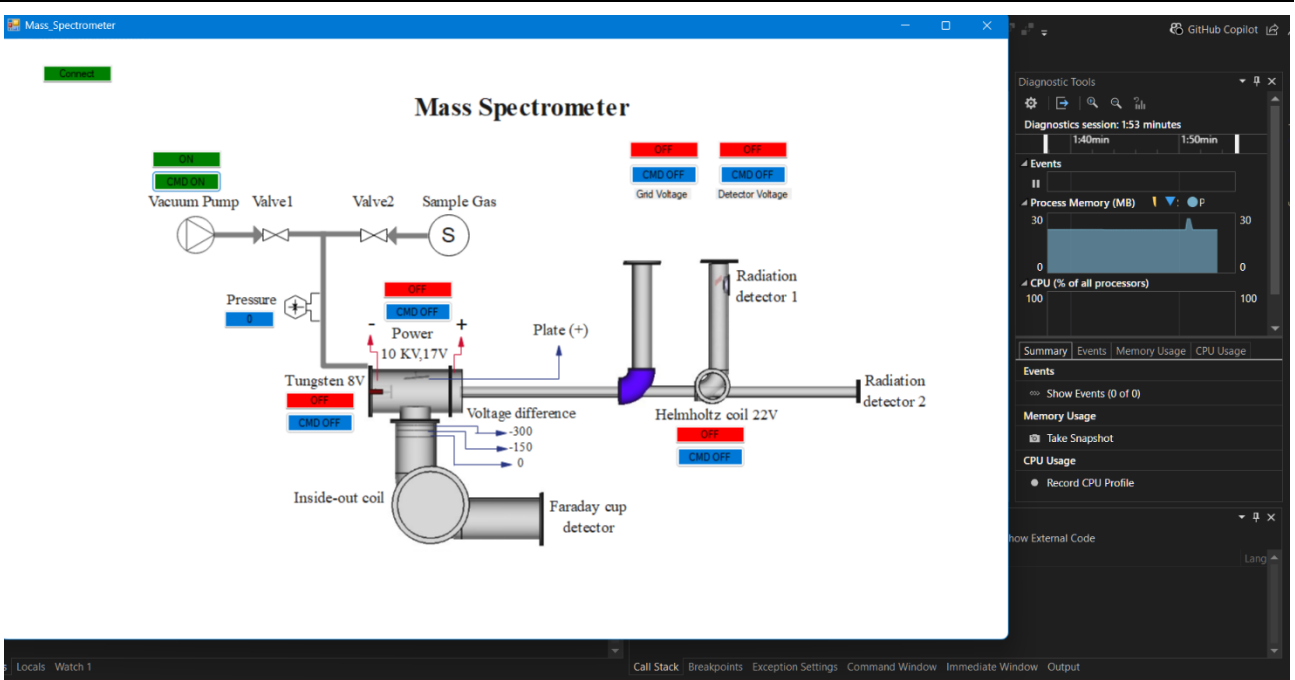


Air leaks were found in various places.

We will close them with silicon and teflon.

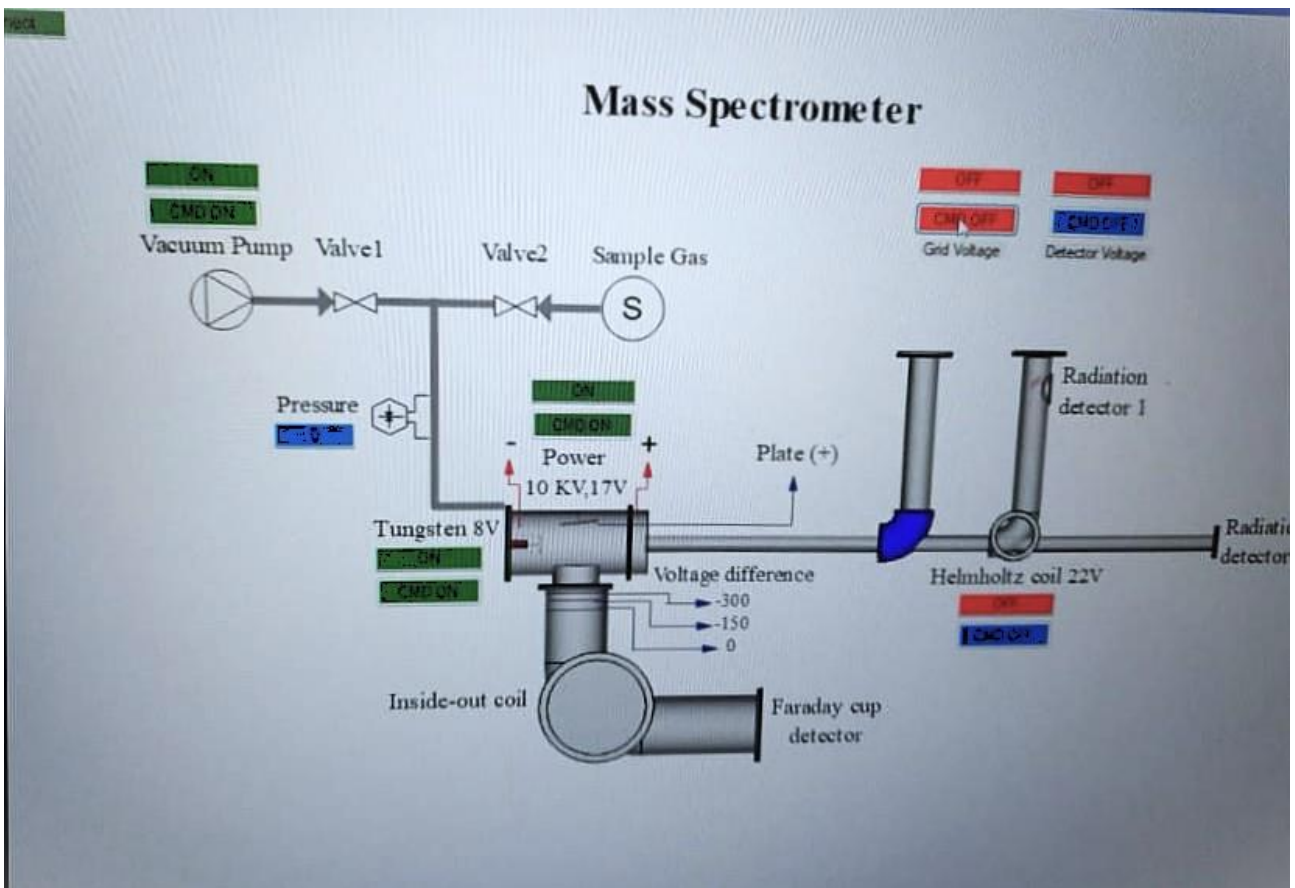
14.4 Electron gun Test (15.3.25)

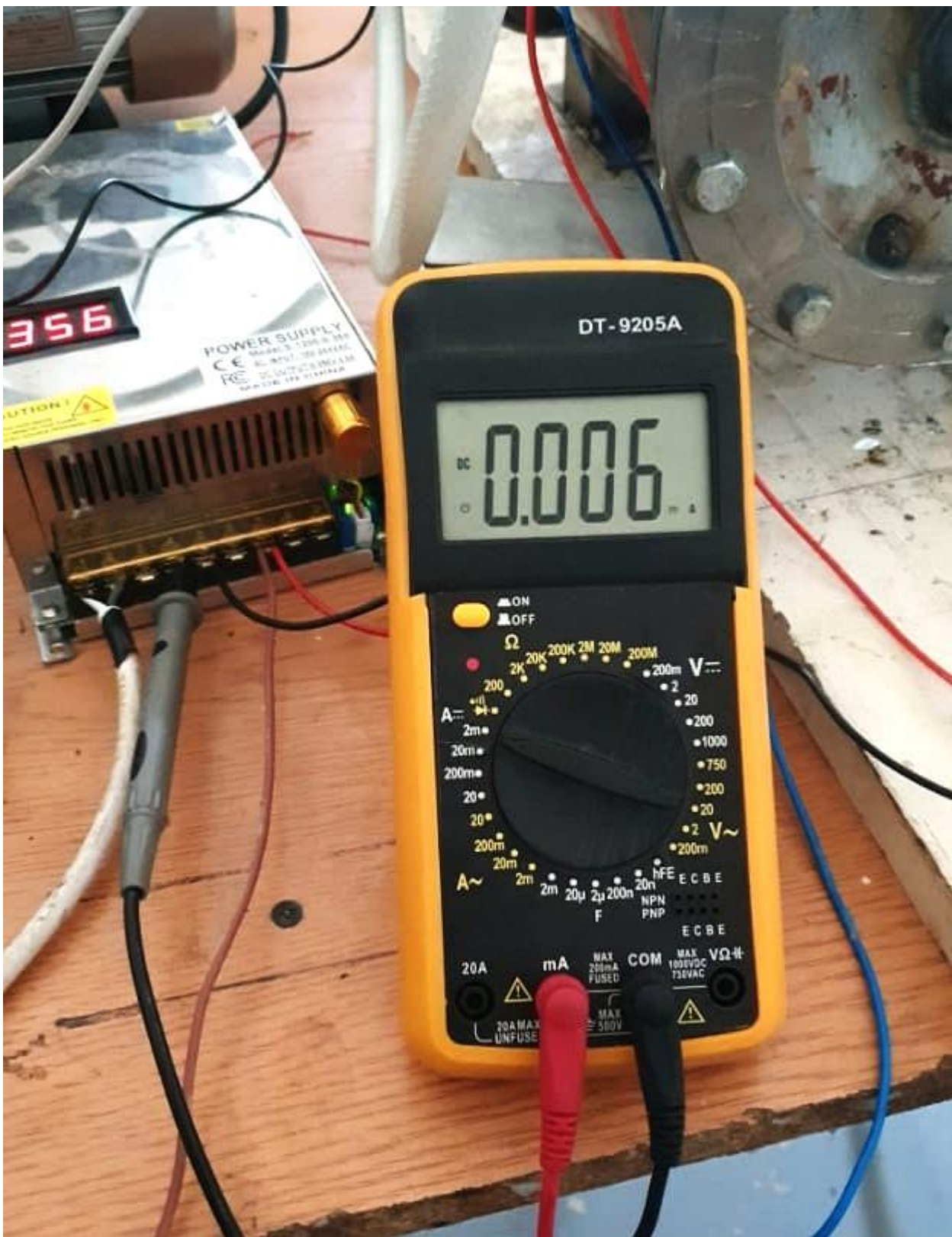
The air leaks are minimized which allowed us to reach 0 Bars on the electronic sensor:



The Tungsten power supply is first turned on, then the high voltage power supply is turned.

A multimeter was connected in series with the power supply to measure the current produced by it. This will help us identify whether there are any arcs, leakage current, (if the current is much higher than zero), or if the electrodes are well insulated and only electron beam is emitted if the current is very close to zero (micro-nano amps range). (KimBall Physics)

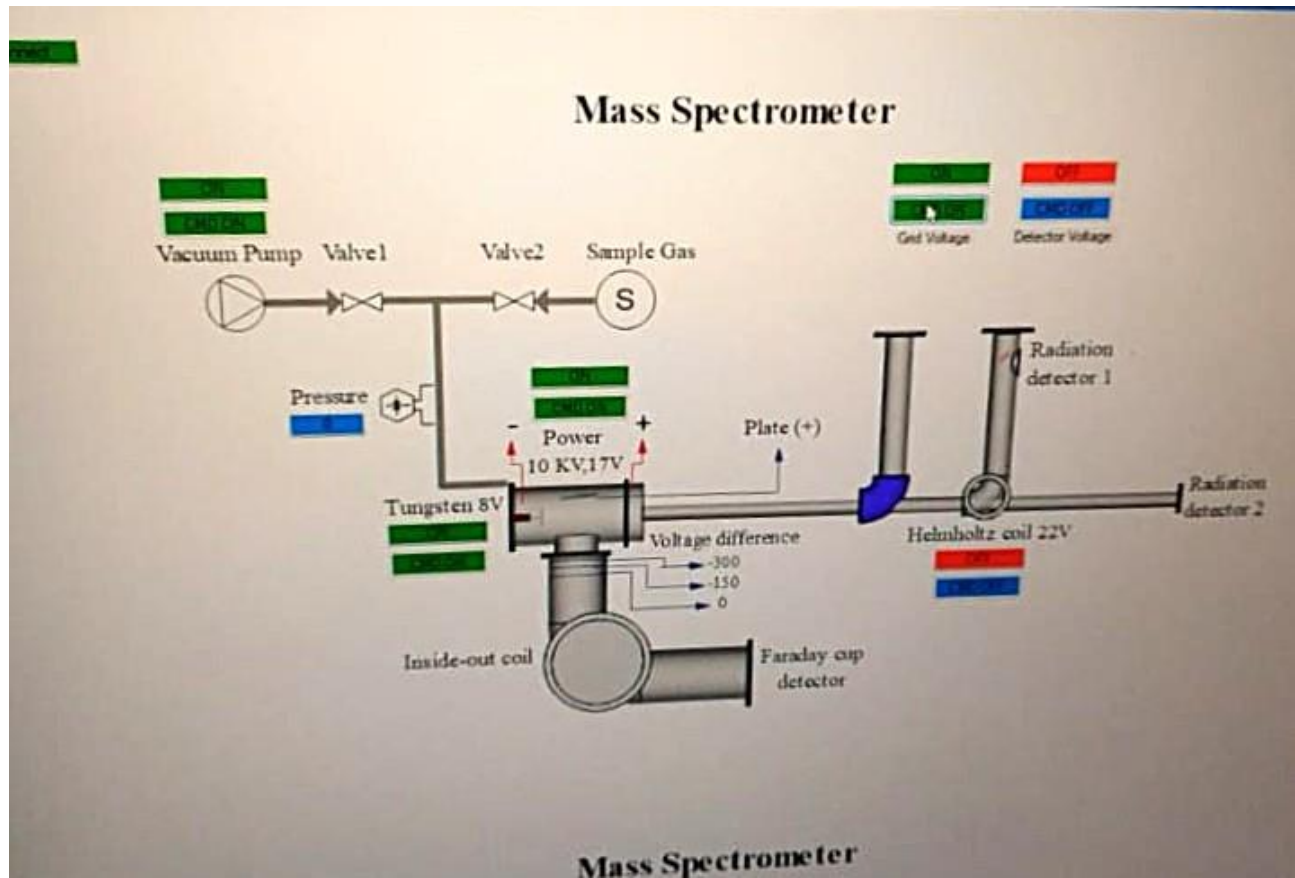




The multimeter read 6 μA , that implies two things:

- No arcs (insulation hold)
- Electron beam of 6 μA going from the cathode to the anode.

After turning on the Grid Voltage, the readings on the multimeter showed an increase in electric current the moment the grid power supply is turned on





The current increased to around 50 μ A which is in range of electron beam at this voltage.

Thus, the test was successful and an electron beam was emitted

14.5 References

- Kimball Physics. "Electron Gun Components and Vacuum Chambers." *Kimball Physics* [Website](<https://www.kimballphysics.com/>).
- Wikipedia. "Vacuum." Accessed at [Wikipedia](<https://en.wikipedia.org/wiki/Vacuum>).
- Knoll, G. (2010). *Radiation Detection and Measurement*. John Wiley & Sons.
- Reimer, L., & Kohl, H. (2008). *Transmission Electron Microscopy: Physics of Image Formation and Microanalysis*. Springer Science & Business Media.

15 Inertial Confinement Fusion (ICF)

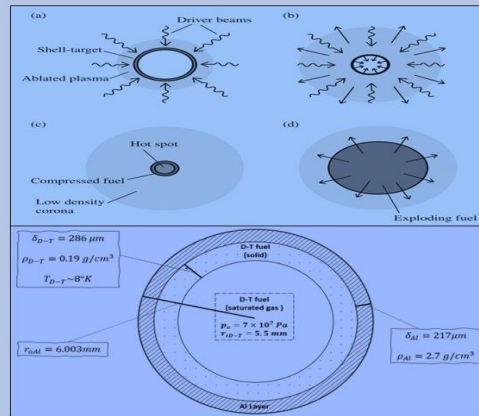
15.1 Fundamentals

Last edited 4/12/2025 6:06:43 PM

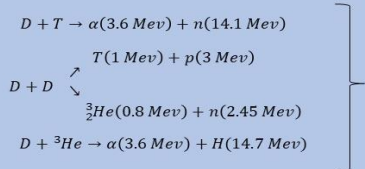
بِسْمِ اللَّهِ الرَّحْمَنِ الرَّحِيمِ

Overview of Inertial Confinement Fusion (ICF)

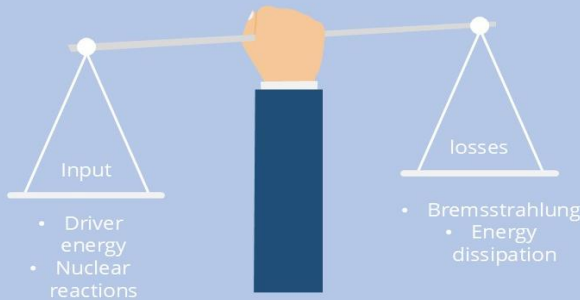
- The object of this method is to exploit *nuclear energy*.
- Confinement is a necessary condition for fusion to occur. In ICF the only mean of confinement is the *fuel's inertia!*
- Nuclear fuel is put in a spherical capsule (typically a couple millimeters in radius) usually made of gold or Aluminum.
- The fuel pellet is irradiated with high intensity Laser beams from all directions, which drive the evaporation of the outer surface, this causes it to ablate outward compressing the fuel with extreme pressure so that the inner core reaches extreme density and temperatures, initiating nuclear fusion. (see figure on the right above)



It is most common to use Deuterium and Tritium (isotopes of Hydrogen) as fuel (D-T fuel) If so, the most occurring nuclear reactions are



Energy Balance

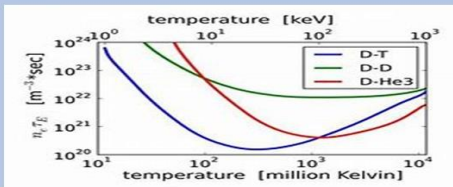


By equating energy losses to gains we arrive at the **Lawson criterion** for ICF

$$n\tau_E = \frac{3kT}{\frac{1}{4} \langle \sigma v \rangle \beta Q_{D-T} - C_b \sqrt{T}}$$

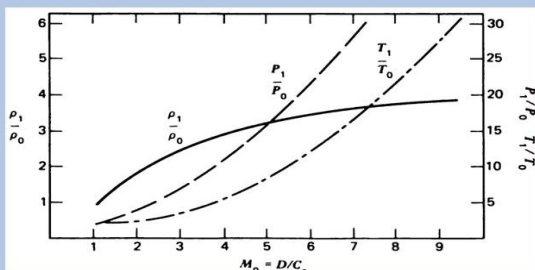
Where

- ✓ $\langle \sigma v \rangle$ is the reaction rate
- ✓ Q_{D-T} is the energy released from D-T reaction
- ✓ β is the fraction of Q_{D-T} that gets absorbed by the fuel
- ✓ T is the temperature, k the Boltzmann constant
- ✓ n is the particle density
- ✓ And most importantly τ_E is the **confinement time**, it is a measure of the time needed by the plasma to dissipate its thermal energy.



Shock-waves propagation

The dominant mechanism for heating the fuel is the shock-heating; as the outer surface is ablated off, shock-waves are created which propagate through the fuel and converge at the center.

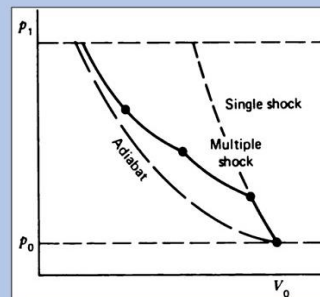


Ratios of the density, pressure and temperature after the shock to their initial values in term of the **Mach number** (Ratio of shock speed to the speed of sound)
Look how density approaches a limit while temperatures and pressure increase indefinitely
This is one downside of shock-heating.

If we treat the ion gas a perfect (with ideal gas ratio γ), then these ratios are given by the **Hugoniot-Rankine** relations;

$$\frac{p_2}{p_1} = \frac{2\gamma}{\gamma+1} M_1^2 - \frac{\gamma-1}{\gamma+1}, \quad \frac{\rho_2}{\rho_1} = \frac{(\gamma+1)M_1^2}{(\gamma-1)M_1^2 + 2}$$

$$\frac{T_2}{T_1} = 1 + \left[2 \frac{\gamma-1}{\gamma+1} \right] \left[\frac{\gamma M_1^2 + 1}{M_1^2} \right] (M_1^2 - 1)$$



One way around this issue is to hit the pellet with multiple light pulses, the effect of the multiple small shocks thus generated is to increase the density with a controllable increase in temperature.

conclusion

The basic ideas of inertial confinement fusion:
Fulfill the Lawson criteria.
Extra density, short time, high temperature by applying strong external forces.

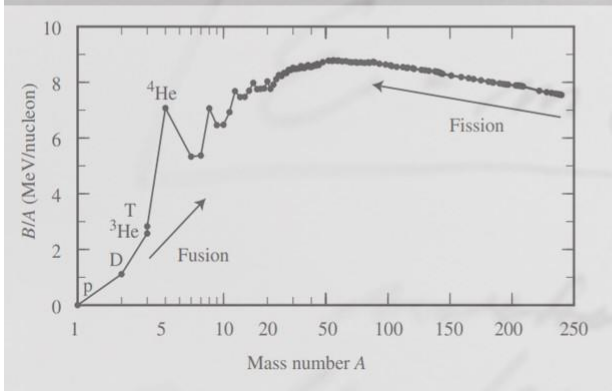
ELAA EO
Ahmad K

§1. Exothermic Nuclear reactions.

It all starts with ,probably, the most popular equation of physics :

$$\mathcal{E} = mc^2$$

due to Einstein. To put it simply , it asserts that to each mass m (at rest) there is a corresponding amount of energy \mathcal{E} , whose ratio to m is the speed of light in vacuum squared. This energy is tremendous even for the tiniest of masses , due to the high magnitude of the speed of light.



The exact circumstances under which mass can become energy remained obscure , until the advent of nuclear physics , where it was noticed that the mass of the nucleus of an atom A_ZX differs from the sum of masses of its constituents , in other words, the quantity

$$\Delta m = Zm_p + (A - Z)m_n - m \quad (1.1)$$

is generally non-zero (m being the actual mass of A_ZX). This fact is best explained in the light of the mass-energy equivalence portrayed above : some of the mass turns into "Binding energy" $B = \Delta m c^2$ that holds the nucleus together ; Atoms with negative B tend to disintegrate , Atoms with positive B tend to be more stable.

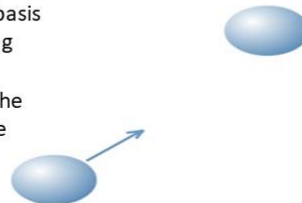
Figure 1.a

A more interesting instance of these ideas is the following fission reaction of ${}^{235}_{92}\text{U}$, The discovery of which marked the genesis of the nuclear bomb ;

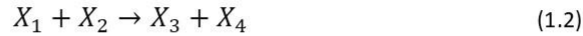


The energy released in a single reaction of this sort is of the order of **210 Mev** .

However , methods of harvesting way more energy from nuclear reactions are yet to come ! It is witnessed that in nature there exist what we call magic numbers , those are special values of Z and A for which the element A_ZX has a surprisingly high binding energy .This is best explained on the basis of Quantum mechanics but we shall not digress to discuss the underlying reasons here . High energy is therefore obtained by "manufacturing" a magic element A_ZX , We consider hence building the element A_ZX from the ground up by combining lighter elements , Let's instead of looking at the detachment of heavy elements , take a look at the collision of two light nuclei , i.e. let's consider their fusion reaction ;



A typical fusion reaction is the following:



Denoting by m_i the mass of X_i ($i=1,\dots,4$), The released energy is calculated to be

$$Q = (m_1 + m_2 - m_3 - m_4)c^2 \quad (1.3)$$

Let A_i be the atomic mass of X_i , Z_i be its atomic number, B_i be its binding energy ($i=1,\dots,4$) - and keeping in mind that the number of protons and neutrons in (1.2) is conserved (for fusion reactions do not involve weak interactions) - it can be shown by some algebra that

$$Q = B_4 + B_3 - B_2 - B_1 \quad (1.4)$$

Equation (1.4) has an important implication ; in order for a fusion reaction be **exothermic** it must be accompanied with an **increase** in the binding energy of the nuclei concerned . Therefore , as figure 1.a shows , the most energy releasing fusion reactions are those that have ${}^4_2\text{He}$ within their product elements.

4

Another constraint on the efficiency of a fusion reaction is obtained by recalling that all nuclei are positively charged , and since like-charges do repel , heavier atoms require more energy to combine . It would therefore be wiser to consider the fusion reactions of light elements.

For the reasons given above , it should not be surprising that the most interesting fusion reaction is that of **Deuterium-Tritium** (D-T reaction)



The energy is released is carried by the newly formed particles , i.e by high speed Neutrons and α -particles (and other elementary particles such as neutrinos whose influence is immaterial) , the former are difficult to capture , but the latter are easy to grab , so basically a single D-T reaction can release about ~ 3 Mev of energy , wich *might appear less* than the output of a single Uranium fission , but there are several factors that make D-T reactions more efficient and more plausible , for instance it does not involve the emission of γ -rays nor the production of harmful nuclear waste.



5

§2. Reaction rate and cross-section.

Collision Processes are characterized by their invariant cross-section, which determines the number of collisions occurring between beams of colliding particles.

Consider two colliding particle beams, let \mathbf{v}_1 and \mathbf{v}_2 be their respective velocities, n_1 and n_2 be their respective densities (i.e. number of particles per unit volume), $d\nu$ be the number of collisions that takes place within the volume dV and during the time interval dt , the cross-section σ is thus defined by

$$d\nu = \sigma v_{rel} n_1 n_2 dV dt \quad (2.1)$$

Where v_{rel} denotes the speed of beam 1 in the rest frame of beam 2, i.e. the relative speed of the first w.r.t the second. In the context of special relativity, one has

$$v_{rel} = \sqrt{(\mathbf{v}_1 - \mathbf{v}_2)^2 - (\mathbf{v}_1 \times \mathbf{v}_2)^2} \quad (2.2)$$

But for our purposes it is enough to restrict ourselves to the limiting case of classical, non-relativistic cinematics;

$$v_{rel} = |\mathbf{v}_1 - \mathbf{v}_2| \quad (2.3)$$

In any case, it is clear that v_{rel} is symmetric in \mathbf{v}_1 and \mathbf{v}_2 , and thus the definition of the cross-section is symmetric in the two particle beams.

The quantity

$$R = \sigma v_1 \quad (2.4)$$

is called the reactivity and is to be interpreted as the probability of reaction per unit time per unit density of target nuclei (which are supposed at rest). In the case the target nuclei are moving, one considers the averaged reactivity

$$\langle \sigma v \rangle = \int \sigma(|\mathbf{v}_1 - \mathbf{v}_2|) |\mathbf{v}_1 - \mathbf{v}_2| f(\mathbf{v}_1) d\mathbf{v}_1 d\mathbf{v}_2 \quad (2.5)$$

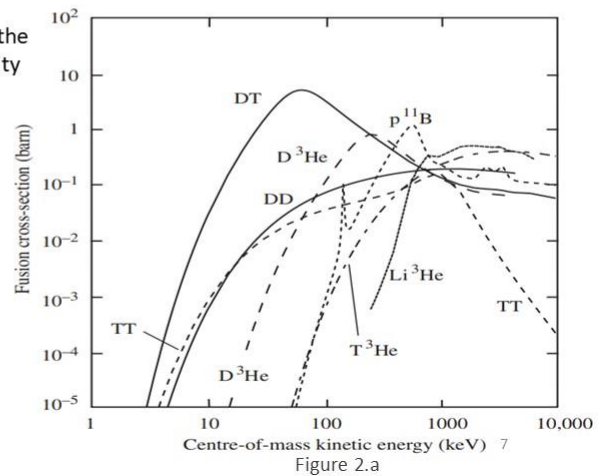
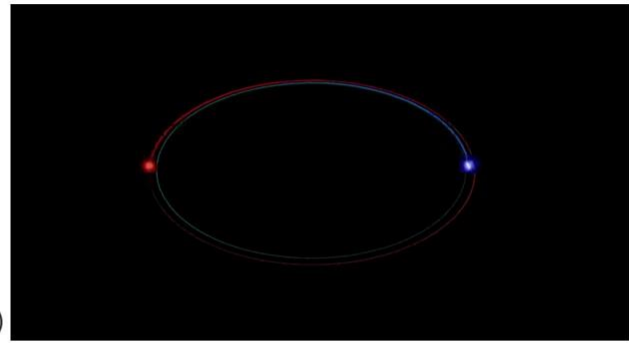
Where f is the distribution function of relative velocities, i.e. the number $f(\mathbf{v})d\mathbf{v}$ determines how many particles have a velocity that lies in the region

$[v_x, v_x + dv_x] \times [v_y, v_y + dv_y] \times [v_z, v_z + dv_z]$
of velocity space.

We may suppose it to be normalized;

$$\int f(\mathbf{v}) d\mathbf{v} = 1 \quad (2.6)$$

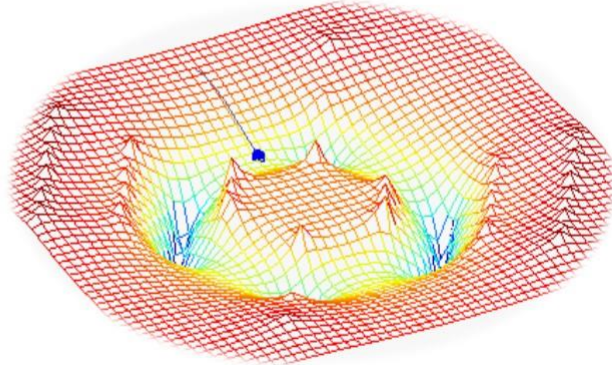
❖ The appropriateness of D-T fuels shows up yet in another important respect; as can be seen from figure 2.a, among all known fusion reactions, D-T reactions have the highest value of cross-section for almost all the energy spectrum.



§§3. Inertial Confinement Fusion (ICF).

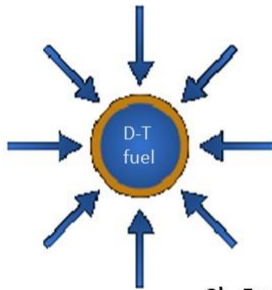
As we have just seen , Fusion requires the high speed collision of nuclei . We know from the statistical interpretation of thermodynamics that temperature isn't but the manifestation of the motion of particles , so in order to achieve high speeds we must heat the fuel up . Moreover one should confine the fuel to a small region of space so that encounters between particles become more likely , thus we must keep the fuel at a high density . But there is an issue ; as temperature arise material tends to expand , making it harder to keep the fuel confined .

One way around that is known as Inertial Electrostatic Confinement (IEC); it consists of heating the fuel up – by depositing extreme energy on its surface via laser beams – turning it into plasma , charged spherical grids are used to create a potential difference across space , the charged ions of the plasma will then move on radial trajectories (as shown in the figure on the right) until they eventually collide at the center .



8

Another clever but similar idea , to which this presentation is devoted , is the regular Inertial Confinement , in which no external means of confinement are involved ,but this method relies solely on the fuel's inertia. The principal stages are briefly outlined below.

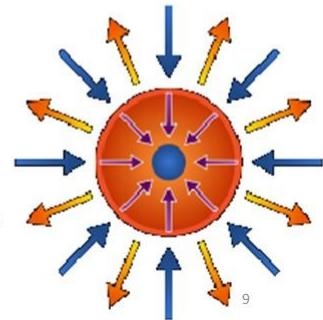


1) Driver energy deposition.

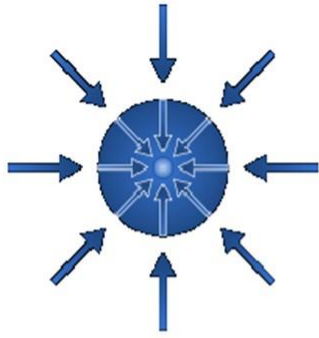
- The D-T fuel is confined to a spherical cavity – usually made of *gold or aluminum* – and is hit from all directions by high intensity laser beams – usually X-rays.
- The means of generating these rays might vary , and it is a matter of design , the discussion of which is deferred to another section.

2) Fuel compression.

- The outer surface will consequently heat up , ionize , and ablate off to surround the pellet by a *plasma corona*.
- The electrons in the corona shield the inner core from incident beams , for the latter can only penetrate to a surface with *critical density* , where the light is completely absorbed by the plasma . This critical density occurs at 10^{21} cm^{-3} for *Nd* laser light ($1.06 \mu\text{m}$) and 10^{19} cm^{-3} for CO_2 laser light ($10.6 \mu\text{m}$).



9



3) Isentropic compression.

- As the ablation of the outer layers continues , extreme pressures are produced at the surface of the fuel , pushing it inward to higher and higher densities (think of it as the fuel bursting out of a rocket).
- Under these conditions , imploding shock-waves are formed , the effect of which is to compress the inner core and to elevate its temperature up to the point where thermonuclear ignition is initiated .
- It is essential here to keep the region surrounding the core as *cold as possible* in order for thermonuclear ignition to start at the center specifically.

4) Thermonuclear burn.

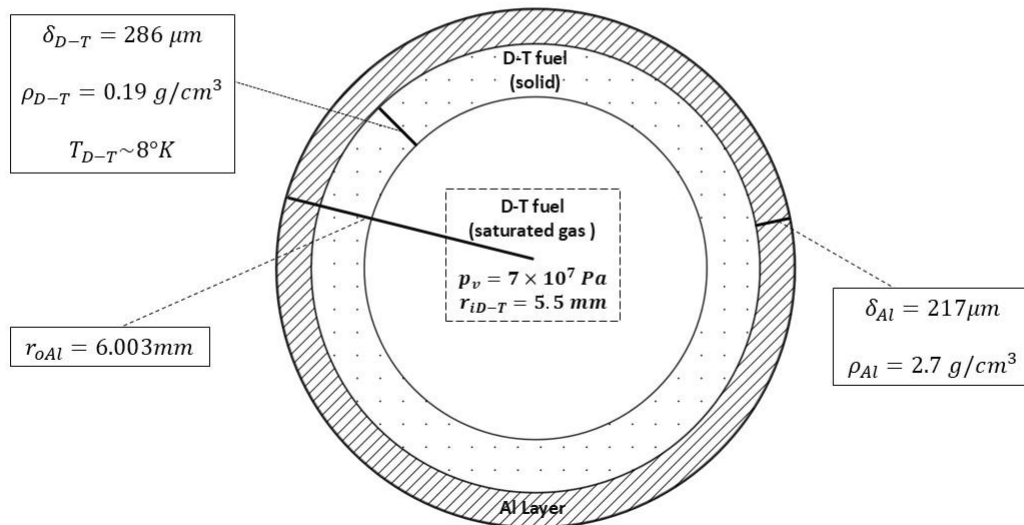
- If $\rho R > 0.5 \text{ g/cm}^2$ α -particles self heating will occur and the intense spark at the center of the inner core will rapidly heat to optimum temperatures of 20 to 100 kev.
- Adjacent layers will burn eventually and a thermonuclear burst expands from the center outward consuming the cold fuel .



10

❖ Numerical application.

We shall digress for a moment and think through an example in order to grasp the order of magnitudes involved in a typical ICF . To this end , consider the following diagram of a fuel pellet;



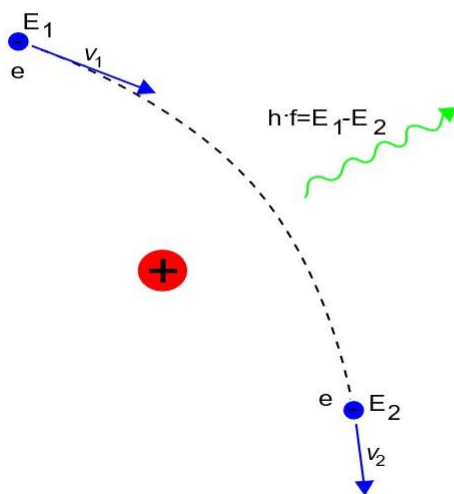
11

- ◇ During 30 ns, the aluminum pusher is homogeneously irradiated from outside by the X-ray, whose initial radiation temperature is $600^\circ K$, the temperature of outer part of pusher layer is elevated to 200 eV ($= 2.3 \text{ Million } ^\circ K$), evaporating outward. As the reaction to this evaporation, the inner surface of the pusher layer pushes the outer surface of the fuel layer with the pressure of $3.8 \times 10^{12} \text{ Pa}$.
- ◇ By this pressure, the fuel layer is accelerated strongly inward. Because the pusher pressure is $p_{iAl} = 3.8 \times 10^{12} \text{ Pa}$ and the area of outer surface of the fuel layer is $S_{oDT} = 421 \text{ mm}^2$, the force of $F = p_{iAl} \times S_{oDT} = 1.6 \times 10^9 \text{ N}$ acts on the fuel layer, whose mass is $M_{DT} = 23 \text{ mg}$.
- ◇ The fuel experiences an inward acceleration $a_{DT} = F/M_{DT} = 7.0 \times 10^{13} \text{ m/s}^2$ during $t_a = 7.1 \text{ ns}$ (because the pusher pressure then decreases), and the implosion velocity reaches $v_{imp} = a_{DT} \times t_a = 5 \times 10^5 \text{ m/s}$. The Mach number of this implosion velocity is about $M = 12$.
- ◇ This supersonic flow collides at the center, being compressed and heated. The mean density of compressed fuel is $\rho_f = 220\rho_s$, where the solid density ρ_s of the DT fuel is 0.19 g/cm^3 . From considerations we shall look into later, the fusion energy can be calculated to be of $E_{out} = 3 \text{ GJ}$ releases from the fuel of 23 mg .
- ◇ At the fuel center, the peak density reaches $\rho_c = 3568\rho_s$ and the temperature arrives at $T_c = 4 \text{ keV}$. Thus, the peak pressure is $p_c = \rho_c \times T_c = 1.55 \times 10^{17} \text{ Pa}$.

12

§3.1. Criteria for an efficient thermo-nuclear burn.

The simple minded exposition of ICF we have given above clarifies the general process, but it does not provide any quantitative insight into the matter.



There are several mechanisms through which energy losses occur. The principal source of radiation losses is the **bremsstrahlung effect**.

When charged particles undergo a deceleration, they suffer a reduction of their kinetic energy, this difference is then emitted in the form of a photon – usually in the X-Ray range. (see the picture on the left)

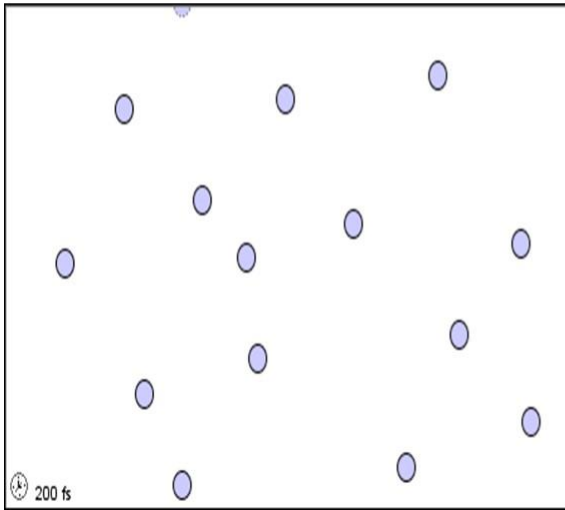
Why is this relevant? Well the plasma created in the first stage of ICF is, broadly, an aggregate of charged particles that are moving randomly while continuously bumping into each other, i.e. they are constantly decelerated, thus, a fraction of the input energy is lost due to bremsstrahlung effects within the plasma, the corresponding volumetric power loss is given by

$$W_b = C_b n_e^2 \sqrt{T} = 5.34 \times 10^{-31} n^2 \sqrt{T} \quad \text{J/s cm}^3 \quad (3.1)$$

Where it was assumed that $n_e = n_i = n$, i.e. ions and electrons have equal densities.

13

Another process of energy dissipation is also at play ; as we know ,the concept of an *isolated system* isn't but a mere **idealization that is unattainable** in practice , for every thermodynamic system is in contact with its environment , and it will consequently lose energy to its surroundings .



The particles of the plasma move at high speeds due to extreme temperature , it is thus permissible to neglect their mutual inter-actions and model the plasma as a **perfect gas** , its volumetric internal energy is therefore

$$W_{thermal} = \frac{3}{2} (n_e + n_i)kT = 3nkT \quad (3.2)$$

Let P_{loss} be the rate of energy loss to the environment we define the **Energy confinement time** by

$$\tau_E = \frac{W_{thermal}}{P_{loss}} \quad (3.3)$$

This parameter will prove to be important in the subsequent. It is a measure of the time taken by a system –i.e. plasma – to reach thermodynamical equilibrium with its environment , and is – in our case– generally small (some *nanosecs*) due to the extreme temperature gradient.

14

Let's now take a look at the procedures through which energy is supplied to the fuel pellet. There is first of all the **driver energy** , i.e. the energy delivered by the high intensity laser beams hitting the surface. It is useful here to define the **target energy gain** as the ratio

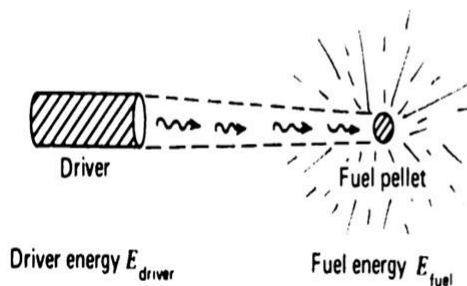
$$G = \frac{E_{fus}}{E_d} \quad (3.4)$$

E_{fus} being the energy released by the fusion. It is given by
number of collisions × *energy released per collision*

Let $W_{fus} = \frac{E_{fus}}{V}$ be the energy density , with the aid of (2.1) and setting $n_D = n_T = \frac{n}{2}$:

$$W_{fus} = \frac{1}{4} n^2 \langle \sigma v \rangle Q_{D-T} \tau_E \quad (3.5)$$

W being the amount of energy released per fusion per unit volume.



In order for a fusion reaction to sustain itself , the energy generated by it must balance the losses , in other words ,

$$\beta W_{fus} = W_{thermal} + W_b \tau_E \quad (3.6)$$

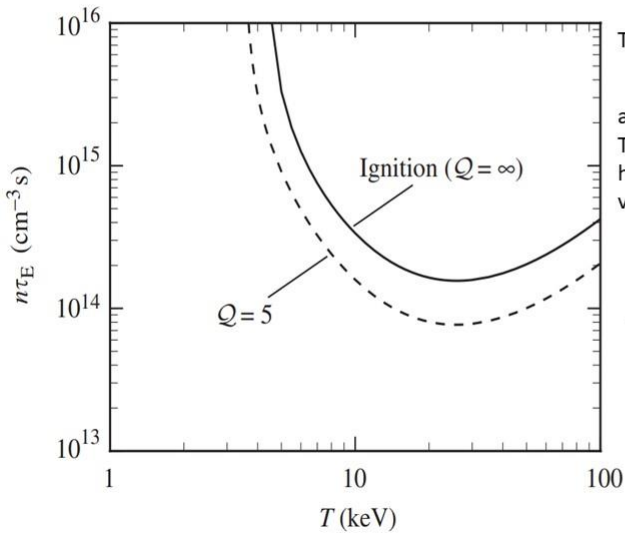
But beware ! Not all the energy released by the fusion is captured but only a fraction β of it - that portion of energy that is carried by α -particles – $\beta=20\%$ for D-T reactions.

15

Rearranging the terms in (3.6) one arrives at the Lawson Criterion

$$n\tau_E = \frac{3kT}{\frac{1}{4}\langle\sigma v\rangle\beta Q_{D-T} - C_b\sqrt{T}} \quad (3.7)$$

This is the confinement parameter



The parameter Q introduced on the left is related to β by

$$\beta = \frac{1}{Q} + \frac{1}{5}$$

and it is a measure of the power input due to auxiliary heating. The aim in ICF is to reach self-sustainability, whence no auxiliary heating methods are required and this corresponds to an infinite value of Q .

Typical values of the temperature that are attained in D-T reactions belong to the range from 20 to 40 keV, The confinement parameter is therefore of the order $\sim 10^{14} \text{cm}^{-3}\text{s}$.

16

§3.2. Rp parameter.

We suppose the fuel pellet to be spherical with radius R , and have a uniform density ρ . As we have already mentioned, for sustainability to be attainable we must make use of the released fusion energy, in the form of α -particles precisely, thus neither R nor ρ can be too low if we want α -particles to ever be captured by the fuel material.

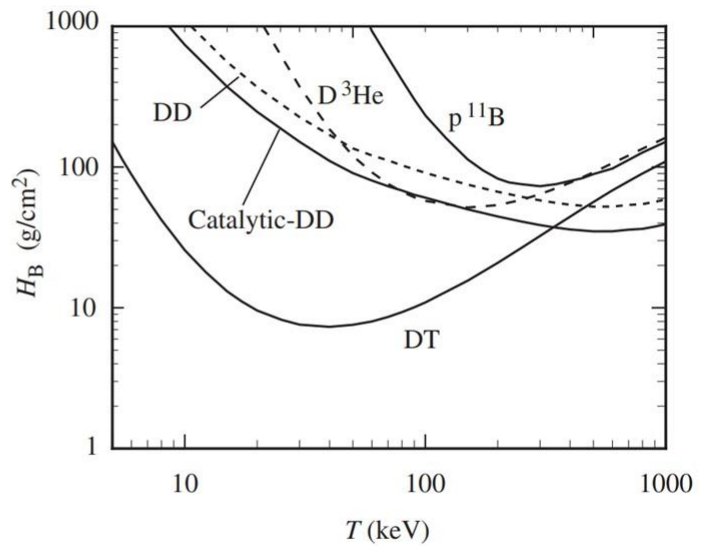
To this end, we define the burn parameter

$$H_B = \frac{8c_s m_f}{\langle\sigma v\rangle} \quad (3.8)$$

Where c_s is the celerity of sound within the plasma, m_f is the average mass of the fuel ions.

Analysis shows that the burn efficiency Φ , i.e. the fraction of fuel that is burnt, is given by

$$\Phi = \frac{R\rho}{R\rho + H_B} \quad (3.9)$$



17

§§4. The Physics of Hydrodynamic compression.

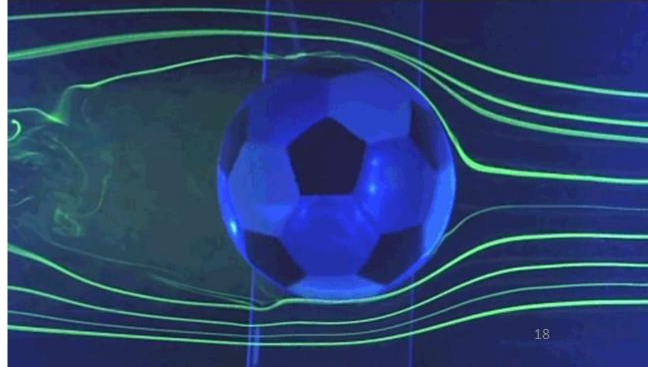
It is the object of inertial confinement fusion to compress a fuel pellet in such a way that only a central region is brought to *ignition temperature*, leaving the rest of the fuel as cold as possible. This is achieved by depositing – through high intensity laser beams – on the surface of the pellet a significant amount of energy, this energy is transported inward to the *ablation surface* through thermal conduction, ablating it outward. This ablation process induces imploding *shock-waves* compressing the fuel to extreme densities.

For an efficient thermo-nuclear reaction to be achieved, we require the *parameter $R\rho$* to overcome a certain threshold ($>1 \text{ g/cm}^2$) on the one hand, on the other hand the *temperature at the center* must exceed that of ignition. It is therefore essential when seeking quantitative insights into the matter to make use of the general theory of Hydrodynamic compression which we outline below.

§4.1. Plasma Hydrodynamics.

The study of the dynamics of plasma belong to the more general branch of *fluid dynamics*.

The mathematical description of a fluid is effected by means of functions which give its velocity field $\mathbf{v}(x, y, z, t)$ and its thermodynamical quantities, such as density $\rho(x, y, z, t)$, temperature $T(x, y, z, t)$ etc...



The evolution of quantities characterizing the state of a fluid is governed by three fundamental equations ;

❖ **Equation of continuity** – The fact that mass is conserved during the motion of the fluid is expressed by:

$$\frac{\partial \rho}{\partial t} + \nabla \cdot (\rho \mathbf{v}) = 0 \quad (4.1)$$

❖ **Euler's equation** – This is basically Newton's second for *ideal – non-viscous* – fluids ;

$$\frac{d\mathbf{v}}{dt} \equiv \frac{\partial \mathbf{v}}{\partial t} + (\mathbf{v} \cdot \nabla) \mathbf{v} = -\frac{1}{\rho} \nabla p + \mathcal{F} \quad (4.2)$$

Where p is the pressure distribution, \mathcal{F} is the acceleration field due to some extraneous force (such as an electric field etc...)

❖ **Conservation of energy** – Taking into account energy dissipation due to viscosity, of course ;

$$\rho c_p \left(\frac{\partial T}{\partial t} + (\mathbf{v} \cdot \nabla) T \right) = \nabla \cdot (\kappa \nabla T) + \sigma_{ik} \frac{\partial v_k}{\partial x_i} \quad (4.3)$$

Where repeated indices are to be summed over, c_p is the specific heat at constant pressure, κ is the heat conductivity, σ_{ik} is the viscosity tensor.

19

§4.2. Shock-Waves.

It is a remarkable feature of gas flow that its properties differ substantially according as it is *subsonic* or *supersonic*, i.e. the velocity is less or greater than that of sound. For in the latter case there is a possibility for what we call *shock-waves* to occur, as we shall see in the subsequent.

To demonstrate this we consider –for simplicity – a uniform flow of gas with velocity \mathbf{v} and consider the effect of a slight perturbation initiated at some point M of the gas. The disturbance will propagate at the speed of sound c *relative to M*, in a direction determined by the unit vector \mathbf{n} . In the fixed frame of reference, the speed of propagation will be $\mathbf{v} + \mathbf{cn}$, we obtain all its possible values by placing one end of the vector \mathbf{v} at M and drawing a sphere of radius c centered at the other end. The vectors thus obtained by joining M with points of the sphere represent all possible magnitudes and directions of the propagation of the perturbation.

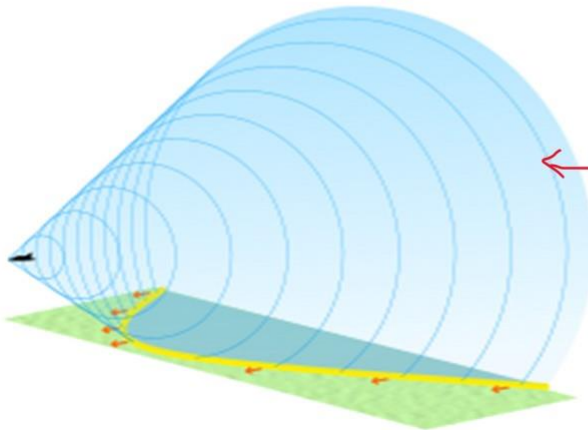


20

As can be seen, the perturbation – in the case of $v < c$ – can propagate in all directions, in other words all points of the gas will eventually be affected by it. If, however, $v > c$ then all possible directions are restricted to a region of space that is bounded by a cone, whose apex is O and contact the sphere centered at M of radius c tangentially. If 2α be the aperture angle of the cone then, obviously;

$$\sin \alpha = \frac{c}{v} \quad (4.4)$$

We shall call the angle α the *Mach angle*, the ratio v/c the *Mach number*.



The surface bounding the region reached by the perturbation initiated from a given point is called the *Mach surface* or the *characteristic surface*.

In the case of general steady flow, the Mach surface is not necessarily a cone through the volume of gas, but it can be asserted as above that it makes with the streamline passing through the point at which the perturbation started a Mach angle, the value of the latter varies through space according to (4.4).

21

➤ Momentum-flux.

Another form of (4.2) is of importance to us, consider the time derivative of the current density $\rho \mathbf{v}$;

$$\frac{\partial(\rho \mathbf{v})}{\partial t} = \rho \frac{\partial \mathbf{v}}{\partial t} + \frac{\partial \rho}{\partial t} \mathbf{v}$$

According to (4.1) ; $\frac{\partial \rho}{\partial t} = -\nabla \cdot (\rho \mathbf{v})$, moreover partial differentiation with respect to time of \mathbf{v} is related to its material derivative – i.e. differentiation w.r.t time along a definite trajectory of some fluid particle – by ; $\frac{\partial \mathbf{v}}{\partial t} = \frac{d\mathbf{v}}{dt} - (\mathbf{v} \cdot \nabla) \mathbf{v}$.

On combining all of these – together with (4.2) – and writing in tensor form :

$$\begin{aligned} \frac{\partial(\rho v_i)}{\partial t} &= \rho \left(\frac{dv_i}{dt} - v_k \frac{\partial v_i}{\partial x_k} \right) - v_i \frac{\partial}{\partial x_k} (\rho v_k) \\ &= -\frac{\partial p}{\partial x_i} - \frac{\partial}{\partial x_k} (\rho v_k v_i) \end{aligned}$$

We finally have :

$$\boxed{\frac{\partial(\rho v_i)}{\partial t} = -\frac{\partial \Pi_{ik}}{\partial x_k}} \quad (4.5)$$

Where we have defined the Momentum-flux density tensor Π_{ik} by ;

$$\Pi_{ik} = p\delta_{ik} + \rho v_k v_i \quad (4.6)$$

In justification of this terminology, we integrate both sides of (4.5) over some volume, and turn the right hand side to a surface integral by *Gauss's Theorem* :

$$\frac{\partial}{\partial t} \int \rho v_i dV = -\oint \Pi_{ik} df_k \quad (4.7)$$

The integral on the right is the amount of momentum flowing out of a given volume element.

22

It is worth noting that in presence of viscous effects – i.e. when internal friction is present – transfer of momentum between different parts of the fluid becomes possible, this is coded into our equations by adding to the ideal momentum-flux tensor (4.6) a term that takes into account the irreversible processes of momentum exchange thus ;

$$\Pi_{ik} = p\delta_{ik} + \rho v_k v_i - \sigma_{ik} \quad (4.7)$$

We dive no deeper into this matter.

This is the definition of the viscosity tensor already mentioned

➤ Energy-flux.

Perhaps we must have discussed energy-flux before momentum flux ; Consider a volume element in space, the total energy contained within it is given by

$$\frac{1}{2} \rho v^2 + \rho \varepsilon$$

The first term is the Kinetic energy, ε denote the internal energy per unit mass. We are interested in the time derivative of the energy density, on the assumption the flow is adiabatic – i.e. energy exchanges between parts of the fluid are absent. We are not displaying the derivation here but content ourselves by stating the result :

$$\frac{\partial}{\partial t} \left(\frac{1}{2} \rho v^2 + \rho \varepsilon \right) = -\nabla \cdot \left(\rho \mathbf{v} \left(\frac{1}{2} v^2 + w \right) \right) \quad (4.8)$$

Or, turning from local to integral form ;

$$\frac{\partial}{\partial t} \int \left(\frac{1}{2} \rho v^2 + \rho \varepsilon \right) dV = -\oint \rho \mathbf{v} \left(\frac{1}{2} v^2 + w \right) \cdot d\mathbf{f} \quad (4.9)$$

23

Where w is the *specific heat function* (the *enthalpy*). The left hand side of (4.9) is the amount of energy leaving the volume element , so one is driven to interpret the vector quantity

$$\rho \mathbf{v} \left(\frac{1}{2} v^2 + w \right) \quad (4.10)$$

As the *energy-flux density*; its magnitude is the amount of energy per unit time passing through unit area in the direction perpendicular to velocity.

➤ Surfaces of discontinuity.

It is a remarkable characteristic of the equations of motion of a fluid that *discontinuous solutions* exist! We arrive thus at the concept of *surface of discontinuity* , these are surfaces that when traversed, the quantities specifying the state of the fluid such as pressure , temperature etc. might vary in a non continuous manner . These surfaces might also be moving through space .

Let us consider an element of such a surface – during a small interval of time – and fix a system of co-ordinates to this element such that the x-axis is along its normal.



Certain boundary conditions must be satisfied on both sides of the surface of discontinuity. First of all –and assuming steady flow – The mass flux through the surface element must be continuous , for a discontinuity in this quantity has the implication that mass is either created or annihilated which , before fusion takes place , is not present . Mathematically;

$$\rho_1 v_{1x} = \rho_2 v_{2x} \quad (\mathcal{A})$$

In similar manner , energy-flux must also be continuous . It is given by (4.10) , thus ;

$$\frac{1}{2} \rho_1 v_{1x}^2 + w_1 = \frac{1}{2} \rho_2 v_{2x}^2 + w_2 \quad (\mathcal{B})$$

Finally , forces exerted on each other by fluid on both sides of the surface must be equal , it therefore should be the case that the components of the Momentum-flux tensor are continuous . All in all this gives;

$$\begin{aligned} \frac{1}{2} \rho_1 v_{1x}^2 + p_1 &= \frac{1}{2} \rho_2 v_{2x}^2 + p_2 \\ \rho_1 v_{1x} v_{1y} &= \rho_2 v_{2x} v_{2y} \\ \rho_1 v_{1x} v_{1z} &= \rho_2 v_{2x} v_{2z} \end{aligned} \quad (\mathcal{C})$$

By contemplating the set of equations (A), (B) & (C) two types of discontinuity become apparent , according as one side – and therefore the other –of (A) is zero or not , the former does not concern us , in the latter one can infer from (A) & (C) that $v_{1y} = v_{2y}$, $v_{1z} = v_{2z}$, i.e. the tangential component of the velocity is continuous and therefore its normal component is necessarily discontinuous , this type of surfaces we shall call a *shock-wave* or simply a *shock*.

The equations (A), (B) & (C) in the case of a shock-wave can be compactly written as

These are called the **Rankine-Hugoniot** relations.

($\mathcal{R} - \mathcal{H}$)

$$\rho_1 v_1 = \rho_2 v_2 \equiv j \quad (4.11)$$

$$\frac{1}{2} v_1^2 + w_1 = \frac{1}{2} v_2^2 + w_2 \quad (4.12)$$

$$\rho_1 v_1^2 + p_1 = \rho_2 v_2^2 + p_2 \quad (4.13)$$

On defining the specific volume $V = 1/\rho$, Algebraic manipulations of the ($\mathcal{R} - \mathcal{H}$) equations give;

$$j^2 = \frac{p_2 - p_1}{V_1 - V_2} \quad (4.14)$$

$$w_2 - w_1 = \frac{1}{2} (p_2 - p_1)(V_2 + V_1) \quad (4.15)$$

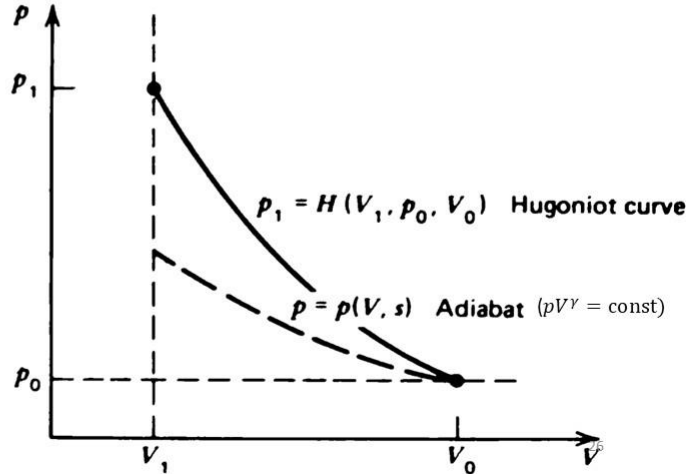
Or on recalling that $w = \varepsilon + pV$;

$$\varepsilon_2 - \varepsilon_1 = \frac{1}{2} (p_1 + p_2)(V_1 - V_2) \quad (4.16)$$

Since thermo-dynamical quantities are related by an **equation of state**; $w = w(\rho, p)$ one can generally arrive to an equation

$$p_2 = H(V_2, V_1, p_1)$$

Relating p_2 to V_2 . It is known as the **shock Hugoniot relation**.



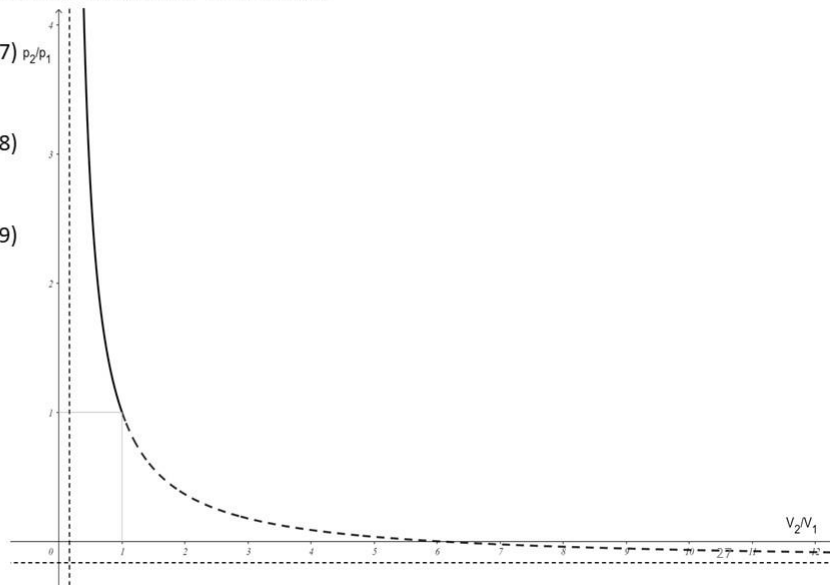
The analysis of the ($\mathcal{R} - \mathcal{H}$) equations can be extended further in the case of a **polytropic gas** for in such a case the specific enthalpy is simply given by $w = \frac{\gamma}{\gamma-1} pV = c_p T$ where $\gamma = c_p/c_v$ is the ratio of specific heats and is a constant in ideal gases. Carrying out the calculations we see that;

$$\frac{p_2}{p_1} = \frac{(\gamma + 1)\rho_2 - (\gamma - 1)\rho_1}{-(\gamma - 1)\rho_2 + (\gamma + 1)\rho_1} \quad (4.17) \quad p_2/p_1$$

$$\frac{\rho_2}{\rho_1} = \frac{(\gamma + 1)p_2 + (\gamma - 1)p_1}{(\gamma - 1)p_2 + (\gamma + 1)p_1} \quad (4.18)$$

$$\frac{T_2}{T_1} = \frac{p_2}{p_1} \cdot \frac{(\gamma - 1)p_2 + (\gamma + 1)p_1}{(\gamma + 1)p_2 + (\gamma - 1)p_1} \quad (4.19)$$

A graph of (4.17) is displayed on the right for $\gamma = 1.4$. It is worth noting that only the part of the curve that is above the point (1,1) has any physical significance. This is due to the fact that **entropy always increases**, dictating the direction of evolution of physical processes, which is the direction of increasing p in our case. We discuss this matter no further.



It is instructive and useful to express the ratios in (4.17)-(4.19) in terms of the *Mach number*. To this end we recall that in an isentropic – i.e. adiabatic and reversible – flow, the *local speed of sound* is given by $c^2 = \frac{dp}{d\rho}$ (= p/ρ , assuming the quantities at hand proportional). By (4.14) & (4.18) one has $v_1^2 = \frac{c_1^2}{2\gamma} \{(\gamma + 1) \frac{p_2}{p_1} + \gamma + 1\}$. By simple transformations;

$$\frac{p_2}{p_1} = \frac{2\gamma}{\gamma + 1} M_1^2 - \frac{\gamma - 1}{\gamma + 1} \quad (4.17)^*$$

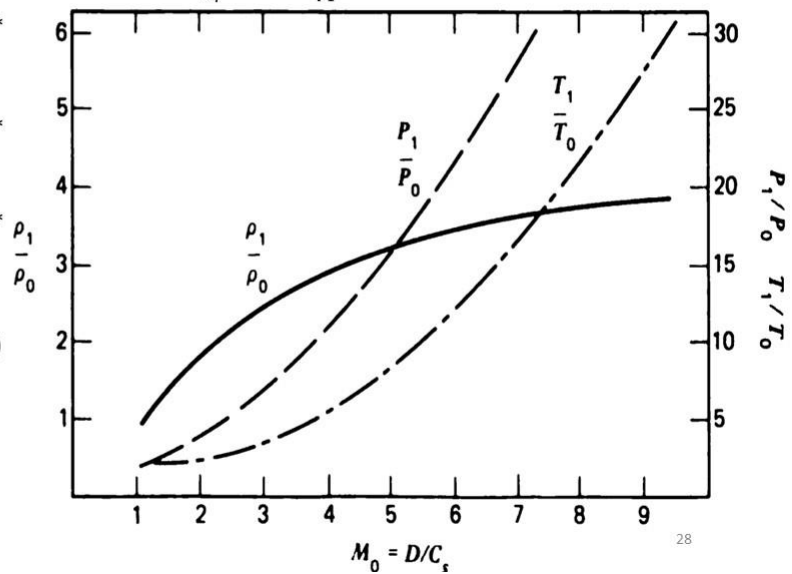
$$\frac{\rho_2}{\rho_1} = \frac{(\gamma + 1) M_1^2}{(\gamma - 1) M_1^2 + 2} \quad (4.18)^*$$

$$\frac{T_2}{T_1} = 1 + \left[2 \frac{\gamma - 1}{\gamma + 1} \right] \left[\frac{\gamma M_1^2 + 1}{M_1^2} \right] (M_1^2 - 1) \quad (4.19)^*$$

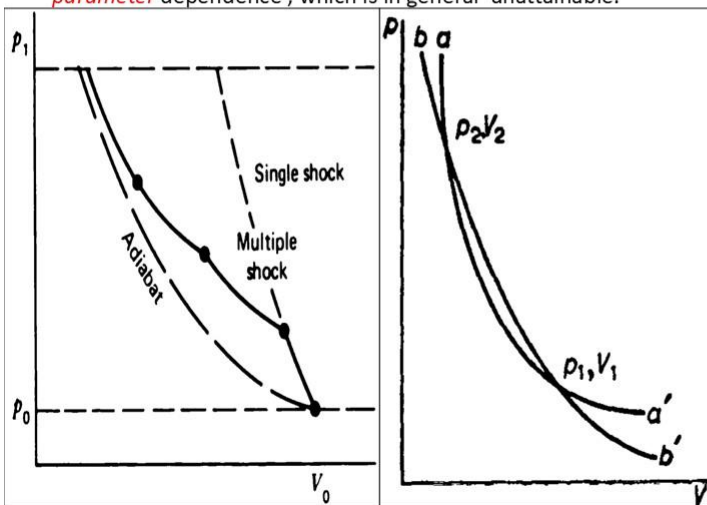
The upstream and downstream Mach numbers are related by

$$2\gamma M_1^2 M_2^2 - (\gamma - 1) \{M_1^2 + M_2^2\} = 2 \quad (4.20)$$

It is remarkable that The ratio T_2/T_1 increases without limit as a function of M_1 (or of the ratio p_2/p_1 for that matter), in contrast, the ratio of densities tends to a definite number, $\rho_2/\rho_1 \rightarrow (\gamma + 1)/(\gamma - 1)$.



We elaborate further on this last point, this is a particular instance of a general result concerning shock adiabatic. The dependence of p_2 on V_2 is determined once we specify the *two-parameters* p_1 & V_1 ; Consider The shock adiabat aa' that has (p_1, V_1) as an initial point, take any point (p_2, V_2) on the curve and take it as the initial point of the shock adiabat bb' , then clearly (p_1, V_1) belongs to bb' – for the $(R - H)$ are symmetric in (p_1, V_1) & (p_2, V_2) – and aa' & bb' intersects at these two points. Asserting however that these two curves are actually identical is generally false; for one would have the simultaneous equations: $p_2 = p_2(V_2, V_1, p_1)$ & $p_1 = p_1(V_1, V_2, p_2)$, implying that $p_2 = p_2(V_2, V_1)$, making it a *one-parameter* dependence, which is in general unattainable.



Now, as a consequence, if we had a series of –two or more – shock-waves taking the gas from the state (p_1, V_1) to (p_2, V_2) and from there to the state (p_3, V_3) , then the transition from (p_1, V_1) to (p_3, V_3) cannot always be effected by a single shock-wave.

This has been concretely seen in the case of a *polytropic gas*; The most a single shock-wave can do is to multiply the density by a factor of $(\gamma + 1)/(\gamma - 1)$ (=4 for monoatomic gases).

Thus if high densities are to be achieved, one is led to consider a series of *weak shock-waves*, we necessitate each step to be weak in order to avoid high increases in temperature.

§5. Spherically imploding Shock-Waves.

Our exploitation of shock-waves and their effect on the thermodynamical quantities has been restricted to *plane shock-waves*, and does not take into account the spherical geometry one meets in an ICF, we therefore devote this section to investigate whether spherical shocks are substantially different, if any difference exists.

In the presence of central symmetry, scalar quantities characterizing the state of the gas can only depend on the distance from the origin, the equations of motion can therefore be turned to equations involving only the variable r together with time. However, *dimensionality considerations* can reduce these equations even further.

Take as origin of time the moment at which the radius $R(t)$ of the shock-wave is zero, then time before focusing correspond to $t < 0$. We shall consider the flow at a stage where The radius R is much smaller than its initial value R_0 , at this point the flow is largely independent of the specific initial conditions.

The only quantities defining the properties of the flow are the time-dependent radius of the shock $R(t)$, the radial velocity of convergence dR/dt

Under these conditions, it is reasonable to assume that there exist a similarity flow in the variable $\xi = r/R(t)$, i.e. the fluid variables ρ, T etc.. Vary with space and time solely through the independent variable ξ .

30

15.2 ICF Simulation Introduction and Theory

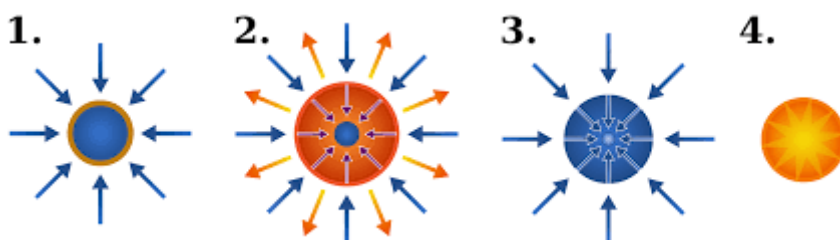
- ICF Simulation

Abstract.

As the general features of Inertial Confinement Fusion have been laid down, we now shall proceed in making numerical estimates of physical quantities of interest (such as released nuclear energy, Lawson's confinement parameter, etc..) that are involved during the extraordinarily short time span of the whole process.

Any accurate description of ICF must take into account a wide variety of factors, and seeking an analytical solution of the problem is simply hopeless; One is therefore lead to resolve the problem numerically. To this end, we discuss in what follows a computer code whose purpose is to simulate the process.

Recall that ICF consists of hitting the surface of a (usually spherical) fuel pellet (most commonly filled with D-T fuel) with high intensity laser beams from all directions. The outer surface will evaporate almost instantly due to intense energy, and will ablate off causing the formation of converging shock-waves throughout the fuel. These shocks will(ideally) converge to the center compressing it to extreme densities and thus inducing thermonuclear reactions. If the conditions for self-sustainability are fulfilled then the burn will propagate and consume the relatively cold fuel surrounding the center;



The purpose of this simulation is to make a (rough) estimate of the temperature and pressure and released energy etc.. during the process of ICF.

Technical details. We shall write our code in C++. We are using the Qtcreator platform, you can download the Qtinstaller [from here](#).(The installation process is straightforward)

When installed you will be asked to choose a Kit, A Qt Kit is a set of a Qt version, compiler and device and some other settings. The one I am using is given below:

```
Desktop Qt 6.7.2 MinGW 64-bit
Device type:
  Desktop
Device:
  Desktop
Build device:
  Desktop
Compiler:
  MinGW 11.2.0 64-bit for C++
Environment:
Debugger:
  GDB Engine using "C:\Qt\Tools\mingw1120_64\bin\gdb.exe"
Sys Root:
Qt version:
  Qt 6.7.2 MinGW 64-bit
mkspec:
Additional Qbs Profile Settings:
CMake:
  CMake 3.29.3 (Qt)
CMake Generator:
  Generator: Ninja
  Extra generator:
CMake Configuration:
  QT_QMAKE_EXECUTABLE:FILEPATH= %{Qt:qmakeExecutable}
  CMAKE_PREFIX_PATH:PATH= %{Qt:QT_INSTALL_PREFIX}
  CMAKE_C_COMPILER:FILEPATH= %{Compiler:Executable:C}
  CMAKE_CXX_COMPILER:FILEPATH= %{Compiler:Executable:Cxx}
```

General references. It must be kept in mind that no ICF code up-to-date takes into account all the occurring physical interactions, and several (simplified) models have been devised over the past decades to describe more or less accurately these phenomena. For starters we shall adhere to the simplest model: The Laser-generated plasma is treated as a single fluid with two temperatures(corresponding to ion and electron populations). This model is addressed in the following:

[Medusa I](#)

[Medusa II](#)

[Wasser](#)

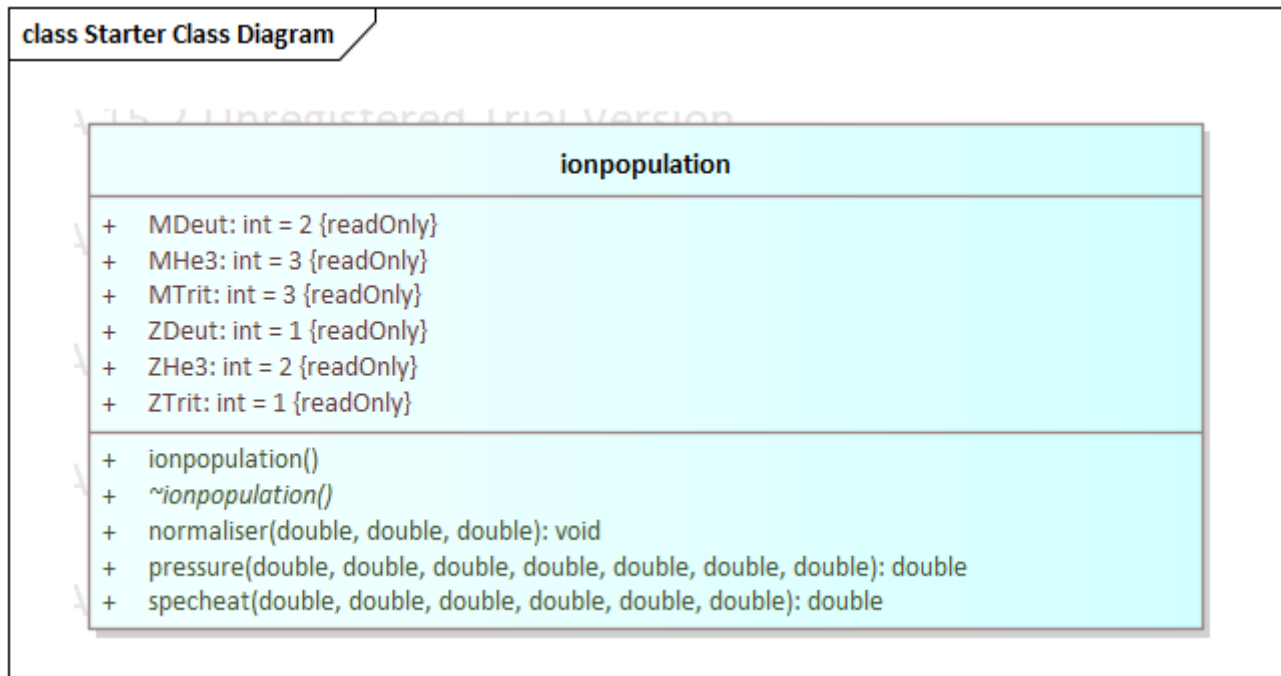
These serve as the theoretical basis for our code, even though i have made several deviations from them, further references are cited when needed.

Code repository

Code Name	Version	Description
<u>ICP- ICF SIMULATION</u>	31.08.2024	Initial Version; one dim. ICF, spherical laser driver; similar to Medusa (<u>Medusa I</u> , <u>Medusa II</u>)

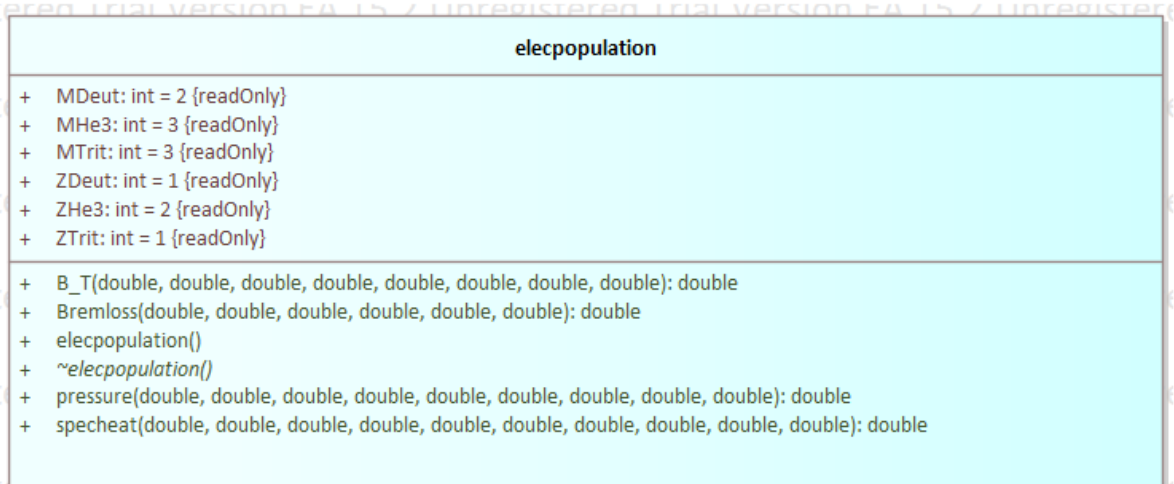
Class Diagram

Our code currently comprises the following classes:



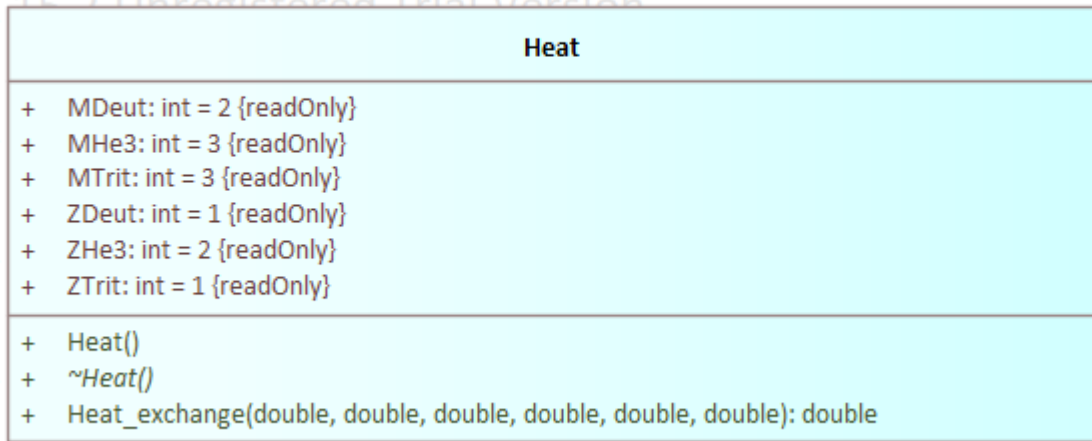
- **normaliser:** imposes the normalisation condition $\sum f_k=1$ on the fractions f_k of each specie in the ion gas
- **pressure:** calculates the ion pressure
- **specheat:** calculates the specific heat at constant volume of the ion gas

class Starter Class Diagram



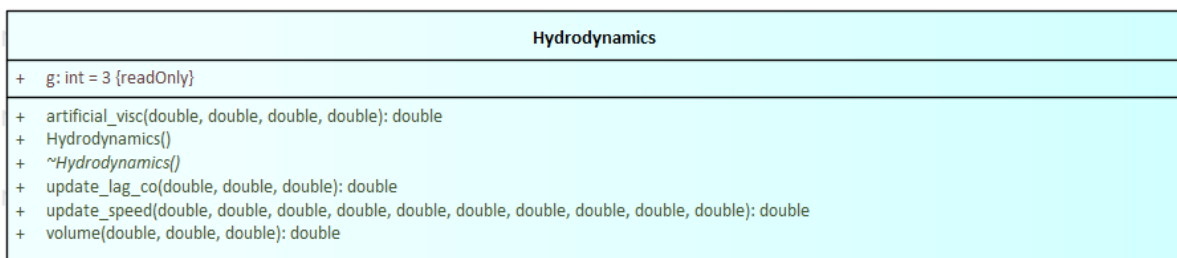
- **B_T**: returns the B_T coefficients of the electron gas
- **Bremloss**: returns the energy losses due to Bremstrahlung radiation in the electron gas
- **pressure**: returns the electron pressure
- **specheat**: returns the electron specific heat at constant volume

class Starter Class Diagram

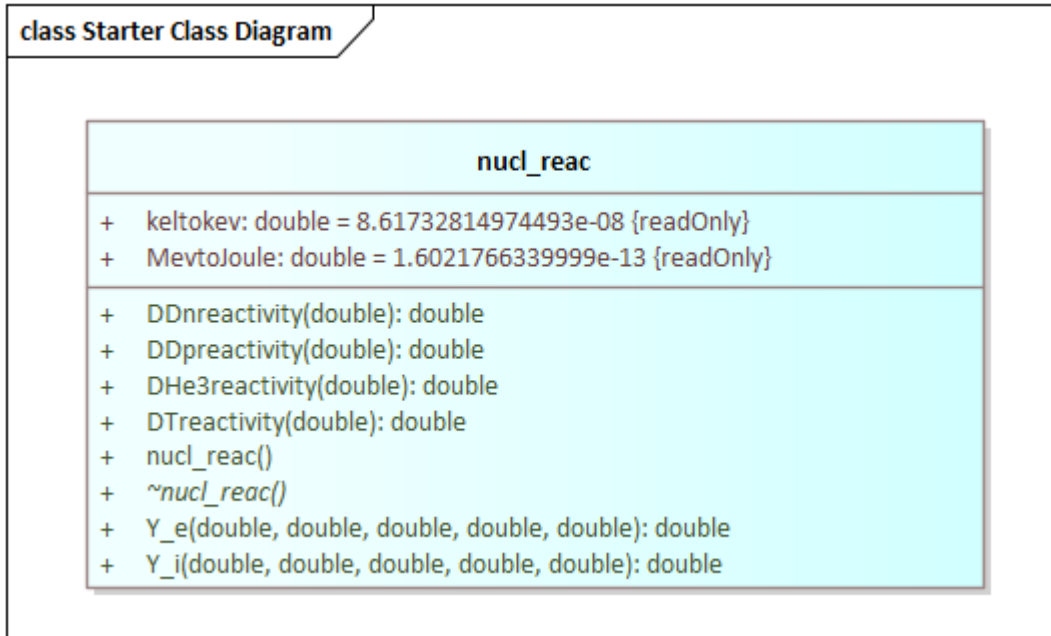


- **Heat_exchange**: returns heat exchange between electrons and ion gases

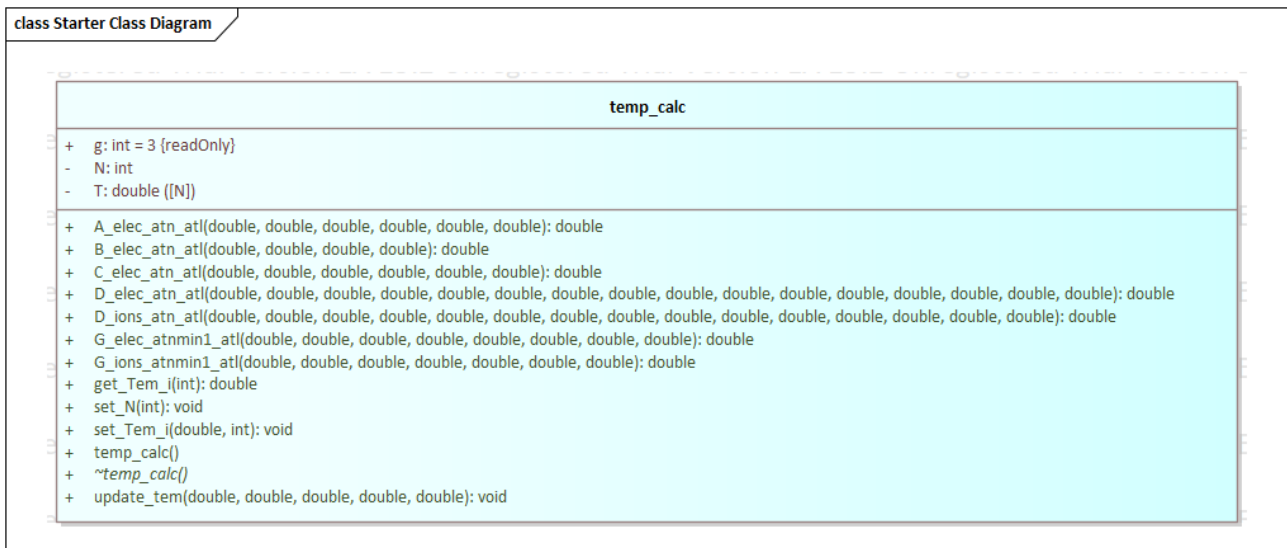
class Starter Class Diagram



- **artificial_visc**: calculates Neuman q
- **update_lag_co**: takes the lagrangian co-ordinate to the next time step
- **update_speed**: takes speed to the next time step
- **volume**: returns the volume of a cell

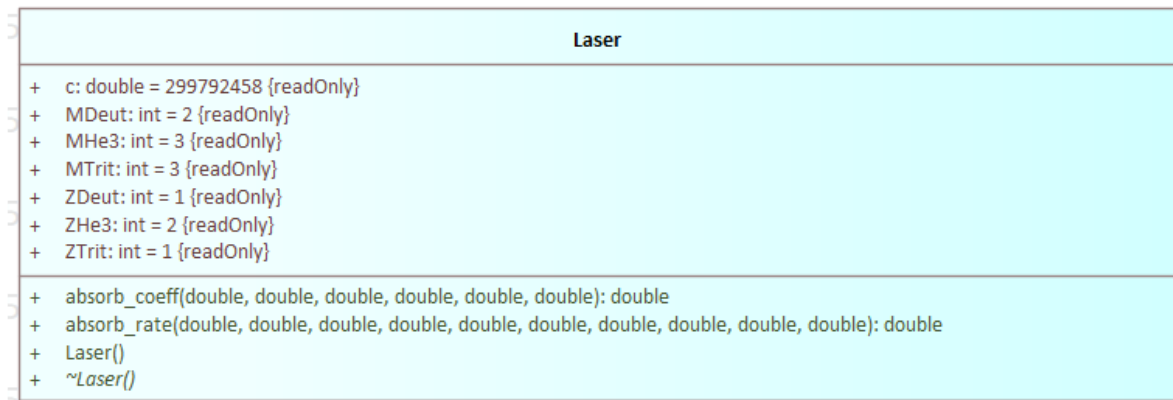


- **DDn, DDp, DHe3, DTreactivity**: returns the reactivity of the corresponding nuclear reaction
- **Y_i, Y_e**: portions of nuclear energy absorbed by ions and electrons respectively



- **A, B, C, D, G coefficients**: return the coefficients of temperature in the discretized heat equation (for ions and electrons)
- **update_tem**: takes temperatures to the next timestep

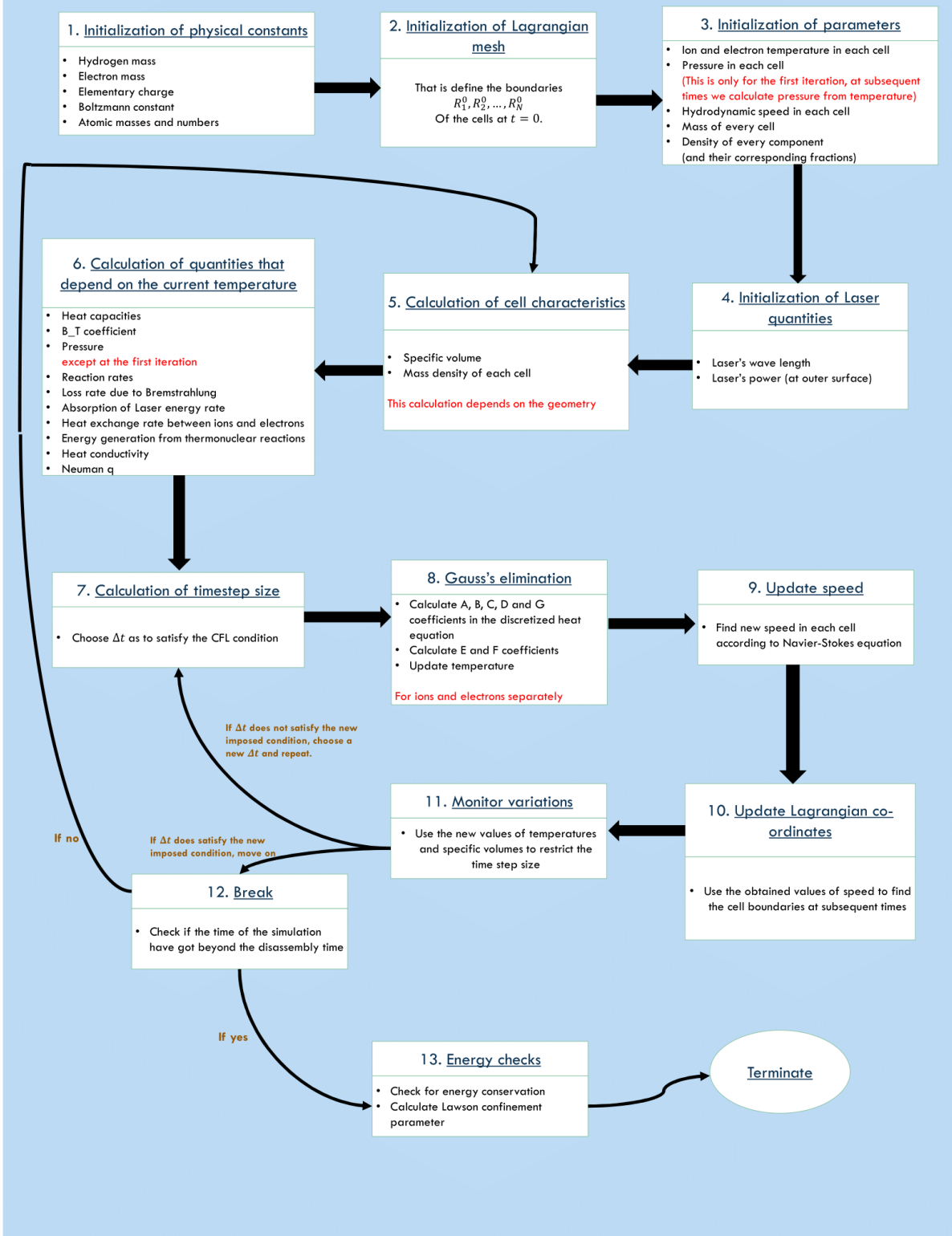
class Starter Class Diagram



- **absorb_coeff**: returns the absorption coefficient of plasma
- **absorb_rate**: returns the absorption rate of laser energy by the plasma

As for the general program flow, we summarize it in the following diagram

Flow chart of the ICF simulation code



Theory. We shall give a brief outline of the underlying theoretical treatment of plasma;

I. Hydrodynamics.

Due to spherical symmetry, the problem can be thought of as one-dimensional, In this case it turns out to be most convenient to work in the *Lagrangian picture*. The equations of motion can thus be written as

$$\frac{dv}{dt} = -\frac{1}{\rho} \frac{\partial p}{\partial r}$$

(Navier-Stokes equation for a non viscous fluid)

p being the hydrodynamic pressure, v the radial velocity
and ρ the mass density

Now the Navier-Stokes equation, as we know, allow discontinuous solutions(shock-waves) which complicate its numerical resolution. To overcome this difficulty we follow Neuman's idea and introduce to the pressure a term q (artificial viscosity). In a ideal fluid, shock-waves have no thickness so quantities characterizing the fluid(such as temperature) change discontinuously on passing through a shock. If viscous effects are present however, the shock surface is "smeared out" and is turned into a very thin layer, throughout which thermodynamical quantities change rapidly yet continuously, Hence we introduce the q term with this purpose in mind. The choice of q can be quiet arbitrary as long as it satisfies some conditions, we shall use the following:

$$q = \begin{cases} [b\Delta m \partial u / \partial m]^2 / V, & \dot{v} < 0 \\ 0, & \dot{v} \geq 0 \end{cases}$$

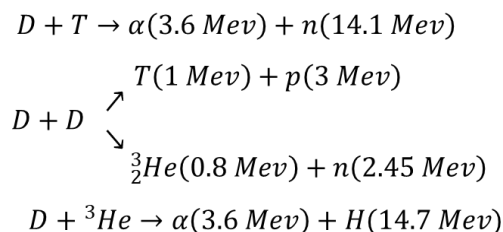
Where b is an adjustable numerical constant, V is the specific volume, m is the mass of the fluid particle, it is related to the Lagrangian co-ordinate by

$$dm = \rho R^2 dR$$

for more details you can consult [this paper](#).

II. Thermo-nuclear reactions.

The four nuclear reactions of interest in ICF are:



Notice that the D-D reaction has two branches: The p-Branch and the n-Branch.

Every reaction has a specific reactivity(that depends on temperature) these are given by formulae of the form:

$$e^{(A_1+A_2|\ln(T/A_3)|^{A_4})}$$

Where T is the ion temperature in keV, A_1 , A_2 , A_3 and A_4 are numerical constants obtained by extrapolation, they can be found [right here](#).

III. Heat equation.

Now on applying the first law of thermo-dynamics for ions and electrons populations we get an equation of the form

$$C_V \dot{T} + B_T \dot{\rho} + p \dot{V} = S$$

Where $C_V = (\partial U / \partial T)_\rho$, $B_T = (\partial U / \partial \rho)_T$, S is the amount of heat entering or leaving the system per unit mass per unit time.

U above is the internal energy. The forms of S for ions and electrons are different, they are given as:

$$S_i = H_i - K + Y_i + Q$$

$$S_e = H_e + K + Y_e + J + X$$

Where;

- H is the heat flux
- K is the exchange rate between ion and electron populations
- Y is the portion of thermo-nuclear energy that is absorbed by ions and electrons
- Q is the shock heating term (Due to artificial viscosity)
- J is the energy loss due to Brehmstrahlung
- X is the absorption rate of Laser energy

The formulae for these terms are given in [Medusa I](#) and [Medusa II](#) so we won't write them down here.

IV. Equations of state.

The ion gas is treated as an ideal gas, so its thermodynamical quantities are most easily given as

- $(C_V)_i = \frac{1}{\gamma_i - 1} \frac{k}{m_H M}$
- $(B_T)_i = 0$
- $p_i = \frac{k}{m_H M} \rho T_i$

Where k is the Boltzmann constant, m_H is the hydrogen mass, M is the average atomic mass, γ is the specific heat ratio.

The electron gas however is poorly handled by the perfect gas model, as it does not take into account degeneracy effects. To this end, we shall make use of the following *quasi-classical* treatment: "the electron gas is modeled as an aggregate of particles that obey the Fermi-Dirac statistics".

The thermodynamical quantities of the electron gas are given in term of the Fermi-Dirac integral:

$$F_s(\alpha) = \int_0^{\infty} \frac{u^s}{e^{\alpha+u} + 1} du$$

Where α is a constant that is fixed by the condition

$$n_e = \frac{4\pi}{h^3} (2mkT_e)^{3/2} F_{1/2}(\alpha)$$

Where n_e is the electronic density, m the electronic mass, h the plank constant.

The equation of state and the pressure are respectivley given by

$$P_e V_e = \frac{2}{3} n_e k T_e, \quad P_e = \frac{8\pi k T_e}{3h^3} (2mkT_e)^{3/2} F_{3/2}(\alpha)$$

Now in order to proceed further we need to expand the Fermi-Dirac integral as a power series, The nature of this expansion will depend on whether the degeneracy is strong, moderate or non-existent.

We find it here useful to define the ratio

$$\zeta = T_e/T_F$$

where the Fermi-temperature T_F is given by

$$kT_F = \frac{h^2}{8m} \left(\frac{3Z\rho}{\pi M m_H} \right)^{2/3}$$

With Z is the average atomic number. We further introduce the parameters ζ_{min} & ζ_{max} That will serve as mean to distinguish between different degrees of degeneracy. Typical values of these parameters would be 0.38 and 1 respectively.

We can now write the expressions for pressure, Specific heat and B_T coefficient as follow:

$$p_e = \frac{k}{m_H M} Z \rho T_e \begin{cases} \frac{2}{5} \zeta^{-1} + \frac{\pi^6}{6} \zeta - \frac{\pi^4}{40} \zeta^3, & \zeta < \zeta_{min} \\ 1 + (3\sqrt{2\pi})^{-1} \zeta^{-3/2}, & \zeta_{min} < \zeta < \zeta_{max} \\ 1, & \zeta_{max} < \zeta \end{cases}$$

$$(C_V)_e = \frac{1}{\gamma_e - 1} \frac{k}{m_H M} Z \begin{cases} \frac{\pi^2}{3} \zeta - \frac{\pi^4}{10} \zeta^3, & \zeta < \zeta_{min} \\ 1 - (6\sqrt{2\pi})^{-1} \zeta^{-3/2}, & \zeta_{min} < \zeta < \zeta_{max} \\ 1, & \zeta_{max} < \zeta \end{cases}$$

$$(B_T)_e = \frac{1}{\gamma_e - 1} p_F \rho^{-2} \begin{cases} \frac{2}{3} - \frac{5\pi^2}{18} \zeta^2 + \frac{\pi^4}{8} \zeta^4, & \zeta < \zeta_{min} \\ 5(6\sqrt{2\pi})^{-1} \zeta^{-\frac{1}{2}}, & \zeta_{min} < \zeta < \zeta_{max} \\ 0, & \zeta_{max} < \zeta \end{cases}$$

Where $p_F = \frac{h^2}{20m} \left(\frac{3}{\pi}\right)^{2/3} \left(\frac{Z\rho}{Mm_H}\right)^{5/3}$ is the *fermi pressure*.

Notice how these values coincide with their values for a perfect gas when ζ is bigger than ζ_{max} , Which correspond to the case of no degeneracy.

for further details consult "**Principles of Stellar formation and nucleo-synthesis, chap.2**" by D.D. Clayton.

V. Chemical composition.

The gas consist of several species, but we are exclusively interested in those elements that undergo nuclear reactions, namely: Deut, Trit, He3, and we denote their densities as

$$n_D, \quad n_T, \quad n_{He3}$$

Together with the total ion density n_i .

The evolution of these quantities with time is governed by the set of differential equations

$$\frac{dn_T}{dt} = \langle \sigma v \rangle_{DDp} n_D^2 - \langle \sigma v \rangle_{DT} n_D n_T$$

$$\frac{dn_D}{dt} = -[\langle \sigma v \rangle_{DDp} + \langle \sigma v \rangle_{DDn}] n_D^2 - \langle \sigma v \rangle_{DT} n_D n_T - \langle \sigma v \rangle_{DHe3} n_D n_{He3}$$

$$\frac{dn_{He3}}{dt} = \langle \sigma v \rangle_{DDn} n_D^2 - \langle \sigma v \rangle_{DHe3} n_D n_{He3}$$

where $\langle \sigma v \rangle$ denotes the reactivity corresponding to each reaction(according to the subscript).

15.3 Our ICP-ICF Simulation Code



310824_12ICF_SIMULATION.zip

CMakeLists.txt	824	401	2024-08-31 09:39
CMakeLists.txt.user	31 105	2 782	2024-08-30 19:16
elecpopulation.cpp	4 176	710	2024-08-13 07:05
elecpopulation.h	1 696	405	2024-08-12 21:16
heat.cpp	760	286	2024-08-23 20:23
heat.h	527	211	2024-08-28 15:05
hydrodynamics.cpp	1 669	409	2024-08-31 11:14
hydrodynamics.h	1 548	494	2024-08-13 07:47
ionpopulation.cpp	760	282	2024-08-13 19:20
ionpopulation.h	1 241	409	2024-08-12 22:52
laser.cpp	1 796	456	2024-08-13 07:03
laser.h	1 470	452	2024-08-31 11:16
main.cpp	1 136	391	2024-08-31 10:07
nucl_reac.cpp	2 729	524	2024-08-13 07:03
nucl_reac.h	914	378	2024-08-13 06:44
temp_calc.cpp	5 345	791	2024-08-30 19:11
temp_calc.h	5 233	806	2024-08-28 15:32

15.3.1 Documentation of the ICF_SIMULATION code

In what follows a documentation of the Inertial confinement fusion simulation code is presented.

15.3.1.1 Description of main.cpp

1. Calculation

The main.cpp file can be found [here](#).

1.1 Physical Constants

The following physical constants are defined for use in various calculations throughout the code:

- m_H: Mass of a hydrogen atom (proton) in kilograms ($1.67262192 \times 10^{-27}$ kg).
- m_e: Mass of an electron in kilograms ($9.1093837 \times 10^{-31}$ kg).
- clight: Speed of light in meters per second (299,792,458 m/s).
- elem_charge: Elementary charge, or the charge of a proton in coulombs ($1.60217663 \times 10^{-19}$ C).
- boltz: Boltzmann constant in joules per kelvin (1.380649×10^{-23} J/K).
- gamma: Specific heat ratio (1.667), commonly used for an ideal diatomic gas.
- zetamax: Upper bound of the zeta parameter (1).
- zetamin: Lower bound of the zeta parameter (0.38).

1.2 Atomic and Nuclear Data

These variables define basic properties of isotopes involved in nuclear reactions:

- **Isotope masses (atomic mass units):**
 - MDeut: Mass of deuterium (2 u).
 - MTrit: Mass of tritium (3 u).
 - MHe3: Mass of helium-3 (3 u).
- **Isotope charge numbers:**
 - ZDeut: Charge number of deuterium (1).
 - ZTrit: Charge number of tritium (1).

-
- ZHe3: Charge number of helium-3 (2).

1.3 Nuclear Reaction Energies (in MeV)

These constants represent the energy released by various fusion reactions:

- E_DT: Energy of deuterium-tritium reaction (3.6 MeV).
- E_DD: Average energy of deuterium-deuterium reaction (2.4 MeV).
- E_DHe3: Energy of deuterium-helium-3 reaction (18.3 MeV).

1.4 Hydrodynamic and Time Step Parameters

Several parameters used for hydrodynamic calculations and time step control:

- b: Parameter for hydrodynamic calculations (0.5).
- a1, a2, a3: Parameters controlling time step calculations (0.75, 0.8, and 1.02 respectively).

1.5 Initial Data

This section initializes the initial conditions for the simulation:

- TotalMass: The total mass of the plasma or fusion fuel (1×10^{-6} kg).
- fD0, fT0: Initial mass fractions of deuterium (70%) and tritium (30%), with helium-3 (fHe3) set to 0 initially.
- R_0: Initial radius of the fusion pellet (25 mm).
- N: Number of spatial cells used in the simulation grid (10).
- M: Number of time steps (20).
- initialtem: Initial temperature of the plasma (300 K).
- p_0: Initial pressure of the plasma (600,000 Pa).
- initialspped: Initial velocity of the plasma (0 m/s).

1.6 Laser Parameters

These variables define the properties of the laser driving the inertial confinement:

- lambda: Wavelength of Laser Light (5×10^{-10} m).
- omega: Frequency of the laser, calculated as c_{light} / λ .
- power: Laser power at the outer boundary (50 kW).

1.7 Object Definitions

Objects representing different physics modules and processes:

- elec, ion: Represent the electron and ion populations.
- hydro: Handles hydrodynamics-related computations.
- heat: Deals with heat transfer processes.
- las: Represents the laser interaction with the plasma.
- nucl: Nuclear reaction handling object.

-
- `elec`: Calculates electron-related properties.
 - `compo`: Handles chemical composition and reaction rates.
 - `eng`: Energy calculation module.

1.8 Time Step and Geometry Initialization

- `dt`: Time step index.
- `deltat[M]`: Array storing time step sizes for each iteration.
- `g`: Dimensionality of the problem, taken from the hydrodynamics module (`hydro.g`).

1.9 Mass Distribution

- `dM[N-1]`: Array storing the mass in each spatial cell. The total mass is distributed uniformly across the cells.
- `dM_mesh[N]`: Mass distribution at mesh points for interpolation or calculations involving the mesh.

1.10 Fuel Fractions and Densities

Arrays used to track the fractions of fuel components and particle densities across space and time:

- `f_Deut[N-1][M]`, `f_Trit[N-1][M]`, `f_He3[N-1][M]`: Fractions of deuterium, tritium, and helium-3, initialized with `f_Deut = 0.7`, `f_Trit = 0.3`, and `f_He3 = 0` at the start.
- `ion_den[N-1][M]`: Ion density (particles per cubic meter).
- `Z[N-1][M]`: Effective charge state (Z value).
- `elecden[N-1][M]`: Electron density (particles per cubic meter).

1.11 Lagrangian Coordinates

- `R[N][M]`: Lagrangian coordinates for each spatial mesh point, initialized based on the pellet radius and number of cells.

1.12 Temperature and Pressure

Arrays for storing temperatures and pressures:

- `electem[N-1][M]`, `iontem[N-1][M]`: Electron and ion temperatures.
- `elecpress[N-1][M]`, `ionpress[N-1][M]`, `p[N-1][M]`: Electron, ion, and total hydrodynamic pressures.

1.13 Main Time-Stepping Loop (`for(dt; dt < M; dt++)`)

This loop handles the time evolution of the system by updating physical properties like specific volume, density, reaction rates, and pressures at each time step.

1.14 Specific Volume and Density Calculation

For each spatial cell (i):

- `SpecVol[i][dt]`: The specific volume of each cell at time dt is calculated using the `hydro.volume()` function, which depends on the current Lagrangian coordinates (`R[i][dt]` and `R[i+1][dt]`) and the mass of the cell (`dM[i]`).

-
- **Density Calculation:**
 - If the specific volume is not zero, the density $\rho[i][dt]$ is calculated as the inverse of specific volume.
 - If the specific volume is zero (to avoid division by zero), the density is set to 1 as a fallback.
 - **Ion Density:**
 - $\text{ion_den}[i][dt]$ represents the ion density, which is calculated using the `ion.Ionden()` function. This function depends on the mass density ($\rho[i][dt]$), hydrogen mass (m_H), and the mass fractions of deuterium, tritium, and helium-3.
 - **Charge and Electron Density:**
 - $Z[i][dt]$ is the effective charge state, calculated based on the charge numbers and mass fractions of deuterium (Z_{Deut}), tritium (Z_{Trit}), and helium-3 (Z_{He3}).
 - $\text{elecden}[i][dt]$ is the electron density, computed as the product of the effective charge state ($Z[i][dt]$) and the ion density ($\text{ion_den}[i][dt]$).

1.15 Heat Capacities Calculation

For each spatial cell (i):

- **Electron Heat Capacity:**
 - $\text{elecCV}[i][dt]$: The specific heat capacity for electrons is calculated using the `elec.speheat()` function. This function depends on electron temperature ($\text{electem}[i][dt]$), mass density ($\rho[i][dt]$), Boltzmann constant (`boltz`), hydrogen mass (m_H), the mass fractions of deuterium, tritium, helium-3, specific heat ratio (γ), and the zeta parameters (`zetamin`, `zetamax`).
- **Ion Heat Capacity:**
 - $\text{ionCV}[dt]$: The ion heat capacity is calculated using the `ion.speheat()` function. This function depends on the specific heat ratio (γ), Boltzmann constant (`boltz`), and the mass fractions of deuterium, tritium, and helium-3.

1.16 B_T Coefficients Calculation

The $B_T[i][dt]$ coefficient is calculated for each cell, which likely represents a temperature-dependent coefficient used in further calculations. The calculation is done using the `elec.B_T()` function, which takes into account the electron temperature, mass density, fuel fractions, specific heat ratio, and the zeta parameters.

1.17 Pressure Calculations

The pressure in each cell is updated based on the electron and ion temperatures:

- **At Initial Time Step ($dt == 0$):**
 - $\text{elecpress}[i][0]$: Initially, the electron pressure is set to zero.
 - $\text{ionpress}[i][0]$: The ion pressure is initialized to the initial plasma pressure (p_0).

-
- **At Later Time Steps ($dt > 0$):**
 - **Electron Pressure:** `elecpress[i][dt]` is calculated using the `elec.pressure()` function, which depends on the electron temperature (`electem[i][dt]`), Boltzmann constant (`boltz`), mass density (`rho[i][dt]`), and the mass fractions of deuterium, tritium, and helium-3.
 - **Ion Pressure:** `ionpress[i][dt]` is calculated using the `ion.pressure()` function, which depends on the ion temperature (`iontem[i][dt]`), Boltzmann constant (`boltz`), mass density (`rho[i][dt]`), and the mass fractions of deuterium, tritium, and helium-3.
 - **Total Hydrodynamic Pressure:** The total pressure `p[i][dt]` is the sum of the electron and ion pressures for each cell.

1.18 Reaction Rates Calculation

For each cell (i), the nuclear reaction rates are calculated:

- **Deuterium-Tritium Reaction Rate ($DT_{\text{reac}}[i][dt]$):** This represents the reaction rate for the deuterium-tritium fusion, calculated using the `nucl.DTreactivity()` function. The input to this function is the ion temperature (`iontem[i][dt]`) multiplied by the Boltzmann constant.
- **Deuterium-Deuterium Reaction Rates:**
 - `DDpreac[i][dt]`: Reaction rate for the D-D proton branch, calculated using `nucl.DDpreactivity()`.
 - `DDnreac[i][dt]`: Reaction rate for the D-D neutron branch, calculated using `nucl.DDnreactivity()`.
- **Deuterium-Helium-3 Reaction Rate ($DHe3_{\text{reac}}[i][dt]$):** This is the rate for the D-He3 fusion reaction, calculated using `nucl.DHe3reactivity()`.

1.19 Heat Conductivity Calculation

This section calculates the thermal conductivity for both electrons and ions in each spatial cell (i):

- **Electron Conductivity ($elec_{\text{kappa}}[i][dt]$):** The function `heat.kappa_elec()` is used to compute the electron heat conductivity based on the electron temperature (`electem[i][dt]`), electron density (`elecden[i][dt]`), and the mass fractions of deuterium, tritium, and helium-3.
- **Ion Conductivity ($ion_{\text{kappa}}[i][dt]$):** The ion heat conductivity is computed using `heat.kappa_ions()` based on ion temperature (`iontem[i][dt]`), electron temperature, electron density, and the fuel fractions.

Next, the values of heat conductivity at mesh points are calculated by averaging adjacent cell conductivities:

- **Mesh Conductivity ($elec_{\text{kappa}}_{\text{mesh}}[i][dt]$, $ion_{\text{kappa}}_{\text{mesh}}[i][dt]$):** The heat conductivity at each mesh point is the average of the conductivities of adjacent cells.

1.20 Heat Exchange Rate Calculation

For each spatial cell (i), the heat exchange rate between ions and electrons is calculated:

-
- **Heat Exchange** ($\text{heatexch}[i][dt]$): The rate of energy exchange between electrons and ions is determined using $\text{heat.Heat_exchange}()$, which depends on ion temperature ($\text{iontem}[i][dt]$), electron temperature, electron density, and the fuel fractions.

1.21 Bremstrahlung Loss Calculation

For each spatial cell (i), the Bremstrahlung radiation loss rate is computed:

- **Bremstrahlung Loss** ($\text{Brem_loss}[i][dt]$): The Bremstrahlung energy loss rate, which represents the energy radiated due to collisions between electrons and ions, is calculated using $\text{elec.Bremloss}()$. This depends on electron temperature, hydrogen mass, fuel fractions, and mass density.

1.22 Laser Energy Absorption Calculation

For each spatial cell (i), the rate of laser energy absorption is calculated:

- **Laser Absorption** ($\text{LaserAbs}[i][dt]$): The rate of laser energy absorbed in each cell is computed using $\text{las.absorb_rate}()$. This depends on electron temperature, laser frequency (ω), fuel fractions, mass density, radial coordinate (r), laser power, pellet radius, and cell mass.

1.23 Thermo-Nuclear Energy Calculation

This section calculates the energy absorbed by electrons and ions due to nuclear fusion reactions:

- **Energy Absorbed by Electrons** ($\text{AbsByElec}[i][dt]$): The energy absorbed by electrons from fusion reactions is computed using $\text{nucl.Y_e}()$. The function takes ion and electron temperatures as inputs, as well as the energy yields from deuterium-tritium (E_{DT}), deuterium-deuterium (E_{DD}), and deuterium-helium-3 (E_{DHe3}) reactions.
- **Energy Absorbed by Ions** ($\text{AbsByIons}[i][dt]$): Similarly, the energy absorbed by ions from fusion reactions is calculated using $\text{nucl.Y_i}()$.

1.24 Artificial Viscosity Calculation

For each spatial cell (i), the artificial viscosity is calculated to handle shock waves:

- **Artificial Viscosity** ($q[i][dt]$): The artificial viscosity is computed using $\text{hydro.artificial_visc}()$, which depends on the parameter b , mass density, and the velocities at adjacent mesh points ($\text{speed}[i][dt]$ and $\text{speed}[i+1][dt]$).

1.25 Time Step Calculation

The time step is calculated based on the Courant-Friedrichs-Lewy (CFL) condition to ensure numerical stability.

1.26 Speed of Sound Calculation

For each spatial cell (i), the speed of sound is calculated:

- **Total Pressure** ($p[i][dt]$): The total pressure in each cell is the sum of the electron pressure ($\text{elecpress}[i][dt]$) and ion pressure ($\text{ionpress}[i][dt]$).

-
- **Speed of Sound ($c[i][dt]$):** The speed of sound is calculated using the relation $c = \sqrt{\frac{\gamma \cdot p}{\rho}}$, where γ is the specific heat ratio, $p[i][dt]$ is the pressure, and $\rho[i][dt]$ is the mass density.

1.27 CFL Condition

The CFL condition is used to determine the maximum allowable time step based on the speed of sound and spatial grid:

- **CFL Value ($CFL[i]$):** The CFL value for each cell is calculated as $(R[i+1][dt] - R[i][dt]) / c[i][dt]$, representing the ratio of the distance between adjacent mesh points to the local speed of sound.
- **Global CFL Condition:** The minimum CFL value across all cells is computed and scaled by the constant $a1$ to determine the time step ($\Delta t[dt]$), ensuring stability in the numerical scheme.

1.28 Chemical Composition Update

This part of the code updates the fuel fractions (deuterium, tritium, helium-3) over time, taking into account the nuclear reactions occurring in each spatial cell.

1. Temporary Arrays for Composition:

- Temporary arrays (`tempf_Deut`, `tempf_Trit`, `tempf_He3`) are created to store the updated fuel fractions. These are initialized with the current values for each species at time dt .

2. Update of Fuel Fractions:

- For each cell i , the fuel fractions of deuterium (f_Deut), tritium (f_Trit), and helium-3 (f_He3) are updated using specific functions from the `compo` object. These updates take into account:
 - The ion density ($ion_den[i][dt]$),
 - The fuel fractions in neighboring cells,
 - The nuclear reaction rates ($DTreac$, $DDpreac$, $DDnreac$, $DHe3reac$), and
 - The current time step ($\Delta t[dt]$).
- After updating the compositions, the `ion.normaliser()` function is called to normalize the fuel fractions, ensuring that the sum of fractions is consistent.

3. Update the Fuel Fractions for the Next Time Step:

- After updating, the new fuel fractions for deuterium, tritium, and helium-3 are stored in $f_Deut[i][dt+1]$, $f_Trit[i][dt+1]$, and $f_He3[i][dt+1]$ for the next time step.

1.29 Discretized Heat Equation Coefficients Calculation

This section calculates the coefficients required to solve the discretized heat equation for ions and electrons. These coefficients are crucial for determining temperature updates in each spatial cell.

1. Coefficients for Heat Equation:

-
- **Aelec[i][dt] & Aions[i][dt]:** These represent the coefficients of the discretized heat equation. They are calculated using `eleccalc.A_elec_atn_atl()`, based on mesh points (`R[i][dt]`), heat conductivity (`eleckappa[i][dt]`, `ionkappa[i][dt]`), mass (`dM[i]`), and time step (`deltat[dt]`).
 - **Celec[i][dt] & Cions[i][dt]:** These represent another set of coefficients for the heat equation. The function `eleccalc.C_elec_atn_atl()` is used here, with similar inputs to the A coefficient calculation, but using mesh-centered conductivities (`eleckappamesh[i+1][dt]`, `ionkappamesh[i+1][dt]`).

2. Additional Coefficients:

- **Belec[i][dt] & Bions[i][dt]:** These are computed using `eleccalc.B_elec_atn_atl()` and depend on the specific heat capacities of electrons and ions (`elecCV[i][dt]`, `ionCV[dt]`).
- **Delec[i][dt] & Dions[i][dt]:** These account for sources and sinks of energy, such as laser absorption (`LaserAbs`), Bremsstrahlung losses (`Brem_loss`), thermonuclear energy absorption (`AbsByElec`, `AbsByIons`), and heat exchange (`heatexch`).
- **Gelec[i][dt] & Gions[i][dt]:** These coefficients handle terms involving the temperatures from the previous time step.

1.30 Solving the Heat Equation

The heat equation for both ions and electrons is solved iteratively using the coefficients calculated in the previous step.

1. Temporary Variables:

- Temporary arrays (`tempelec`, `tempions`, etc.) store the intermediate results for the temperatures and coefficients during the iterative solving process.

2. Updating Temperatures:

- The functions `eleccalc.update_tem()` are called to update the electron and ion temperatures based on the A, B, C, D, and G coefficients.
- After updating, the new temperatures are stored in `electem[i][dt+1]` and `iontem[i][dt+1]` for the next time step.

1.31 Iteration Control

The iteration is controlled by the do-while loop, ensuring that the chemical composition and temperature updates are applied repeatedly until the desired convergence is reached (not specified here but likely based on a convergence criterion).

- **numbOfIterations:** This variable tracks the number of iterations.

1.32 Hydrodynamic Update

The code updates the hydrodynamic quantities, specifically the speed and position, for each cell in the simulation.

1. Temporary Arrays:

-
- tempSpeed[] and tempR[] store the current speed and position at time step dt.
 - tempNewSpeed[] and tempNewR[] store the updated speed and position, which will be calculated and then assigned to the next time step dt+1.

2. Update Speed and Position:

- For each cell, the new speed (tempNewSpeed[i]) is updated using the function hydro.update_speed(). This function takes into account:
 - Pressures (elecpress, ionpress),
 - Heat flux (q),
 - Mass (dM), and
 - Time step (deltat).
- The new position (tempNewR[i]) is updated using the function hydro.update_lag_co(), which uses the new speed and time step.

3. Store Updated Values:

- The updated speed and position values are stored in speed[i][dt+1] and R[i][dt+1] for the next time step.

1.33 Restrict Time Variation

This part restricts the time step to ensure numerical stability based on the relative variation of ion temperature, electron temperature, and speed.

1. Relative Variations:

- The relative changes between consecutive time steps (dt and dt+1) are calculated for:
 - Ion temperature (iontemVar[]),
 - Electron temperature (electemVar[]), and
 - Speed (speedVar[]).
- Each variation is normalized by the sum of the current and previous values to avoid division by zero.

2. Find Minimum Variation:

- MinIonTemVar, MinElecTemVar, and MinspeedVar store the minimum variation for ion temperature, electron temperature, and speed, respectively, across all cells.
- Maxrestriction is the overall minimum variation, which will be used to adjust the time step.

3. Time Step Adjustment:

- A new time step (newdeltat) is calculated based on Maxrestriction and a factor a2.
- If the current time step (deltat[dt]) is smaller than the newly calculated one, the loop is terminated. Otherwise, the time step is updated to the new value.

1.34 Energy Checks

This section evaluates various forms of energy in the system at each time step, including thermal, kinetic, input energy, fusion energy, and Bremstrahlung loss energy. The difference between the input and output energies provides an estimate of the system's energy conservation.

1. **Energy Arrays:**

- Arrays like ThermEng[], KinEng[], InEng[], FusEng[], BremEng[], and DeltaE[] store energy values at each time step.

2. **Bremstrahlung and Fusion Energy Calculation:**

- totBremEng[]: The total Bremstrahlung energy loss is computed by summing contributions from neighboring time steps, weighted by the mass of each cell (dM[]).
- totNuclEng[]: The total nuclear energy from ions and electrons is computed similarly, accounting for absorption rates.

3. **Thermal and Kinetic Energy:**

- **Thermal energy** is calculated using eng.ThermalEng() with inputs like pressure, specific volume, mass, and the adiabatic index (gamma).
- **Kinetic energy** is computed using eng.kineticEng() based on the speed at the current and previous time steps.

4. **Input Energy:**

- The rate of energy input into the system is calculated using eng.InputEngRate() with boundary pressures and speeds.
- The cumulative input energy over time is computed using eng.InputEng().

5. **Fusion and Bremstrahlung Energy:**

- Fusion energy (FusEng[]) and Bremstrahlung energy loss (BremEng[]) are updated over time using eng.BremEngAtn().

6. **Energy Conservation Check:**

- The energy balance is checked using DeltaE[], which is the difference between the thermal and kinetic energy on one side and the input, fusion, and Bremstrahlung energy on the other. This value estimates how well energy is conserved during the simulation.

1.35 Lawson Parameter Calculation

The Lawson parameter is a measure of the confinement quality in fusion simulations, crucial for determining whether a system achieves the conditions necessary for sustained fusion.

1. **Total Mass and ρR :**

- The total mass (totmass) is accumulated by summing over all cells.
- The confinement parameter ρR_{dM} is computed by summing the product of density ($\rho[i][j]$), position ($R[i][j]$), and mass for each cell.

2. **Lawson Parameter:**

-
- For each time step, the Lawson parameter is calculated as the ratio of ρR_{dM} to the total mass. This provides insight into the confinement efficiency of the plasma at each time step.

2. Output/Visualization of computation results

This section of the code is responsible for **writing simulation results** to various output files. Each file corresponds to a different physical property or parameter, such as ion temperature, electron temperature, pressure, etc. The files are created in specific directories, and the simulation data for each time step and mesh point is written to them.

1. Output File Streams:

- Various `std::ofstream` objects are created to handle the writing of data to files, each representing a different property:
 - **Ion temperature** (`outputfile_iontem`)
 - **Electron temperature** (`outputfile_electem`)
 - **Ion pressure** (`outputfile_ionpress`)
 - **Electron pressure** (`outputfile_elecpress`)
 - **Mesh points** (`outputfile_Cellbounds`)
 - **Speed** (`outputfile_speed`)
 - **Deuterium fraction** (`outputfile_fDeut`)
 - **Tritium fraction** (`outputfile_fTrit`)
 - **Helium-3 fraction** (`outputfile_fHe3`)
 - **Energy error** (`outputfile_EngErr`)
 - **Lawson parameter** (`outputfile_Lawson`)
 - **Density** (`outputfile_rho`)

2. Opening Files:

- Each file is opened using `open()`, with paths specified for directories such as `"ICFsim_output\\Temperature\\..."` for temperature-related data, `"ICFsim_output\\Hydrodynamics\\..."` for hydrodynamic properties, and so on.
- If the file opens successfully, data for each time step and cell is written to it. Otherwise, an error message is printed to `std::cout`.

3. Writing Data:

- For each file, the program loops over time steps (M) and mesh points (N).
- At each time step, data for all cells in the mesh is written, and a new line is added between time steps to separate the data.

4. Specific Data Files:

-
- **Ion and Electron Temperature:** These files log the temperature of ions and electrons at each cell for all time steps.
 - **Ion and Electron Pressure:** These files log the pressure values at each cell for each time step.
 - **Cell Boundaries (Mesh Points):** This file logs the positions of cell boundaries ($R[j][i]$).
 - **Speed:** This file logs the speed of each cell at each time step.
 - **Density (ρ):** Logs the density of the material in each cell.
 - **Fuel Fractions (f_{Deut} , f_{Trit} , f_{He3}):** These files log the fraction of deuterium, tritium, and helium-3 in the plasma.
 - **Energy Error (ΔE):** This file records the energy conservation error.
 - **Lawson Parameter:** This file records the Lawson parameter for each time step.

5. Formatting Output:

- The code includes newline ($\backslash n$) and empty line (`std::endl`) separators between time steps to make the output more readable.

15.4 Design of IAP-ICF Device

Tbd

16 ICF Light-Ion Driver: Marx Generator and Pulsed Powered Diode

Association for Economic and Technological Cooperation in the Euro-Asian and North-African Region
www.aecenar.com

Pulsed diode accelerator

General features:

Considered E.M pulse compressors; consists of discharging electrical energy from the Marx generator into a pulse forming line where a short high energy pulse is formed and then applied to the diode via the transmission line.

Marx Generator

(energy storage + voltage multiplication from the charge-discharge phenomenon of the capacitor)

E.M high voltage but

Pulse rise time is too slow

Pulse forming lines

(compress electrical energy into a short, fast pulse, this will multiply the voltage)

E.M of high voltage

+ Short and fast

Transmission line

(make the E.M more intense (beam))

E.M intense high voltage

+ Short and fast

Diode

(when the high voltage pulse reaches the cathode, its voltage will create an intense field on the cathode tip which produces a plasma on the surface of the cathode and is translated by an intense current of electrons directing towards the anode)

Types of accelerators:

1-Marx Generator:

- The Marx generator designed for voltage multiplication.
- The generator is used as an energy storage element, at relatively low voltages; and when triggered, the 1st switching voltage drops, which increases the voltages across the remaining switches, causing a self-triggering chain reaction, until a high voltage pulse is obtained at the load.

Wave erection Marx:

- The Marx transient wave erection differs from the previous Marx circuit in its use of stray capacitance effects.
- A voltage wave propagates towards the load with increasing intensity, triggering successive switchings faster and faster until it reaches the load with a rise time inside (ns) and low jitter for output voltages of several certain (kv) at moderate energies per pulse.

Large and Moderate generator systems	Compact and Solid state generator systems
<ul style="list-style-type: none"> • Used as pulse charging subsystems in larger pulsed power applications. 	<ul style="list-style-type: none"> • Designed to have pulse widths narrow enough to directly drive some applications.
<ul style="list-style-type: none"> • Have low repetition rates, either because of the capacity of the power supply or because of the thermal stability of the load. 	<ul style="list-style-type: none"> • Tend to run at higher rep rates to increase the average energy delivered to the load.
<ul style="list-style-type: none"> • Resistive load works well (resistors reduce load efficiency). 	<ul style="list-style-type: none"> • Resistors are replaced by inductors to allow fast and efficient charging (the addition of mutual coupling between the two inductors increases system performance).

2-linear accelerator:

Linear Particle Accelerator (LINAC) is a type of particle accelerator that dramatically increases the kinetic energy of charged subatomic particles or ions by subjecting the charged particles to a series of oscillating electrical potentials along a line of linear beam.

How it works:

- The source gives electrons which are accelerated towards the 1st drift tube due to their negative potential and the (+) tube; when these electrons enter the tube, the R.F source changes the polarity.
- The electrons leave the tube due to its inertia and then they are pushed by the 1st tube and attracted by the second in the same direction.
- When these electrons accelerate, their speed increases and they travel greater distances at the same time. As the electron velocity approaches C, the velocity increase will be small, and the electrode lengths will be ~ct.

Pulse forming line (PFL):

-A transmission line of any geometry of length l and characteristic impedance Z_0 makes a pulse forming line (PFL), which when combined with a closing switch SS makes the simple transmission line pulser.

-But the impulse generated in a suitable load is only equal to $(V_0/2)$; to avoid this problem, we will use Bulmeint PFL.

Electron Gun:

Electron guns include a cathode (tungsten filament), where electrons are produced, the cathode is at negative potential in the range [-30kv to -150kv], there is a vacuum gap between cathode and anode which is at ground potential. The anode has a hole, so electrons are accelerated towards it and then pass through the hole. They then move at constant speed until they hit the target, where they release their kinetic energy in the form of heat and X-rays.

The electron beam is visible because there is low pressure gas in the tube. The electrons strike the gas molecules and give them energy, which is then released as light.

Notes:

When the slit is disconnected, the electrons stayed around the tungsten filament (cathode).

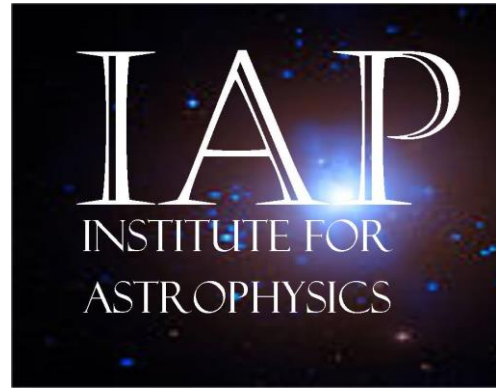
When the slit anode is connected, the electrons are accelerated and then pass through the slit.

The best type of power supply to use would probably be a (roughly) 20kV DC flyback transformer. However, we did not have a flyback power supply on hand, so I used a rectified sign transformer.

Vacuum of the tube accelerator (Amocanal pump)

The transformer (of 12 kv) is an output in AC mode; for converted to DC mode, we use 4 diodes; and to multiply the applied voltage, this transformer is connected to a 2-stage voltage multiplier circuit, which provides a total voltage of 48 Kv [U_{out} = 2 × n × U_{in}]. To avoid jumping the voltage of the capacitor pins, this multiplier circuit is isolated and made in an oil bath.

Rouwayda Sakka, Asmaa El Mir & Ali Obeid
@AECENAR/August 2022



Pulsed power diode accelerator

Author:

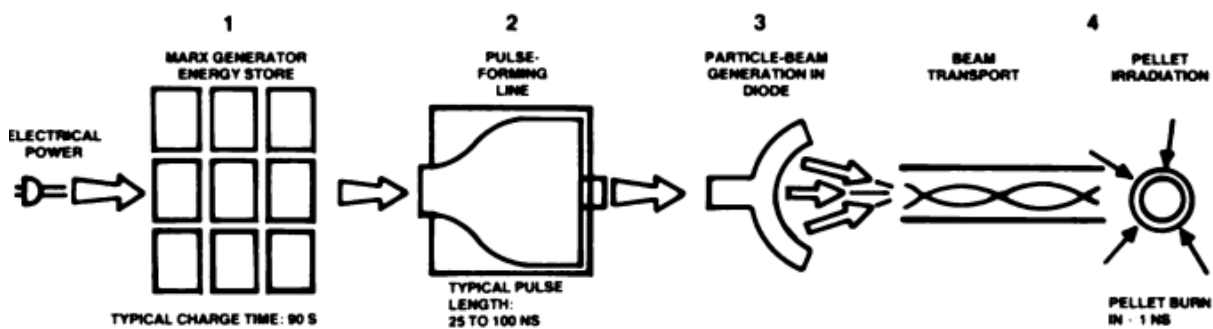
Ali Obeid

Last Update: 31.03.2022

16.1 Pulsed power diode accelerator

16.1.1 General Features:

Pulsed diode accelerators are not charged particle accelerators in the usual sense familiar from high energy physics research. Alternatively they can be considered as electromagnetic pulse compressors. The general operation of these devices involves discharging electrical energy from capacitive storage devices known as Marx generators into a pulse modulation line where a short, high-energy pulse is formed and then applied to the diode via the transmission line. An intense electromagnetic wave travels inward along the transmission line and appears on a pair of face-to-face particle accelerator electrodes. One electrode, the cathode, is charged with a negative pulse relative to the other electrode, the anode. When millions of volts are applied to the electrodes, the electric fields produced are enough to pull electrons from the cathode material into the vacuum. Electrons withdrawn from the cathode dissipate enough energy at both the cathode and anode to vaporize their surface layers and form a plasma. The cathode plasma becomes the electron source and the anode plasma provides a source of positive charge to neutralize the static field electric current of the beam. The basic components of a pulse diode accelerator include:



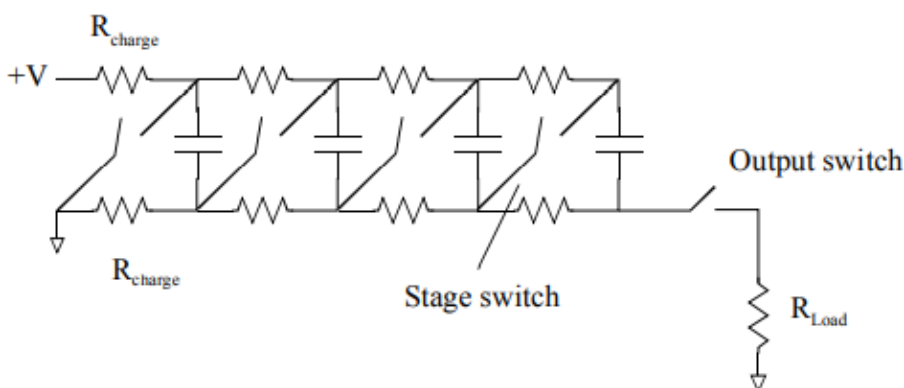
Basic components of a pulsed power diode accelerator.

1. A capacitive energy storage system: Usually this is a Marx generator that acts as a storage device and a voltage multiplier. The Marx The alternator charges the capacitors in parallel and then discharges them in series to achieve a very high voltage. The rise time of the pulse produced by a Marx generator is too slow for ICF drive applications, so one must then compress the pulse in time.
2. Pulse forming lines: A pulse modulating network is used to compress electrical energy into a short, fast pulse, nearly doubling the output voltage in the process. This can be both one or more pulse lines and a complex transmitter such as the Blumlein network.
3. Transmission line: Then the energy pulse is transmitted as an intense electromagnetic wave through a transmission line to the diode. High voltage isolation of the transmission line is of particular concern because it determines the maximum allowable voltage pulse.
4. Diode: The diode consists of a cathode and an anode chip, separated by a short gap. When the high voltage pulse reaches the cathode, its voltage causes an intense field to be emitted from the cathode tip which produces plasma on the surface of the cathode and results in an intense current of electrons moving towards the anode. At higher energies, electrons can easily penetrate a thin anode wafer and continue to form a relativistic electron beam with radial currents of several mega-amperes. The polarity of the diode can be reversed and the electron current suppressed to produce an ion beam in the device.

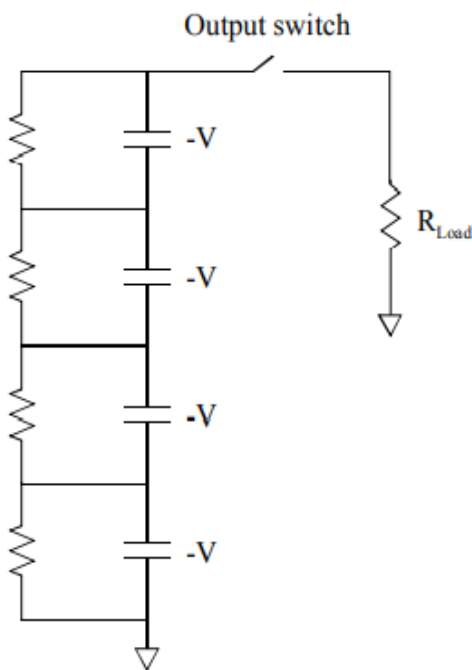
16.1.1.1 Marx generator

The term Marx Generator describes a unique circuit designed for voltage multiplication. In general, all Marx generators follow the same fundamental operation. However, similarities between Marx systems diverge in their construction and performance characteristics as a function of their application. Typical applications of the Marx generator has been with pulse charging circuits. In essence, the generator is used as an energy storage element, at relatively low voltages, and when fired, pulse charges a transmission line at a high voltage, with typical applications seen in High Power Microwave, and accelerators. Generators in this role tend to be large, as well as slow devices. Smaller versions of the Marx generator have filled the role of trigger generator for larger systems. These generators are typically characterized by their low per pulse energies, but with several hundreds of kV. The main attraction to these pulses lies in their rise times and compact geometries. Recent work has extended the use of these compact generators into the Ultra WideBand (UWB) genre. With rise times as short as 250 ps, these compact generators are finding their way into UWB radar systems and RF weapon systems and come packages that may be hand held. The Marx circuit, on the solid state level has also found applications in laser systems as Pockel's cell drivers and trigger generators. The "credit card" devices can deliver voltages of 10's of kV, with sub-Joule energies. This paper attempts to provide a broad overview of Marx generators, their fundamental operation, and some perspective on electrical characteristics and associated volumes. Fundamental trigger techniques are presented and include information for low jitter operation. Finally, the wave-erection generator is presented.

The Marx generator is a capacitive energy storage circuit which is charged to a given voltage level and then quickly discharged, delivering its energy quickly to a load at very high power levels. A typical Marx circuit uses resistors to charge N capacitors in parallel to a voltage V , as shown in Figure 1. When triggered, the first switch voltage drops which increases the voltages across the remaining switches, causing a chain reaction of self-triggering. The capacitors are then momentarily switched into a series configuration, delivering a voltage pulse to the load that is theoretically $N \times V$, depicted in Figure 2. The output switch is present to isolate the load while charging the Marx, and to insure full Marx erection before energy is transferred to the load. The charging resistors grade the output voltage from the charging supply during firing, providing electrical isolation.



Marx generator charging circuit.



Marx generator discharging circuit.

Marx generator:

A) Large Generator Systems Large Marx generator systems may be found in the ever-expansive high energy systems such as with the Z-machine and large HPM systems, and often reside in very large rooms. These systems offer Mega-volts and Mega-Joules at relatively long pulse durations. The pulses are slow in their rise time (10's of ns), and due to their massive energy requirements, offer very low repetition rates (essentially single events).

B) Moderate Generator Systems Moderate Marx generators may be categorized as small room to large desktop-sized systems, offering voltages from 100's of kV to several MV's. Pulse energies may rate into the low MJ's. Pulse widths vary from 10's of ns to μ s. Their rise times typically remain slow, on the order of several ns to 10's of ns. However, repetition rates are more achievable and as high as several 10's of Hz.

C) Compact Generator Systems Compact Marx generators fit into the range of handheld to desktop-sized systems. These systems offer relatively low pulse energies, < 10 J – 1kJ, and high voltages of 100's kV to MV. Fast rise times, 100's ps, are achievable, as well as high repetition rates (> 1 kHz).

D) Solid State Generator Systems Solid state Marx generators are circuit board size systems with voltages up to the several kV range and less than 1 Joule energy storage. Rise times in the 100 ps range have been demonstrated. Repetition rates could potentially be in the 10's to 100's of kHz. Large and moderate Marx generators are typically used as pulse charging sub-systems in larger pulsed power applications. In systems such as Z pinch machines Marx generators are initial energy stores which deliver energy to a pulse compression circuit before reaching the load. Compact and solid state generators can be designed to have pulse widths that are narrow enough to drive some applications directly. These include ultra wide band antennas, jamming systems, and pulse radar systems. Multi-pulse systems can also be directly driven, with serial temporal signals spaced apart

in the 10's of ns for driving a common antenna, or phased array systems with sub-ns jitter and sub-ns phase differences firing into an array of antennas.

MARX TRIGGERING TECHNIQUES

The choice of Marx switches is dependent on the operating voltage, pulse repetition frequency, and lifetime, and switching support requirements. Solid state switches may be used in low voltage applications. However, many Marx generators operate in regimes where the only viable alternative is a spark gap. Spark gap technology is broadly split into liquid filled and gas filled systems. For both cases, the medium provides both the cooling and switching characteristics. Maximum repetition rates are achieved by flowing the medium through the switching region to carry away heat and recover voltage hold-off capability quickly. Liquid systems typically use oil or water, but can be based on a variety of other liquids. Liquid systems have excellent thermal mitigation properties. However, these systems tend to use pumps and filters to remove contamination, adding to volume and complexity. Gas systems can be based on a variety of gases, depending on repetition rates, spark gap lifetime, and safety concerns the highest repetition rate systems use high pressure hydrogen due to its ability to recover its insulating properties quickly after firing.

V. REPETITION RATE ISSUES An important parameter for any pulsed power system is the time it requires after firing to recharge and be ready to fire again. Large and moderate generator systems typically have low repetition rates which are dictated by either the power supply's ability to recharge the system or thermal stabilization of the load. Compact and solid state generator systems obtain size reductions by storing less energy per shot. Typically these systems still have reasonably high peak power levels with narrow pulse widths, so that thermal heating of the system from a single event is low. These systems tend to be operated at higher repetition rates in order to raise the average energy deliver to the load. High repetition rate systems can still be power supply limited. However, the recovery time of the switches used becomes a key concern Resistive charging works well for low repetition rates. However, the charging time required by the Marx before firing is approximately equal to $2N^2 RC$ and the resistors reduce the charging efficiency. Therefore, for high repetition rate systems the resistors are replaced with inductors to accommodate fast, efficient charging. The addition of mutual coupling between the two inductors associated with a Marx stage can further increase the system performance. For this case, the individual inductances appear smaller during charging and larger during firing, allowing for faster charging with increased firing isolation.

MARX DESIGN EXAMPLE

The following example demonstrates key elements of designing a Marx generator for single output pulse delivery into a known real load. A first order approximation of the Marx generator circuit is a single loop LRC circuit where L_{eq} and C_{eq} are the lumped inductance and capacitance of the Marx circuit and R is the load resistance. The period of oscillation for an underdamped circuit is given in equation (1) and the Marx impedance in equation (2).

$$T = 2\pi\sqrt{L_{eq} C_{eq}} \quad (1)$$

$$Z = \sqrt{L_{eq}/C_{eq}} \quad (2)$$

Critical damping is chosen as a compromise between maximum voltage amplitude and overshoot, as defined by equation 3. For this choice, the FWHM pulse width is about 80% of half the period of underdamped oscillation and that the output voltage will be near 70% of theoretical, shown in equations (4) and (5) where n is the number of stages and Vcharge is the Marx input voltage.

$$Z = R/2 \quad (3)$$

$$T_{\text{pulse}} = 0.8 \pi \sqrt{L_{\text{eq}} C_{\text{eq}}} \quad (4)$$

$$V_{\text{out}} = 0.7 (n V_{\text{charge}}) \quad (5)$$

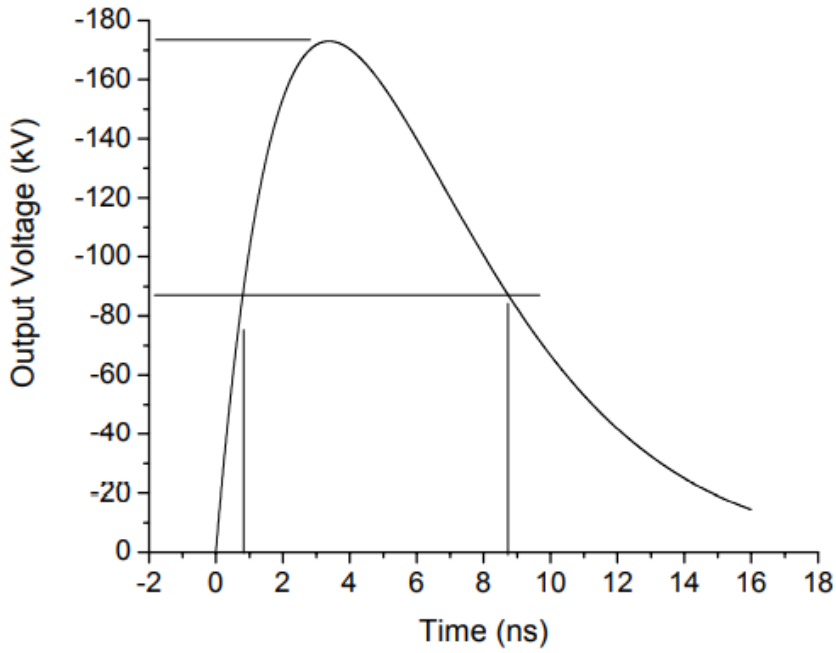
Therefore, a first pass Marx design is obtained in the following way: 1. Choose the desired T_{pulse} , V_{out} , and R. 2. Solve equations (2), (3), and (4) to find L_{eq} and C_{eq} . 3. Choose n and V_{charge} to satisfy equation (5). 4. Calculate the stage inductances and capacitances according to equations (6) and (7).

$$L_{\text{stage}} = L_{\text{eq}}/n \quad (6)$$

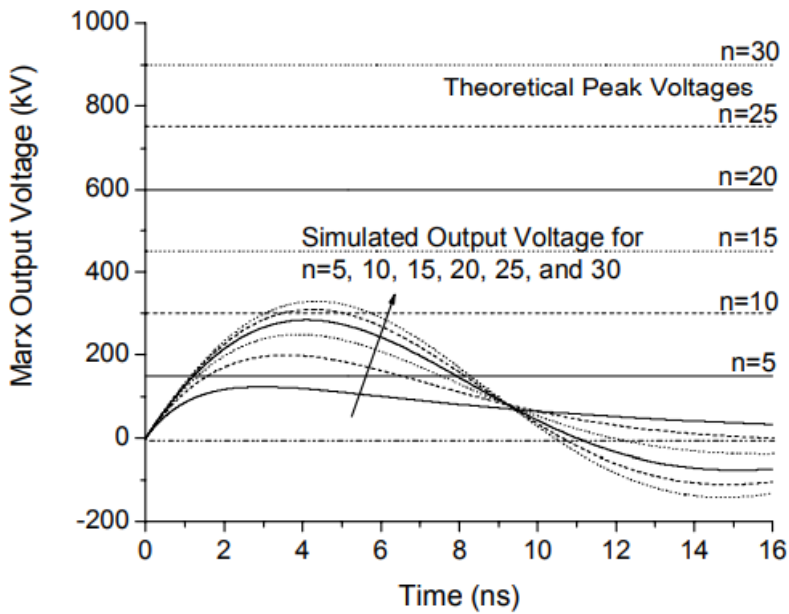
$$C_{\text{stage}} = n C_{\text{eq}} \quad (7)$$

It should be noted that the additional inductance associated with both ends of the Marx has been neglected. They can be easily included by subtracting them from L_{eq} before calculating L_{stage} . This simplification has been made to more easily show the results of adding stages in the following paragraphs. Consider the design of a Marx generator with a FWHM pulse width of 8ns with an amplitude of -170kV into 50 Ohms. These require $L_{\text{eq}} = 80\text{nH}$ and $C_{\text{eq}} = 127\text{pF}$. A charge voltage of 240kV is required, so an 8 stage Marx is chosen with 30 kV charging. The simulated result is shown in Figure 3. The design process shown has been straightforward, and a Marx designed as described typically performs reasonably close to specifications. It is now assumed that a Marx has been designed and constructed as described. The system works as planned, but now it is decided to increase the output voltage. It seems reasonable to construct more stages just like are presently in use and lengthen the Marx. How will these additional equivalent stages affect circuit performance, other than changing the charging time? Equation 8, derived from 2, 6 and 7 shows that the impedance of the Marx increases with n. Figure 4 illustrates that the LRC circuit model becomes increasingly underdamped. The pulse length does not change significantly, but more energy is lost in the overshoot, decreasing the voltage efficiency as shown in Figure

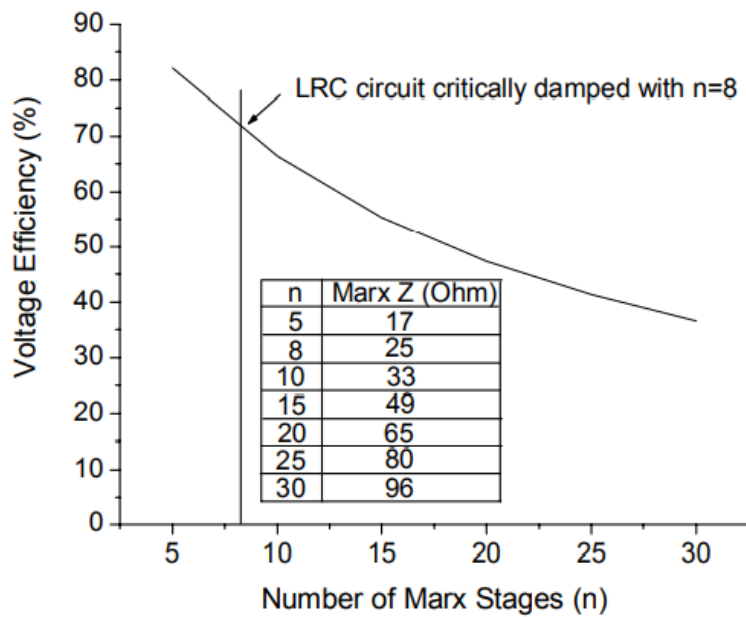
$$Z = n \sqrt{L_{\text{stage}}/C_{\text{stage}}} \quad (8)$$



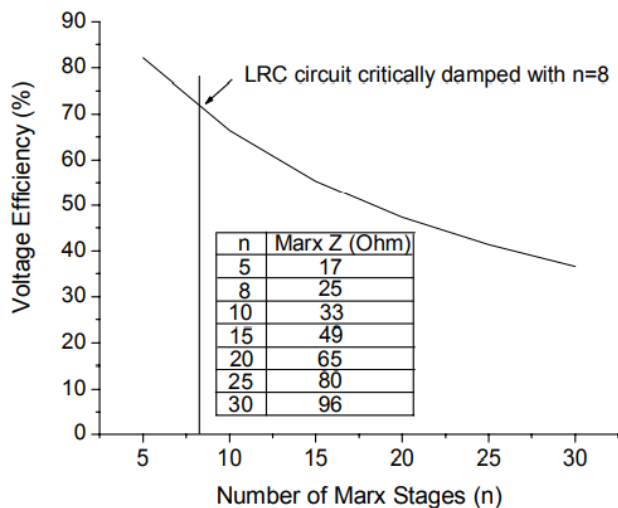
Simulation Marx generator design example.



Marx LRC circuit approximation performance when equivalent stages are added.



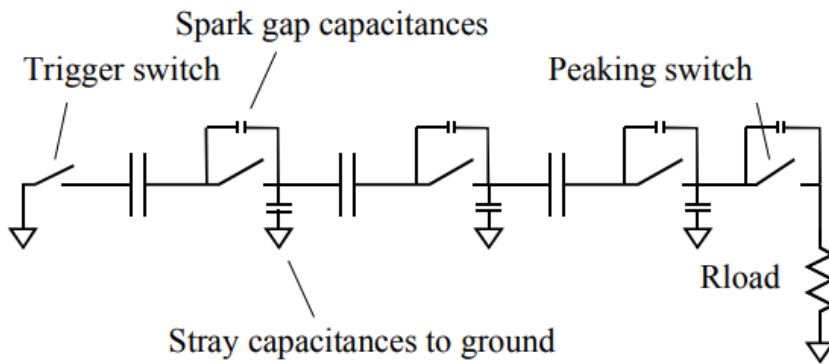
Voltage efficiency of a Marx generator as equivalent stages are added, changing the circuit damping.



Voltage efficiency of a Marx generator as equivalent stages are added, changing the circuit damping.

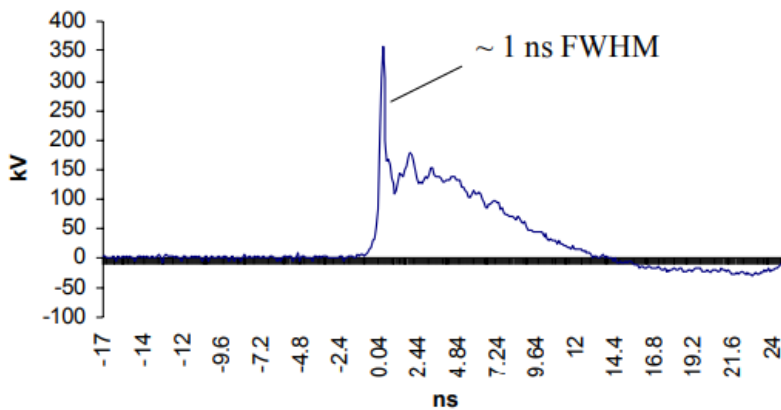
WAVE ERECTION MARX

The transient wave erection Marx shown in Figure 6 differs from the Marx circuit of Figures 1 and 2 in its use of stray capacitance effects. The general Marx circuit does not force switches to close in succession. Therefore, switches can fire randomly, adding temporal jitter to the system's performance. The transient wave Marx insures that after closure of the first switch, stray capacitances hold one side of each successive switch near ground until the switch fires. A voltage wave propagates toward the load with increasing intensity, triggering successive switches faster and faster until it reaches the load with sub-ns rise time and low jitter for output voltages of several hundred kV at moderate per pulse energies.



Transient wave erection Marx circuit.

The output waveform from a 17 stage transient wave Marx generator is shown in Figure 7. Notice the characteristic Marx output pulse shape, except for the front spike. The risetime is 250ps. A temporal jitter of 114ps RMS has been demonstrated by a 17 stage transient Marx, excluding the 15kV trigger generator circuitry.

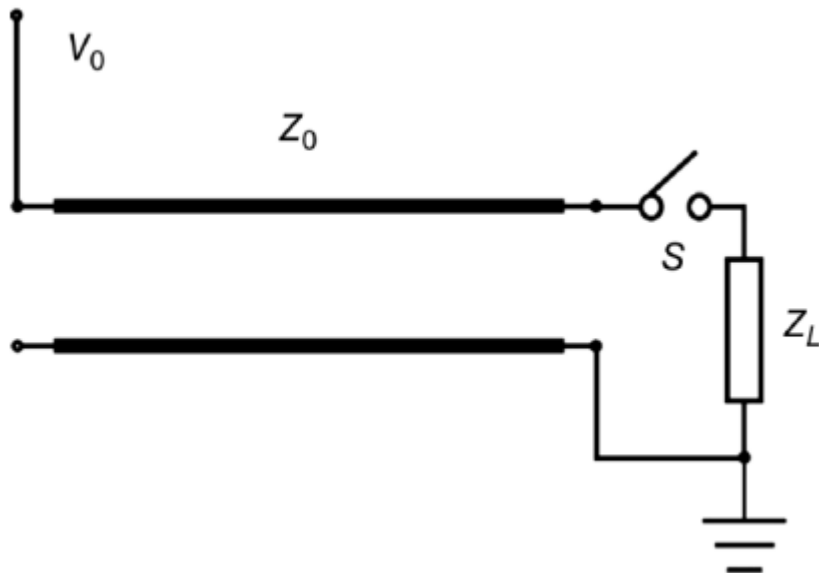


Transient wave Marx output waveform

Marx generators are effective systems for efficient voltage multiplication. For short pulse generation the Marx should operate near its critical damping due to a balance between voltage efficiency and overshoot. The transient wave erection Marx should be used where fast rise times are critical.

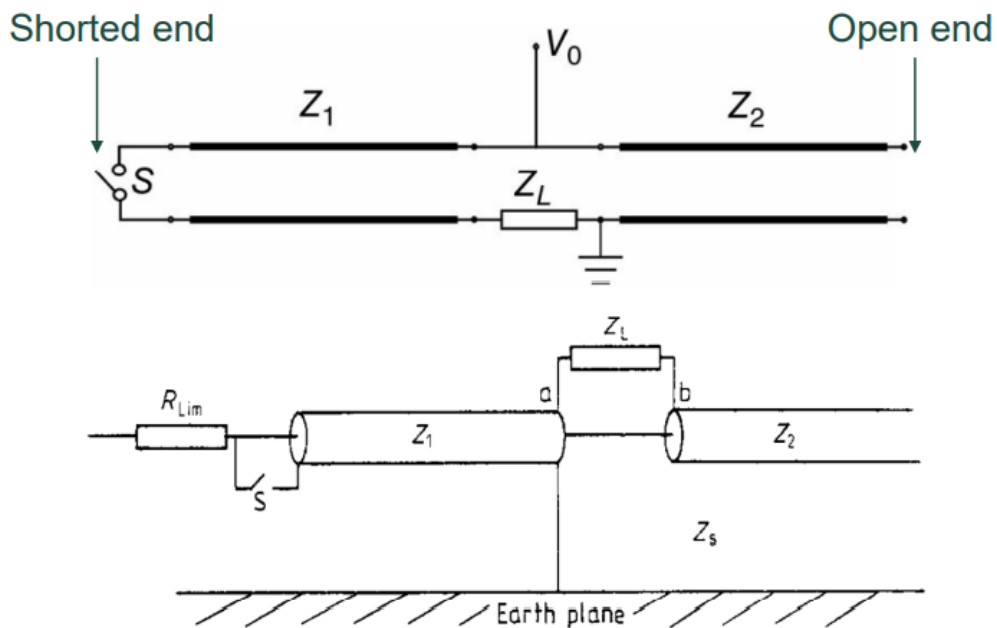
16.1.1.2 Pulse forming line (PFL)

- There are numerous applications in both physics and electrical engineering for short ($\sim 10 \text{ ns} < t_p < 100 \mu\text{s}$) electrical pulses. These applications often require that the pulses have a “good” square shape.
- Although there are many ways for generating such pulses, the pulse-forming line (PFL) is one of the simplest techniques and can be used even at extremely high pulsed power levels.
- A transmission line of any geometry of length l and characteristic impedance Z_0 makes a pulse forming line (PFL), which when combined with a closing switch SS makes the simple transmission line pulser.



Blumlein PFL

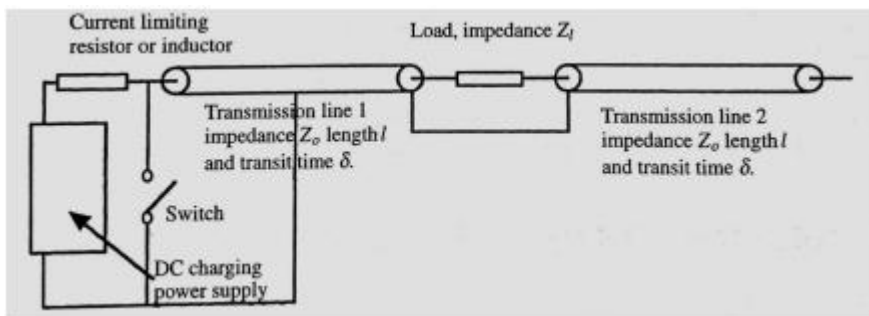
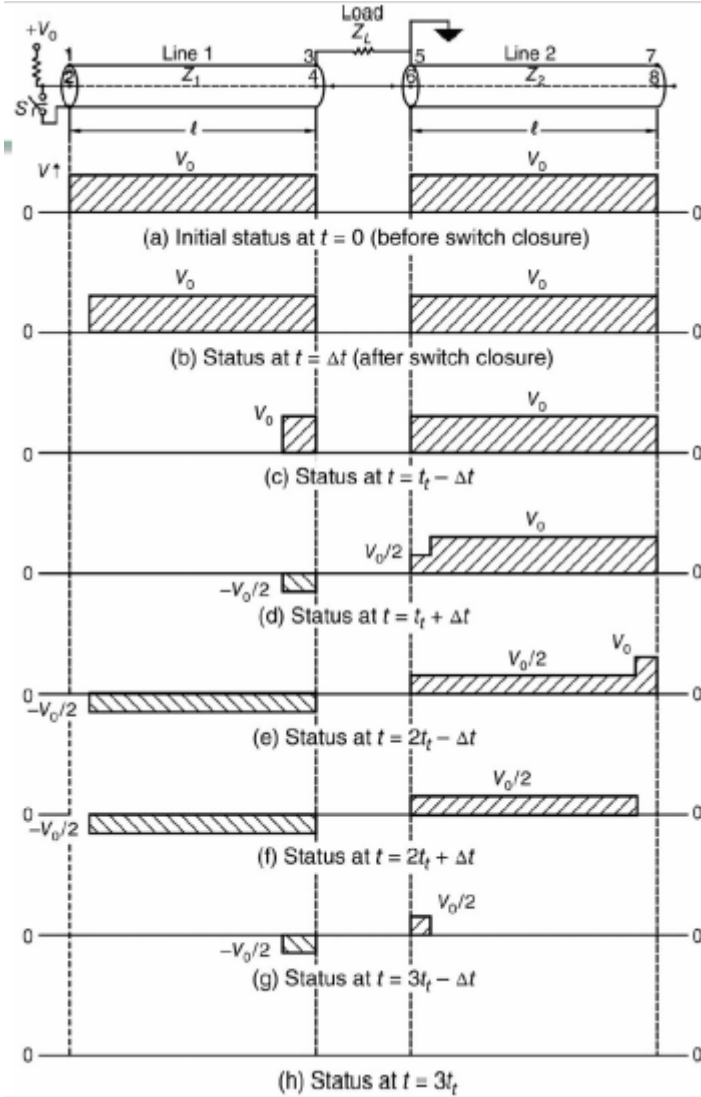
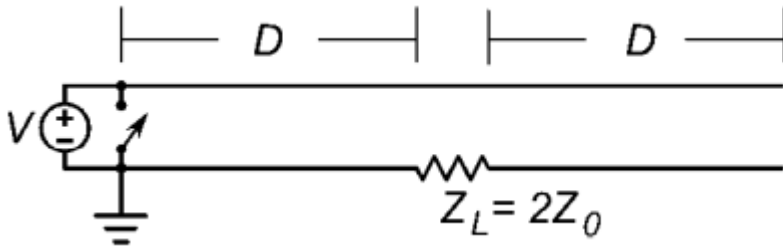
- An important disadvantage of the simple PFL is that the pulse generated into a matched load is only equal to $VV_0/2$.
- This problem can be avoided using the Blumlein PFL invented by A. D. Blumlein.
- Two transmission lines and one switch is used to construct the generator.



- After switch closure, the end of line 1 is effectively shorted; thus the reflection coefficient is +1.
- At the junction of line 1 and the load, the reflection coefficient is given by

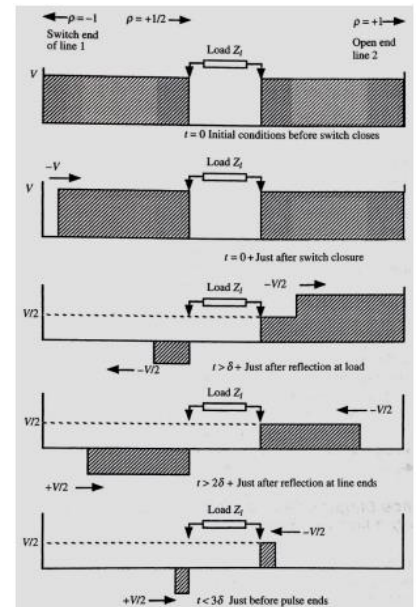
$$\rho = \frac{(Z_L + Z_2) - Z_1}{(Z_L + Z_2) + Z_1} = \frac{Z_L}{Z_L + 2Z_0} = \frac{1}{2}$$

- λ Matching condition: $ZL = 2Z_0$



- The reflection coefficient at the load

$$\rho = \frac{Z_L}{Z_L + 2Z_0}$$



- The reflected step at the load

$$V_- = \rho(-V) = -V \frac{Z_L}{Z_L + 2Z_0}$$

- The step V_{TT} transmitted to the load and the line 2

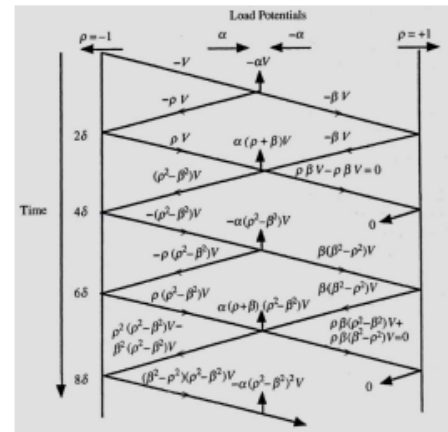
$$V_T = V_+ + V_- = -2V \frac{Z_L + Z_0}{Z_L + 2Z_0}$$

- The fraction of the step to the load and the line 2

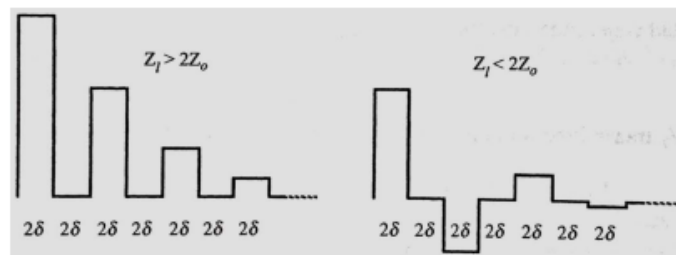
$$V_L = -2V \frac{Z_L + Z_0}{Z_L + 2Z_0} \times \frac{Z_L}{Z_L + Z_0} = -\alpha V$$

$$V_{2T} = -2V \frac{Z_L + Z_0}{Z_L + 2Z_0} \times \frac{Z_0}{Z_L + Z_0} = -\beta V$$

$$\alpha = \frac{2Z_L}{Z_L + 2Z_0} \quad \beta = \frac{2Z_0}{Z_L + 2Z_0}$$



$$V_L = -\alpha V [1 - 1 + (\rho - \beta) - (\rho - \beta) + (\rho - \beta)^2 - (\rho - \beta)^2 + \dots]$$



References

The following reports and articles (with submenus) are included:

2021 (X-Ray Detector):

[X-Ray Detector - Presentation Master Thesis of Yahya Abbouchi \(pptx\), Dec 2021](#)

[PhysicsLab Test Rigs PCS \(Dec2021\) \(docx\)](#)

2022 (IECF,

[Electrofilter Measurement with Rogowski Coil \(pdf\)](#)

[Electrofilter Measurement with Rogowski Coil \(docx\)](#)

2024 (Mass Spectrometer):

[OZ, Measuring of Incineration Flue Gas Heavy Metals Residues with Mass Spectrometer Introduction \(Presentation\) \(pptx\)](#)

[OZ, Measuring of Incineration Flue Gas Heavy Metals Residues with Mass Spectrometer \(Master Thesis Report\) \(docx\) \(Oct 2024\)](#)

[Mass Spectrometer PCS Poster \(pptx\)](#)

IAP-PhysicsLab Design and X-Ray 2023

[Master Thesis Of Rouwayda \(docx\)](#)

Mass Spectrometer 2023

[Master Thesis Of Asmaa \(docx\)](#)

[Memoire De Master Asmaa \(docx\)](#)

[IAP Report 2022 \(docx\)](#)

[IAP Report 2022 \(PDF\)](#)

Fusion (Presentation and Simulation) (2024)